



National Library
of Canada

Bibliothèque nationale
du Canada

Canadian Theses Service

Service des thèses canadiennes

Ottawa, Canada
K1A 0N4

NOTICE

The quality of this microform is heavily dependent upon the quality of the original thesis submitted for microfilming. Every effort has been made to ensure the highest quality of reproduction possible.

If pages are missing, contact the university which granted the degree.

Some pages may have indistinct print especially if the original pages were typed with a poor typewriter ribbon or if the university sent us an inferior photocopy.

Reproduction in full or in part of this microform is governed by the Canadian Copyright Act, R.S.C. 1970, c. C-30, and subsequent amendments.

AVIS

La qualité de cette microforme dépend grandement de la qualité de la thèse soumise au microfilmage. Nous avons tout fait pour assurer une qualité supérieure de reproduction.

S'il manque des pages, veuillez communiquer avec l'université qui a conféré le grade.

La qualité d'impression de certaines pages peut laisser à désirer, surtout si les pages originales ont été dactylographiées à l'aide d'un ruban usé ou si l'université nous a fait parvenir une photocopie de qualité inférieure.

La reproduction, même partielle, de cette microforme est soumise à la Loi canadienne sur le droit d'auteur, SRC 1970, c. C-30, et ses amendements subséquents.



National Library
of Canada

Bibliothèque nationale
du Canada

Canadian Theses Service Service des thèses canadiennes

Ottawa, Canada
K1A 0N4

The author has granted an irrevocable non-exclusive licence allowing the National Library of Canada to reproduce, loan, distribute or sell copies of his/her thesis by any means and in any form or format, making this thesis available to interested persons.

The author retains ownership of the copyright in his/her thesis. Neither the thesis nor substantial extracts from it may be printed or otherwise reproduced without his/her permission.

L'auteur a accordé une licence irrévocable et non exclusive permettant à la Bibliothèque nationale du Canada de reproduire, prêter, distribuer ou vendre des copies de sa thèse de quelque manière et sous quelque forme que ce soit pour mettre des exemplaires de cette thèse à la disposition des personnes intéressées.

L'auteur conserve la propriété du droit d'auteur qui protège sa thèse. Ni la thèse ni des extraits substantiels de celle-ci ne doivent être imprimés ou autrement reproduits sans son autorisation.

ISBN 0-315-55333-2

Canada

THE UNIVERSITY OF ALBERTA

Field Monitoring of Anchored Sheet Pile Retaining Walls

by

Peter Gaffran



A THESIS

SUBMITTED TO THE FACULTY OF GRADUATE STUDIES AND RESEARCH
IN PARTIAL FULFILMENT OF THE REQUIREMENTS FOR THE DEGREE
OF MASTER OF SCIENCE

DEPARTMENT OF CIVIL ENGINEERING

EDMONTON, ALBERTA

FALL 1989

THE UNIVERSITY OF ALBERTA

RELEASE FORM

NAME OF AUTHOR Peter Gaffran
TITLE OF THESIS Field Monitoring of Anchored Sheet
Pile Retaining Walls
DEGREE FOR WHICH THESIS WAS PRESENTED MASTER OF SCIENCE
YEAR THIS DEGREE GRANTED FALL 1989

Permission is hereby granted to THE UNIVERSITY OF ALBERTA LIBRARY to reproduce single copies of this thesis and to lend or sell such copies for private, scholarly or scientific research purposes only.

The author reserves other publication rights, and neither the thesis nor extensive extracts from it may be printed or otherwise reproduced without the author's written permission.

(SIGNED) *P. Gaffran*

PERMANENT ADDRESS:

..4. Horns Hill Drive

..Aurora, Ontario

..M1S 2Y2

DATED ... *Mar. 23* 198*8*

THE UNIVERSITY OF ALBERTA
FACULTY OF GRADUATE STUDIES AND RESEARCH

The undersigned certify that they have read, and recommend to the Faculty of Graduate Studies and Research, for acceptance, a thesis entitled Field Monitoring of Anchored Sheet Pile Retaining Walls submitted by Peter Gaffran in partial fulfilment of the requirements for the degree of MASTER OF SCIENCE in CIVIL ENGINEERING.

..... *A. Seg.*

..... Supervisor
P. Peteres

..... *P. Bou*

..... *W. H. ...*

Date... *Aug. 29* ... *1928*

Abstract

Canadian National Railways, during the spring of 1984, was twinning its track in the vicinity of Boston Bar, British Columbia. In order to support the new track it was necessary to construct two anchored sheet pile retaining walls just north of the townsite. In conjunction with the Department of Civil Engineering at the University of Alberta a program was established to monitor the performance of these walls. Load cells, wall and anchor mounted strain gauges, a survey network, vertical slope indicators, and multi-point magnetic extensometers were installed at the site. Field data was collected on a regular basis over the course of 33 months providing the opportunity to observe the behavior of the walls over a considerable time period.

The project's objectives are as follows: reduce the data collected from the field and present the results; interpret the results so that the observed behavior of the walls can be described; compare the measured performance with predictions for the loads and deformations sustained by retaining walls.

The lateral earth pressures behind the walls were noted to conform to a rectangular distribution. Loads were, however, increased over the top half of the distributions as a result of the influence of the train traffic. Lateral pressures were approximately $0.25\gamma H$ and $0.15\gamma H$ over the upper and lower portions of the wall respectively.

Measurements of displacements at one of the walls indicated concave outward deflected shapes. Maximum movements of approximately $0.0015H$ were noted at ends of the wall. Movements over the mid-section of the wall were approximately one half of the maximum.

Available measurements also suggest that one of the walls has experienced considerable differential settlement. As well, vertical movements in the backfill behind this wall exceeded 200 mm.

Reasonable prediction of the observed lateral loads was achieved by combining the Terzaghi and Peck (1967) recommendation with a modified Boussinesq procedure (Canadian Foundation Engineering Manual, 1985). Poorer predictions for the observed displacements were obtained using finite element analysis. However, results indicate that wall movements can be adequately modelled based on the bending moment distribution associated with an assumed pressure distribution.

Acknowledgements

The research program described here was carried out under the supervision of Professor D.C. Sego. It has been a privilege and a pleasure to work for Professor Sego. I express sincere appreciation and many thanks for his guidance and contributions.

Mr. B. Jubien of Canadian National Railways initiated this project. Thanks are extended to him for providing the opportunity to conduct a long term field monitoring program and for committing CN's support and assistance.

I am grateful to Professor A.E. Peterson who has been an integral part of this project since its inception. I extend thanks for the many hours of work he has generously contributed, both in the field and at the computer. I also wish to thank him for the many discussions we have had, the many books he has loaned me and the encouragement he has provided over the past two years.

This project would not have been possible without the expertise and skill of Mr. G. Cyre. He was responsible for the installation of all the instrumentation at the site and has made numerous field visits. His dedication has been much appreciated.

I am very much indebted to my friend and colleague Mr. Henk Aik Khoo. He possesses a powerful intellect combined with an uncommon ability to relate higher concepts to lesser mortals. This he did for me with understanding and enthusiasm on many occasions.

Professor A. Elwi has acted as the project's unofficial structural consultant. His involvement in the planning phase of the project is acknowledged. Thanks are due for the useful advise he has provided over the course of this research.

Mr. J. Rodgers was of great assistance both in the field and at the office. He made an art out of being indispensable and I thank him for his efforts.

I would like to thank Professor Sego for providing financial support from the National Research Council of Canada. Thanks are also due to Professor D. Chan for whom I worked as a research assistant.

I extend special thanks to Barbara Hofmann. She is familiar with every detail of this work and has contributed much to its completion. I am very grateful for her support and especially her skillful listening.

To my Parents, to whom I dedicate this work, I express my profound thanks. Thanks, Mom and Dad, for everything.

Table of Contents

Chapter	Page
1. Introduction	1
1.1 General	1
1.2 The Project and the Research Objectives	2
1.3 Thesis Organization	2
2. Literature Review	6
2.1 Nature of the Problem	6
2.2 Coulomb Theory	7
2.3 Rankine Theory	12
2.4 Subsequent Developments	15
2.5 Strutted Excavations	17
2.6 Tied Back Walls	25
3. Site Description	44
3.1 Introduction	44
3.2 General Description	44
3.3 Instrumentation	46
3.4 Construction Procedure	49
3.5 Monitoring History	53
4. Instrumentation	72
4.1 Introduction	72
4.2 Anchor and Wall Mounted Strain Gauges	72
4.3 Load Cells	79
4.4 Surveying	83
4.5 Slope Indicator	89
4.6 Magnetic Extensometer	92
5. Field Results	97
5.1 Introduction	97

5.2	Loads on the Wall	97
5.2.1	Anchor Loads	97
5.2.1.1	East Wall Load Cells	98
5.2.1.2	West Wall Load Cells	101
5.2.1.3	East Wall Anchor Strain Gauge Loads	102
5.2.1.4	West Wall Anchor Strain Gauge Loads	103
5.2.2	Stress Distribution In the Anchors	104
5.2.3	Loads Inferred from the Wall Mounted Strain Gauges	106
5.2.3.1	East and West Section Earth Pressure Results	107
5.3	Lateral Displacement of the East Wall	109
5.3.1	Surveying	109
5.3.2	Slope Indicators	111
5.3.2.1	VSI1	113
5.3.2.2	VSI2	115
5.3.2.3	VSI3	116
5.3.3	Displacement Inferred from the Wall Mounted Strain Gauges	117
5.4	Extensometer Results	118
5.5	Correlation Between East Wall Loads and Movement	119
5.6	Conclusions	122
6.	Performance Predictions for the East Wall	126
6.1	Introduction	126
6.2	Field Results	127
6.2.1	Measured Loads	127
6.2.2	Measured Deformations	129

6.3	Predicted Results	129
6.3.1	Rankine Earth Pressure	132
6.3.2	Coulomb Earth Pressure	133
6.3.3	Dubrova Solution	134
6.3.4	Terzaghi and Peck	136
6.3.5	Tschebotarioff	137
6.3.6	Hanna and Matallana	138
6.3.7	Effect of Train Loads	138
6.3.8	The Finite Element Method	140
6.4	Comparison of Field and Predicted Results	146
6.4.1	Load	147
6.4.2	Deformation	154
6.5	Conclusions	156
7.	Conclusions and Recommendations	180
7.1	Conclusions	180
7.2	Recommendations	182
	References	185
	<i>Appendix A</i>	
	<i>Anchor Loads</i>	<i>192</i>
	<i>Appendix B</i>	
	<i>Anchor Strain Gauge Results</i>	<i>209</i>
	<i>Appendix C</i>	
	<i>Earth Pressure Distributions based on the Wall</i>	
	<i>Mounted Strain Gauges</i>	<i>228</i>
	<i>Appendix D</i>	
	<i>Displacements of the East Wall as Determined by</i>	
	<i>Surveying.</i>	<i>239</i>
	<i>Appendix E</i>	
	<i>Slope Indicator Results</i>	<i>250</i>
	<i>Appendix F</i>	
	<i>East Wall Displacements based on the Wall Mounted</i>	
	<i>Strain Gauges</i>	<i>283</i>

Appendix G	
Extensometer Results	290
Appendix H	
Bending Moments Based on the Wall Mounted Strain	
Gauge Results	292
Appendix I	
Data Reduction Procedure for the Load Cells	339
I.1 Introduction	339
I.2 Calculation Procedure	340
I.3 Operating Procedure	342
I.4 Datafile and Program Listings	343
Appendix J	
Data Reduction Procedure for the Anchor Strain	
Gauges	344
J.1 Introduction	355
J.2 Calculation Procedure	355
J.3 Operating Procedure	358
J.4 Datafile and Program Listings	358
Appendix K	
Data Reduction Procedure for the Wall Mounted Strain	
Gauges	359
K.1 Introduction	368
K.2 Calculation Procedure	368
K.2.1 Calculation of the bending and axial	
stresses and the bending moments	369
K.2.2 Establish a bending moment distribution	
over the height of the wall	373
K.2.3 Determine the shear and pressure	
distributions	379
K.2.4 Determine the theoretical bending	
deflection of the wall	381
K.2.5 Comments on the data reduction procedure	
.....	383
K.3 Operating Procedure	384

K.4	Datafile and Program Listings	385
<i>Appendix L</i>		
	<i>Data Reduction Procedure for the Survey</i>	386
L.1	Introduction	414
L.2	Calculation Procedure	414
L.2.1	Survey Data Preparation	415
L.2.1.1	Horizontal Angles	415
L.2.1.2	Vertical Angles	416
L.2.1.3	Chained Distances	417
L.2.1.4	Distance Measured with the Wild Distomat (DI4)	419
L.2.2	Least Squares Adjustment	420
L.2.3	Calculation of the Deflection Profile	430
L.3	Operating Procedure	431
L.4	Datafile and Program Listings	432
<i>Appendix M</i>		
	<i>Data Reduction Procedure for the Slope Indicator</i>	433
M.1	Introduction	446
M.2	Calculation Procedure	446
M.3	Operating Procedure	455
M.4	Datafile and Program Listings	455
<i>Appendix N</i>		
	<i>Data Reduction Procedure for the Extensometer</i>	456
N.1	Introduction	466
N.2	Calculation Procedure	466
N.3	Operating Procedure	468
N.4	Datafile and Program Listings	468
<i>Appendix O</i>		
	<i>Earth Pressure Results</i>	469
O.1	Introduction	472

Appendix P
Factor of Safety Analyses494
 P.1 Sliding Factor of Safety494
 P.2 Factor of Safety based on Force Equilibrium496
Appendix Q
Miscellaneous Computer Programs499

List of Tables

Table	Page
3.1	Locations of the wall mounted strain gauges on the east wall.55
3.2	Locations of the survey positions on the east wall.56
3.3	Instrument measurement dates.57
6.1	Weighted average anchor loads per metre width and per unit area.157
6.2	Materials used in the finite element analysis and their parameters.158
6.3	Summary of measured and predicted anchor loads.159
A.1	Load readings for anchor A.193
A.2	Load readings for anchor B.193
A.3	Load readings for anchor C.194
A.4	Load readings for anchor D.194
A.5	Load readings for anchor E.195
A.6	Load readings for anchor F.195
A.7	Load readings for anchor G.196
A.8	Load readings for anchor G.196
B.1	Strain gauge results for Anchor A.210
B.2	Strain gauge results for Anchor B.211
B.3	Strain gauge results for Anchor C.212
B.4	Strain gauge results for Anchor D.213
B.5	Strain gauge results for Anchor E.214
B.6	Strain gauge results for Anchor F.215
D.1	Survey displacement results, east wall.240
E.1	VSI1, calibration values, 21/06/84.251
E.2	VSI1, results from 05/08/84.252
E.3	VSI1, results from 03/10/84.253

Table	Page
E.4 VSI1, results from 05/12/84.	254
E.5 VSI1, results from 11/02/85.	255
E.6 VSI1, results from 29/08/85.	256
E.7 VSI1, results from 25/03/86.	257
E.8 VSI1, results from 29/07/86.	258
E.9 VSI1, results from 09/12/86.	259
E.10 VSI1, results from 16/02/87.	260
E.11 VSI1, results from 25/03/87.	261
E.12 VSI2, calibration values, 29/07/86.	262
E.13 VSI2, results from 09/12/86.	263
E.14 VSI2, results from 16/02/87.	264
E.15 VSI2, results from 25/03/87.	265
E.16 VSI3, calibration values, 29/07/86.	266
E.17 VSI3, results from 09/12/86.	267
E.18 VSI3, results from 25/03/87.	268
H.1 Wall mounted strain gauge results for June 20, 1984, east section.	293
H.2 Wall mounted strain gauge results for June 21, 1984, east section.	293
H.3 Wall mounted strain gauge results for July 10, 1984, east section.	294
H.4 Wall mounted strain gauge results for August 5, 1984, east section.	294
H.5 Wall mounted strain gauge results for October 3, 1984, east section.	295
H.6 Wall mounted strain gauge results for December 5, 1984, east section.	295
H.7 Wall mounted strain gauge results for February 11, 1985, east section.	296
H.8 Wall mounted strain gauge results for August 29, 1985, east section.	296

Table	Page
H.9 Wall mounted strain gauge results for March 25, 1986, east section.	297
H.10 Wall mounted strain gauge results for July 29, 1986, east section.	297
H.11 Wall mounted strain gauge results for December 10, 1986, east section.	298
H.12 Wall mounted strain gauge results for February 16, 1987, east section.	298
H.13 Wall mounted strain gauge results for March 25, 1987, east section.	299
H.14 Wall mounted strain gauge results for June 20, 1984, west section.	300
H.15 Wall mounted strain gauge results for June 21, 1984, west section.	300
H.16 Wall mounted strain gauge results for July 10, 1984, west section.	301
H.17 Wall mounted strain gauge results for August 5, 1984, west section.	301
H.18 Wall mounted strain gauge results for October 3, 1984, west section.	302
H.19 Wall mounted strain gauge results for December 5, 1984, west section.	302
H.20 Wall mounted strain gauge results for February 11, 1985, west section.	303
H.21 Wall mounted strain gauge results for August 29, 1985, west section.	303
H.22 Wall mounted strain gauge results for March 25, 1986, west section.	304
H.23 Wall mounted strain gauge results for July 29, 1986, west section.	304
H.24 Wall mounted strain gauge results for December 10, 1986, west section.	305
H.25 Wall mounted strain gauge results for February 16, 1987, west section.	305
H.26 Wall mounted strain gauge results for March 25, 1987, west section.	306

Table	Page
O.1 Rankine earth pressure results, low wall, no soil surcharge.	474
O.2 Rankine earth pressure results, high wall, no soil surcharge.	474
O.3 Rankine earth pressure results, low wall, soil surcharge.	475
O.4 Rankine earth pressure results, high wall, soil surcharge.	475
O.5 Coulomb earth pressure results, low wall, no train.	476
O.6 Coulomb earth pressure results, low wall, train.	477
O.7 Coulomb earth pressure results, high wall, no train.	478
O.8 Coulomb earth pressure results, high wall, train.	479
O.9 Dubrova earth pressure results, low wall, no train.	480
O.10 Dubrova earth pressure results, low wall, train.	481
O.11 Dubrova earth pressure results, high wall, no train.	482
O.12 Dubrova earth pressure results, high wall, train.	483
O.13 Terzaghi & Peck (1948) earth pressure results, low wall, no soil surcharge.	484
O.14 Terzaghi & Peck (1948) earth pressure results, high wall, no soil surcharge.	485
O.15 Terzaghi & Peck (1948) earth pressure results, low wall, soil surcharge.	486
O.16 Terzaghi & Peck (1948) earth pressure results, high wall, soil surcharge.	487
O.17 Terzaghi & Peck (1967) earth pressure results, low wall, no soil surcharge.	488
O.18 Terzaghi & Peck (1967) earth pressure results, high wall, no soil surcharge.	488

Table	Page
O.19 Terzaghi & Peck (1967) earth pressure results, low wall, soil surcharge.	489
O.20 Terzaghi & Peck (1967) earth pressure results, high wall, soil surcharge.	489
O.21 Tschebotarioff (1951) earth pressure results, low wall, no soil surcharge.	490
O.22 Tschebotarioff (1951) earth pressure results, high wall, no soil surcharge.	490
O.23 Tschebotarioff (1951) earth pressure results, low wall, soil surcharge.	490
O.24 Tschebotarioff (1951) earth pressure results, high wall, soil surcharge.	490
O.25 Tschebotarioff (1973) earth pressure results, low wall, no soil surcharge.	491
O.26 Tschebotarioff (1973) earth pressure results, high wall, no soil surcharge.	491
O.27 Tschebotarioff (1973) earth pressure results, low wall, soil surcharge.	491
O.28 Tschebotarioff (1973) earth pressure results, high wall, soil surcharge.	491
O.29 Hanna & Matallana earth pressure results, low wall, no soil surcharge.	492
O.30 Hanna & Matallana earth pressure results, high wall, no soil surcharge.	492
O.31 Hanna & Matallana earth pressure results, low wall, soil surcharge.	493
O.32 Hanna & Matallana earth pressure results, high wall, soil surcharge.	493

List of Figures

Figure	Page
2.1	Terms involved in the Coulomb solution showing the force polygon. Soil has no cohesion36
2.2	Stress state under active and passive lateral earth pressure conditions, cohesive soil, horizontal back slope.36
2.3	Terms involved in Rankine earth pressure solution for; a) active case, b) passive case.37
2.4	Terzaghi and Peck's (1948) apparent earth pressure distribution for sand.38
2.5	Terzaghi and Peck's (1967) apparent earth pressure distribution for sand.38
2.6	Tschebotarioff's (1951) recommendation for the earth pressure distribution in sand.39
2.7	Tschebotarioff's (1973) recommendation for the earth pressure distribution in sand.39
2.8	Peck's (1943) earth pressure distribution for normally consolidated clay.40
2.9	Tschebotarioff's (1951) recommendations for earth pressure distributions in; a) temporary cuts in stiff clay, b) permanent cuts in medium clay.40
2.10	Terzaghi and Peck's (1967) apparent earth pressure distribution for soft to medium clay.41
2.11	Terzaghi and Peck's (1967) apparent earth pressure distribution for stiff clay.41
2.12	Danish earth pressure distribution for anchored bulkheads.42
2.13	Deformation condition and the pressure distribution associated with the free earth support method.42
2.14	Deformation condition and the pressure distribution associated with the fixed earth support method.42

Figure	Page
2.15 Ohde's prediction for the earth pressure distribution behind a wall with fixed top and bottom as reported by Terzaghi (1953).	43
2.16 Tschebotarioff's (1973) design envelope incorporating a hinge at the dredge level.	43
2.17 Hanna and Matallana's (1970) apparent earth pressure distribution for cuts in granular material supported by multiple anchor rows.	43
3.1 General site plan.	58
3.2 East wall elevation view.	59
3.3 West wall elevation view.	60
3.4 Cross section at the reference sheet pile joint of the east wall	61
3.5 Plan view of east wall showing surface instrumentation installed.	62
3.6 Location of elements in the survey network (excluding elements mounted on the surface of the east wall).	63
3.7 Location of survey positions on the east wall.	64
3.8 Dimensions and characteristics of the sheet pile section.	65
3.9 Details of the waler, anchor and load cell arrangement.	65
4.1 The Wheatstone bridge.	94
4.2 Connection of the strain gauge to the Wheatstone bridge via: a) a two wire system; b) a three wire system.	94
4.3 Load cell used at Boston Bar shown in; a) elevation view, b) plan view.	95
4.4 a) load cell divided into quadrants; b) an "unrolled" load cell showing the positions of the strain gauges around its circumference; c) the positions of the strain gauges in the Wheatstone bridge.	96

Figure	Page
6.1 Horizontal earth pressure based on east wall load cell results.	160
6.2 Pressure distributions based on wall mounted strain gauges, reference epochs, east section.	161
6.3 Pressure distributions based on wall mounted strain gauges, reference epochs, west section.	162
6.4 Displacement based on wall mounted strain gauges, reference epochs, east section.	163
6.5 Displacement based on wall mounted strain gauges, reference epochs, west section.	164
6.6 Predicted pressure envelopes, low wall, no train.	165
6.7 Predicted pressure envelopes, low wall, no train.	166
6.8 Predicted pressure envelopes, low wall, train present.	167
6.9 Predicted pressure envelopes, low wall, train present.	168
6.10 Predicted pressure envelopes, high wall, train present.	169
6.11 Predicted pressure envelopes, high wall, train present.	170
6.12 Boussinesq pressures from line loads due to train traffic, wall unextended.	171
6.13 Boussinesq pressures from line loads due to train traffic, wall extended.	172
6.14 Lateral earth pressure predicted by finite element analysis.	173
6.15 Displacement of SPW referenced to load step 5 as predicted by the finite element analysis.	174
6.16 Terms involved in the Dubrova (1963) solution.	175

Figure	Page
6.17 Boussinesq procedure for calculating lateral pressures induced by line loads; a) as presented in CFEM (1985), b) as applied to Boston Bar to account for batter of wall and the sloped backfill.	175
6.18 The finite element grid.	176
6.19 Load steps 1 to 3 in the finite element analysis.	177
6.20 Load steps 4 and 5 in the finite element analysis.	178
6.21 Load steps 6 and 7 in the finite element analysis.	179
A.1 Load versus time for Anchor A.	197
A.2 Load versus time for Anchor B.	198
A.3 Load versus time for Anchor C.	199
A.4 Load versus time for Anchor D.	200
A.5 Load versus time for Anchor E.	201
A.6 Load versus time for Anchor F.	202
A.7 Load versus time for Anchor G.	203
A.8 Load versus time for Anchor H.	204
A.9 Load versus time for east wall load cells.	205
A.10 Load versus time for west wall load cells.	206
A.11 Load versus time for east wall ASG.	207
A.12 Load versus time for west wall ASG.	208
B.1 Stress vs length for Anchor A, early epochs.	216
B.2 Stress vs length for Anchor A, late epochs.	217
B.3 Stress vs length for Anchor B, early epochs.	218

Figure	Page
B.4 Stress vs length for Anchor B, late epochs.	219
B.5 Stress vs length for Anchor C, early epochs.	220
B.6 Stress vs length for Anchor C, late epochs.	221
B.7 Stress vs length for Anchor D, early epochs.	222
B.8 Stress vs length for Anchor D, late epochs.	223
B.9 Stress vs length for Anchor E, early epochs.	224
B.10 Stress vs length for Anchor E, late epochs.	225
B.11 Stress vs length for Anchor F, early epochs.	226
B.12 Stress vs length for Anchor F, late epochs.	227
C.1 Earth pressure distributions, east section.	229
C.2 Earth pressure distributions, east section.	230
C.3 Earth pressure distributions, east section.	231
C.4 Earth pressure distributions, east section.	232
C.5 Summary of east section earth pressure distributions.	233
C.6 Earth pressure distributions, west section.	234
C.7 Earth pressure distributions, west section.	235
C.8 Earth pressure distributions, west section.	236
C.9 Earth pressure distributions, west section.	237

Figure	Page
C.10 Summary of west section earth pressure distributions.	238
D.1 Survey displacements, Column A.	241
D.2 Survey displacements, Column B.	242
D.3 Survey displacements, Column C.	243
D.4 Survey displacements, early epochs, Column D.	244
D.5 Survey displacements, late epochs, Column D.	245
D.6 Survey displacements with time, Column A.	246
D.7 Survey displacements with time, Column B.	247
D.8 Survey displacements with time, Column C.	248
D.9 Survey displacements with time, Column D.	249
E.1 VSI1, A direction absolute displacements, early epochs.	269
E.2 VSI1, A direction absolute displacements, late epochs.	270
E.3 VSI1, B direction displacements, early epochs.	271
E.4 VSI1, B direction displacements, late epochs.	272
E.5 VSI1, A direction absolute displacements/time.	273
E.6 VSI1, B direction displacements/time.	274
E.7 VSI2, A direction absolute displacements.	275
E.8 VSI2, B direction absolute displacements.	276
E.9 VSI2, A direction absolute displacements/time.	277
E.10 VSI2, B direction absolute displacements/time.	278
E.11 VSI3, A direction absolute displacements.	279
E.12 VSI3, B direction absolute displacements.	280

Figure	Page
E.13 VSI3, A direction absolute displacements/time.	281
E.14 VSI3, B direction absolute displacements/time.	282
F.1 Theoretical displacements (sheet pile only), east section, early epochs.	284
F.2 Theoretical displacements (sheet pile only), east section, late epochs.	285
F.3 Theoretical displacements (sheet pile only), west section, early epochs.	286
F.4 Theoretical displacements (sheet pile only), west section, late epochs.	287
F.5 Theoretical displacement versus time, east section.	288
F.6 Theoretical displacement versus time, west section.	289
G.1 Extensometer results.	291
H.1 Field determined moments, east section, early epochs.	307
H.2 Field determined moments, east section, late epochs.	308
H.3 Interpolated bending moment, east section, June 21, 1984.	309
H.4 Interpolated bending moment, east section, July 10, 1984.	310
H.5 Interpolated bending moment, east section, August 5, 1984.	311
H.6 Interpolated bending moment, east section, October 3, 1984.	312
H.7 Interpolated bending moment, east section, December 5, 1984.	313
H.8 Interpolated bending moment, east section, February 11, 1985.	314
H.9 Interpolated bending moment, east section, August 29, 1985.	315

Figure	Page
H.10 Interpolated bending moment, east section, March 25, 1986.	316
H.11 Interpolated bending moment, east section, July 29, 1986.	317
H.12 Interpolated bending moment, east section, December 10, 1986.	318
H.13 Interpolated bending moment, east section, February 11, 1987.	319
H.14 Interpolated bending moment, east section, March 25, 1987.	320
H.15 Shear diagram, east section, early epochs.	321
H.16 Shear diagram, east section, late epochs.	322
H.17 Field determined moments, west section, early epochs.	323
H.18 Field determined moments, west section, late epochs.	324
H.19 Interpolated bending moment, west section, June 21, 1984.	325
H.20 Interpolated bending moment, west section, July 10, 1984.	326
H.21 Interpolated bending moment, west section, August 5, 1984.	327
H.22 Interpolated bending moment, west section, October 3, 1984.	328
H.23 Interpolated bending moment, west section, December 5, 1984.	329
H.24 Interpolated bending moment, west section, February 11, 1985.	330
H.25 Interpolated bending moment, west section, August 29, 1985.	331
H.26 Interpolated bending moment, west section, March 25, 1986.	332
H.27 Interpolated bending moment, west section, July 29, 1986.	333

Figure	Page
H.28 Interpolated bending moment, west section, December 10, 1986.	334
H.29 Interpolated bending moment, west section, February 11, 1987.	335
H.30 Interpolated bending moment, west section, March 25, 1987.	336
H.31 Shear diagram, west section, early epochs.	337
H.32 Shear diagram, west section, late epochs.	338
P.1 Forces involved in sliding factor of safety analysis; a) general case, b) with the original timber retaining wall considered.	498
P.2 Forces involved with factor of safety analysis based on force equilibrium.	498

List of Plates

Plate	Page
3.1 The east wall.	66
3.2 The sheet pile section of the east wall.	66
3.3 View of the east wall looking eastbound.	67
3.4 View of the east wall looking westbound.	67
3.5 Survey monuments; M1 in foreground and M2 in background.	68
3.6 Instrument mount on survey monument.	68
3.7 Circular wall surveying target.	69
3.8 Backsite target plate.	69
3.9 Backsite pin.	70
3.10 Waler, anchor and load cell arrangement.	70
3.11 Drill rig drilling anchor holes at the east wall.	71

1. Introduction

1.1 General

The problem of predicting the lateral pressure exerted by a soil is a common one in civil engineering. Despite two centuries of study it is an area of continued academic interest. This stems from the fact that the performance of a structure engineered to withstand earth pressures depends on a large number of factors: soil properties including density, strength and deformation characteristics; stress and strain history and the initial stress conditions in the soil; the strength and rigidity of the structure in contact with the soil; the nature of the soil/structure interface; the boundary conditions and the influence of the construction procedure.

A design approach simultaneously incorporating all of these considerations would be exceedingly complex. Substantial progress has been made, particularly with the application of numerical techniques such as the finite element method. Nevertheless, empirical procedures remain a common basis for the design of retaining structures. With this approach the experience derived from previous projects, particularly projects where detailed observations of performance have been made, provide the framework for design.

Performance monitoring of new projects, such as the one discussed in this work, allows an evaluation of the

applicability of current design practices. This in turn may provide an opportunity to expand the existing body of knowledge.

1.2 The Project and the Research Objectives

Canadian National Railways (CN Rail), during the summer of 1984, was twinning its track in the vicinity of Boston Bar, British Columbia. To support the new line it was necessary to construct two retaining walls just north of the townsite. CN Rail, in conjunction with the Department of Civil Engineering at the University of Alberta, installed instrumentation in order to conduct a monitoring program. The program was designed to allow earth pressures and wall deformations to be determined.

The objectives of the research project are as follows:

1. Reduce the data collected from the field and present the results.
2. Interpret the results so that some explanation of the observed behavior can be provided.
3. Compare the measured performance of the walls with that predicted by the more commonly used methods currently available.

1.3 Thesis Organization

This work is organized in the conventional manner with a series of chapters followed by a number of appendices containing ancilliary material. The appendices also contain

all of the reduced field results. The results from each type of instrumentation are contained in an individual appendix. Inclusion of this material into the main body of the thesis is prohibited by the volume involved. The organization is described in detail below.

Chapter 2 traces the development of lateral earth pressure theory and introduces the need for the research conducted in this endeavor.

Chapter 3 provides a general description of the field site. The geometries of the walls being studied are detailed. The types of instrumentation installed and their locations are given. The procedure used to construct the walls is described as well. Finally, the monitoring history of the walls is given.

Chapter 4 provides specific descriptions of the instrumentation used at the site. The manner in which readings are made, the operating principles and the accuracies involved with the instruments are detailed.

Chapter 5 discusses and interprets the results which have been obtained from the field measurements. The chapter is divided into two broad categories: the first deals with the loads on the walls; the second focusses on the wall displacements.

Chapter 6 gives performance predictions for the more heavily instrumented east wall. These predictions are based on the more commonly used design procedures including the finite element method. The calculated results are presented

graphically and are compared to the results obtained from the field measurements. This allows an assessment of the validity of current practice as related to the design of retaining structures.

The thesis is concluded in Chapter 7. All of the findings related to the research objectives are summarized. The experience gained in conducting the field project also allow recommendations to be made. These detail improvements which would enhance the effectiveness of any subsequent monitoring program.

All of the field results are presented in Appendices A through H. Their contents are as follows:

- A - the load cell results.
- B - the anchor mounted strain gauge results.
- C - the earth pressure distributions based on the wall mounted strain gauges.
- D - the survey results.
- E - the slope indicator results.
- F - the displacements based on the wall mounted strain gauge results.
- G - the extensometer results.
- H - the bending moment results based on the wall mounted strain gauges.

The procedures used to reduce the data from each type of instrumentation are presented in individual sections in Appendices I through N. Each appendix also gives: listings of the computer programs used to reduce the raw

measurements; sample datafiles with an explanation of their format; and the procedures required to operate the programs and produce the results.

With only minor exceptions the instruments are dealt with in the same order established above:

- I - the load cells.
- J - the anchor mounted strain gauges.
- K - the wall mounted strain gauges.
- L - the survey.
- M - the slope indicators.
- N - the extensometer.

Appendix O contains tabular results from analyses carried out in Chapter 6 to predict the loads on the east wall. Appendix P discusses two forms of factor of safety analysis that have been carried out on the east wall. Finally, Appendix Q contains miscellaneous computer programs used in various analyses of the east retaining wall.

2. Literature Review

2.1 Nature of the Problem

Any structure in intimate contact with a mass of soil will experience an earth pressure. A successful design requires that the forces, and perhaps also the deformations, resulting from the earth pressure be accurately quantified. In many situations, however, particularly in view of the interdependence of displacement and load, this is not a trivial undertaking.

The essence of the problem lies in the fact that soil is composed of discrete grains. Ultimately, it is the forces transferred through individual soil particles that gives rise to earth pressure. Calculating the multitude of these forces is statically indeterminate and simplifying strategies are required. Two general techniques are available: 1) modelling the soil as a homogeneous, isotropic elastic or plastic medium; 2) using empirical procedures based on collected observational data.

Within the former category two approaches exist: a) based on a unique definition of the stress-strain relationship the stress and deformation for every point in the soil mass can be determined. The finite element method solves this problem numerically and is useful for a wide range of problems. Alternatively, compatibility and equilibrium equations can be formulated to yield a set of differential equations. This rigorous approach has limited

applicability due to the difficult mathematics involved. b) Conditions at failure can be analyzed by considering the limiting equilibrium of the mass of soil adjacent to the structure. This is the approach taken by Coulomb who considers the soil to have failed along a single shear surface. Rankine, on the other hand, evaluates conditions in the soil just when shear failure is about to occur throughout its mass. This is defined as plastic equilibrium.

The classical theories formulated by Coulomb and Rankine were used to predict the lateral loads imposed on vertical or near vertical earth retaining structures. From this fundamental framework numerous advances, spurred primarily by laboratory and field observations, have been made in the design of retaining walls. These developments, together with the original theories, will be reviewed in the following.

2.2 Coulomb Theory

Coulomb (1776) developed his theory of lateral earth pressure as a designer of gravity retaining walls for military fortifications. The theory considers the stability of a wedge of soil bounded by the back of the retaining wall and a failure surface extending from the bottom of the wall to the surface of the soil behind the wall. The forces acting on the wedge, assuming cohesionless soil, are: its self weight, W ; the shearing resistance, R , along the surface of sliding and inclined at ϕ degrees to the normal

to the shear plane; and the support, P_s , provided by the wall and inclined at δ degrees to the wall. See Figure 2.1 for an illustration of the terms involved. The quantity ϕ represents the angle of internal friction of the backfill; δ is the maximum angle of friction that can develop between the soil and the wall.

The following assumptions are inherent in the method:

1. The soil is assumed to be isotropic and homogeneous and obeys the Mohr-Coulomb failure criterion;
2. The backfill surface is planar but may be inclined;
3. The back of the wall is planar but may have any inclination;
4. The wedge behaves as a rigid body;
5. Plane strain conditions prevail;
6. The friction forces are distributed uniformly along the rupture surface and the back of the wall;
7. The friction angle between the soil and the wall cannot exceed ϕ ;
8. The failure surface is planar.

The last assumption is invalid for rough walls as the effect of wall friction is to cause the failure surface to curve near the heel of the wall. Coulomb neglected this curvature. However, the error involved for the active case is not large and is on the safe side. For the passive case the error is more substantial, particularly if $\delta > \phi/3$, and is on the unsafe side. Therefore, the curvature should be accounted for if the Coulomb theory is applied to passive earth

pressure problems.

In the active case, failure is induced by outward displacement of the retaining structure and movement of the backfill into the space previously occupied by the wall. For the passive case the opposite occurs, with the wall moving into the zone formerly filled with soil. For both cases the result is a mobilization of the shearing resistance of the backfill soil. When sufficient movement has occurred the shearing resistance of the soil is completely mobilized. At this stage the soil is in a state of limiting equilibrium and failure is said to have occurred.

To solve for the magnitude of the earth thrust acting on the retaining wall a force polygon incorporating the forces acting on a trial soil wedge is used. For the cohesionless case the force polygon is made up of the three forces shown in Figure 2.1. For cohesive soil two additional forces, the resultant cohesion along the slip surface and the wall, also exist. The weight, W , of the trial wedge is known along with the orientation of all the other forces. Using geometrical relations obtained from the force polygon the earth thrust can be expressed as a function of the geometry and the soil parameters: H , W , α , β , θ , ϕ and δ . In order to determine the critical wedge this function is differentiated with respect to θ , the failure plane orientation, and set to zero. Solving this equation gives rise to the maximum value P_a of the lateral earth force for the active case or the minimum value P_p for the passive

case. The active and passive equations are:

$$P_a = \frac{1}{2}K_a \gamma H^2 \quad [2.1]$$

where:

$$K_a = \frac{\sin^2(a+\phi)}{(\sin^2 a) \sin(a-\delta) (1 + \sqrt{A})^2} \quad [2.2]$$

$$A = \frac{\sin(\phi+\delta) \sin(\phi-\beta)}{\sin(a-\delta) \sin(a+\beta)}$$

$$P_p = \frac{1}{2}K_p \gamma H^2 \quad [2.3]$$

where:

$$K_p = \frac{\sin^2(a-\phi)}{(\sin^2 a) \sin(a+\delta) (1 - \sqrt{B})^2} \quad [2.4]$$

$$B = \frac{\sin(\phi+\delta) \sin(\phi+\beta)}{\sin(a+\delta) \sin(a+\beta)}$$

A solution can also be obtained using graphical methods. Terzaghi (1943) lists several methods, the most commonly used being that developed by Culmann. Such an approach can be useful for cases where the top of the backfill or the back of the wall are composed of more than one plane section.

Coulomb's theory does suffer from several shortcomings. For it to be applicable, sufficient deformation must occur. No attempt is made, however, to quantify this movement. As a result the designer is left to judge on the basis of experience whether an adequate amount of movement will occur. If not, the active and passive forces may be respectively larger and smaller than those predicted by

theory.

An additional kinematic requirement is demanded by the theory. Not only must the quantity of movement be sufficient but it must be of a specific nature. Considering the active case the theory does not prove valid for cases where outward bulging of the mid-section of the wall occurs or for rotation about the top of the wall.

Ignoring the curvature of the failure surface precludes satisfaction of moment equilibrium and in the passive case can give rise to appreciable error. Finally, although the magnitude and direction of the active or passive forces can be calculated the method does not determine their lines of action.

Nevertheless, for the application intended by Coulomb, his theory performed admirably. He worked with massive gravity retaining walls usually backfilled with cohesionless soil. These walls were rigid and moved not by deforming but rather by translation or by rotating about their lower edge. This movement could be counted on to equal or exceed that required for complete shear strength mobilization to occur in the soil.

Terzaghi (1941) identified the Coulomb theory as being suitable for the design of walls which provide lateral support independent of their yield, i.e. stiff structures such as reinforced concrete walls. Coulomb's success as a designer can be attributed to his staying within the limitations of his theory.

2.3 Rankine Theory

Rankine's (1857) theory, although following Coulomb's by some 80 years represents a less general treatment of the lateral earth pressure problem. Unlike Coulomb, Rankine investigated the state of stress in a soil mass when shear failure is pending throughout the mass. Instead of approaching the problem by considering limit equilibrium Rankine's derivation is based on the state of stress throughout the soil at failure. The following assumptions are made:

1. Sufficient deformation has occurred in the soil to mobilize full shear strength;
2. The soil is represented by a semi-infinite, homogeneous and isotropic mass with an upper planar boundary;
3. A lateral boundary is formed by a smooth vertical semi-infinite wall;
4. Plane strain conditions apply.

The stress conditions associated with the above assumptions are illustrated using a Mohr's Circle diagram in Figure 2.2. A wall containing cohesive soil with a horizontal backslope is considered in the figure. No shear stresses exist on horizontal or vertical planes so $\sigma_2 = \gamma z = \sigma_1$. σ_x is some fraction of σ_2 and is also a principal stress, i.e. $\sigma_x = K_0 \sigma_2 = \sigma_3$. With outward movement of the wall σ_x decreases as the soil dilates. If the expansion is large enough the Mohr circle representing the state of stress will become tangent to the failure envelope. At this stage the

soil is in a state of plastic equilibrium and exerts a maximum pressure on the retaining structure. Two sets of failure planes, inclined at $45^\circ + \phi/2$ to the horizontal, will be present. Under such circumstances an infinitely small increase in stress produces a steady increase in strain.

With inward movement of the wall the soil is compressed and σ_x increases. Prior to failure σ_x becomes the major principal stress. When the Mohr circle representing the state of stress expands sufficiently in size plastic equilibrium is again reached, this time in the passive state. Failure planes develop at inclinations of $45^\circ - \phi/2$ to the horizontal.

Rankine's approach can be interpreted with the Mohr circle to determine the ratio between the principal stresses for the active and passive failure conditions. These relationships are easily determined by solving the geometry of the Mohr diagram. One of the principal stresses, the overburden, remains constant. Therefore, the other principal stress, the lateral earth pressure, can be obtained by applying the stress ratio to γz . The orientation of the failure planes can also be obtained from the Mohr diagram.

Rankine originally based his work on cohesionless soil. This was extended to include cohesive soil by Résal (1910). The earth pressure equations for a horizontal ground surface are given below. The terms are defined in Figure 2.3.

Active case:

$$p_a = K_a \gamma z - 2c\sqrt{K_a} \quad [2.5]$$

$$\text{where } K_a = \tan^2(45 - \phi/2)$$

$$P_a = \frac{1}{2} K_a \gamma (H - z_o)^2 \quad [2.6]$$

$$\text{where } z_o = \frac{2c}{\gamma\sqrt{K_a}}$$

Passive case:

$$p_p = K_p \gamma z + 2c\sqrt{K_p} \quad [2.7]$$

$$\text{where } K_p = \tan^2(45 + \phi/2)$$

$$P_p = \frac{1}{2} K_p \gamma H^2 + 2c\sqrt{K_p} H \quad [2.8]$$

For cohesive soils the effective height of the supported soil is reduced by the quantity z_o in the active case. This is attributed to the fact that expansion causes a tensile zone to develop in the upper reaches of the soil. For cohesionless soil the 'c' term drops out of the equations. Note also that a solution exists for inclined backfills.

Inherent in the application of the Rankine theory is the assumption that deformation sufficient to cause plastic equilibrium in the soil has occurred. Thus, as with the Coulomb method, Rankine's theory can only be safely used where one is certain that this is the case. Most unsupported structures, such as gravity or cantilevered retaining walls, satisfy the deformation requirement. Because Rankine's theory does not account for wall friction the values of

active and passive pressure predicted will be slightly conservative. The error for smooth walls such as steel sheet piles is negligible. For the passive case the ease of computation and the error involved in the Coulomb method means that Rankine's theory is generally more popular.

2.4 Subsequent Developments

Numerous workers continued investigations of the earth pressure problem subsequent to publication of Coulomb's theory. Feld (1923) chronicles a host of researchers whose methods or conclusions portray either ignorance or complete misinterpretation of Coulomb's findings.

Gouthey in 1785 conducted theoretical work which was reported by Navier (1809). His discussion was based on the incorrect premise that the sliding plane will form at an inclination equal to the angle of repose of the backfill. Woltmann (1799) reported on experiments where active earth pressures were measured. His results were at odds with what theory would predict because he ignored wall friction. Mayniel (1808) repeated this mistake.

Woltmann, however, made an error with far broader implications. Coulomb identified the friction coefficient of the backfill as $1/\eta$. He did not make any reference to a relationship between this quantity and the natural angle of repose of the soil. Woltmann wrongly assumed that these two quantities were one and the same. He included this assumption in his widely distributed translation of

Coulomb's work.

It was some 130 years before this fallacy was corrected by Crosthwaite (1920). He inferred the angle of internal friction, ϕ , by using a plunger which was pushed into several different materials. Correspondence between the angle of repose and the friction angle was found only for very loose materials; otherwise none existed. The difference between the two measures could be quite large, especially for cohesive soils. Terzaghi (1920) cites several failures which he attributes to designs based on the angle of repose.

Hagen (1833) seems to be the first researcher to successfully confirm Coulomb's predictions in the laboratory. Several others followed. Winkler (1865) determined that the resultant earth force had an inclination equal to the angle of friction of the wall. Consid re (1870) obtained a similar result by reanalyzing experimental work done by Aude (1848).

Leygue (1885) conducted the most rigorous experimental tests of Coulomb's work done to date. He observed that the failure surface was essentially planar in cohesionless materials. He noted that its shape was independent of the angle of repose of the backfill; the height and batter of the wall; and whether failure was induced by wall rotation or translation. As well, he incidentally validated Coulomb's assertion that soil strength consisted of two independent components: friction and cohesion. This had been challenged by some researchers.

With scientific acceptance of Coulomb's (and by inference Rankine's) theory came its widespread use as a design method. It was with this broader application, however, that problems arose. The theory itself was not at fault. Rather, it was being employed in situations incompatible with the fundamental assumptions involved. The chief examples of this misuse are the design of braced excavations and anchored bulkheads. The support provided by the struts or anchors may inhibit the deformation required for full mobilization of the shear strength of the soil. In addition, these structures were often constructed from very flexible soldier or sheet piles. The deformations of these walls can be different from those originally envisioned by Coulomb. The net result was designs that were dangerously unsafe or extravagantly over-conservative. These issues are discussed in greater detail in the following sections.

2.5 Strutted Excavations

The first critical evaluation of the established theory with respect to strutted excavations was performed by Meem (1908, 1910). With observations made during the construction of the New York subway Meem noted that the pressure distribution behind the timbers supporting the cut was not hydrostatic. Braces near the top of the excavation which should have been carrying low load were in fact highly stressed. He also had opportunity to notice that a failure plane which had developed intersected the surface at a right

angle. He carried out extensive experiments designed to investigate soil arching behind walls and attempted to incorporate his findings into a design method for braced cuts. He proposed the following pressure distribution. The thrust at any point on the wall is proportional to the width at that particular elevation of the wedge of soil between the wall and the angle of repose. These results are exactly opposite to that predicted by Rankine, where the maximum pressure exists at the bottom of the wall. Although widely used, Meem's hypothesis did not survive subsequent scrutiny. He did, nonetheless, make a valuable contribution. He realized that unless the deformation conditions demanded by the classical theories were met they could not be properly employed. The strutted excavation was correctly identified as not satisfying these requirements.

Moulton (1920) substantiated this conclusion as did Terzaghi (1934) with a series of tests on a large model retaining wall. Terzaghi's experiment provided the first quantitative study of the effects of wall movement on the coefficient of lateral earth pressure. He noted that the centre of pressure acted at a height greater than $H/3$ (where H equals the wall height), the height specified by Rankine. As well, under certain conditions, the failure surface was seen to have a marked curvature.

A theoretical study was performed by Terzaghi (1936). He determined the conditions required for different pressure distributions to develop. He also demonstrated that unless a

retaining wall displaces by sufficient rotation about its base, the centre of pressure will be located above $H/3$. The centre of active earth pressure may occur anywhere between $0.33H$ and $0.66H$ above the base of the wall. The nature of the horizontal movement influences the actual position of the centre of pressure.

It was also determined that the process of excavation in a cut supported by timber lagging led to deformation similar to rotation of a wall about its upper edge. Terzaghi (1941) quoted Ohde's (1938) calculations which established the centre of pressure at $0.55H$ for this type of displacement. Ohde also found that the lateral pressure for this situation is considerably higher than predicted by Coulomb's theory. This satisfies intuition. If the soil is not as active in its own support because it has not developed all of its shear strength then the wall must be expected to provide the difference and sustain a higher load.

The instrumentation of sections of the Berlin subway excavation provided the opportunity to analyze comprehensive field data. The cut was internally braced, 12m deep and in fine uniform sands. Terzaghi's theoretical prediction for the earth pressure on a timbered cut gives a parabolic distribution. This in turn demands that arching occurs in the soil. Measurements of the strut loads in Berlin were consistent with these findings.

Based on the Berlin data Terzaghi and Peck (1948) recommended the adoption of a trapezoidal earth pressure envelope for cohesionless soil. This is illustrated in Figure 2.4. Review of later field data, particularly from Munich and New York, led to the introduction of a new apparent pressure envelope (Terzaghi and Peck, 1967). Refer to Figure 2.5 for an illustration.

Tschebotarioff (1951) in his first edition text suggested modifications to Terzaghi and Peck's 1948 envelope for granular soils. His proposal, illustrated in Figure 2.6, was based on a reanalysis of the New York subway construction records. His recommendation is independent of ϕ , a quantity which Tschebotarioff felt could vary widely and was rarely known with any accuracy.

In Tschebotarioff's second edition text (1973) he modified his earlier recommendation with a more conservative envelope that adopted a rectangular shape. This is shown in Figure 2.7.

Work very similar to Terzaghi's in Berlin was conducted by Peck during the construction of the Chicago subway. The predominant soil at this location was normally consolidated clay. Peck had two objectives: 1) to infer a pressure distribution from the measured strut loads; 2) to determine what proportion of the maximum available shear stress was mobilized and the amount of wall movement this corresponded to.

Results presented by Peck (1943) showed that the magnitude of the total earth pressure compared well with that predicted by Coulomb. The distribution of the pressure, however, was found to vary considerably. Peck attributed this difference to the nature of the excavation and to the manner in which the supporting struts were installed. Yielding that resulted produced a parabolic distribution with the centre of pressure at approximately midheight.

The average shear stress developed was about 75% of the available strength. Deformation of 0.25% of the wall height was noted to be enough for full strength mobilization. This is in line with the data quoted by DiBiagio and Roti (1972) for excavations in the Oslo clay.

By considering the statistical variation in the strut loads measured in Chicago Peck (1943) proposed a trapezoidal earth pressure envelope that encompassed all the actual pressure distributions. This is illustrated in Figure 2.8. For safety the area of the trapezoid is approximately 50% larger than the maximum measured distribution.

A very interesting observation, hitherto unnoticed, was also reported. Most of the deformation at a given point occurred prior to the excavation reaching that elevation. Thus movement occurs below the base of the excavation. This suggests that lateral movement can never be eliminated but only reduced by closer vertical spacing of the support braces.

Peck (1943) pointed out that then current understanding was still limited. Although he suggested a means of calculating strut spacing it was not completely endorsed. Nor was the question of pile penetration depth resolved. He identified this to be primarily a function of the stiffness of the soil and how this stiffness changes with depth below the excavation.

Several authors raised questions concerning Peck's proposal; notably Tschebotarioff (1951). He pointed out that the strut loads in the Chicago cut were underestimated by the pressure envelope when the cut was at shallow depth. A more serious shortcoming concerns the prediction of negative pressure or tension when $\gamma H/q_u$ is less than 2. q_u is the unconfined compressive strength of the soil. With this the case the equation $K_a = 1 - 2q_u/\gamma H$ becomes negative. This situation can arise when H is small or q_u is large.

Golder (1948) measured high strut loads in a cut in stiff clay which on the basis of Peck's scheme should have been self supporting. Similar results were reported by DiBiagio and Bjerrum (1957). Tschebotarioff (1951) proposed an alternate pressure envelope in an effort to correct these discrepancies. This is illustrated in Figure 2.9.

In addition to this experience, observations from sites in England, Oslo, Tokyo and elsewhere became available (Megaw, 1951; Skempton and Ward, 1952; Wu and Berman, 1953; and Humphreys, 1962). Based on this expanded database Terzaghi and Peck (1967) concluded that the behavior of deep

cuts in soft to medium clays was related to a parameter they identified as the stability number, N .

$$N = \frac{\gamma H}{c_u} \quad [2.9]$$

They noted that as N approaches 4 a plastic zone appears in the clay near the corners of the excavation. The extent of this plastic zone grows considerably as N increases to six or seven and may exceed the dimensions of the failure wedge predicted by Coulomb's theory. This can result in earth pressures much higher than predicted by classical theory

The field data cited above shows a wide scatter so it was with reservations that Terzaghi and Peck (1967) proposed the design envelope illustrated in Figure 2.10. The equation governing K_a in this distribution reflects this uncertainty by incorporating a reduction factor m . This parameter depends on the stress history of the clay. As a rule of thumb m equals one for most clays where the stability number is less than four. The presence of normally consolidated clay at depth below the cut can reduce m to as low as 0.4. Previous experience provides the only reliable rationale for choosing m .

For stiffer clays a separate envelope was proposed. Caution was again urged in its application as it is based on only two sets of observations (DiBiagio and Bjerrum, 1957 and Golder, 1948). Refer to Figure 2.11 for an illustration. Terzaghi and Peck (1967) suggested that the lower bound of

pressure should only be used when movement can be minimized and construction exposure time is limited.

Peck (1969), in a state-of-the-art review, reaffirmed the 1967 recommendations. He did, however, emphasize that strength change with depth, wall embedment, stratification and the effects of construction procedures were all poorly understood phenomena.

Several additional case studies have since been documented. Chapman *et al.* (1972) observed pressures equivalent to $0.15\gamma H$ at 30 feet increasing progressively to $0.23\gamma H$ at 60 feet. These measurements were obtained from strut loads for the construction of the Washington subway. Armento (1972), working on the BART subway at a braced excavation in Oakland, determined loads of $0.2\gamma H$. The soil at this site consisted of stiff sandy clay.

Harr (1966) reports on a semi-empirical technique developed by Dubrova (1963). It calculates the earth pressure distribution behind a retaining wall but gives consideration to the type of deformation the structure experiences. The particulars of the procedure are discussed in greater detail in Section 6.3.3. However, Scott *et al.* (1972) found that the solution provided good results for a braced cut in sand.

Although quantifying strutted wall behavior still relies more on empirical procedures than rigorous theory, the general mechanisms involved are fairly well understood. The deformations associated with a braced cut are usually

sufficient to ensure the active condition. The influence of the supports, however, causes the distribution to deviate from hydrostatic. The new distribution is commonly parabolic and is adequately modelled by a trapezoid. The total active earth pressure is often close to that determined by Coulomb. The soil characteristics play a large role in determining the magnitude of the wall displacements. Displacements in clay can be expected to exceed those in sand. As most of the movement of a wall occurs below the excavation depth deformations can be minimized by installing more strut levels. The increased number of supports will reduce the quantity of deformation.

2.6 Tied Back Walls

The use of tied back walls in excavation support offers a distinct advantage over internal bracing by keeping the working area clear of obstructions. The difficulty with installing complete crosscut bracing in large excavations also favours the use of anchored walls. As a result tied back walls are increasingly used. Prior to the development of pressure grouting, however, the application of this support system was limited. Historically, anchored walls were employed almost exclusively as quay walls. In these designs support was provided by fixing usually a single row of anchors to large blocks. These were placed some distance behind the wall and just below the ground surface.

Terzaghi (1953) noted that earth pressure computations were traditionally not involved in the design process of these bulkheads. Attempts to do so ran into difficulties when it was noted that on the basis of Coulomb theory most existing walls should have failed. Stroyer (1927) referred to numerous examples where the dimensions of the retaining structure appear to be inadequate to accommodate the apparent stresses. He concluded that the earth pressures are lower than classical theory predicts and that a method more appropriate to the prevailing conditions should be used. His work is notable because he suggested that a reduction in the bending moments in anchored bulkheads might be related to the stiffness of the wall. At the same time he acknowledged the difficulties involved in rationalizing what had previously been a rule of thumb design process.

The first attempt at doing so must be credited to the Danish Society of Engineers who put forward a design code in 1906. The basis of their procedure rests on the assertion that the minimum earth pressure acting on a wall exists midway between the anchor and dredge levels. This conclusion was arrived at by noting that a simply supported beam has maximum deflection at midspan. Soil behind such a structure would also experience maximum deformation at this location. Soil at the supports remains stationary. This differential movement means the development of friction between soil grains. Through this action load is transferred from those regions which move to those which do not. Thus the resulting

earth pressure is largest at the supports and smallest where the most deformation has occurred.

The proposal makes numerous practical suggestions but the essence of the procedure involves the replacement of Coulomb's triangular pressure distribution with one based on a parabolic shape. The resulting bending moments are greatly reduced, sometimes by as much as half. The details are shown in Figure 2.12. Although the method became widely and successfully employed the procedure had minimal theoretical foundation.

Terzaghi (1953) reports that the next contribution was made by H. Krey working in Berlin around 1910. Subsequent developments, including a design method put forth by Pennoyer (1933), led to the procedures commonly referred to as the free and fixed earth support methods. The deformations and the assumed earth pressures associated with these methods are shown in Figures 2.13 and 2.14. Both these procedures revert back to classical theory in order to calculate the earth pressures. Unfortunately, tests performed by Terzaghi (1934) cast doubt on the validity of these methods.

Stroyer (1935), in a series of experiments with flexible steel bulkheads, reported results which indicated a pressure distribution similar to the Danish code. This in turn supported the original Danish contention that arching has an important influence on the earth pressure against flexible walls. In 1938 Ohde, as quoted by Terzaghi (1953),

calculated the pressure distribution on a flexible wall with fixed supports. In relation to the hydrostatic distribution it was found to be reduced at midheight and increased at the supports. This is illustrated in Figure 2.15.

Enough evidence had by now been accumulated to allow Terzaghi (1941) to state that "the arching between the upper and the lower support of flexible bulkheads eliminates Coulomb's theory from application to bulkhead problems". He admitted, though, that the mechanisms involved were poorly understood. The properties of the backfill, the stiffness of the wall, anchor location and yield and the amount of embedment were identified as likely having an effect on the problem. Complete understanding of how deformation affected the pressure distribution had not yet been attained. So for the lack of a better approach design practice remained unchanged.

An in depth study was undertaken by Tschebotarioff between 1944 and 1948 at Princeton. He conducted large scale tests on anchored bulkhead models. The results, reported by Tschebotarioff and Brown (1948) and Tschebotarioff and Welch (1948), indicated earth pressure distributions similar to that shown in Figure 2.15. The envelope put forth as a design recommendation is shown in Figure 2.16. It is notable in that it does not extend below the dredge line. The bending moments based on this distribution compared well with those determined from strain gauge measurements assuming a hinge at the dredge level. These results, in

agreement with Ohde's theoretical predictions, stimulated considerable interest and controversy. This was especially true among those who had experience and faith in the Danish Code of Practice.

In response, Tschebotarioff maintained that the actual mechanism of moment reduction in anchored walls was quite different from that envisioned by the Danish. He suggested that a higher passive resultant was largely responsible. This contention was shortly to be proved correct by Rowe.

The publication of work done by Rowe (1952) marked a significant advance. He had performed model studies with walls of different flexibilities. The wall was 1.07 meters (3.5 feet) high with freestanding heights ranging from 50.8 to 91.4 centimeters (20 to 36 inches). The wall was instrumented with pressure and strain gauges. Four different backfills were used: crushed rock, pea gravel, sand, and ashes.

Rowe noted pressure distributions similar to those seen by Tschebotarioff. As Rowe did not assume a hinge at the dredge level his pressure envelopes extended over the full height of the wall. He demonstrated, however, that an anchor yield of as little as $0.001H$ resulted in a hydrostatic pressure distribution. This led him to recommend that any benefits obtained from a pressure distribution that deviated from Coulomb's prediction be ignored. Anchor yield less than $0.001H$ could not be guaranteed nor could the possibly detrimental effects of wave or traffic induced vibrations be

completely avoided. This directly contradicted the Danish philosophy and pointed to the existence of some other moment reducing action.

Rowe also discovered that as the flexibility of the model bulkhead increased the maximum bending moment on the wall reduced dramatically. This effect was found to be more pronounced as the backfill density increased. Rowe introduced a flexibility coefficient, ρ .

$$\rho = \frac{H^4}{EI} \quad [2.10]$$

where H = the length of the pile

E = the modulus of elasticity

I = the moment of inertia of the pile

For very stiff walls the maximum observed bending moment is independent of ρ . The moments can be accurately determined on the basis of the free earth support method. For less stiff walls with larger values of ρ the maximum bending moment decreases. This decrease can be as large as 70%. Beyond this, more wall flexibility affords no further reduction.

Rowe recognized that the primary cause of the decreased bending moments was due to the deflection of the pile below the dredge level. With increasing wall flexibility this movement becomes less like that assumed by the free earth support method and more like that associated with fixed earth support. With fixed earth support, movement occurs by

rotation about the base of the wall. This has two beneficial effects. First, the resultant passive earth pressure in front of the wall is larger and acts closer to the dredge line than classical theory predicts. This had been Tschebotariff's contention four years earlier. Secondly, the active earth pressure at the base of the back of the wall is also increased in response to the diminished movements at this location. These changes induce a bending moment that counteracts the maximum moment in the wall. The net result is a reduced maximum bending moment.

Rowe concluded his paper by making the following recommendations. He proposed that the free earth support method, in conjunction with Coulomb theory, be used as the basis for design. The depth of penetration for the pile is calculated by summing moments about the anchor level. The anchor force can then be determined by summing horizontal forces. The passive resultant is to be reduced by a factor of 1.5 and a shear force at the base of the wall is to be accounted for. He suggested that wall friction angles of $2/3\phi$ be used for the active side and zero for the passive side. With the wall dimensions and the forces found the maximum bending moment can be calculated and reduced on the basis of the flexibility coefficient.

Rowe (1955 a,b) followed up his laboratory work with a theoretical analysis which agreed well with his experimental results. He later (Rowe, 1956) identified an additional source of moment reduction for dredged walls that exhibit

elastic anchor yield. Inward deflection above the tie level and a rise in the active earth pressure at this location were seen to have a beneficial influence on the moments. In 1957 Rowe extended his work to include anchored bulkheads in clay.

Rowe's findings were validated by field experience and independent work carried out by Frinch Hansen (1953). Thus, significant progress had been made in the design methods used for anchored bulkheads. The mechanisms involved in anchored wall behavior, for so long misunderstood, were now adequately described by a semi-empirical procedure. The theory was, however, limited to walls with only one row of anchors.

Traditionally, research was concentrated on this area because when investigations began harbour front structures were the only common use for tie backs. The designs of these walls usually employed only a single row of anchors. It was not foreseen that multiple rows of drilled and pressure grouted anchors would one day supplant internal bracing for excavation support. As late as 1972 Bjerrum *et al.* discussed the need for more research because "in the future we will face the problem of designing structures with greater dimensions than those we build today and structures which will be built and will operate under conditions which deviate from those on which our experience was derived". This situation was, by then, already prevalent.

Hanna and Matallana (1970) undertook model studies of walls supported with multi-level anchors. Their results showed trapezoidal pressure envelope similar to those put forth for braced excavations. This was an encouraging result. It suggested that the years of experience obtained with strutted excavations could be transferred to cuts supported with more than one row of anchors. They recommended the rectangular earth pressure distribution shown in Figure 2.17 for design purposes. Unfortunately, the relevance of Hanna and Matallana's work may be questioned on the grounds that their model anchors were essentially unyielding. This perhaps explains the slightly higher earth pressure their distribution involves.

Morgenstern and Sego (1981) reported on a steel sheet pile wall constructed in the Edmonton region which was the subject of a monitoring program. The wall was built with two rows of anchors and supported a railway line built above a clay soil. The distribution used for the design of the structure was trapezoidal with a maximum earth pressure of $0.42\gamma H$.

The Edmonton Convention Centre employed seven rows of anchors to support a concrete tangent pile wall. It was also designed on the basis of a trapezoidal earth pressure distribution with a magnitude of $0.4\gamma H$ (Balanko *et al.*, 1982).

However, to cloud the issue, as recently as 1985 the Canadian Foundation Engineering Manual recommended a

triangular pressure distribution for use with multi-row anchor systems. This is an approach similar to that followed by the designers of the walls considered in this study.

In the absence of much laboratory or field experience the finite element method has been very successfully applied to the design of excavations with several rows of anchors. Morgenstern and Eisenstein (1970) discuss the techniques involved in the application of the method to predict loads and deformations in excavations. The Edmonton Convention Centre, previously mentioned, is a prime example.

Clough *et al.* (1972) studied a wall in clay with five anchor rows using this method. They obtained detailed information concerning wall deflections, surface settlements, excavation heave, earth pressure and overall excavation stability. It is interesting to note that with minor variations their pressure distribution followed Terzaghi and Peck's 1967 recommendation for stiff clay very closely.

Egger (1972) studied the effects of changing wall stiffness and anchor prestressing on the distribution of earth pressure behind a wall with three anchor rows. In contrast to Clough *et al.* (1972), the earth pressure envelope he obtained resembled the fixed earth support distribution. The stiffness of the wall was found to have no appreciable effect on the earth pressure. This agrees with Clough *et al.* (1972) who recommended the use of a soldier pile wall over a much stiffer concrete one for the

construction site they were evaluating.

Not enough evidence has been presented to make conclusive statements about the nature of the pressure distributions behind walls with multi-level anchors. Differences of opinion have been documented. It is apparent from the literature that for specific cases the finite element method can be used to estimate what such a distribution might look like. The usefulness of this approach is further endorsed by its application to strutted excavations where the base of empirical knowledge is much larger. Eisenstein and Medeiros (1983) and Wong (1985) are given as examples.

As more experience develops the nature of the behavior of walls with several rows of anchors will become better understood. This work is intended to contribute to this goal.

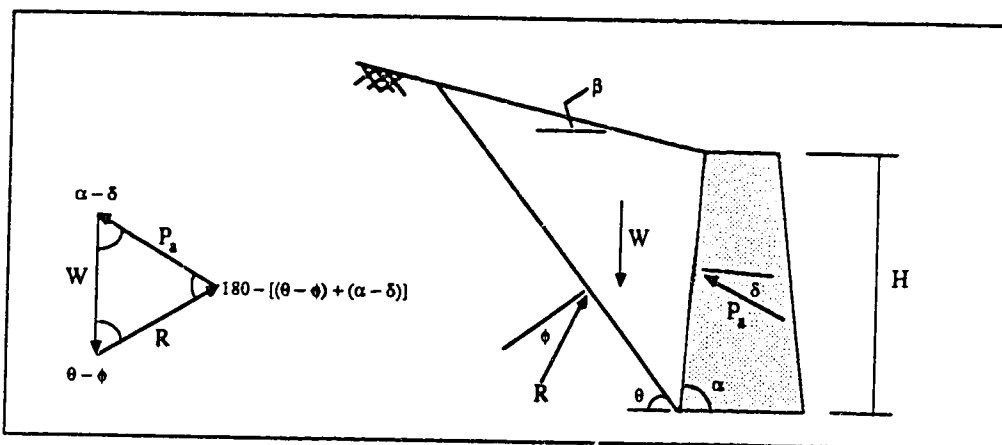


Figure 2.1: Terms involved in the Coulomb solution showing the force polygon. Soil has no cohesion.

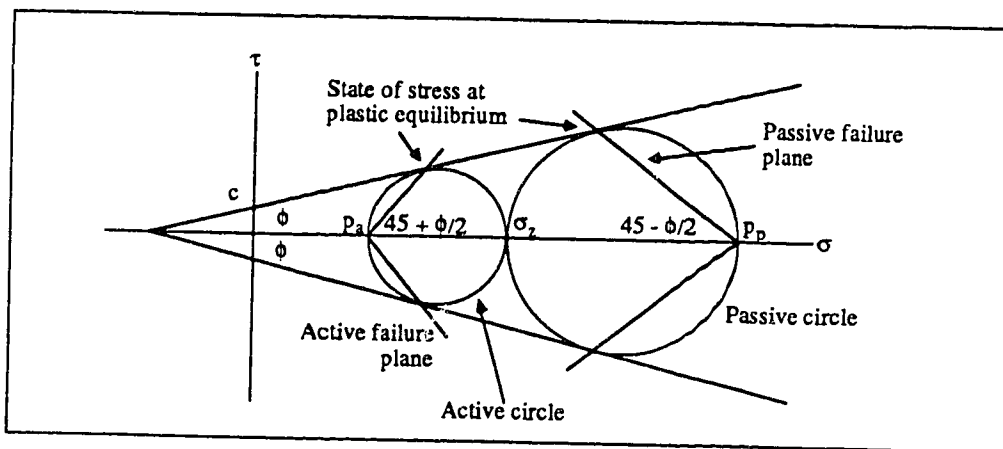
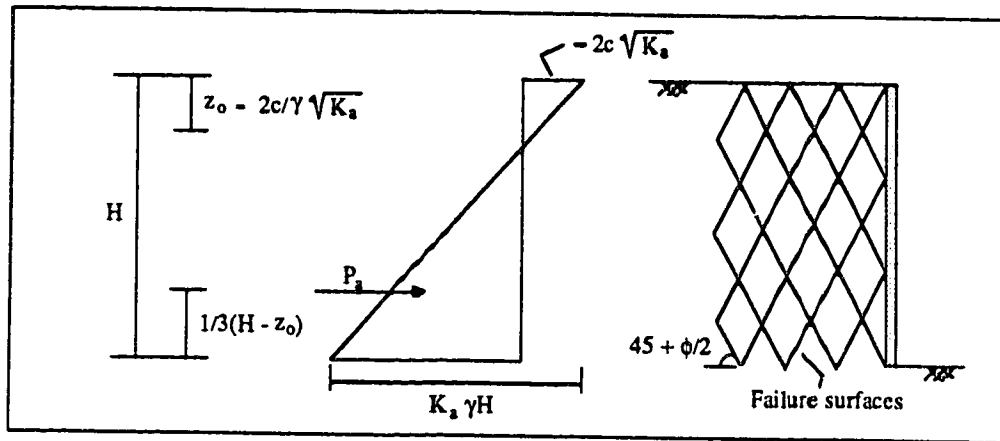
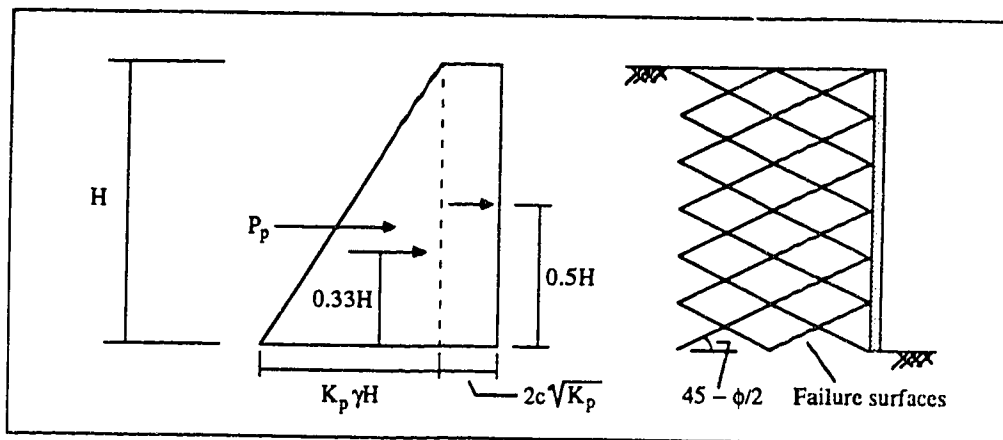


Figure 2.2: Stress state under active and passive lateral earth pressure conditions, cohesive soil, horizontal back slope.



(a)



(b)

Figure 2.3: Terms involved in Rankine earth pressure solution for; a) active case, b) passive case.

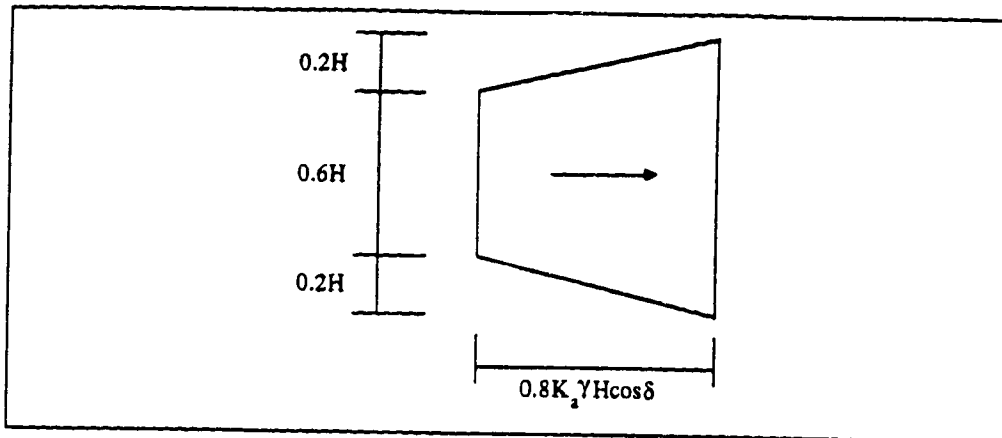


Figure 2.4: Terzaghi and Peck's (1948) apparent earth pressure distribution for sand. (modified from)

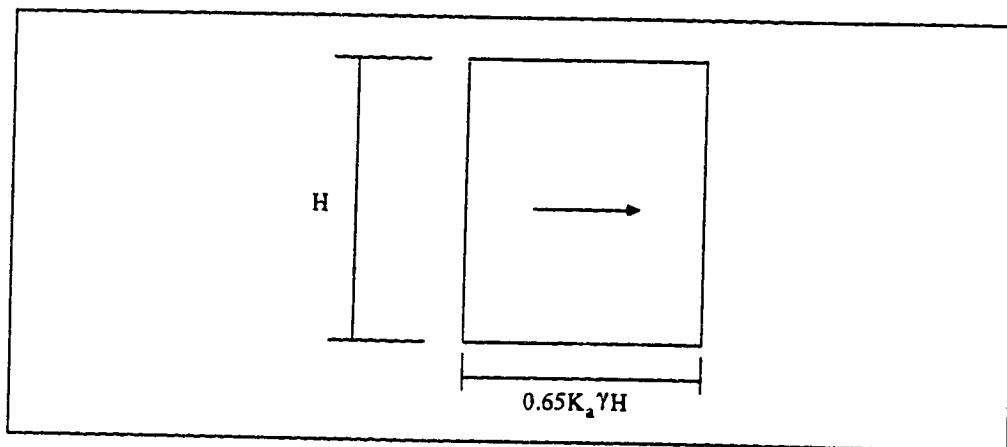


Figure 2.5: Terzaghi and Peck's (1967) apparent earth pressure distribution for sand. (modified from)

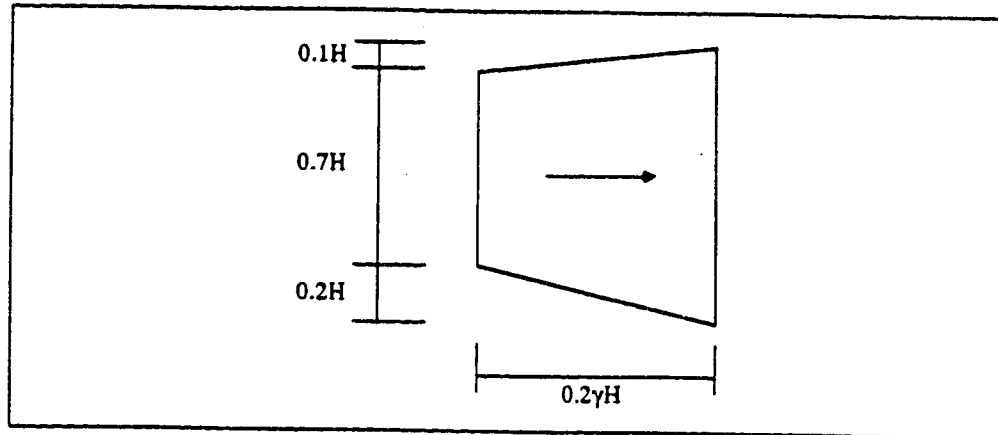


Figure 2.6: Tschebotarioff's (1951) recommendation for the earth pressure distribution in sand.(modified from)

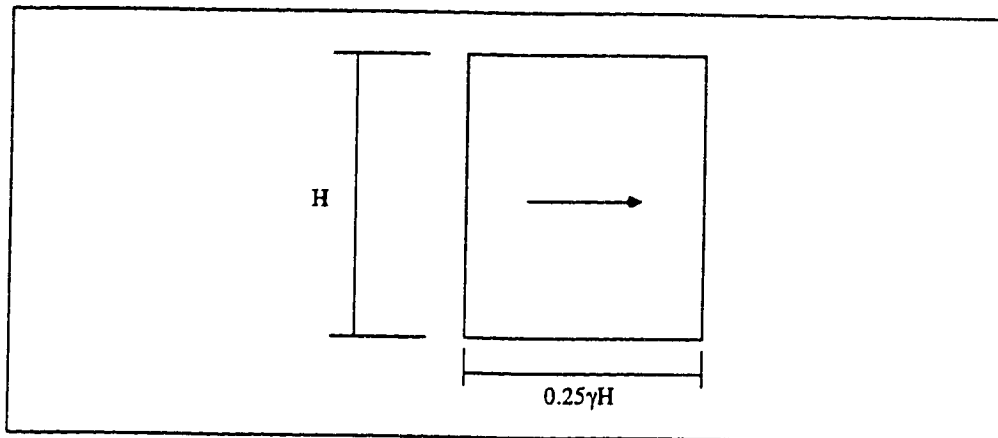


Figure 2.7: Tschebotarioff's (1973) recommendation for the earth pressure distribution in sand.(modified from)

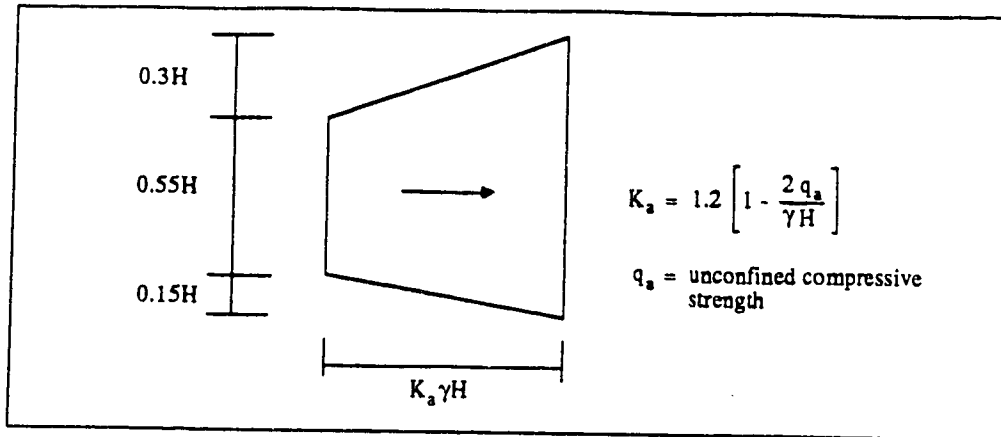
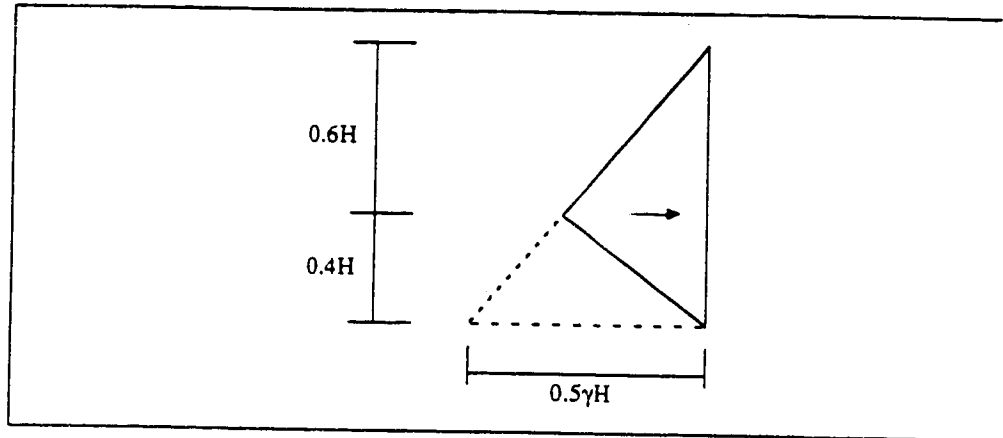
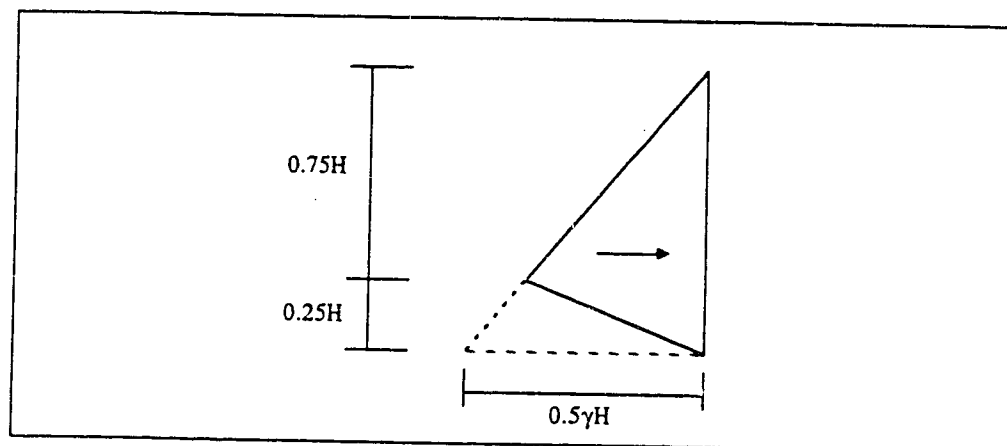


Figure 2.8: Peck's (1943) earth pressure distribution for normally consolidated clay.(modified from)



(a)



(b)

Figure 2.9: Tschebotarioff's (1951) recommendations for earth pressure distributions in; a) temporary cuts in stiff clay, b) permanent cuts in medium clay.(modified from)

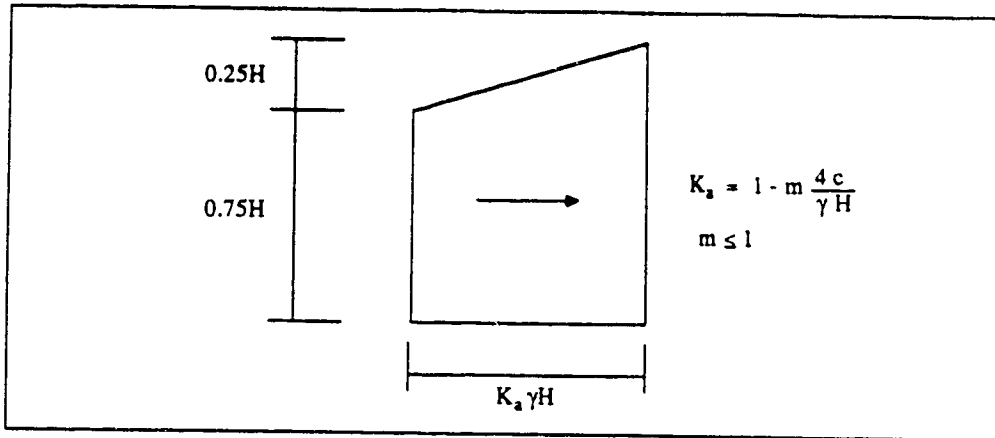


Figure 2.10: Terzaghi and Peck's (1967) apparent earth pressure distribution for soft to medium clay.(modified from)

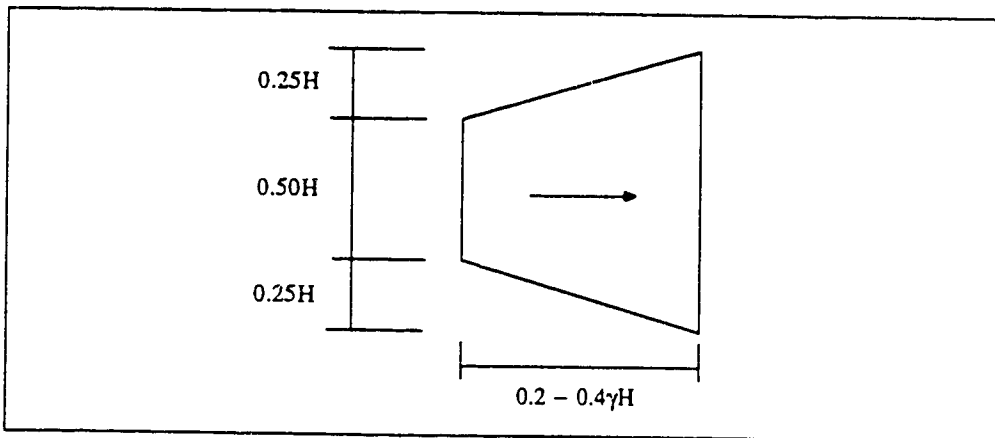


Figure 2.11: Terzaghi and Peck's (1967) apparent earth pressure distribution for stiff clay.(modified from)

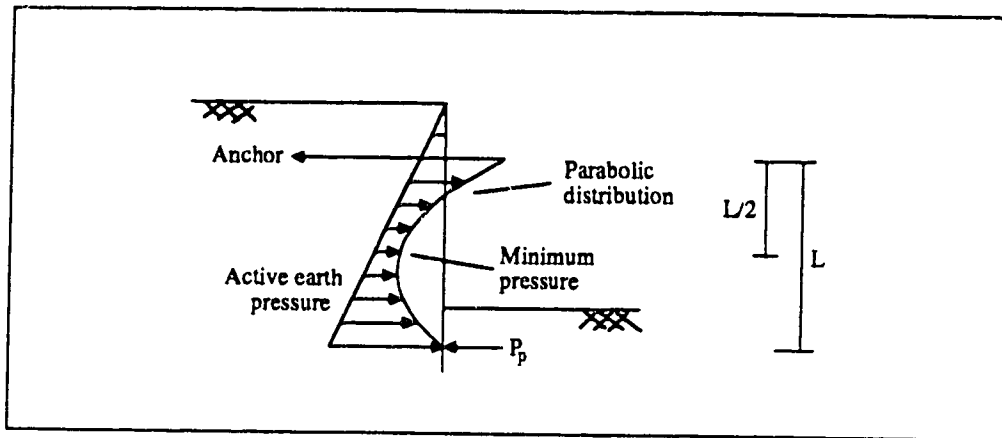


Figure 2.12: Danish earth pressure distribution for anchored bulkheads.

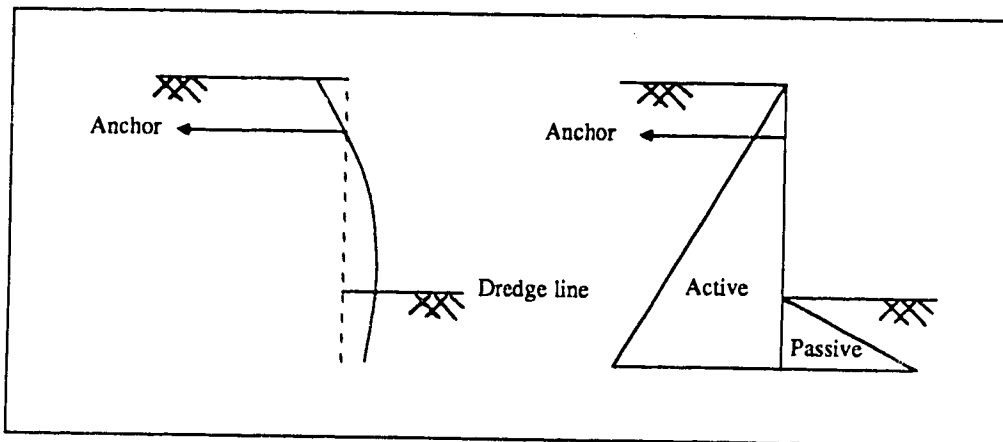


Figure 2.13: Deformation condition and the pressure distribution associated with the free earth support method.

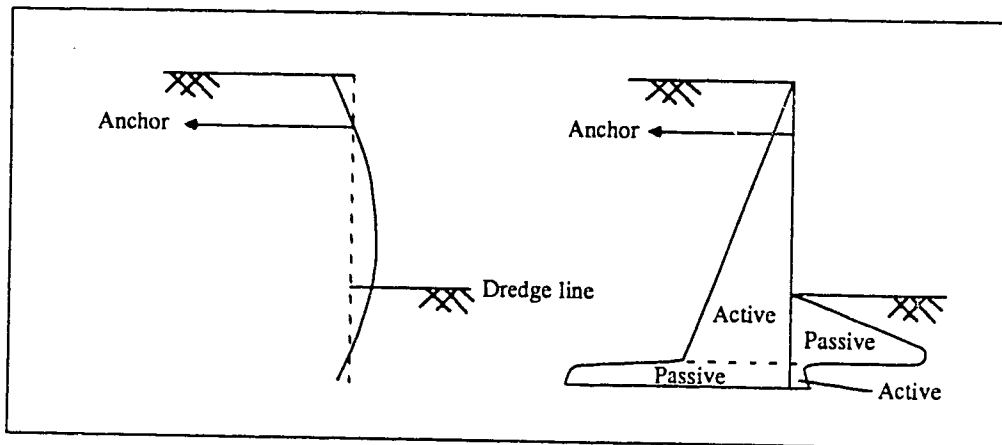


Figure 2.14: Deformation condition and the pressure distribution associated with the fixed earth support method.

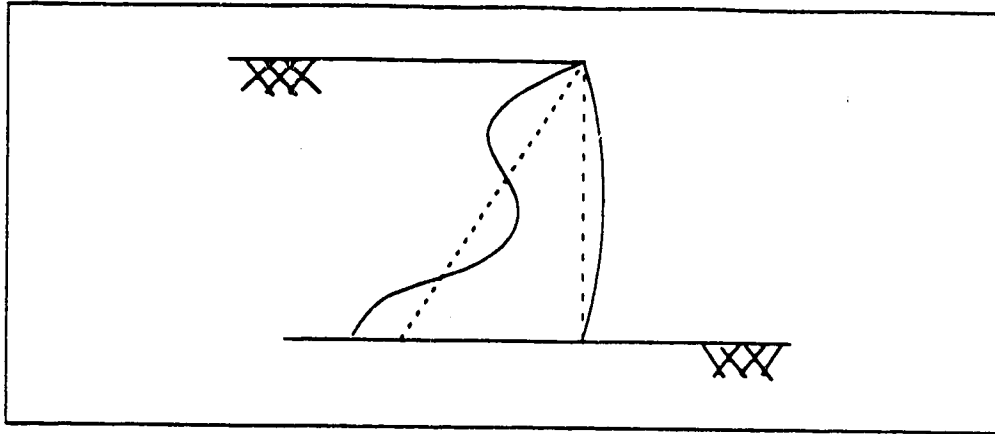


Figure 2.15: Ohde's prediction for the earth pressure distribution behind a wall with fixed top and bottom as reported by Terzaghi (1953). (modified from)

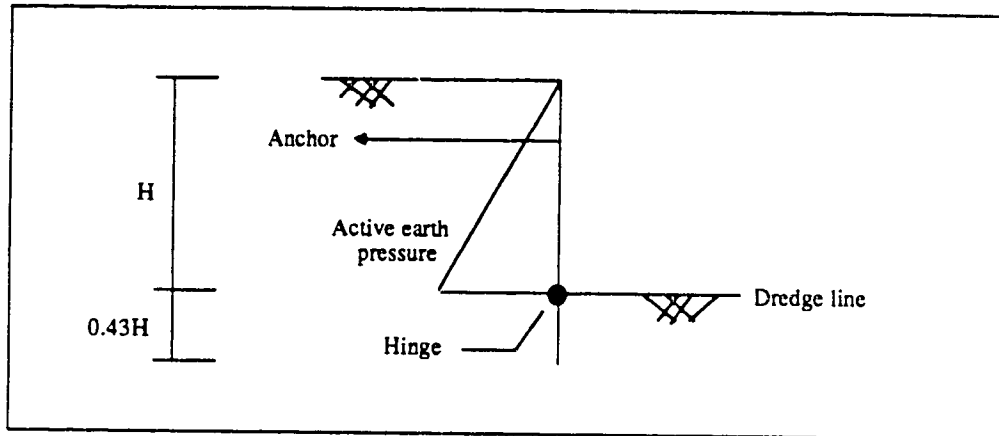


Figure 2.16: Tschebotarioff's (1973) design envelope incorporating a hinge at the dredge level. (modified from)

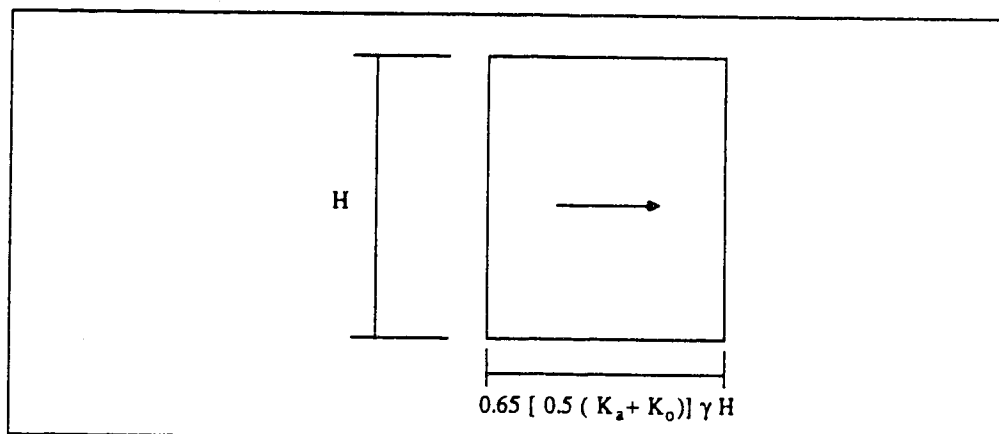


Figure 2.17: Hanna & Matallana's (1970) apparent earth pressure distribution for cuts in granular material supported by multiple anchor rows. (modified from)

3. Site Description

3.1 Introduction

The test site at Boston Bar is described primarily through the use of figures and plates. Maps of the site illustrate the general plan of the area and specifically show the locations of the instrumented sections of the retaining walls. Elevation views of the two instrumented sections of wall indicate their geometries. A cross section is also provided at one location. The diagrams also serve to show the locations of the instrumentation which has been installed at the site.

Brief discussions of the instrumentation, construction procedure and the monitoring history of the site are provided. These follow a general description of the site.

3.2 General Description

The test site is situated along the CN Rail mainline track between Hope and Kamloops, British Columbia, approximately 2 kilometers north of the village of Boston Bar. CN Rail twinned the track through this area in the summer of 1984. The right of way is located directly on the east wall of the Fraser River valley. The valley wall consists to a large extent of exposed bedrock which has been identified as mildly metamorphosed argillaceous phyllite. The slopes both above and below the tracks exceed 45° . In order to provide a level platform on which the new track could be

constructed retaining walls were necessary.

The locations of these structures are illustrated in Figure 3.1, a general plan of the site. Two separate walls were built in the area. These are identified in the figure as the east and west walls (based on the east and westbound track directions). The instrumented sections on each wall are also shown.

The walls at both test sections are constructed from steel sheet pile supported by two rows of walers and anchors. Elevation views of the east and west test sections are given in Figures 3.2 and 3.3 respectively. These illustrate the wall geometries and the instrument locations. Photographs of the east wall are also available. The complete length of wall is shown in Plate 3.1; the instrumented central sheet pile section is shown in Plate 3.2. Plates 3.3 and 3.4 show views along the east wall looking eastbound and westbound respectively.

A cross section of the east wall appears in Figure 3.4. The section is located at what is identified in Figure 3.2 as the reference sheet pile wall joint. This region is of interest because it corresponds to the centre of the instrumented section of the east wall. Of note is the fact that a timber and lagging retaining wall is located behind the steel sheet pile structure. The inner wall, approximately the length of the sheet pile section, served to support CN's original track where the valley wall is particularly steep.

All references to elevations have been established relative to an arbitrary benchmark. The top of the mount for Pin 1 in the survey network has been declared 500 metres above mean sea level.

3.3 Instrumentation

The instrumentation used at the Boston Bar test site includes: load cells; anchor and wall mounted strain gauges; vertical slope indicators; an extensometer and a survey network. Thermistors, a horizontal slope indicator, surface settlement points and additional extensometers were installed in the backfill behind the east wall. They were, however, destroyed shortly after installation.

The locations of the load cells are given in Figures 3.2 and 3.3. At the east wall the load cells are mounted on anchors E through H. At the west wall anchors A through D are equipped with load cells.

All of the above mentioned anchors, with the exceptions of G and H, are instrumented with seven weldable wire strain gauges. These gauges are mounted along the anchor rods at : 1 m, 2 m, 3 m, 4 m, 5 m, 6.5 m and 8 m relative to the start of the grouted section.

Weldable wire strain gauges are also mounted on the outside surface of the east wall. Four columns of gauges have been placed on two adjacent sections of sheet pile. These piles are connected at the reference sheet pile joint. The two columns of gauges on the pile east of this joint are

referred to as the east section strain gauges. The two remaining columns are correspondingly labelled the west section strain gauges. The locations of all the gauges are indicated in Figure 3.2. Table 3.1 gives the elevations of the gauges and their offsets relative to the reference sheet pile joint.

The wall mounted strain gauges provide data which ultimately yields bending moments. This information, in turn, is used to calculate pressure distributions behind the wall as well as the wall's displacement.

Three vertical slope indicators, identified as VSI1, VSI2 and VSI3, have been installed at the east wall. VSI1 is mounted directly along the outer surface of the wall adjacent to the reference sheet pile joint. The top of the casing is at an elevation of 498.35 m. Measurements can be made to a depth of 16 feet or to an elevation of 493.48 m. VSI2 and VSI3 are located within the backfill 1.8 m behind the east wall at the locations indicated in Figure 3.5. The casings are respectively 34 and 39 feet deep. Elevations at the tops of each casing are approximately 499.0 m for VSI2 and 499.2 m for VSI3.

Two magnetic multipoint extensometers are also installed in the backfill behind the east wall. One, however, was damaged early in the project and provided no data. The location of the remaining instrument is shown in Figure 3.5. The extensometer provides a means of determining the settlement profile through the depth of the backfill.

A surveying program was implemented to monitor the horizontal movements of the east wall. A survey network incorporating two observation monuments, wall targets and fixed backsites was installed at the site to fulfil this objective. The observation monuments are box like cribs constructed from stacked railroad ties. In the centre of the cribs a concrete pedestal 30 cm square was formed to a height approximately 1.5 m above the top of the crib. A mounting plate was grouted on to the top of the pedestals which allowed a theodolite, a target or a reflector to be positioned.

The crib was filled with soil so as to provide a working platform from which the surveying could be conducted. The locations of the monuments, identified as M1 and M2, are shown in Figure 3.5 and 3.6. Plate 3.5 illustrates the railway tie cribs which make up monuments M1 and M2 (the monuments are also visible in the backgrounds of Plates 3.3 and 3.4). Plate 3.6 shows the instrument mounting plate on a survey monument.

Observations were made from the survey monuments to survey positions on the sheet pile. A survey position consisted of a credit card sized rectangle painted on to the surface of the wall. These were arranged in four vertical columns, labelled A through D. Two columns were located on each side of the reference sheet pile joint in close proximity to the wall mounted strain gauges. Their exact positions are illustrated in Figure 3.7 and listed in Table

3.2.

Observations to the wall were actually made to a circular target aligned perpendicular to the wall. The target, shown in Plate 3.7, was attached to the sheet pile by a magnet and connecting rod. The magnet was mounted directly on top of a survey position for each measurement.

A series of fixed backsites were also used in the survey to establish the coordinates of those points in the network which move. A total of five backsites, identified as BS1, BS2, BS3, P1 and P2, were used. Their locations are indicated in Figure 3.6. BS2 and BS3 are target plates 135 mm square. An example is illustrated in Plate 3.8. BS1, originally a target plate, was destroyed and replaced by a nail hammered into a large tree. P1 and P2 are pins located immediately across the tracks opposite monuments M1 and M2 respectively. An illustration of a pin is provided in Plate 3.9.

Both the target plates and pins are supported by reinforcing bars grouted in to holes drilled in to the rock wall adjacent to the inside track.

3.4 Construction Procedure

In the following discussion attention is focussed on the anchored sheet pile sections of the retaining walls at Boston Bar. This corresponds to the type of wall at the instrumented sections. Construction commenced with the excavation of a platform into the slope beneath the original

track. At the test section of the east wall this took place downslope but immediately adjacent to the existing timber wall. Thus, as the excavation proceeded downwards more of the embedded portion of the timber wall became exposed.

The platform provided a surface from which drilling of the anchor holes could be carried out. When the platform had reached the desired elevation the upper row of anchor holes were drilled. The platform was then lowered by further excavation allowing the bottom row of anchor holes to be drilled. Plate 3.11 provides an illustration of the drilling platform at the east wall with the drill rig at work. This plate also illustrates the anchors and walers which were installed in the timber wall to replace the support provided by the excavated soil.

The anchor holes have a typical diameter of 100 mm and are inclined 10° below horizontal. They were drilled through any fill or ballast which may have been encountered on the surface of the rock slope. Once solid rock was encountered the holes were advanced a further 9 m.

With the anchor holes drilled Dwidag anchor bars were installed in the holes. Thirty two mm diameter bars were used for the upper anchors; 36 mm bars for the lower anchors. The bars, which extended some length beyond the hole openings were grouted into place over the complete depth of the hole.

The next stage of construction involved lowering the working platform to an elevation equal to the base of the

new wall. It was necessary to excavate only the outer portion of the platform. This was followed by placement of the sections of the sheet pile. K95Z sheet pile manufactured by Casteel were used. The specifications of this pile are provided in Figure 3.8. The piles were placed at a 10° batter and with no embedment depth. Wooden timbers acting as rakers served to temporarily support the free standing wall.

The anchors were then extended using additional Dwidag bar and couplers. Corrugated plastic pipe placed over the rod extensions and filled with grout provided corrosion protection for the exposed length of the anchors. Holes were cut through the sheet pile to allow the anchor rod to pass through the wall. Walers were then placed over the portions of the rods extending beyond the outer surface of the piles. Two C230x30 C channel sections placed web to web but separated by spacers made up the walers at the lower level. The upper walers were made from two C310x37 C channels.

Following the walers bearing plates and then nuts were placed over the ends of the anchor rods. The details of this arrangement are illustrated in Figure 3.9 which also includes a load cell. Plate 3.10 provides an illustration. Note that because both the wall and the anchors are inclined at 10° the two components are perpendicular. At this stage the nuts were tightened only enough to remove any slack between the components along the anchor rods.

With construction almost complete the empty space behind the walls was backfilled. The backfill was obtained

from a borrow area just north of the site. The material consisted of crushed rock excavated from the argillaceous bedrock indigenous to the area. This grey, generally weak, rock is characterized by roughly planar partings which give rise to elongated chunks or slabs when broken. The exact size gradation of the backfill is unknown. Gravel and cobbles sizes were, however, the predominant constituents. The remainder of the material consisted of sand sized fractions. Trace quantities of clay derived from weathered bedrock may also be included.

The backfill was transported to the site by truck and dumped in to place. Details of the compaction applied to the fill are also unavailable. It is known that hand operated vibrating tampers were used but not to what extent.

The final stage in the construction of the wall involved tensioning the anchors. This was accomplished by tightening the nut on the threaded anchor bars. This occurred on June 8, 1984 at the west test section and on June 21, 1984 at the east wall test section.

Normal practise has the anchors tightened to some percentage, usually 50%, above their design load. This increased load is maintained for typically 15 minutes. The outward deformation of the anchor is noted over this interval and if not excessive the anchor is declared fit. The load is then reduced to the design level. The details of this type of testing at Boston Bar are unavailable.

The completion of construction of the retaining wall was followed by the placement of ballast and the laying of the new track. Traffic on the new line commenced in the late fall of 1984. This was accompanied by excessive movements in the unanchored bin walls to either side of the sheet pile at the east wall. Train traffic was halted until February, 1985 while anchors were installed at these locations. During this interval the height of the sheet pile at the east wall was also extended with 0.5 m of bin wall.

3.5 Monitoring History

Monitoring of the walls at Boston Bar continued from June of 1984 to March, 1987. During this interval a total of thirteen site visits were made. Each visit is referred to as an epoch. Table 3.3 gives the dates of each epoch as well as the types of instrumentation read during each visit. Not all instrumentation was read at every occasion. The most notable example of this are survey measurements from monument 2. This monument was destroyed following the October, 1984 epoch as a result of the remedial anchoring of the bin walls referred to above. It was not serviceable again until March, 1987 so measurements are unavailable for several consecutive epochs.

Table 3.3 also indicates when zero readings of the instrumentation were made. Zero reading of the load cells, anchor strain gauges and the wall mounted strain gauges were made just prior to tensioning of the anchors. The zero

readings for the slope indicators and the survey were made just after the anchors were tensioned.

East Section			West Section		
Strain Gauge	X (mm)	Y (m)	Strain Gauge	X (mm)	Y (m)
2	160	497.547	22	120	497.547
3	450	497.547	23	410	497.547
4	160	497.360	24	120	497.350
5	450	497.320	25	410	497.350
6	130	496.936	26	110	496.956
7	475	496.956	27	400	496.956
8	140	496.710	28	130	496.729
9	475	496.729	29	400	496.739
10	130	495.853	30	110	495.882
11	470	495.922	31	400	495.922
12	160	494.789	32	140	494.789
13	470	494.858	33	400	494.838
14	135	494.543	36	100	493.952
15	450	494.523	37	400	493.952
16	130	493.952	38	120	493.558
17	470	494.001	39	410	493.509

Notes: 1) X represents lateral distance between strain gauge and reference sheet pile joint.

2) Y represents elevation.

Table 3.1: East Wall strain gauge locations.

Survey Position	X (mm)	Y (m)
A1	470 W	493.048
A2	470 W	493.509
A3	460 W	493.952
A4	480 W	494.819
A5	470 W	495.902
A6	460 W	496.828
A7	480 W	497.448
A8	470 W	497.960
B2	110 W	494.917
B3	110 W	495.991
B4	110 W	496.542
B5	140 W	497.645
C2	150 E	494.917
C3	140 E	495.971
C4	150 E	496.532
C5	160 E	497.645
D1	390 E	493.051
D2	370 E	493.607
D3	400 E	494.001
D4	390 E	494.494
D5	410 E	494.789
D6	400 E	495.853
D7	400 E	496.808
D8	400 E	497.448
D9	400 E	497.941

- Notes: 1) X represents lateral distance between survey position and reference sheet pile joint. E equals east of joint, W equals west.
- 2) Y represents elevation.

Table 3.2: East wall survey point locations.

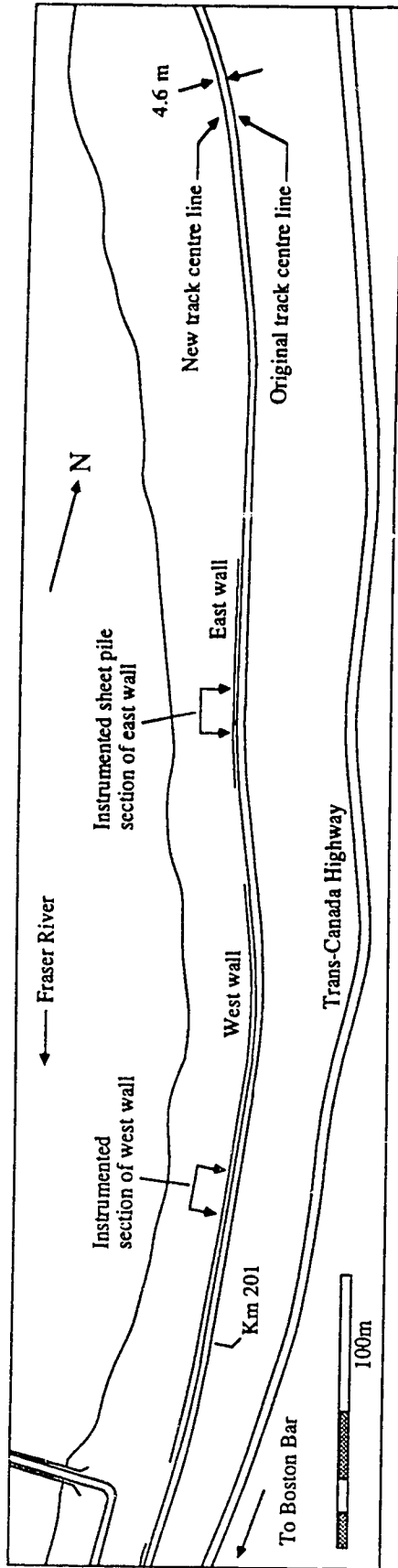


Figure 3.1: General site plan.

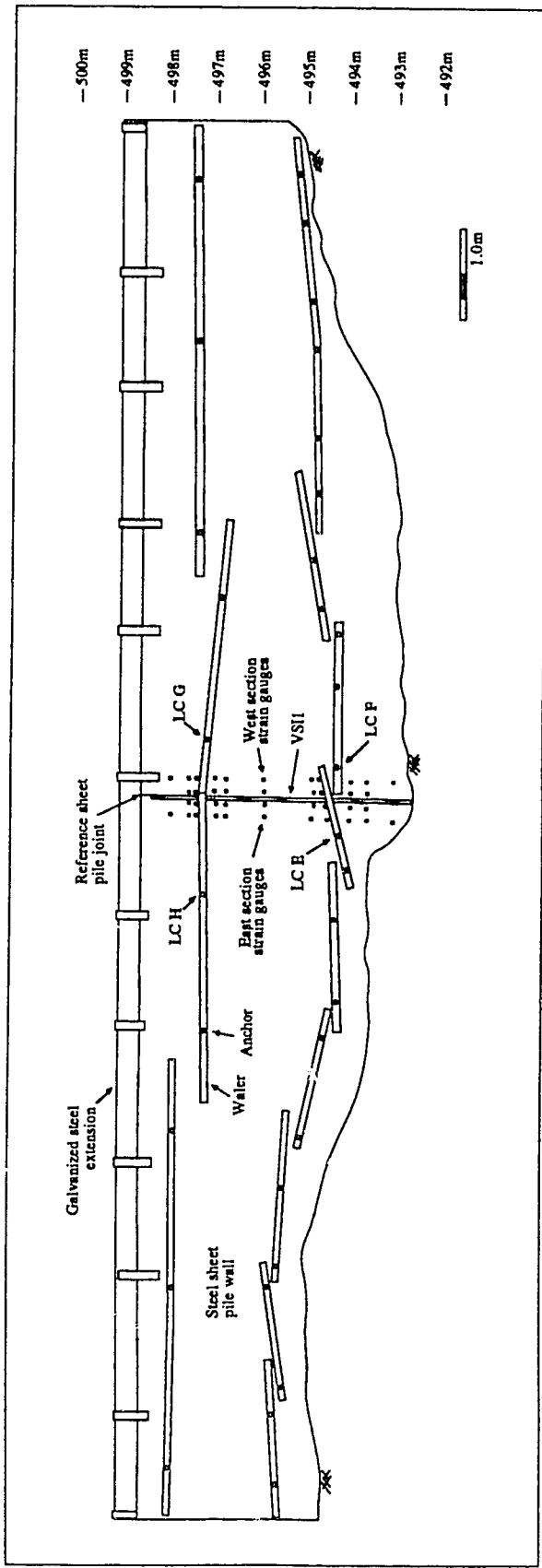


Figure 3.2: East wall elevation view.

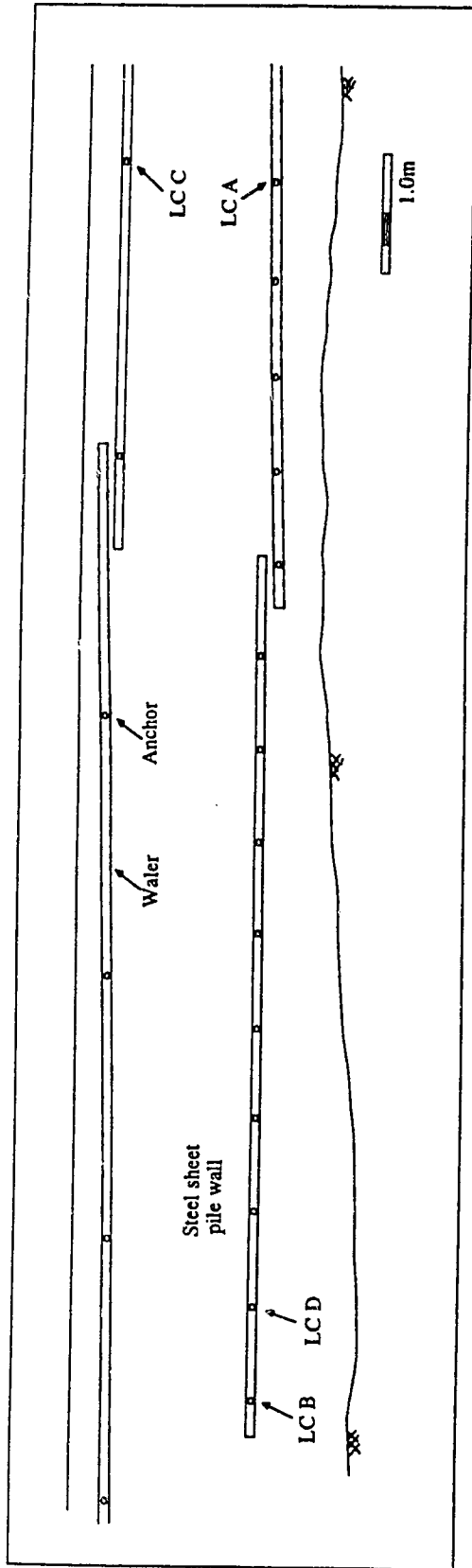


Figure 3.3: West wall elevation view.

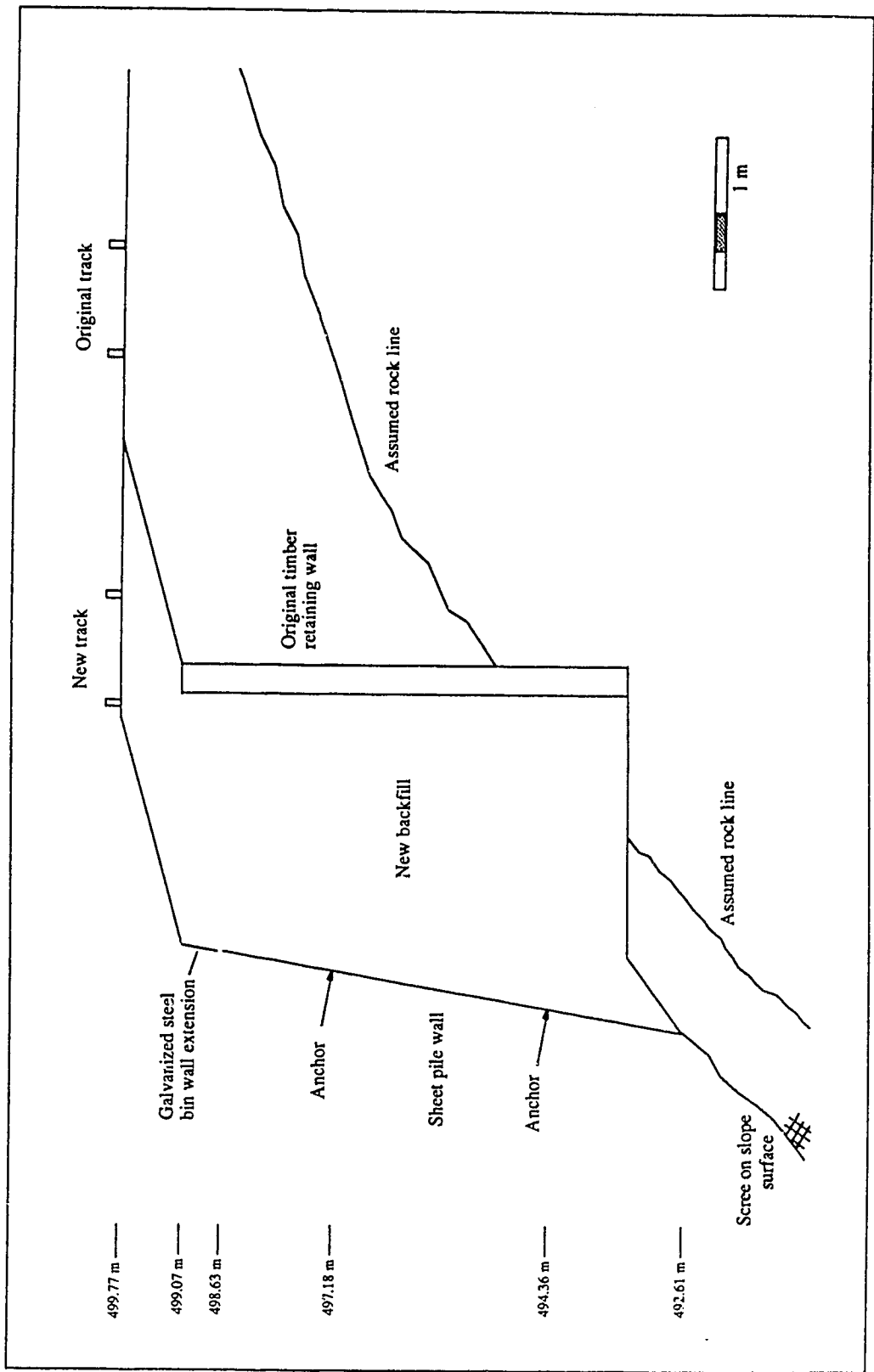


Figure 3.4: Cross section at the reference sheet pile joint of the east wall.

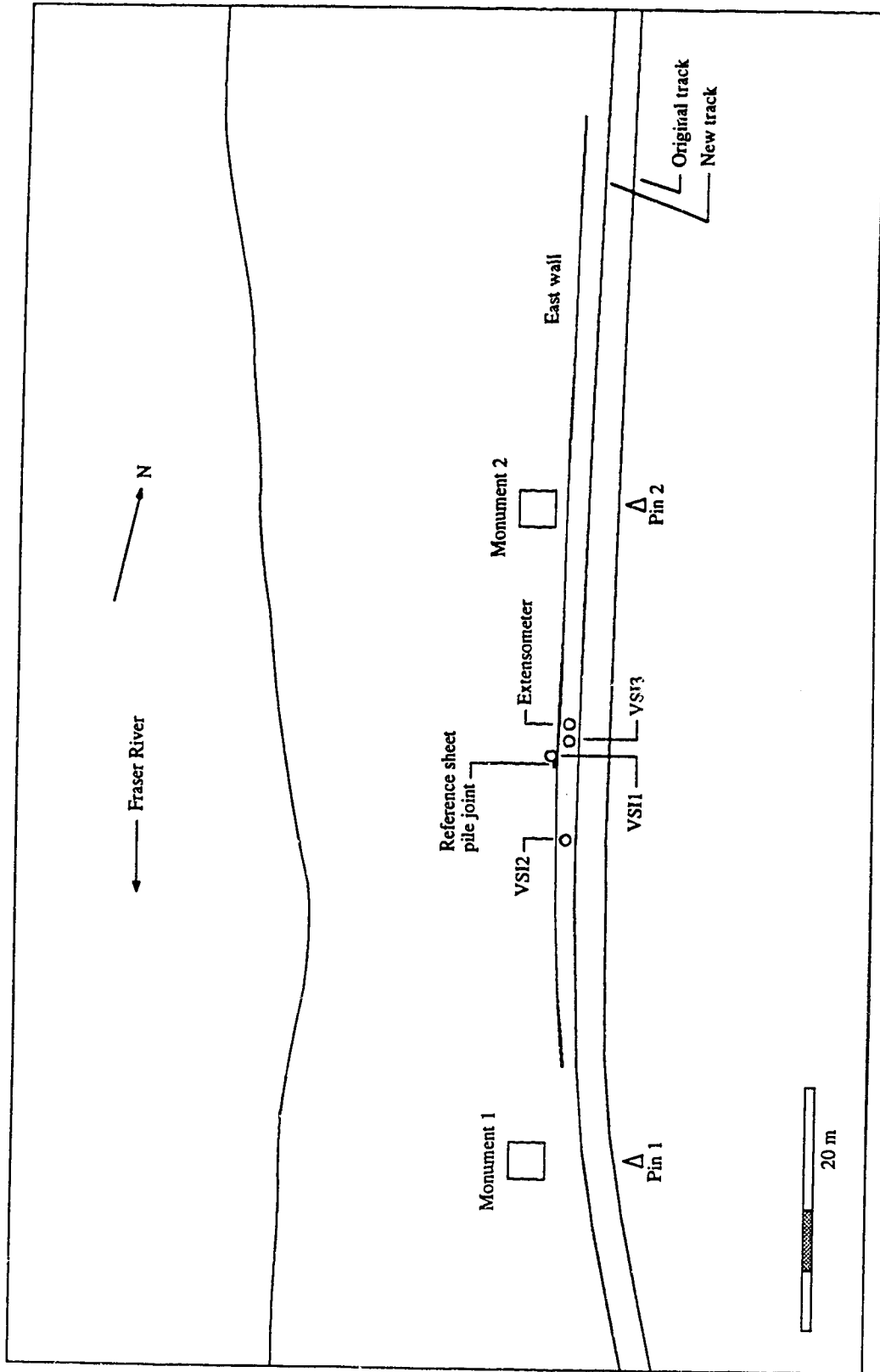


Figure 3.5: Plan view of east wall showing surface instrumentation installed.

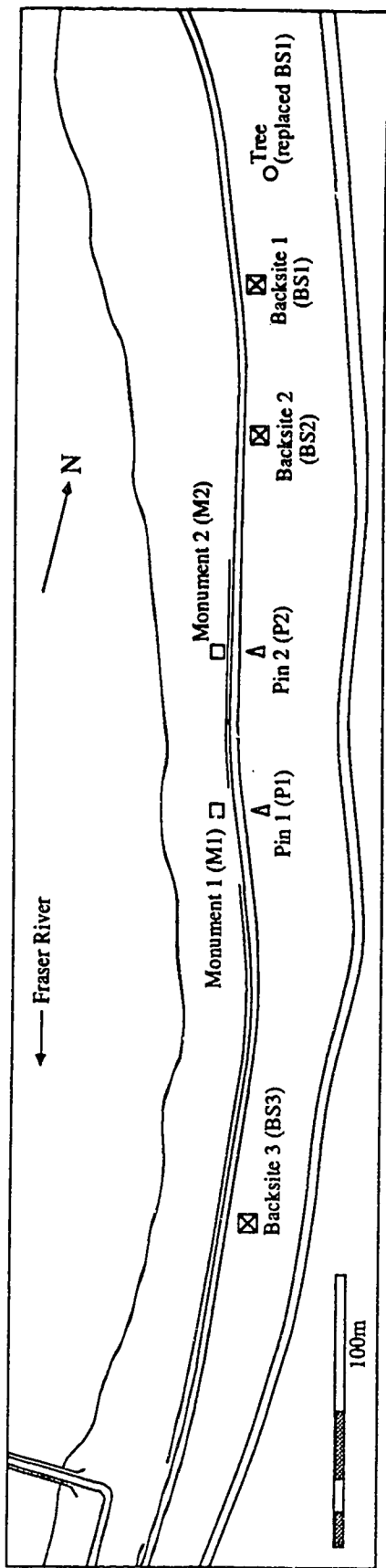


Figure 3.6: Location of elements in the survey network (excluding elements mounted on the surface of the east wall).

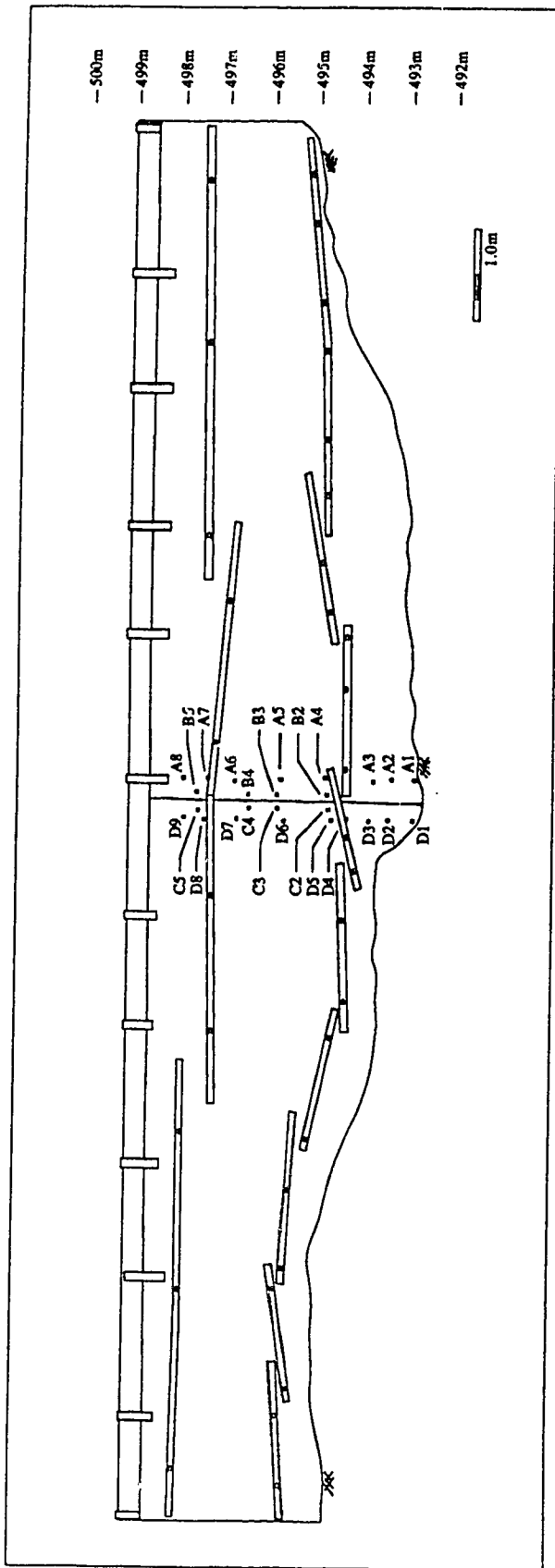


Figure 3.7: Location of survey positions on the east wall.

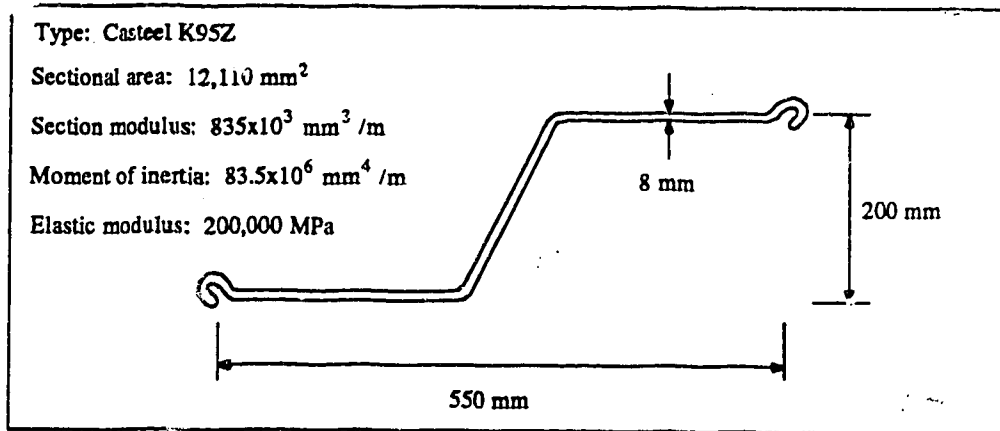


Figure 3.8: Dimensions and characteristics of the sheet pile section.

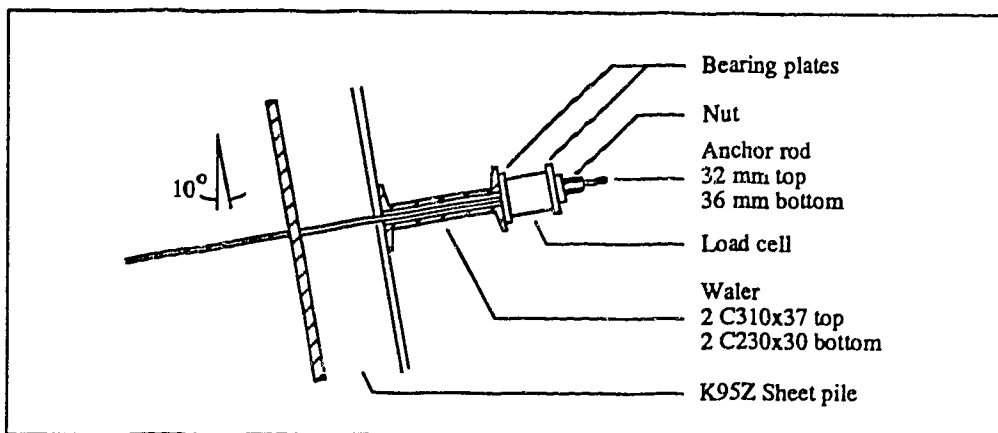


Figure 3.9: Details of waler, anchor and load cell arrangement.

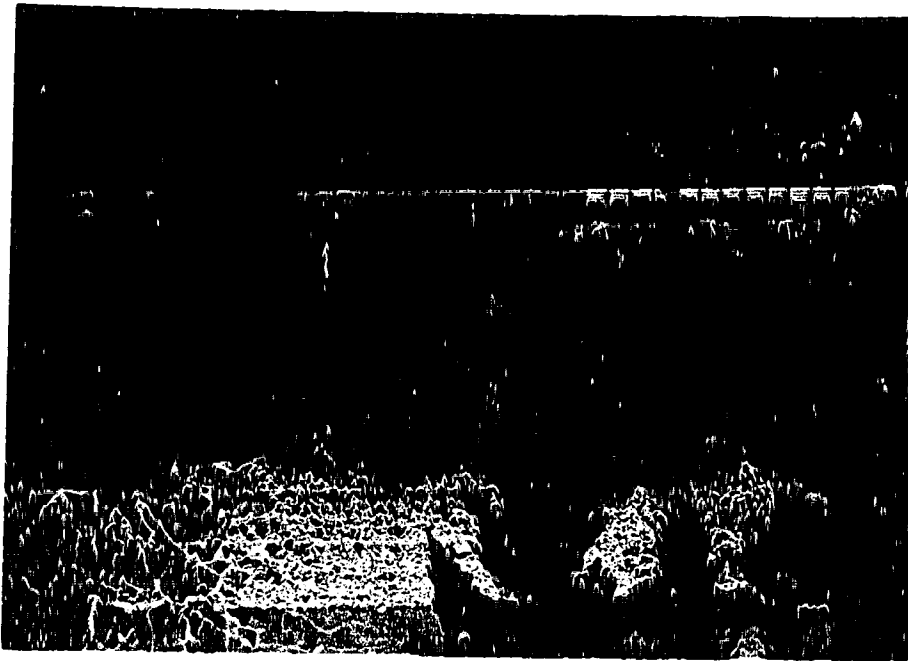


Plate 3.1 The east wall.

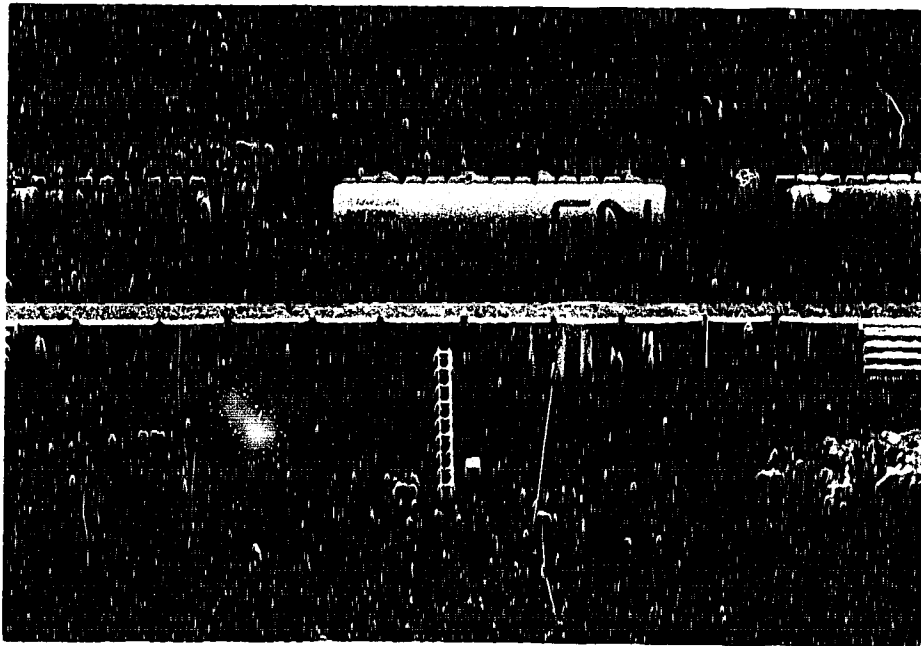


Plate 3.2 The sheet pile section of the east wall.

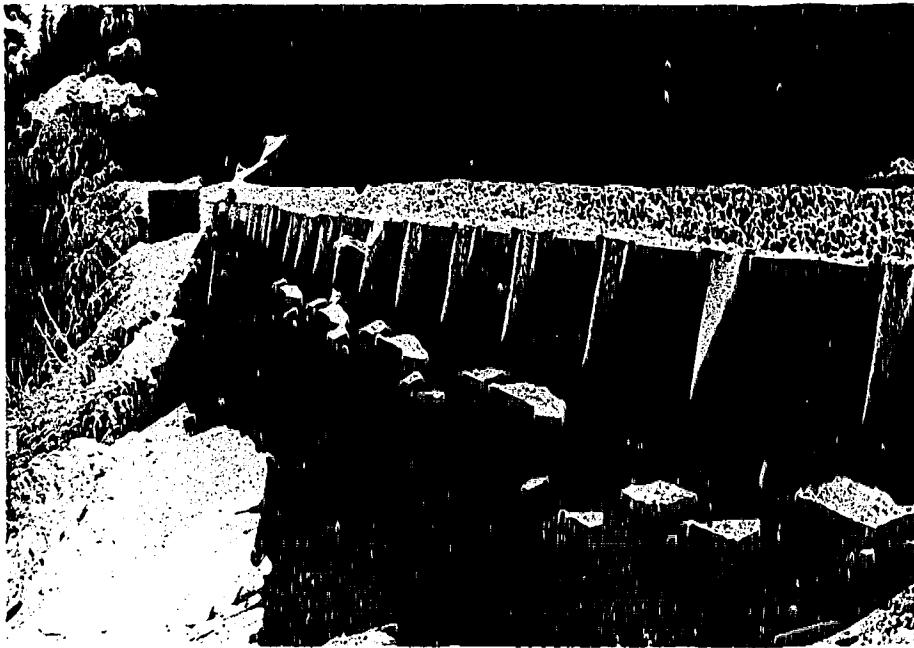


Plate 3.3 View of the east wall looking eastbound.



Plate 3.4 View of the east wall looking westbound.

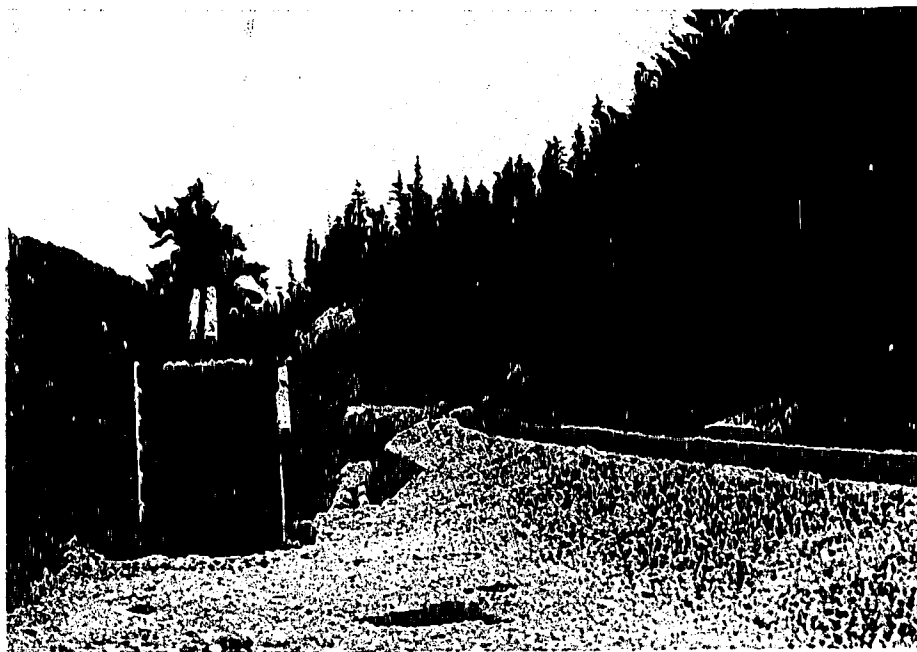


Plate 3.5 Survey monuments; M1 in foreground and M2 in background.

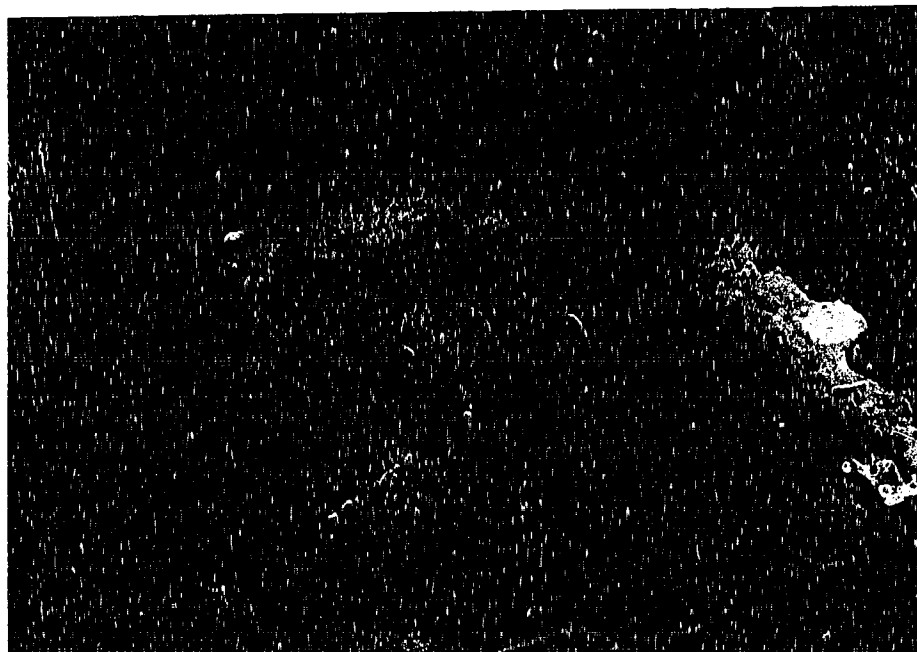


Plate 3.6 Instrument mount on survey monument.



Plate 3.7 Circular wall surveying target.

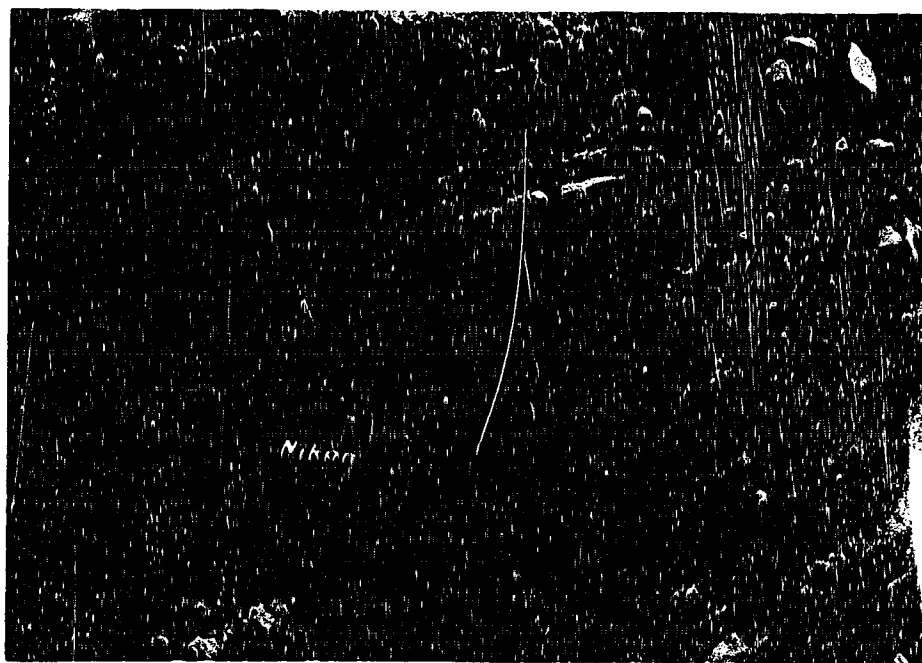


Plate 3.8 Backsite target plate.

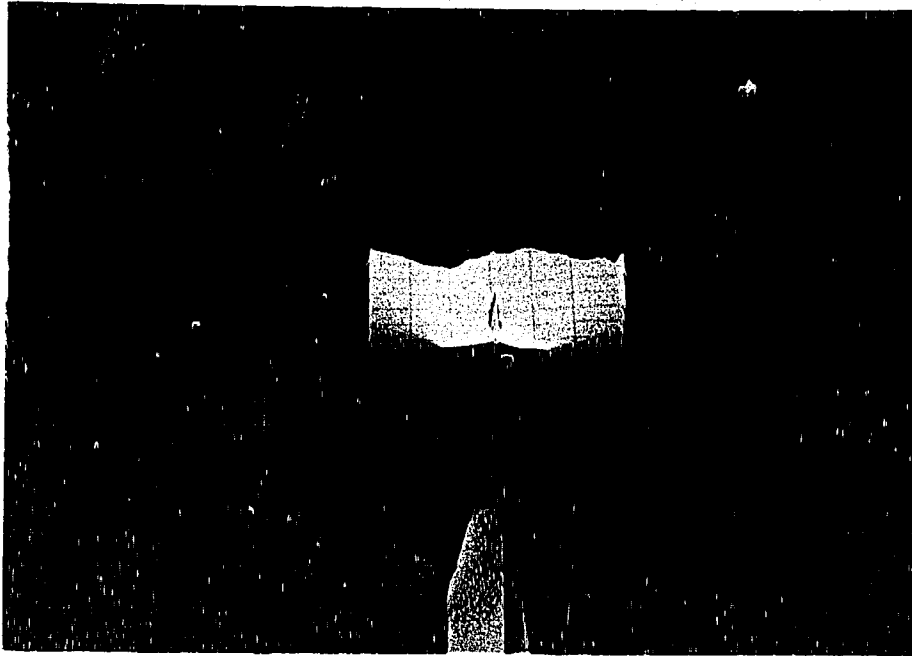


Plate 3.9 Backsite pin.

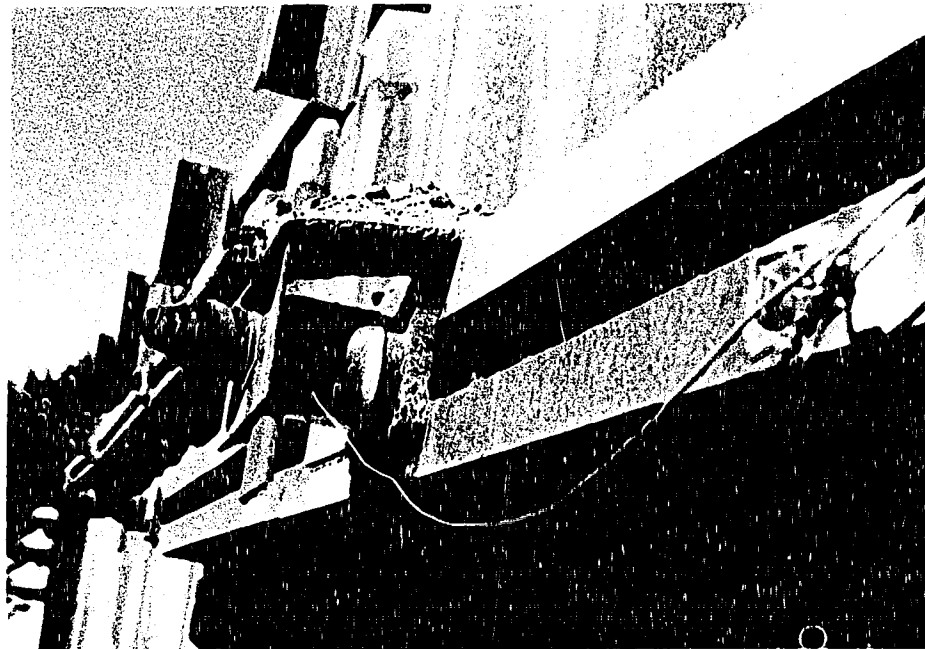


Plate 3.10 Waler, anchor and load cell arrangement.



Plate 3.11 Drill rig drilling anchor holes at the east wall.

4. Instrumentation

4.1 Introduction

This chapter describes the operating principles and the accuracy of the field instrumentation used in the Boston Bar monitoring program. Discussion of measurement errors is limited to inaccuracies intrinsic in the instrumentation only. Errors introduced during the reduction of the data are not dealt with here. These are considered in the discussions of the data reduction procedures which appear in the appendices. Each instrument type is considered separately in the following sections.

4.2 Anchor and Wall Mounted Strain Gauges

The strain gauge is an electrical conductor which experiences a change in resistance when strained. When bonded to a test material under load the changes in resistance experienced by the gauge can be related to the surface strains. A parameter called the gauge factor, F , gives the sensitivity of the strain gauge to strain. This is a dimensionless quantity provided by the manufacturer for each specific gauge type. It is defined by the following expression.

$$F = \frac{\Delta R/R_0}{\Delta L/L_0} \quad [4.1]$$

The quantities R and L are resistance and length

respectively. For high quality gauges working in the elastic range the gauge factor is essentially constant. Thus, the change in resistance experienced by a strain gauge as its length changes is linear.

A strain gauge is used as a part of an electrical measuring system which includes lead wires, a readout device and a power supply. These elements are configured in a circuit called a Wheatstone bridge. At Boston Bar each of the wall and anchor mounted strain gauges are read using what is referred to as a quarter bridge arrangement. As is illustrated in Figure 4.1 this means that one of the four resistors in the bridge circuit is a strain gauge.

The principles governing the operation of a quarter bridge system are described in the following. R_{sg} in Figure 4.1 represents the strain gauge which has been temporarily wired into the bridge for reading. R_2 represents an element of variable resistance. Prior to commencement of the loading test the resistance R_2 is adjusted so that the voltage drop between points A and B, given by ΔV , equals zero.

$$\Delta V = V_a - V_b = 0 \quad [4.2]$$

$$\therefore V_a = V_b$$

V_a and V_b , the voltages at points A and B, can be expressed in terms of resistance values.

$$V_a = \frac{R_2}{R_{sg} + R_2} V \quad [4.3]$$

$$V_b = \frac{R_4}{R_3 + R_4} V \quad [4.4]$$

Equating these two expressions and rearranging terms gives rise to:

$$R_2 R_3 = R_{sg} R_4 \quad [4.5]$$

$$\frac{R_{sg}}{R_2} = \frac{R_3}{R_4} \quad [4.6]$$

This implies that the voltage drop through each half of the bridge will be identical when the ratio of the resistances in vertically adjacent arms of the bridge are equal.

When loading commences the resistance in the strain gauge changes becoming $R_{sg} + \Delta R_{sg}$. ΔV will assume a non-zero value as a result of an imbalance in the bridge.

$$\begin{aligned} \Delta V &= V_a - V_b \\ &= \left[\frac{R_2}{R_{sg} + \Delta R_{sg} + R_2} - \frac{R_4}{R_3 + R_4} \right] V \\ &= \frac{R_2 R_3 - R_{sg} R_4 - \Delta R_{sg} R_4}{(R_{sg} + \Delta R_{sg} + R_2)(R_3 + R_4)} V \quad [4.7] \end{aligned}$$

Recall that Equation 4.5 is valid when the bridge is balanced. Therefore:

$$\Delta V = - \frac{\Delta R_{sg} R_4}{(R_{sg} + \Delta R_{sg} + R_2)(R_3 + R_4)} V \quad [4.8]$$

The following equation results if: $R_{sg}=R_2=R_3=R_4$ and $\Delta R_{sg}=\Delta R$ is much less than R .

$$\Delta V = \frac{\Delta R}{4R} V \quad [4.9]$$

Rearranging Equation 4.1 gives:

$$\begin{aligned} \frac{\Delta R}{R} &= F \frac{\Delta L}{L} \\ &= F \epsilon \end{aligned} \quad [4.10]$$

Substituting Equation 4.10 into Equation 4.9 gives:

$$\epsilon = 4 \frac{\Delta V}{FV} \quad [4.11]$$

Thus the strain acting at the strain gauge can be determined by measuring the voltage change ΔV across the bridge.

The quarter bridge system, as it is implemented in the field, differs slightly from the above description. It is not necessary to balance the bridge prior to the start of the loading test and the first strain gauge reading. An initial reading can be made prior to loading with an unbalanced bridge, noting, however, the balance setting of the bridge. This corresponds in effect to the resistance of the variable resistor R_2 . All subsequent readings are made with the same setting. The net strain can be determined by subtracting the initial reading from all subsequent readings.

The second difference between the procedure described above and field practice concerns how the strain gauge is connected to the Wheatstone circuit. The strain gauge is separated from the three remaining resistors making up the bridge. A connection is afforded by lead wires. Figure 4.2a shows how this would be accomplished according to the configuration given in Figure 4.1.

The lead wires introduce a resistance, $2r$, of their own along the AC leg of the circuit. This is not a problem so long as r remains constant over the duration of the test. This cannot be guaranteed, however, as the resistance of a conductor is dependent upon the temperature. A change in temperature results in r becoming $r + \Delta r$. Unless accounted for an additional resistance of $2\Delta r$ would be spuriously interpreted as resulting from strain in the strain gauge.

An alternate wiring scheme, shown in Figure 4.2b, obviates the need to account for temperature effects on the lead wires. This arrangement, called a three wire system, provides a built in compensation mechanism. Consider that the bridge shown is in balance. The ratio of the resistances along the left branch of the bridge is given by:

$$\frac{R_{sg} + r}{R_2 + r}$$

If the temperature changes the ratio becomes:

$$\frac{R_{sg} + r + \Delta r}{R_2 + r + \Delta r}$$

So long as Δr remains small compared to $R+r$ the ratio remains constant and the bridge remains balanced. Thus the change in resistance due to temperature effects on the lead wires does not register as a voltage change across the bridge.

A number of sources of error exist in the operation of a strain gauge. The gauge factor specified by the manufacturer is usually within plus or minus 0.5% of the actual value. As well the gauge factor will vary with temperature; up to 1% per 100°C.

Thermal effects change the resistance of the strain gauge just as was described for the lead wires. As well, temperature changes induce thermal strains in both the test material and the strain gauge. Collectively, these errors are referred to as temperature induced apparent strains. Unless accounted for this error can be the largest source of inaccuracy associated with the operation of strain gauges.

Apparent strain can be largely nullified through the use of self temperature compensated (STC) strain gauges. These gauges have been specially manufactured so that when matched to a particular material their resistance response with temperature is almost constant. This adjusted behavior mitigates, to a large degree, both of the sources of apparent strain error.

Any residual apparent strain which remains despite the use of STC gauges can be eliminated with the use of a dummy strain gauge. A dummy gauge is mounted on an unstressed

portion of the test material. As a result, its output will reflect any residual apparent strain. Strain gauges are also prone to drift error. This is a time dependent change in gauge resistance under no load conditions which can amount to several microstrains per year. This will also be reflected in the dummy strain gauge reading. Subtracting the dummy gauge value from each of the other strain gauge readings eliminates both of these errors. This assumes, of course, that the dummy strain gauge behaves similarly to the loaded gauges.

There are a number of other less significant effects which introduce error. These include transverse sensitivity, creep, strain transmission error, reinforcement effects, strain extrapolation, non-linearity and densification. None of these effects are deemed to have any appreciable influence on the results at Boston Bar. Nevertheless for a discussion of these errors refer to Perry (1984) and Window and Holister (1982).

Perry (1984) states that operational and environmental variables have a much larger influence on strain gauge accuracy than the properties of the strain gauges themselves. Unfortunately, the influence of the user and the severity of the testing conditions are difficult to quantify. Perry has nevertheless attempted to do so based on the analysis of a large number of tests. Graphically, the percent uncertainty of a strain gauge reading is given as a function of a user expertise index and a test severity

index. Both indices are scaled from 1 to 7 (1 being least expert and least severe). Histograms for each variable are given showing the majority of users at an expertise level of 3. Test severity most commonly rates at 4.

For Boston Bar expertise and severity numbers of 5 and 4 have been used respectively. This gives an uncertainty ranging from 4% to 8%. Thus, an approximate error of plus or minus 6% may be associated with the wall and anchor mounted strain gauge readings.

4.3 Load Cells

The load cells used at Boston Bar can be described as an aluminium donut instrumented with strain gauges. An illustration is provided in Figure 4.3. The load cell fits over the end of the anchor rod between the waler and the anchor locking nut as was illustrated in Figure 3.9.

The operating principles of the load cell are detailed below. The arrangement of strain gauges on the load cell and in the Wheatstone bridge when being read is of importance. A total of eight strain gauges are used; four are aligned parallel to the direction of loading and four are oriented transversely. This is illustrated in Figure 4.4. The strain gauges are shown and numbered on an "unrolled" load cell so that their relative positions around the circumference can be seen.

The strain gauges are read using a full bridge Wheatstone circuit. This means that strain gauges make up

the resistors along all four arms of the bridge. This is illustrated in Figure 4.4c. The numerals in the figure correspond to those in Figure 4.4b and identify the position each strain gauge occupies in the circuit. Each arm contains either two axial or two transverse strain gauges wired in series. The wiring is completed so that adjacent strain gauges on the same arm are from opposite sides of the load cell. Note also that the "axial" and "transverse" arms of the bridge are diagonally opposed. This ensures that an unbalance in the bridge will occur when the load cell experiences deformation.

Recall from the previous section that the voltage drop across the bridge, ie. from A to B, is some function of the difference between the ratios of the resistances in vertically adjacent arms of the bridge.

$$\Delta V = f \left[\frac{R_{AC}}{R_{AD}} - \frac{R_{CB}}{R_{BD}} \right] \quad [4.12]$$

where R_{AC} = the resistance along the AC arm of the bridge

When subjected to load the load cell deforms and the resistances along the four arms of the bridge change. This gives rise to a voltage drop across the Wheatstone bridge. This change could be related to axial strain in a procedure similar to that used in the previous section. The calculations are more involved because of the increased

number of strain gauges in the bridge and the presence of transversely mounted gauges. They are unnecessary, however.

The load cells have been calibrated to give a direct relationship between the Wheatstone bridge output and the force in the load cell. This process is described by Morgenstern and Segó (1981) and gives a calibration factor for each individual load cell. The change in a load cell's readings since the start of a test multiplied by the calibration factor gives the force in the load cell. Because the conversion of strain gauge resistance to strain is effectively bypassed the gauge factor used in calibrating and subsequently to read the load cells is irrelevant. It is convenient to use a gauge factor of one.

The strain gauges used to monitor the load cells are similar to those mounted on the anchor rods and the sheet pile. They are susceptible to the same, mostly minimal, errors. Temperature effects are, theoretically at least, automatically compensated for by the strain gauges used on the load cells. Thus a "dummy" load cell is not required to provide a correction for uncorrected residual temperature effects.

Recall that apparent strains results from temperature dependent resistance changes as well as thermally induced strains. For the strain gauges, changes in resistance due to both effects are minimized because they are self temperature compensated. Nevertheless, any small shift in resistance which does occur will affect all the arms of the Wheatstone

bridge equally. The same applies to temperature induced resistance changes in the lead wires. This stems from the fact that in the full bridge configuration all arms of the bridge are identical. Each contains two strain gauges and an equal amount of lead wire. Thus, as long as the resistance changes remain small the ratio of resistances in vertically adjacent arms of the bridge will stay constant with temperature.

Morgenstern and Sego (1981) report that in practice this is not the case. In the load cell application they discuss, a correction for the output change of the cell with temperature was done. This was based on calibration data obtained by testing the load cell under no load conditions at various temperatures. Similar data is not available for the load cells used at Boston Bar. As a result any anomalies in the readings of these load cells remain uncorrected. However, Sego (1988) reports that this error has an insignificant effect on the accuracy of the load cells.

Morgenstern and Sego (1981) point out what does amount to a significant error in the load cell readings. At the conclusion of the testing program described, the calibration factor for each load cell was re-established. A variation of up to 13% was noted from the value determined before the load cells were installed. An average variation of 8% was quoted. This error is likely due to drift, mentioned earlier, as well as creep. Creep manifests itself as a change in the resistance of a strain gauge under constant

load conditions.

The load cells used in this field program were identical to those used by Morgenstern and Seg0 (1981). Based on their experience then, the load cells can be considered to be accurate to within approximately 8%.

4.4 Surveying

The survey program at Boston Bar involves a network of positions to which direction and distance measurements are made. The network was illustrated and described in the previous chapter. The measurements allow the horizontal coordinates, referred to as the northing and easting, of the points to be determined. Comparison of the northing coordinates for the wall positions at successive epochs allows the lateral deflection of the wall to be determined. This is the ultimate objective of the surveying program.

The two surveying monuments, M1 and M2, serve as theodolite stations from which the various measurements are made. The procedure followed at each station is identical. Assuming that M1 is the active monument the survey measurements made during a typical epoch are described below.

The first measurements usually made were the distances from the pins, P1 and P2, to the monuments M1 and M2, respectively. Refer to Figure 3.6 for an illustration of the locations of these elements. This was done with a standard survey chain and tension handle. The same pieces of

equipment were used for all epochs. At least three pulls each were made at tensions of 15, 20 and 25 pounds.

For eventual reduction of the readings it is important that the temperature of the chaining tape is known. Care was taken not to expose the chain to direct sunlight prior to use. The tape was assumed to be at a temperature equal to the air temperature in the shade.

Horizontal angles were usually the next set of measurements made. With the theodolite mounted and levelled on the monument, left face measurements were made from M1 to; M2, BS1, BS2, P1 and BS3. This was followed by measurements made to Column A of the wall mounted survey positions (refer to Figure 3.7). Angles were read to a portable target that was mounted at each of the survey positions in turn. Plate 3.4 shows a measurement being made.

Measurements were started from the top of Column A and progressed downwards. After the lowest position in the column (A1) was measured the theodolite was plunged so that right face measurements could be made. These progressed from A1 upwards. When the column was complete right face angles were measured to BS3, P1, P2, BS2, BS1 and finally back to M2 again. This completed the first set of horizontal angle measurements. The entire process was repeated for each of the remaining columns; B, C and D.

Note that it was usual practice to set the theodolite so that the left face horizontal angle from M1 to M2 was approximately 90° for the column A measurements. For each

subsequent set the horizontal circle of the theodolite was randomly turned. This was done in an effort to minimize any effects of graduation errors in the horizontal circle.

With the exception of the distance between M1 and P1 (and M2 and P2) which is too short to effectively use electronic measurement all other distances were measured using the Wild DI4 Distomat. From M1 lengths were measured to M2, BS1, BS2, P2 and BS3. This involved mounting the DI4 atop the theodolite and mounting a prismatic reflector at each of the above mentioned positions. At M2 and P2 this was achieved by a screw mount. At the backsites a specially machined mounting clamp was used. This positioned the centre of the reflector directly above the plate which made up the backsite. Note that BS1, which was eventually destroyed, was replaced by a nail hammered into a large tree. In this case the reflector was held against the tree directly in front of the nail. A correction of half the thickness of the reflector had to be applied to the measured distance.

Distances were measured by aiming the DI4 at the reflector using the theodolite. Several measurements were made and the average taken. The results given by the DI4 are dependent upon the atmospheric conditions. This must be accounted for in the results. The unit has dial switches which could be set to automatically provide atmospheric compensation according to the conditions at the time. Standard practice at Boston Bar, however, was to set the DI4 to 8+0 which gave no atmospheric correction. Temperature and

pressure at the time of measurement were noted. This allowed a distance correction to be subsequently calculated using an equation provided by the manufacturer.

For both the DI4 and the chaining tape the distances measured are slope distances. For the former measurements the horizontal distance can be obtained by measuring the vertical angle between the theodolite and the centre of the reflector. Several left and right face measurements are made allowing the vertical circle error and the average vertical angle to be determined.

The same procedure is followed for measuring the vertical angle between M1 and P1. In this case, however, a correction for the height of the theodolite must be applied. This results from the fact that the distance between the two positions is measured using the chaining tape between two pins. The elevation difference between the two pins differs from the elevation difference between the theodolite at M1 and the pin at P1 when vertical angle measurements are made.

At the conclusion of the survey measurements the distances between the monuments and the pins immediately opposite them were measured once again. The repetition is appropriate as these distances are in the direction of the principle wall deformation.

All the survey measurements made at Boston Bar have been briefly described for a typical epoch. During the initial epoch additional measurements were made. These consisted of distance and vertical angle measurements from

the monuments to the wall targets. This data allowed the easting coordinates of these positions to be determined. As only movements perpendicular to the wall were expected these are of no particular interest and were assumed to remain constant. Therefore, no further distance or vertical angle measurements were made to the wall targets.

In assessing the accuracy of the survey it is more informative to consider the entire system of measurements rather than the errors associated with each individual type of measurement. This stems from the manner in which the measurements are reduced to yield position coordinates. The technique, called Survey Adjustment by Least Squares (Cooper, 1987), utilizes the fact that there are more measurements than unknown coordinates. Inconsistencies in the results are inevitable in this situation because of errors associated with each measurement.

The survey adjustment procedure uses all available measurements to calculate the planar coordinates so that the uncertainty in each result is minimized. In this manner the calculated values are likely to be closer to the true values than if fewer measurements were made.

The theory involved in the technique is discussed in Appendix L. The calculations used to reduce the survey data are implemented in a computer program called Plane Adjustment by Least Squares or PALS (Peterson, 1987). The program and its operation are also described in Appendix L.

Of note in this context, however, is the fact that the adjustment procedure provides a statistical method of assessing the reliability of the results. The procedure calculates, along with the position coordinates, the standard deviation, S , of each result. The standard deviation has the following interpretation: the adjusted coordinate has approximately a 0.68 probability of lying within plus or minus S of its true value. Clearly then, the smaller S is the more reliable the results. For the northing coordinates of the wall targets S is predominantly in a range of ± 1.5 mm. This figure is directly associated with the uncertainty of the horizontal angle measurements made to the wall targets. At Boston Bar this is 5 seconds.

The results of the PALS analysis also allows a check of whether the movement experienced by a wall target between two successive epochs is statistically significant. This procedure is a statistical comparison of the standard deviation from two epochs with the movement that has occurred during the interval. In this case the northing coordinates of the wall targets are of interest. The method tests the hypothesis: is d , the amount of movement, significantly different from zero. A 95% confidence limit based on the Student t distribution is employed to test the hypothesis. The analysis on the wall target results from epochs 1 and 2 indicate that movements in excess of 2 mm are statistically significant.

4.5 Slope Indicator

A slope indicator system consists of: a grooved casing installed permanently at a test site; a probe or sensing device which is compatible with the casing; a readout device; and a connection cable which, in addition to linking the probe and readout device vertically, supports the probe when it is in the casing.

The casing has four sets of grooves machined into ABS plastic pipe at equal intervals around the inside circumference. When installed the casing is positioned so that one set of oppositely opposed grooves is oriented parallel to the direction of the expected maximum movement. This is referred to as the A direction. The remaining pair of grooves are thus aligned orthogonally to this, in the B direction.

The probe is a torpedo like device equipped with two sets of guide wheels. The guide wheels, all lying in the same plane, support the probe horizontally when it is in the casing. Measurements are made by lowering the probe to the bottom of the casing with the guide wheels oriented parallel to the A direction. The probe is then raised with readings being made at two foot intervals. The device makes concurrent measurements in both the A and B directions. The two foot measuring interval corresponds to the separation of the probe's guide wheels. This in turn marks the length over which the inclination of the probe is measured.

When the readings are completed a second set is obtained with the probe oriented 180° away from the original run. This provides a reciprocal or nearly reciprocal set of readings which together with the first set are averaged.

The connection cable which supports the probe when it is in the casing is banded at one foot intervals. This provides the means for establishing the measurement points. Alternate bands are simply held against the top edge of the casing.

The probe's measurements are transferred via the connection cable to the readout device. A switch setting allows either the A or B direction reading to be displayed. The data is given by a four digit bipolar voltmeter. The instrument is calibrated so that the readings are equivalent to $2\sin\theta$ where θ is the inclination of the casing between the support wheels. Because the wheel spacing is two feet the readout value can also be directly interpreted as displacement in feet. This follows from the trigonometric relation between θ and the two foot measurement length. Integrating these quantities over the depth of the casing allows the deflection profile of the hole to be determined. The exact procedure is detailed in Appendix M.

The accuracy of the slope indicator system is dependent on several factors; the most fundamental being the probe's sensitivity to inclination. The SINCO probe measures inclination with two null-balance closed loop servo-accelerometers (Savigny, 1980). The sensors are

mounted parallel and perpendicular to the guide wheels. A voltage is applied to the sensors which is stabilized in response to tilt by a change in current flow. The resulting voltage is proportional to the angle of inclination as cited above. Savigny reports that the probe does not suffer significant inaccuracies due to non-linearity, hysteresis, temperature change or zero drift. The manufacturer quotes the sensitivity of the tilt sensor to be within plus or minus 0.5×10^{-4} m of deflection per metre depth. This corresponds to a trifling plus or minus 0.3 mm over the length of VSI1 at Boston Bar.

There are, however, operational factors which influence the system's performance. Savigny (1980) discusses among other things casing irregularities, repeatability, changing stress conditions around the casing and sensor axis rotation. The net effect is that in practice the accuracy of the slope indicator may be less than that of the tilt sensor alone. Bromwell *et al.* (1971) report field precision from 0.4×10^{-4} to 1.0×10^{-4} ; Peters and Ellis (1972) report field precision of 1.3×10^{-4} (metres of deflection per metre depth). The manufacturers themselves provide a figure of 0.0076 m per 30 metres of casing which converts to 3.0×10^{-4} m/m. From the references cited it is likely that performance is better than SINCO's estimate. Nevertheless, applying this figure to the 6 metre length of VSI1 gives a maximum uncertainty of plus or minus 1.5 mm at the top of the casing.

4.6 Magnetic Extensometer

The magnetic extensometer is a simple audio device that is used at Boston Bar to measure the settlement profile of the backfill behind the wall. It consists of: a vertical casing installed in the backfill; ring magnets surrounding the casing at set intervals but which are free to move vertically with the backfill; a probe which operates inside the casing; a lead wire which supports the probe and transmits its signals to the surface; a measuring tape which is connected to the probe when it is in the casing; an audio speaker.

When the probe is moved through the casing and passes a magnet the speaker emits three beeps. The first is of short duration and signifies that a magnet will be imminently encountered. The middle beep continues for as long as the probe is adjacent to the magnet. When the probe has passed completely beyond the magnet a third short beep is heard. The readings on the measuring tape are noted against some reference (usually the top of the casing) at the start and end of the middle beep. In this manner the positions of the magnets in the backfill can be determined.

At any particular epoch it is usual to take two sets of readings. The first is made by lowering the probe into the casing reading the locations of successive magnets until the lowest is encountered. Readings are then repeated by pulling the probe up and out of the casing. The two sets of reading defining the top and bottom of each magnet are averaged to

determine the location of the middle of the magnets. These figures are compared to corresponding values from an initial epoch. This allows the changes in the vertical position's of the magnets to be determined.

The measurements are not subject to substantial errors. The tape allows measurements to the nearest millimeter. Thus the maximum error in the position of the middle of a magnet is 0.5 mm. This figure assumes that the measuring tape is free from defects and temperature effects.

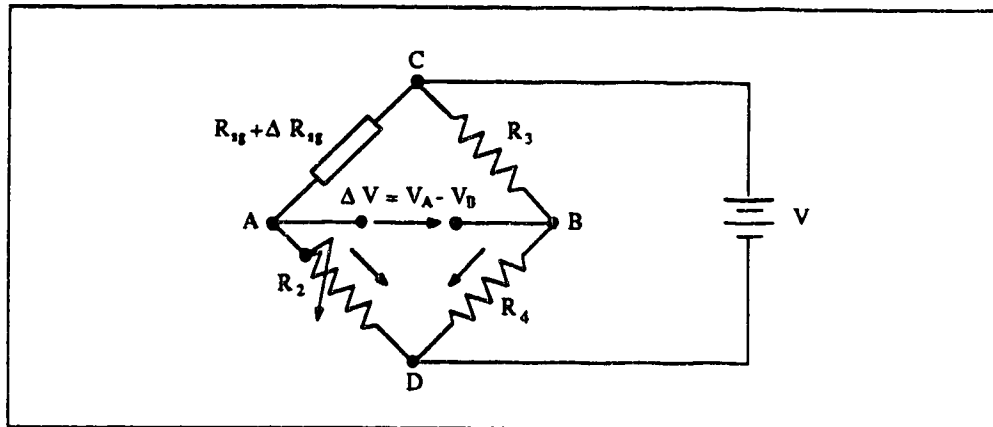
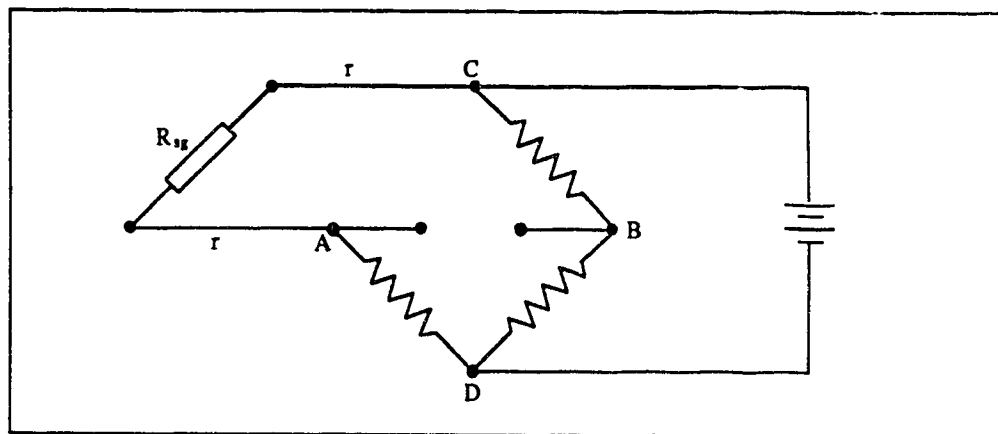
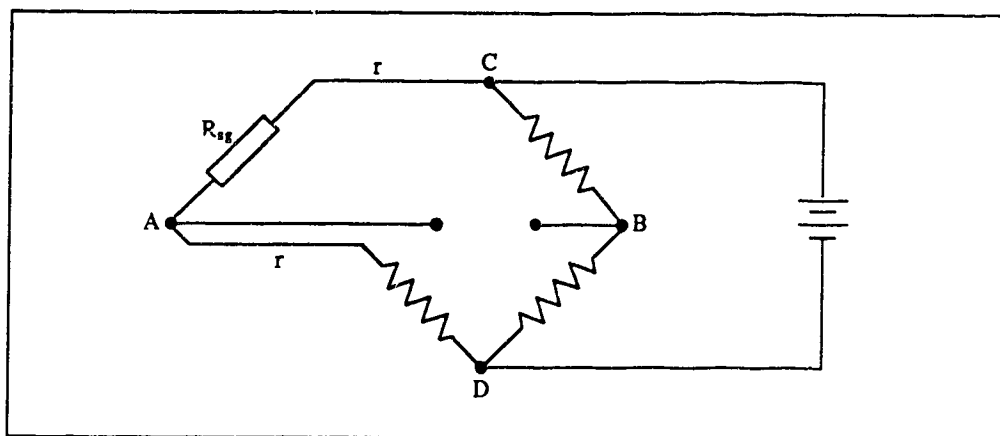


Figure 4.1: The Wheatstone bridge.

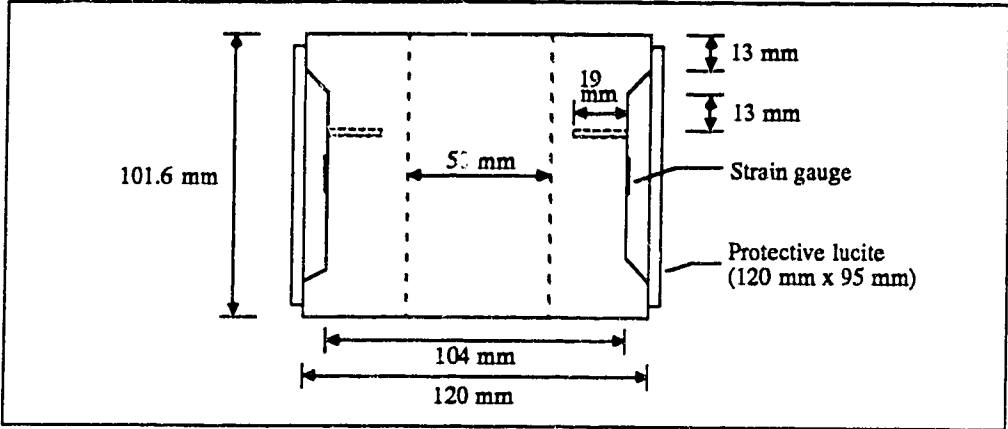


(a)

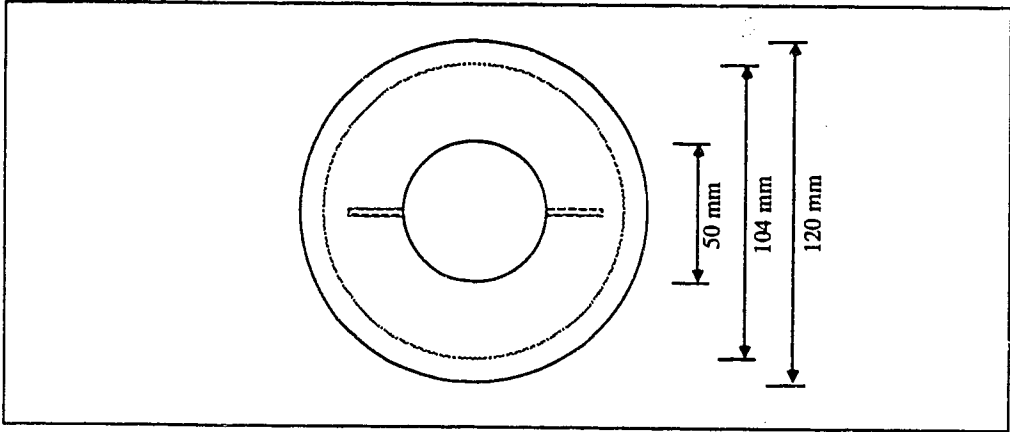


(b)

Figure 4.2: Connection of the strain gauge to the Wheatstone bridge via:
a) a two wire system; b) a three wire system.

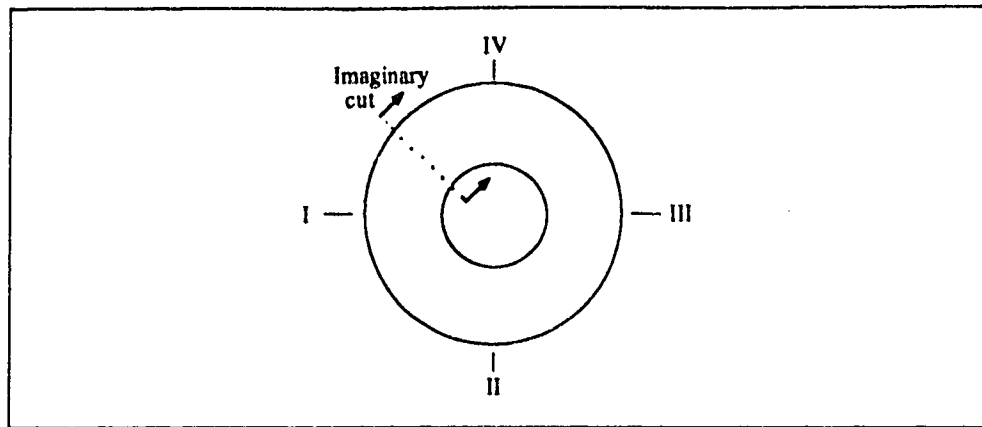


(a)

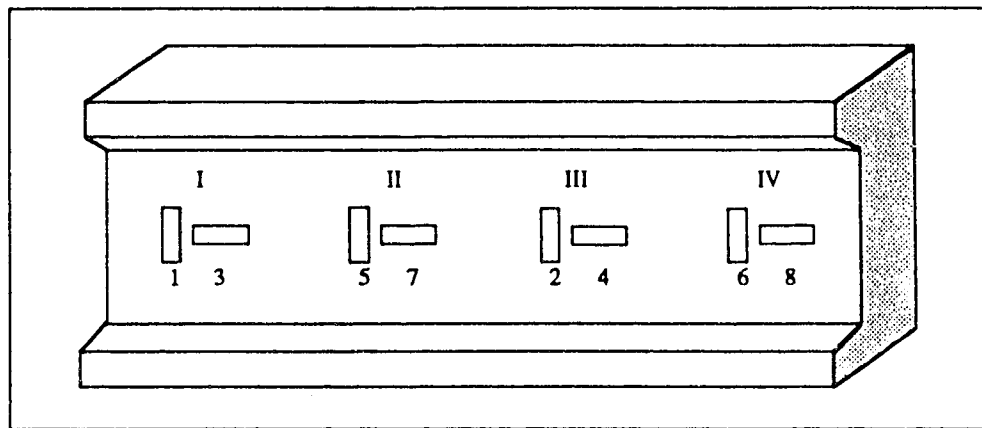


(b)

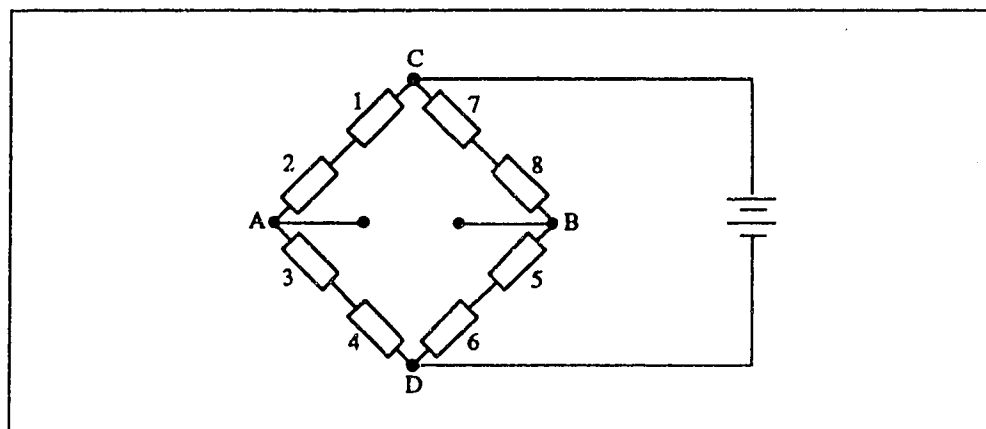
Figure 4.3: Load cell used at Boston Bar shown in; a) elevation view, b) plan view.



(a)



(b)



(c)

Figure 4.4: a) load cell divided into quadrants; b) an "unrolled" load cell showing the positions of the strain gauges around its circumference; c) the positions of the strain gauges in the Wheatstone bridge.

5. Field Results

5.1 Introduction

This chapter discusses the behavior of the wall as determined from the field measurements. Two broad categories are discussed; the loads on the wall and the deformation that it experiences. This will provide the basis for a subsequent assessment of the appropriateness of current design practice.

5.2 Loads on the Wall

The anchors provide the most direct means of determining the loads acting on the wall. The anchor loads are measured using load cells and strain gauges mounted along the grouted section of the anchors. The shortcoming with this information is that it applies only to discrete points on the wall. A means does exist, however, for inferring the distribution of pressure on the wall. This is achieved by combining the anchor loads with information provided by the wall mounted strain gauges. These results will be examined following a discussion of the anchor loads.

5.2.1 Anchor Loads

The anchor load results are given in Appendix A. The procedures used to obtain the results from the field data are discussed in Appendix I.

In Appendix A a table of results is given for each instrumented anchor. For every epoch for which measurements are available the following quantities are given: the total load in the anchor; the load per unit width of wall; the load per unit area of wall. When both load cell and anchor strain gauge data is available this information is provided for each type of instrumentation.

The load per unit area is of most interest because it facilitates comparison of the loads in the variably spaced anchors. This quantity has been plotted against time for each anchor on an individual graph. Results from both the load cells and the anchor strain gauges are included on each plot when both are available.

Several summary plots are also included in Appendix A. These include: the east wall load cell results; the west wall load cell results; the east wall anchor strain gauge results; the west wall anchor strain gauge results.

The behavior of the anchors, as revealed by the load cells and the anchor strain gauges, will be discussed in the following.

5.2.1.1 East Wall Load Cells

The load cell results for the east wall anchors are summarized in Figure A.9. Refer to Figure 3.2 for the locations of the instrumented anchors.

Figure A.9 suggests that the load cell results can be divided into two stages. The initial stage is marked by fairly rapid load changes and lasts until December,

1984. The following stage is characterized by more gradual load changes.

The upper load cells, G and H, give consistent readings during the initial period. They both indicate moderate increases in load up to October, 1984. This is followed by a sharp rise in load registered at the December, 1984 epoch. During this interval the new rail line was commissioned. Thus the increased loads can be directly attributed to the surcharge imposed by the train traffic on the wall.

Load cells E and F, positioned along the lower walers, show less consistent results during the early stage. Load cell E, with an initial load substantially higher than the other anchors, registers a large decrease by December, 1984. Load cell F essentially maintains a constant load. The lack of response in the lower load cells between October and December, 1984 is significant. It suggests that the train traffic has little influence over the lower portion of the retaining wall.

The initial stage appears to be characterized by a trend towards a redistribution of load. The sum of the loads in the lower load cells decreases while the opposite occurs in the upper load cells. This indicates a shift away from the triangular pressure distribution which was used to design the wall. This process is hastened by the train traffic on the new line. By

December, 1984 the average load in load cells E and F is identical to the loads in G and H. This suggests that the actual earth pressure distribution is likely some form of trapezoid.

Changes registered by the load cells during the second stage are more gradual. Load cells G and H give very similar readings. Both show a slow but steady increase in load which continues until December, 1986. Load cell E maintains its decreasing trend but at a reduced rate. The reduction halts by December, 1986 when its load is equivalent to that given by load cells G and H. Load cell F continues to maintain a constant load.

Thus it appears that the load redistribution noted during the first stage continues during the second period but at a slower rate. The process seems to have been completed by December, 1986. At this time the average load in the upper and lower anchors suggests a trapezoidal earth pressure distribution weighted in favour of the top half of the wall. The higher pressures over the upper region of the wall can be attributed to the increased effects of the train loads at shallower depths.

The influence of the train traffic on the wall loads warrants further discussion. As was noted above, the upper loads cells registered increased loads once trains started running on the new track. From this time on an increased load was maintained regardless of the

presence of absence of a train. It appears, therefore, that the train traffic worked to lock in a permanently increased load on the wall. This is corroborated by load cell measurements made when a loaded train was present on the outer track (March and December, 1986). The anchor forces were not significantly different from readings made when no trains were present.

5.2.1.2 West Wall Load Cells

The load cell results for the west wall anchors are summarized in Figure A.10. Refer to Figure 3.3 for the locations of the instrumented anchors.

Each of the load cells; A, B, C, and D, exhibit similar patterns of behavior. This pattern can be divided into three stages. Initially all the load cells register a sharp reduction. This suggests that the initial loads established in the anchors were inappropriately high.

The next stage consists of a rebound in load. This is most significant during the interval between October and December, 1984 when the trains started running on the new track. The magnitude of the increase at this time is approximately equal to that noted at the east wall. At the lower west wall, however, the increases occur at both the top and bottom walers.

The final stage from December, 1984 to March, 1987 has all the load cells, with the exception of A, staying constant. Load cell A experiences a gradual decrease

which halts by July, 1986.

As was seen at the east wall it appears that some vertical redistribution of load is occurring. This can be noted by considering the vertically adjacent pair of load cells, A and C. Initially load cell A, positioned on a lower waler, registers the higher load. By December, 1984 the two load cells have equal loads. As the load in A decreases the advantage swings to load cell C. The redistribution appears to be complete by February, 1987. It is likely that the earth pressure distribution changes from triangular to trapezoidal and eventually to a trapezoid weighted at its upper end. Thus the pattern of load transfer is similar to that noted at the east wall.

5.2.1.3 East Wall Anchor Strain Gauge Loads

At the east wall only anchors E and F are instrumented with strain gauges along the grouted sections. The loads calculated from this data have been plotted against time in Figure A.11.

Comparing the anchor strain gauge results to the load cell curve for anchor E indicates excellent agreement (Figure A.5). Good agreement is observed between the patterns of the strain gauge and load cell results for anchor F (Figure A.6). However, the strain gauge loads are approximately 10 kN/m^2 less than the load cell values.

This difference may be attributable to the following. The load in the grouted portion of the anchor is determined using the reading from the outer most strain gauge. Shedding of load through friction along the portion of the anchor between the strain gauge and the load cell may be occurring. This would cause a discrepancy in the readings given by the instruments.

5.2.1.4 West Wall Anchor Strain Gauge Loads

The load/time curves from the west wall anchor strain gauge data appear in Figure A.12. With one prominent exception they match the load cell results fairly well.

An extremely large increase in load is indicated by the strain gauges in all the anchors at the December, 1984 epoch. However, several factors cast suspicion on these results. The response is inconsistent with the load cells of either the west or east walls as well as the east wall anchor strain gauges. While load increases at this time have been noted none are on the order of the 500% indicated by some of the west wall anchor strain gauges. Further doubt is raised by the fact that the loads drop to normal levels immediately after the high readings. If the December, 1984 readings are ignored trends similar to those observed for the east wall anchor strain gauges would emerge. Thus, it seems likely that the results are anomalous.

The behavior of anchor A should be noted. It has a strain gauge load higher than the load cell reading. In this case the former gives readings that are on average 40 kN higher than the latter. Friction along the anchor rod may be acting in the same direction as the applied external force. Then the load measured in the grouted section would exceed that at the load cell. Such a situation could arise if the fill was moving outwards with respect to the anchor shaft.

5.2.2 Stress Distribution In the Anchors

The anchor mounted strain gauges allow the distribution of stress along the grouted section of the anchors to be determined. These are illustrated in Appendix B in Figures B.1 through B.12. The field data and results are also presented in the Appendix in tabular form. The procedure used to reduce the field data is described in Appendix J.

Several features are common to all the anchors. The most prominent is the fact that with few exceptions the highest stress levels occur at the outer most strain gauge. In only one case does a peak stress occur at a depth of greater than three metres. The lowest stress is for the most part registered at the deepest strain gauge. A similar pattern is observed by Indraratna (1987) in work with rock bolts.

This behavior is a direct consequence of the manner in which an anchor responds to loading. Upon loading, the

anchor shaft strains. The strain is transmitted through the rod to the grouted section of the anchor, where further straining is partially inhibited. This occurs first at the outer most part of the grouted section. At this location a friction force is developed opposite in direction to the applied load which is correspondingly reduced. Thus the load left to be sustained is diminished and less response is required from the rest of the anchor.

The difference between the outer most and the deepest stresses along a rod is most pronounced during the early epochs. With time, however, the difference reduces as the outer stresses decline and the stresses deeper along the anchor rise. This suggests that the steepness of the stress distribution along an anchor is a direct indication of how much of its capacity is being utilized. If load increases the reaction is provided by those parts of the anchor not already highly stressed. As a result the stress distribution flattens.

There appears to be a limit to how much stress readjustment is possible. In all the anchors this limit is reached by the August, 1985 epoch. The stress distribution at this time sets the pattern for all the remaining measurements. Thus if a load change occurs it affects the entire stress distribution equally. The effect is simply to translate the distribution either up or down the vertical axis of the graphs.

Mention has been made in the previous section of the high anchor strain gauge readings recorded at the west wall during the December, 1984 epoch. These show up clearly on the stress distribution plots. Although the stress levels increase by up to four times the pattern of the distributions change little if at all. Given the large magnitudes of the increases some change in the stress distribution would seem likely. Thus, additional weight is given to the contention that the readings at this time are incorrect.

5.2.3 Loads Inferred from the Wall Mounted Strain Gauges

As was outlined in Section 3.3 weldable wire strain gauges are mounted on the outside surface of the sheet pile at the east wall. The strain gauges are arranged in four vertical columns which are divided into two groups. These are called the east and west sections. The data provided by each section is used in conjunction with the load cell readings to infer an earth pressure distribution.

The results are presented in Appendix C. Pressure distributions for the east section are given in Figures C.1 through C.5. The west section distributions appear in Figures C.6 through C.10. Each figure, with the exception of C.5 and C.10 which are summary plots, include the results from three consecutive epochs.

It should be noted at the outset that the earth pressure results discussed in the following are highly

dependent on the methods used in their calculation. The calculation procedure is discussed in detail in Appendix K. Very briefly, however, the pressure results are obtained by double differentiation of bending moment distributions. These in turn are obtained by interpolation of the strain gauge results. In this case the curve fitting is done using cubic polynomial regression in three linked sections. Lagrangian multipliers are used to enforce boundary conditions upon the interpolation.

Note, however, that as a direct consequence of the nature of the bending moment curves, the earth pressure distributions are composed of three linear sections. It cannot be expected that the pressure distribution in the field would adhere to so simple a pattern. It is important to recognize, therefore, that the results are based on "best fits" which likely only approximate actual conditions.

5.2.3.1 East and West Section Earth Pressure Results

All of the earth pressure distributions show more or less trapezoidal shapes. Variations do occur, however. The initial epoch has distributions that are slightly triangular. These subsequently change to a more trapezoidal shape. The influence of the train loads is readily apparent from the December, 1984 epoch onwards. A bulge in the pressure over the top half of the wall occurs in all of the distributions. With time the pressure behind the lower water experiences a general decrease. This reflects the redistribution of load from

the lower to the upper regions of the wall discussed earlier.

The west section results provide more consistent distributions. This is not unexpected because more strain gauge data was available at this location. Earth pressures range from 5 kPa near the lower waler to approximately 30 kPa behind the upper waler.

At the east section the maximum pressures are in the range of 30 to 35 kPa behind the upper waler. Minimum pressures in the negative range are indicated at the lower waler for some epochs. These results stem from inadequacies in the interpolation of the bending moment distributions. Ideally, the results should provide the pressures acting from the soil only. This pressure is due to the self weight of the backfill, surcharges, and reactions to the anchor forces. The negative pressures which occur reflect to some extent the net effect of earth pressure acting in one direction and an anchor force acting in the opposite direction. Thus the actual earth pressure at the lower waler is likely in the 5 to 10 kPa range for the east section.

The results indicate the inappropriateness of the triangular earth pressure distribution used for the design of the wall. This is discussed in greater detail in Chapter 6. However, it appears that a trapezoidal or rectangular distribution coupled with line load predictions would have adequately matched the results

discussed here.

5.3 Lateral Displacement of the East Wall

The movement of the east wall has been measured with surveying, slope indicators and indirectly by the wall mounted strain gauges. The results from each technique will be discussed in turn.

5.3.1 Surveying

Recall from Section 3.3 that four columns of survey positions were established on the sheet pile at the east wall. The locations of these positions are shown in Figure 3.7. The surveying program was designed to allow the horizontal displacement of these positions to be determined. Thus a column of survey positions gives the horizontal displacement profile for a vertical section of the wall at a particular time. These results are presented in Appendix D in Figures D.1 through D.5.

Also given are plots of deflection versus time for each of the survey positions. One graph is produced for each column of positions in Figure D.6 through D.9. Note that in these plots only data points spaced consecutively in time are connected. Because the slope of the deflection/time curves represent the rate of movement connection of non consecutive data points would distort interpretation of the results.

The procedure used to reduce the survey data is presented in Appendix L. Note, however, that all the survey deflections are referenced to measurements made immediately following the loading of the anchors.

The four columns of survey positions provide a fairly consistent picture of the horizontal movements experienced by the east wall. The measurements made at the July, 1984 epoch indicate that the wall moved inwards or towards the backfill. The mid-height region of the wall experienced the most movement ranging from 2 to 4 mm. The ends of the wall showed less inward movement resulting in the wall assuming a concave outward shape.

The period from July to December, 1984 has the wall moving sharply outwards. This movement occurs as a rigid body translation of the wall and is approximately 7 mm in magnitude. Thus the concave shape of the wall is preserved.

The results provided by columns C and D indicate that by the next set of measurements in August, 1985, the wall has retreated. The inward movement is fairly uniform over the height of the wall and is on the order of 4 mm.

The next phase of behavior, lasting from August, 1985 to the latter half of 1986, has the wall resuming its outward movement. The displacement occurs at a more moderate rate than previous trends but is less uniform. Nevertheless, on average the wall experiences about 2 mm of outward deflection.

The final recognizable stage of behavior has the wall halting its outward shift and then moving inwards. The inward movement is approximately 1 mm. The final profile of the wall is still a pronounced concave shape at column A. At column D this is less evident with the bottom of the wall displaced further outwards than the top.

Columns B and C, which are located over shorter heights in the middle region of the wall display more vertical profiles throughout the monitoring. They also move more than the remaining columns over similar elevations. This can be attributed to the fact that columns B and C are located on inner bends of the corrugated sheet pile. These surfaces are therefore not in contact with the walers as are the outer bends upon which columns A and D are mounted.

The maximum range of movement that the wall undergoes is from -4 mm to 10 mm. Both of these figures are registered at column A, the former near mid-height of the wall and the latter near the bottom of the wall. For the most part, however, movements of the wall are in the range from -3 mm to 7 mm. As was mentioned most of the movement occurs as rigid body translation with the wall in a concave shape.

5.3.2 Slope Indicators

Recall from Section 3.3 that three vertical slope indicators were installed at the east wall. Refer to Figure 3.5 for the locations of the instruments identified as VSI1, VSI2 and VSI3.

The results are presented in graphical and tabular form in Appendix E. Before the results are discussed, however, some preliminary comments are warranted.

The procedure used to reduce the slope indicator data is described in Appendix M. All of the results are referenced to an initial set of measurements made immediately following the loading of the anchors. This is consistent with the procedure established for the survey results.

Note that the A direction measures horizontal displacement perpendicular to the wall. The B direction measures displacement parallel to the wall.

VSI1 is mounted along the outer surface of the sheet pile and as a result is free to move over its entire length. Therefore, it cannot, on its own, provide absolute displacements. Unfortunately, provisions were not made to survey the slope indicator casing. As a result survey position C2 has been used to establish the location of the casing in space so that absolute displacements can be obtained. The shortcomings with this technique are discussed in Appendix M.

Establishing the absolute displacements for the B direction movements of VSI1 is not possible because the survey does not provide measurements transverse to the wall.

Both VSI2 and VSI3, located behind the wall, are socketed into the bedrock underlying the backfill. Their bases are stationary and so the results given by these

instruments can be interpreted directly as absolute displacements.

5.3.2.1 VSI1

The results for VSI1 appear in Figures E.1 through E.6. The first four of these figures give the displacement profiles in the A and B directions. The results are divided into late and early epochs. The final two figures provide deflection versus time plots for the A and B directions.

The A direction results compare moderately well with the survey results. The slope indicator initially shows a concave outward appearance. This diminishes with time, however, as a kink develops in the lower region of the casing and the wall displays a more pronounced outward tilt.

More favourable comparisons occur between VSI1 and survey columns B and C. These three elements are in close proximity. Over similar elevations they show magnitudes and patterns of movement that are in good agreement.

An exception occurs during the interval between August, 1985 and July 1986. During this time the slope indicator shows a retreat while the survey indicates outward movement.

The very sharp outward movement registered at the top of the slope indicator casing at the December, 1986 epoch cannot be corroborated. No survey positions exist

in this vicinity. The fact that higher than normal displacements are maintained at this location for the next two epochs suggests that the slope indicator results are legitimate.

The B direction of VSI1 shows dramatic movements. With time the slope indicator has become progressively more inclined to the north. The difference in readings between the top and bottom of the casing steadily increases and by December, 1986 approaches 90 mm.

These results indicate that the wall experienced rotation about an axis perpendicular to the wall. Because all movements along the slope indicator are referenced to the bottom of the casing this location appears to be the centre of rotation. However, this need not be the case; the rotation could be occurring about any point on the wall.

Differential settlement is the most probable cause of the rotational movement. Frictional downdrag caused by settling of the backfill would cause wall settlement. Variations in either this force or the bearing capacity of the soil underneath the wall would cause differential settlement.

Whatever the exact nature of the B direction movement it stops by December, 1986. Both subsequent measurements do not register any further relative motion between the top and bottom of the casing.

5.3.2.2 VSI2

The results for VSI2 appear in Figures E.7 through E.10. The original set of zeros for this instrument were lost so a new set was established at the July, 1986 epoch. Even over the shortened interval of measurement substantial movement has been recorded. Considering first the A direction, up to 5 mm of outward displacement is noted by the December, 1986 epoch. The deflected shape assumes a vertical profile over the elevation range of the wall. This suggests uniform outward translation of the fill. This presents an interesting anomaly because during the same interval the survey shows little or no movement of the wall. VSI1, which experienced a large increase in the relative separation of its base and top through this duration, supports the measurements of VSI2.

The first measurement of the B direction indicates a roughly parabolic profile. The top of the casing experiences the most movement; about 9 mm to the north. Further northward movement is registered by the next epoch, to be followed by a retreat at the March, 1987 reading. At this time the top of the casing is displaced 6 mm from its July, 1986 position.

The curved nature of the deflected profiles of VSI2 contrast the very straight shapes recorded in the B direction by VSI1. This may be attributable to the fact that VSI1, without a fixed base, can respond to

rotational movements without bending. In addition, the magnitudes of movement measured by VSI1 and VSI2 are very different. Over the interval between July and December, 1986 the former shows displacement of 23 mm at the top of its casing, three times that registered by VSI2 at a similar elevation. This is not a surprising result as one would expect movement to decrease with distance from the wall. An exception to this observation is available, however. Comparing the increments of movement at the tops of VSI1 and VSI2 over the last two epochs shows identical results.

5.3.2.3 VSI3

The results for VSI3 appear in Figures E.11 through E.14. VSI3 also has calibration readings dating from the July, 1986 epoch. The first set of results from December, 1986 record outward translation on the order of 2 mm over most of the instrument in the A direction. The only other available data, from March, 1987, records a backward tilt that places the upper half of the casing behind its zero position by 1 to 2 mm. The shape at this final reading is quite irregular. Agreement between VSI2 and VSI3 is in general quite good although the latter experiences smaller movements.

The B direction indicates first a fairly uniform northward tilt with the top of the casing moving a total of 4 mm. The tilt reverses direction by the next reading but does not display the same degree of uniformity. The

top of the casing is 3 mm to the westward. The 7 mm shift is significant, especially considering the short interval over which it occurred. Similar movement is not noted at the other slope indicators.

5.3.3 Displacement Inferred from the Wall Mounted Strain Gauges

The wall mounted strain gauge results allow theoretical displacement profiles for the wall to be calculated. The procedure is described in Appendix K. As was the case for the calculated earth pressure distributions, however, the results must be considered approximations only.

The results are presented graphically in Appendix F. Figures F.1 and F.2 give the theoretical displacement profiles for the east section. Figures F.3 and F.4 provide the same for the west section. Figure F.5 and F.6 are displacement versus time plots for the east and west sections respectively.

The displacement profiles show some similarity to the results of VSI1. A concave outwards shape is seen in the wall for both the east and west sections. The backwards kink noted in VSI1 near the bottom of the wall is also in evidence in the east section results, particularly in the early epochs. During the later epochs the displacement profiles adopt more of a tilted shape although some concavity is preserved. This is again similar to behavior seen with VSI1.

The magnitudes of the calculated displacements show better agreement with the measured results over the top half of the wall than the lower regions. About 2.5 mm of inward movement is predicted for the bottom of the east section for the later epochs. As well, the pattern of movement through time does not exactly match those established with the measurements.

The fairly uniform backwards movement of the wall following loading of the anchors does not appear in the theoretical results. The rapid outward movement experienced prior to December, 1984 is predicted but only for the upper half of the wall. Following this stage the calculated displacements either increase slowly or stay constant. The inward and outward movements seen in the surveying result between December, 1984 and December, 1986 are not repeated in the calculated results.

Nevertheless, in light of the many assumptions involved in their calculation the theoretical displacements are a reasonable match of the field measurements.

5.4 Extensometer Results

The results from the multi-point magnetic extensometer appear in Appendix G. The procedure used to reduce the data is provided in Appendix N. Refer to Figure 3.5 for an illustration of the extensometer's location.

The results show that since the initial set of readings settlement in excess of 200 mm has occurred by February,

1987. The largest settlements are restricted to the upper magnets. Settlement of the magnet near the middle of the instrument is less than 100 mm. The lower magnets register small settlements.

Curious response is noted at the last epoch of results. Each magnet, with the exception of the lowest one, is shown to rise approximately 10 mm. This may be related to the fact that during the same time period the wall was observed to move in towards the fill. This may have acted to compress the fill marginally raising the magnets.

5.5 Correlation Between East Wall Loads and Movement

The displacement and load results for the east wall exhibit a dependence that is evident through five distinct stages. The initial phase commences upon loading of the anchors and lasts 20 days until July 10, 1984. During this period, as was discussed earlier, the wall was observed to move in towards the backfill. Closer scrutiny of the movements, however, indicates that more movement occurred at the bottom of the wall than at the top. The upper survey positions register very minimal inward movement and at position C5 outward movement is indicated. This agrees with the results from VSI1 and the wall mounted strain gauges in the same region of the wall.

During this stage the lower anchors, E and F, in sum show a 9 percent decrease in load. At the same time the upper anchors experience a 28 percent increase in load. Thus

one can hypothesize that as the loads on the wall decrease it moves inward and vice versa.

The correlation at this stage is tentative because distinct outward movement at the top of the wall is not indicated by all displacement measurements. As well, some portion of the load changes mentioned are likely due to redistribution of forces. This was referred to earlier and probably occurred under the influence of a trapezoidal earth pressure distribution. This would cause the anchor forces to change as they were originally loaded on the basis of a triangular distribution.

The next stage, from July to December, 1984, is characterized by rapid outward movement of the wall. At the same time the anchor loads, with the exception of E, increase. The rate of increase is more pronounced for anchors G and H following the October, 1984 epoch. This has already been linked to the start of train traffic on the new rail line.

Notwithstanding anchor E, the trend conditionally identified in the first stage is supported by the observations made in this period. As the loads increase outward movement of the wall occurs.

The third stage commences as of the December, 1984 epoch. The load cell results suggest that it continues until February, 1985. During this interval all of the anchors show a decrease in load. This corresponds to the temporary suspension of train traffic on the new line. The

displacement measurements indicate that the wall moves back toward the fill during this stage. Unfortunately, survey measurements at the February, 1985 epoch were not made. This means that end of the load decrease cannot be correlated to a halt in the backward movement of the wall. The strain gauge displacements do indicate, however, that the backward movement of the wall stops as of February, 1985.

The fourth stage is considered to last from February, 1985 until December, 1986. During this period the anchor forces increase slightly. This is matched by moderate outward movement of the wall. Initially, however, the available survey results show backwards movement occurring from December, 1984 to August, 1985.

Recall that survey measurements were not made during the intervening epoch at February, 1985. Hypothetically, results at this time could have shown that the retreat of the wall actually ended sooner than the available survey measurements indicate. Extending this argument allows speculation that the outward movement that characterized this stage actually started as of February, 1985.

Thus the behavior inferred and observed during this stage remains consistent with the relationship established between the loads on the wall and its movement.

The fifth and final stage lasts from December, 1986 to the last epoch in March, 1987. The displacement measurements show a backward movement of the wall. This is accompanied by a decrease in the anchor forces.

Although exceptions can be noted, in general, load increases on the wall cause it to move outwards. Conversely, load decreases are accompanied by inward wall movement. Neither of these relationships are unexpected. Nevertheless, the links between the displacement and load measurements do serve to indirectly substantiate one another.

5.6 Conclusions

The following list summarizes the observed behavior of the retaining walls.

1. The load cell results suggest a vertical redistribution of the loads on the walls. The initial anchor loads were established on the basis of a triangular earth pressure distribution. The presence of some form of trapezoidal earth pressure distribution would result in load transfer between the upper and lower anchors.
2. The train traffic on the new track acted to lock in permanently increased loads on the retaining walls. At the east wall this was noted only over the upper half of the wall. At the lower west wall the load increase occurred over the entire height of the wall.
3. The field data indicates that the loads on the walls range from $0.2-0.25\gamma H$ over the top half and $0.1-0.15\gamma H$ over the lower portion of the walls. The west wall, although lower than the east wall, experiences higher loads. This may be linked to the fact that the west wall anchors were initially loaded to higher levels.

4. Changes in anchor loads occur most rapidly prior to December, 1984. The most significant changes in the anchor loads can be linked to the initiation of train traffic on the new track. Following this, changes occur more gradually.
5. With only some exceptions the loads based on the anchor strain gauges and the load cells show good agreement.
6. The results from the wall mounted strain gauges suggest some form of trapezoidal earth pressure distribution. These results also show that the train loads from the new track have an appreciable effect on the lateral pressures. The influence is restricted, however, to the top half of the wall.
7. A direct correspondence between loads and wall movement has been established. As loads increase outward movement occurs. The opposite also was observed to occur.
8. Movement of the wall and the load in the anchors do not appear to be seasonal. Thus frost effects can be discounted.
9. In general a flattening of the anchor stress distributions is observed with time. This occurs as load is distributed more evenly along the anchor. Nevertheless, stress levels in the anchor rods remain highest near the outer portion of the grouted sections of the anchors.
10. The survey and slope indicator results show reasonable agreement. The east wall was observed to experience a

series of inward and outward movements that for the most part resembled uniform translations. Movements were predominantly in the range from -3 mm to 7 mm.

11. The most notable discrepancy between the survey and slope indicator results concerns the deflected profile of the east wall. The survey results from columns A and D indicated that the wall had assumed a concave outward shape. The maximum deflections occurred at the bottom of wall. The slope indicator, VSI1, did not illustrate as distinct a concave profile. VSI1 gave maximum displacements at the top of the wall as the deflected shape had more of a tilted nature. Part of this difference may be due to the fact that the slope indicator is located on an inner bend of the sheet pile wall. Survey columns A and D, on the other hand, are situated on outer bends of the wall. Greater agreement between VSI1 and survey columns B and C was noted as all these elements are in close proximity to one another.
12. The displacements calculated from the wall mounted strain gauges agree fairly well with VSI1.
13. The east wall has experienced substantial differential settlement which has caused a northward tilt. This halted as of December, 1986.
14. The backfill behind the east wall has experienced considerable settlement. As of February, 1987, however, the settlement has stopped. One can speculate that had measurements been available from the December, 1986

epoch, the halt may have been detected earlier. This is based on the fact that the rotational movement of the east wall stopped at this time. It seem likely that both phenomena are linked as down drag of the settling backfill is probably the cause of the wall settlements.

6. Performance Predictions for the East Wall

6.1 Introduction

A number of procedures are available for predicting the performance of earth retaining structures. These include theoretical, empirical and numerical methods. Examples of each have been applied to the instrumented section of the east wall at Boston Bar. The loads sustained by the wall and the deformations it undergoes have been calculated. These results are subsequently compared to the field measurements.

Calculations have been carried out for several configurations of the wall to reflect the changes that it has undergone during its history. Three stages can be identified:

1. The wall before being extended and prior to train traffic on the new track.
2. The wall before extension but after the new track became operational.
3. The wall after extension with the new track operational.

All calculations have been carried out for the cross section illustrated in Figure 3.4. This corresponds to the wall at the reference sheet pile joint in the middle of the instrumented section of the east wall. This allows for a comparison between the predicted and the measured performance of the wall. This subsequently permits an evaluation of the methods most appropriate for the design of tied back walls.

The field results used in this comparative analysis are described below. This is followed by presentation of the methods used to predict the performance of the wall. Finally, the predicted results are compared to the field measurements of load and deformation.

6.2 Field Results

Field results are sampled from epochs representative of the three stages mentioned above. The results from June 21, 1984 are used as they represent conditions immediately after completion of the wall. This date is prior to the height of the wall being increased and before the new track was brought into service. The results from December 05, 1984 are used because it is the first epoch following commissioning of the new rail line. Finally, the results from December 10, 1986 are considered. The wall has by this time been extended in height and has also been subjected to repeated train loads. Conditions appear to have stabilized with the anchor loads reaching their maximum values. Collectively, these three epochs are hence forth referred to as the reference epochs.

6.2.1 Measured Loads

The field measurements of load used in this comparative analysis come from two sources: the anchor mounted load cells and the pressure distributions calculated from the strain gauge data. Direct comparison between the measured

and the predicted anchor loads is not possible because the calculated loads are based on a metre width of wall. The anchors have a variable spacing that is in excess of one metre.

An additional point must also be considered. The section of wall used for the prediction calculations lies between the instrumented anchors at both the upper and lower walers. Therefore, the average load/unit width of the two top and the two bottom anchors is appropriate for comparison to the predicted loads. These quantities are given in Table 6.1 for the reference epochs.

The anchor forces, normalized to a load per unit area, can also be used to obtain pressure distributions. For the lower half of the wall an average load per unit area is calculated based on the results of load cells E and F. This quantity is assumed to be acting uniformly from the base of the wall to midway between the walers. A similar procedure is used for load cells G and H with the results applied over the top half of the wall. Note that this region does not include the galvanized steel extension above the sheet pile until after December, 1984.

The average anchor loads per unit area, again for the reference epochs, are given in Table 6.1. They are also illustrated as pressure distributions in Figure 6.1. These distributions, based solely on the tributary areas of the anchors, are admittedly arbitrary. There is precedent for this approach, however (Terzaghi and Peck, 1948). The fact

that the loads per unit area for the upper and lower anchors are similar in magnitude also encourages the approach.

The pressure distributions inferred from the wall mounted strain gauges for the reference epochs are presented in Figures 6.2 and 6.3. The former shows the results from the reference epochs for the east section; the latter the west section of the east wall. Recall that the east and west sections straddle the reference sheet pile wall joint. This in turn marks the location of the cross section used for all of the calculations.

6.2.2 Measured Deformations

The displacement of the east wall is given by the survey and the slope indicator VSI1. As well, deformations have been calculated using the wall mounted strain gauge data. For each of these cases it should be noted that the zero displacement condition is assumed to exist immediately after the tensioning of the anchors. The survey and slope indicator results appear respectively in Appendices D and E. The displacements based on the wall mounted strain gauges for the reference epochs have been summarized in Figures 6.4 and 6.5.

6.3 Predicted Results

The majority of the methods used to predict the performance of the retaining wall are based upon a theoretical or empirical earth pressure distribution. These

include the Rankine (1857) and Coulomb (1776) theories as well as the recommendations by Terzaghi and Peck, (1948, 1967), Tschebotarioff (1951,1973), Dubrova (1963), and Hanna and Matallana (1970). Based on the calculated earth pressure distributions anchor loads can be determined using tributary areas. Note that the Coulomb and Dubrova procedures will be referred to as the force polygon methods. The remaining procedures will be referred to collectively as the pressure envelope methods.

The finite element method, a numerical solution, has also been applied to the wall. The results it provides have been interpreted to give the horizontal stresses in the backfill behind the wall as well as the anchor loads. The method also provides the only available *a priori* means of calculating displacements. It has therefore been used to predict the deformation profile of the wall.

The effects of the train loads are directly considered by the force polygon and finite element methods. For the remaining procedures the surcharge imposed by the train traffic is dealt with separately using Boussinesq (1885) elastic theory.

Prediction of the behavior of the retaining wall is complicated by the fact that the properties of the backfill are not known. Each of the calculation procedures discussed (with the exception of the Boussinesq method) require soil parameters as input. The pressure envelope and force polygon methods are not computationally demanding. This permits

ranges of values for the required soil parameters to be used.

The angle of shearing resistance, ϕ , was varied from 30° to 50° using 5° increments. The total unit weight, γ , was given values of 17, 19 and 21 kN/m^3 . The wall friction angle, δ , was taken as 0, $\phi/2$ and $2\phi/3$. These ranges are considered broad enough to bracket the backfill's actual properties.

For the finite element method, where the expense of the analysis prohibits numerous runs, best estimates of the necessary properties are used. This is discussed in greater detail in Section 6.3.8.

Each of the methods listed above are presented in individual sections. The calculations involved are described as are the assumptions made. Where appropriate each method has been applied to all of the three wall stages identified in Section 6.1.

The results are presented in Figures 6.6 through 6.15. For the pressure envelope and force polygon methods, however, these figures provide only a sample of the results. This is explained in greater detail in Section 6.4. Complete results for the pressure envelope and force polygon methods are presented in tabular form in Appendix O. These tables are included for reference only.

6.3.1 Rankine Earth Pressure

The Rankine (1857) theory was discussed in Section 2.3. Of note, however, is the fact that the method is applicable to vertical walls only. Therefore, without some approximations, the procedure cannot be used for Boston Bar where the wall has a 10° batter.

The batter of the wall could simply be ignored. While this would allow direct application of the procedure the results would clearly be in error. Schnabel (1982) states that "it is not unusual to batter a wall 10° from vertical and find the earth pressure reduced by a third". Unfortunately the origin of this reduction is not specified.

A more rational approach would apply a reduction equivalent to that predicted by Coulomb theory for an inclined wall. This amounts to using the Coulomb equation directly since, notwithstanding wall inclination, both Coulomb and Rankine give identical results for walls with zero friction. The Coulomb equation for the lateral earth pressure coefficient, K_a , for a wall without wall friction and with a horizontal backslope is as follows:

$$K_a = \frac{\sin^2(a+\phi)}{\sin^3 a (1+(\sin\phi/a))^2} \quad [6.1]$$

With K_a established the earth pressure at any depth can be found using:

$$p = K_a \gamma z \quad [6.2]$$

Calculations are applied to two separate cases. The first assumes that because of the shallow slope of the fill above the wall no soil surcharge acts. The second considers the 0.7 metre height of fill above the wall to be acting as a surcharge.

6.3.2 Coulomb Earth Pressure

The Coulomb theory is described in Section 2.2. Direct application of Coulomb's earth pressure coefficient equation (Equation 2.1) is not possible because of the irregular geometry of the backslope. As a result a force polygon solution has been implemented as a computer program. The program, called Z-FP, appears in Appendix Q along with instructions for its operation.

The program considers a series of trial slip surfaces. For each trial a force polygon is constructed. This includes: the weight vector for the wedge of soil bounded by the wall and the slip surface; the reaction force along the slip surface; and P_a , the active earth thrust equivalent to the lateral force exerted by the wedge. For a general case a trial slip surface, together with the forces acting on the sliding wedge, are shown in Figure 2.1. A force polygon is also indicated. The weight of the soil wedge and the orientation of all the vectors are known. By geometry the magnitude of P_a can be calculated. The slip surface which yields the largest value of P_a defines the critical wedge.

The irregular geometry of the backslope also means that the calculated earth thrust cannot be assumed to be acting over a triangular pressure distribution. To calculate the pressure distribution earth thrusts are found using slip surfaces originating from numerous heights along the wall. The difference in successive earth thrusts divided by the distance separating the points being considered gives the earth pressure over that section of wall.

If train traffic is accounted for the calculations are modified slightly. If the trial slip surface intersects the ground beyond a rail then the weight vector is increased by the amount of the train load. Darrach (1984) quotes this as 150 kN per metre per rail.

A final note concerns the orientation of the pressure which is calculated. Because the Coulomb method accounts for wall friction the pressure is oriented at a specified inclination, δ , away from the normal to the wall. This must be accounted for when the anchor loads are calculated.

6.3.3 Dubrova Solution

Harr (1966) discusses a solution developed by Dubrova (1963) which allows for an earth pressure distribution to be calculated for a variety of deformation conditions. On the basis of its successful application by Scott *et al.* (1972) it has been used here. The method is based on the original Coulomb theory with an important addition. Dubrova allows an assumption concerning the mobilization of ϕ along what Harr

(1966) refers to as quasi-rupture lines. The degree of mobilization, represented by ψ , is some function of the depth z . This in turn is related to the type of deformation the wall undergoes. Refer to Figure 6.16 for an illustration of the terms discussed.

For the case of a wall rotating about its top Dubrova assumes that ψ is related to z as follows:

$$\psi = \frac{\phi z}{H} \quad [6.3]$$

As can be readily noted $\psi=0$ at the top of the wall where no movement occurs. At the base of the wall where movement is a maximum $\psi=\phi$.

The particular expression for ψ replaces ϕ in Coulomb's lateral earth pressure coefficient equation (Equation 2.2). The lateral earth pressure equation (Equation 2.1), which includes K_a as a term, is differentiated with respect to z . The result is an expression which gives the variation of earth pressure as the mobilization of friction varies.

The mathematics involved is cumbersome. As a result all the solutions given by Harr (1966) are restricted to cases with vertical walls, horizontal backfills and simple deformation conditions.

The technique has, however, been extended by using a numerical procedure based on the computerized force polygon solution discussed in 6.3.2. A series of slip surfaces or quasi-rupture lines are considered from $z=0$ to $z=H$. For each

wedge the maximum active earth thrust is calculated based on the angle ψ . The difference between two successive thrusts divided by Δz gives the earth pressure acting over that interval.

For conditions at Boston Bar ψ is considered to be a quadratic function of z . At the ends of the wall $\psi = \phi$. Halfway between the walers $\psi = 0.8\phi$. This corresponds to outward rotation of the upper and lower halves of the wall about a point midway between the walers. Some translation is also accounted for by the mobilization of friction at the point of rotation. The ψ distribution is intended to mimic the concave deformation pattern indicated by the survey results. Mobilization of soil friction is highest where deformation is a maximum.

As was the case for the Coulomb analysis two situations are considered. The first does not account for any train loads; the second does if the slip surface intersects the ground beyond a rail.

6.3.4 Terzaghi and Peck

Both Terzaghi (1941) and Peck (1943) related experience that had been gained in dealing with braced cuts. Together they later proposed an apparent earth pressure envelope that became widely used (Terzaghi and Peck, 1948). Their recommendation is illustrated in Figure 2.4. Observations made over subsequent years, in particular at New York, Berlin and Munich subway construction sites, led them to

modify their proposal (Terzaghi and Peck, 1967). This envelope is shown in Figure 2.5.

Both methods are applied to the two cases considered in Section 6.3.1 for the Rankine procedure. That is, the 0.7 metres of fill above the wall is first ignored and then considered. Also in keeping with the convention adopted in 6.3.1 the wall batter is accounted for by using Equation 6.1 to calculate K_a .

6.3.5 Tschebotarioff

The two earth pressure envelopes proposed by Tschebotarioff (1951, 1973) for cohesionless soil were discussed in Section 2.5. Illustrations of each of his envelopes are given in Figure 2.6 and 2.7.

Because neither recommendation includes K_a the Coulomb equation cannot be directly used to account for the wall batter as had been done previously. For the range of friction angles being considered the Coulomb method predicts a 12% to 27% decrease in earth pressure for a wall with 10° batter. The average reduction is approximately 20%. This figure has been applied to the pressures calculated by the Tschebotarioff procedures in an effort to account for the inclination of the wall.

Again, the analysis considers the two cases of soil surcharge already discussed.

6.3.6 Hanna and Matallana

Hanna and Matallana (1970) published results from scale model test of a retaining wall with multiple rows of tiebacks supporting sand. Measurements of anchor loads and earth pressures led them to propose the pressure envelope illustrated in Figure 2.17. Application of their recommendation has been done for the two soil surcharge cases. Again, Equation 6.1 is used to calculate K_o , so as to account for the batter of the wall. K_o is calculated according to Jaky (1944):

$$K_o = 1 - \sin\phi \quad [6.4]$$

6.3.7 Effect of Train Loads

The Canadian Foundation Engineering Manual (1985) provides a modified version of Boussinesq's theory (1885). This method has been applied to calculate the loads imposed on the sheet pile wall by the train traffic. The procedure is illustrated in Figure 6.17a. An equation for σ_h , the horizontal stress, is given in the figure. It is applied at a desired number of depths allowing the pressure distribution due to a surface line load to be determined.

There are several difficulties involved in using the procedure as outlined in Figure 6.17a. The method is applicable to vertical walls with horizontal backslopes. Neither of these conditions are present at Boston Bar. The solution has therefore been modified to take the geometry at

Boston Bar into account.

The batter of the wall, as shown in Figure 6.17b, has the effect of increasing the value of the parameter m with depth. In the conventional solution m stays constant. Using an m appropriate to the depth being considered allows the inclination of the wall to be taken into account.

The inclined backfill has the effect of raising the train load a distance, 0.7m, above the top of the wall. This is accounted for by considering an effective depth. This is measured not from the top of the wall as in shown in Figure 6.17a but rather from the upper surface of the backfill.

An approximation is also required in applying the train loads. A train represents a series of usually moving point loads. Darrach (1984) quotes CN procedure and recommends using a line load of 150 kN per metre per rail to model the trains. This quantity has been used in this analysis.

The results are presented in graphical form in Figures 6.12 and 6.13. The former gives the results for the unextended wall; the latter for the wall once its height is increased. The influence of each of the four rails making up the two sets of tracks is investigated. The pressure distributions for each individual rail are shown as is the sum of the effects of the two outer rails. Note that the rails are numbered in the figures, with "1" referring to the outer most rail, "4" the inner most rail.

6.3.8 The Finite Element Method

A linear, elastic, plane strain finite element analysis has been carried out to fulfil two objectives. The distribution of horizontal stress behind the sheet pile wall and resulting from the backfill and train loads is desired. The deformation of the wall due to the soil and train loads is also to be investigated.

The FEARS (Chalaturnyk, 1988) version of the SAFE (Chan, 1986) program has been used. FEARS incorporates a one dimensional reinforcing element. The element can be used to model an un-tensioned or passive anchor, an application useful for this analysis.

The finite element grid used is shown in Figure 6.18. It is based on the field geometry known or inferred at the location of the reference sheet pile joint. The grid consists of 250 isoparametric rectangular or triangular elements and three reinforcing elements. The latter are two noded and have linear force/deformation response. The system contains a total of 759 nodes. Those along the lower boundary have their vertical degree of freedom fixed. Those along the right boundary have their horizontal degree of freedom fixed.

The finite element analysis incorporates seven load steps. These are illustrated in Figures 6.19 through 6.21. This sequence of steps represents the history of the wall with one important exception. In the field the anchors were tensioned once backfilling of the wall was completed. In

this analysis, however, the anchors are never "externally" tensioned. The forces in the anchors develop only in response to the loads sustained by the wall.

Tensioned anchors could be modelled using point loads. Assumptions as to the magnitudes of these point loads would be required, however. This would defeat the purpose of an analysis that attempts to predict behavior.

A number of different materials are included in the cross section represented by the finite element grid. The material zones are indicated by numerals in the load step diagrams. The reader is referred to Table 6.2 which identifies the material associated with each number. The properties required to define the material for the finite element analysis are also given in this table. Very few of the material properties are precisely known. Therefore some explanation is required as to how the parameters were established.

The properties of material 1, the backfill behind the new retaining wall, are unknown. The values used have been established based on best estimates available from the literature. Unfortunately, the backfill can be expected to exert the greatest influence on the behavior being investigated.

K_0 for granular soil is quoted by Holtz and Kovacs (1981) to range from 0.4 to 0.6 with 0.5 being a good average. With $K_0=0.5$ Poisson's ratio is calculated as 0.33 using the following relation.

$$\nu = \frac{K_o}{1+K_o} \quad [6.5]$$

The unit weight of the backfill is taken as 19 kN/m³, the average of the range of values considered in the other analyses. The elastic modulus of the material was calculated using the Janbu (1963) expression:

$$E = Kp_a(\sigma_3/p_a)^n \quad [6.6]$$

where K = modulus number

p_a = atmospheric pressure

n = modulus exponent

For a well graded granular fill Duncan *et al.* (1980) quote values for K and n of 600 and 0.4 respectively. σ_3 is calculated based on:

$$\sigma_3 = K_o \gamma z \quad [6.7]$$

With z taken at mid-depth of the backfill σ_3 becomes 24.7 kPa. The calculations give rise to an elastic modulus of 34,567 kPa. This has been arbitrarily reduced to 30,000 kPa to account for the fact that the backfill used at Boston is likely not ideal.

The properties of material 2, the scree along the lower slope surface, are also unknown. This zone has been given the same properties as the backfill which lies immediately above it. This simplifies the stress conditions at the

interface between the materials.

The material in zone 3, the region behind the timber wall, has also been given the same properties as material 1. It is not expected that the characteristics of the fill in this area will have an appreciable effect on the behavior of the sheet pile wall.

Material 4 represents the bedrock foundation. Its unit weight has been set at 22.5 kN/m^3 , a value common for rock. ν has been set at 0.15 based on independent laboratory tests conducted on quartzite and sandstone by the author. E has been established as 10 GPa based on information provided by Peck *et al.* (1953) and the laboratory tests referred to above. As with material 3 it is not expected that the properties of the rock will have much influence on the behavior of the sheet pile wall.

Material 5, the timber wall, has been given properties of 5 kN/m^3 , 5 GPa and 0.31 for γ , E and ν respectively. These quantities have been obtained from Eshbach (1952). The difficulty in establishing an elastic modulus should be noted. It differs widely with the type of wood, the direction of loading with respect to the grain and size effects. The elements representing the timber wall have been dimensioned on the basis of an estimated average wall thickness. The wall consists of spaced vertical timber piles supporting heavy timber lagging. Its thickness is thus variable. Based on dimensions obtained from photographs an average thickness of 400 mm has been used in the analysis.

Material 6 is made up of a reinforcing element used to model the upper anchor of the sheet pile wall. The reinforcing elements are defined by two parameters; a tensile strength and an elastic modulus both in units of force. The tensile strength for mild steel is quoted by the Tennent (1971) as 460 MPa. This quantity is converted to a force through multiplication by the average anchor area per unit width of wall. Along the upper waler at the reference sheet pile joint two 32mm diameter anchors are spaced over an interval of 6.634m. The average anchor area per unit width is calculated as follows.

$$\begin{aligned}
 A &= \frac{2\pi(32\text{mm}/2)^2}{6.634\text{m}} & [6.8] \\
 &= 2.425 \times 10^{-4} \text{ m}^2/\text{m width of wall}
 \end{aligned}$$

This value gives rise to a tensile strength of 111 kN. Similarly, the standard modulus for mild steel, 200 Gpa, is converted to 48,500 kN using this area.

Material 7 is used for the lower sheet pile wall anchors. Its reinforcing element has a tensile strength and elastic modulus of 325 kN and 141,000 kN respectively. These figures differ from those for material 6 because the lower anchors have a larger diameter and are more closely spaced.

Material 8 represents the anchors installed in the timber wall during construction of the new wall. The anchor diameters and spacings are not known. As a result the reinforcing element used to model the anchors has been given

the same properties as material 6.

Material 9 represents the steel sheet pile wall. E for mild steel has already been quoted as 200 GPa. ν is given as 0.29 from Tennent (1971). Some explanation concerning the dimensions of the elements making up the wall is required. The thickness, t , of the elements is defined as the dimension in the plane of the finite element grid and perpendicular to the height of the wall. The thickness has been calculated so that the section modulus of the wall elements, if they were considered as a beam, would be equivalent to the figure quoted for the sheet pile. The calculations are shown below.

$$\begin{aligned}
 S &= \frac{I}{y} \\
 &= \frac{6t^3/12}{t/2} \\
 &= 835 \times 10^3 \text{ mm}^3
 \end{aligned}
 \tag{6.9}$$

Solving for t gives an element thickness of 71 mm.

The results of the finite element analyses are presented graphically. The horizontal stress distribution in the backfill immediately behind the sheet pile wall is given in Figure 6.14. The results for load steps 5, 6 and 7 are included. This graph has been produced by sampling the Gauss points closest to the wall in those elements adjacent to the wall.

The deformation of the sheet pile is shown in Figure 6.15. This plot has been produced by sampling the displacements of the nodes along the outer face of the wall. Again, the results from load step 5 and onwards are given. All of the displacements have been referenced to load step 5, however. This establishes the zero displacement condition for the finite element results at a time consistent with that used for the field measurements.

6.4 Comparison of Field and Predicted Results

The predicted and measured performance of the retaining wall are compared in the next two sections. The first section deals with the loads on the wall; the second discusses the wall's deformation. This allows an assessment of the applicability of each of the calculation procedures that have been considered.

Recall, however, that for the pressure envelope and force polygon methods results were obtained using ranges of soil parameters. Therefore, to facilitate comparison, attention must be focussed on those results calculated with the most likely values of the soil parameters.

Establishing the most likely values of the backfill's properties can best be described as an educated guess. Some assistance is provided by initial comparison of the predicted results to the field measurements. A wide variation between the two is an indication that the parameters used in the calculations are not reasonable. This

approach can be relied upon only to a certain extent, however. The lack of consistency between predictions and measurements could well be due to a poor model.

Factor of safety analyses have been carried out to assist in determining backfill parameters which are most appropriate. The analyses are presented and described in Appendix P. Assuming that the calculation procedure is valid a factor of safety less than one must be based on incorrect soil properties.

The above considerations suggest that ϕ , γ and δ can be established as 40° , 19 kN/m^3 and 20° respectively. For a compacted granular backfill these values are not unreasonable. Thus, for the pressure envelope and force polygon methods only the results obtained with the above quantities will be compared to the measured performance.

For all of the results comparisons are made for each of the three stages identified in the history of the wall. Results calculated for a particular stage are compared to field measurements made at a similar time.

6.4.1 Load

As was mentioned in Section 6.2.1 earth pressure envelopes derived from the field measurements are presented in Figures 6.1, 6.2 and 6.3. Results from Section 6.3 have been extracted to provide load predictions for the three stages in the history of the wall. The results from the pressure envelope and force polygon methods are presented in

Figures 6.6 through 6.11. These figures show the pressure distributions obtained with the best estimate backfill parameters discussed in the previous section.

Figures 6.6 and 6.7 give the calculated envelopes for the unextended wall prior to the new rail line becoming operational. These results should therefore be compared to the first reference epoch; June 21, 1984.

Figures 6.8 and 6.9 give earth pressure predictions for the unextended wall once train traffic has commenced on the new line. This corresponds to conditions at the second reference epoch; December 05, 1984. The effects of the train loads upon the pressure distributions have been obtained by adding the Boussinesq results to the envelopes shown in Figure 6.6 and 6.7.

For the unextended wall the Boussinesq results are given in Figure 6.12. Only the pressure due to the outer most rail, identified as Rail 1 in the figure, has been included in the summation. As will become apparent, consideration of the loads from the remaining rails would lead to over prediction of the earth pressure on the wall.

The Coulomb and Dubrova procedures, unlike the pressure envelope methods, can account directly for the influence of surcharge line loads. As a result two additional pressure envelopes, shown in Figure 6.9 and labelled Coulomb (D) and Dubrova (D) (D for direct), are given. These distributions are obtained from the force polygon solutions with the train load considered.

Figures 6.10 and 6.11 give the predicted pressure distributions for the extended wall with the new track operational. The convention outlined for the previous stage has again been followed. The distributions have been obtained by summing the results from each of the pressure envelope and force polygon methods with the Boussinesq loads. For the extended wall the Boussinesq results are given in Figure 6.13. Two additional distributions, due to the Coulomb and Dubrova methods with direct consideration of the train loads, are also given.

Additional clarification is required for the results extracted from the pressure envelope methods. For each of these procedures two cases were considered. In the first case the height of backfill above the top of the wall was not considered; in the second case it was. This was done because of uncertainty concerning whether or not the additional height of sloping fill would influence the lateral earth pressure.

Results indicate that it does not. Therefore, all of the pressure envelope results presented in the figures do not account for the height of backfill above the top of the wall. The lack of influence of the sloping backfill on the earth pressure can be noted in Figure 6.7. Comparison of the Rankine and Coulomb distributions shows very minimal differences. This occurs despite the fact that the Coulomb solution accounts for the height of fill above the top of the wall.

Finally, the lateral earth pressures predicted by the finite element results are illustrated in Figure 6.14. Pressure distributions from load steps 5 through 7 are given. Recall that load step 5 involves placement of the third lift of backfill. This corresponds to the first stage in the wall's history. The train load is applied in load step 6, modelling the second stage of the wall. The last load step increases the height of the wall and places the final lift of soil. This models the last stage of the wall.

A summary of the predicted and measured anchor loads for each of the three wall stages is given in Table 6.3.

For the initial stage of the wall the measured results give roughly rectangular pressure distributions with an average magnitude of approximately 12 kPa. The pressure is increased at the base of the wall, however. The best predicted pressure distribution is that due to Terzaghi and Peck (1967). This is a rectangular envelope, and although it does not match the peak of pressure at the base of the wall, it matches the measured anchor loads fairly well.

The distributions due to Tschebotarioff and Hanna and Matallana over predict both the earth pressures and the anchor loads by a substantial margin. The Rankine, Coulomb, Terzaghi and Peck (1948), Dubrova and finite element (load step 5) solutions all under predict the earth pressures and anchor loads.

The most obvious shortcoming with the finite element results is the zone of negative stress at the base of the

wall. By the sign convention being used this indicates compression in this region. The compression results because the base of the wall is inhibited from moving by being directly connected to the soil elements underneath it. This prevents lateral expansion of the soil elements behind the lower portion of the wall.

As has been mentioned the predicted pressures over the remaining height of the wall are less than those indicated by the field measurements. Part of this difference must be attributed to the tension applied to the anchors in the field. The field determined pressure distributions will reflect the effects of this and thus give larger pressures. As was mentioned in Section 6.3.8 the anchors in the finite element analysis are never "externally" tensioned.

The results of load step 5, therefore, give the stresses generated by the backfill only. This distribution could be approximated by a trapezoid with a magnitude of about 12 kPa. The trapezoid would of course not reflect the negative pressure region nor the decreased pressure acting midway between the walers.

The most notable behavior during the second stage is the increase in the lateral pressure over the upper region of the wall. This is due to the effects of the train traffic. The pressure at the lower anchor stays constant or decreases slightly while at the base of the wall they stay constant or increase slightly. The general indication, however, is that the train has minimal effect over the lower

portion of the wall.

Both of the envelopes due to Terzaghi and Peck provide reasonable predictions for the pressures and anchor loads. Recall that these distributions incorporate the Boussinesq results. Their later recommendation gives a better fit of the field determined distributions while their original envelope gives better predictions of the anchor forces. Note that both of these procedures, together with most of the other methods, over predict the anchor forces. The exceptions are the Coulomb (D) and finite element methods.

The Coulomb (D) and Dubrova (D) procedures provide the closest predictions for the measured anchor forces but give unrealistic pressure distributions. The surcharge due to the train loads has the effect of curving the failure surface (Terzaghi, 1943). This behavior is not accounted for by the force polygon solution which assumes planar slip surfaces. This discrepancy manifests itself with the irregular pressure distributions shown in Figure 6.9.

The finite element results for this stage are given by load step 6. The train is shown to have a very small influence upon the lateral pressures. The horizontal stresses increase by a maximum of less than 5 kPa in the upper reaches of the wall. This is an unexpected result for which no definitive explanation can be provided. It is possible that the model allows the timber retaining wall to exercise a larger role in supporting the train loads than actually occurs. The pressure distribution for load step 6

is an under prediction for the same reason cited for load step 5. However, it would be expected that the relative difference between the two distributions should approximate the changes observed in the field.

The third stage in the history of the wall corresponds to its increased height. The field determined pressures are observed to increase moderately in the upper half of the wall and decrease or stay constant in the lower half. Again, both of the Terzaghi and Peck envelopes give reasonable fits for the pressure distribution as well as the anchor loads. Each recommendation over predicts on both counts with the 1948 envelope giving slightly better results for the anchor forces.

The recommendations due to Tschebotarioff and Hanna and Matallana are conservative. Once again the Coulomb (D) and Dubrova (D) methods provide the closest predictions for the anchor loads. However, the pressure distributions they give are again in error due to the problem discussed above. The Rankine, Coulomb and Dubrova procedures do not adequately model the increased pressure over the upper half of the wall.

The finite element results show no increase in pressure with the extension of the wall and the placement of the small final lift of soil. This contradicts both the field results as well as the other prediction methods.

6.4.2 Deformation

The finite element method provides the only *a priori* means of predicting the deformation of the wall. The displacement profiles for load steps 6 and 7 are given in Figure 6.15. These profiles correspond to the second and third reference epochs.

The results are identical for both load steps and indicate a uniform outward tilt about the base of the wall accompanied by a small amount of translation. The maximum displacement is approximately 1 mm at the top of the sheet pile and about 0.25 mm at its base. This pattern of displacement reflects that given by the results of VSI1 and the wall mounted strain gauges. The predicted magnitudes are, however, substantially smaller. The additional displacement seen to occur in the field between the second and third reference epochs is also not correctly predicted. This is consistent with the fact that the finite element analyses showed no increase in earth pressures between these two epochs.

The poor displacement results may be attributable to a number of sources. Some of the discrepancy between the observed and the calculated movements is likely due to the presence of plastic deformations in the field. Terzaghi (1953) states that the fully active earth pressure condition, and thus the limits of elastic behavior, are reached with movements equal to 0.001 of the wall height. At the east wall this corresponds to about 6 mm. Displacements

of this magnitude and larger have been measured. Thus the possibility exists that plastic deformations in excess of the purely elastic movements have occurred. These movements would be beyond the range of predictions by an elastic analysis. Unfortunately, the finite element results are well under this 6 mm threshold of elastic movement.

Assumptions and simplifications concerning material properties, geometry and boundary conditions contribute the remaining error. Of these the material properties are likely the most significant. The estimates made to establish many of the material parameters used in the analysis are recalled. This conclusion also follows, indirectly at least, from a consideration of the stress results. The stress calculations, by the Airy stress function, are independent of material properties. The fact that fairly reasonable stress results have been obtained endorses the geometric and boundary condition assumptions that have been made.

Incorrect material properties should not be given an inordinate amount of blame, however. Additional analysis indicated that wall displacements are inversely proportional to the elastic modulus of the backfill behind the wall. The elastic modulus used for the backfill in the analysis being considered was 30,000 kPa. Increasing the calculated displacements by one magnitude would bring them more in line with field results. This would require a backfill modulus of 3,000 kPa if the above relationship still applies. This figure is unfortunately more representative of a soft clay

than a compacted granular material. It is unlikely, therefore, that material parameter estimates are in error by one magnitude.

6.5 Conclusions

The results of this comparative analysis indicate that the loads on the wall can be adequately predicted. The measured displacements, on the other hand, have been poorly matched.

The best fits of the measured loads was provided by the Terzaghi and Peck (1948, 1967) apparent pressure envelopes. Matching either of these distributions with the loads given by the Boussinesq procedure gives good predictions for the sum of the influence of the backfill and the train loads. However, the slightly more conservative nature of the later envelope would favour its use in future designs similar to Boston Bar.

The finite element analysis carried out, while giving fairly reasonable stress results, provided very poor displacement predictions. As has been recorded by numerous other workers the sensitivity of displacement calculations to material parameters is emphasized. It can be concluded on the basis of this experience that the prediction of displacements using the finite element method is not a straightforward undertaking.

Epoch	Average Anchor Load per metre width (kN)		Average Anchor Load per unit area (kPa)	
	E & F	G & H	E & F	G & H
June 21, 1984	54.64	21.62	18.12	6.36
Dec. 05, 1984	47.24	57.82	15.10	19.61
Dec. 10, 1986	44.88	69.68	14.89	20.48

Table 6.1: Weighted average anchor loads per metre width and per unit area.

Material Number	Material Type	Elastic Modulus	Poisson's Ratio	Total Unit Weight (kN/m)	Tensile Strength (kN)
1	Backfill behind new wall	30,000 kPa	0.5	19	-
2	Scree material on slope surface	30,000 kPa	0.5	19	-
3	Backfill and/or scree behind original timber wall	30,000 kPa	0.5	19	-
4	Bedrock	10 GPa	0.15	22.5	-
5	Timber wall	5 GPa	0.31	5	-
6	Upper anchor in new wall	48,500 kN	-	0	111
7	Lower anchor in new wall	141,000 kN	-	0	325
8	Anchor in timber wall	48,500 kN	-	0	111
9	Steel sheet pile wall	200 GPa	0.29	0	-

Table 6.2: Materials used in the finite element analysis and their parameters.

	Low Wall No Train		Low Wall Train		High Wall Train	
	Top Anchor	Bottom Anchor	Top Anchor	Bottom Anchor	Top Anchor	Bottom Anchor
Jun. 21/84 Load Cells	21.62	54.64				
Dec. 05/84 Load Cells			57.82	47.24		
Dec. 10/84 Load Cells					69.68	44.88
Tschebotarloff (1973)	64.40	71.19	110.46	96.63	132.2	101.76
Hanna and Mataliana	53.90	59.65	99.96	85.09	119.34	89.37
Tschbotarloff (1951)	46.10	46.10	92.16	71.54	110.04	73.99
Dubrova (D)	-	-	56.42	55.30	59.14	44.96
Dubrova	20.68	41.48	66.74	66.92	76.52	59.82
Terzaghi & Peck (1967)	33.10	36.64	79.16	62.08	93.54	64.69
Terzaghi & Peck (1948)	26.70	30.33	72.75	55.77	86.24	57.36
Coulomb (D)	-	-	20.28	74.40	27.14	76.96
Coulomb	12.71	42.45	58.77	67.89	67.84	68.49
Rankine	12.10	41.58	58.16	67.02	64.64	66.95
Finite Elements	3.26	11.27	3.84	16.97	3.84	16.97

Table 6.3: Summary of anchor loads from field measurements and from prediction calculations.

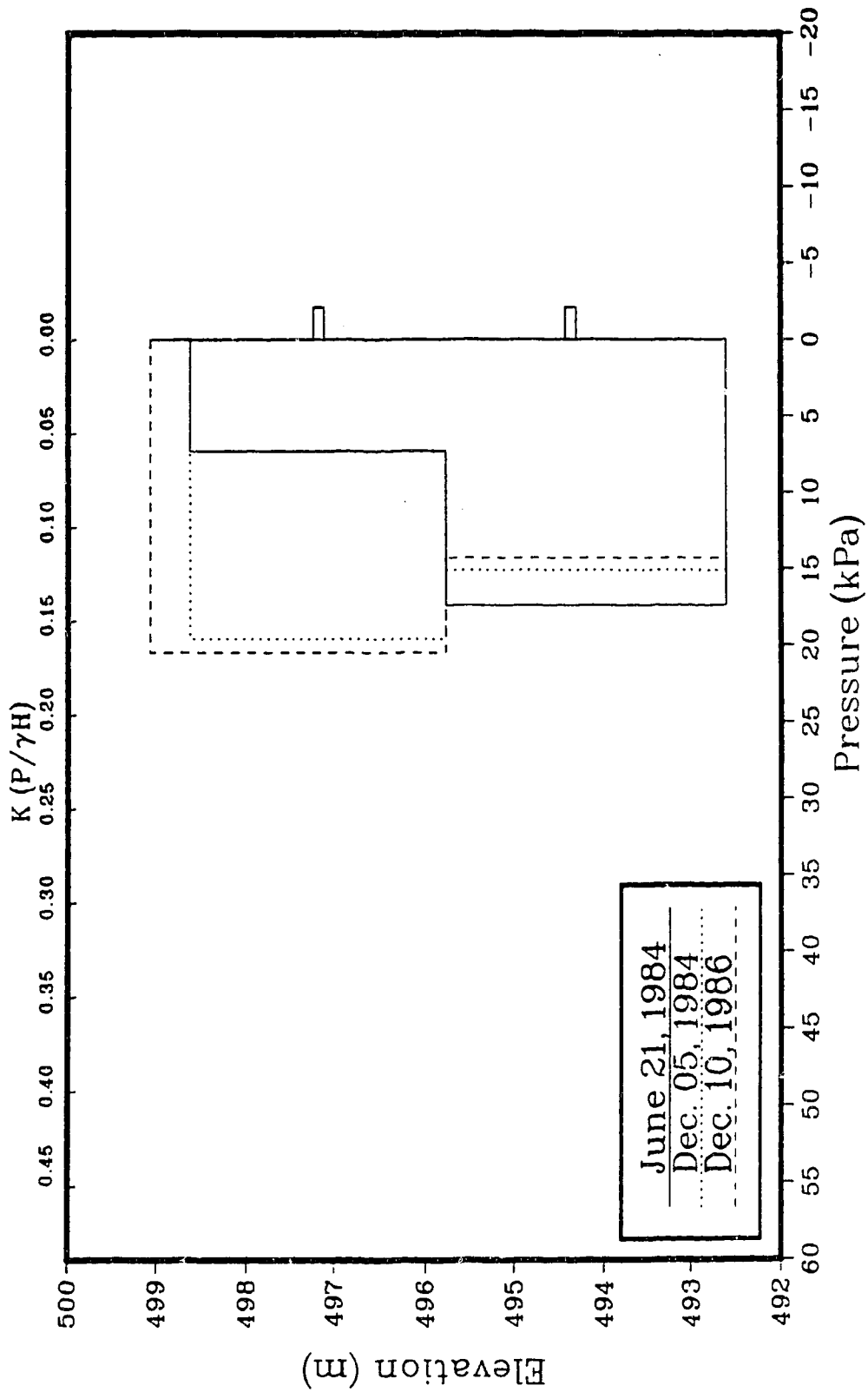


Figure 6.1: Horizontal earth pressure based on east wall load cell results.

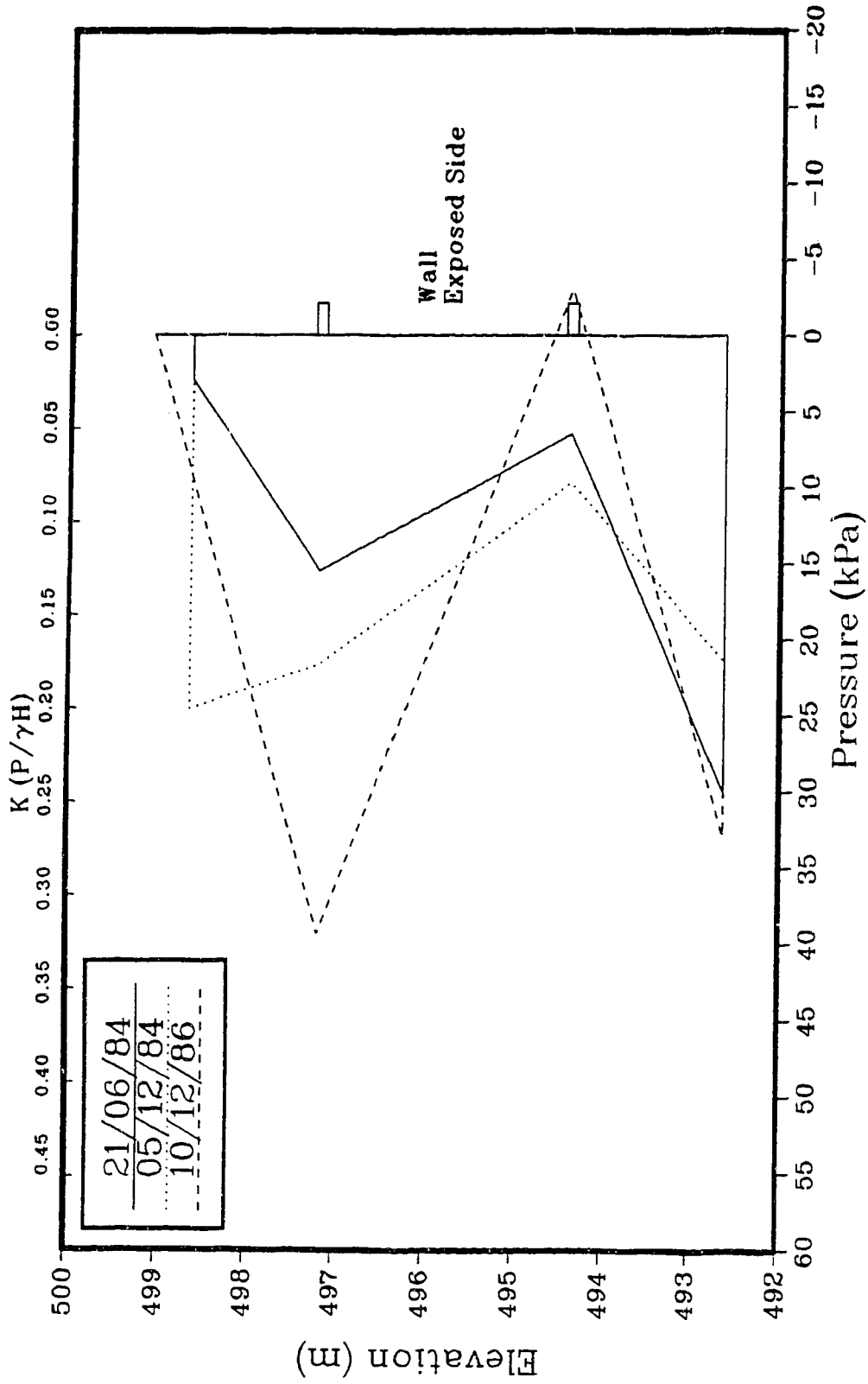


Figure 6.2: Pressure distributions based on wall mounted strain gauges, reference epochs, east section.

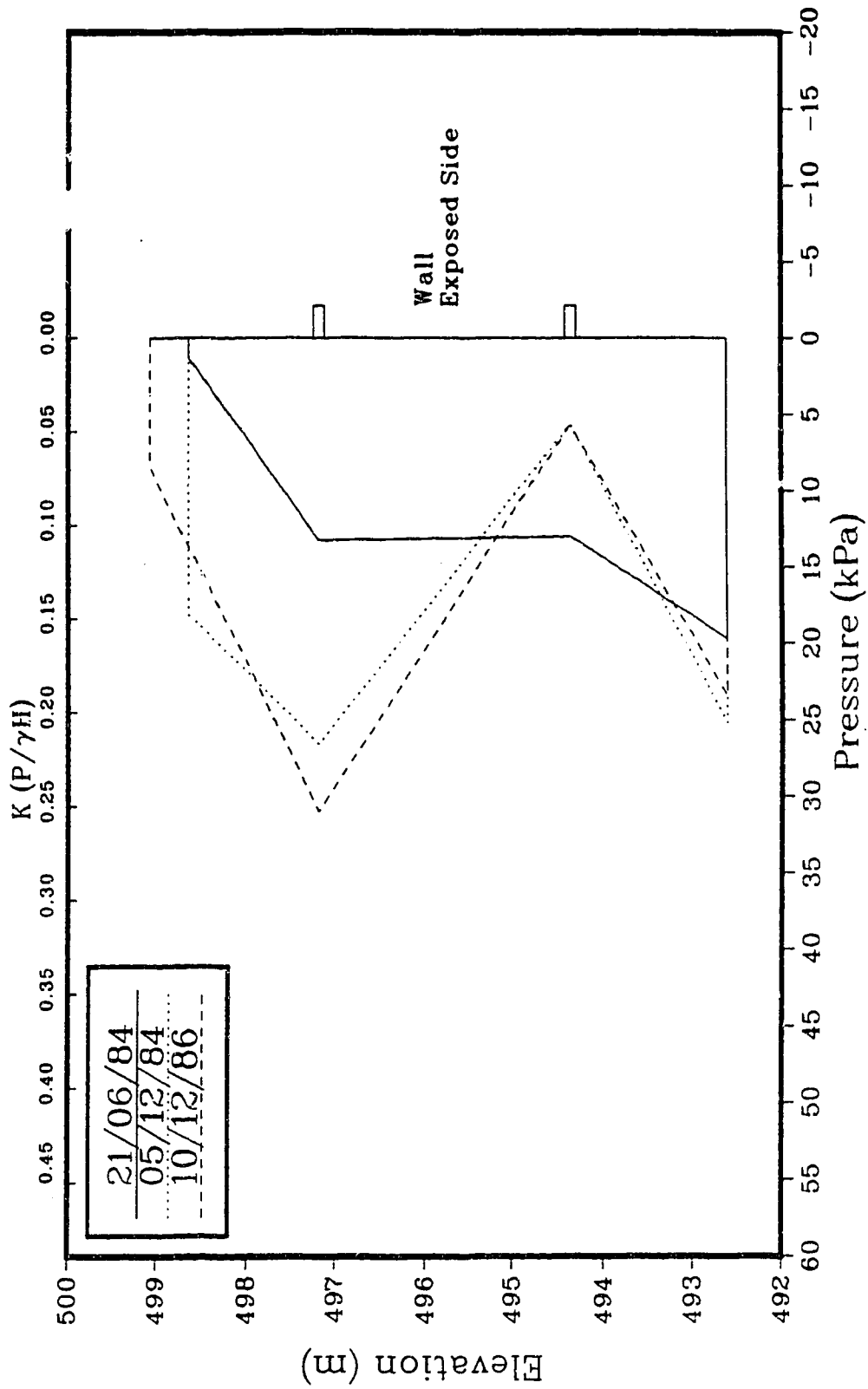


Figure 6.3: Pressure distributions based on wall mounted strain gauges, reference epochs, west section.

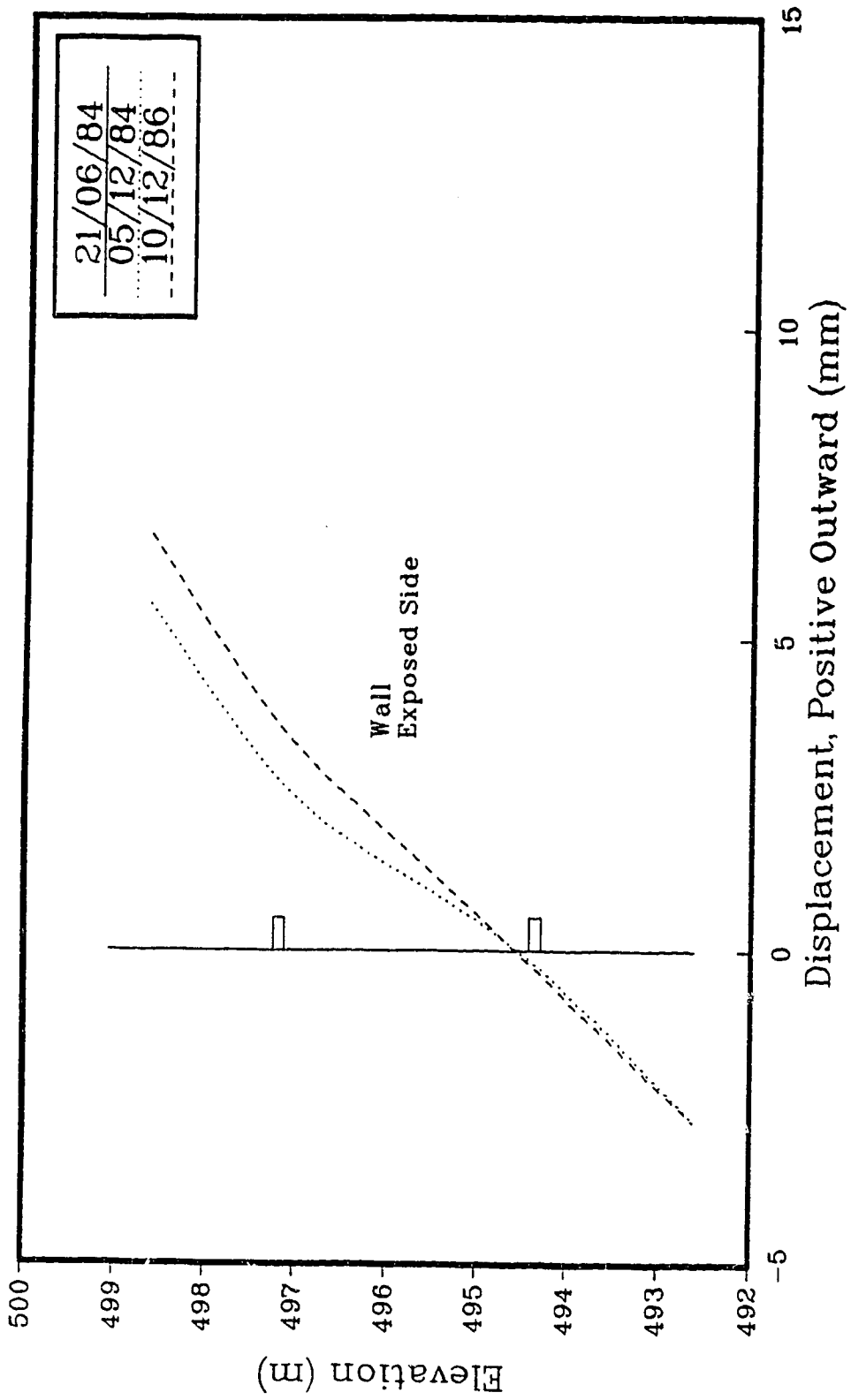


Figure 6.4: Displacements based on wall mounted strain gauges, reference epochs, east section.

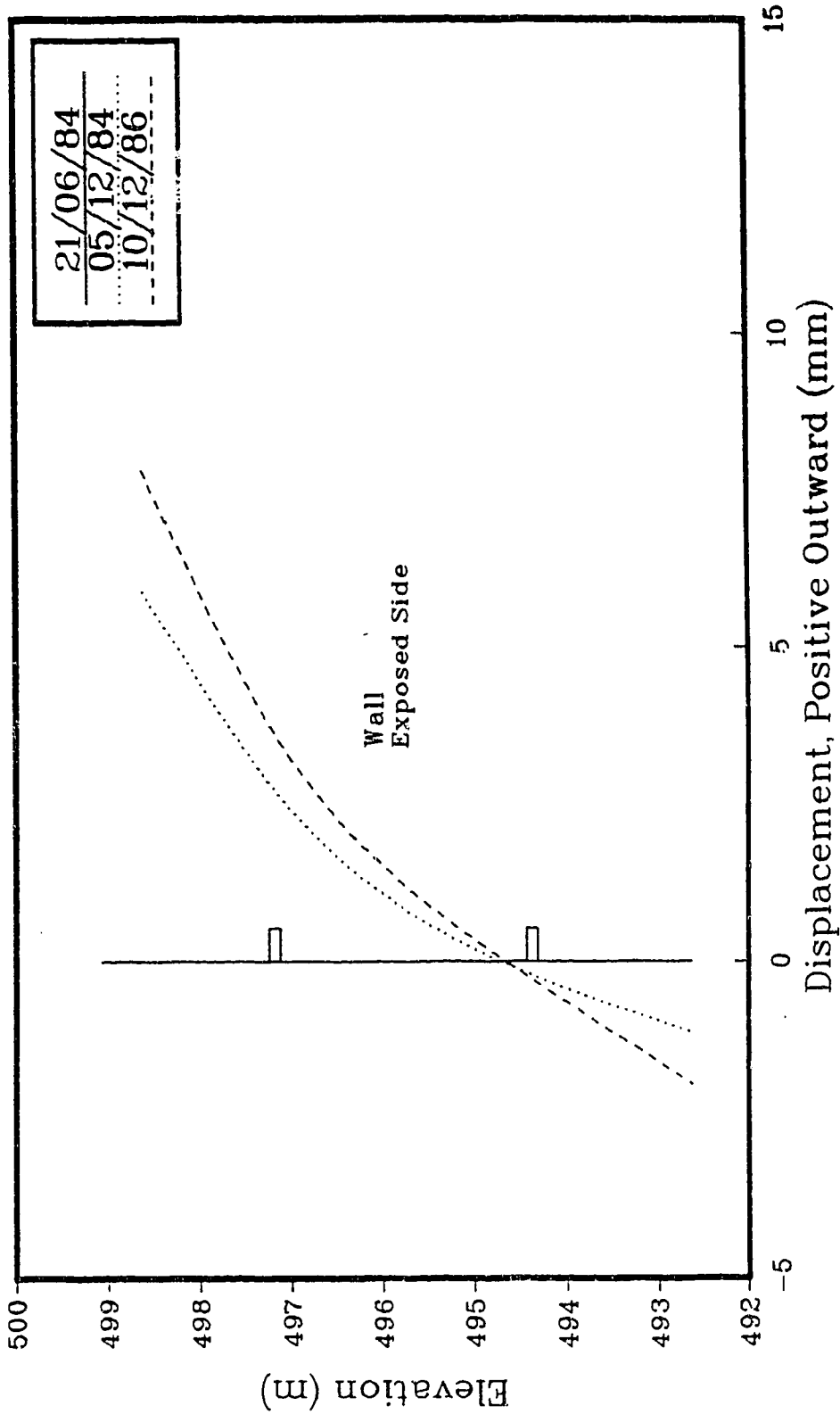


Figure 6.5: Displacements based on wall mounted strain gauges, reference epochs, west section.

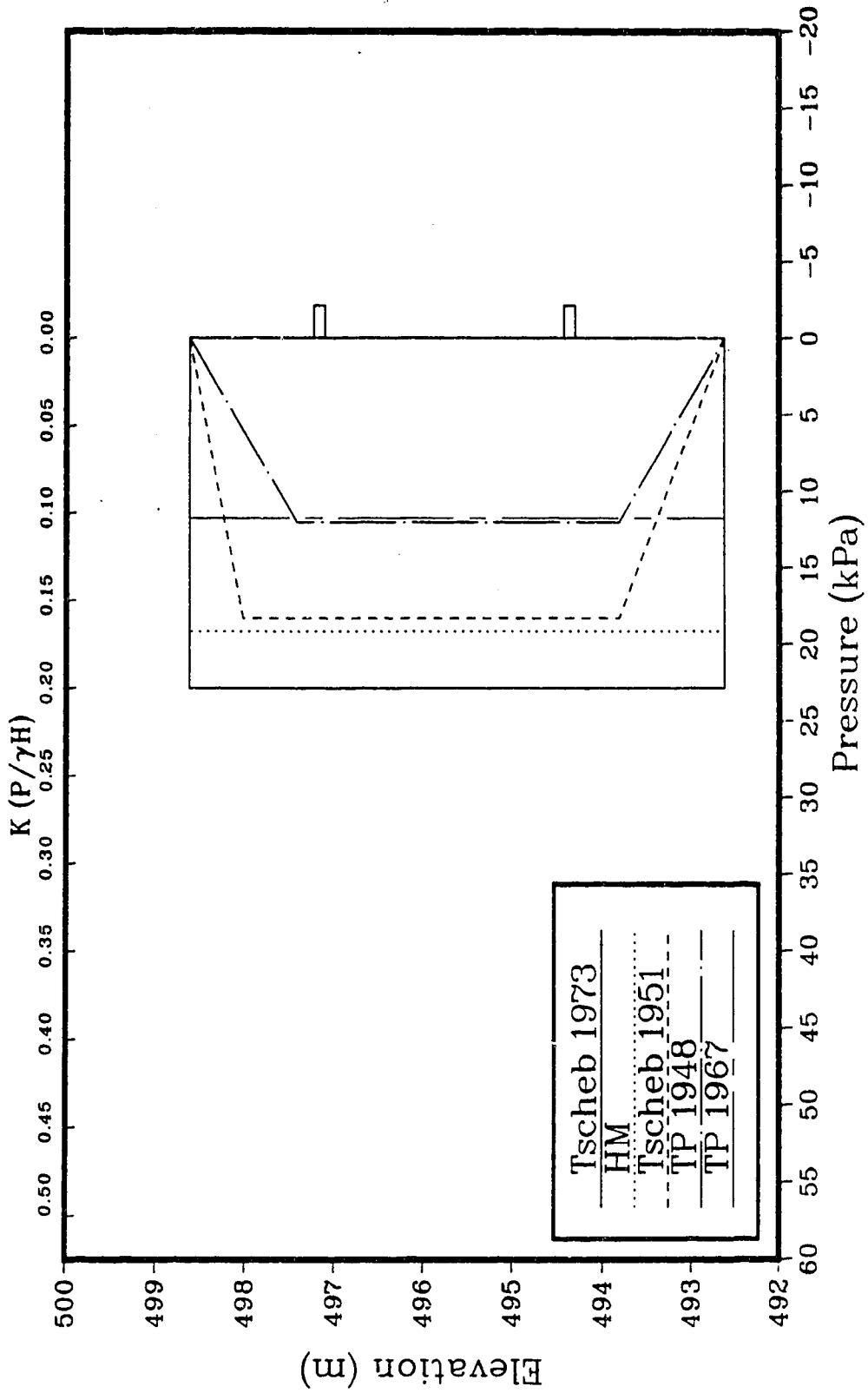


Figure 6.6: Predicted pressure envelopes; low wall, no train.

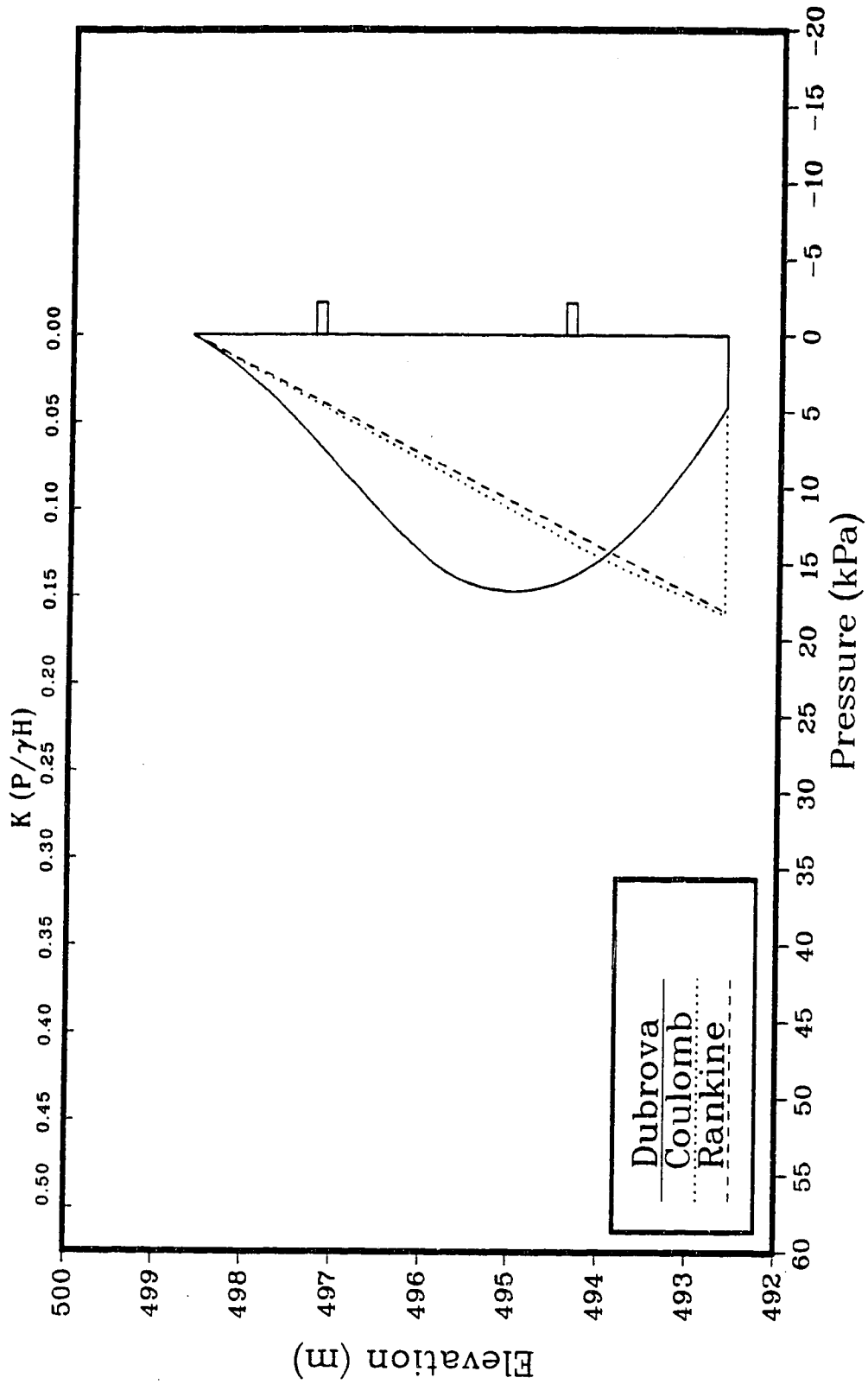


Figure 6.7: Predicted pressure envelopes; low wall, no train.

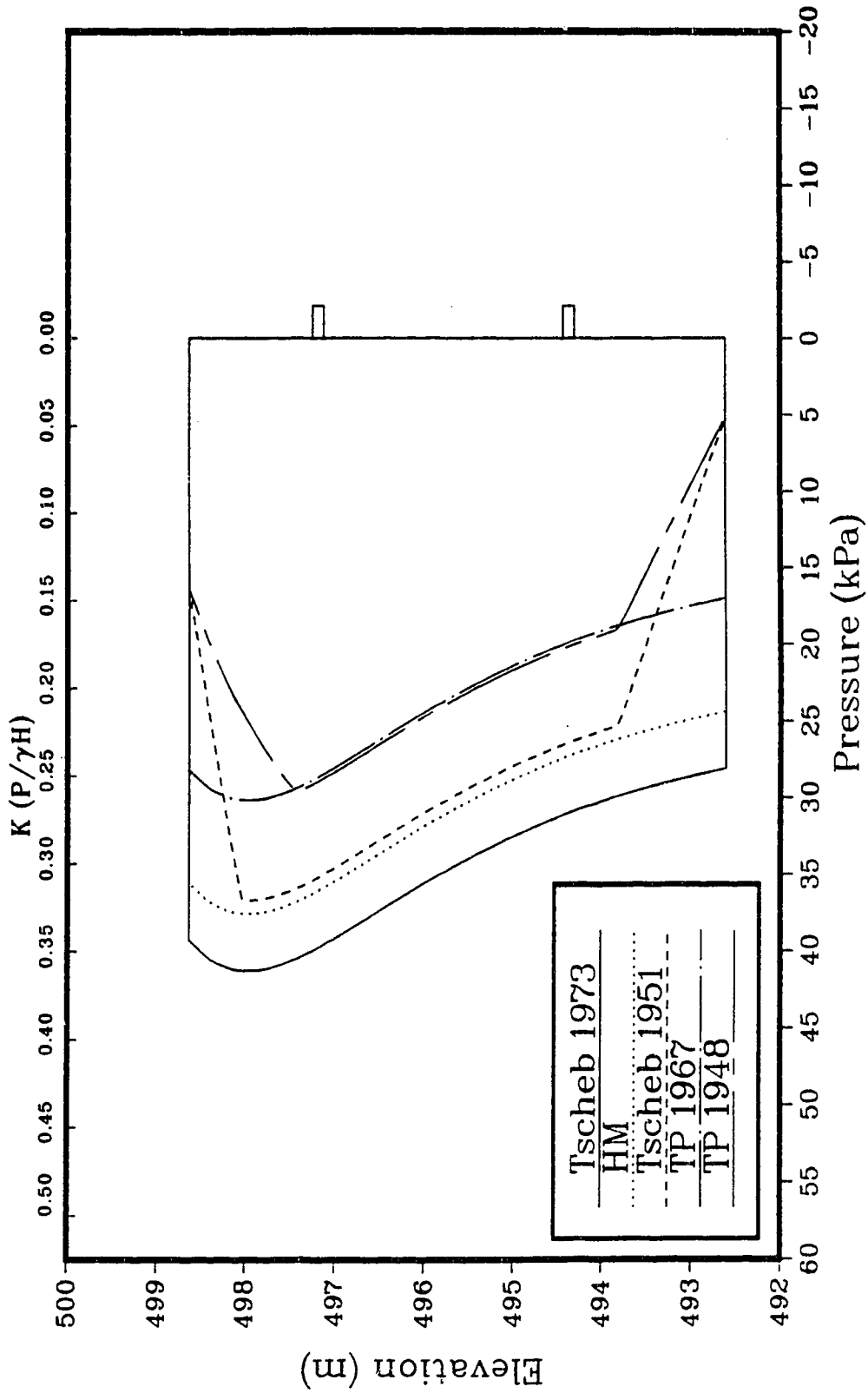


Figure 6.8: Predicted pressure envelopes; low wall, train present.

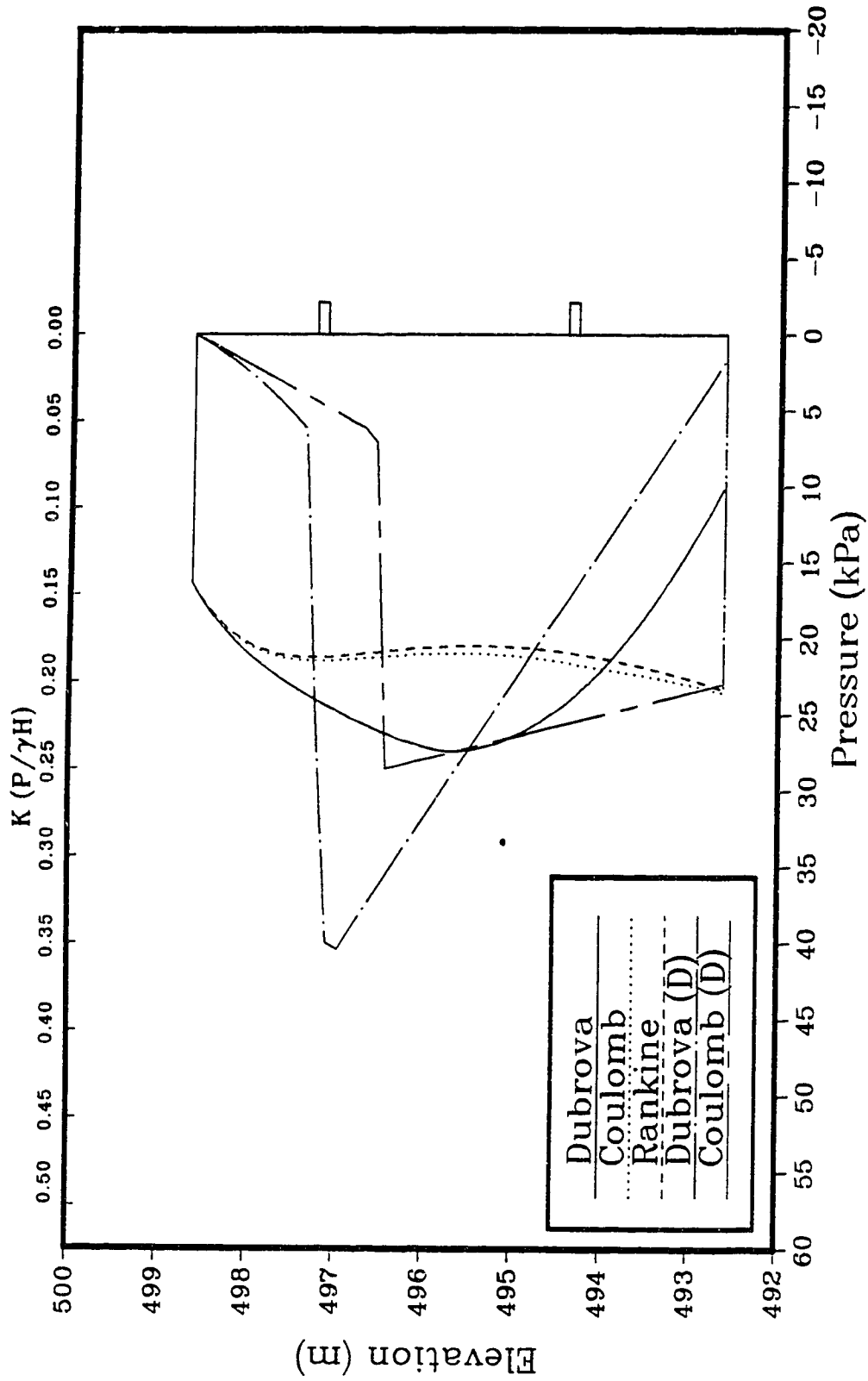


Figure 6.9: Predicted pressure envelopes; low wall, train present.

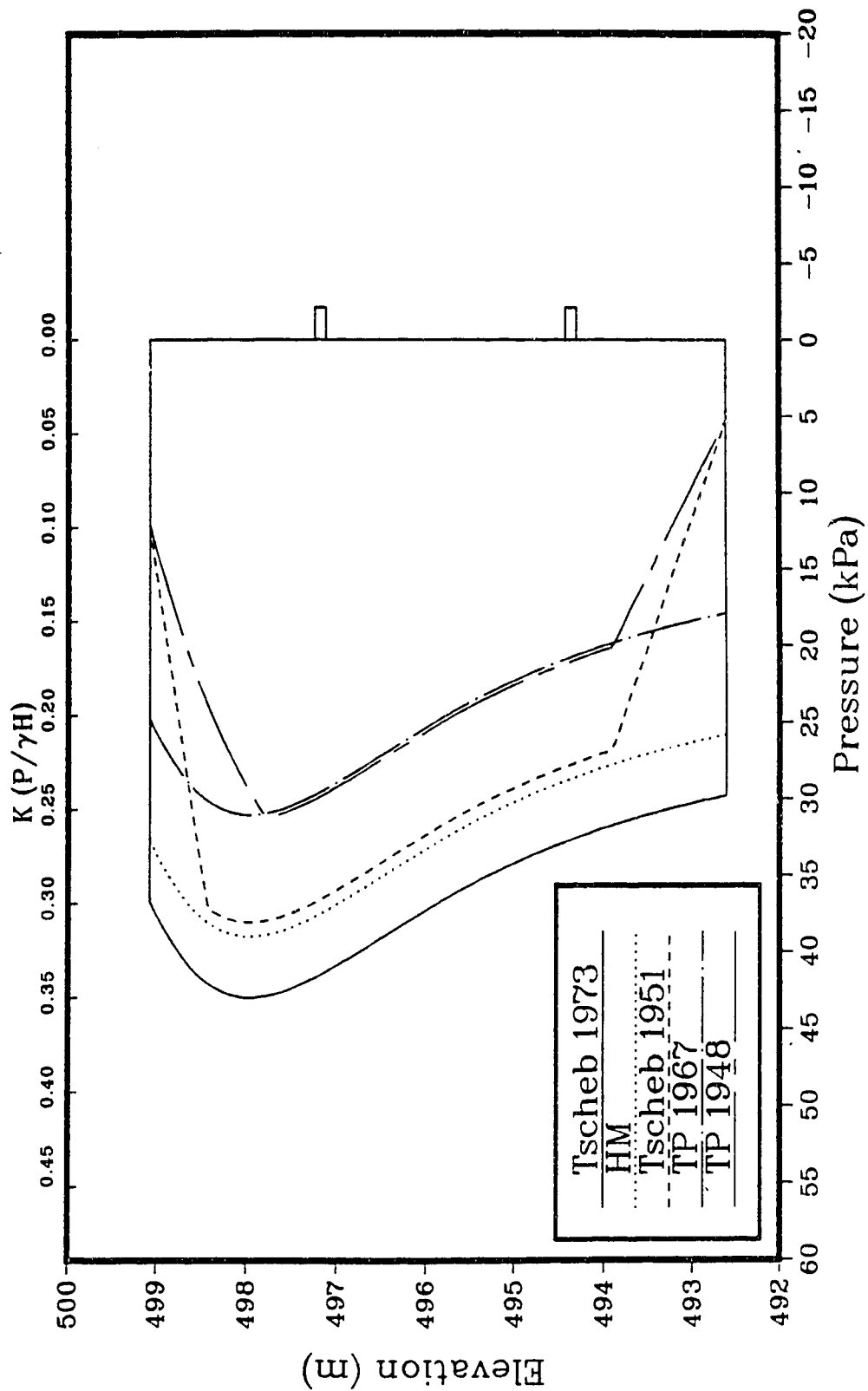


Figure 6.10: Predicted pressure envelopes; high wall, train present.

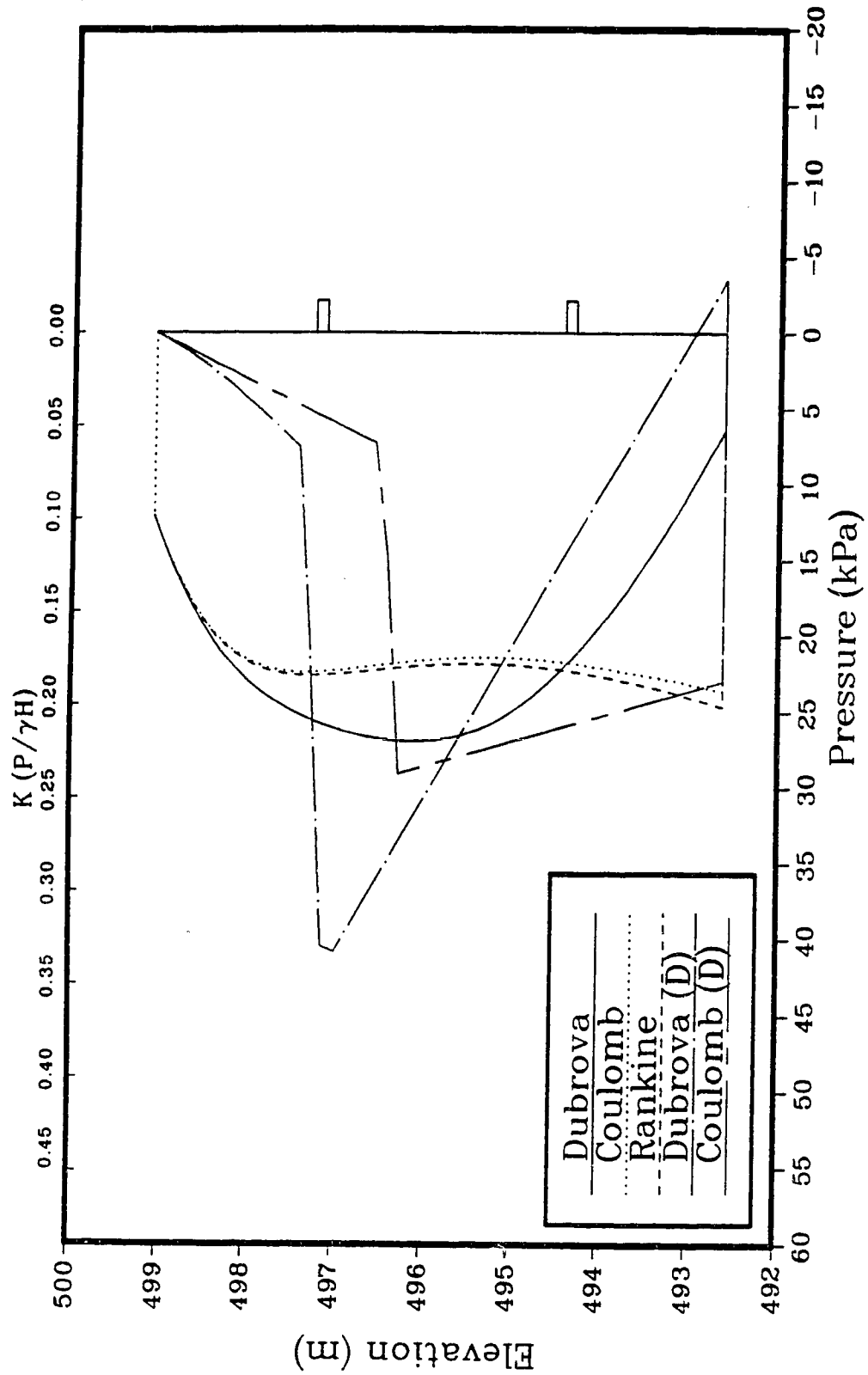


Figure 6.11: Predicted pressure envelopes; high wall, train present.

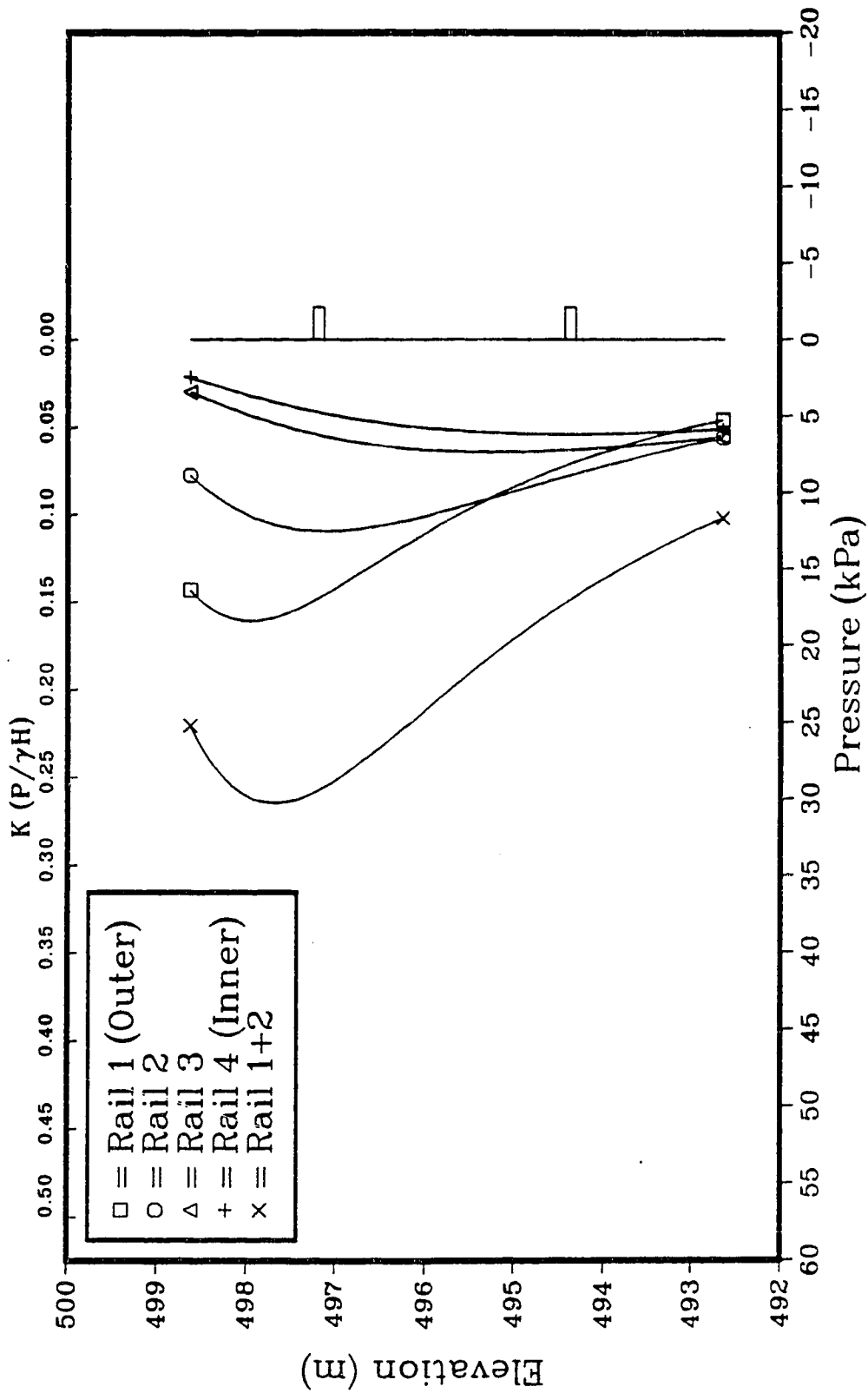


Figure 6.12: Boussinesq pressures from line loads due to train traffic, wall unextended.

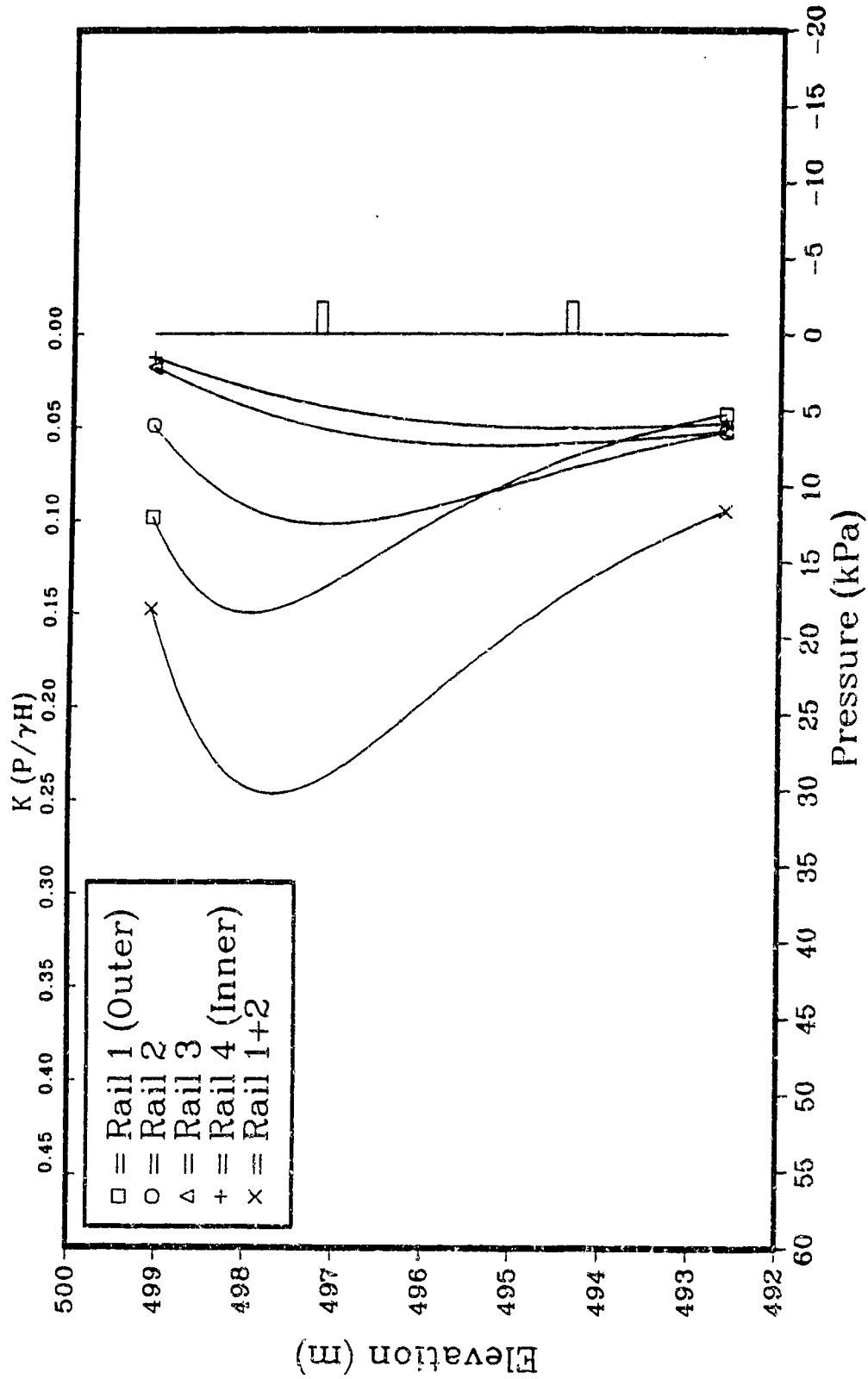


Figure 6.13: Boussinesq pressures from line loads due to train traffic, wall extended.

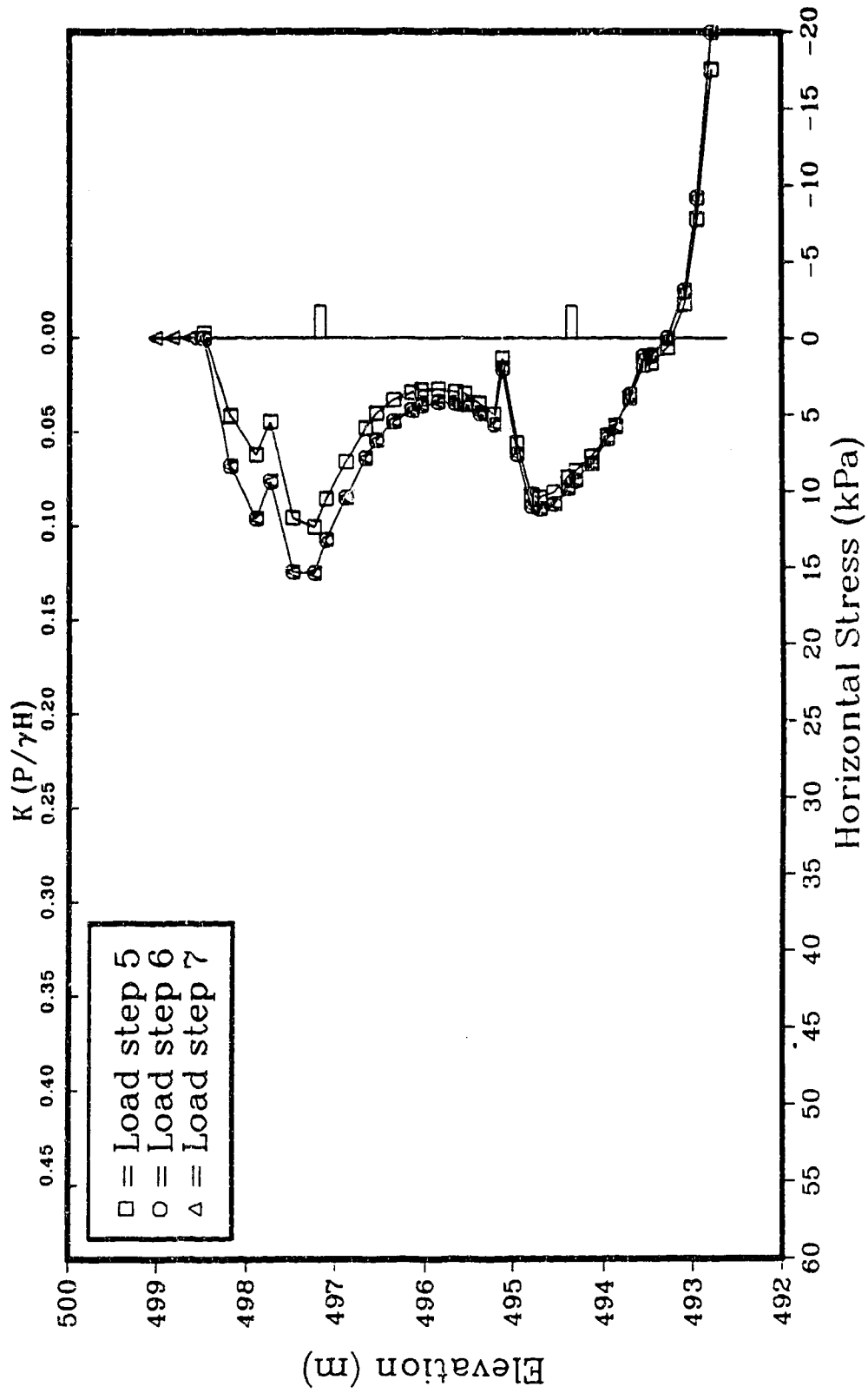


Figure 6.14: Lateral earth pressure predicted by finite element analysis.

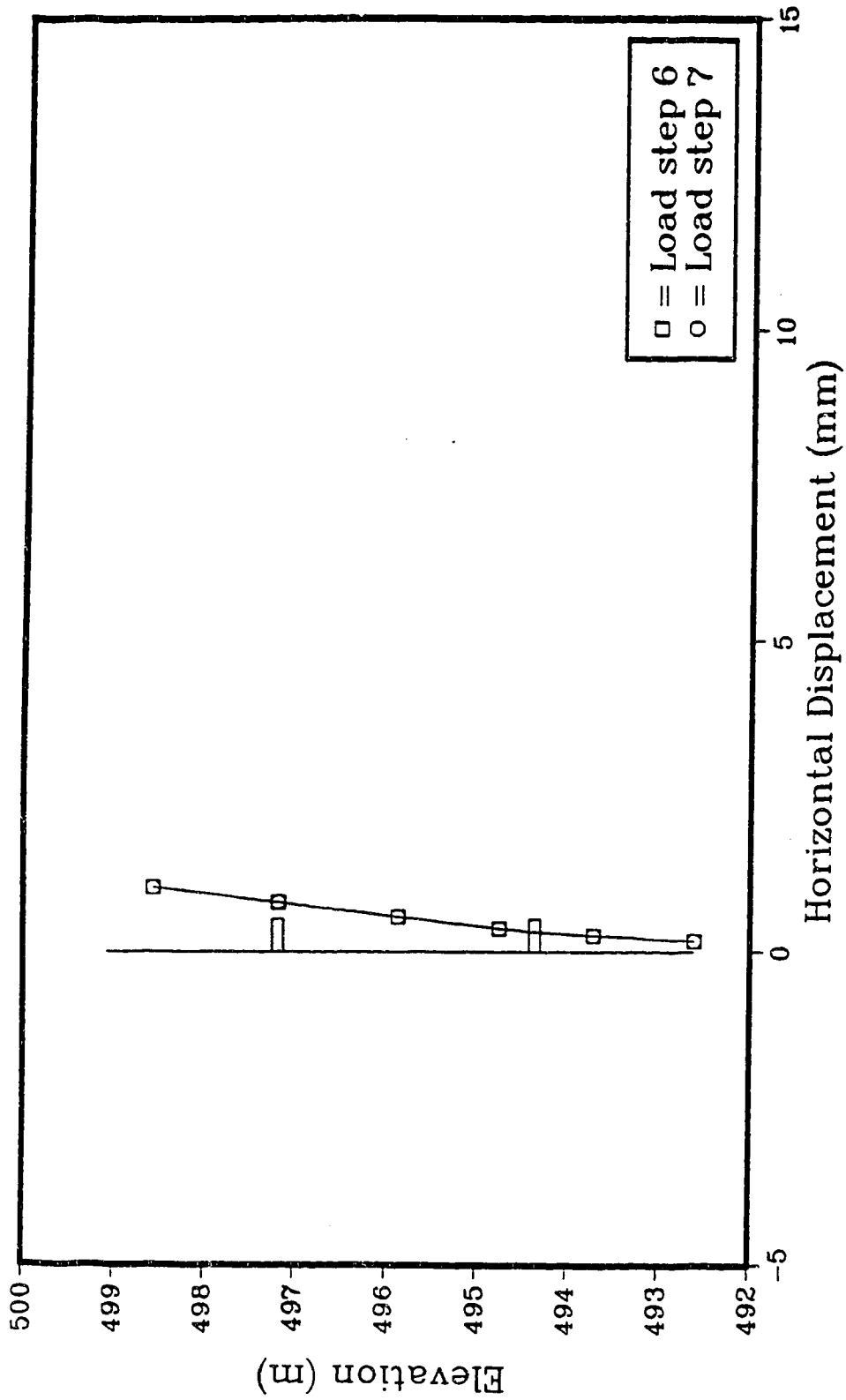


Figure 6.15: Displacement of SPW referenced to initial epoch as predicted by finite element analysis.

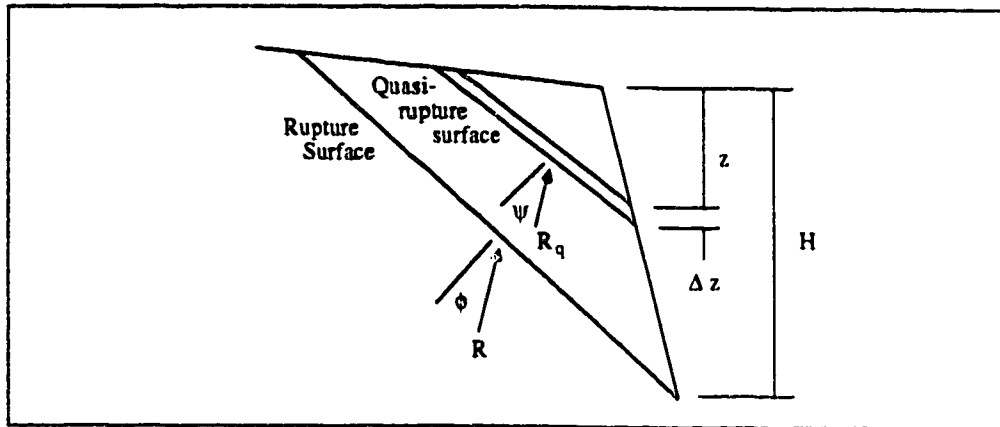
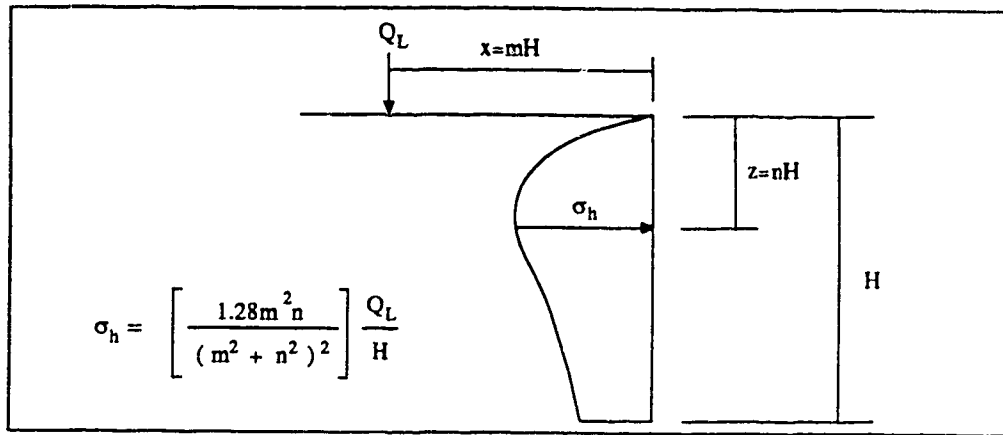
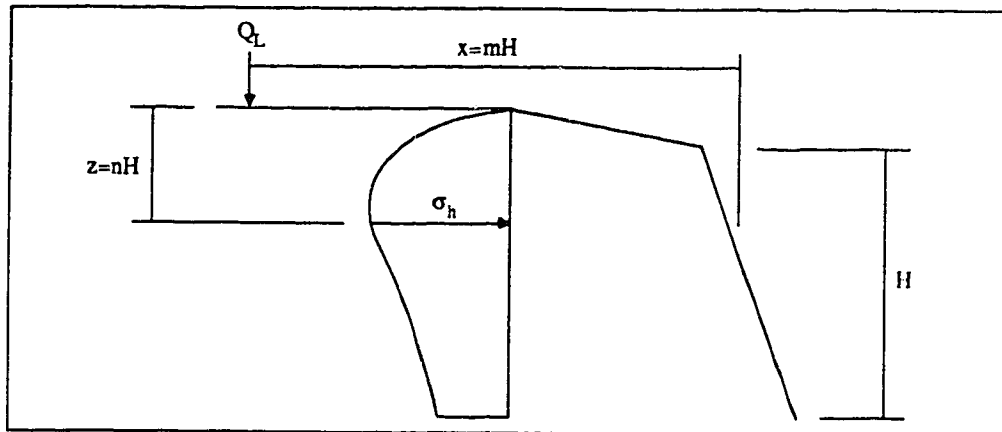


Figure 6.16: Terms involved with the Dubrova (1963) solution.



(a)



(b)

Figure 6.17: Boussinesq procedure for calculating lateral pressures induced by line loads; (a) as presented in CFEM (1985), (b) as applied to Boston Bar to account for batter of wall and the sloped backfill.

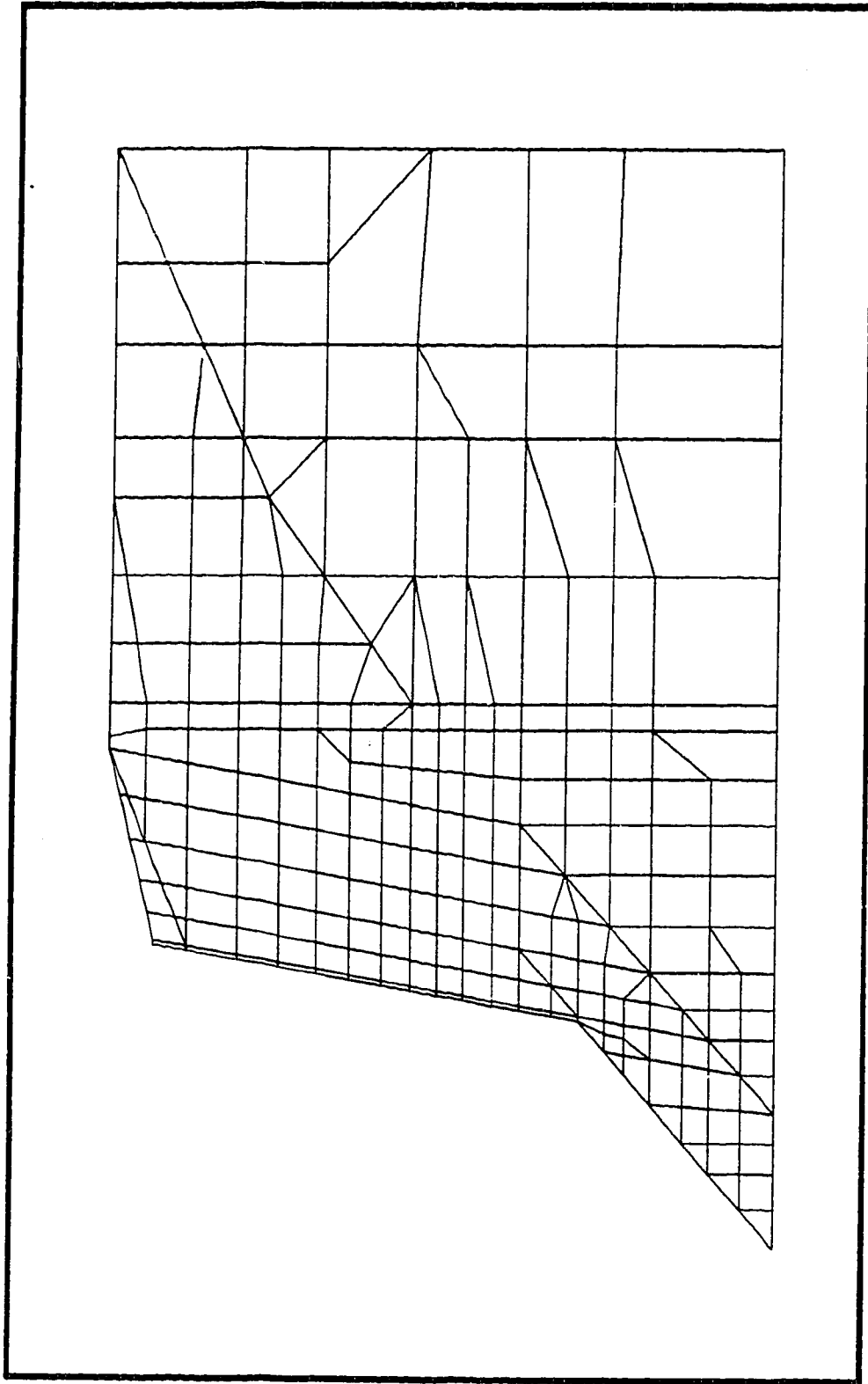
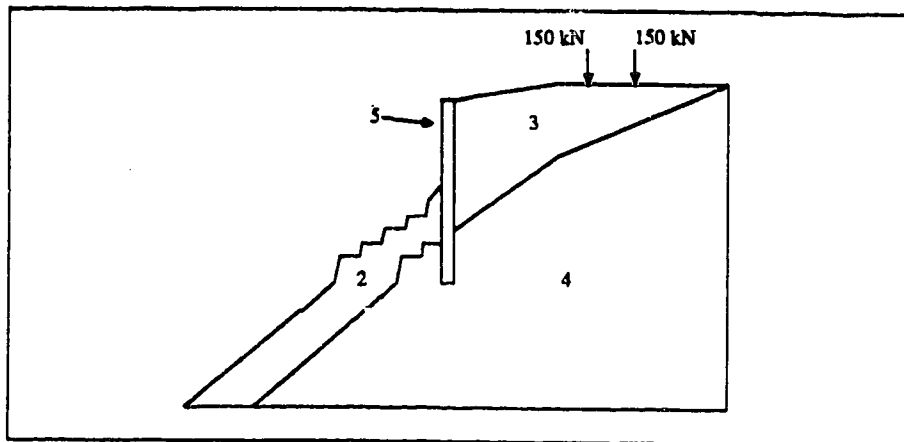
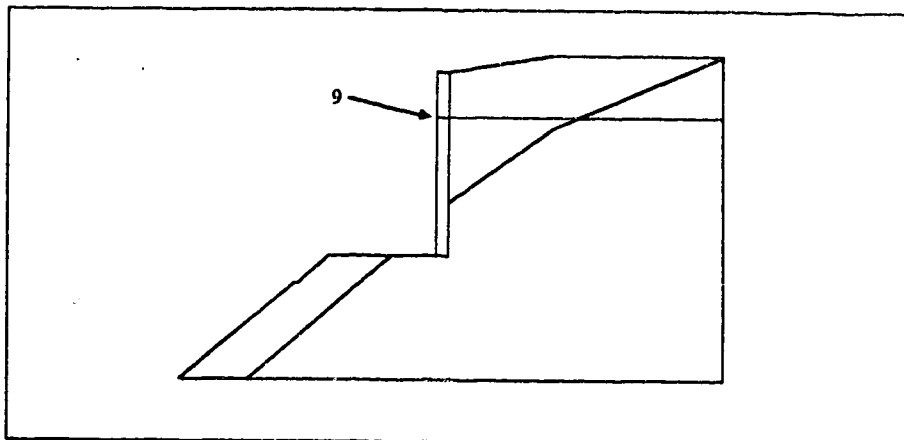


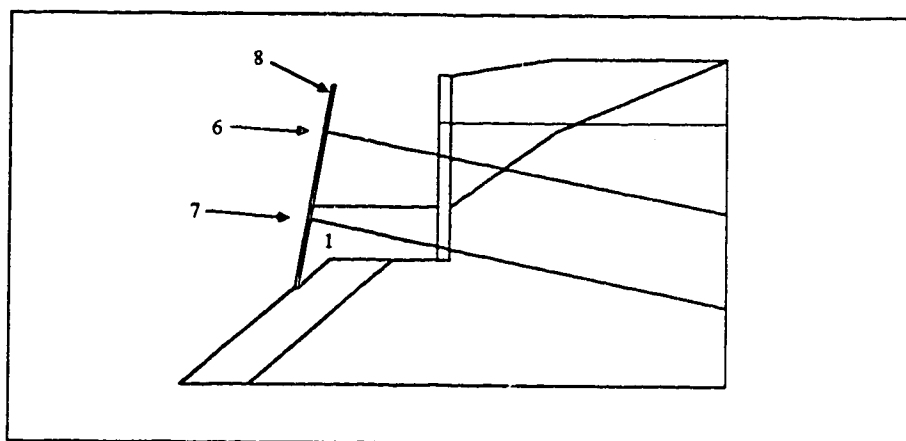
Figure 6.18: Finite element mesh; cross section at the reference sheet pile wall joint of the east wall.



(a) Load step 1. Switch on gravity in foundation and apply train load from original track.

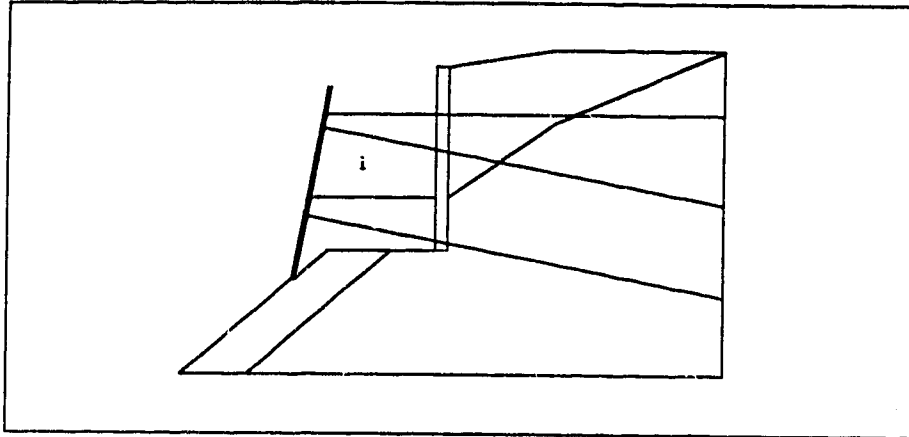


(b) Load step 2. Reset strains and displacements from load step 1 to zero. Excavate material in front of old wall and place anchor.

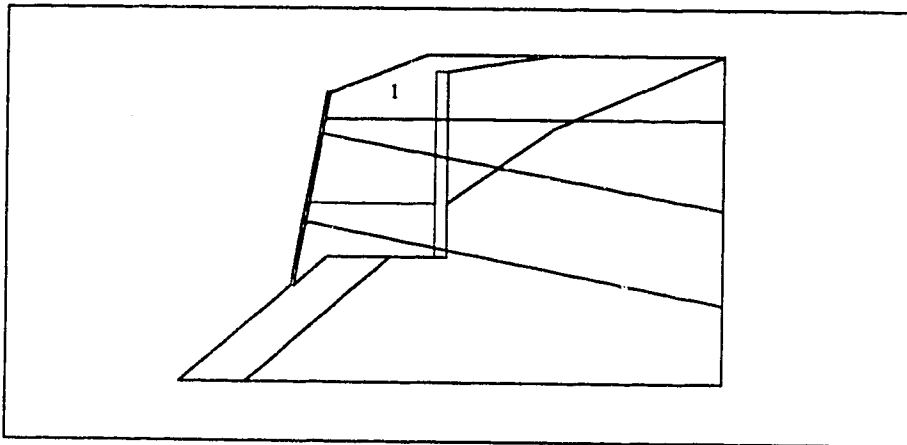


(c) Load step 3. Place wall and its anchors and the first lift of backfill.

Figure 6.19: Load steps 1 to 3 in the finite element analysis.

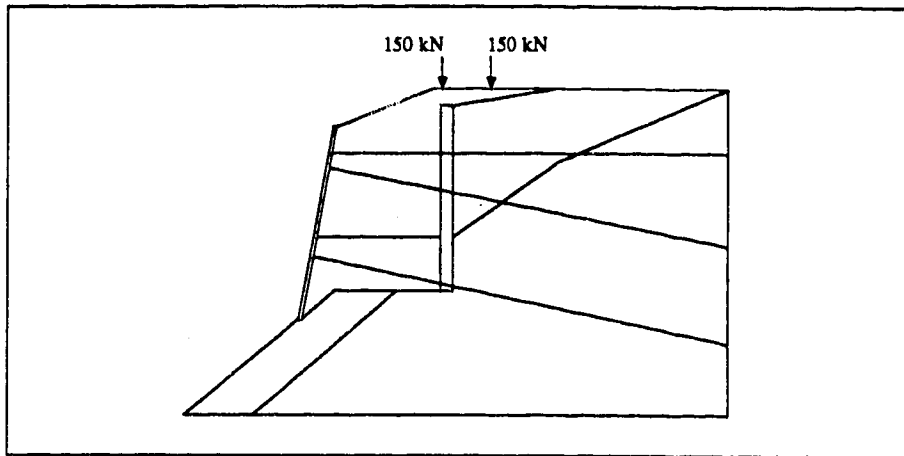


(a) Load step 4. Place second lift of backfill.

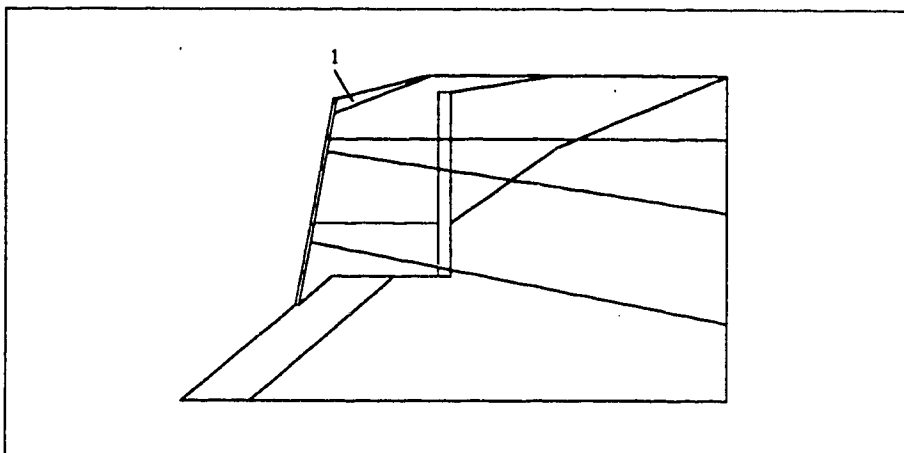


(b) Load step 5. Place third lift of backfill.

Figure 6.20: Load steps 4 and 5 in the finite element analysis.



(a) Load step 6. Apply train load from new track.



(b) Load step 7. Increase wall height and add fourth lift of backfill.

Figure 6.21: Load steps 6 and 7 in the finite element analysis.

7. Conclusions and Recommendations

7.1 Conclusions

As was mentioned in Section 1.2 the Boston Bar field monitoring program was established in conjunction with CN Rail's track twinning project. The instrumentation of the retaining walls was motivated by CN's desire to collect information on which to base the design of much larger walls. These new structures were also a part of the track twinning project. They were required to support the approaches to a bridge in the vicinity of Boston Bar.

A number of conclusions concerning the behavior observed at Boston Bar were made in Section 5.5. Similarly, comments regarding the ability to predict the observed behavior of the walls appear in the concluding remarks of Chapter 6. However, the findings most relevant for the design of the structures described above are reiterated in the following.

The most significant finding concerns the nature of the earth pressure distribution at the site. The earth pressures inferred from the field measurements conformed to a rectangular shape. The empirical pressure envelop due to Terzaghi and Peck (1967) was noted to adequately match the field observations with pressures in the $0.10\gamma H$ to $0.15\gamma H$ range.

The influence of the train traffic was significant but limited predominantly to the upper half of the walls. The

lateral pressures were seen to increase to $0.20\gamma H$ to $0.25\gamma H$ in this region once trains started running on the new track. The Boussinesq procedure predicted the influence of the train loads well. It also illustrated that only train loads on the outer track had any appreciable effect on the wall loads.

The lateral pressure on the walls can be predicted by combining the results from the Terzaghi and Peck (1967) recommendation with the Boussinesq procedure. The triangular earth pressure distribution which was used to design the wall has been shown to be inappropriate.

This has several implications for the design of similar walls. At Boston Bar the upper anchors are spaced at greater intervals than the lower ones. As well, smaller diameter anchor rods were used for the upper anchors. Actual conditions show that both of these situations should be reversed.

Most of the lateral movements of the east retaining wall fell within the range $-0.0005H$ to $0.0010H$ where H is the wall height. Maximum movements were approximately $0.0015H$. The wall was observed to undergo periods of both outward movement and retreat which were directly related to changing loads.

An application of the finite element method for displacement prediction was unsuccessful. However, reasonable wall displacements were obtained from the bending moment results based on the field data. This suggests that

displacements based on the bending moments associated with an assumed lateral pressure distribution would provide an adequate prediction technique.

The settlement observed and inferred at the east wall is also an important finding. Settlement of close to 200 mm has been recorded in the backfill behind the east wall. The wall itself has also undergone considerable differential settlement as is evidenced by the wall mounted slope indicator. These developments may be attributed to the following: inadequate compaction of the backfill; lack of embedment depth for the sheet piles. If the larger walls mentioned above are built in a similar manner excessive settlement could become an operational consideration.

7.2 Recommendations

Shortcomings in the field monitoring program at Boston Bar existed. Several improvements became apparent during the course of the project. For the benefit of researchers embarking on similar monitoring programs these are listed as recommendations below.

1. At least three pairs of strain gauges above the upper waler and below the lower waler should be installed on each instrumented section of the wall. At Boston Bar only two pairs of strain gauges were located in both of these regions. This affords less reliable curve fitting.
2. The wall mounted strain gauges should be at least 250 mm away from the nearest waler. Localized effects due to

the proximity of a waler appears to affect the readings of the gauges.

3. Survey positions should have been established on the ends of the anchor rods instrumented with load cells. This would have allowed the direct measurement of the movement of the wall at a point coincident with a load measurement.
4. Permanent survey levelling positions should have been established along the tops of the two retaining walls. This would have allowed regular elevation profiles of the walls to be obtained. Part of the reason these measurements were not made was that appreciable vertical movement of the walls was not anticipated.
5. Provisions should have been made to allow the wall mounted slope indicator, VSI1, to be surveyed. It was not foreseen that the casing of this instrument would not be visible from the survey monuments. This was inevitable, however, given that the casing was installed on an inner bend of the sheet pile. This, in turn, was required so that the casing could pass by the walers mounted across the outer bends of the sheet pile.
6. The chaining tape used in the survey measurements gives temperature dependent results which require compensation. The correction was based on the ambient air temperature which was assumed to apply to the tape. It would have been more accurate, however, to measure the tape temperature directly.

7. Survey pins were installed at various locations in the survey network every time a set of measurements was made. Provisions should have been made via labels to ensure that the same pins were mounted at the same locations for every epoch. In addition the survey pins were mounted via threads. The pins and the mounts should have been notched to ensure that the pins were always positioned in an identical manner from epoch to epoch.
8. Load cells B and D at the west wall should have been vertically adjacent instead of side by side. A vertical distribution of load would have provided more information.
9. The wall target used to survey the wall mounted survey positions consisted of a rod approximately 500 mm in length. This length was insufficient for many of the positions in columns B and C. For these points the rod often did not extend far enough beyond the outer surface of the wall to ensure that views would be unobstructed.

References

- Armento, W.J., 1972. Criteria for lateral pressures for braced cuts. Proceedings of the American Society of Civil Engineers, Specialty Conference on Performance of Earth and Earth Supported Structures, Volume 1, pp. 1283-1302.
- Aude, 1848. Memorial de l'officier du Gnie, Volume 9.
- Balanko, L.A., Morgenstern, N.R., and Yacyshyn, R., 1982. Tangent pile wall, Edmonton Convention Centre. Presented at ASCE National Conference, April 29, 1982, Las Vegas, Nevada, pp. 1-18.
- Bjerrum, L., Frimann Clausen, C.J., and Duncan, J.M., 1972. Earth pressures on flexible structures, A-state-of-the-art-report. Fifth European Conference on Soil Mechanics and Foundation Engineering, Madrid, pp. 169-196.
- Boussinesq, J., 1885. Application des Potentiels a l'Etude de l'Equilibre et du Mouvement des Solides Elastiques. Paris, Gauthier-Villard.
- Brinch Hansen, J., 1953. Earth pressure calculation. The Danish Technical Press, Copenhagen, 254 p.
- Bromwell, L.G., Ryan, C.R. and Toth, W.E., 1971. Recording inclinometer for measuring soil movement. Proceeding of the 4th Panamerican Conference on Soil Mechanics and Foundation Engineering, San Juan, Volume 2, pp. 333-343.
- Canadian Geotechnical Society, 1985. Canadian foundation engineering manual, Second Edition. Canadian Geotechnical Society, Technical Committee on Foundations, 456 p.
- Chalaturnyk, R., 1988. The behavior of a reinforced soil slope. Unpublished M.Sc. Thesis, University of Alberta, 320 p.
- Chan, D.H.K., 1986. Finite element analysis of strain softening material. Unpublished Ph.D. Thesis, University of Alberta, 345 p.
- Chapman, K.R., Cording, E.J., and Schnabel, H., 1972. Performance of a braced excavation in granular and cohesive soils. Proceedings of the American Society of Civil Engineers, Specialty Conference on Performance of Earth and Earth-Supported Structures, Volume 3, pp. 271-293.

- Clough, G.W., Weber, P.R. and Lamont, J., 1972. Design and observation of a tied-back wall. Proceedings of the American Society of Civil Engineers, Specialty Conference on Performance of Earth and Earth-Supported Structures, Volume 1, Part 2, pp. 1367-1389.
- Consideré, 1870. Annales des Ponts et Chaussées Volume 19, 547 p.
- Cooper, M.A.R., 1987. Control surveys in civil engineering. Collins, London, 381 p.
- Coulomb, C.A., 1776. Essai sur une application des regles des maximis et minimis a quelques problemes de statique relatifs a l'architecture. Reprint of Coulomb's Memoir on Statics, (in French and English), Heyman, J., 1972.
- Crosthwaite, P.M., 1920. Experiments on the horizontal pressure of sand. Minutes of Proceedings of Institution of Civil Engineers, London, Volume CCIX, Part I, pp. 252-283.
- Darrach, I.D., 1984. Discussion of earth pressure acting against a tied-back sheet pile wall. Unpublished M.Eng. Report, University of Alberta, 41 p.
- Davis, R.E., Foote, F.S., Anderson, J.M. and Mikhail, E.M., 1981. Surveying theory and practice, Sixth Edition. McGraw-Hill, New York, 992 p.
- DiBiagio, E. and Bjerrum, L., 1957. Earth pressure measurements in a trench excavated in stiff marine clay. International Conference on Soil Mechanics and Foundation Engineering, London, Proceedings, Volume 2, pp. 196-202.
- DiBiagio, E. and Roti, J., 1972. Earth pressure measurements on a braced slurry trench wall in soft clay. Proceedings of the Fifth European Conference on Soil Mechanics and Foundation Engineering, Madrid, Volume 1, pp. 473-483.
- Dubrova, G.A., 1963. Interaction of soil and structures. Rechnoy Transport, Moscow.
- Duncan, J.M., Byrne, P., Wong, K.S., and Mabry, P., 1980. Strength, stress-strain and bulk modulus parameters for finite element analyses of stresses and movements in soil masses. Report No. UCB/GT/80-01, College of Engineering, Office of Research Services, University of California, Berkeley.
- Egger, P., 1972. Influence of wall stiffness and anchor prestressing on earth pressure distribution. Proceedings of the Fifth European Conference on Soil Mechanics and

- Foundation Engineering, Madrid, Volume 1, Theme 3a, pp. 259-264.
- Eisenstein, Z. and Medeiros, L.V., 1983. A deep retaining structure in till and sand, part 2: Performance and analysis. Canadian Geotechnical Journal, Volume 20, pp. 131-140.
- Elwi A., 1988. Personal communication. Professor of Civil Engineering, Department of Civil Engineering, University of Alberta.
- Eshbach, O.W., 1952. Handbook of engineering fundamentals. John Wiley and Sons, Inc., New York, 1314 p.
- Feld, J., 1923. The accurate experimental determination of the lateral earth pressure, together with a resume of previous experiments. Transactions of the American Society of Civil Engineers, Volume LXXXVI, pp. 1448-1505.
- Golder, H.Q., 1948. Earth pressure against flexible vertical walls. Proceedings of the Second International Conference on Soil Mechanics and Foundation Engineering, London, Volume 2, pp.76-81.
- Hagen, 1833. Druck und reibung des sandes. Annalen der Physik und Chemie, Volume 116, pp. 17-48.
- Hanna, T.H. and Matallana, G.A., 1970. The behavior of tied-back retaining walls. Canadian Geotechnical Journal, Volume 7, pp. 372-396.
- Harr, M.E., 1966. Foundations of theoretical soil mechanics. McGraw-Hill, New York, 381 p.
- Hoek, E. and Bray, J., 1981. Rock slope engineering, third edition. The Institution of Mining and Metallurgy, London, 358 p.
- Holts, R.D. and Kovacs, P.E., 1981. An introduction to geotechnical engineering. Prentice-Hall, Inc., Englewood Cliffs, New Jersey, 733 p.
- Hooke, R., 1678. De potentia restitutiva. Royal Society of London, Philosophical Collections.
- Humphreys, J.D., 1962. The measurement of loads on timber supports in a deep trench. Géotechnique, Volume 12, Number 1, pp. 44-54.
- Indraratna, B., 1987. Application of fully grouted bolts in yielding rock. Unpublished Ph.D. Thesis, University of Alberta, 286 p.

- Jaky, J., 1944. The coefficient of earth pressure at rest. Journal of the Society of Hungarian Architects and Engineers, pp. 355-358.
- Janbu, N., 1963. Soil compressibility as determined by oedometer and triaxial tests. European Conference on Soil Mechanics and Foundation Engineering, Wisbaden, Germany, Volume 1, pp. 19-25.
- Leygue, 1885. Nouvell resherche sur le pousse des terres. Annales des Ponts et Chaussées, Volume 10, pp. 780-1000.
- Mayniel, 1808. Traite experimental, analytique et pratique de la pousse des terres et des murs revetement.
- Meem, J.C., 1908. The bracing of trenches and tunnels with practical formulas for earth pressure. Transactions of the American Society of Civil Engineers, Volume LX, p. 1-23. Discussions, pp. 24-100.
- Meem, J.C., 1910. Pressure, resistance, and stability of earth. Transactions of the American Society of Civil Engineers, Volume 70, pp. 352-411.
- Megaw, T.M., 1951. Foundations at Poole power station. Géotechnique, Volume 2, pp. 280-292.
- Mikhail, E.M. and Gracie, G., 1981. Analysis and adjustment of survey measurements. Van Nostrand Reinhold Company, New York, 340 p.
- Morgenstern, N.R. and Eisenstein, Z., 1970. Method of estimating lateral loads and deformations. Proceedings of the American Society of Civil Engineers, Specialty Conference on Lateral Stresses and Retaining Structures, State of the art report, Cornell University, pp. 51-102.
- Morgenstern, N.R. and Sego, D.C., 1981. Performance of temporary tie-backs under winter conditions. Canadian Geotechnical Journal, Volume 18, Number 4, pp. 566-572.
- Moulton, H.G., 1920. Earth and rock pressures. Transactions of the American Society of Mineral and Metallurgical Engineers, Volume LXIII, pp. 327-369.
- Navier, 1809. Ouvres, Vol 1.
- Ohde, J., 1938. Zur theorie des erddruckes unter besonderer berucksichtigung der erddruck verteilung. Die Bautechnik, Volume 16, pp. 480-487.
- Peck, R.B., 1943. Earth pressure measurements in open cuts Chicago (Illinois) subway. Transactions of the American Society of Civil Engineers, Volume 108, pp. 1008-1036.

- Peck, R.B., 1969. Deep excavations and tunneling in soft ground. State of the art report, Seventh International Conference on Soil Mechanics and Foundation Engineering, Mexico, pp. 215-290.
- Peck, R.B., Hanson, W.E., and Thornburn, T.H., 1953. Foundation engineering. John Wiley and Sons, Inc., New York, 410 p.
- Pennoyer, R.A., 1933. Design of steel sheet-piling bulkheads. Civil Engineering, Volume 3, pp. 615-619.
- Perry, C.C., 1984. The resistance strain gauge revisited. Experimental Mechanics, Volume 24, pp. 286-299.
- Peters, N. and Ellis, J.H., 1972. Instrumentation for the Gardiner Dam. Proceedings, 25th Canadian Geotechnical Conference, Ottawa.
- Peterson, A.E., 1987. Plane adjustment by least squares. Computer program, Department of Civil Engineering, University of Alberta.
- Rankine, 1857. Theory on the stability of loose earth, based on the ellipse of stress. Philosophical Transactions of the Royal Society of London, Volume 147.
- Résal, J., 1910. Poussée des terres, stabilité des murs de soutènement. Encyclopedia des travaux publics. Paris.
- Rowe, P.W., 1952. Anchored sheet-pile walls. Proceedings of the Institution of Civil Engineers, London, Volume 1, pp. 27-70.
- Rowe, P.W., 1955a. A theoretical and experimental analysis of sheet pile walls. Proceedings of the Institution of Civil Engineers, London, Volume 4, Part I, pp. 32-69.
- Rowe, P.W., 1955b. Sheet-pile walls encastré at the anchorage. Proceedings of the Institution of Civil Engineers, London, Volume 4, Part I, pp. 70-87.
- Rowe, P.W., 1956. Sheet-pile walls at failure. Proceedings of the Institution of Civil Engineers, London, Volume 5, Part I, pp. 276-315.
- Rowe, P.W., 1957. Sheet-pile walls in clay. Proceedings of the Institution of Civil Engineers, London, Volume 7, pp. 629-654.
- Savigny, K.W., 1980. *in situ* analysis of naturally occurring creep in ice-rich permafrost soil. Unpublished Ph.D. Thesis, University of Alberta, 439 p.

- Schnabel, H., 1982. Tiebacks in foundation engineering and construction. McGraw-Hill, New York, 170 p.
- Scott, J.D., Wilson, N.E. and Bauer, G.E., 1972. Analysis and performance of a braced cut in sand with large deformations. Canadian Geotechnical Journal, Volume 9, pp. 384-406.
- Sego D.C.C., 1988. Personal communication. Professor of Civil Engineering, Department of Civil Engineering, University of Alberta.
- Skempton, A.W., and Ward, W.H., 1952. Investigations concerning a deep cofferdam in the Thames estuary clay at Shellhaven. Géotechnique, Volume 3, Number 3, pp. 119-139.
- Stroyer, R.N., 1927. Earth pressure on flexible bulkheads. Minutes of Proceedings of the Institution of Civil Engineers, London, Volume 226, pp. 116-134.
- Stroyer, R.N., 1935. Earth-pressure on flexible walls. Journal of the Institution of Civil Engineers, London, Volume 1, pp. 94-139.
- Tennent, R.M., 1971. Science data book. Oliver and Boyd, Edinburgh, 104 p.
- Terzaghi, K., 1920. Old earth-pressure theories and new test results. Engineering News-Record, Volume 85, Number 14, pp. 632-637.
- Terzaghi, K., 1934. Large retaining wall tests. Engineering News-Record, Volume 112, pp. 136-140.
- Terzaghi, K., 1936. Distribution of the lateral pressure of sand on the timbering of cuts. Proceeding of the First International Conference on Soil Mechanics and Foundation Engineering, Volume 1, Cambridge, Mass., pp. 211-218.
- Terzaghi, K., 1941. General wedge theory of earth pressure. Transactions of the American Society of Civil Engineers, Volume 106, pp. 68-97.
- Terzaghi, K., 1943. Theoretical soil mechanics, John Wiley and Sons, New York, 510 p.
- Terzaghi, K., 1953. Anchored bulkheads. Proceedings of the American Society of Civil Engineers, Volume 79, Separate Number 262, pp. 1-39.
- Terzaghi, K. and Peck, R.B., 1948. Soil mechanics in engineering practice, First Edition, John Wiley and

- Sons, Inc., New York, 566 p.
- Terzaghi, K. and Peck, R.B., 1967. Soil mechanics in engineering practice, Second Edition, John Wiley and Sons, Inc., New York, 729 p.
- Tschebotarioff, G.P., 1951. Soil mechanics, foundations, and earth structures. McGraw-Hill Book Company, Inc., New York, Toronto, London. 655 p.
- Tschebotarioff, G.P., 1973. Foundations, retaining and earth structures, Second Edition. McGraw-Hill, New York, 612 p.
- Tschebotarioff, G.P. and Brown, P.P., 1948. Lateral earth pressure as a problem of deformation or of rupture. Proceedings, Second International Conference on Soil Mechanics and Foundation Engineering, Rotterdam, Volume 2, pp. 81-86.
- Tschebotarioff, G.P. and Welch, J.D., 1948. Effect of boundary conditions on lateral earth pressure. Proceedings, Second International Conference on Soil Mechanics and Foundation Engineering, Rotterdam, Volume 3, pp. 308-313.
- Window, A.L. and Holister, G.S., 1982. Strain gauge technology. Applied Science Publishers, London and New Jersey, 356 p.
- Winkler, 1865. Neue theorie des erddrucks. Der Civilingenieur, Volume 2, pp. 1-11.
- Wolf, P.R., 1980. Adjustment computations, second edition. P.B.L. Publishing Company, Monona, Wisconsin, 284 p.
- Woltmann, 1799. Beitrage zur Hydraulischen Architektur. Volume 4.
- Wong, O.H., 1985. Measured and predicted performance of deep excavations in Edmonton till. Unpublished M.Sc. Thesis, University of Alberta, 249 p.
- Wu, T.-H. and Berman, S., 1953. Earth pressure measurements in open cut, contract D-8, Chicago subway. Géotechnique, Volume 3, Number 6, pp. 248-258.

Appendix A
Anchor Loads

Time (Days)	Load Cell			Anchor Strain Gauges		
	kN	kN/m Width	kN/m**2	kN	kN/m Width	kN/m**2
	8.	81.99	54.66	24.19	0.0	0.0
9.	-	-	-	120.11	80.07	35.43
20.	60.45	40.30	17.83	95.68	63.79	28.22
40.	36.27	24.18	10.70	83.87	55.92	24.74
65.	43.09	28.72	12.71	73.90	49.27	21.80
123.	41.63	27.75	12.28	72.27	48.18	21.32
185.	63.72	42.48	18.80	-	-	-
187.	-	-	-	315.54	210.36	93.08
454.	46.54	31.03	13.73	99.14	66.09	29.25
662.	46.90	31.27	13.84	96.49	64.33	28.46
788.	44.45	29.63	13.11	96.09	64.06	28.34
921.	61.99	41.33	18.29	113.59	75.73	33.51
990.	41.54	27.69	12.25	96.29	64.19	28.40
1027.	42.72	28.48	12.60	93.03	62.02	27.44

Table A.1: Load readings for Anchor A.

Time (Days)	Load Cell			Anchor Strain Gauges		
	kN	kN/m Width	kN/m**2	kN	kN/m Width	kN/m**2
	8.	135.50	90.33	31.15	0.0	0.0
9.	-	-	-	71.66	47.77	16.47
20.	116.11	77.41	26.69	51.91	34.61	11.93
40.	78.49	52.33	18.04	41.94	27.96	9.64
65.	99.36	66.24	22.84	30.74	20.49	7.07
123.	102.08	68.06	23.47	29.31	19.54	6.74
185.	124.18	82.79	28.55	-	-	-
187.	-	-	-	273.40	182.27	62.85
454.	123.13	82.09	28.31	134.77	89.84	30.98
662.	125.85	83.90	28.93	145.35	96.90	33.41
788.	131.11	87.11	30.14	144.95	96.63	33.32
921.	129.45	86.30	29.76	162.86	108.57	37.44
990.	120.68	80.45	27.74	146.78	97.85	33.74
1027.	121.64	81.09	27.96	146.78	97.85	33.74

Table A.2: Load readings for Anchor B.

Time (Days)	Load Cell			Anchor Strain Gauges		
	kN	kN/m Width	kN/m**2	kN	kN/m Width	kN/m**2
8.	122.52	30.63	16.04	0.0	0.0	0.0
9.	-	-	-	110.83	17.71	14.51
20.	77.96	19.49	10.20	69.49	17.37	9.10
40.	50.23	12.56	6.58	71.74	17.93	9.39
64.	-	-	-	64.02	16.00	8.38
65.	76.59	19.15	10.02	-	-	-
123.	78.23	19.56	10.24	66.75	16.69	8.74
185.	144.02	36.01	18.85	-	-	-
187.	-	-	-	289.85	72.46	37.94
454.	131.76	32.94	17.25	115.65	28.91	15.14
662.	143.01	35.75	18.72	127.07	31.77	16.63
788.	138.35	34.59	18.11	114.36	28.59	14.97
921.	144.02	36.01	18.85	132.38	33.09	17.33
990.	144.84	36.21	18.96	129.00	32.25	16.88
1027.	142.65	35.66	18.67	124.82	31.20	16.34

Table A.3: Load readings for Anchor C.

Time (Days)	Load Cell			Anchor Strain Gauges		
	kN	kN/m Width	kN/m**2	kN	kN/m Width	kN/m**2
8.	153.35	102.23	33.30	0.0	0.0	0.0
9.	-	-	-	134.16	89.44	29.13
20.	123.26	82.17	26.77	108.30	72.20	23.52
40.	88.03	58.69	19.12	104.03	69.35	22.59
65.	109.02	72.68	23.67	91.41	60.94	19.85
123.	104.97	69.98	22.79	89.78	59.85	19.50
185.	134.43	89.62	29.19	-	-	-
187.	-	-	-	254.47	169.65	55.26
454.	120.64	80.43	26.20	111.36	74.24	24.18
662.	129.92	86.62	28.21	122.35	81.57	26.57
788.	130.55	87.04	28.35	118.89	79.26	25.82
921.	142.72	95.15	30.99	134.16	89.44	29.13
990.	127.04	84.69	27.59	122.96	81.97	26.70
1027.	125.42	83.61	27.24	120.52	80.34	26.17

Table A.4: Load readings for Anchor D.

Time (Days)	Load Cell			Anchor Strain Gauges		
	kN	kN/m Width	kN/m**2	kN	kN/m Width	kN/m**2
20.	-	-	-	0.0	0.0	0.0
21.	108.11	90.09	31.36	109.52	91.27	31.77
40.	94.74	78.95	27.48	90.39	75.32	26.22
65.	88.27	73.56	25.60	81.43	67.86	23.62
123.	93.26	77.71	27.05	81.43	67.86	23.62
185.	79.27	66.06	22.99	88.35	73.63	25.63
251.	72.11	60.09	20.91	77.15	64.30	22.38
454.	79.71	66.42	23.12	68.60	57.17	19.90
662.	70.62	58.85	20.48	67.18	55.98	19.49
788.	75.43	62.86	21.88	64.33	53.61	18.66
921.	66.86	55.72	19.39	75.12	62.60	21.79
990.	66.16	55.13	19.19	60.46	50.38	17.54
1027.	66.16	55.13	19.19	56.80	47.33	16.47

Table A.5: Load readings for Anchor E.

Time (Days)	Load Cell			Anchor Strain Gauges		
	kN	kN/m Width	kN/m**2	kN	kN/m Width	kN/m**2
20.	-	-	-	0.0	0.0	0.0
21.	49.25	29.44	9.40	-18.53	-11.07	-3.54
40.	48.43	28.95	9.24	-18.73	-11.19	-3.57
65.	47.89	28.62	9.14	-20.15	-12.05	-3.85
123.	45.98	27.49	8.78	-17.91	-10.71	-3.42
185.	56.78	33.94	10.84	13.44	8.03	2.56
251.	52.79	31.55	10.07	8.14	4.87	1.55
454.	57.05	34.10	10.89	2.04	1.22	0.39
662.	55.96	33.45	10.68	6.11	3.65	1.17
788.	54.69	32.69	10.44	2.65	1.58	0.51
921.	62.40	37.30	11.91	25.04	14.97	4.78
990.	54.60	32.64	10.42	12.83	7.67	2.45
1027.	53.15	31.77	10.14	7.74	4.62	1.48

Table A.6: Load readings for Anchor F.

Time (Days)	Load Cell			Anchor Strain Gauges		
	kN	kN/m Width	kN/m**2	kN	kN/m Width	kN/m**2
21.	96.57	28.37	8.37	-	-	-
40.	111.87	32.86	9.70	-	-	-
65.	113.33	33.29	9.82	-	-	-
123.	122.26	35.92	10.60	-	-	-
185.	203.52	59.79	17.64	-	-	-
251.	190.58	55.99	16.52	-	-	-
454.	210.35	61.79	18.23	-	-	-
662.	226.20	66.45	19.61	-	-	-
788.	229.57	67.44	19.90	-	-	-
921.	238.68	70.12	20.69	-	-	-
990.	233.31	68.54	20.22	-	-	-
1027.	231.03	67.87	20.03	-	-	-

Table A.7: Load readings for Anchor G.

Time (Days)	Load Cell			Anchor Strain Gauges		
	kN	kN/m Width	kN/m**2	kN	kN/m Width	kN/m**2
21.	46.89	14.45	4.25	-	-	-
40.	71.69	22.09	6.50	-	-	-
65.	72.30	22.28	6.55	-	-	-
123.	84.30	25.98	7.64	-	-	-
185.	180.09	55.50	16.32	-	-	-
251.	161.99	49.92	14.68	-	-	-
454.	201.84	62.20	18.29	-	-	-
662.	211.24	65.10	19.15	-	-	-
788.	219.24	67.56	19.87	-	-	-
921.	223.59	68.90	20.27	-	-	-
990.	219.24	67.56	19.87	-	-	-
1027.	220.28	67.88	19.97	-	-	-

Table A.8: Load readings for Anchor H.

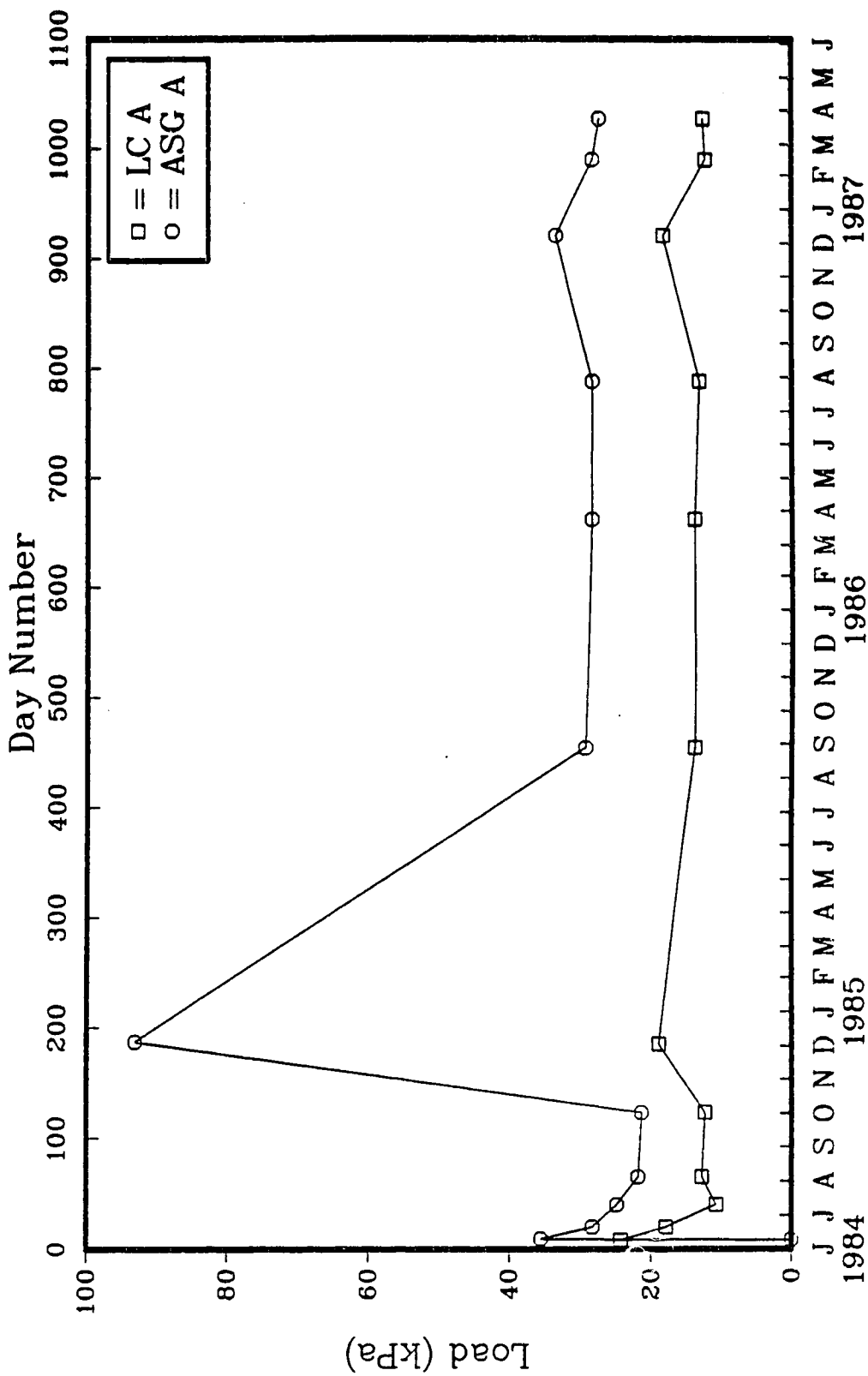


Figure A.1: Load versus time for Anchor A.

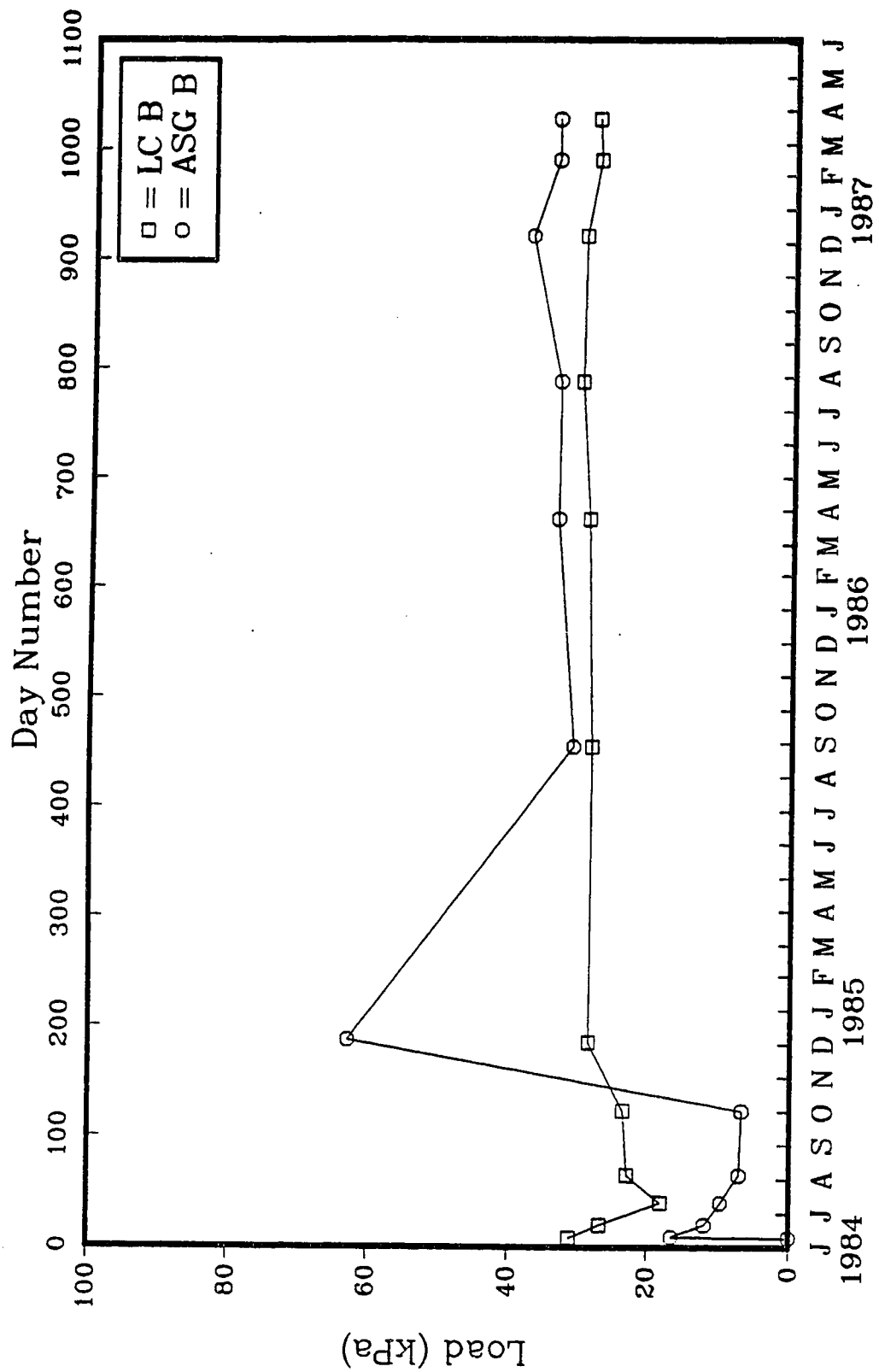


Figure A.2: Load versus time for Anchor B.

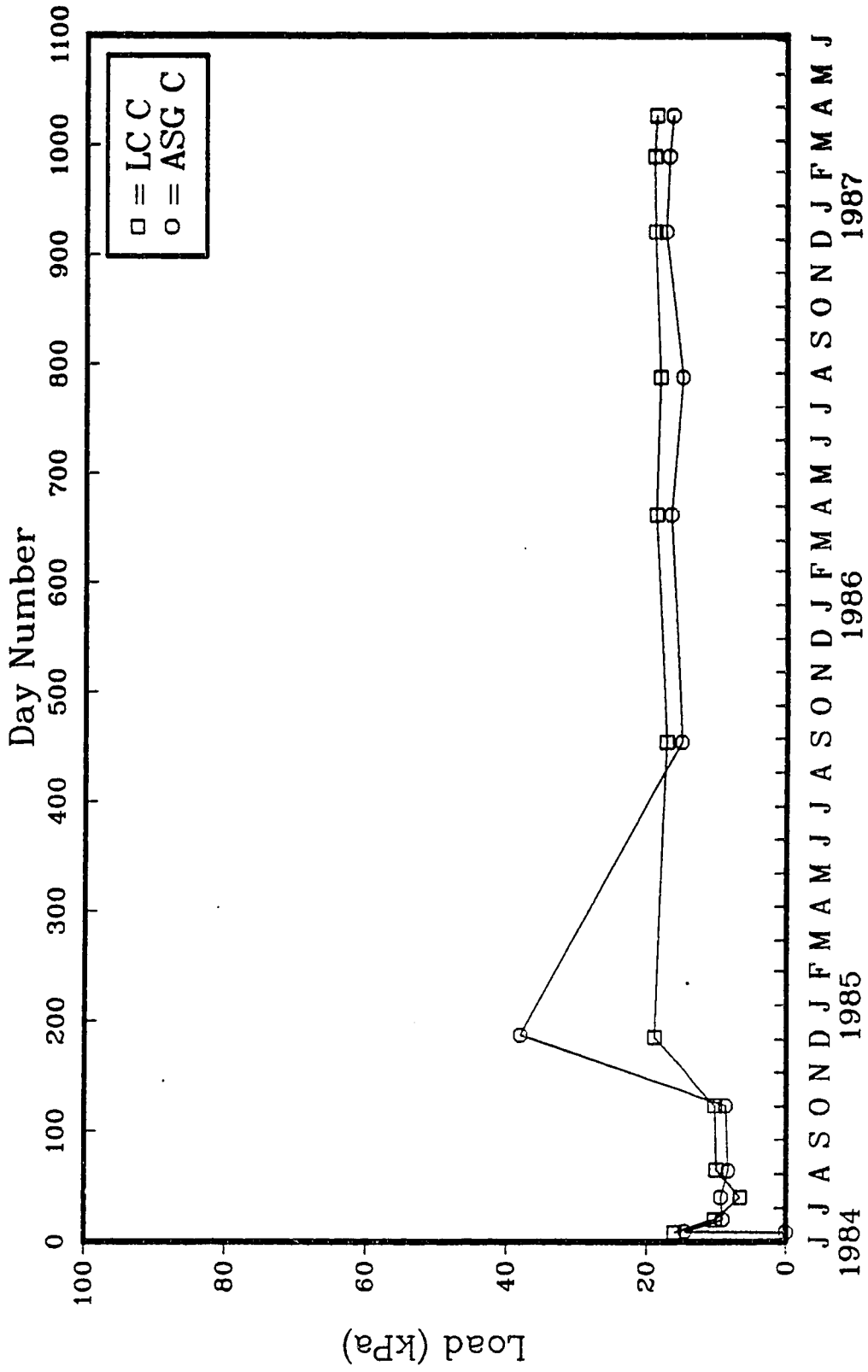


Figure A.3: Load versus time for Anchor C.

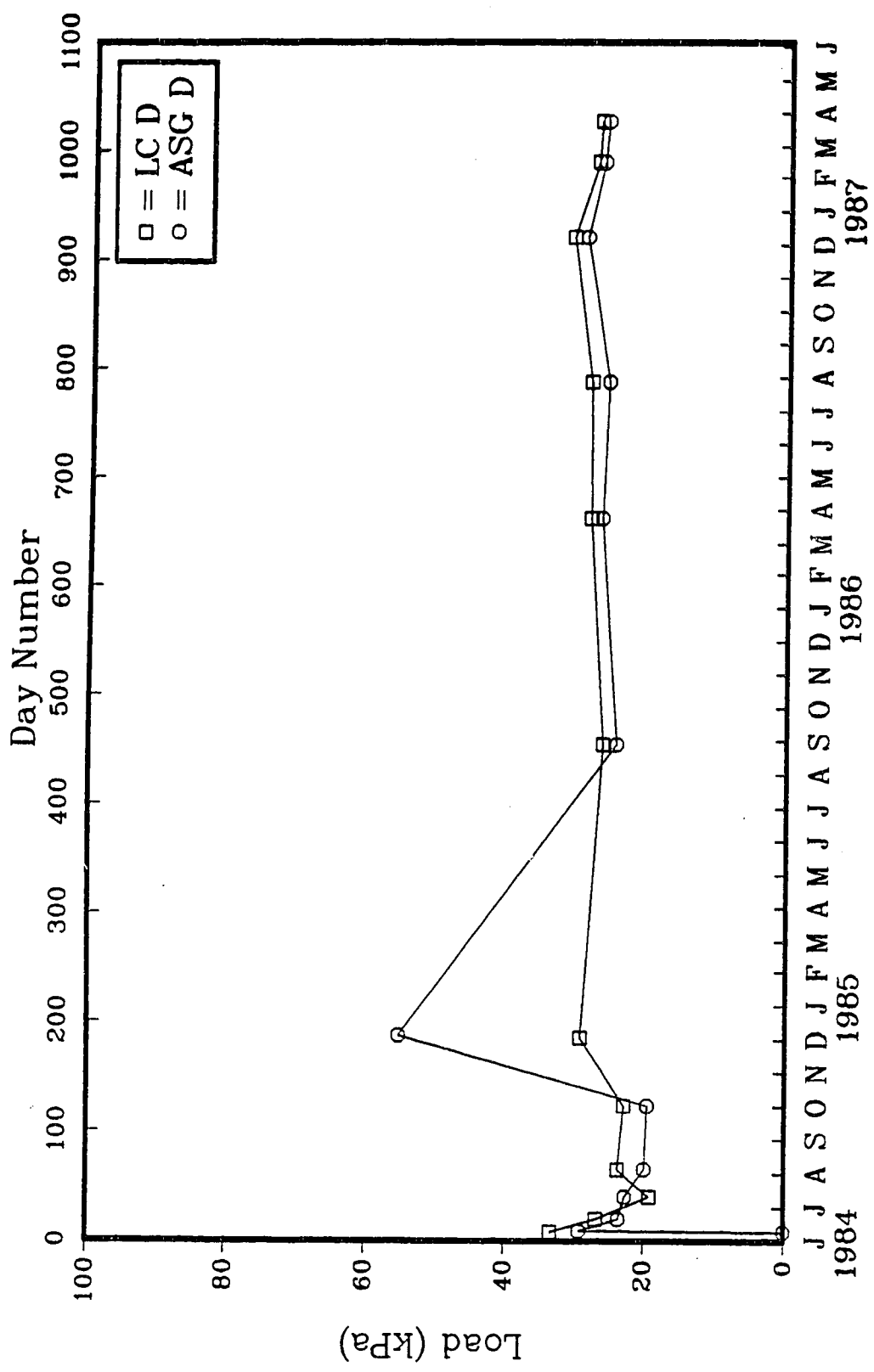


Figure A.4: Load versus time for Anchor D.

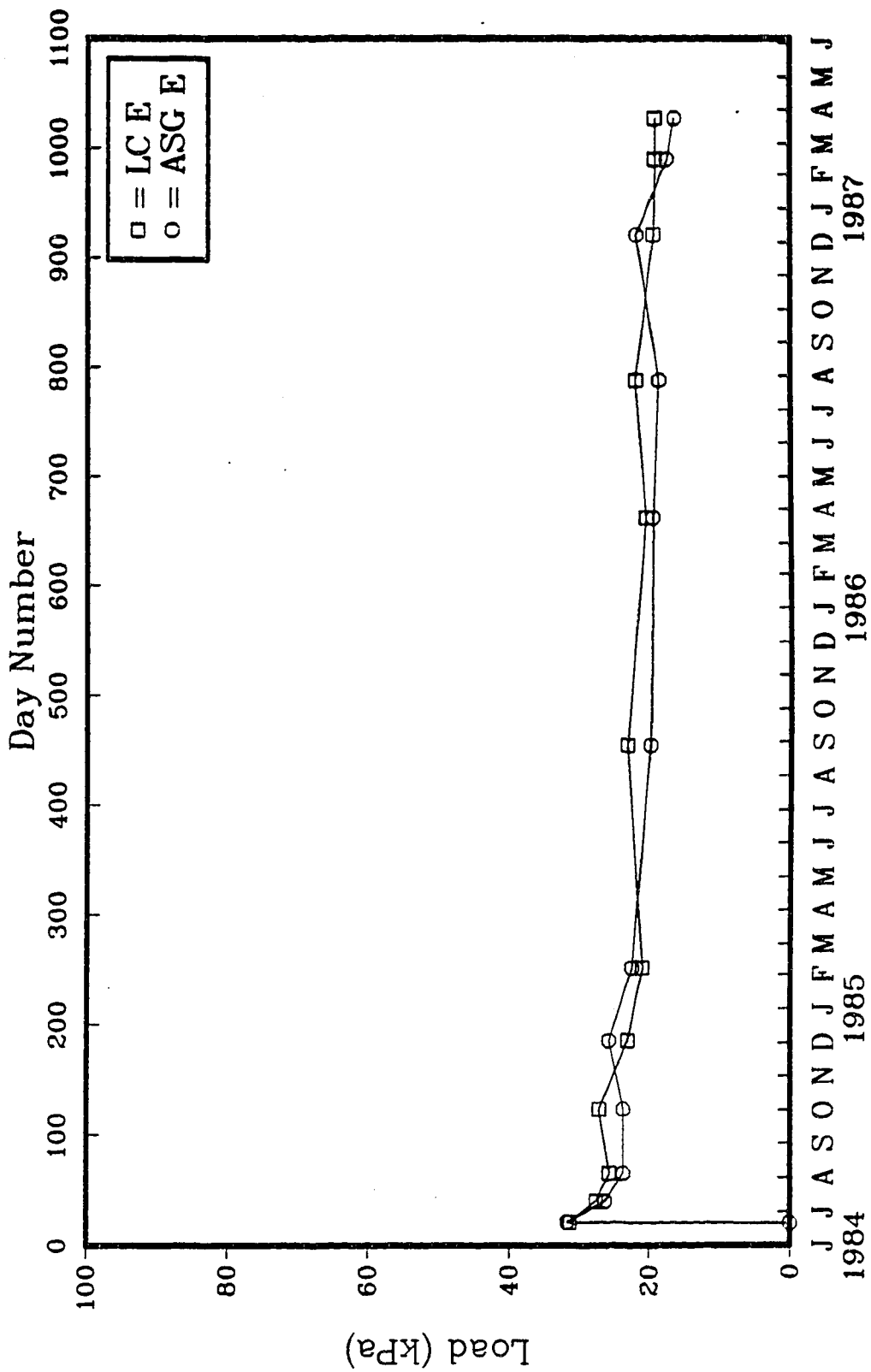


Figure A.5: Load versus time for Anchor E.

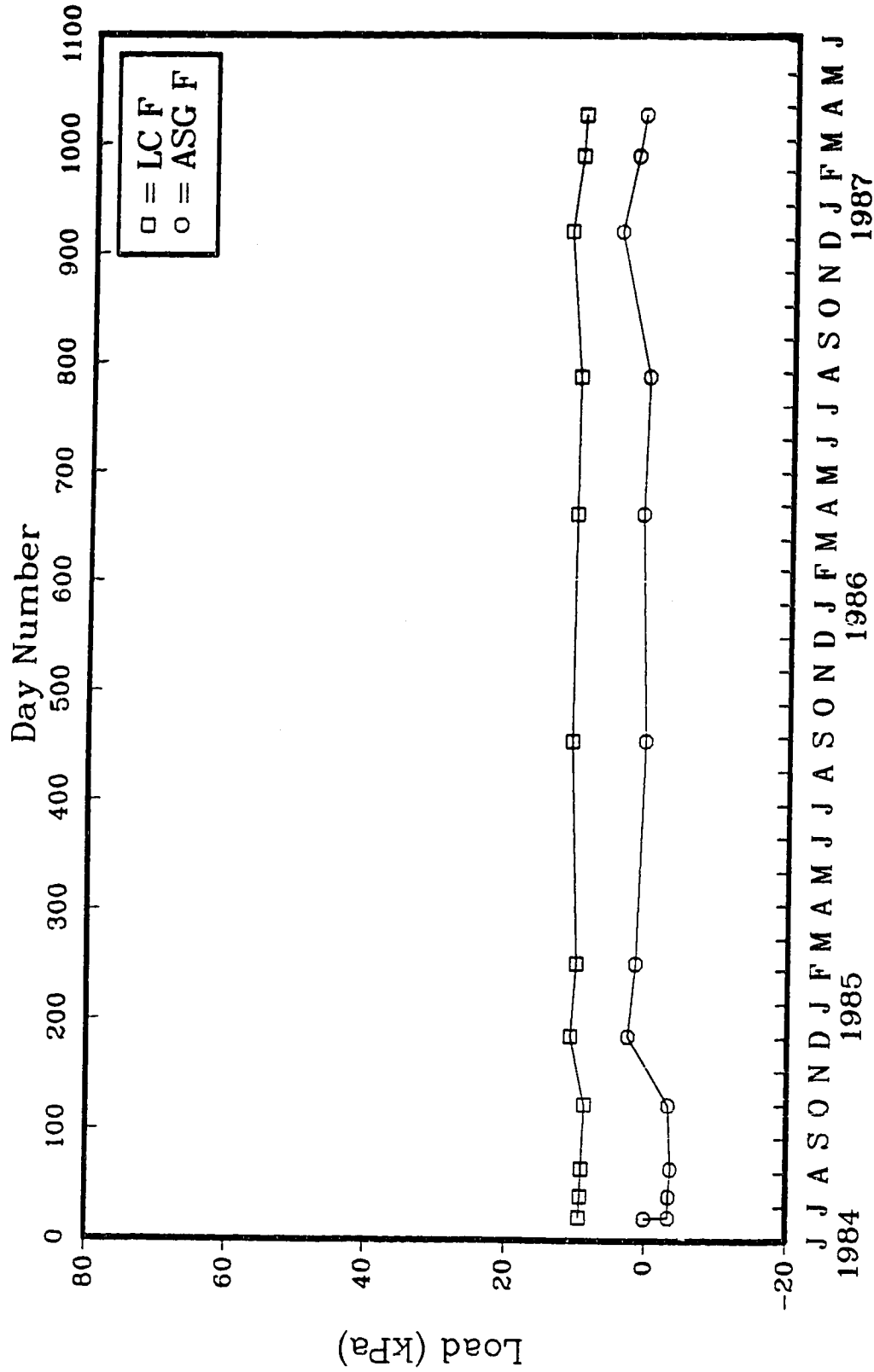


Figure A.6: Load versus time for Anchor F.

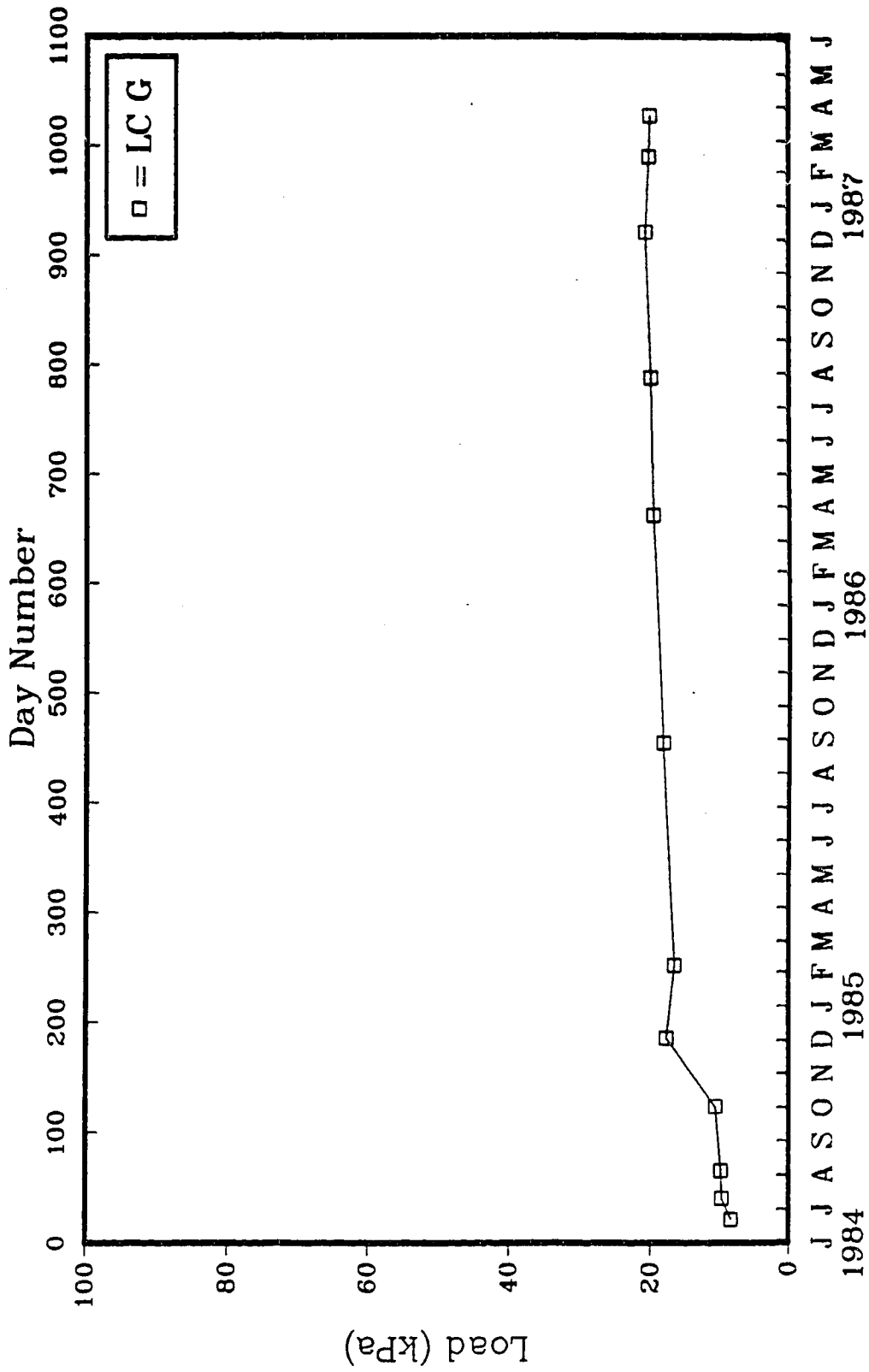


Figure A.7: Load versus time for Anchor G.

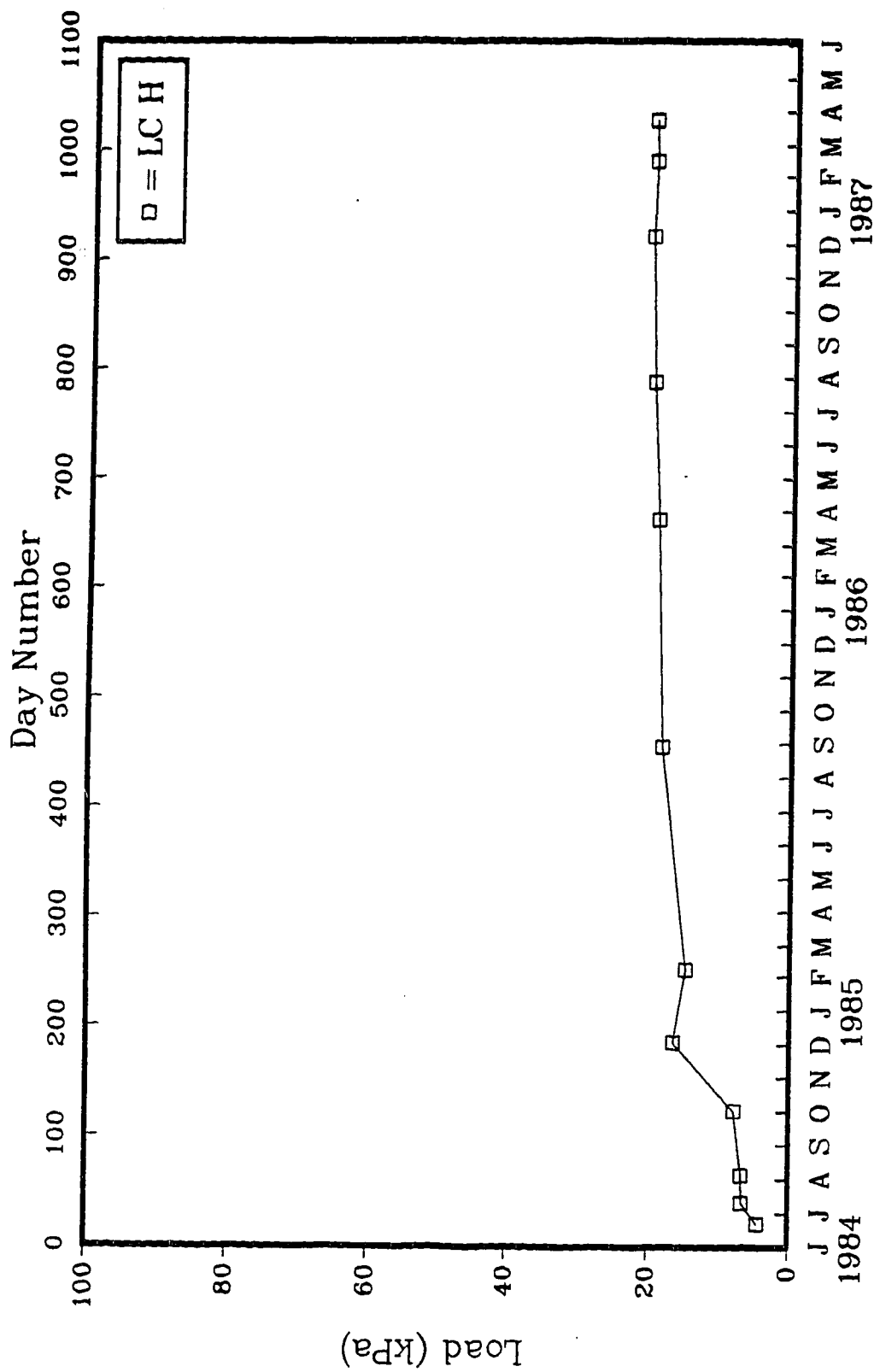


Figure A.8: Load versus time for Anchor H.

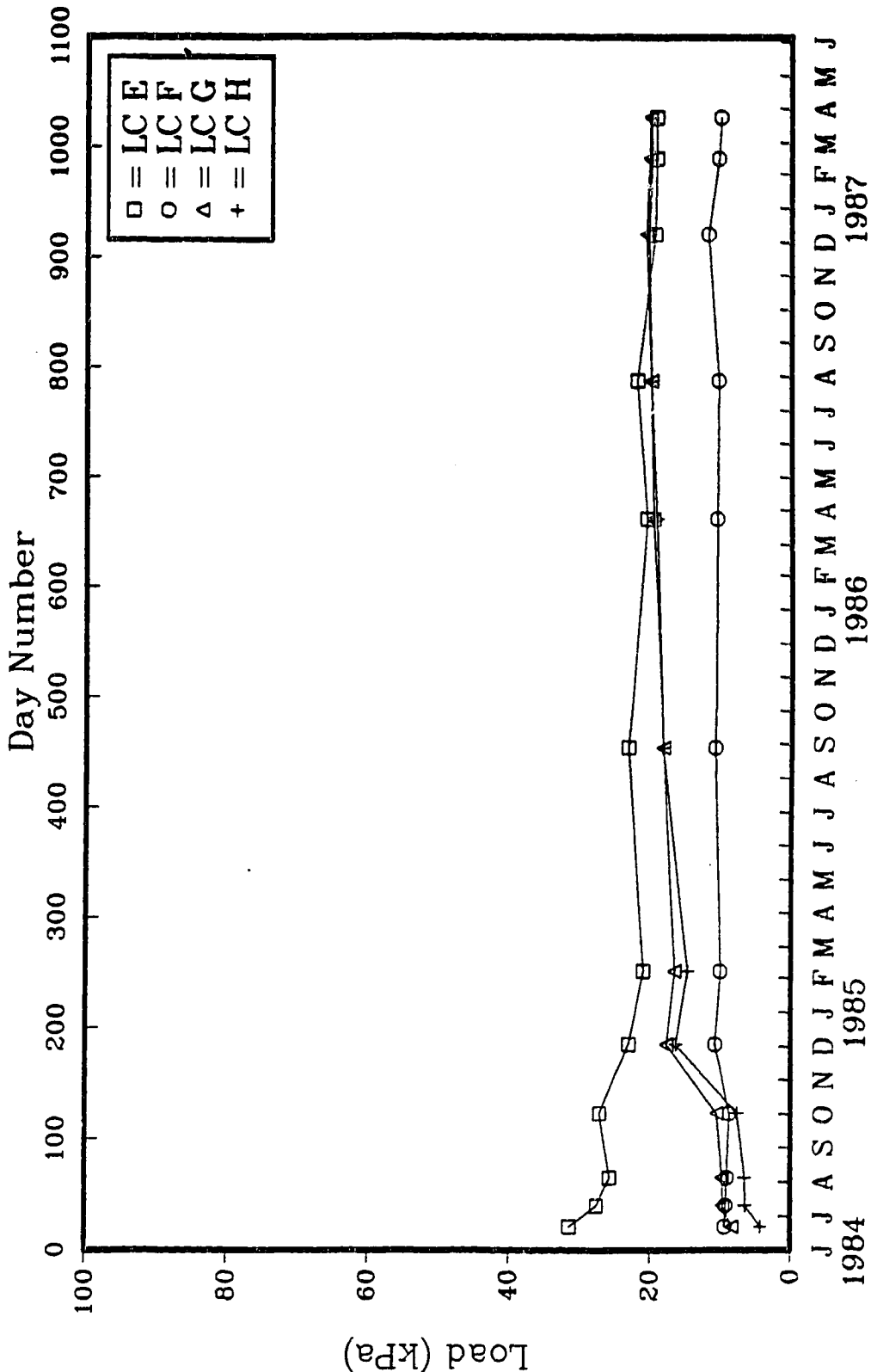


Figure A.9: East wall load cells.

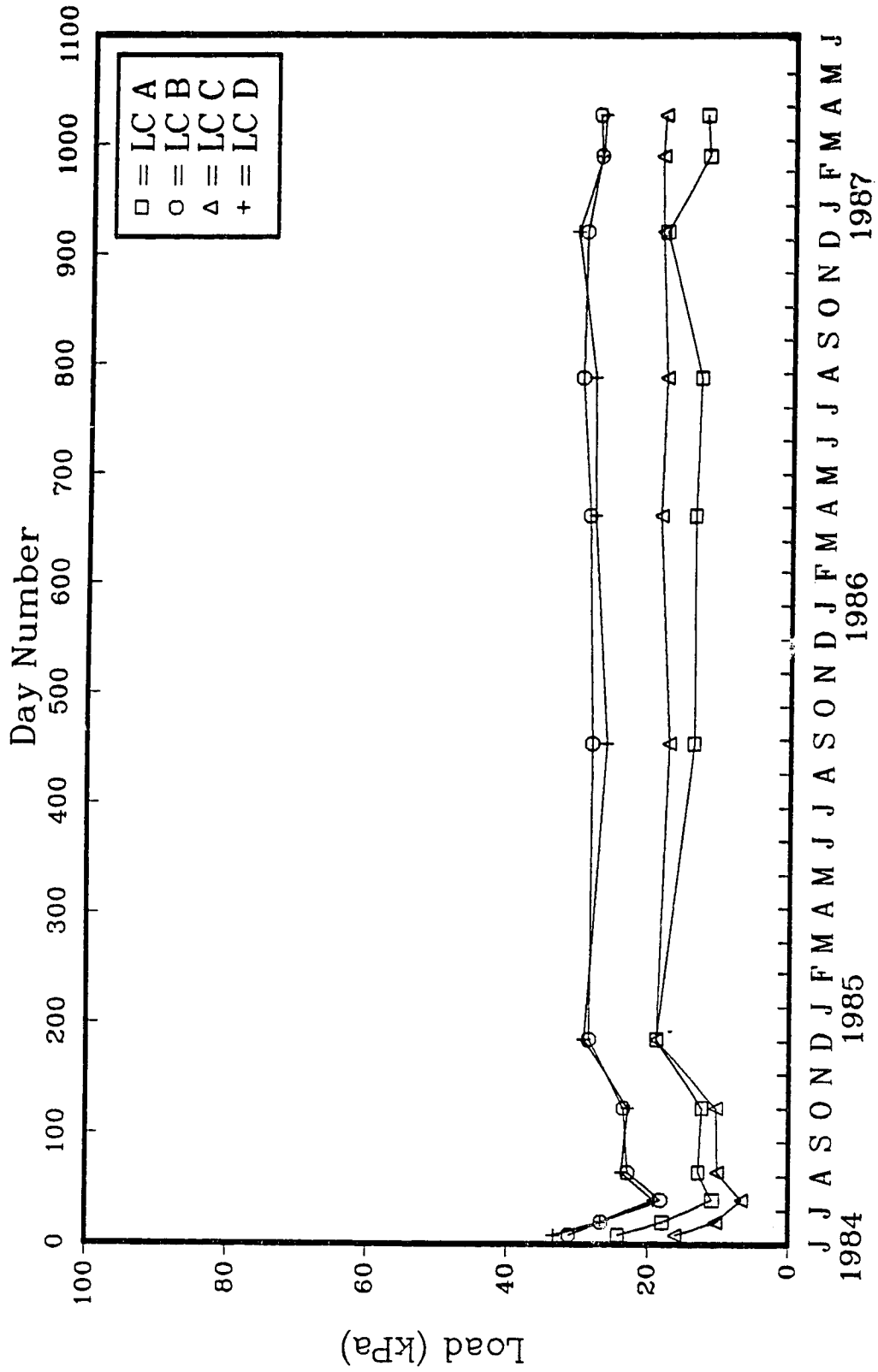


Figure A.10: West wall load cells.

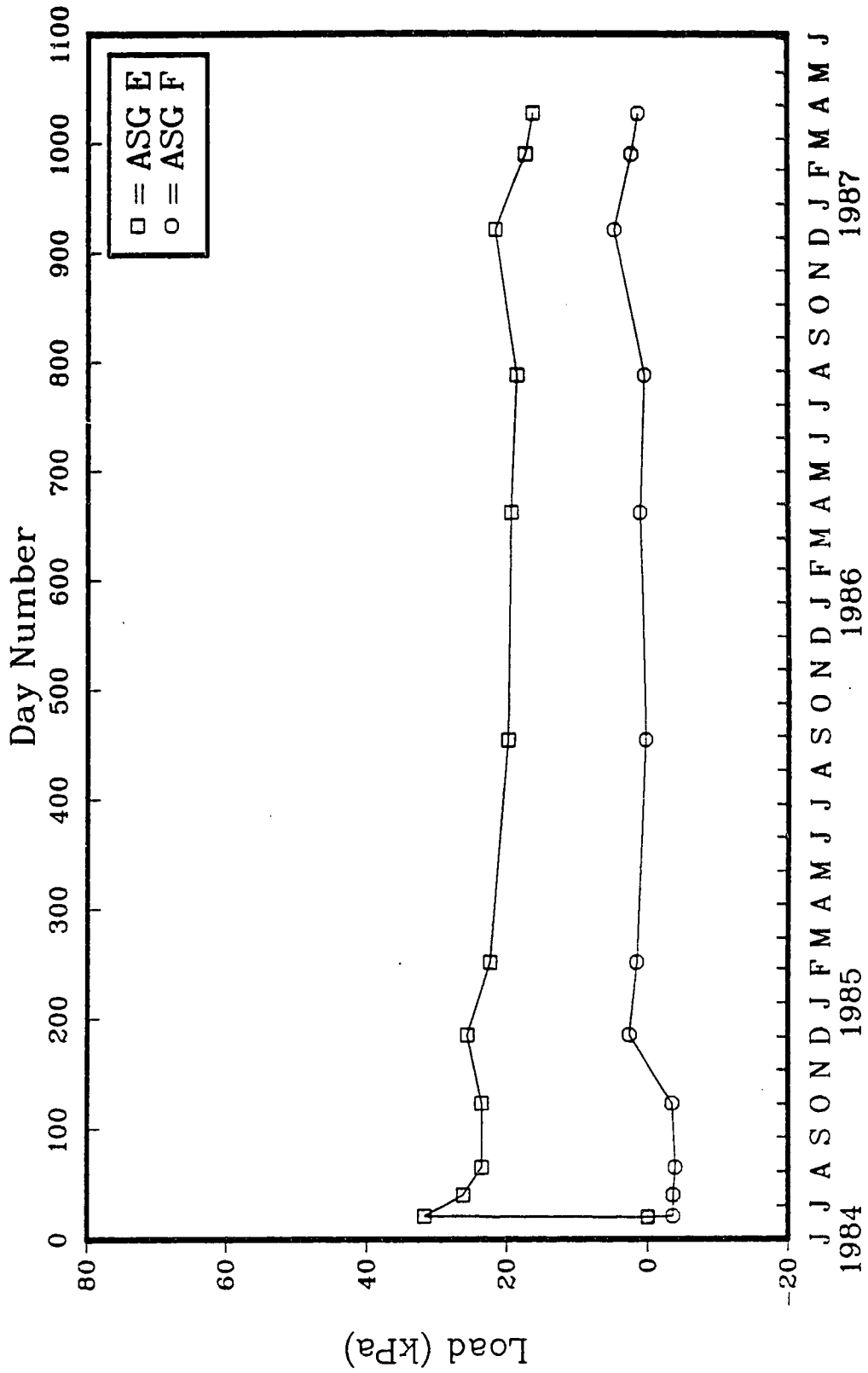


Figure A.11: East wall ASG loads.

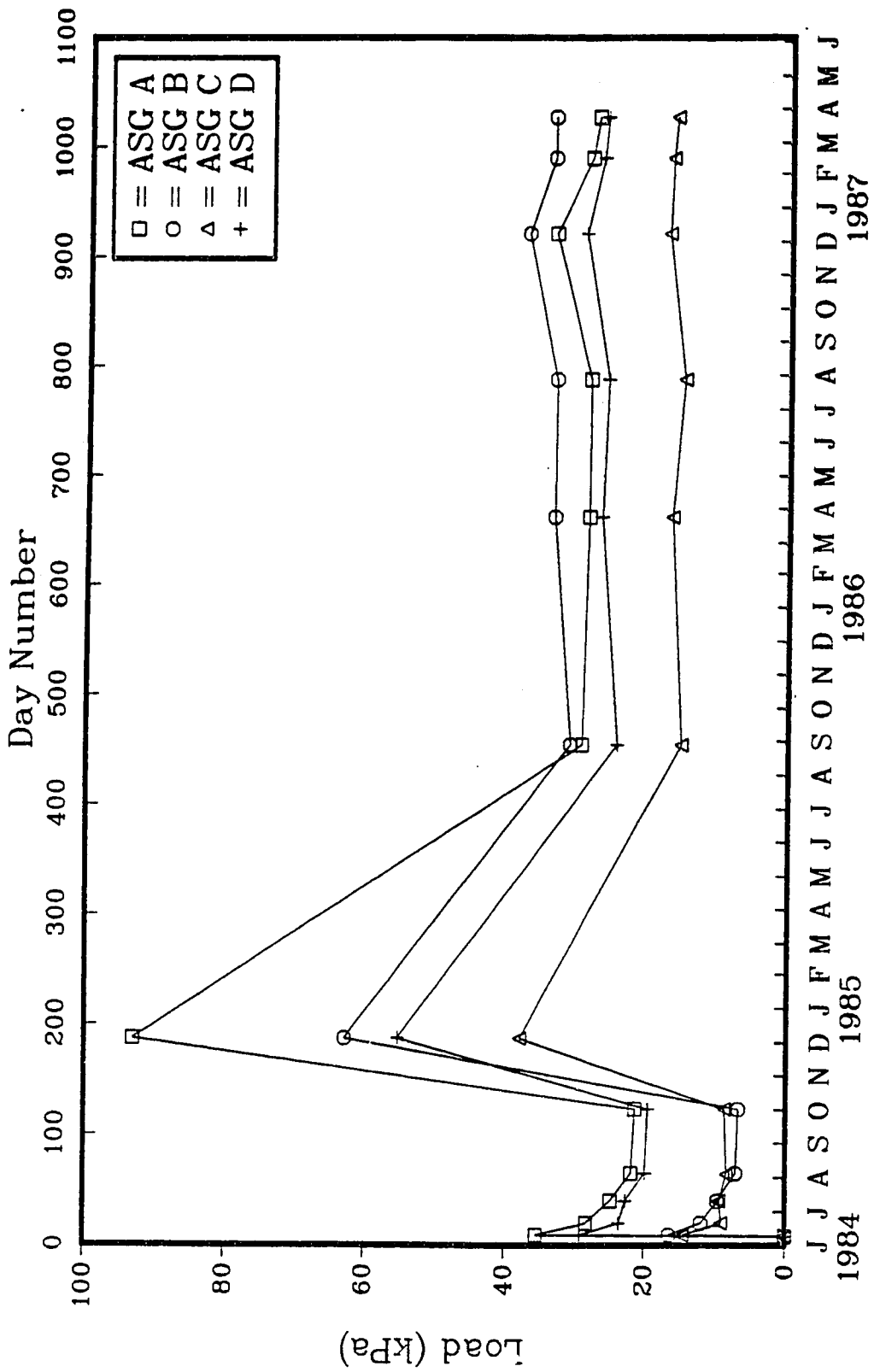


Figure A.12: West wall ASG loads.

Appendix B
Anchor Strain Gauge Results

Time (Days)	Net Strain (mmE-6/mm)						
	SG 1	SG 2	SG 3	SG 4	SG 5	SG 6	SG 7
8	0.	0.	0.	0.	0.	0.	0.
9	590.	320.	420.	504.	491.	532.	68.
20	470.	428.	423.	431.	397.	427.	252.
40	412.	404.	394.	393.	358.	381.	252.
65	363.	393.	375.	372.	334.	353.	254.
123	355.	384.	357.	364.	325.	350.	260.
187	1550.	1372.	1350.	1386.	1350.	1394.	1255.
454	487.	362.	319.	433.	321.	376.	276.
662	474.	384.	299.	566.	354.	395.	298.
788	472.	358.	226.	574.	333.	380.	285.
921	558.	378.	160.	682.	396.	447.	345.
990	473.	382.	123.	686.	358.	393.	317.
1027	457.	367.	107.	685.	339.	375.	304.

Time (Days)	Stress (MPa)						
	SG 1	SG 2	SG 3	SG 4	SG 5	SG 6	SG 7
8	0.0	0.0	0.0	0.0	0.0	0.0	0.0
9	118.00	64.00	84.00	100.80	98.20	106.40	13.60
20	94.00	85.60	84.60	86.20	79.40	85.40	50.40
40	82.40	80.80	78.80	78.60	71.60	76.20	50.40
65	72.60	78.60	75.00	74.40	66.80	70.60	50.80
123	71.00	76.80	71.40	72.80	65.00	70.00	52.00
187	310.00	274.40	270.00	277.20	270.00	278.80	251.00
454	97.40	72.40	63.80	86.60	64.20	75.20	55.20
662	94.80	76.80	59.80	113.20	70.80	79.00	59.60
788	94.40	71.60	45.20	114.80	66.60	76.00	57.00
921	111.60	75.60	32.00	136.40	79.20	89.40	69.00
990	94.60	76.40	24.60	137.20	71.60	78.60	63.40
1027	91.40	73.40	21.40	137.00	67.80	75.00	60.80

Table B.1: Strain gauge results for Anchor A.

Time (Days)	Net Strain (mmE-G/mm)						
	SG 1	SG 2	SG 3	SG 4	SG 5	SG 6	SG 7
8	0.	0.	0.	0.	0.	0.	0.
9	352.	345.	302.	240.	139.	18.	-1.
20	255.	268.	264.	239.	212.	167.	200.
40	206.	228.	247.	230.	210.	179.	221.
65	151.	183.	213.	197.	180.	165.	210.
123	144.	172.	206.	186.	167.	169.	221.
187	1343.	968.	937.	888.	864.	856.	888.
454	662.	289.	280.	227.	186.	225.	258.
662	714.	385.	344.	278.	236.	274.	284.
788	712.	348.	317.	259.	201.	262.	279.
921	800.	423.	388.	321.	259.	333.	340.
990	721.	391.	357.	293.	238.	310.	320.
1027	721.	368.	339.	279.	220.	302.	310.

Time (Days)	Stress (MPa)						
	SG 1	SG 2	SG 3	SG 4	SG 5	SG 6	SG 7
8	0.0	0.0	0.0	0.0	0.0	0.0	0.0
9	70.40	69.00	60.40	48.00	27.80	3.60	-0.20
20	51.00	53.60	52.80	47.80	42.40	33.40	40.00
40	41.20	45.60	49.40	46.00	42.00	35.80	44.20
65	30.20	36.60	42.60	39.40	36.00	33.00	42.00
123	28.80	34.40	41.20	37.20	33.40	33.80	44.20
187	268.60	193.60	187.40	177.60	172.80	171.20	177.60
454	132.40	57.80	56.00	45.40	37.20	45.00	51.60
662	142.80	77.00	68.80	55.60	47.20	54.80	56.80
788	142.40	69.60	63.40	51.80	40.20	52.40	55.80
921	160.00	84.60	77.60	64.20	51.80	66.60	68.00
990	144.20	78.20	71.40	58.60	47.60	62.00	64.00
1027	144.20	73.60	67.80	55.80	44.00	60.40	62.00

Table B.2: Strain gauge results for Anchor B.

Time (Days)	Net Strain (mmE-6/mm)						
	SG 1	SG 2	SG 3	SG 4	SG 5	SG 6	SG 7
8	0.	0.	0.	0.	0.	0.	0.
9	689.	481.	757.	663.	335.	144.	50.
20	432.	164.	472.	417.	316.	258.	254.
40	446.	172.	475.	412.	315.	258.	249.
64	398.	127.	433.	373.	302.	244.	247.
123	415.	132.	450.	384.	309.	247.	249.
187	1802.	1688.	1944.	1801.	1481.	1370.	1323.
454	719.	590.	834.	679.	475.	373.	326.
662	790.	687.	940.	780.	570.	475.	409.
788	711.	599.	858.	708.	503.	380.	359.
921	823.	694.	990.	807.	578.	473.	447.
990	802.	667.	970.	793.	571.	462.	450.
1027	776.	650.	946.	774.	547.	445.	430.

Time (Days)	Stress (MPa)						
	SG 1	SG 2	SG 3	SG 4	SG 5	SG 6	SG 7
8	0.0	0.0	0.0	0.0	0.0	0.0	0.0
9	137.80	96.20	151.40	132.60	67.00	28.80	10.00
20	86.40	32.80	94.40	83.40	63.20	51.60	50.80
40	89.20	34.40	95.00	82.40	63.00	51.60	49.80
64	79.60	25.40	86.60	74.60	60.40	48.80	49.40
123	83.00	26.40	90.00	76.80	61.80	49.40	49.80
187	360.40	337.60	388.80	360.20	296.20	274.00	264.60
454	143.80	118.00	166.80	135.80	95.00	74.60	65.20
662	158.00	137.40	188.00	156.00	114.00	95.00	81.80
788	142.20	119.80	171.60	141.60	100.60	76.00	71.80
921	164.60	138.80	198.00	161.40	115.60	94.60	89.40
990	160.40	133.40	194.00	158.60	114.20	92.40	90.00
1027	155.20	130.00	189.20	154.80	109.40	89.00	86.00

Table B.3: Strain gauge results for Anchor C.

Time (Days)	Net Strain (mmE-6/mm)						
	SG 1	SG 2	SG 3	SG 4	SG 5	SG 6	SG 7
8	0.	0.	0.	0.	0.	0.	0.
9	659.	527.	486.	182.	39.	87.	3.
20	532.	451.	430.	238.	120.	159.	173.
40	511.	397.	418.	250.	140.	177.	189.
65	449.	351.	375.	229.	124.	164.	178.
123	441.	336.	359.	230.	128.	168.	181.
187	1250.	1067.	1074.	913.	801.	842.	851.
454	547.	361.	340.	241.	151.	181.	203.
662	601.	409.	408.	292.	182.	225.	239.
788	584.	339.	350.	262.	163.	202.	219.
921	659.	407.	412.	327.	233.	267.	285.
990	604.	425.	403.	309.	202.	238.	262.
1027	592.	404.	385.	296.	185.	224.	251.

Time (Days)	Stress (MPa)						
	SG 1	SG 2	SG 3	SG 4	SG 5	SG 6	SG 7
8	0.0	0.0	0.0	0.0	0.0	0.0	0.0
9	131.80	105.40	97.20	36.40	7.80	17.40	0.60
20	106.40	90.20	86.00	47.60	24.00	31.80	34.60
40	102.20	79.40	83.60	50.00	28.00	35.40	37.80
65	89.80	70.20	75.00	45.80	24.80	32.80	35.60
123	88.20	67.20	71.80	46.00	25.60	33.60	36.20
187	250.00	213.40	214.80	182.60	160.20	168.40	170.20
454	109.40	72.20	68.00	48.20	30.20	36.20	40.60
662	120.20	81.80	81.60	58.40	36.40	45.00	47.80
788	116.80	67.80	70.00	52.40	32.60	40.40	43.80
921	131.80	81.40	82.40	65.40	46.60	53.40	57.00
990	120.80	85.00	80.60	61.80	40.40	47.60	52.40
1027	118.40	80.80	77.00	59.20	37.00	44.80	50.20

Table B.4: Strain gauge results for Anchor D.

Time (Days)	Net Strain (mmE-6/mm)					
	SG 1	SG 2	SG 3	SG 4	SG 5	SG 6
20	0.	0.	0.	0.	0.	0.
21	538.	317.	187.	54.	-8.	-6.
40	444.	294.	171.	48.	-3.	-6.
65	400.	272.	163.	42.	-12.	-9.
123	400.	278.	152.	37.	-27.	-9.
185	434.	369.	255.	114.	50.	46.
251	379.	373.	266.	131.	65.	52.
454	337.	329.	197.	70.	-7.	-2.
662	330.	380.	234.	107.	32.	15.
788	316.	359.	211.	83.	-6.	0.
921	369.	424.	261.	131.	71.	33.
990	297.	406.	228.	104.	37.	16.
1027	279.	412.	210.	94.	27.	8.

Time (Days)	Stress (MPa)					
	SG 1	SG 2	SG 3	SG 4	SG 5	SG 6
20	0.0	0.0	0.0	0.0	0.0	0.0
21	107.60	63.40	37.40	10.80	-1.60	-1.20
40	88.80	56.80	34.20	9.60	-0.60	-1.20
65	80.00	54.40	32.60	8.40	-2.40	-1.80
123	80.00	55.60	32.40	7.40	-5.40	-1.80
185	86.80	73.80	51.00	22.80	10.00	9.20
251	75.80	74.60	53.20	26.20	13.00	10.40
454	67.40	65.80	39.40	14.00	-1.40	-0.40
662	66.00	76.00	46.80	21.40	6.40	3.00
788	63.20	71.80	42.20	16.60	-1.20	0.0
921	73.80	84.80	52.20	26.20	14.20	6.60
990	59.40	81.20	45.60	20.80	7.40	3.20
1027	55.80	82.40	42.00	18.80	5.40	1.60

Table B.5: Strain gauge results for Anchor E.

Time (Days)	Net Strain (mmE-6/mm)						
	SG 1	SG 2	SG 3	SG 4	SG 5	SG 6	SG 7
20	0.	0.	0.	0.	0.	0.	0.
21	-91.	-21.	31.	34.	9.	1.	-3.
40	-92.	-28.	10.	23.	6.	-1.	-6.
65	-99.	-29.	-2.	14.	4.	-10.	-7.
123	-88.	-9.	-15.	6.	-2.	-26.	-20.
185	66.	133.	107.	71.	75.	28.	32.
251	40.	132.	104.	52.	91.	28.	35.
454	10.	94.	59.	-31.	40.	-88.	-13.
662	30.	133.	44.	-44.	79.	-84.	4.
788	13.	115.	24.	-81.	60.	-131.	4.
921	123.	163.	51.	-31.	115.	-82.	64.
990	63.	114.	-5.	-58.	89.	-112.	31.
1027	38.	96.	-34.	-72.	77.	-121.	18.

Time (Days)	Stress (MPa)						
	SG 1	SG 2	SG 3	SG 4	SG 5	SG 6	SG 7
20	0.0	0.0	0.0	0.0	0.0	0.0	0.0
21	-18.20	-4.20	6.20	6.80	1.80	0.20	-0.60
40	-18.40	-5.60	2.00	4.60	1.20	-0.20	-1.20
65	-19.80	-5.80	-0.40	2.80	0.80	-2.00	-1.40
123	-17.60	-1.80	-3.00	1.20	-0.40	-5.20	-4.00
185	13.20	26.60	20.80	14.20	15.00	5.60	6.40
251	8.00	26.40	21.40	10.40	18.20	5.60	7.00
454	2.00	18.80	11.80	-6.20	8.00	-17.60	-2.60
662	6.00	26.60	8.80	-8.80	15.80	-16.80	0.80
788	2.60	23.00	4.80	-16.20	12.00	-26.20	0.80
921	24.60	32.60	10.20	-6.20	23.00	-16.40	12.80
990	12.60	22.80	-1.00	-11.60	17.80	-22.40	6.20
1027	7.60	19.20	-6.80	-14.40	15.40	-24.20	3.60

Table B.6: Strain gauge results for Anchor F.

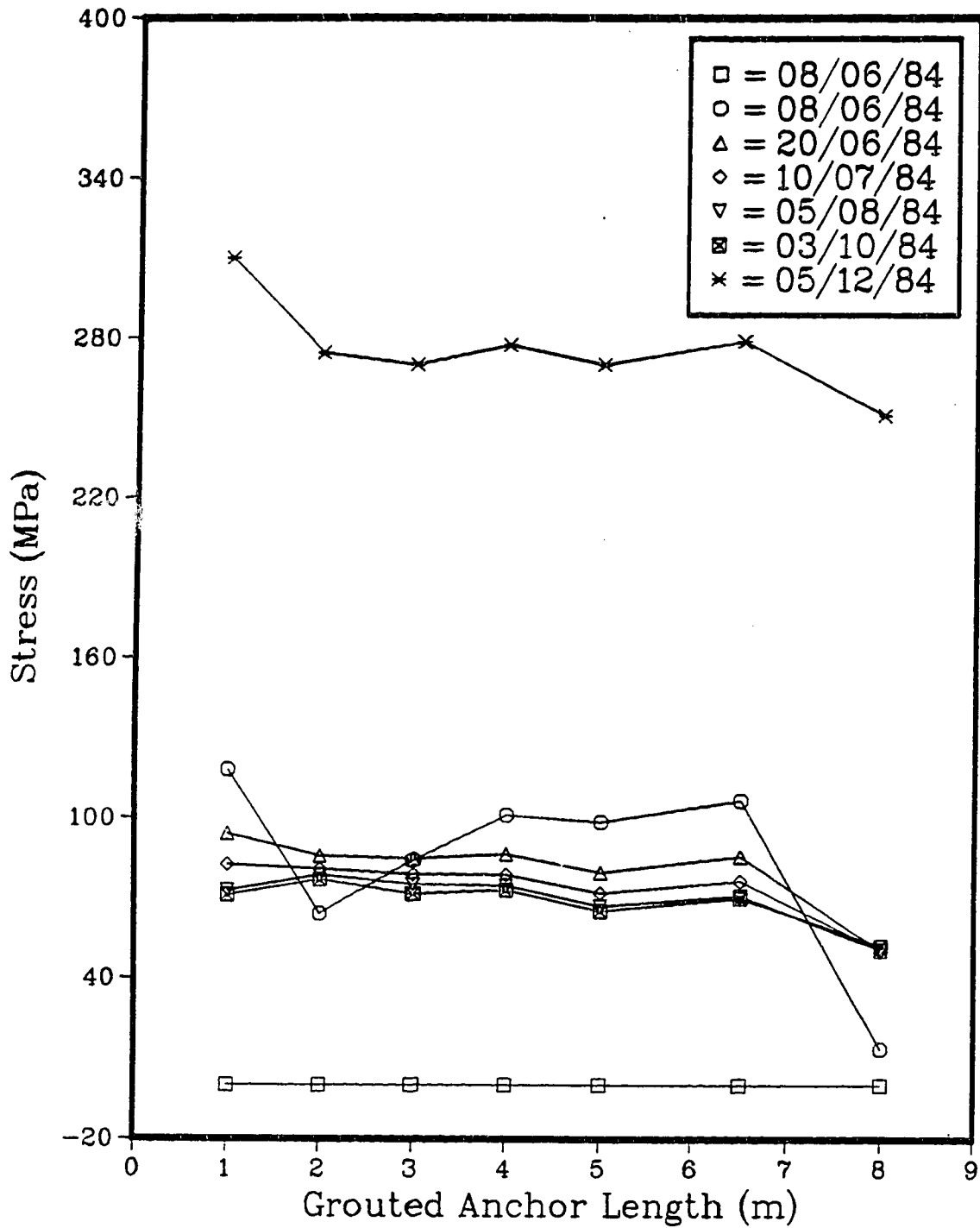


Figure B.1: Stress vs length for Anchor A, early epochs.

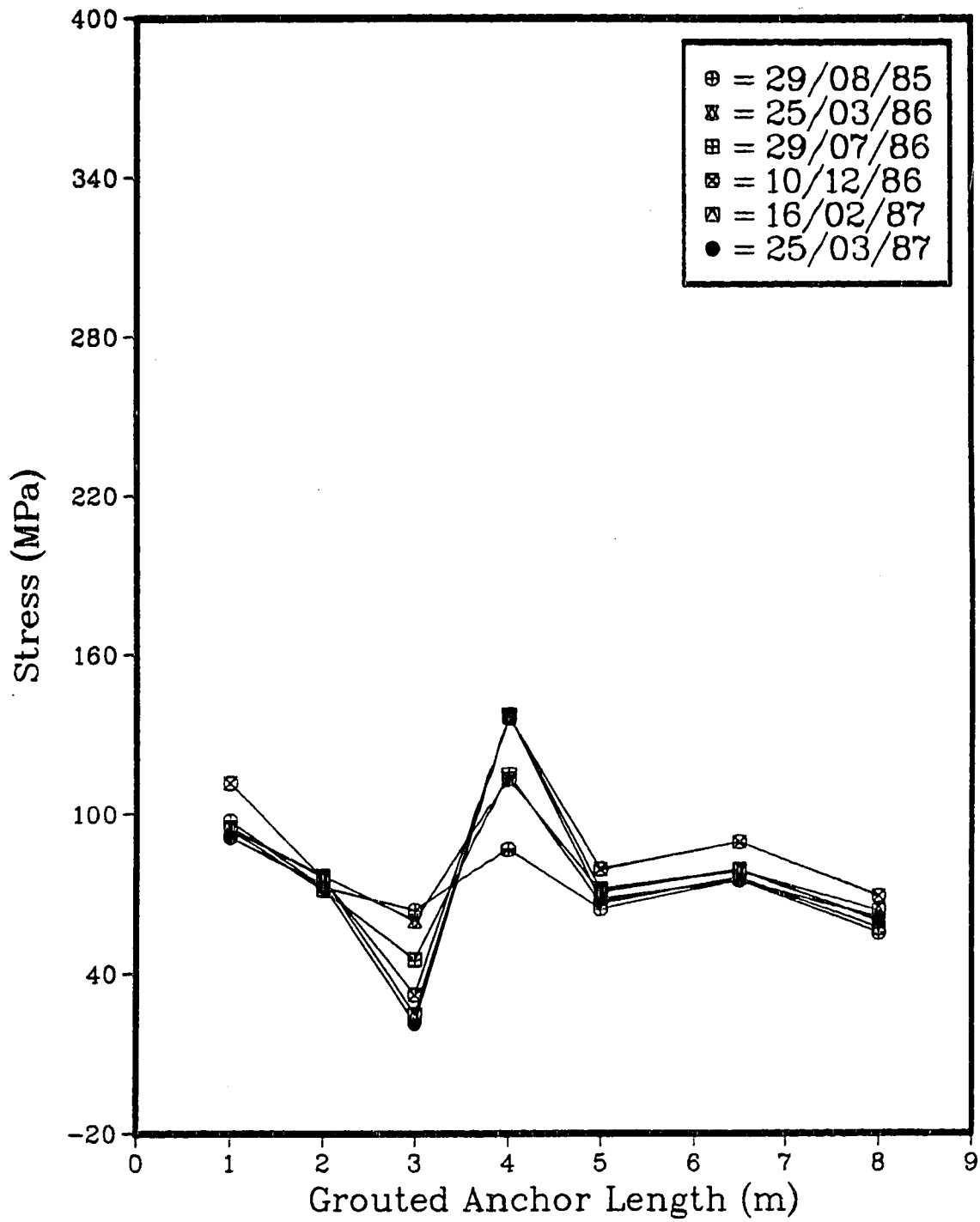


Figure B.2: Stress vs length for Anchor A, late epochs.

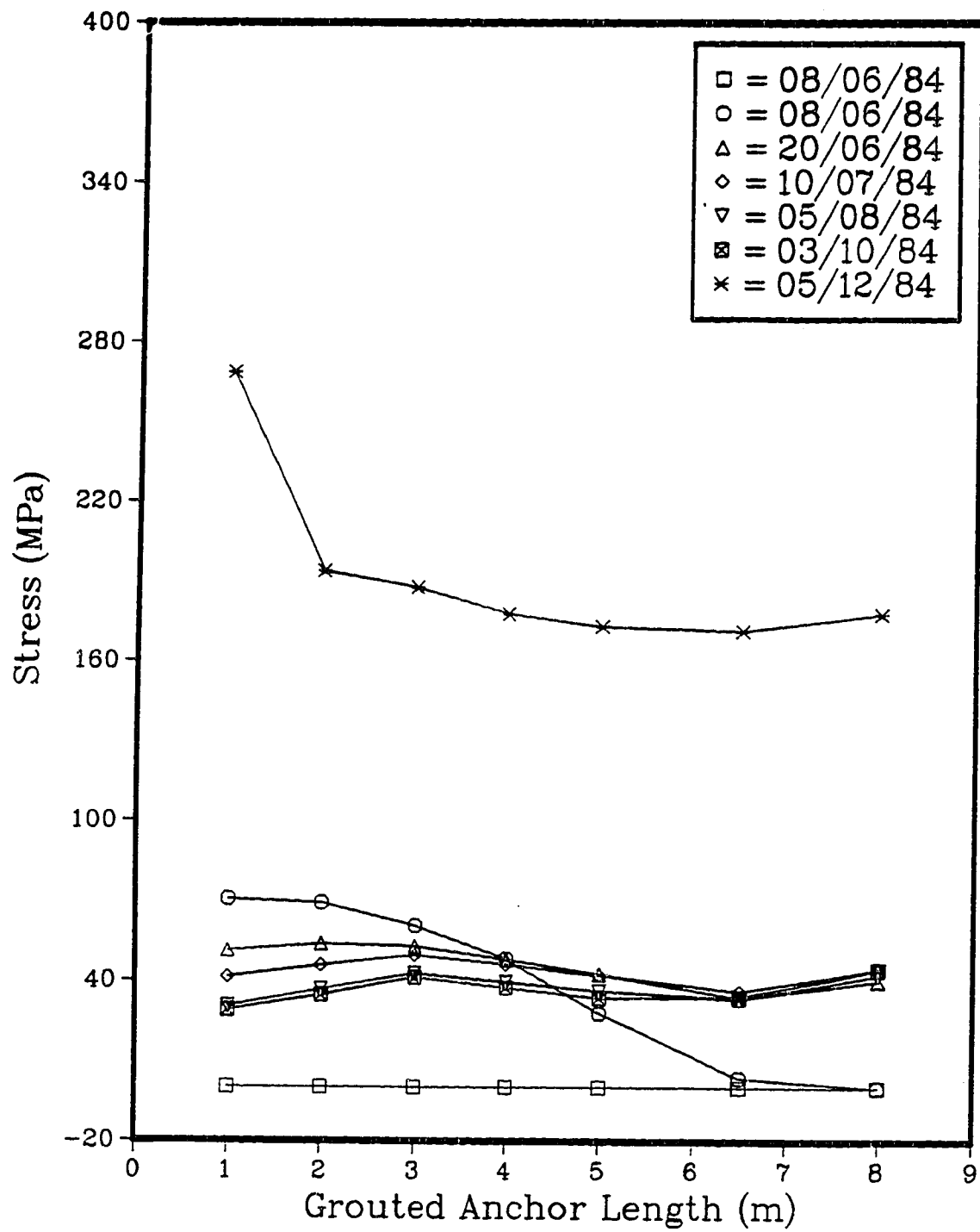


Figure B.3: Stress vs length for Anchor B, early epochs.

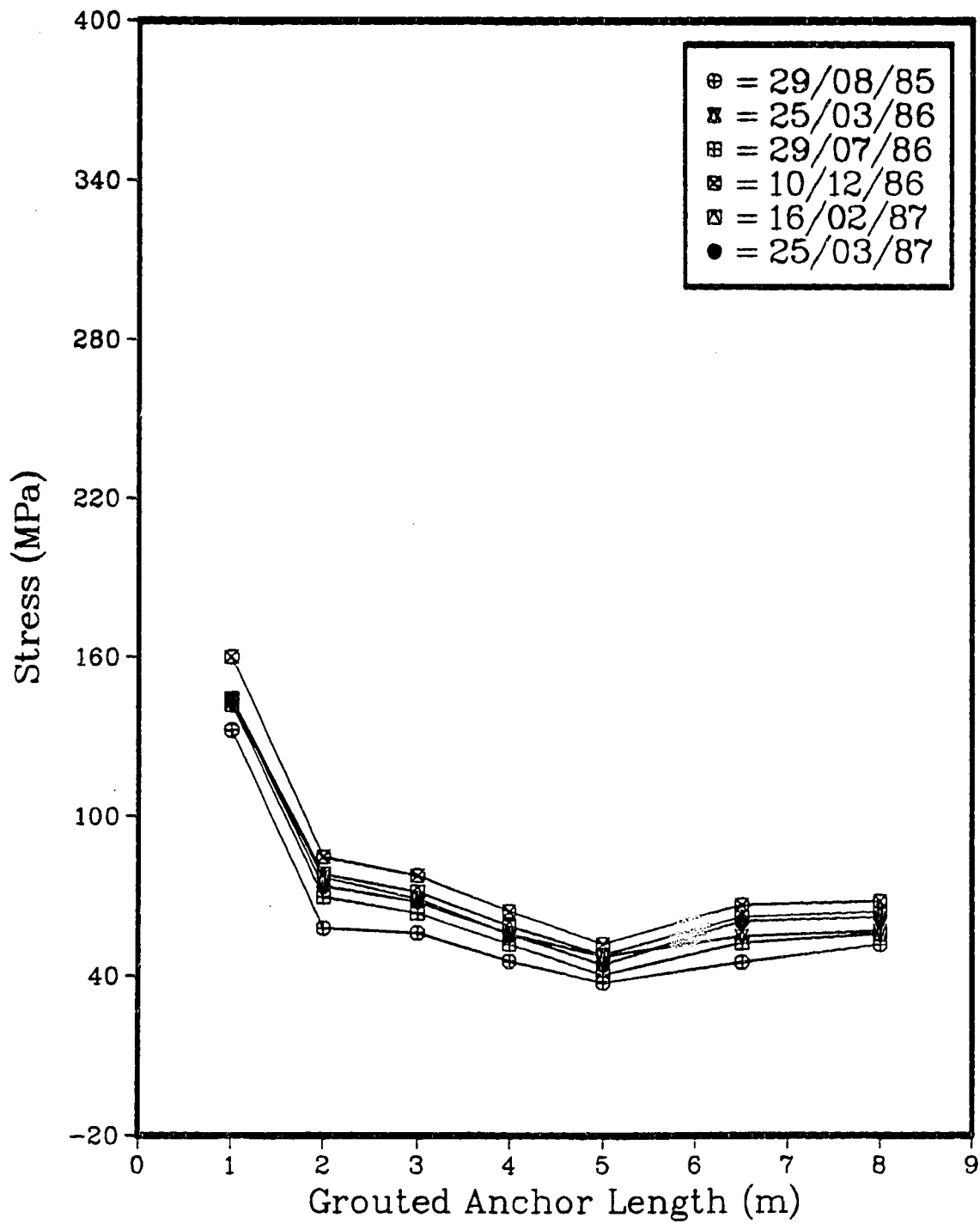


Figure B.4: Stress vs length for Anchor B, late epochs.

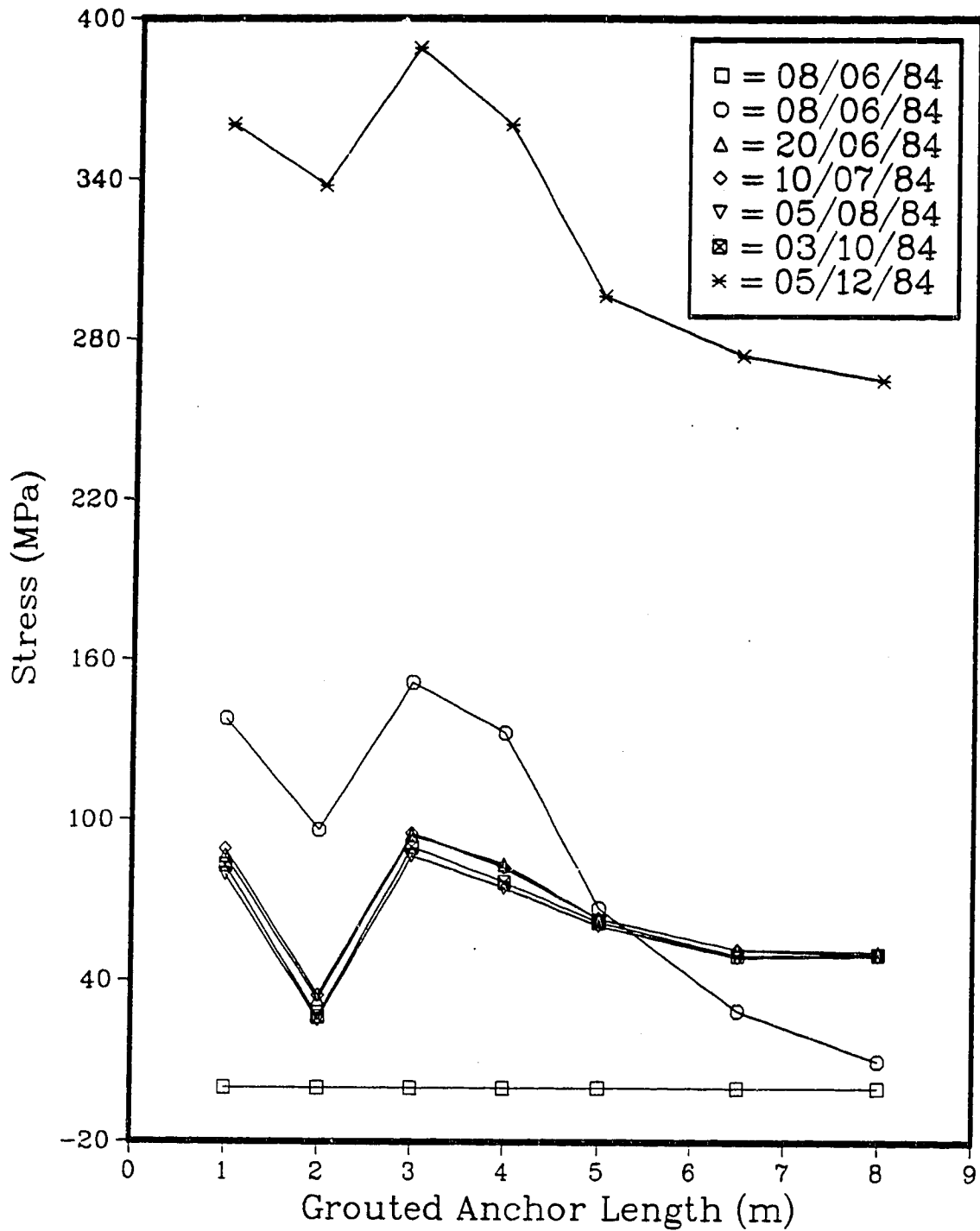


Figure B.5: Stress vs length for Anchor C, early epochs.

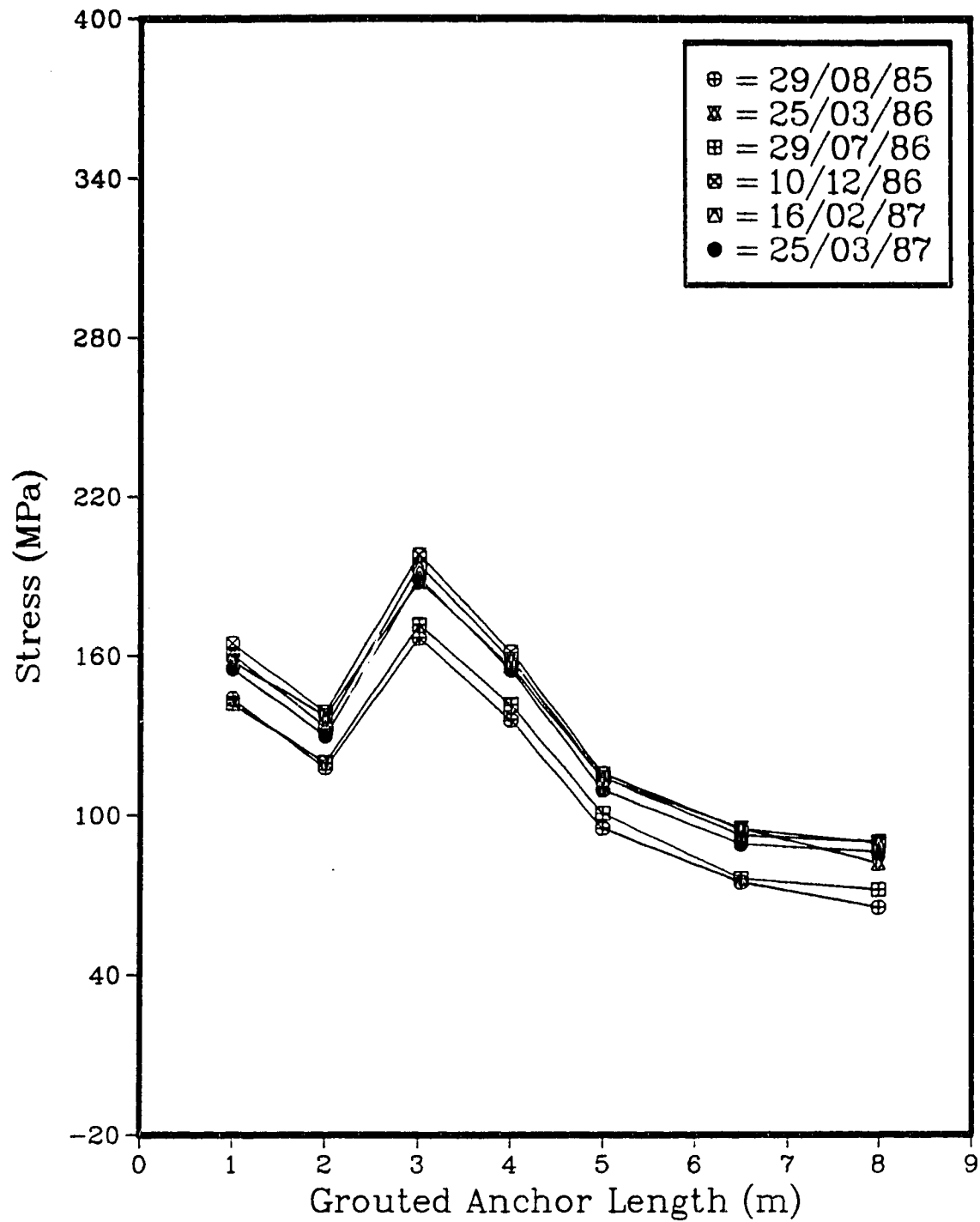


Figure B.6: Stress vs length for Anchor C, late epochs.

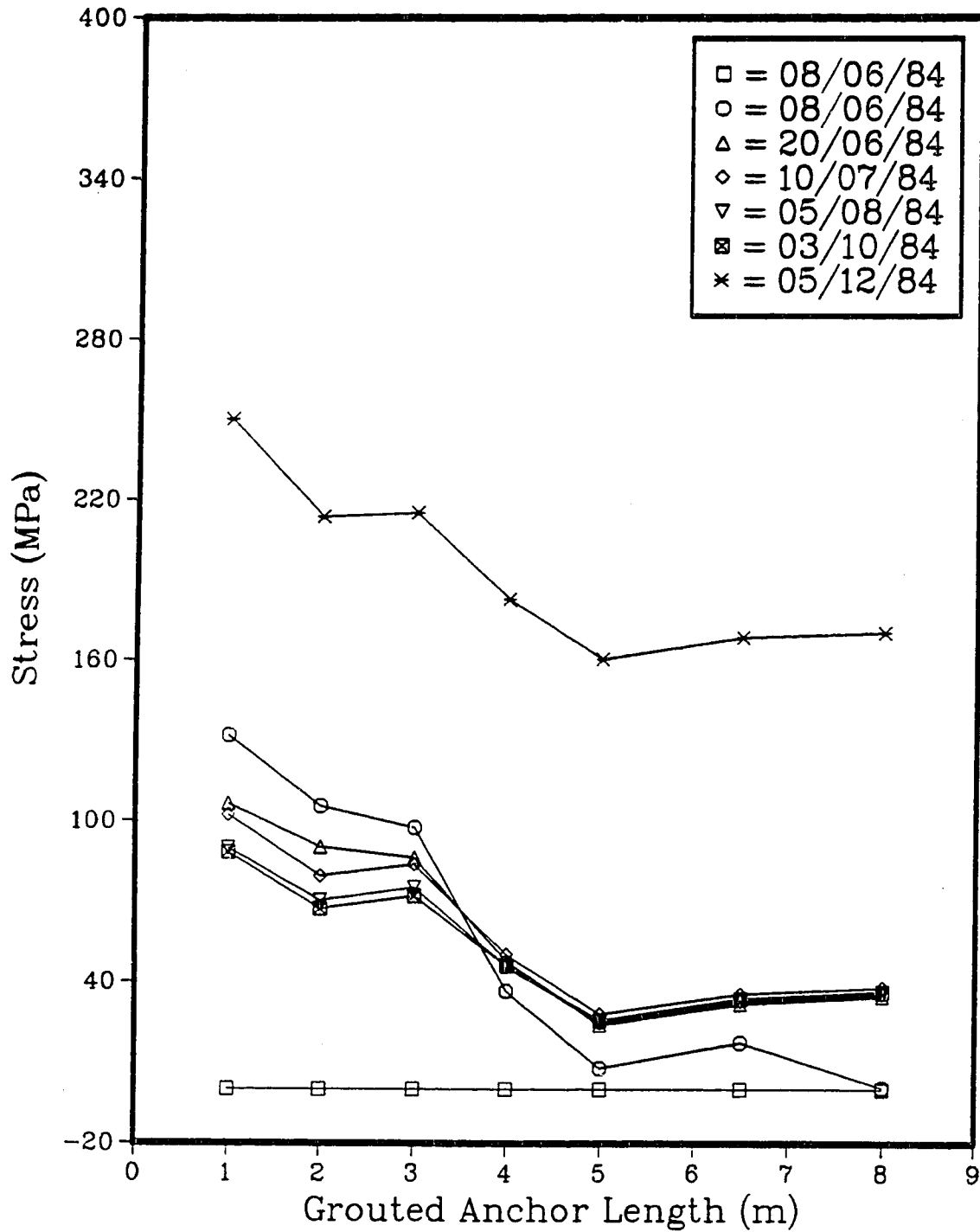


Figure B.7: Stress vs length for Anchor D, early epochs.

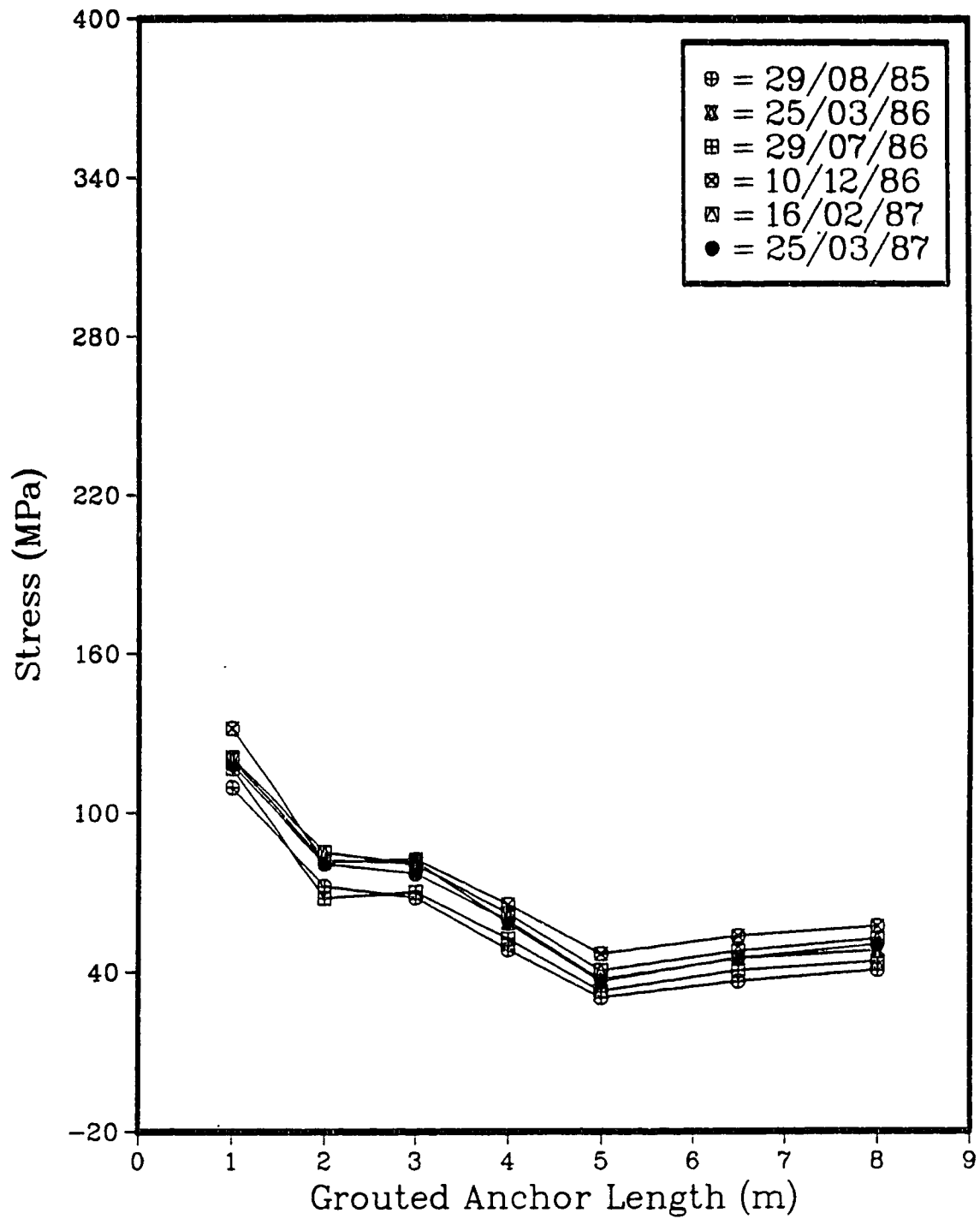


Figure B.8: Stress vs length for Anchor D, late epochs.

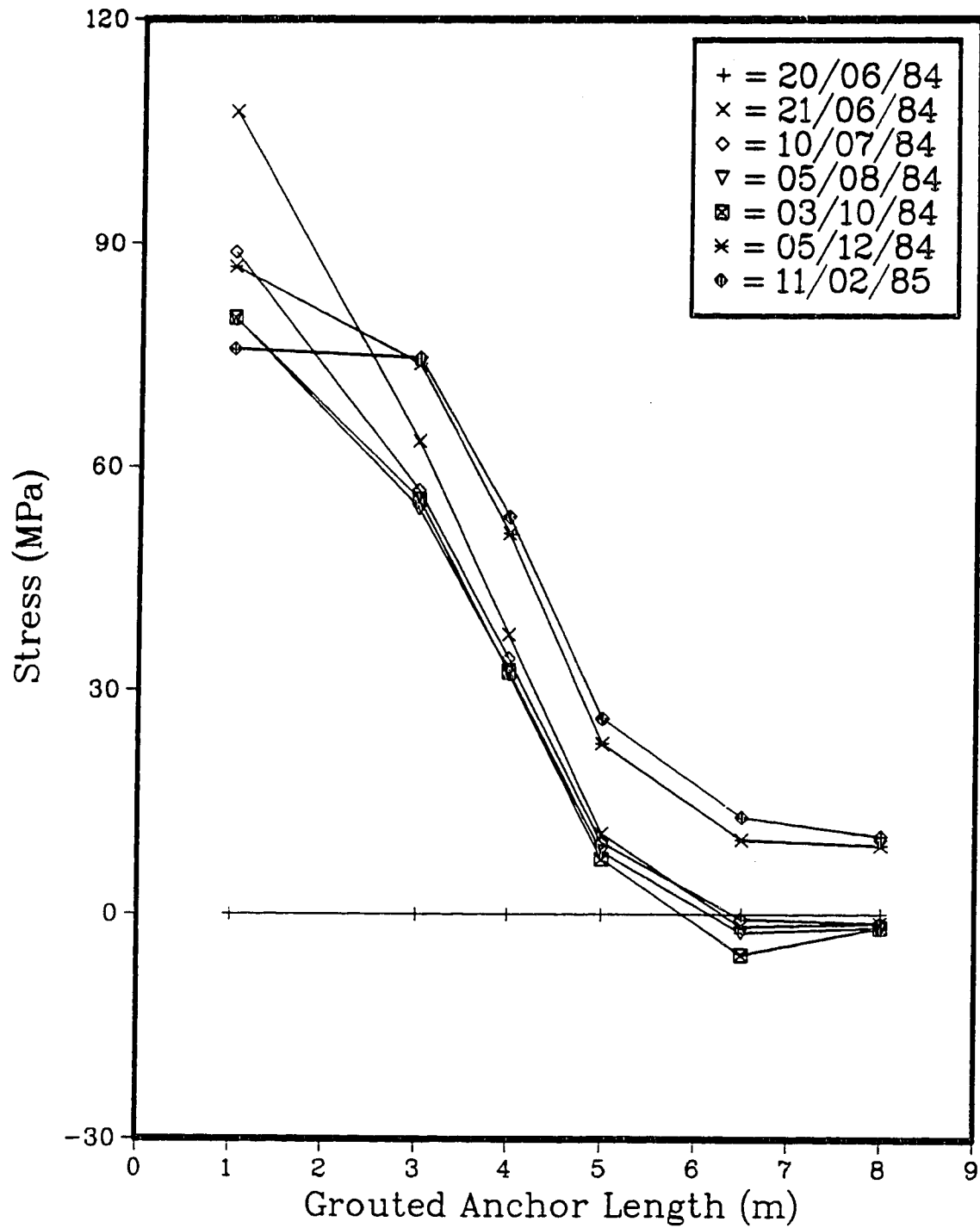


Figure B.9: Stress vs length for Anchor E, early epochs.

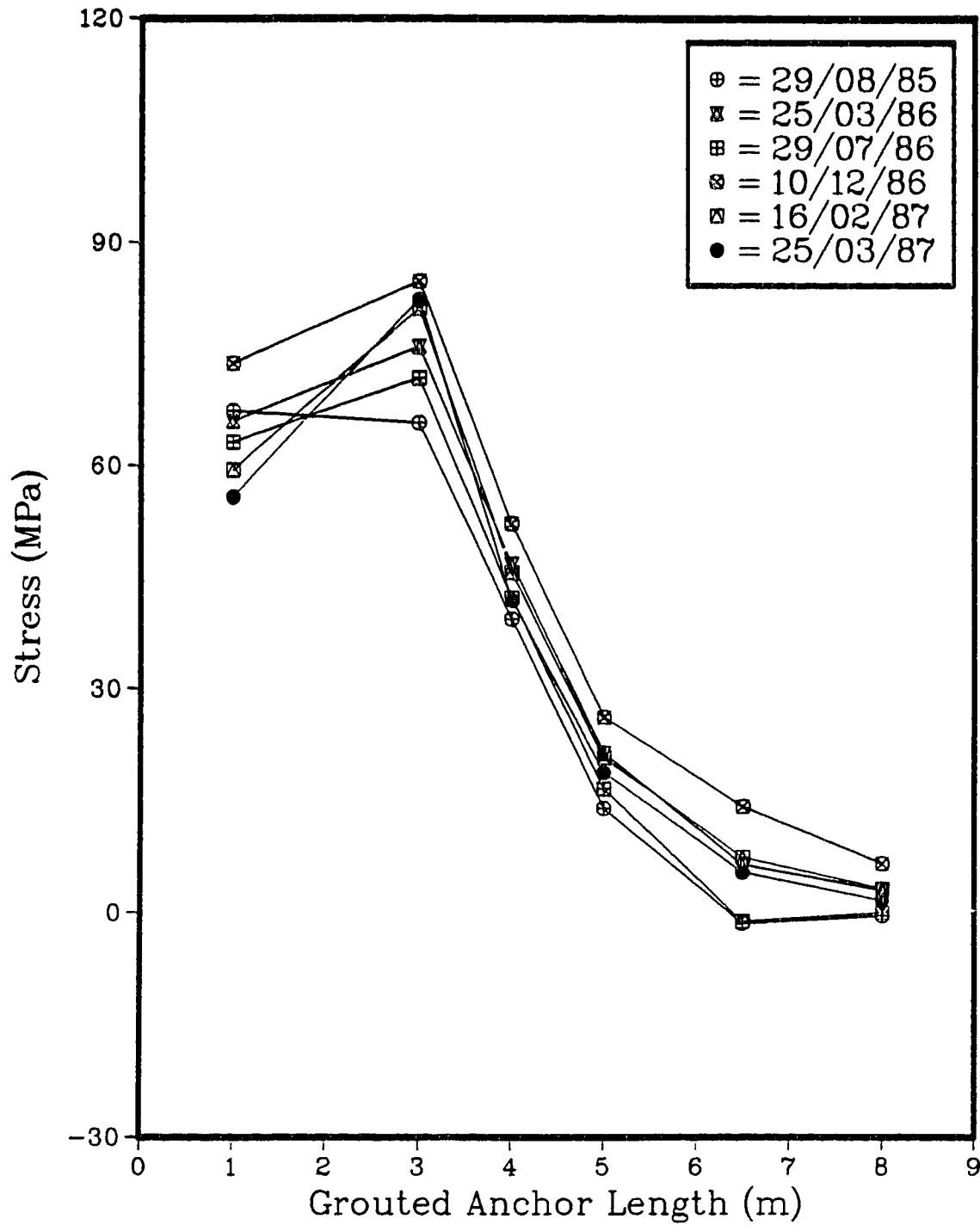


Figure B.10: Stress vs length for Anchor E, late epochs.

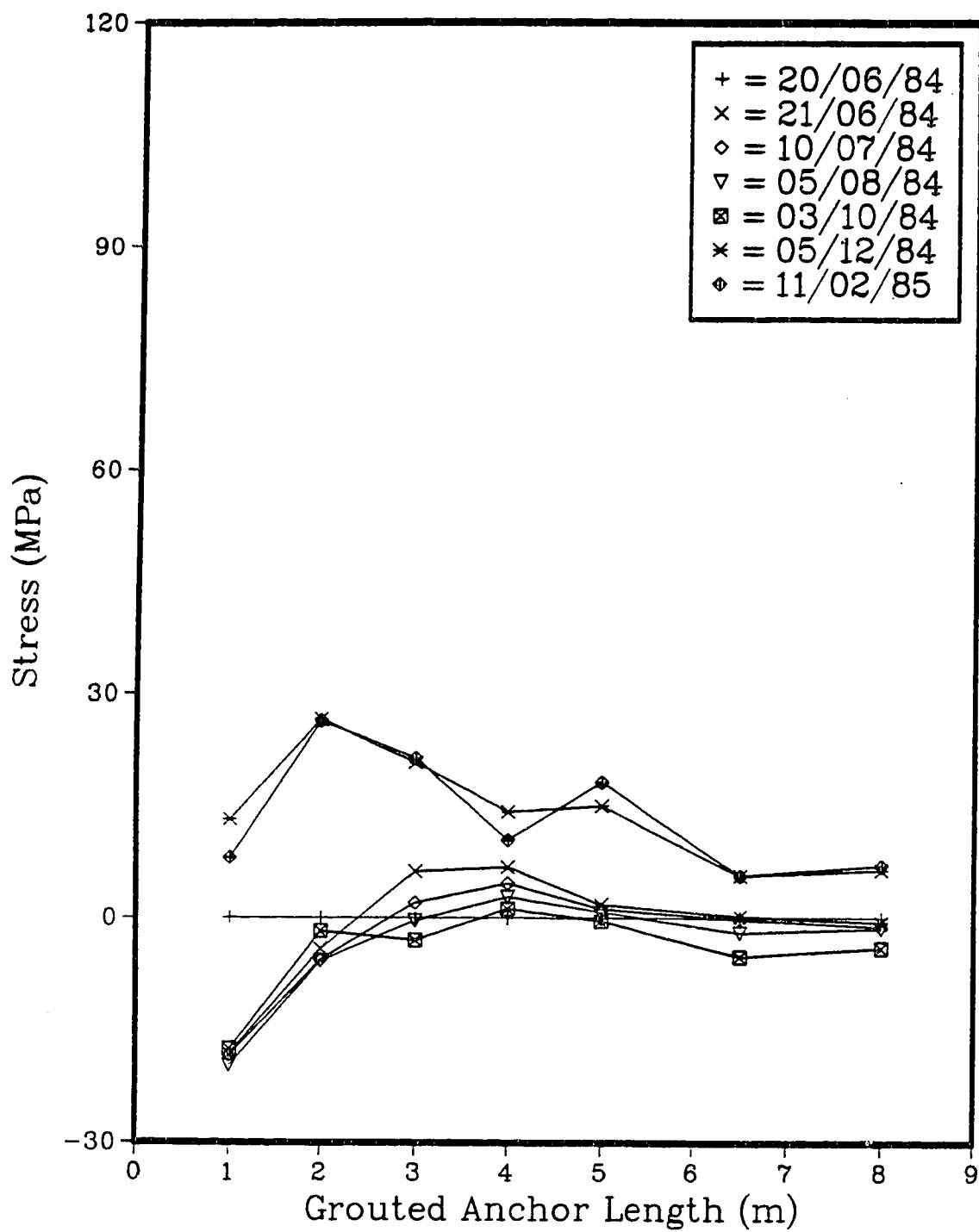


Figure B.11: Stress vs length for Anchor F, early epochs.

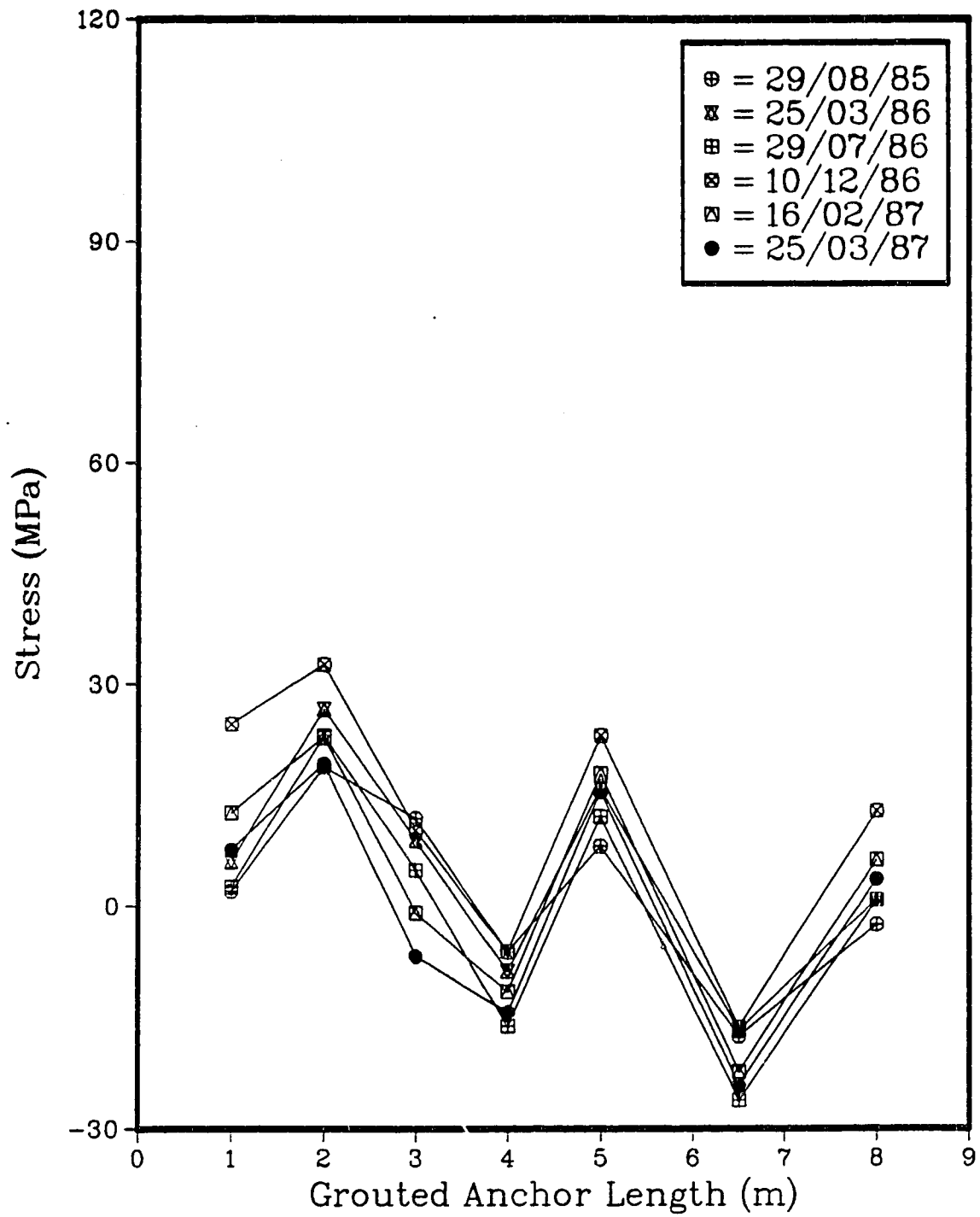


Figure B.12: Stress vs length for Anchor F, late epochs.

Appendix C
Earth Pressure Distributions based on the Wall Mounted
Strain Gauges

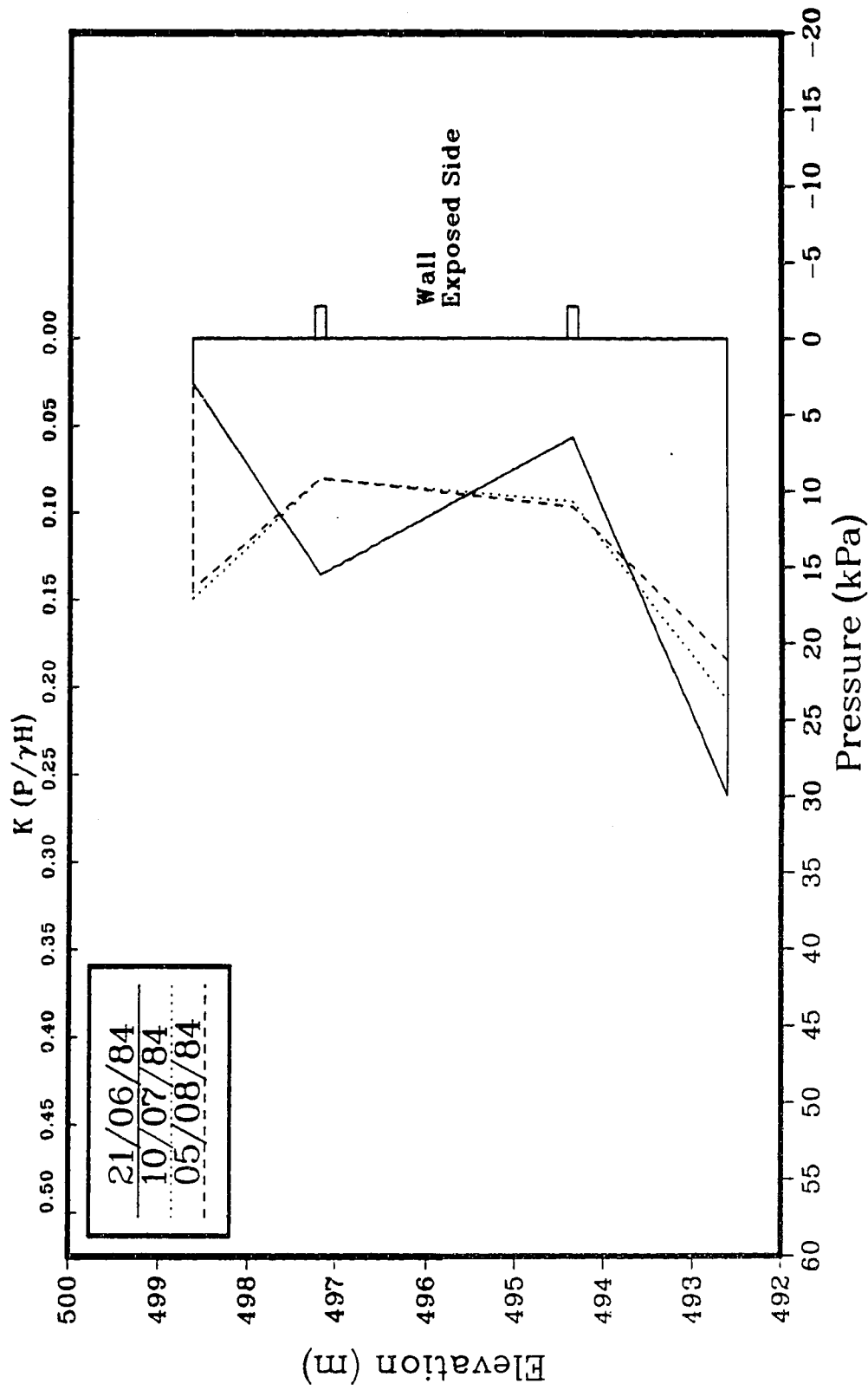


Figure C.1: Earth pressure distributions, east section.

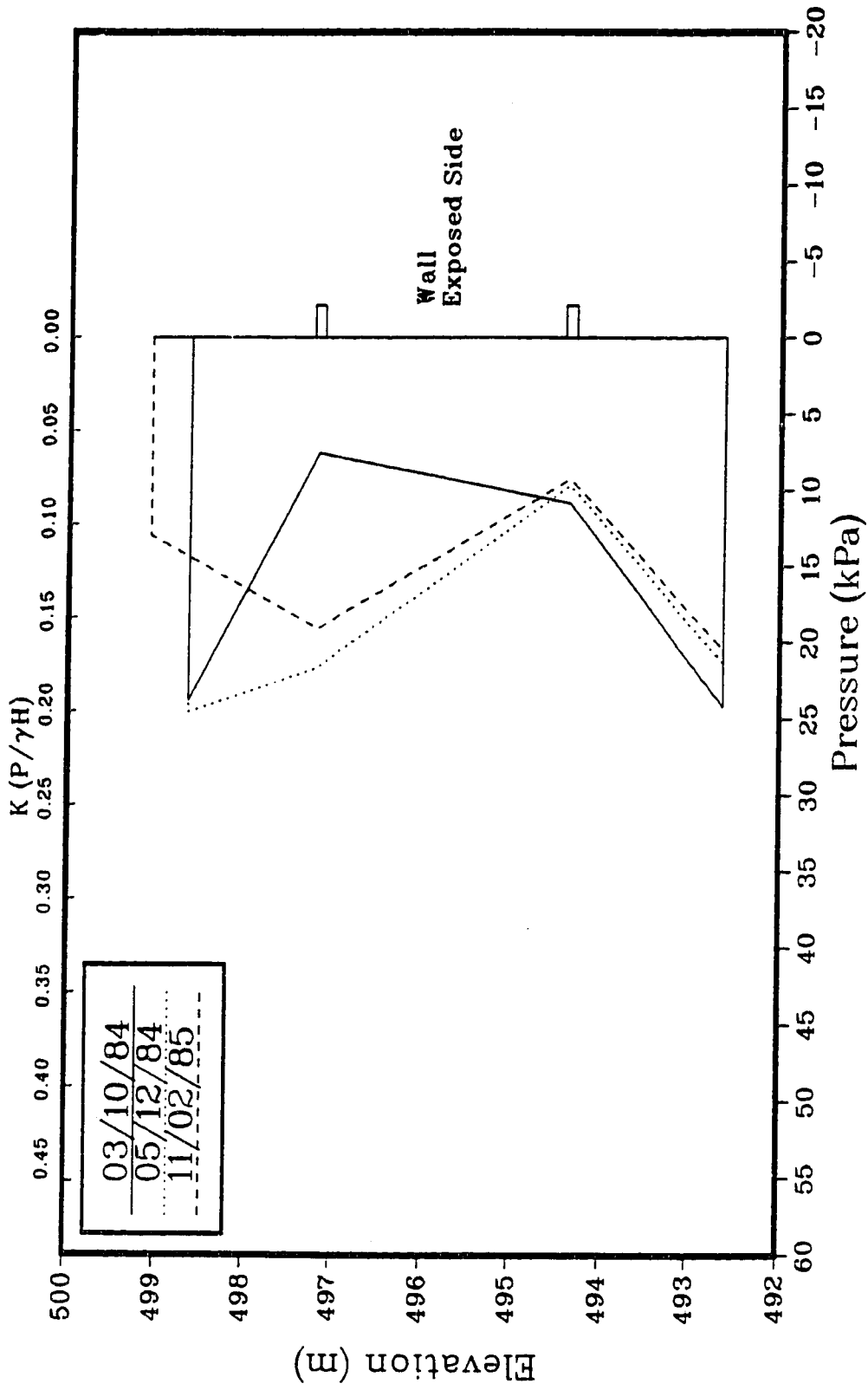


Figure C.2: Earth pressure distributions, east section.

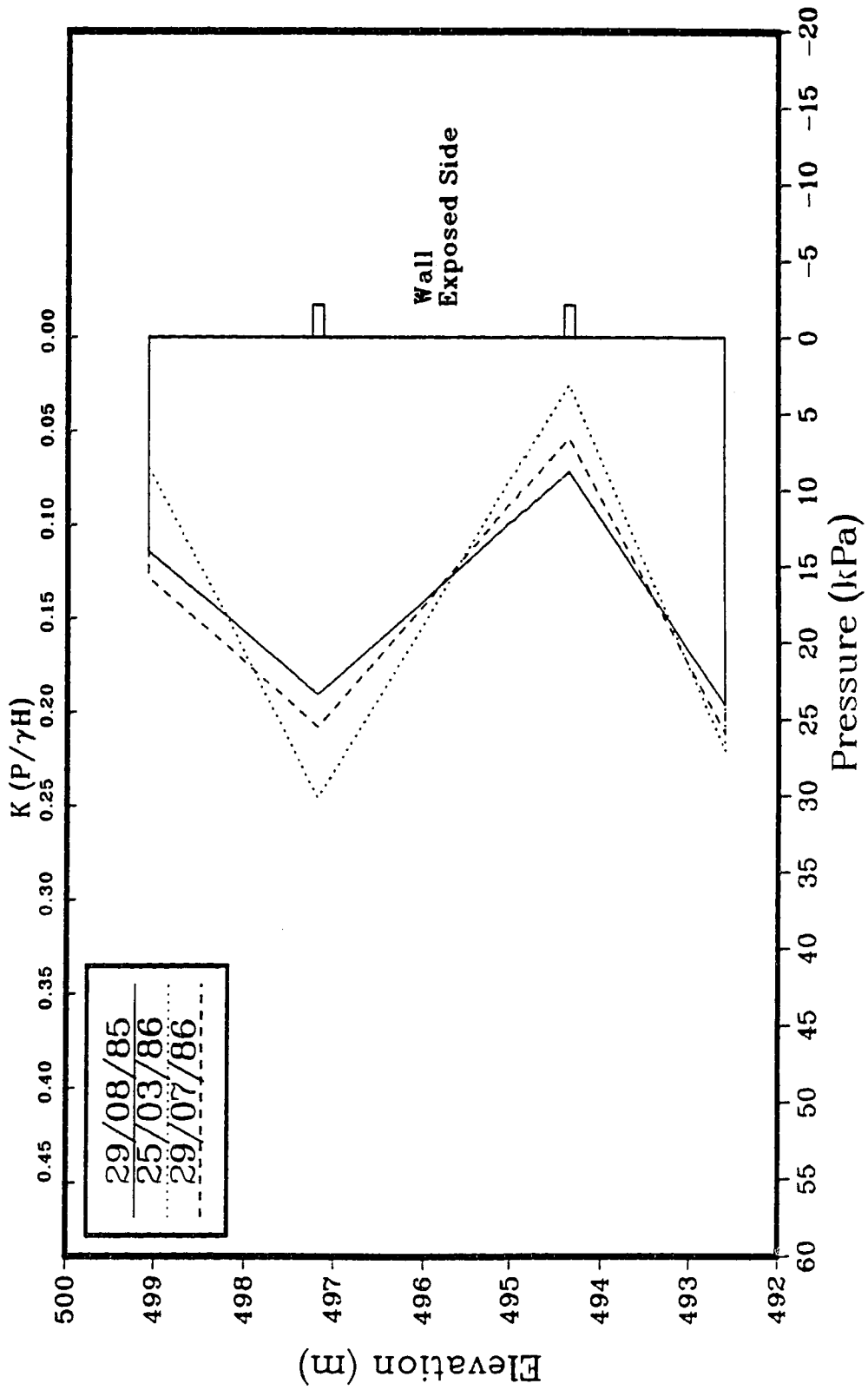


Figure C.3: Earth pressure distributions, east section.

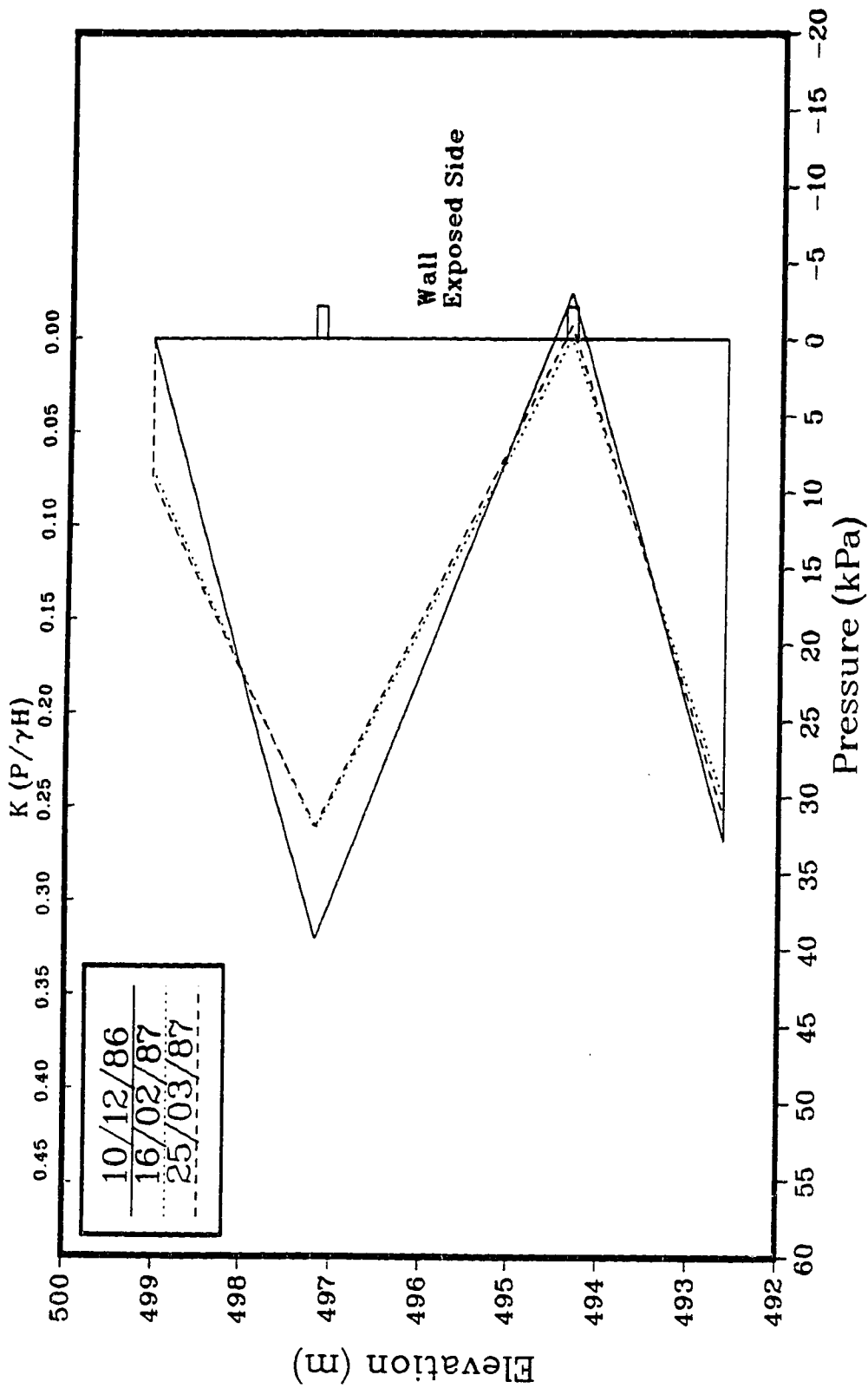


Figure C.4: Earth pressure distributions, east section.

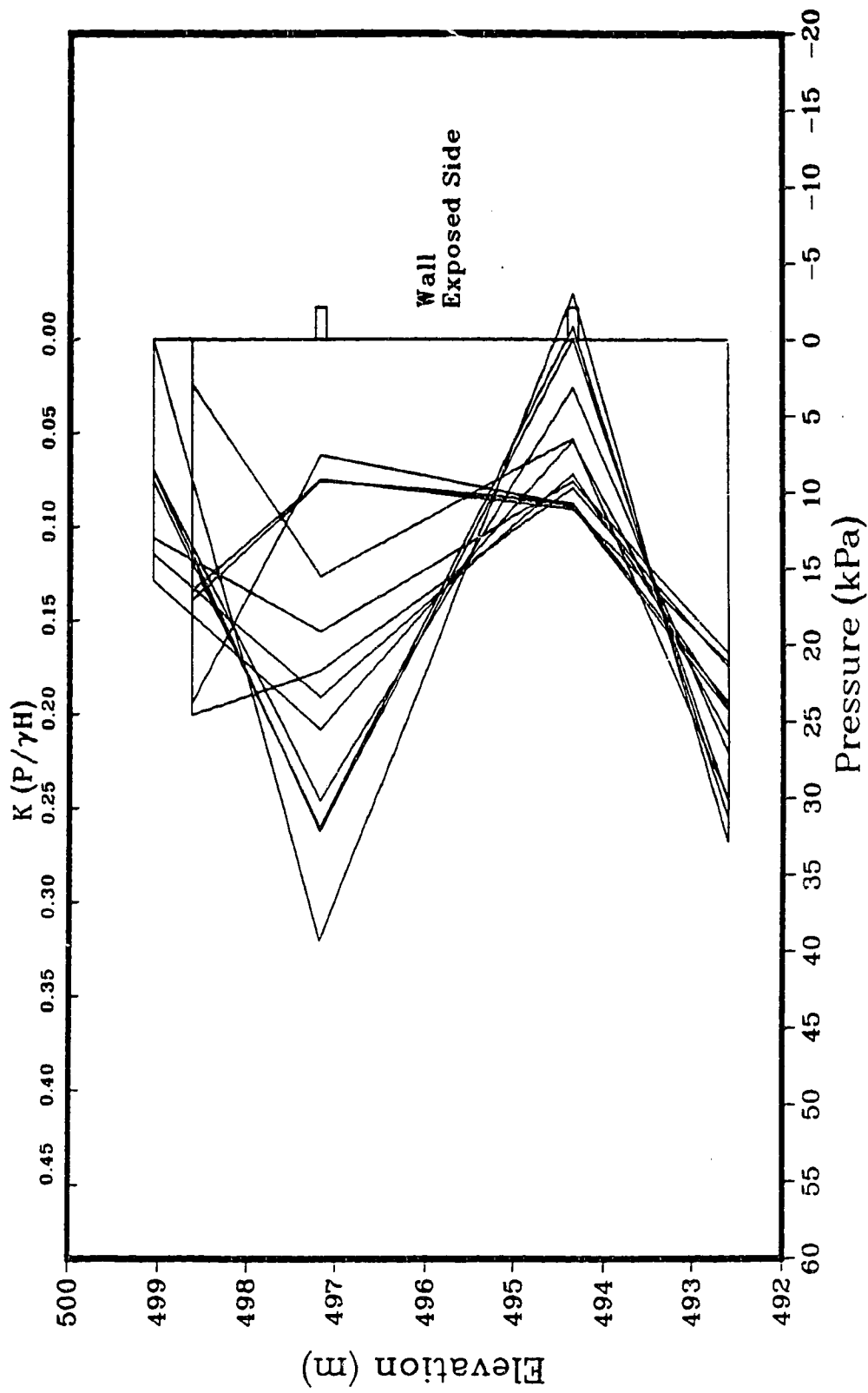


Figure C. 5: Summary of east section, earth pressure distributions.

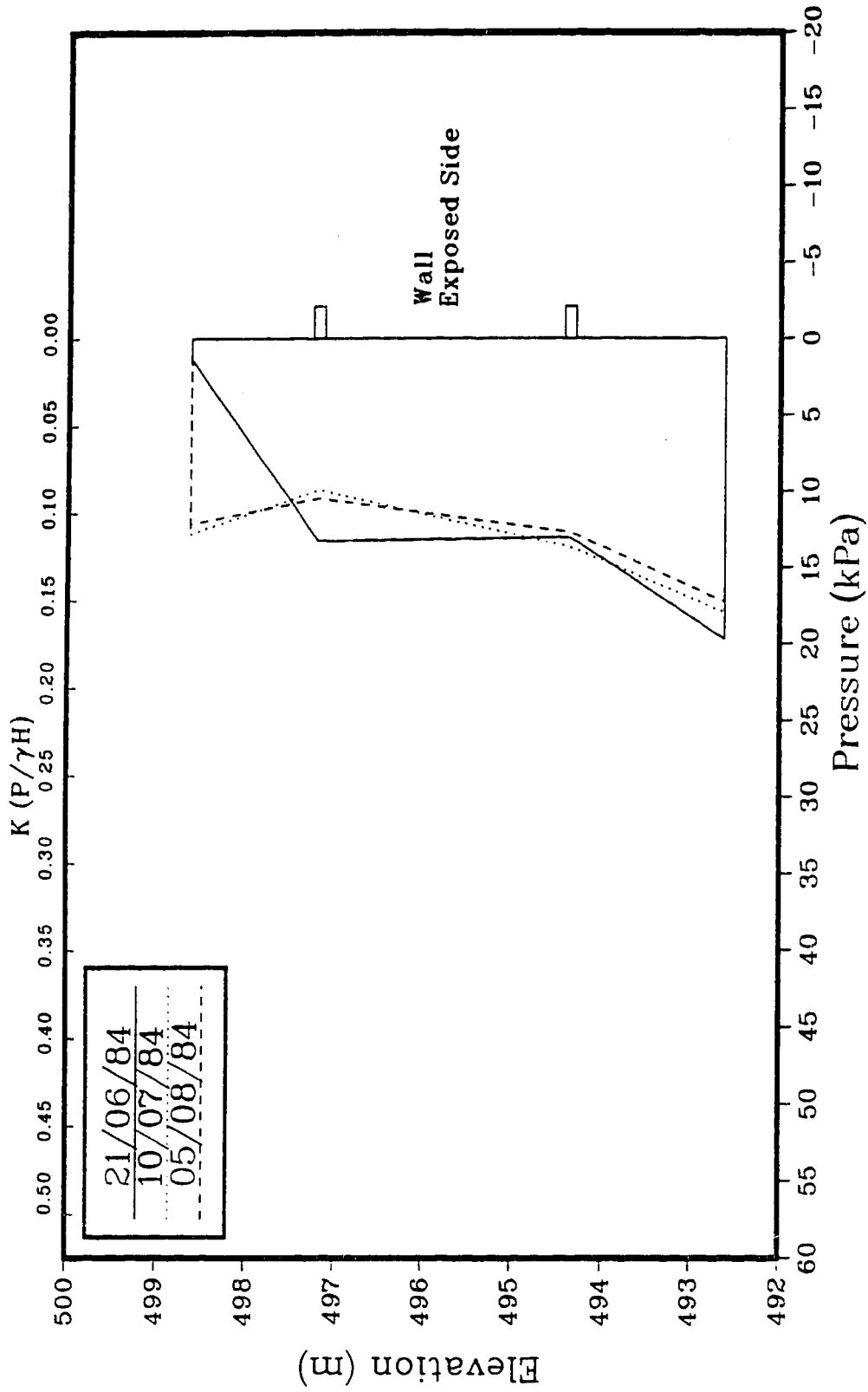


Figure C.6: Earth pressure distributions, west section.

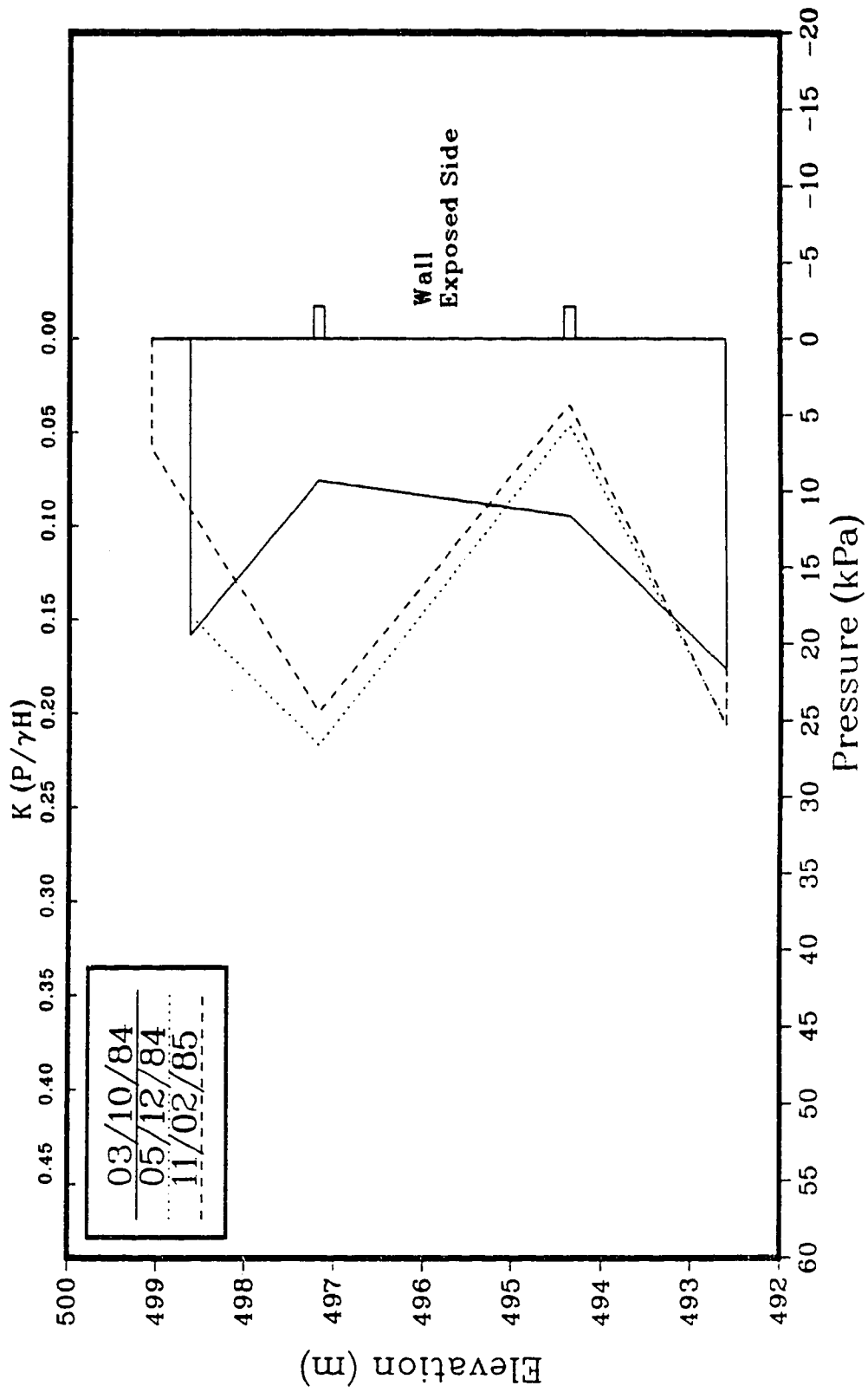


Figure C.7: Earth pressure distributions, west section.

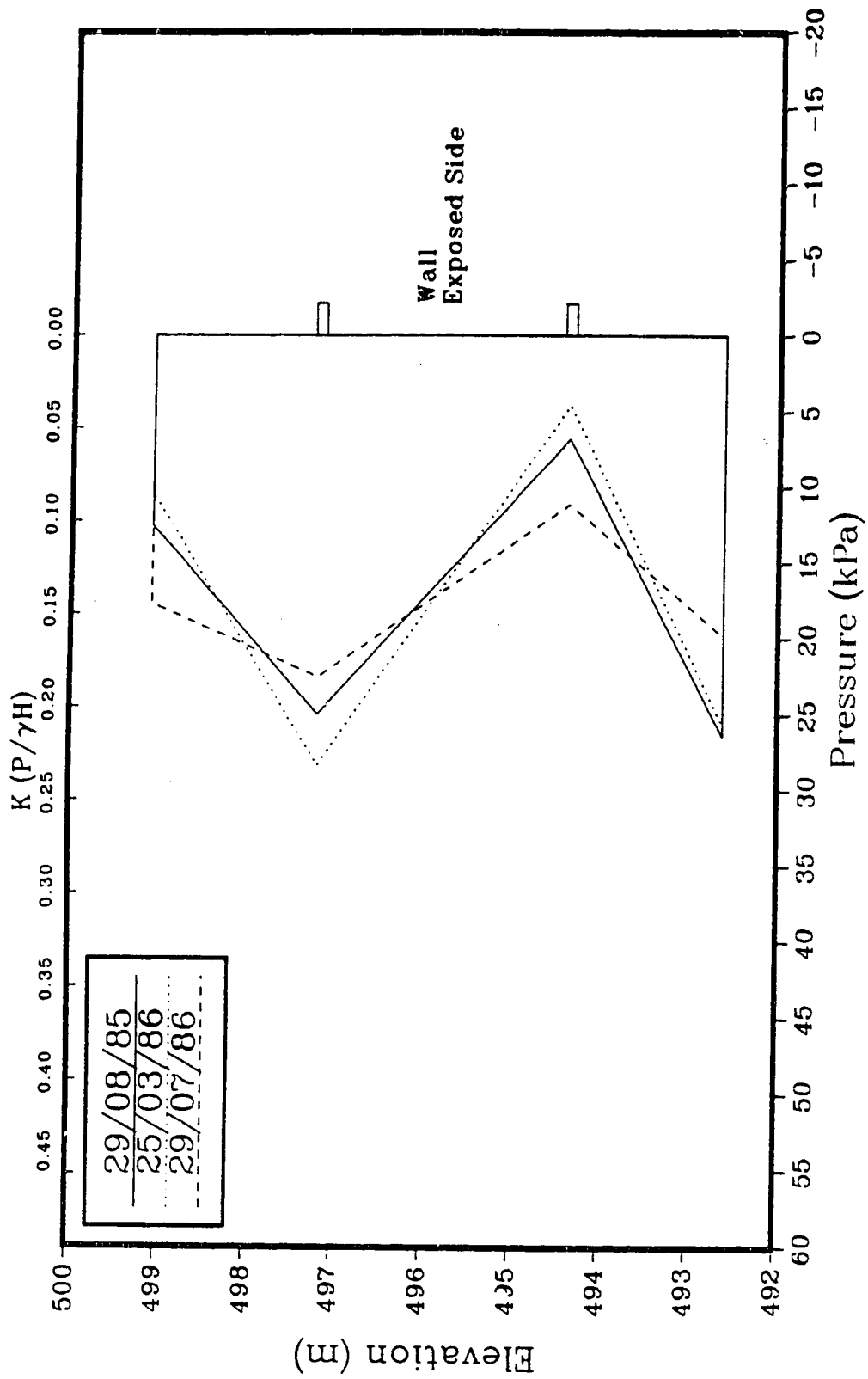


Figure C.8: Earth pressure distributions, west section.

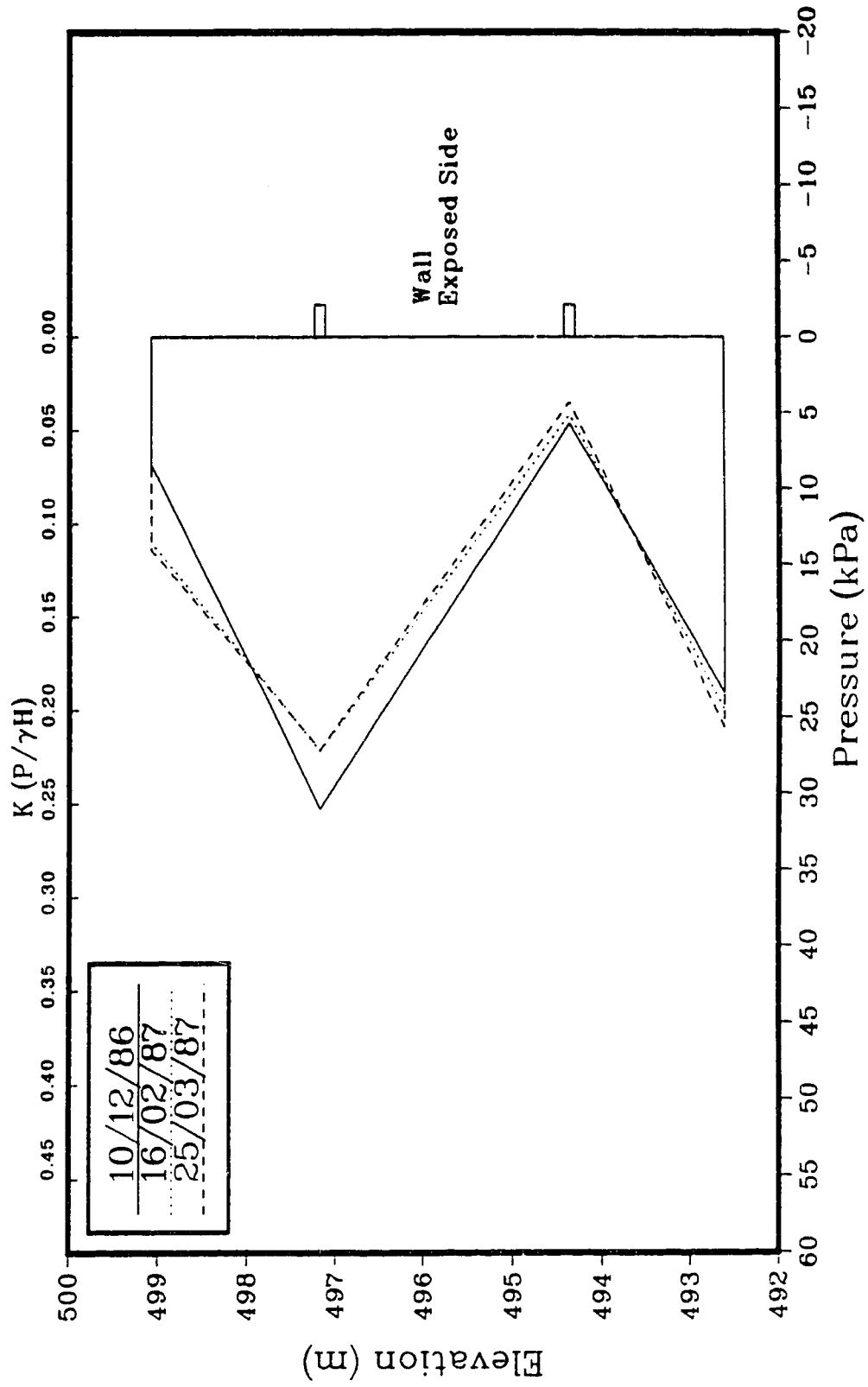


Figure C.9: Earth pressure distributions, west section.

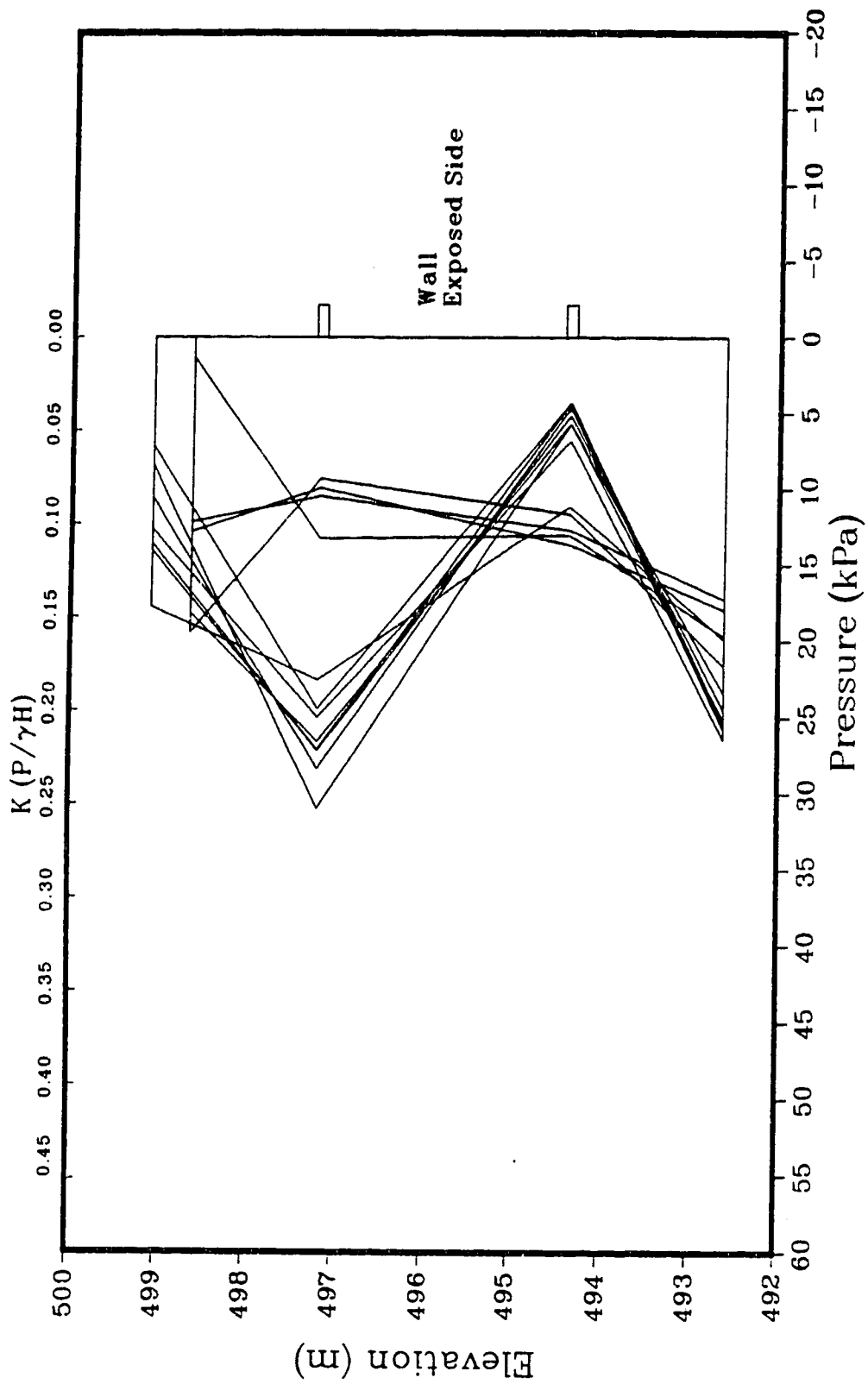


Figure C.10: Summary of west section, earth pressure distributions.

Appendix D
Displacements of the East Wall as Determined by Surveying.

Survey Position (Elevation)	Date (Day Number)										
	21/06/84 (21)	10/07/84 (40)	05/08/84 (66)	03/10/84 (125)	05/12/84 (185)	25/08/85 (451)	30/07/86 (789)	10/12/86 (925)	28/03/87 (1028)		
A1 (493.05)	0.0	-2.7	1.7	-	-	8.3	9.8	10.0	6.8		
A2 (493.51)	0.0	-1.7	2.4	-	-	5.4	6.6	7.6	5.4		
A3 (493.95)	0.0	-3.9	-1.2	-	-	6.1	8.1	7.6	7.1		
A4 (494.82)	0.0	-3.9	-1.7	-	-	1.2	3.7	3.4	2.0		
A5 (495.90)	0.0	-1.2	0.7	-	-	1.2	1.5	1.5	0.5		
A6 (496.83)	0.0	-0.7	0.5	-	-	1.2	2.0	2.0	0.7		
A7 (497.45)	0.0	-	3.4	-	-	2.4	5.4	3.2	2.4		
A8 (497.96)	0.0	-	-	-	-	4.4	6.6	6.1	4.2		
B2 (494.92)	0.0	-3.2	-0.7	-	-	-	-	3.7	4.2		
B3 (495.99)	0.0	-2.0	-0.7	-	-	2.2	3.7	3.4	2.0		
B4 (496.54)	0.0	-1.0	1.0	-	-	3.4	2.9	4.4	2.9		
B5 (497.65)	0.0	-0.2	1.5	-	-	2.4	3.7	4.9	2.9		
C2 (494.92)	0.0	-1.7	-0.5	2.4	6.8	-	3.7	5.1	4.2		
C3 (495.97)	0.0	-2.4	0.5	3.4	6.1	2.0	4.4	4.4	2.9		
C4 (496.53)	0.0	-2.4	0.0	2.7	5.1	0.2	3.4	3.4	1.2		
C5 (497.65)	0.0	0.7	2.2	7.1	6.6	2.9	3.9	4.2	2.7		
D1 (493.05)	0.0	-2.2	0.2	-	7.3	-	-	-	-		
D2 (493.61)	0.0	-3.9	0.0	2.2	5.9	1.7	5.4	4.9	4.6		
D3 (494.00)	0.0	-4.2	-0.5	-	-	-	-	2.9	2.4		
D4 (494.49)	0.0	-	0.2	-	-	-	-	2.4	1.7		
D5 (494.79)	0.0	-	-1.2	-	-	0.7	3.2	2.0	1.5		
D6 (495.85)	0.0	-3.2	-1.5	1.5	3.9	-0.2	1.7	0.2	-1.0		
D7 (496.81)	0.0	-0.7	0.5	3.9	5.4	0.7	2.4	1.0	0.2		
D8 (497.45)	0.0	-1.2	0.0	4.4	3.9	0.2	0.0	-0.2	-0.7		
D9 (497.94)	0.0	-0.2	1.2	5.1	5.1	-1.2	2.0	0.2	-0.2		

Table D.1: Survey displacement results, east wall.

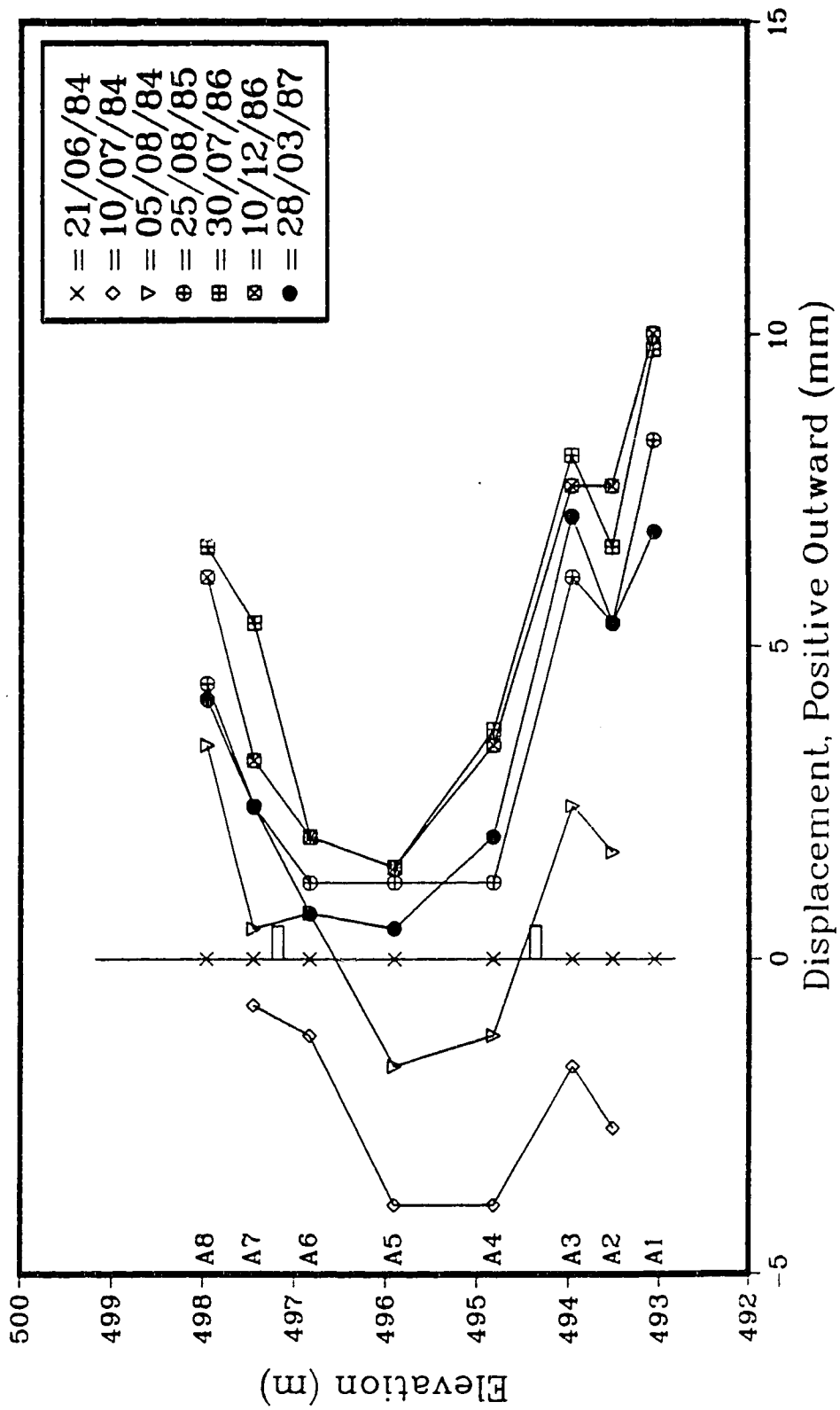


Figure D.1: Survey displacements, Column A.

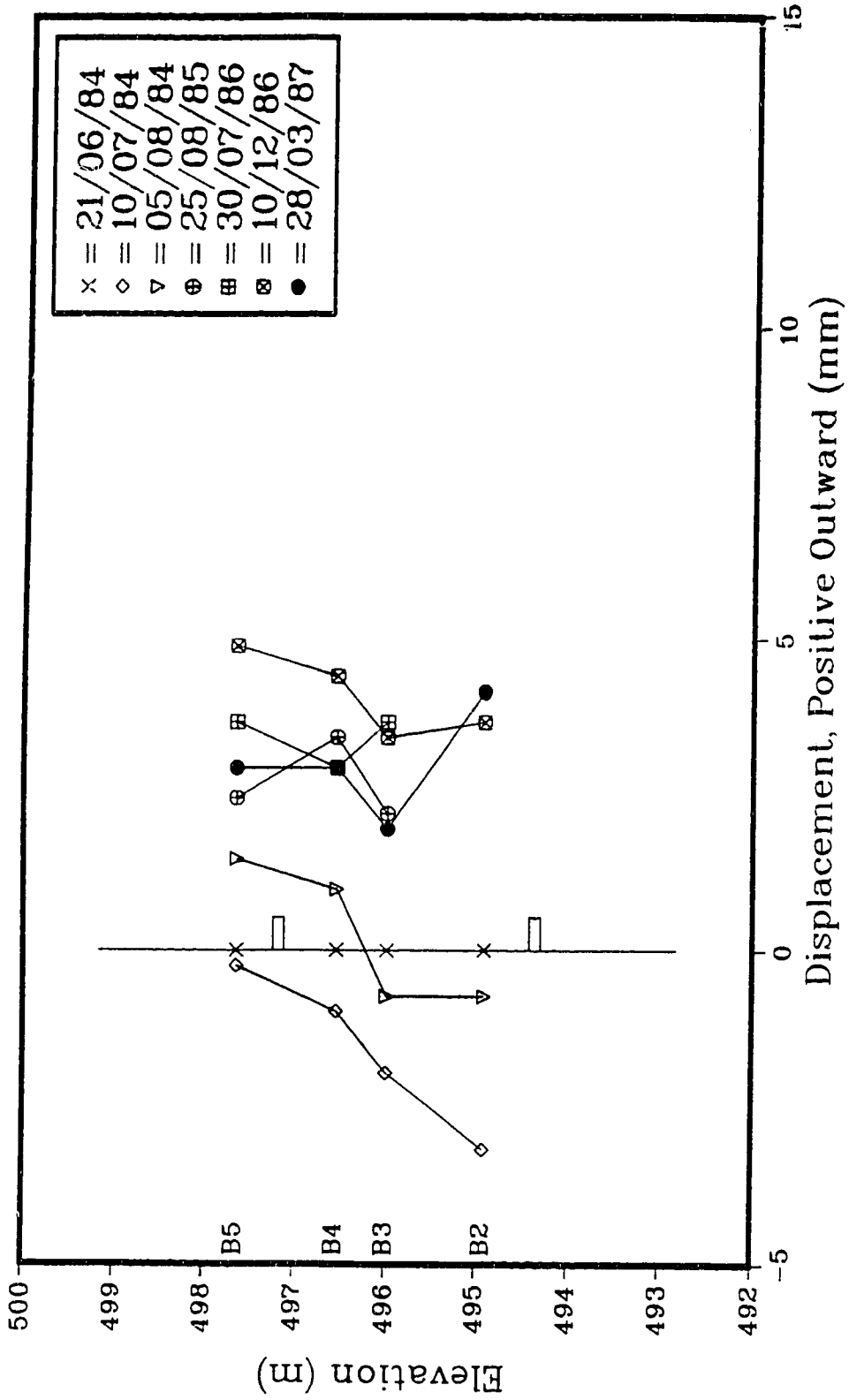


Figure D.2: Survey displacements, Column B.

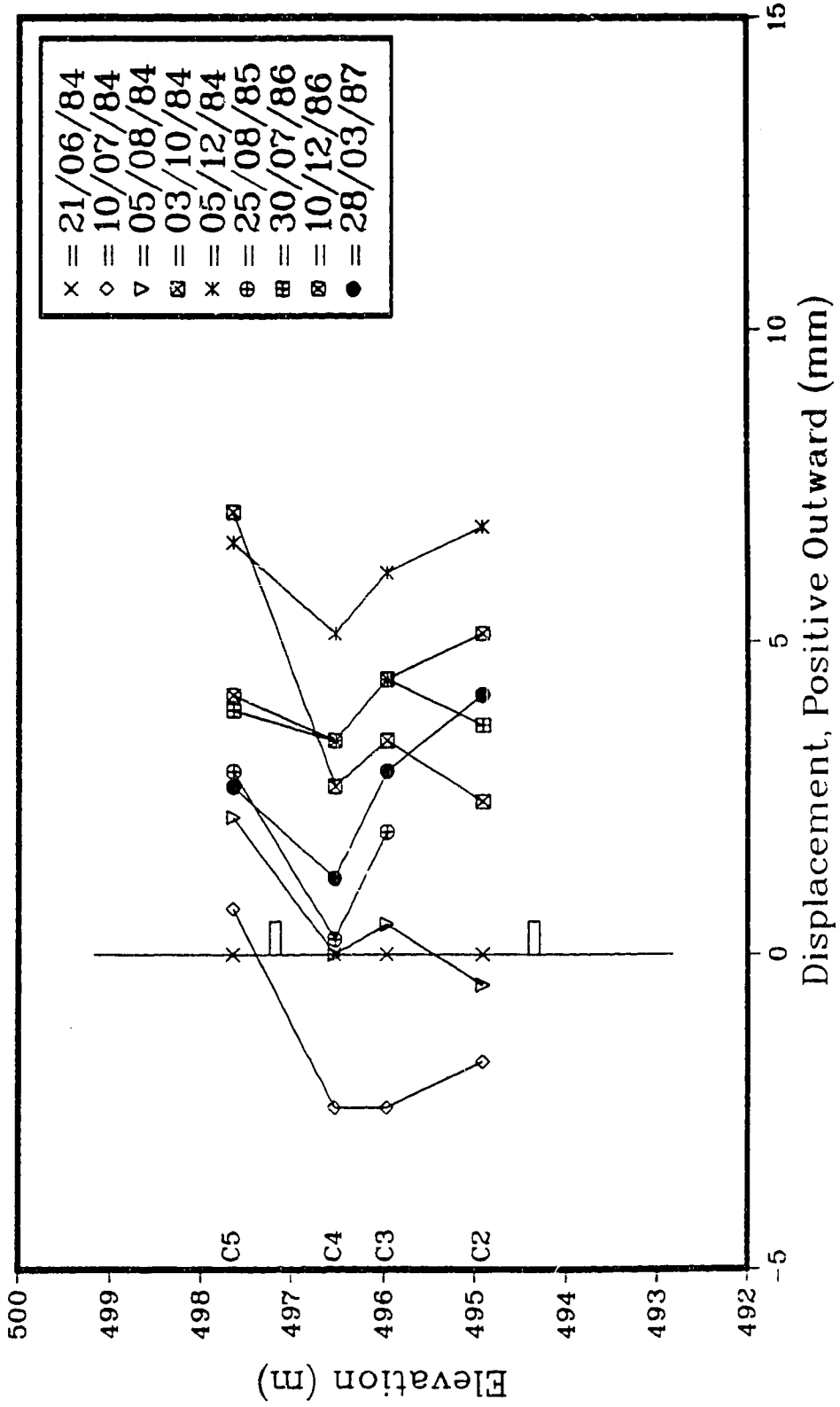


Figure D.3: Survey displacements, Column C.

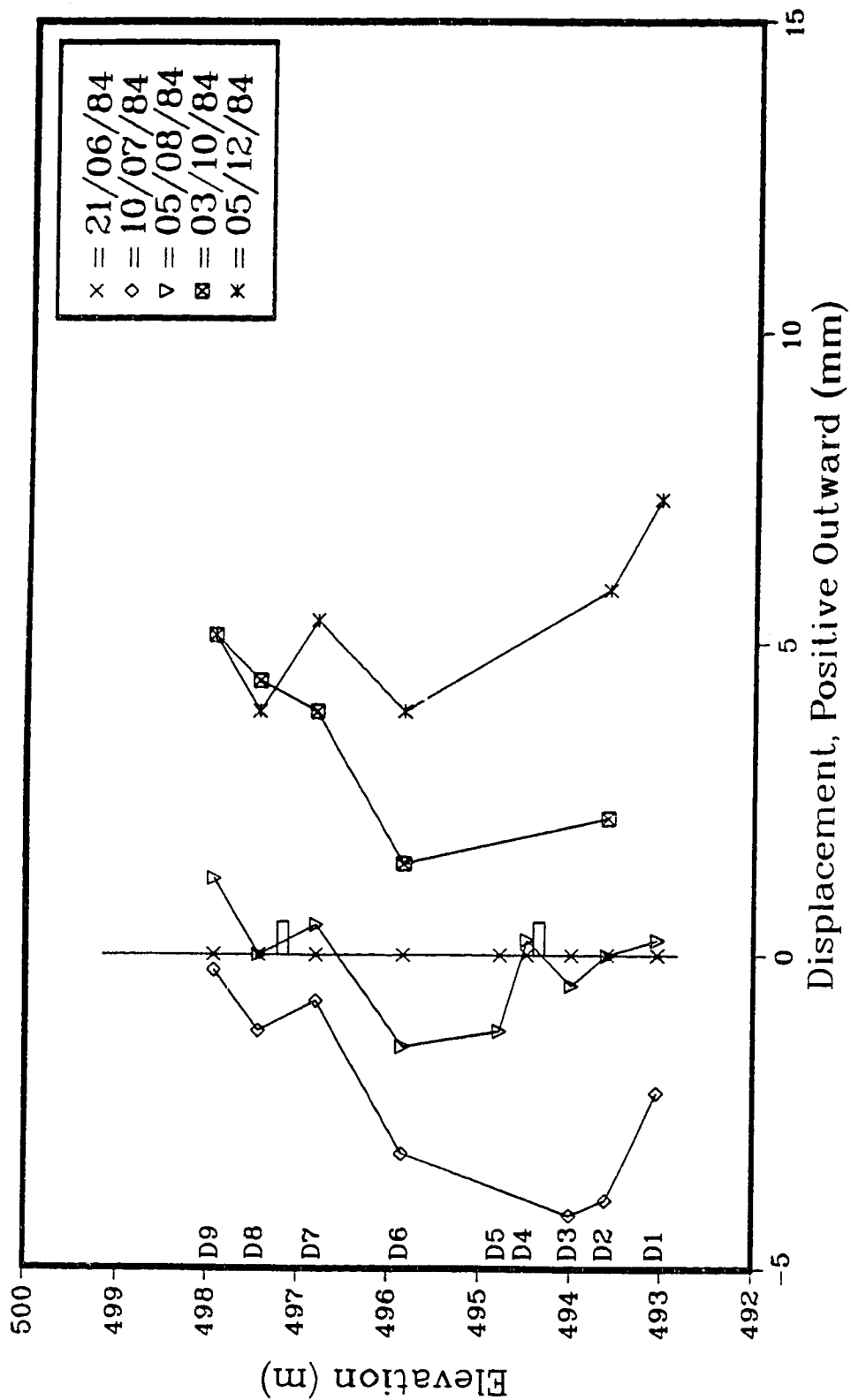


Figure D.4: Survey displacements, early epochs, Column D.

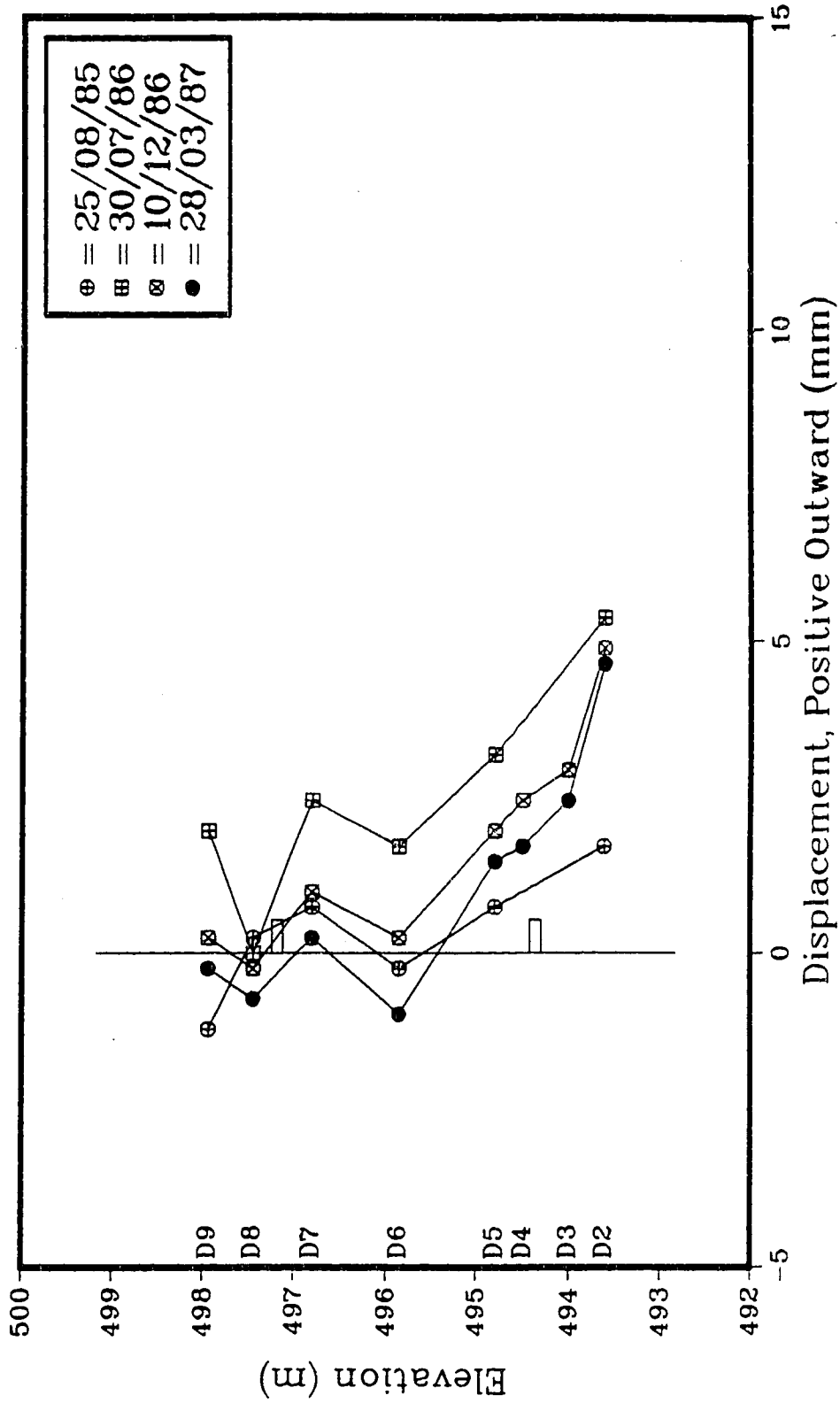


Figure D.5: Survey displacements, late epochs, Column D.

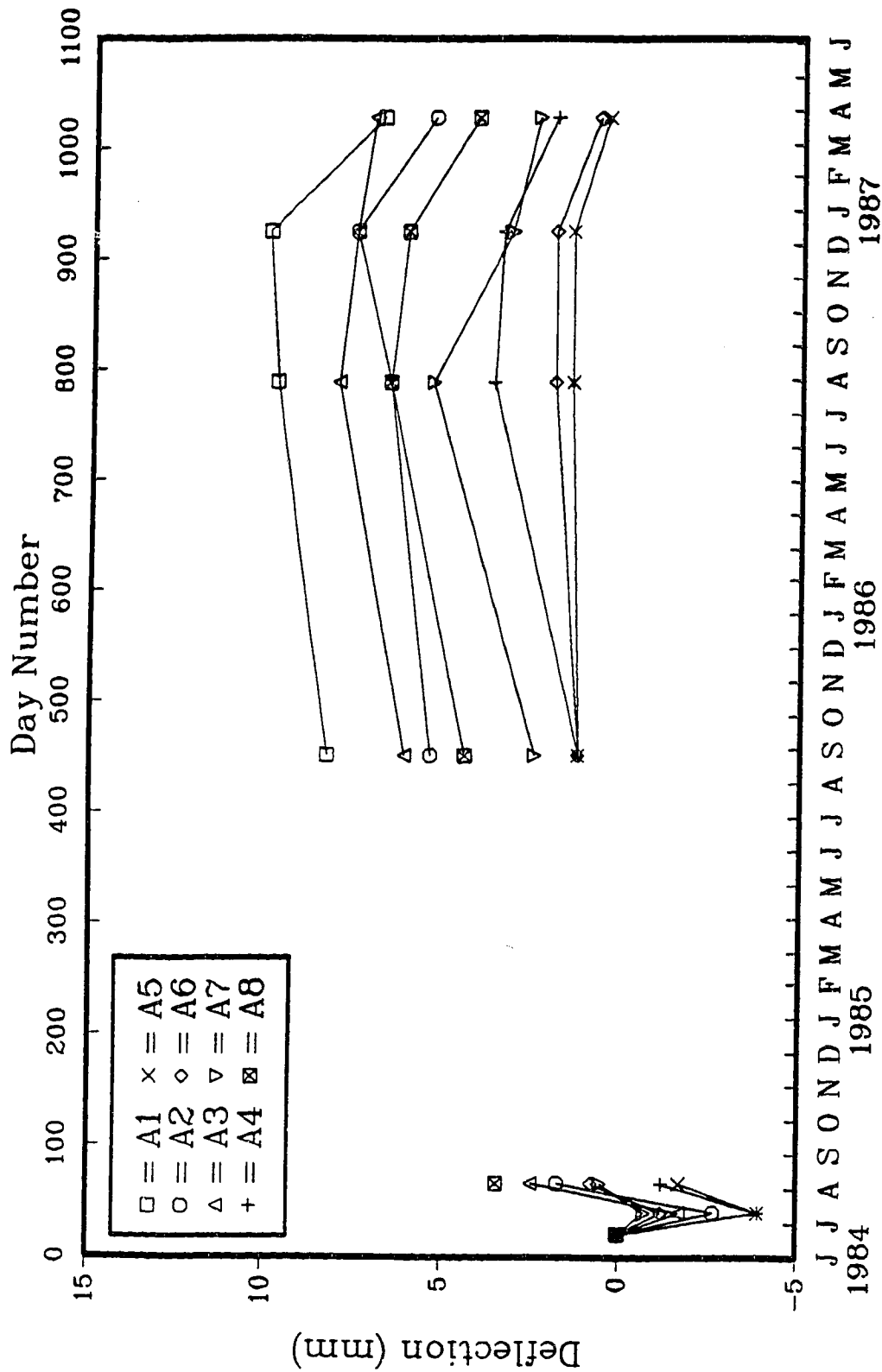


Figure D.6: Survey displacements with time, Column A.

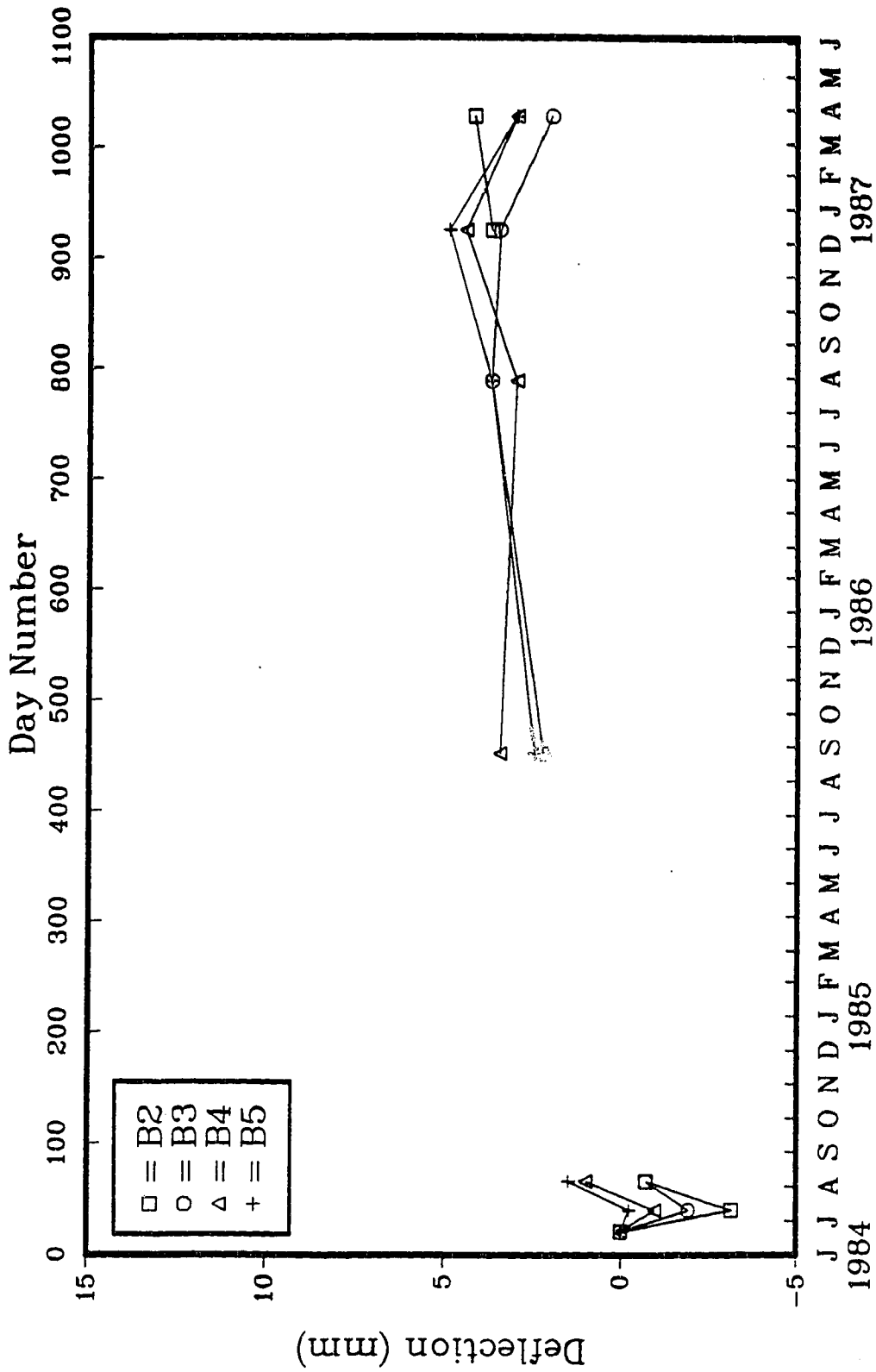


Figure D.7: Survey displacements with time, Column B.

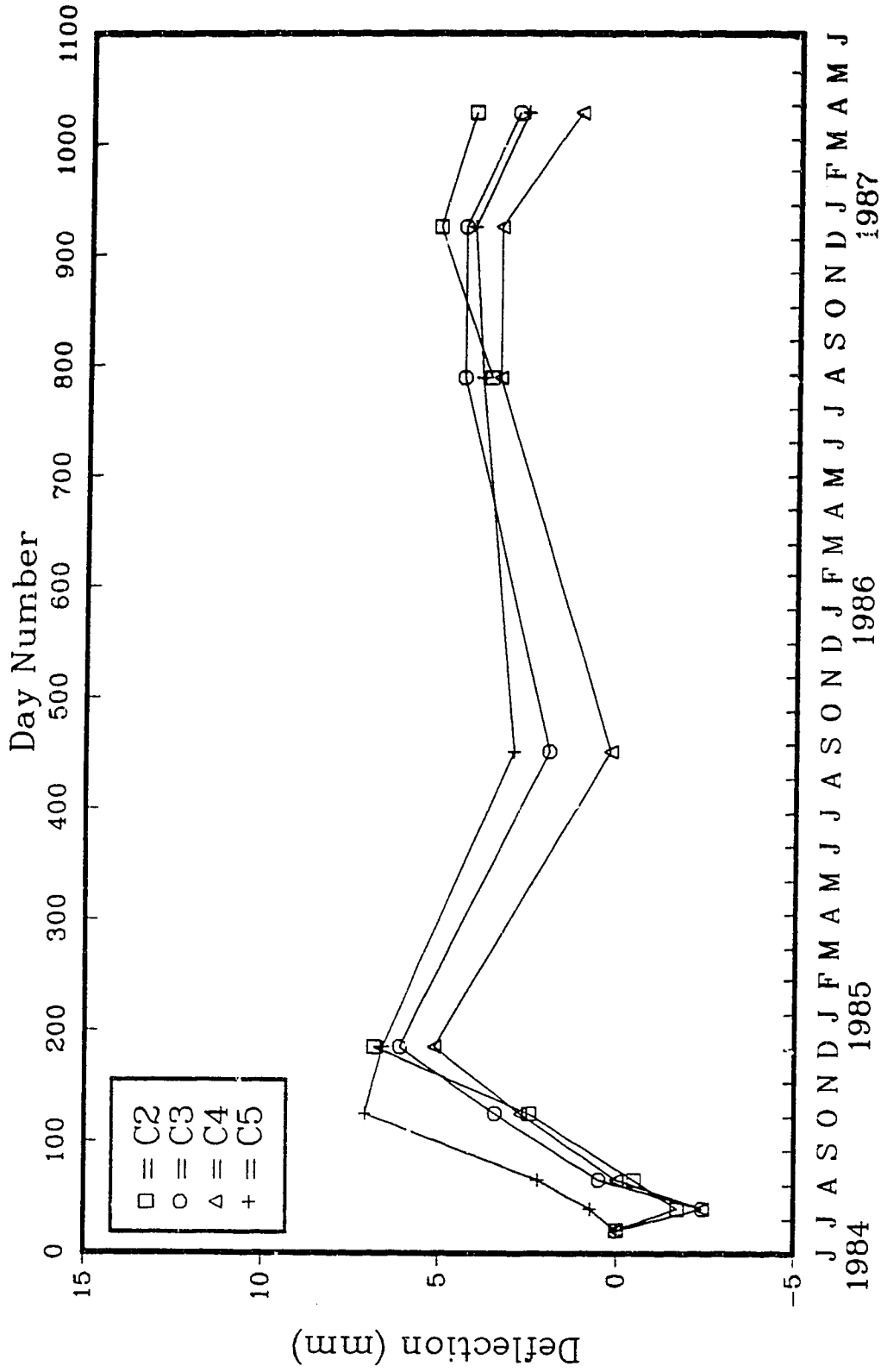


Figure D.8: Survey displacements with time, Column C.

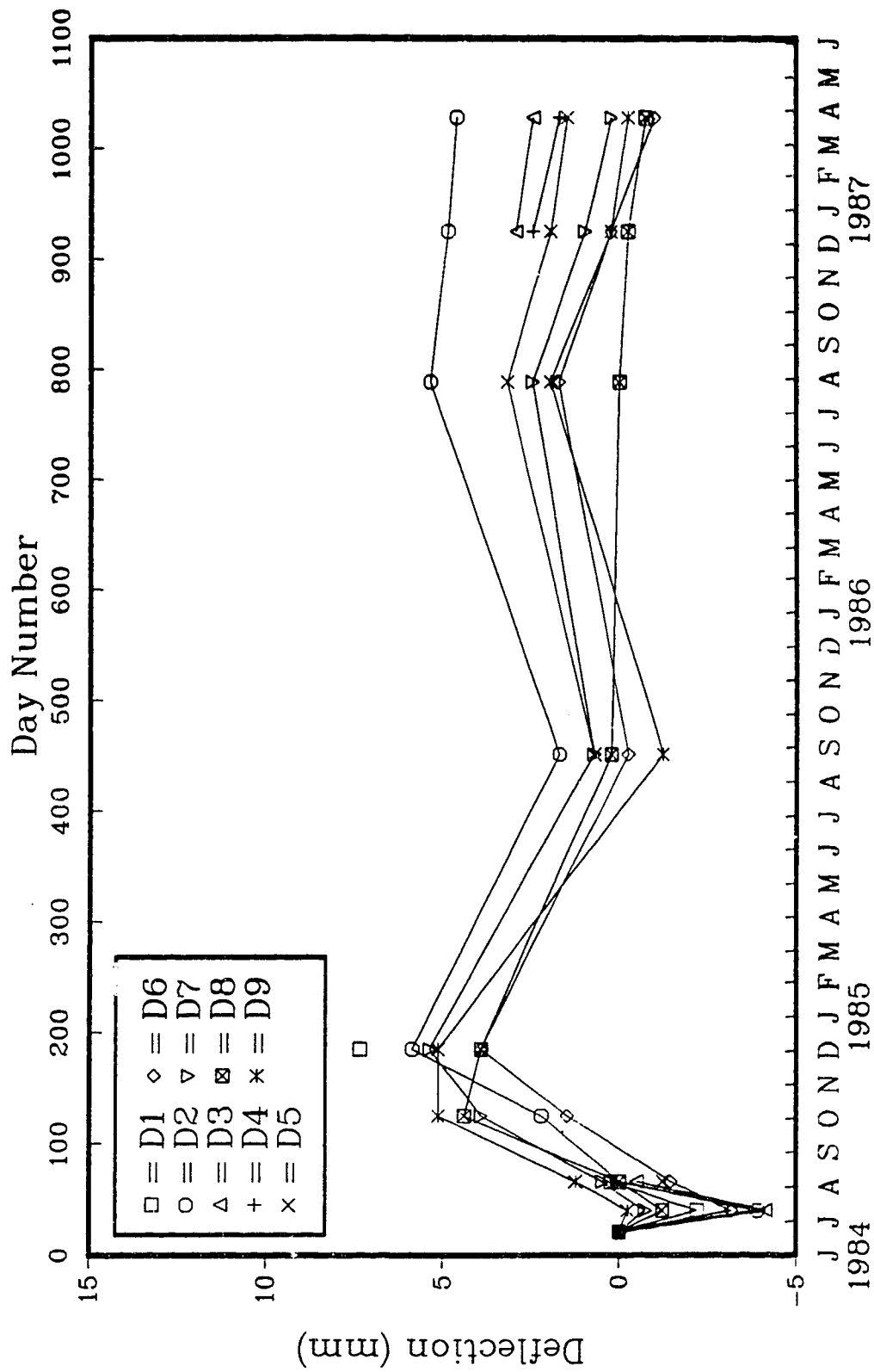


Figure D.9: Survey displacements with time, Column D.

Appendix E
Slope Indicator Results

A Direction

Elev. (m)	A1	A2	A1-A2
493.55	-3268	3306	-6574
494.15	-3226	3262	-6488
494.75	-3204	3236	-6440
495.35	-3143	3159	-6302
495.95	-3208	3260	-6468
496.55	-3214	3238	-6452
497.15	-3156	3182	-6338
497.75	-3110	3144	-6254

B Direction

Elev. (m)	B1	B2	B1-B2
493.55	154	-128	282
494.15	151	-116	267
494.75	119	-89	208
495.35	179	-152	331
495.95	52	-7	59
496.55	86	-51	137
497.15	104	-62	166
497.75	90	-54	144

Table E.1: VSI1, calibration values, 21/06/84

A Direction

Elev. (m)	A1	A2	A1-A2	CHANGE	SOC	Deflec (mm)
493.55	-3275	3309	-6584	-10	-10	-0.20
494.15	-3226	3268	-6494	-6	-16	-0.29
494.75	-3209	3245	-6454	-14	-30	-0.50
495.35	-3138	3163	-6301	1	-29	-0.49
495.95	-3200	3249	-6449	19	-10	-0.20
496.55	-3185	3219	-6404	48	38	0.53
497.15	-3123	3140	-6263	75	113	1.68
497.75	-3046	3090	-6136	118	231	3.47

B Direction

Elev. (m)	B1	B2	B1-B2	CHANGE	SOC	Deflec (mm)
493.55	154	-158	312	30	30	0.46
494.15	134	-126	260	-7	23	0.35
494.75	162	-153	315	107	130	1.98
495.35	198	-181	379	48	178	2.71
495.95	25	-6	31	-28	150	2.29
496.55	77	-70	147	10	160	2.44
497.15	123	-104	227	61	221	3.37
497.75	94	-72	166	22	243	3.70

Table E.2: VS11, results from 05/08/84.

A Direction

Elev. (m)	A1	A2	A1-A2	CHANGE	SOC	Deflec (mm)
493.55	-3285	3328	-6613	-39	-39	2.99
494.15	-3230	3276	-6506	-18	-57	2.71
494.75	-3210	3251	-6461	-21	-78	2.39
495.35	-3147	3177	-6324	-22	-100	2.06
495.95	-3203	3259	-6462	6	-94	2.15
496.55	-3193	3224	-6417	35	-59	2.68
497.15	-3120	3144	-6264	74	15	3.81
497.75	-3047	3096	-6143	111	126	5.50

B Direction

Elev. (m)	B1	B2	B1-B2	CHANGE	SOC	Deflec (mm)
493.55	175	-128	303	21	21	0.32
494.15	164	-138	302	35	56	0.85
494.75	180	-154	334	126	182	2.77
495.35	218	-189	407	76	258	3.93
495.95	38	-9	47	-12	246	3.75
496.55	100	-79	179	42	288	4.39
497.15	135	-111	246	80	368	5.61
497.75	122	-101	223	79	447	6.81

Table E.3: VSI1, results from 03/10/84.

A Direction

Elev. (m)	A1	A2	A1-A2	CHANGE	SOC	Deflec (mm)
493.55	-3273	3306	-6579	-5	-5	5.72
494.15	-3206	3246	-6452	36	31	6.27
494.75	-3180	3214	-6394	46	77	6.97
495.35	-3221	3144	-6365	-63	14	6.01
495.95	-3203	3258	-6461	7	21	6.12
496.55	-3190	3212	-6402	50	71	6.88
497.15	-3115	3138	-6253	85	156	8.17
497.75	-3048	3088	-6136	118	274	9.97

B Direction

Elev. (m)	B1	B2	B1-B2	CHANGE	SOC	Deflec (mm)
493.55	260	-268	528	246	246	3.75
494.15	235	-251	486	219	465	7.09
494.75	274	-292	566	358	823	12.54
495.35	309	-315	624	293	1116	17.01
495.95	129	-136	265	206	1322	20.15
496.55	187	-208	395	258	1580	24.08
497.15	252	-274	526	360	1940	29.57
497.75	231	-238	469	325	2265	34.52

Table E.4: VSI1, results from 05/12/84.

A Direction

Elev. (m)	A1	A2	A1-A2	CHANGE	SOC	Deflec (mm)
493.55	-3282	3324	-6606	-32	-32	4.68
494.15	-3208	3247	-6455	33	1	5.18
494.75	-3180	3218	-6398	42	43	5.82
495.35	-3127	3157	-6284	18	61	6.10
495.95	-3215	3262	-6477	-9	52	5.96
496.55	-3207	3234	-6441	11	63	6.13
497.15	-3117	3148	-6265	73	136	7.24
497.75	-3033	3078	-6111	143	279	9.42

B Direction

Elev. (m)	B1	B2	B1-B2	CHANGE	SOC	Deflec (mm)
493.55	286	-277	563	281	281	4.28
494.15	265	-257	522	255	536	8.17
494.75	293	-295	588	380	916	13.96
495.35	318	-315	633	302	1218	18.56
495.95	135	-128	263	204	1422	21.67
496.55	192	-192	384	247	1669	25.44
497.15	245	-251	496	330	1999	30.46
497.75	205	-209	414	270	2269	34.58

Table E.5: VSI1, results from 11/02/85.

A Direction

Elev. (m)	A1	A2	A1-A2	CHANGE	SOC	Deflec (mm)
493.55	-3302	3332	-6634	-60	-60	4.27
494.15	-3213	3250	-6463	25	-35	4.65
494.75	-3190	3218	-6408	32	-3	5.14
495.35	-3137	3151	-6288	14	11	5.35
495.95	-3224	3272	-6496	-28	-17	4.93
496.55	-3220	3242	-6462	-10	-27	4.77
497.15	-3140	3162	-6302	36	9	5.32
497.75	-3082	3118	-6200	54	63	6.15

B Direction

Elev. (m)	B1	B2	B1-B2	CHANGE	SOC	Deflec (mm)
493.55	388	-332	720	438	438	6.68
494.15	340	-300	640	373	811	12.36
494.75	376	-352	728	520	1331	20.28
495.35	400	-359	759	428	1759	26.81
495.95	207	-163	370	311	2070	31.55
496.55	301	-280	581	444	2514	38.31
497.15	344	-301	645	479	2993	45.61
497.75	304	-261	565	421	3414	52.03

Table E.6: VSI1, results from 29/08/85.

A Direction

Elev. (m)	A1	A2	A1-A2	CHANGE	SOC	Deflec (mm)
493.55	-3283	3329	-6612	-38	-38	2.62
494.15	-3196	3246	-6442	46	8	3.32
494.75	-3170	3211	-6381	59	67	4.22
495.35	-3116	3143	-6259	43	-110	4.87
495.95	-3214	3274	-6488	-20	90	4.57
496.55	-3204	3234	-6438	14	104	4.78
497.15	-3123	3154	-6277	61	165	5.71
497.75	-3049	3095	-6144	110	275	7.39

B Direction

Elev. (m)	B1	B2	B1-B2	CHANGE	SOC	Deflec (mm)
493.55	483	-407	890	608	608	9.27
494.15	450	-390	840	573	1181	18.00
494.75	486	-426	912	704	1885	28.73
495.35	495	-428	923	592	2477	37.75
495.95	336	-259	595	536	3013	45.92
496.55	399	-349	748	611	3624	55.23
497.15	436	-392	828	662	4286	65.32
497.75	372	-307	679	535	4821	73.47

Table E.7: VSI1, results from 25/03/86.

A Direction

Elev. (m)	A1	A2	A1-A2	CHANGE	SOC	Deflec (mm)
493.55	-3283	3334	-6617	-43	-43	2.69
494.15	-3200	3256	-6456	32	-11	3.18
494.75	-3196	3216	-6412	28	17	3.61
495.35	-3123	3157	-6280	22	39	3.94
495.95	-3209	3279	-6488	-20	19	3.64
496.55	-3213	3251	-6464	-12	7	3.45
497.15	-3127	3169	-6296	42	49	4.09
497.75	-3056	3116	-6172	82	131	5.34

B Direction

Elev. (m)	B1	B2	B1-B2	CHANGE	SOC	Deflec (mm)
493.55	438	-425	863	581	581	8.85
494.15	427	-389	816	549	1130	17.22
494.75	436	-434	870	662	1792	27.31
495.35	484	-458	942	611	2403	36.62
495.95	286	-254	540	481	2884	43.95
496.55	374	-362	736	599	3483	53.08
497.15	406	-379	785	619	4102	62.51
497.75	417	-353	770	626	4728	72.05

Table E.8: VSI1, results from 29/07/86.

A Direction

Elev. (m)	A1	A2	A1-A2	CHANGE	SOC	Deflec (mm)
493.55	-3256	3315	-6571	3	3	1.84
494.15	-3172	3227	-6399	89	92	3.19
494.75	-3148	3200	-6348	92	184	4.60
495.35	-3088	3120	-6208	94	278	6.03
495.95	-3175	3249	-6424	44	322	6.70
496.55	-3155	3198	-6353	99	421	8.21
497.15	-3083	3129	-6212	126	547	10.13
497.75	-3048	3025	-6073	181	728	12.89

B Direction

Elev. (m)	B1	B2	B1-B2	CHANGE	SOC	Deflec (mm)
493.55	565	-544	1109	827	827	12.60
494.15	499	-501	1000	733	1560	23.77
494.75	543	-537	1080	872	2432	37.06
495.35	553	-546	1099	768	3200	48.77
495.95	409	-385	794	735	3935	59.97
496.55	465	-467	932	795	4730	72.09
497.15	504	-485	989	823	5553	84.63
497.75	416	-408	824	680	6233	94.99

Table E.9: VSI1, results from 09/12/86.

A Direction

Elev. (m)	A1	A2	A1-A2	CHANGE	SOC	Deflec (mm)
493.55	-3286	3330	-6616	-42	-42	2.10
494.15	-3187	3236	-6423	65	23	3.09
494.75	-3164	3198	-6362	78	101	4.28
495.35	-3112	3139	-6251	51	152	5.06
495.95	-3197	3252	-6449	19	171	5.35
496.55	-3205	3235	-6440	12	183	5.53
497.15	-3122	3148	-6270	68	251	6.57
497.75	-3048	3090	-6138	116	367	8.34

B Direction

Elev. (m)	B1	B2	B1-B2	CHANGE	SOC	Deflec (mm)
493.55	561	-543	1104	822	822	12.53
494.15	534	-496	1030	763	1585	24.16
494.75	551	-545	1096	888	2473	37.69
495.35	564	-546	1110	779	3252	49.56
495.95	410	-394	804	745	3997	60.91
496.55	456	-445	901	764	4761	72.56
497.15	501	-484	985	819	5580	85.04
497.75	434	-429	863	719	6299	96.00

Table E.10: VSI1, results from 16/02/87.

A Direction

Elev. (m)	A1	A2	A1-A2	CHANGE	SOC	Deflec (mm)
493.55	-3273	3328	-6601	-27	-27	1.77
494.15	-3182	3240	-6422	66	39	2.78
494.75	-3163	3211	-6374	66	105	3.79
495.35	-3109	3143	-6252	50	155	4.55
495.95	-3194	3262	-6456	12	167	4.73
496.55	-3195	3238	-6433	19	186	5.02
497.15	-3118	3150	-6268	70	256	6.09
497.75	-3039	3096	-6135	119	375	7.90

B Direction

Elev. (m)	B1	B2	B1-B2	CHANGE	SOC	Deflec (mm)
493.55	545	-539	1084	802	802	12.22
494.15	519	-516	1035	768	1570	23.93
494.75	540	-543	1083	875	2445	37.26
495.35	550	-551	1101	770	3215	49.00
495.95	392	-375	767	708	3920	59.79
496.55	463	-460	923	786	4709	71.77
497.15	492	-518	1010	844	5553	84.63
497.75	408	-430	838	694	6247	95.20

Table E.11: VS11, results from 25/03/87.

A Direction

Elev. (m)	A1	A2	A1-A2
488.64	-1775	1822	-3597
489.25	-1554	1603	-3157
489.86	-1433	1482	-2915
490.47	-1313	1360	-2673
491.08	-1235	1287	-2522
491.68	-1242	1286	-2528
492.29	-1181	1235	-2416
492.90	-1096	1142	-2238
493.51	-981	1031	-2012
494.12	-762	806	-1568
494.73	-500	546	-1046
495.34	-481	529	-1010
495.95	-363	409	-772
496.56	-57	103	-160
497.17	-204	252	-456
497.78	-100	147	-247
498.39	618	-564	1182

B Direction

Elev. (m)	B1	B2	B1-B2
488.64	164	-151	315
489.25	204	-191	395
489.86	235	-216	451
490.47	300	-286	586
491.08	325	-316	641
491.68	268	-252	520
492.29	261	-237	498
492.90	176	-170	346
493.51	47	-19	66
494.12	-116	123	-239
494.73	-277	282	-559
495.34	-340	364	-704
495.95	-443	463	-906
496.56	-482	501	-983
497.17	-519	530	-1049
497.78	-395	420	-815
498.39	-305	326	-631

Table E.12: VSI2, calibration values, 29/07/86

A Direction

Elev. (m)	A1	A2	A1-A2	CHANGE	SOC	Deflec (mm)
488.64	-1757	1802	-3559	38	38	0.58
489.25	-1535	1581	-3116	41	79	1.20
489.86	-1418	1461	-2879	36	115	1.75
490.47	-1296	1342	-2638	35	150	2.29
491.08	-1221	1269	-2490	32	182	2.77
491.68	-1226	1268	-2494	34	216	3.29
492.29	-1170	1219	-2389	27	243	3.70
492.90	-1083	1125	-2208	30	273	4.16
493.51	-970	1014	-1984	28	301	4.59
494.12	-758	793	-1551	17	318	4.85
494.73	-502	541	-1043	3	321	4.89
495.34	-483	527	-1010	0	321	4.89
495.95	-367	412	-779	-7	314	4.79
496.56	-64	106	-170	-10	304	4.63
497.17	-210	255	-465	-9	295	4.50
497.78	106	141	-35	212	507	7.73
498.39	584	-539	1123	-59	448	6.83

B Direction

Elev. (m)	B1	B2	B1-B2	CHANGE	SOC	Deflec (mm)
488.64	194	-184	378	63	63	0.96
489.25	228	-226	454	59	122	1.86
489.86	256	-255	511	60	182	2.77
490.47	318	-321	639	53	235	3.58
491.08	339	-346	685	44	279	4.25
491.68	293	-285	578	58	337	5.14
492.29	276	-264	540	42	379	5.78
492.90	202	-182	384	38	417	6.36
493.51	60	-37	97	31	448	6.83
494.12	-98	112	-210	29	477	7.27
494.73	-257	274	-531	28	505	7.70
495.34	-331	336	-667	37	542	8.26
495.95	-437	444	-881	25	567	8.64
496.56	-480	483	-963	20	587	8.95
497.17	-515	510	-1025	24	611	9.31
497.78	-398	407	-805	10	621	9.46
498.39	-313	321	-634	-3	618	9.42

Table E.13: VSI2, results from 09/12/86.

A Direction

Elev. (m)	A1	A2	A1-A2	CHANGE	SOC	Deflec (mm)
488.64	-1781	1808	-3589	8	8	0.12
489.25	-1551	1582	-3133	24	32	0.49
489.86	-1434	1460	-2894	21	53	0.81
490.47	-1312	1340	-2652	21	74	1.13
491.08	-1235	1266	-2501	21	95	1.45
491.68	-1238	1262	-2500	28	123	1.87
492.29	-1182	1212	-2394	22	145	2.21
492.90	-1097	1125	-2222	16	161	2.45
493.51	-983	1011	-1994	18	179	2.73
494.12	-777	794	-1571	-3	176	2.68
494.73	-513	536	-1049	-3	173	2.64
495.34	-495	522	-1017	-7	166	2.53
495.95	-383	407	-790	-18	148	2.26
496.56	-71	100	-171	-11	137	2.09
497.17	-211	254	-465	-9	128	1.95
497.78	-140	145	-285	-38	90	1.37
498.39	568	-539	1107	-75	15	0.23

B Direction

Elev. (m)	B1	B2	B1-B2	CHANGE	SOC	Deflec (mm)
488.64	201	-191	392	77	77	1.17
489.25	235	-226	461	66	143	2.18
489.86	264	-256	520	69	212	3.23
490.47	327	-319	646	60	272	4.15
491.08	348	-346	694	53	325	4.95
491.68	299	-284	583	63	388	5.91
492.29	282	-263	545	47	435	6.63
492.90	213	-201	414	68	503	7.67
493.51	68	-50	118	52	555	8.46
494.12	-97	101	-198	41	596	9.08
494.73	-250	263	-513	46	642	9.78
495.34	-326	336	-662	42	684	10.42
495.95	-428	443	-871	35	719	10.96
496.56	-474	492	-966	17	736	11.22
497.17	-510	514	-1024	25	761	11.60
497.78	-399	413	-812	3	764	11.64
498.39	-323	333	-656	-25	739	11.26

Table E.14: VSI2, results from 16/02/87.

A Direction

Elev. (m)	A1	A2	A1-A2	CHANGE	SOC	Deflec (mm)
488.64	-1771	1819	-3590	7	7	0.11
489.25	-1544	1592	-3136	21	28	0.43
489.86	-1426	1474	-2900	15	43	0.66
490.47	-1308	1354	-2662	11	54	0.82
491.08	-1226	1277	-2503	19	73	1.11
491.68	-1231	1273	-2504	24	97	1.48
492.29	-1175	1228	-2403	13	110	1.68
492.90	-1089	1135	-2224	14	124	1.89
493.51	-972	1022	-1994	18	142	2.16
494.12	-761	807	-1568	0	142	2.16
494.73	-498	542	-1040	6	148	2.26
495.34	-481	527	-1008	2	150	2.29
495.95	-370	412	-782	-10	140	2.13
496.56	-58	102	-160	0	140	2.13
497.17	-208	260	-468	-12	128	1.95
497.78	-104	147	-251	-4	124	1.89
498.39	699	-643	1342	160	284	4.33

B Direction

Elev. (m)	B1	B2	B1-B2	CHANGE	SOC	Deflec (mm)
488.64	186	-192	378	63	63	0.96
489.25	219	-226	445	50	113	1.72
489.86	247	-250	497	46	159	2.42
490.47	314	-321	635	49	208	3.17
491.08	334	-350	684	43	251	3.83
491.68	280	-285	565	45	296	4.51
492.29	268	-263	531	33	329	5.01
492.90	197	-188	385	39	368	5.61
493.51	51	-40	91	25	393	5.99
494.12	-120	109	-229	10	403	6.14
494.73	-270	269	-539	20	423	6.45
495.34	-337	342	-679	25	448	6.83
495.95	-440	447	-887	19	467	7.12
496.56	-484	491	-975	8	475	7.24
497.17	-522	509	-1031	18	493	7.51
497.78	-399	409	-808	7	500	7.62
498.39	-308	326	-634	-3	497	7.57

Table E.15: VSI2, results from 25/03/87.

A Direction

Elev. (m)	A1	A2	A1-A2
487.62	-843	886	-1729
488.23	-683	722	-1405
488.84	-626	675	-1301
489.45	-947	995	-1942
490.06	-1275	1320	-2595
490.67	-1342	1383	-2725
491.28	-1199	1238	-2437
491.88	-1112	1155	-2267
492.49	-975	1021	-1996
493.10	-941	996	-1937
493.71	-1127	1169	-2296
494.32	-821	856	-1677
494.93	-768	815	-1583
495.54	-846	883	-1729
496.15	-666	703	-1369
496.76	-834	882	-1716
497.37	-913	950	-1863
497.98	-168	291	-459
498.59	504	-597	1101

B Direction

Elev. (m)	B1	B2	B1-B2
487.62	-169	198	-367
488.23	-101	119	-220
488.84	58	-35	93
489.45	286	-268	554
490.06	421	-400	821
490.67	282	-261	543
491.28	32	-8	40
491.88	-80	102	-182
492.49	-162	184	-346
493.10	-413	434	-847
493.71	-597	622	-1219
494.32	-61	76	-137
494.93	120	-94	214
495.54	-166	200	-366
496.15	-263	274	-537
496.76	-274	287	-561
497.37	-78	98	-176
497.98	-503	441	-944
498.59	-2172	2143	-4315

Table E.16: VSI3, calibration values, 29/07/86

A Direction

Elev. (m)	A1	A2	A1-A2	CHANGE	SOC	Deflec (mm)
487.62	-840	885	-1725	4	4	0.06
488.23	-681	727	-1408	-3	1	0.02
488.84	-617	664	-1281	20	21	0.32
489.45	-934	976	-1910	32	53	0.81
490.06	-1258	1300	-2558	37	90	1.37
490.67	-1331	1373	-2704	21	111	1.69
491.28	-1193	1236	-2429	8	119	1.81
491.88	-1108	1152	-2260	7	126	1.92
492.49	-974	1019	-1993	3	129	1.97
493.10	-942	990	-1932	5	134	2.04
493.71	-1134	1175	-2309	-13	121	1.84
494.32	-817	853	-1670	7	128	1.95
494.93	-763	809	-1572	11	139	2.12
495.54	-845	882	-1727	2	141	2.15
496.15	-669	706	-1375	-6	135	2.06
496.76	-823	878	-1701	15	150	2.29
497.37	-908	952	-1860	3	153	2.33
497.98	-166	319	-485	-26	127	1.94
498.59	611	-536	1147	46	173	2.64

B Direction

Elev. (m)	B1	B2	B1-B2	CHANGE	SOC	Deflec (mm)
487.62	-175	177	-352	15	15	0.23
488.23	-111	105	-216	4	19	0.29
488.84	60	-48	108	15	34	0.52
489.45	286	-282	568	14	48	0.73
490.06	418	-424	842	21	69	1.05
490.67	280	-284	564	21	90	1.37
491.28	34	-41	75	35	125	1.90
491.88	-80	83	-163	19	144	2.19
492.49	-163	165	-328	18	162	2.47
493.10	-417	408	-825	22	184	2.80
493.71	-611	607	-1218	1	185	2.82
494.32	-66	78	-144	-7	178	2.71
494.93	117	-109	226	12	190	2.90
495.54	-172	187	-359	7	197	3.00
496.15	-267	249	-516	21	218	3.32
496.76	-278	276	-554	7	225	3.43
497.37	-84	88	-172	4	229	3.49
497.98	-521	395	-916	28	257	3.92
498.59	-2167	2137	-4304	11	268	4.08

Table E.17: VSI3, results from 09/12/86.

A Direction

Elev. (m)	A1	A2	A1-A2	CHANGE	SOC	Deflec (mm)
487.62	-853	891	-1744	-15	-15	-0.23
488.23	-700	738	-1438	-33	-48	-0.73
488.84	-615	661	-1276	25	-23	-0.35
489.45	-922	973	-1895	47	24	0.37
490.06	-1251	1305	-2556	39	63	0.96
490.67	-1351	1387	-2738	-13	50	0.76
491.28	-1205	1247	-2452	-15	35	0.53
491.88	-1119	1163	-2282	-15	20	0.30
492.49	-985	1034	-2019	-23	-3	-0.05
493.10	-932	989	-1921	16	13	0.20
493.71	-1145	1183	-2328	-32	-19	-0.29
494.32	-830	867	-1697	-20	-39	-0.59
494.93	-761	806	-1567	16	-23	-0.35
495.54	-849	888	-1737	-8	-31	-0.47
496.15	-677	713	-1390	-21	-52	-0.79
496.76	-821	873	-1694	22	-30	-0.46
497.37	-920	956	-1876	-13	-43	-0.66
497.98	-176	307	-483	-24	-67	-1.02
498.59	527	-581	1108	7	-60	-0.91

B Direction

Elev. (m)	B1	B2	B1-B2	CHANGE	SOC	Deflec (mm)
487.62	-190	188	-378	-11	-11	-0.17
488.23	-123	114	-237	-17	-28	-0.43
488.84	43	-30	73	-20	-48	-0.73
489.45	268	-279	547	-7	-55	-0.84
490.06	412	-422	834	13	-42	-0.64
490.67	274	-285	559	16	-26	-0.40
491.28	26	-25	51	11	-15	-0.23
491.88	-89	90	-179	3	-12	-0.18
492.49	-174	175	-349	-3	-15	-0.23
493.10	-420	411	-831	16	1	0.02
493.71	-631	637	-1268	-49	-48	-0.73
494.32	-87	90	-177	-40	-88	-1.34
494.93	108	-107	215	1	-87	-1.33
495.54	-191	200	-391	-25	-112	-1.71
496.15	-273	265	-538	-1	-113	-1.72
496.76	-300	294	-594	-33	-146	-2.23
497.37	-106	102	-208	-32	-178	-2.71
497.98	-521	424	-945	-1	-179	-2.73
498.59	-2168	2146	-4314	1	-178	-2.71

Table E.18: VSI3, results from 25/03/87.

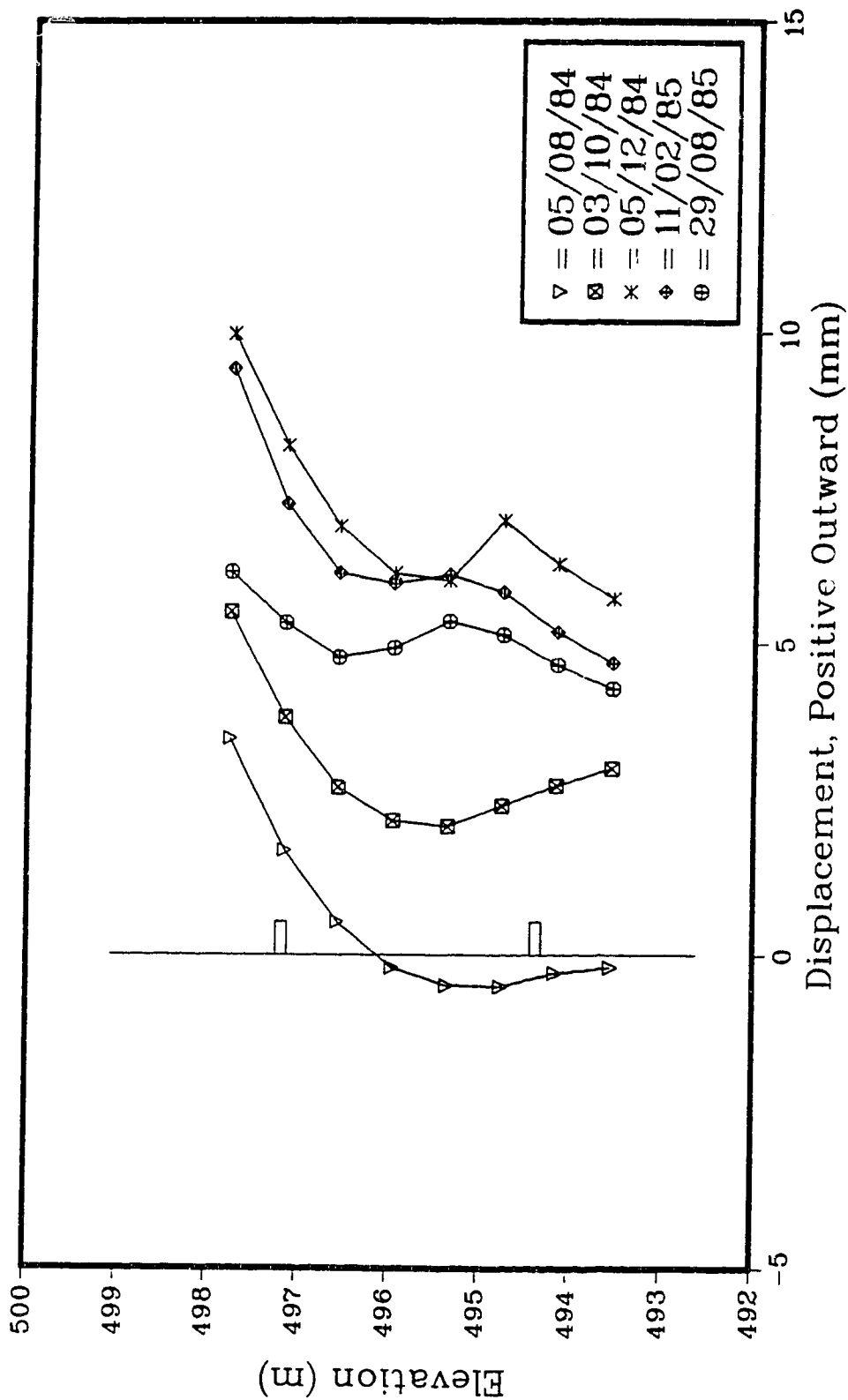


Figure E.1: VSI1, A direction absolute displacements, early epochs.

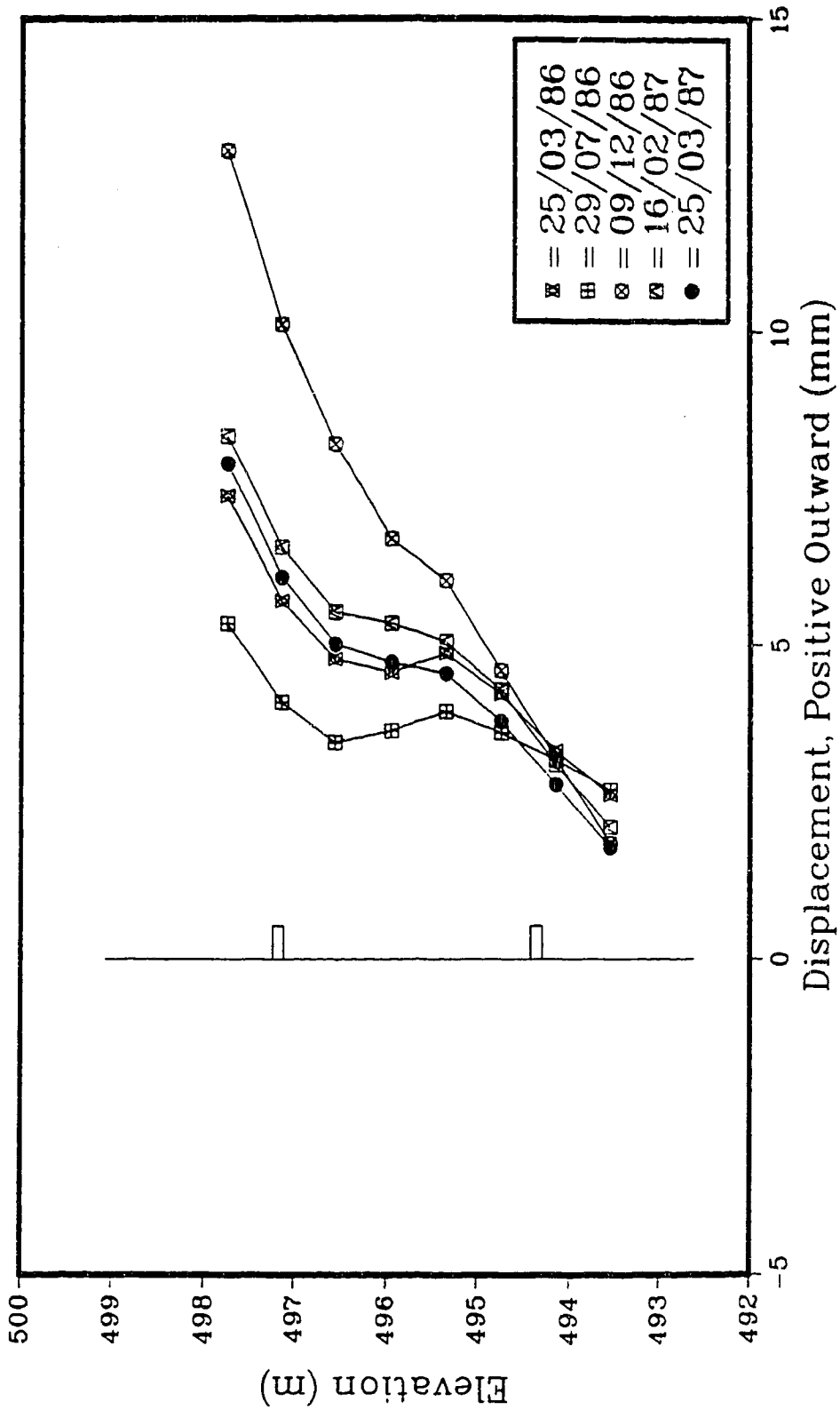


Figure E.2: VSII, A direction absolute displacements, late epochs.

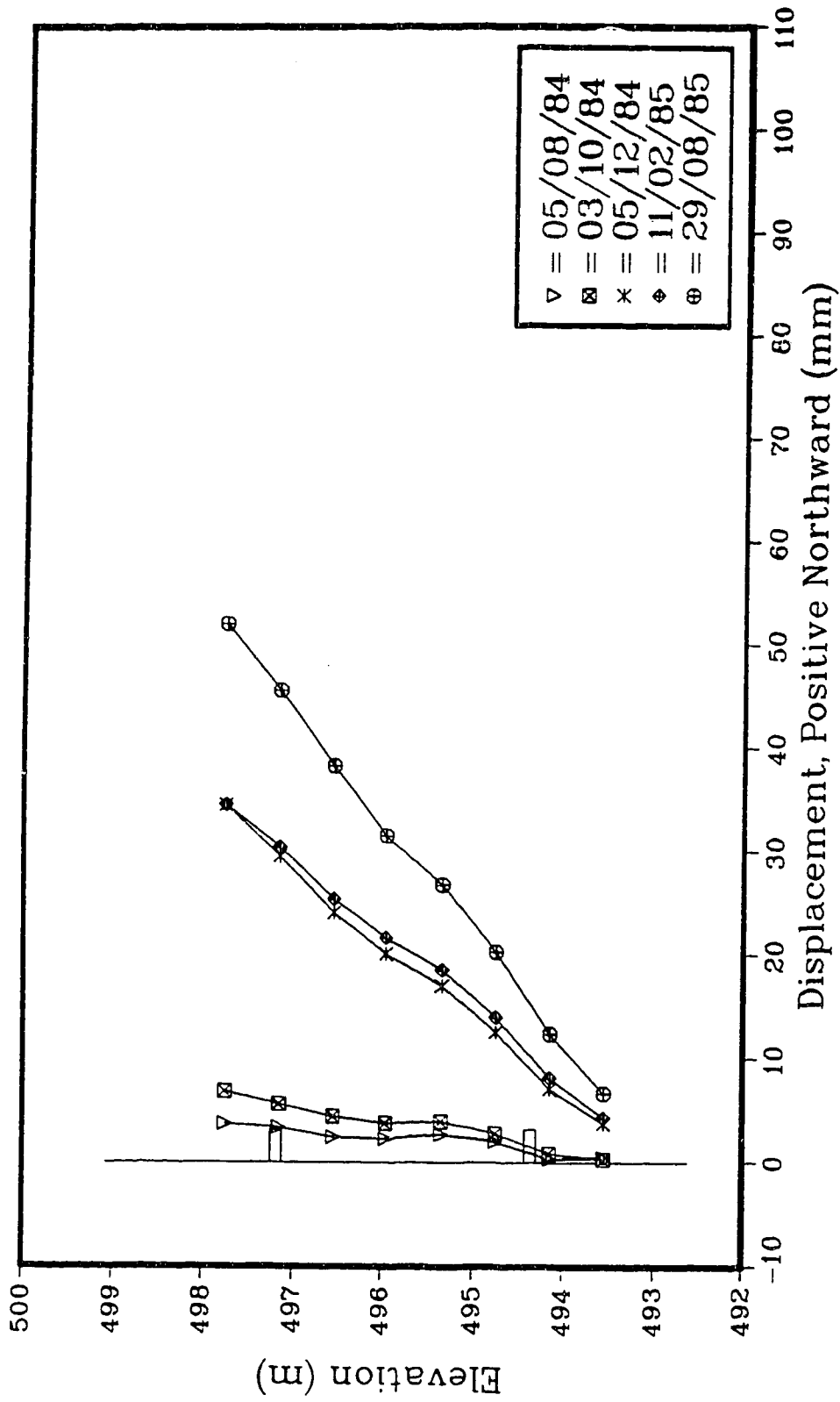


Figure E.3: VSI1, B direction displacements, early epochs.

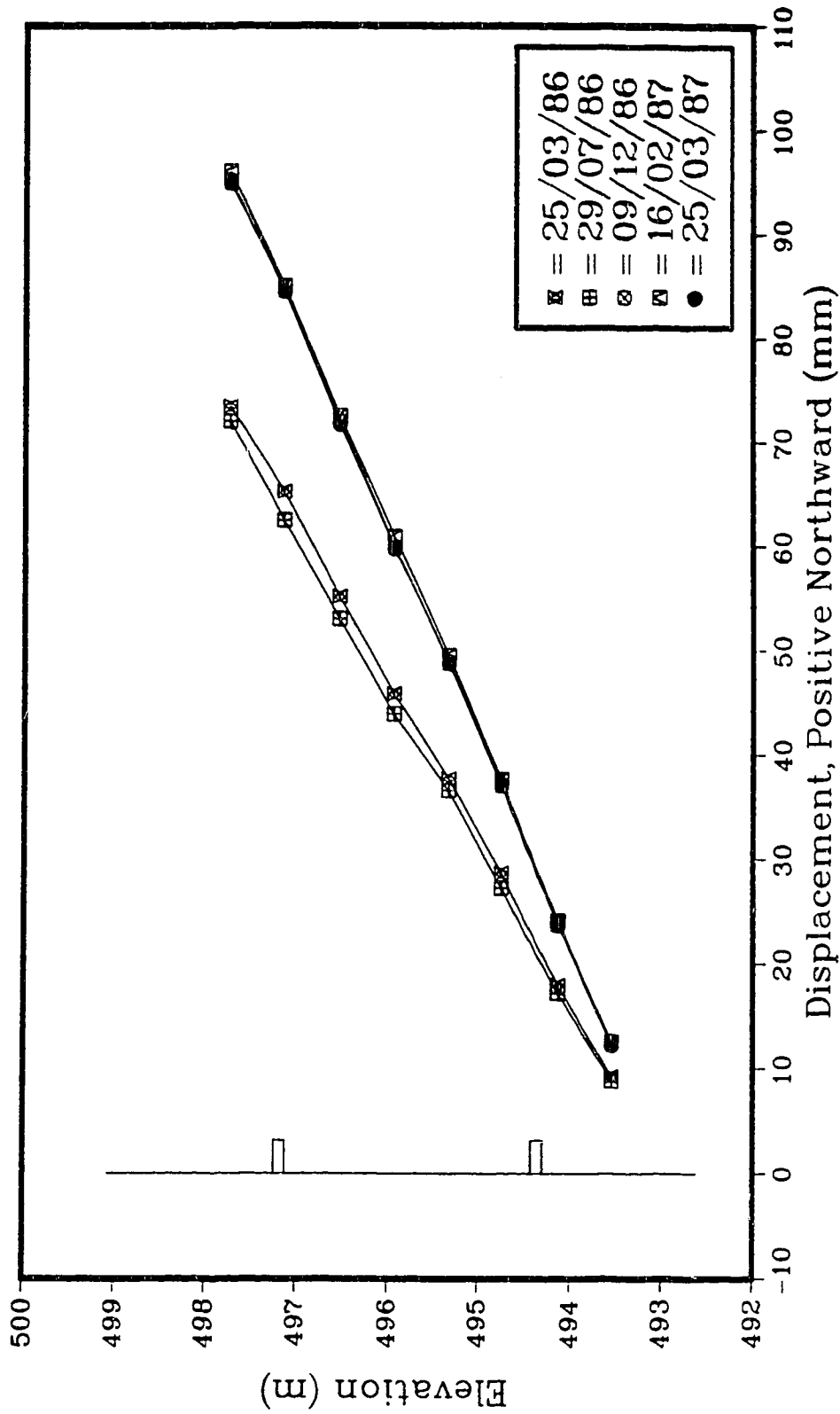


Figure E.4: VSII, B direction displacements, late epochs.

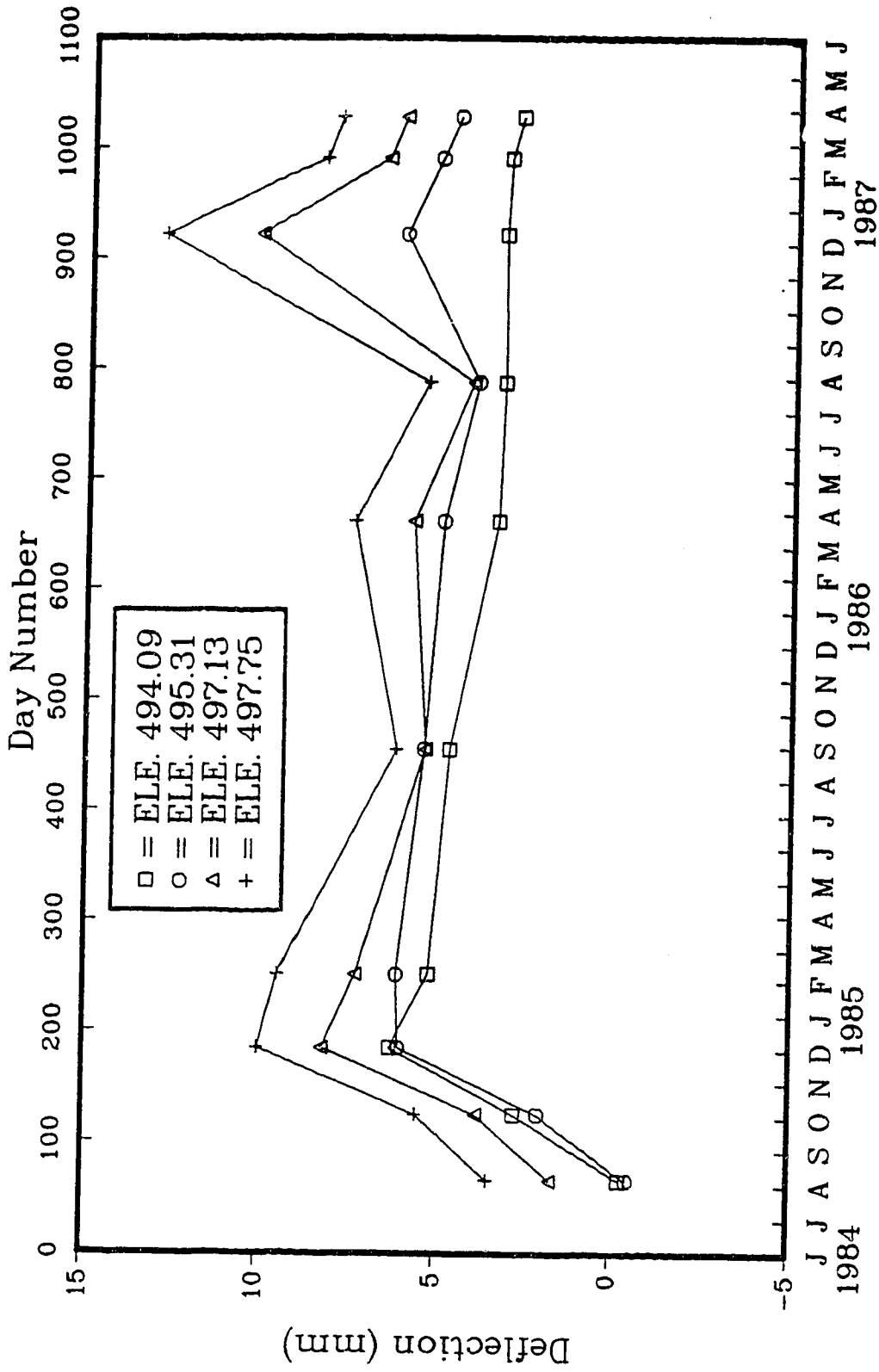


Figure E.5: VSI1, A direction absolute displacements/time.

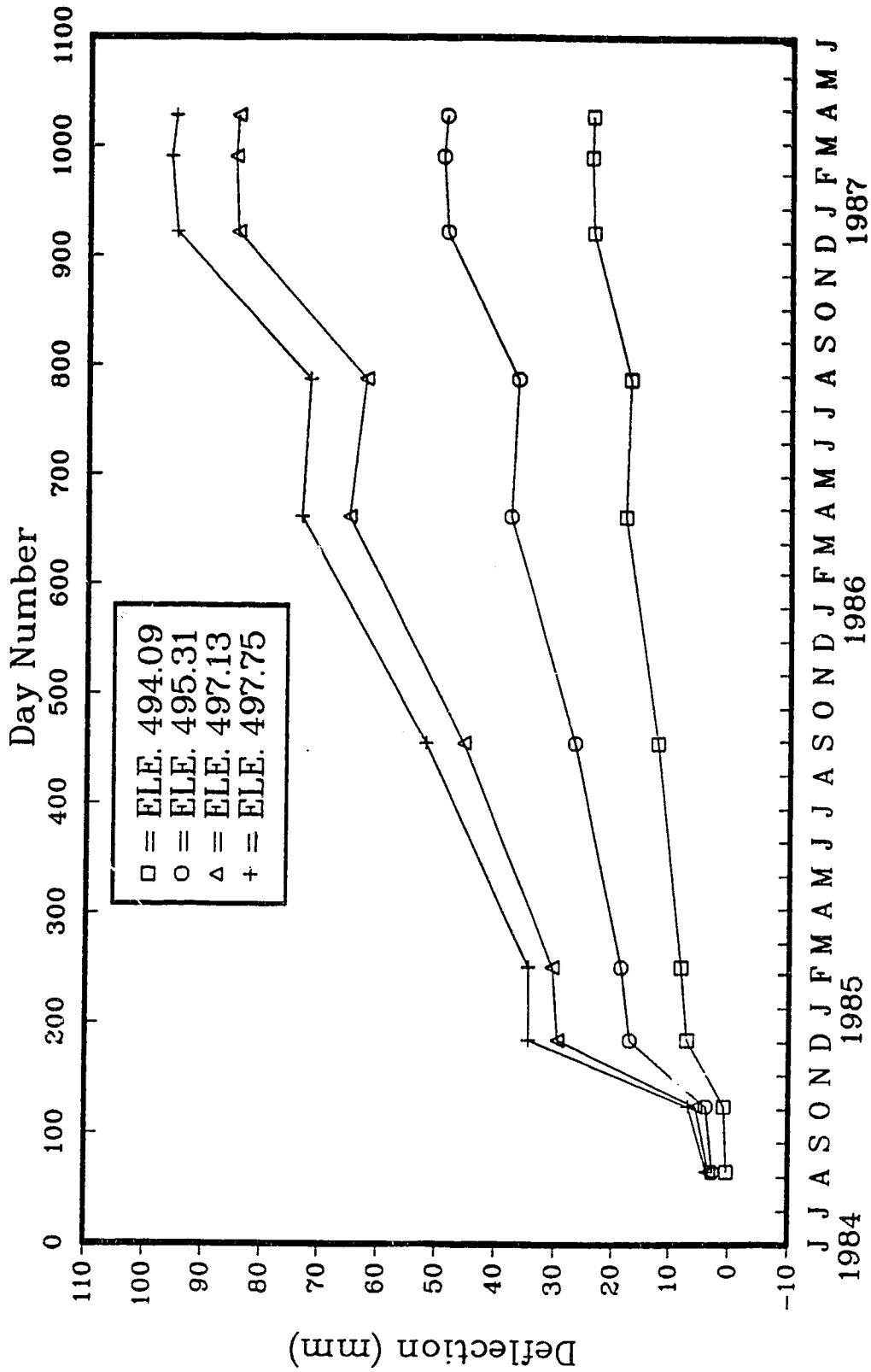


Figure E.6: VS11, B direction displacements/time.

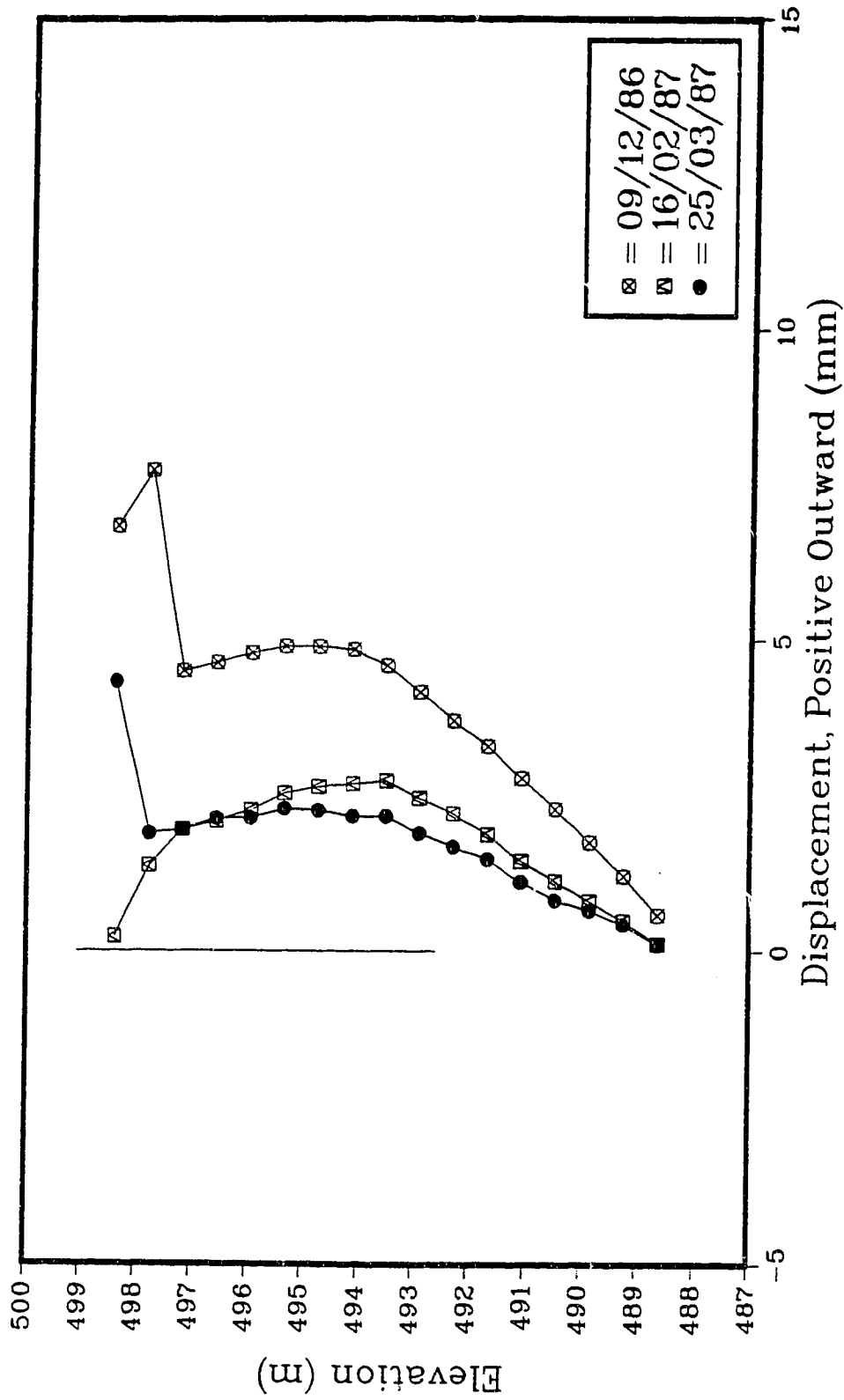


Figure E.7: VSI2, A direction absolute displacements.

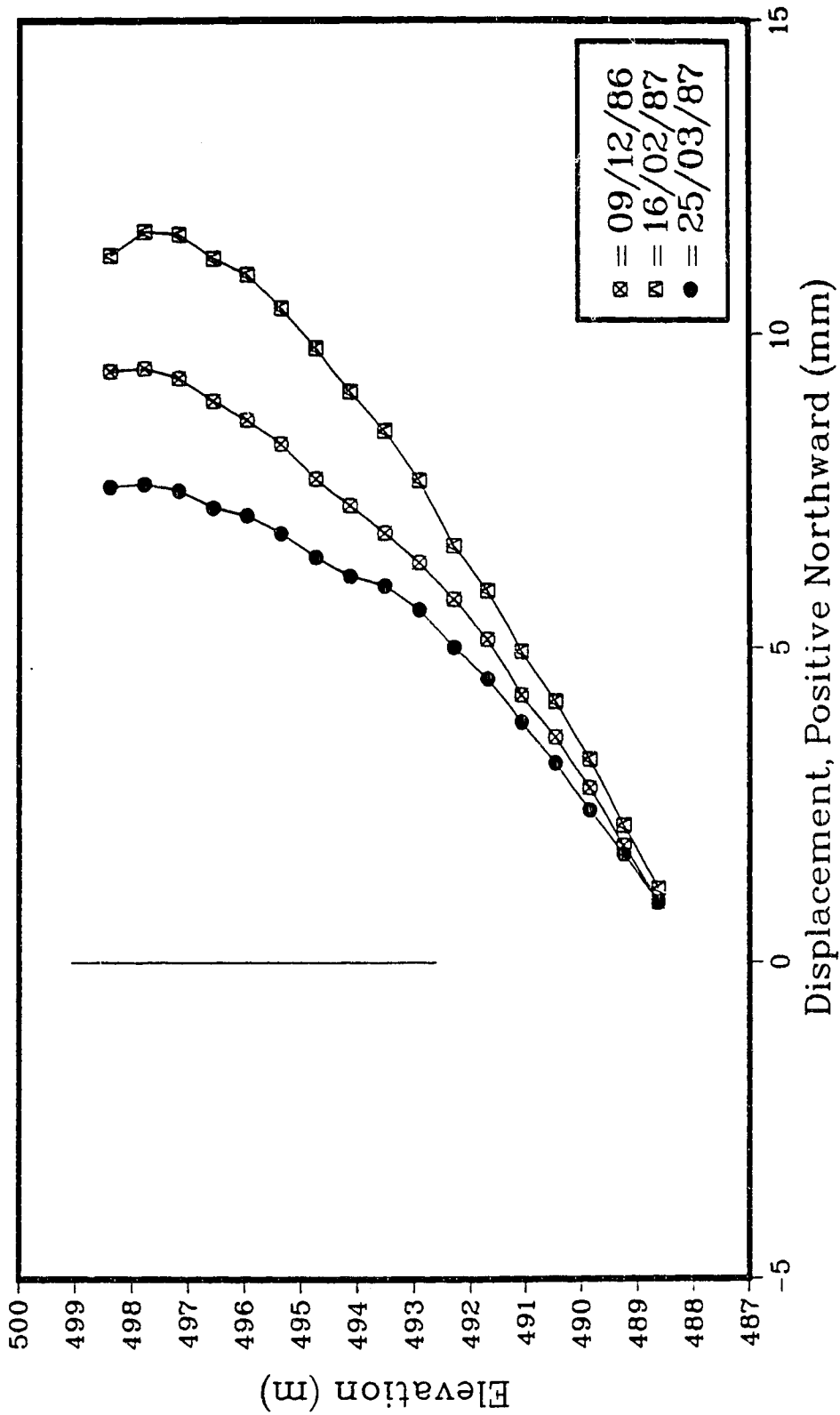


Figure E.8: VSI2, B direction absolute displacements.

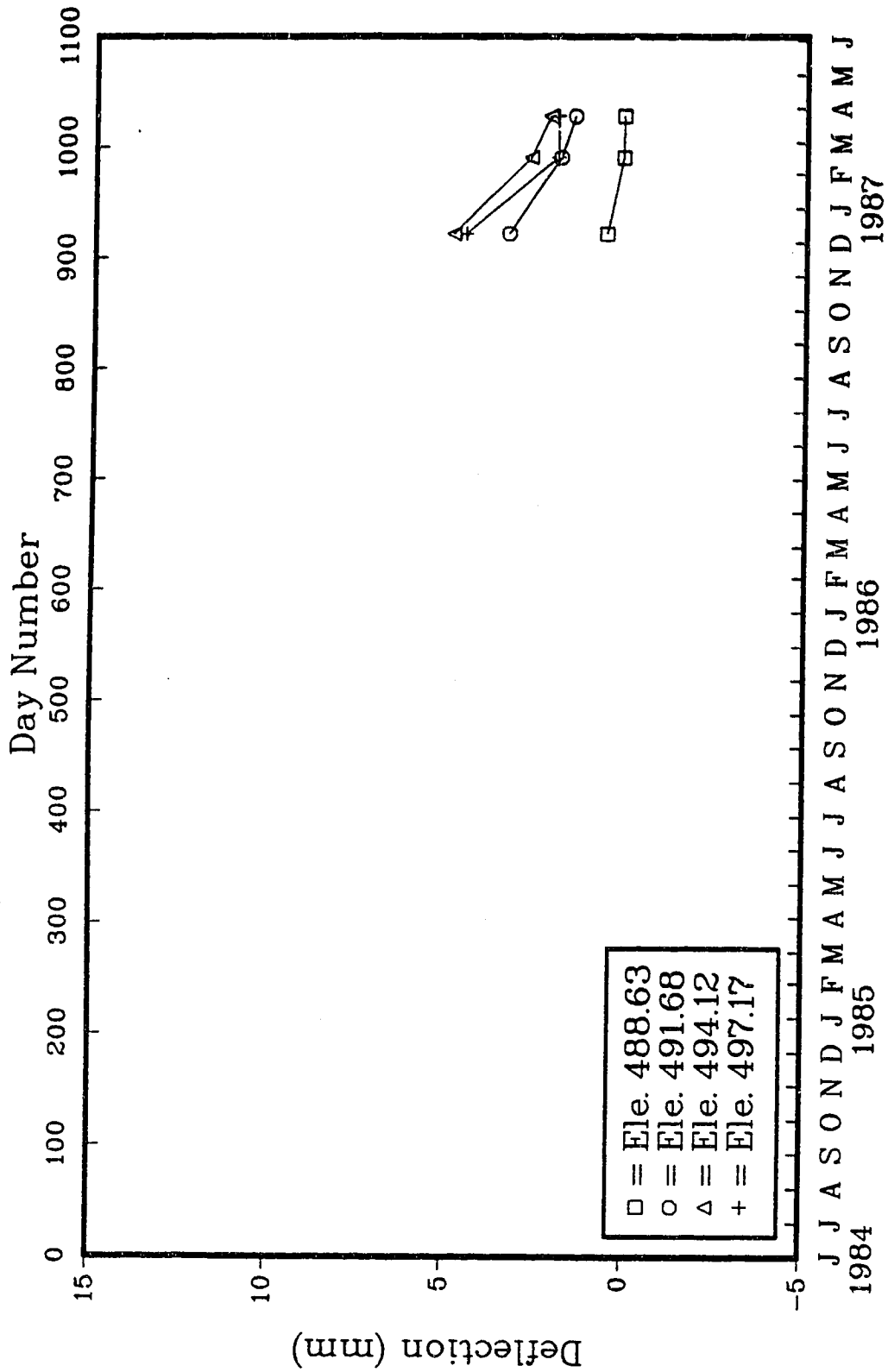


Figure E.9: VSI2, A direction absolute displacements/time.

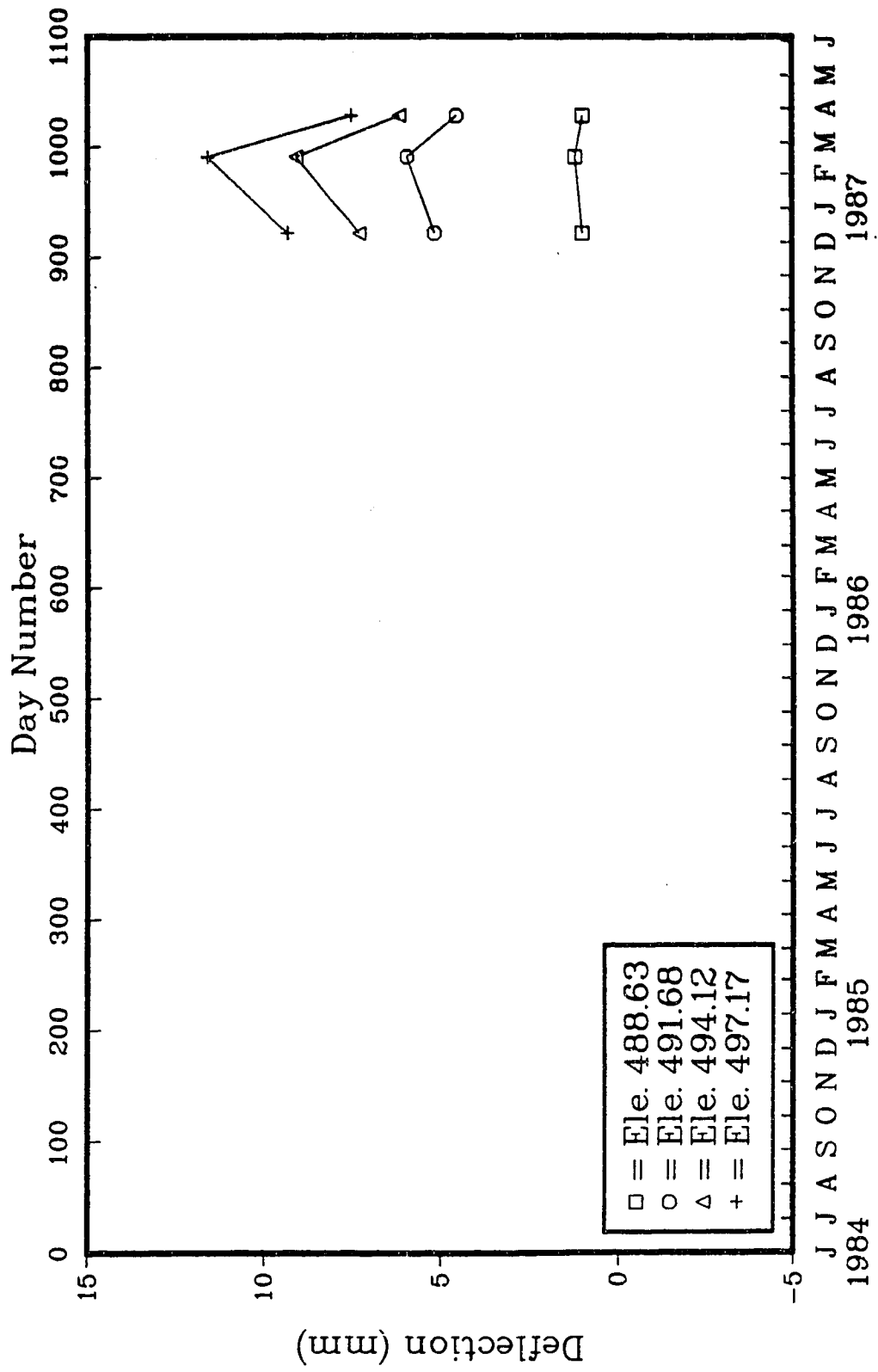


Figure E.10: VSI2, B direction absolute displacements/time.

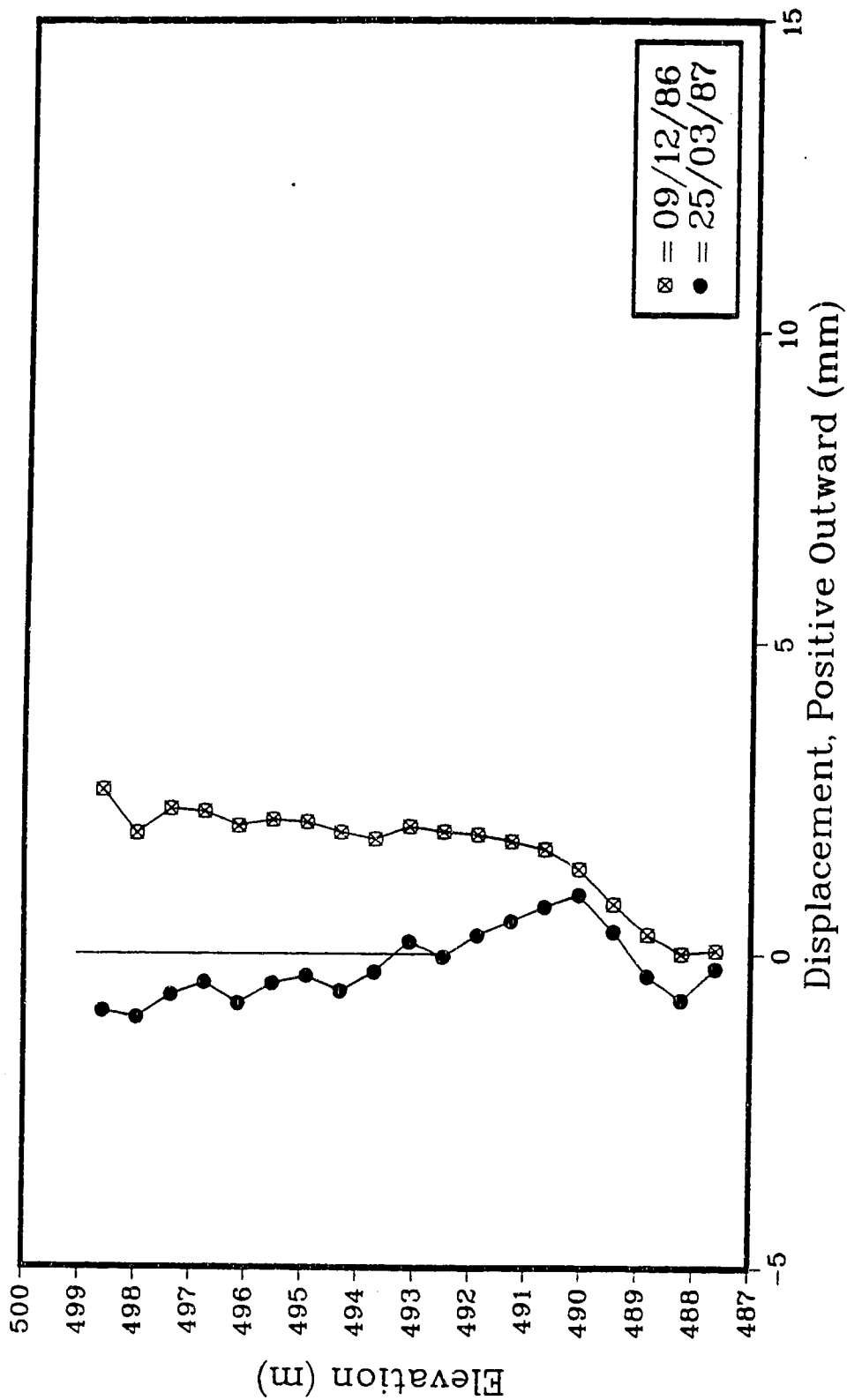


Figure E.11: VSI3, A direction absolute displacements.

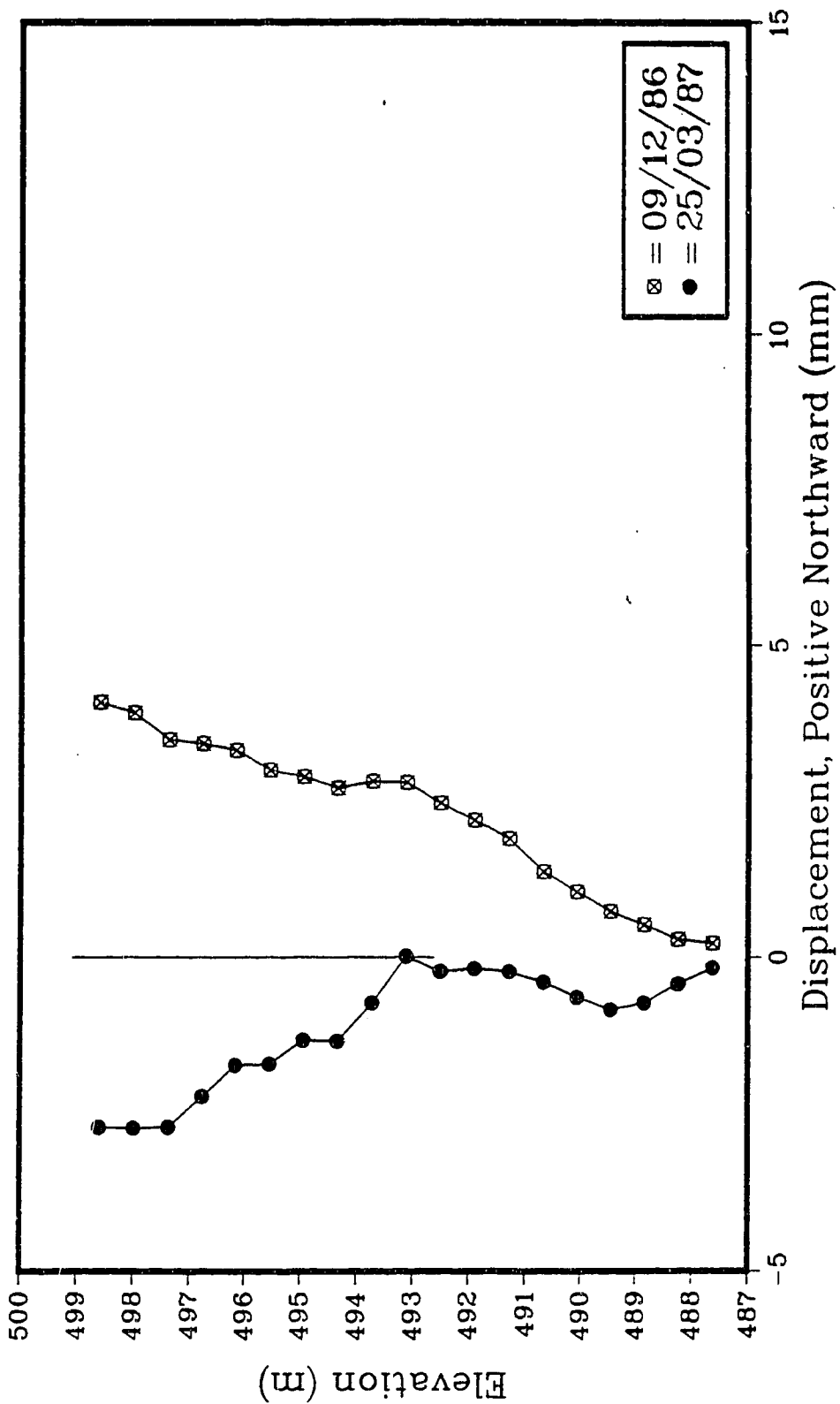


Figure E.12: VSI3, B direction absolute displacements.

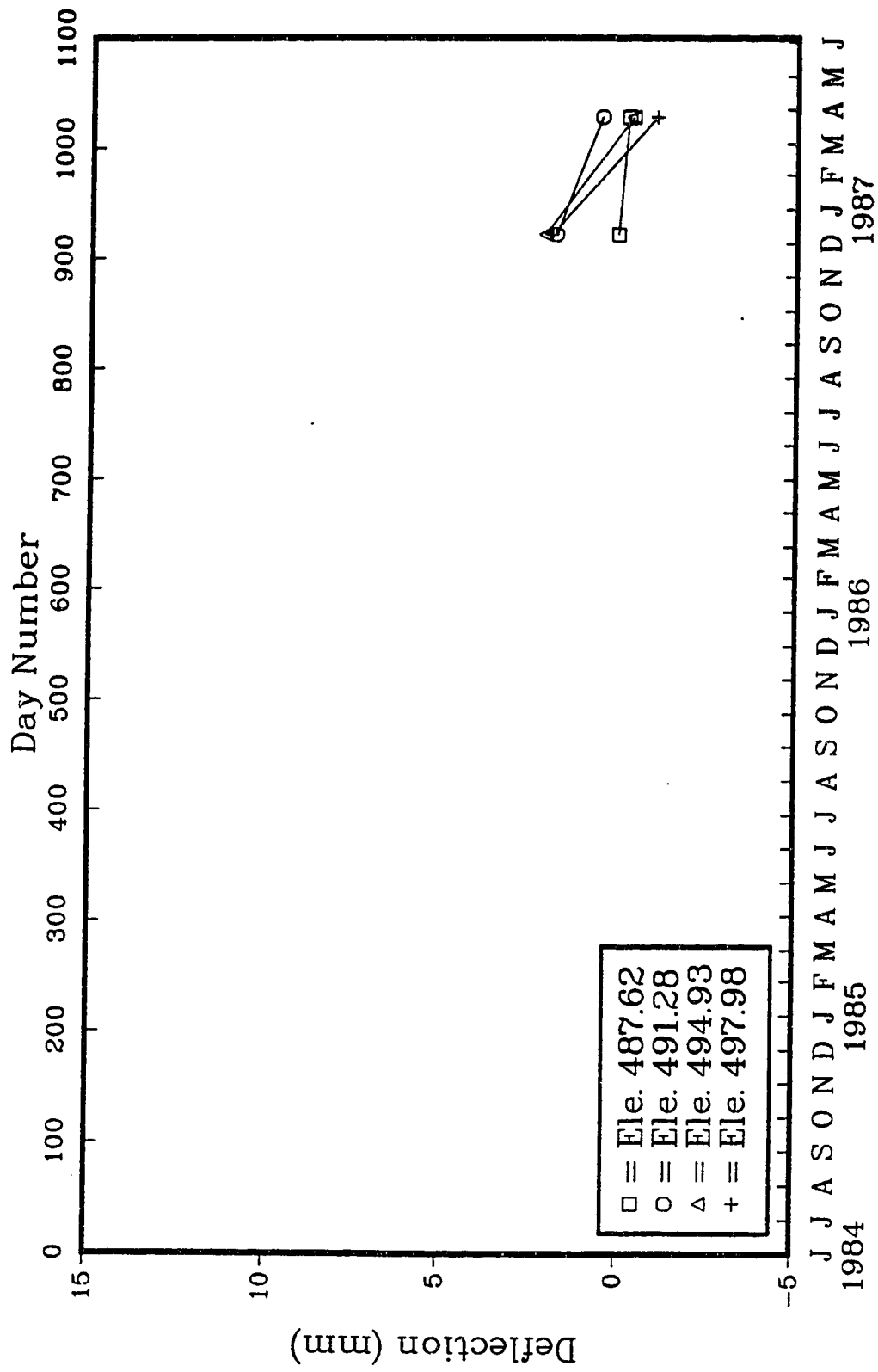


Figure E.13: VSI3, A direction absolute displacements/time.

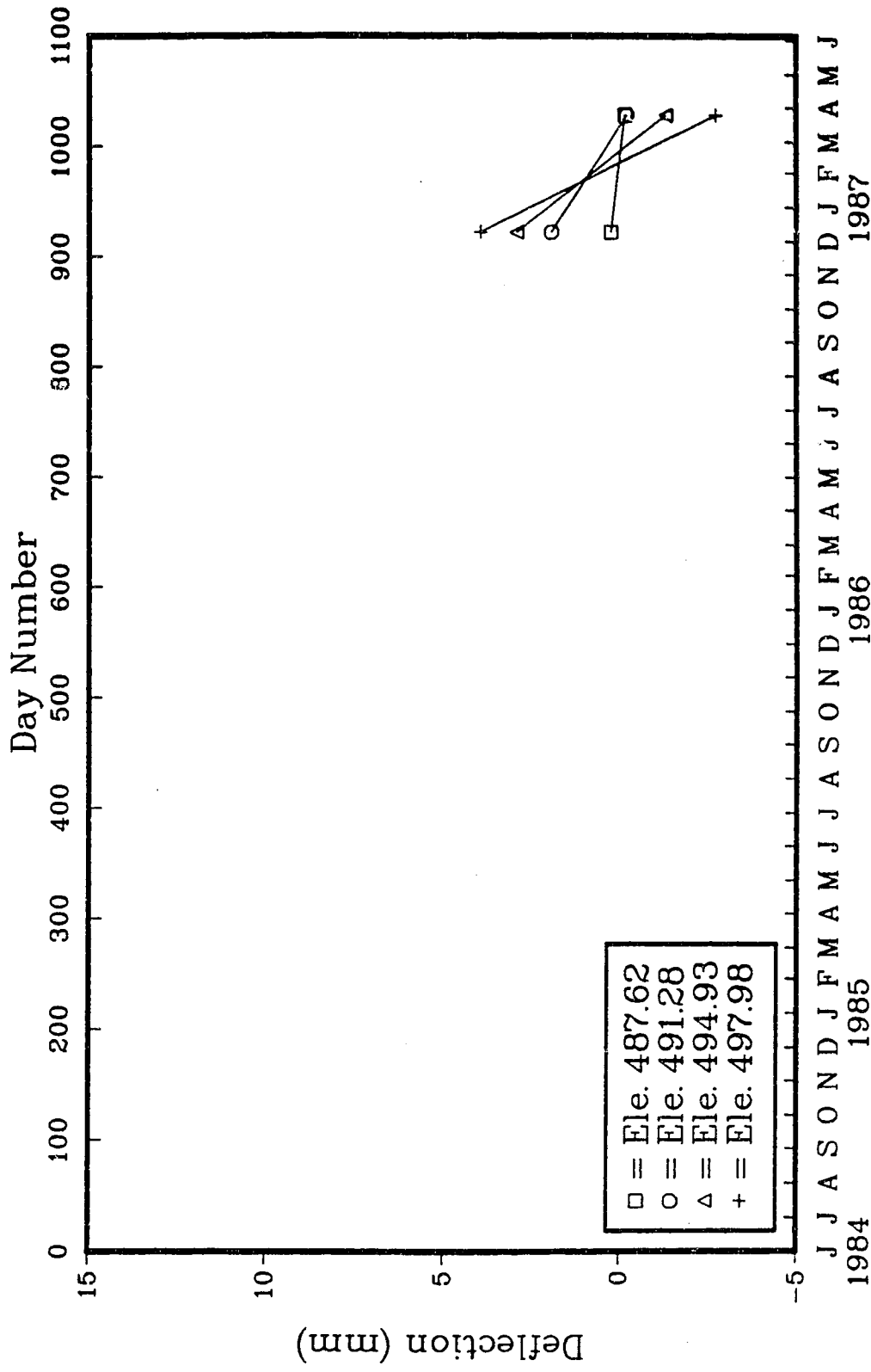


Figure E.14: VSI3, B direction absolute displacements/time.

Appendix F
East Wall Displacements based on the Wall Mounted Strain
Gauges

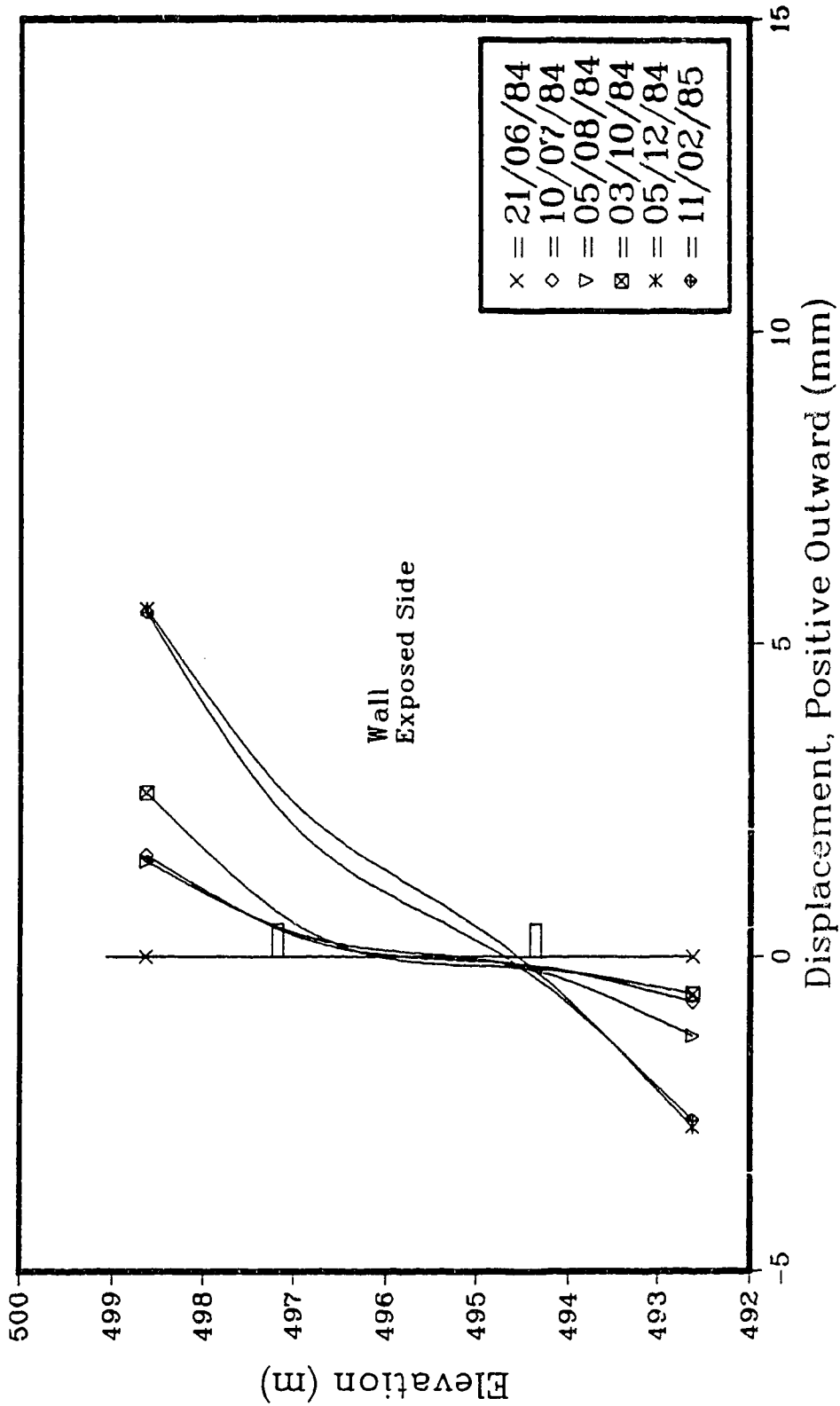


Figure F.1: Theoretical displacement (sheet pile only), east section, early epochs.

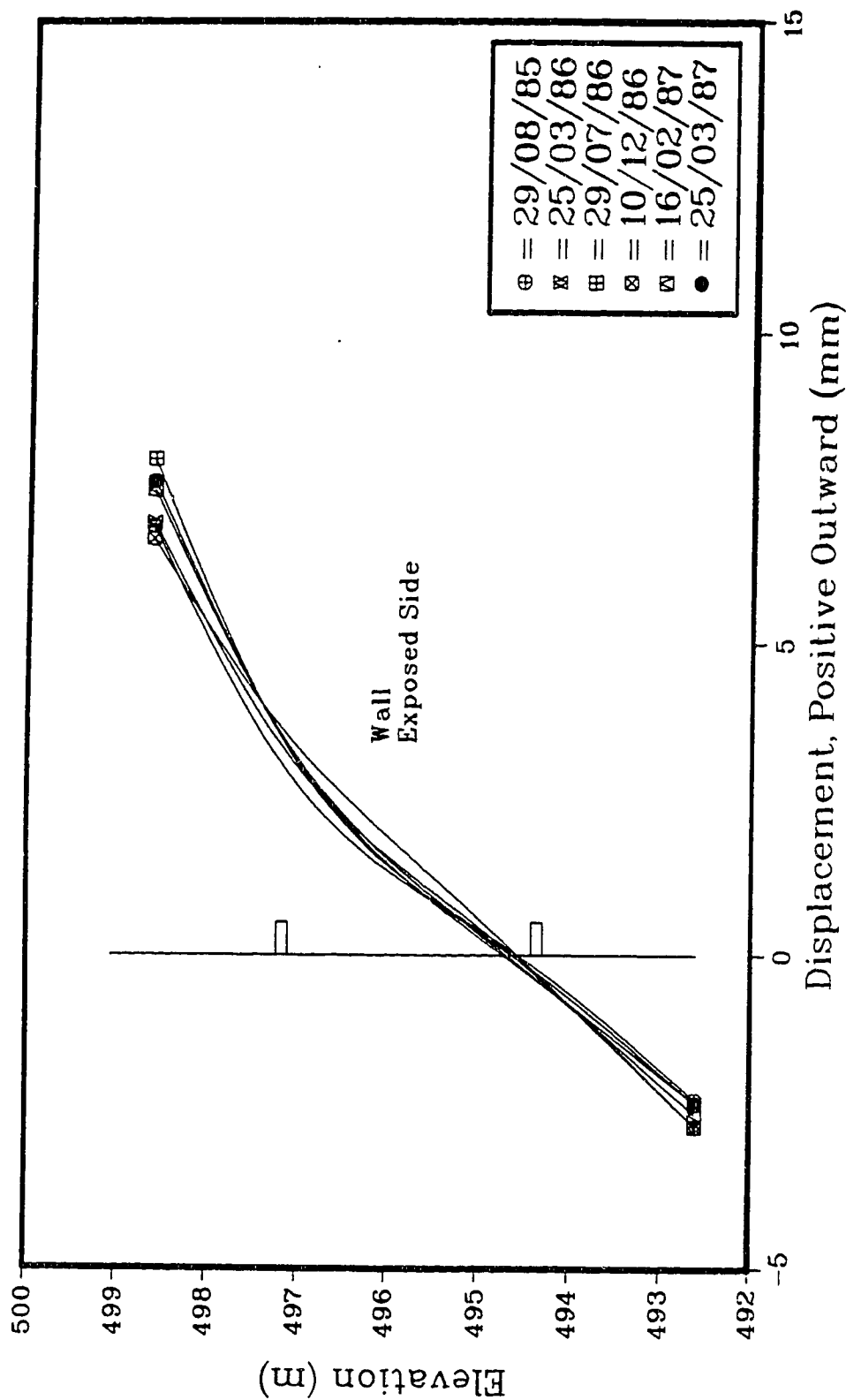


Figure F.2: Theoretical displacement (sheet pile only), east section, late epochs.

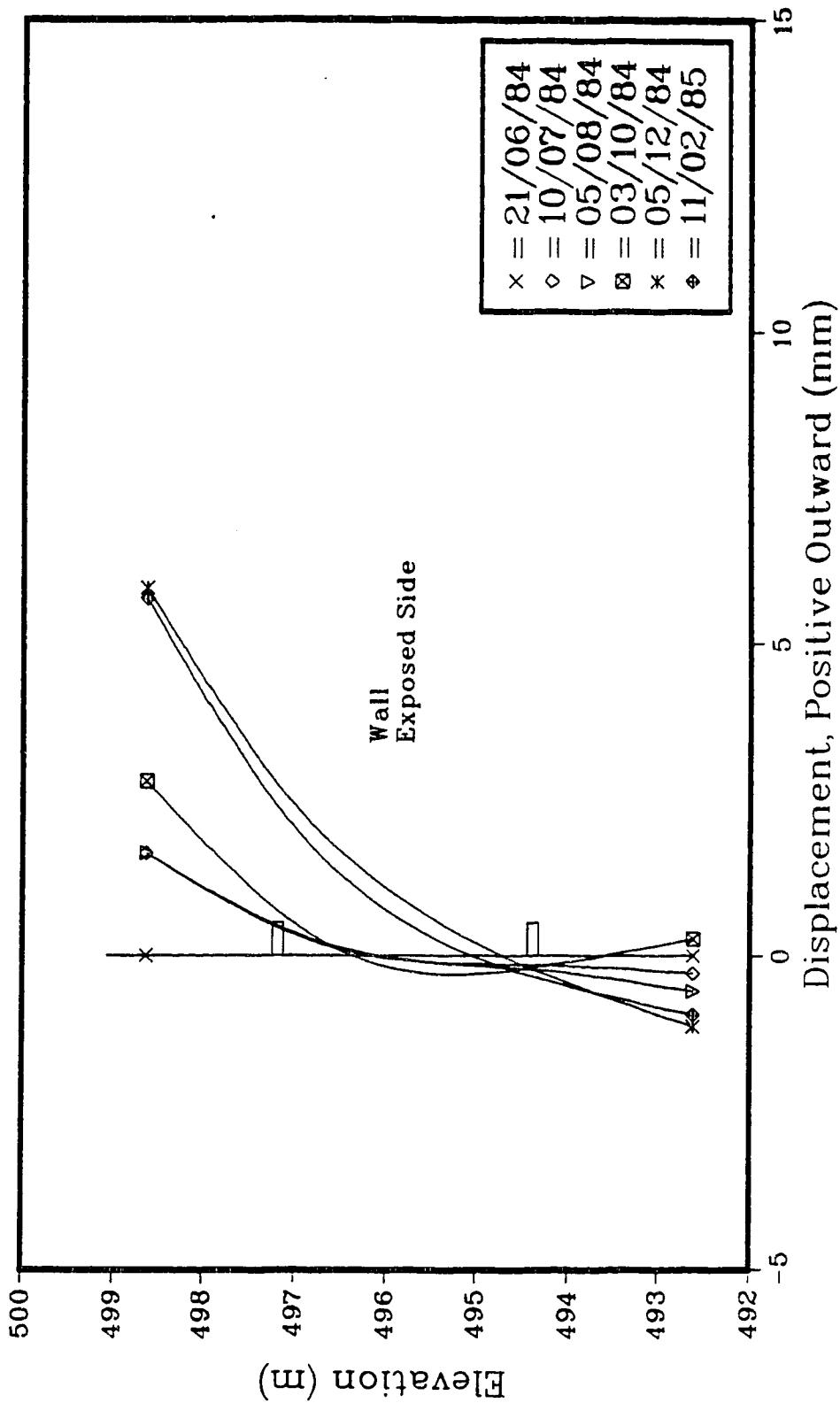


Figure F.3: Theoretical displacement (sheet pile only), west section, early epochs.

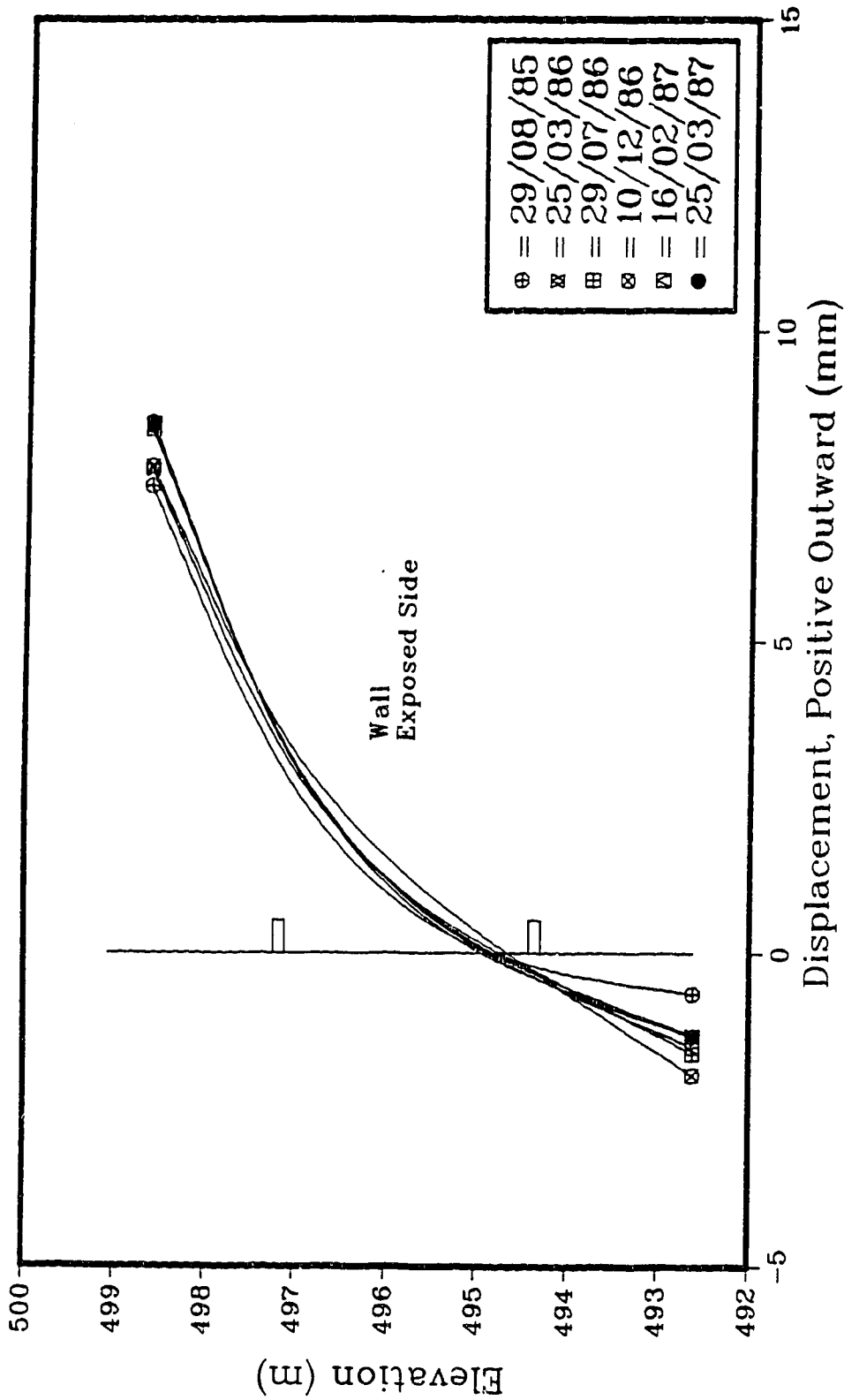


Figure F.4: Theoretical displacement (sheet pile only), west section, late epochs.

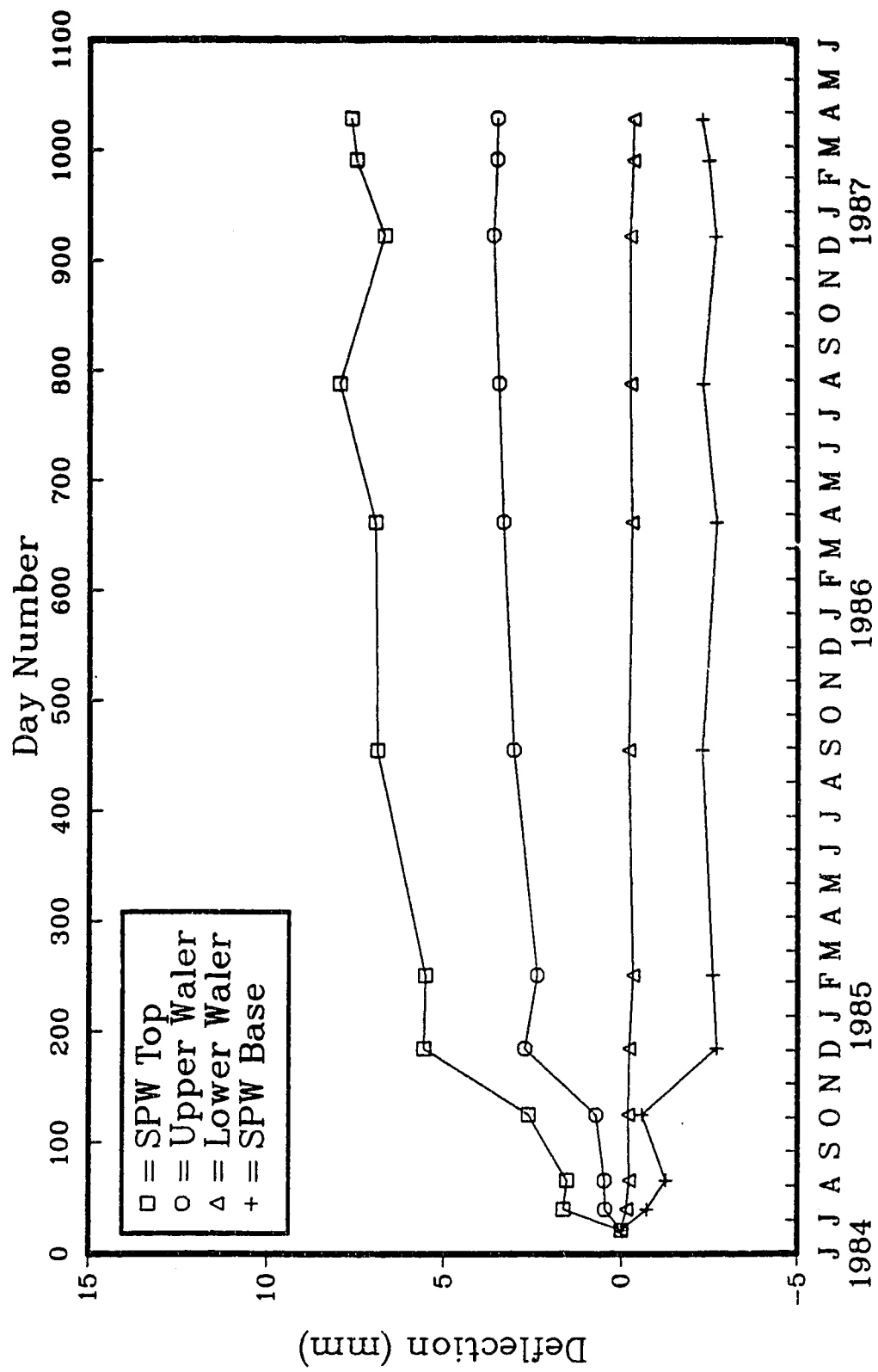


Figure F.5: Theoretical displacement versus time, east section.

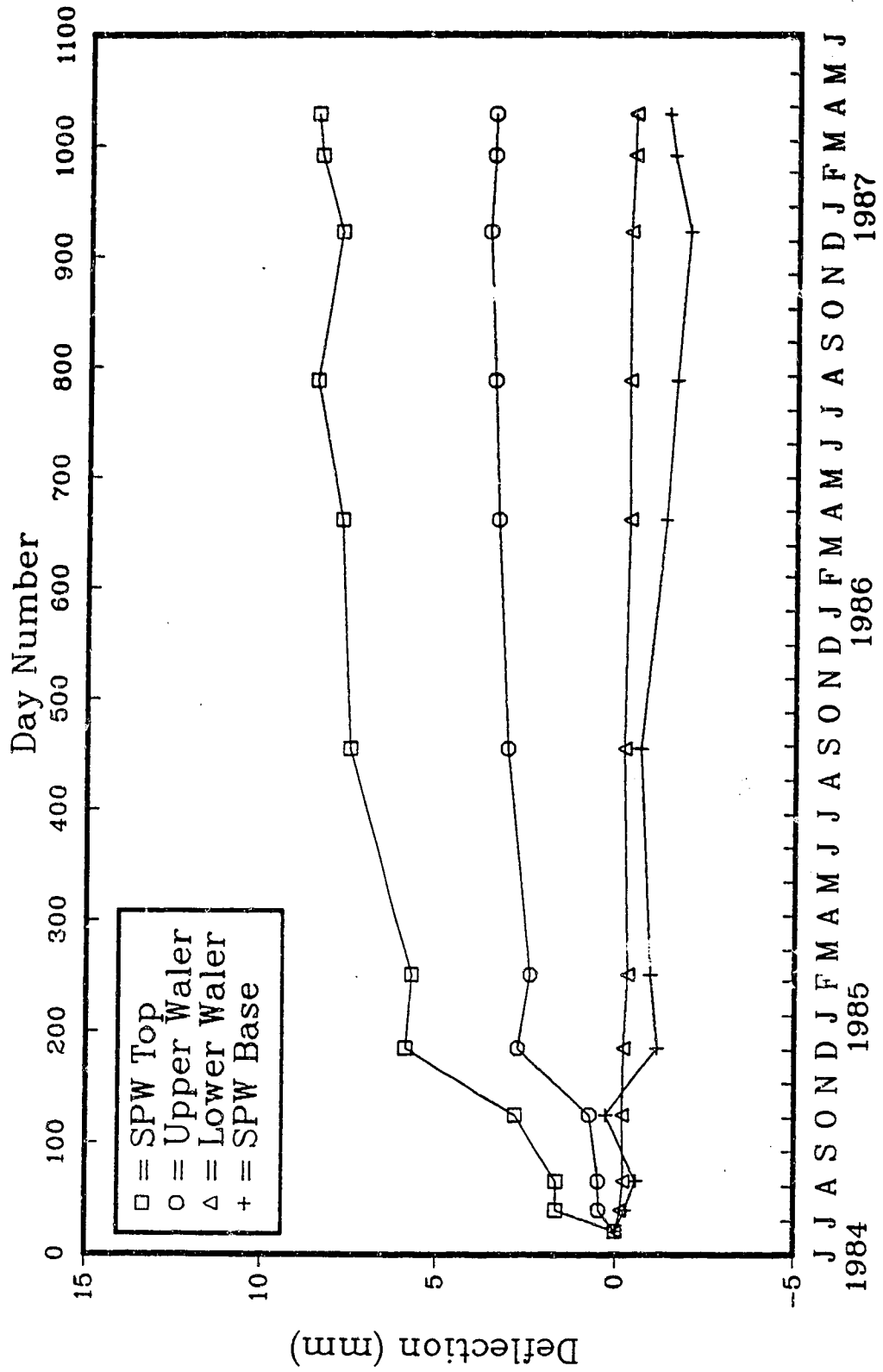


Figure F.6: Theoretical displacement versus time, west section.

Appendix G
Extensometer Results

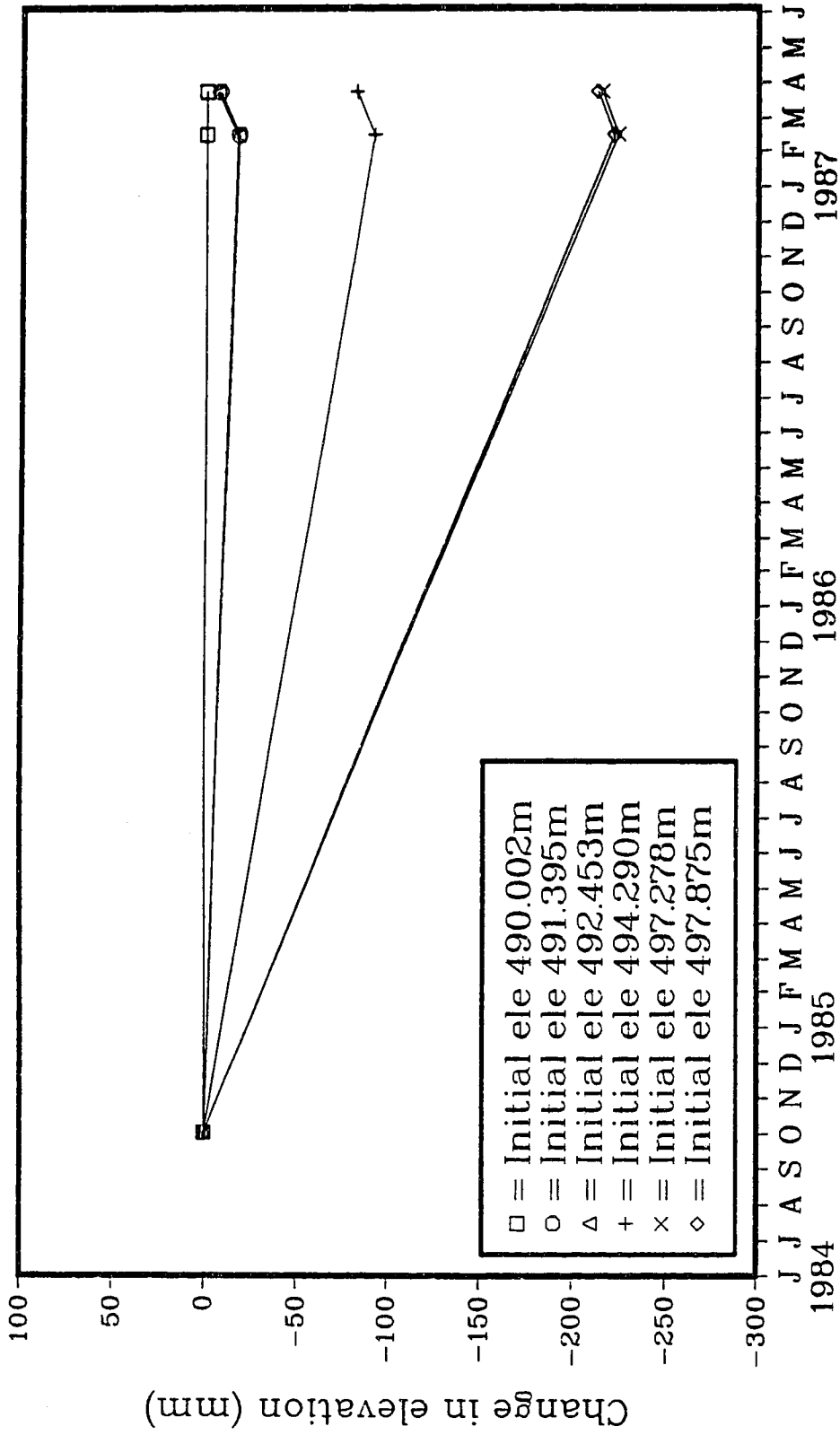


Figure G.1: Extensometer results.

Appendix H
Bending Moments Based on the Wall Mounted Strain Gauge
Results

SG Number	"Inner" Column				Outer Column				Axial Stress (MPa)	Bending Stress (MPa)	Moment (kN m)
	Strain (E-6)	Net Strain	Stress (MPa)	Adjusted Stress	SG Number	Strain (E-6)	Net Strain	Stress (MPa)			
2	-3935	0	0.0	0.0	3	-3665	0	0.0	0.0	0.0	0.0
4	-729	0	0.0	0.0	5	-459	0	0.0	0.0	0.0	0.0
6	-959	0	0.0	0.0	7	-2292	0	0.0	0.0	0.0	0.0
8	-1677	0	0.0	0.0	9	-4433	0	0.0	0.0	0.0	0.0
10	-600	0	0.0	0.0	11	-666	0	0.0	0.0	0.0	0.0
12	-5831	0	0.0	0.0	13	-2997	0	0.0	0.0	0.0	0.0
14	-240	0	0.0	0.0	15	-4213	0	0.0	0.0	0.0	0.0
16	-5899	0	0.0	0.0	17	-2535	0	0.0	0.0	0.0	0.0

Temperature dependence correction applied to SG readings (micro strain units): 0.

Table H.1: Wall mounted strain gauge results, east section, June 20, 1984.

SG Number	"Inner" Column				Outer Column				Axial Stress (MPa)	Bending Stress (MPa)	Moment (kN m)
	Strain (E-6)	Net Strain	Stress (MPa)	Adjusted Stress	SG Number	Strain (E-6)	Net Strain	Stress (MPa)			
2	-3933	2	0.40	0.52	3	-3678	-13	-2.60	-1.04	-1.56	-1.30
4	-726	3	0.60	0.65	5	-462	-3	-0.60	0.02	-0.62	-0.52
6	-954	5	1.00	1.37	7	-2332	-40	-8.00	-3.31	-4.69	-3.91
8	-1659	18	3.60	4.05	9	-4469	-36	-7.20	-1.58	-5.63	-4.70
10	-550	50	10.00	11.13	11	-751	-85	-17.00	-2.94	-14.06	-11.74
12	-5709	122	24.40	26.64	13	-3144	-147	-29.40	-1.38	-28.02	-23.40
14	-112	128	25.60	28.22	15	-4400	-187	-37.40	-4.59	-32.81	-27.40
16	-5783	116	23.20	25.52	17	-2697	-162	-32.40	-3.44	-28.96	-24.18

Temperature dependence correction applied to SG readings (micro strain units): 0.

Table H.2: Wall mounted strain gauge results, east section, June 21, 1984.

"Inner" Column						Outer Column				Axial Stress (MPa)	Bending Stress (MPa)	Moment (kN m)
SG Number	Strain (E-6)	Net Strain	Stress (MPa)	Adjusted Stress	SG Number	Strain (E-6)	Net Strain	Stress (MPa)				
2	-3906	66	13.20	13.77	3	-3705	-3	-0.60	6.59	-7.19	-6.00	
4	-690	76	15.20	15.39	5	-443	53	10.60	13.00	-2.40	-2.00	
6	-914	82	16.40	17.17	7	-2340	-11	-2.20	7.49	-9.69	-8.09	
8	-1619	95	19.00	20.10	9	-4507	-37	-7.40	6.35	-13.75	-11.48	
10	-530	107	21.40	22.91	11	-777	-74	-14.80	4.05	-18.85	-15.74	
12	-5714	154	30.80	32.88	13	-3130	-96	-19.20	6.84	-26.04	-21.74	
14	-129	148	29.60	31.86	15	-4373	-123	-24.60	3.63	-28.23	-23.57	
16	-5806	130	26.00	27.91	17	-2671	-99	-19.80	4.05	-23.85	-19.92	

Temperature dependence correction applied to SG readings (micro strain units): 37.

Table H.3: Wall mounted strain gauge results, east section, July 10, 1984.

"Inner" Column						Outer Column				Axial Stress (MPa)	Bending Stress (MPa)	Moment (kN m)
SG Number	Strain (E-6)	Net Strain	Stress (MPa)	Adjusted Stress	SG Number	Strain (E-6)	Net Strain	Stress (MPa)				
2	-3911	19	3.80	4.36	3	-3708	-48	-9.60	-2.62	-6.98	-5.83	
4	-693	31	6.20	6.23	5	-426	28	5.60	5.91	-0.31	-0.26	
6	-913	41	8.20	8.75	7	-2312	-25	-5.00	1.87	-6.87	-5.74	
8	-1617	55	11.00	12.02	9	-4496	-68	-13.60	-0.79	-12.81	-10.70	
10	-544	51	10.20	11.52	11	-769	-108	-21.60	-5.04	-16.56	-13.83	
12	-5720	106	21.20	23.12	13	-3116	-124	-24.80	-0.84	-23.96	-20.01	
14	-142	93	18.60	20.63	15	-4359	-151	-30.20	-4.78	-25.42	-21.22	
16	-5816	78	15.60	17.29	17	-2655	-125	-25.00	-3.85	-21.15	-17.66	

Temperature dependence correction applied to SG readings (micro strain units): -5.

Table H.4: Wall mounted strain gauge results, east section, August 5, 1984.

"Inner" Column										Outer Column				Axial Stress (MPa)	Bending Stress (MPa)	Moment (kN m)
SG Number	Strain (E-6)	Net Strain	Stress (MPa)	Adjusted Stress	SG Number	Strain (E-6)	Net Strain	Stress (MPa)	Adjusted Stress	SG Number	Strain (E-6)	Net Strain	Stress (MPa)			
2	-3883	72	14.40	15.29	3	-3720	-35	-7.00	4.15	3	-3720	-35	-7.00	-11.15	-9.31	
4	-666	83	16.60	17.17	5	-464	15	3.00	10.08	5	-464	15	3.00	-7.08	-5.91	
6	-881	98	19.60	20.67	7	-2342	-30	-6.00	7.33	7	-2342	-30	-6.00	-13.33	-11.13	
8	-1590	107	21.40	22.92	9	-4529	-76	-15.20	3.86	9	-4529	-76	-15.20	-19.06	-15.92	
10	-525	95	19.00	20.75	11	-801	-115	-23.00	-1.13	11	-801	-115	-23.00	-21.88	-18.27	
12	-5712	139	27.80	29.96	13	-3137	-120	-24.00	2.98	13	-3137	-120	-24.00	-26.98	-22.53	
14	-127	133	26.60	29.02	15	-4390	-157	-31.40	-1.19	15	-4390	-157	-31.40	-30.21	-25.22	
16	-5802	117	23.40	25.39	17	-2677	-122	-24.40	0.50	17	-2677	-122	-24.40	-24.90	-20.79	

Temperature dependence correction applied to SG readings (micro strain units): 20.

Table H.5: Wall mounted strain gauge results, east section, October 3, 1984.

"Inner" Column										Outer Column				Axial Stress (MPa)	Bending Stress (MPa)	Moment (kN m)
SG Number	Strain (E-6)	Net Strain	Stress (MPa)	Adjusted Stress	SG Number	Strain (E-6)	Net Strain	Stress (MPa)	Adjusted Stress	SG Number	Strain (E-6)	Net Strain	Stress (MPa)			
2	-3822	63	12.60	13.70	3	-3684	-69	-13.80	-0.05	3	-3684	-69	-13.80	-13.75	-11.48	
4	-597	82	16.40	16.81	5	-375	33	6.60	11.70	5	-375	33	6.60	-5.10	-4.26	
6	-812	97	19.40	20.94	7	-2330	-88	-17.60	1.67	7	-2330	-88	-17.60	-19.27	-16.09	
8	-1538	89	17.80	19.33	9	-4478	-95	-19.00	0.17	9	-4478	-95	-19.00	-19.17	-16.00	
10	-497	53	10.60	11.82	11	-709	-93	-18.60	-3.39	11	-709	-93	-18.60	-15.21	-12.70	
12	-5679	102	20.40	22.12	13	-3052	-105	-21.00	0.56	13	-3052	-105	-21.00	-21.56	-18.00	
14	-83	107	21.40	23.33	15	-4288	-125	-25.00	-0.83	15	-4288	-125	-25.00	-24.17	-20.18	
16	-5752	97	19.40	21.32	17	-2619	-134	-26.80	-2.74	17	-2619	-134	-26.80	-24.06	-20.09	

Temperature dependence correction applied to SG readings (micro strain units):-50.

Table H.6: Wall mounted strain gauge results, east section, December 5, 1984.

"Inner" Column				Outer Column				Axial Stress (MPa)	Bending Stress (MPa)	Moment (kN m)	
SG Number	Strain (E-6)	Net Strain	Stress (MPa)	Adjusted Stress	SG Number	Strain (E-6)	Net Strain				Stress (MPa)
2	-3812	68	13.60	14.95	3	-3704	-94	-18.80	-1.93	-16.87	-14.09
4	-594	80	16.00	16.77	5	-417	-13	-2.60	7.09	-9.69	-8.09
6	-814	90	18.00	19.62	7	-2341	-104	-20.80	-0.59	-20.21	-16.87
8	-1533	89	17.80	19.62	9	-4507	-129	-25.80	-3.09	-22.71	-18.96
10	-492	53	10.60	12.03	11	-730	-119	-23.80	-5.88	-17.92	-14.96
12	-5684	92	18.40	20.19	13	-3065	-123	-24.60	-2.20	-22.40	-18.70
14	-94	91	18.20	20.02	15	-4285	-127	-25.40	-2.69	-22.71	-18.96
16	-5758	86	17.20	19.01	17	-2611	-131	-26.20	-3.60	-22.60	-18.87

Temperature dependence correction applied to SG readings (micro strain units):-55.

Table H.7: Wall mounted strain gauge results, east section, February 11, 1985.

"Inner" Column				Outer Column				Axial Stress (MPa)	Bending Stress (MPa)	Moment (kN m)	
SG Number	Strain (E-6)	Net Strain	Stress (MPa)	Adjusted Stress	SG Number	Strain (E-6)	Net Strain				Stress (MPa)
2	-3853	85	17.00	18.82	3	-3802	-134	-26.80	-3.99	-22.81	-19.05
4	-640	92	18.40	19.15	5	-460	2	0.40	9.77	-9.37	-7.83
6	-861	101	20.20	21.80	7	-2386	-91	-18.20	1.80	-20.00	-16.70
8	-1580	100	20.00	21.88	9	-4562	-126	-25.20	-1.66	-23.54	-19.56
10	-552	51	10.20	11.77	11	-806	-137	-27.40	-7.82	-19.58	-16.35
12	-5719	115	23.00	24.90	13	-3113	-113	-22.60	1.15	-23.75	-19.83
14	-131	112	22.40	24.65	15	-4374	-158	-31.60	-3.48	-28.13	-23.48
16	-5793	109	21.80	23.94	17	-2686	-148	-29.60	-2.83	-26.77	-22.35

Temperature dependence correction applied to SG readings (micro strain units): 3.

Table H.8: Wall mounted strain gauge results, east section, August 29, 1985.

"Inner" Column				Outer Column				Axial Stress (MPa)	Bending Stress (MPa)	Moment (kN m)
SG Number	Strain (E-6)	Net Strain	Stress (MPa)	Adjusted Stress	SG Number	Strain (E-6)	Net Strain			
2	-3856	80	16.00	17.68	3	-3788	-122	-24.40	-3.36	-17.57
4	-642	88	17.60	18.22	5	-446	14	2.80	10.51	-6.44
6	-856	104	20.80	22.14	7	-2350	-57	-11.40	5.37	-14.00
8	-1578	100	20.00	21.59	9	-4525	-91	-18.20	1.70	-16.61
10	-549	52	10.40	11.64	11	-764	-37	-19.40	-3.88	-12.96
12	-5704	128	25.60	27.58	13	-3108	-110	-22.00	2.79	-20.70
14	-120	121	24.20	26.37	15	-4353	-139	-27.80	-0.72	-22.61
16	-5766	134	26.80	29.18	17	-2688	-152	-30.40	-0.61	-24.88

Temperature dependence correction applied to SG readings (micro strain units): 1.

Table H.9: Wall mounted strain gauge results, east section, March 25, 1986.

"Inner" Column				Outer Column				Axial Stress (MPa)	Bending Stress (MPa)	Moment (kN m)
SG Number	Strain (E-6)	Net Strain	Stress (MPa)	Adjusted Stress	SG Number	Strain (E-6)	Net Strain			
2	-3840	107	21.40	23.57	3	-3830	-153	-30.60	-3.52	-22.61
4	-621	120	24.00	25.28	5	-505	-34	-6.80	9.24	-13.39
6	-842	129	25.80	27.45	7	-2373	-69	-13.80	6.82	-17.22
8	-1561	128	25.60	27.73	9	-4573	-128	-25.60	1.07	-22.27
10	-540	72	14.40	16.07	11	-807	-129	-25.80	-4.86	-17.48
12	-5709	134	26.80	28.79	13	-3114	-105	-21.00	3.90	-20.79
14	-134	118	23.60	25.86	15	-4378	-153	-30.60	-2.37	-23.57
16	-5771	140	28.00	30.50	17	-2707	-160	-32.00	-0.75	-26.09

Temperature dependence correction applied to SG readings (micro strain units): 12.

Table H.10: Wall mounted strain gauge results, east section, July 29, 1986.

"Inner" Column				Outer Column				Axial Stress (MPa)	Bending Stress (MPa)	Moment (kN m)	
SG Number	Strain (E-6)	Net Strain	Stress (MPa)	Adjusted Stress	SG Number	Strain (E-6)	Net Strain				Stress (MPa)
2	-3848	34	6.80	7.97	3	-3718	-106	-21.20	-6.62	-14.58	-12.18
4	-619	57	11.40	11.64	5	-378	28	5.60	8.62	-3.02	-2.52
6	-826	80	16.00	16.85	7	-2261	-22	-4.40	6.22	-10.62	-8.87
8	-1556	68	13.60	14.68	9	-4442	-62	-12.40	1.14	-13.54	-11.31
10	-497	50	10.00	11.04	11	-688	-75	-15.00	-1.98	-13.02	-10.87
12	-5653	125	25.00	27.15	13	-3077	-133	-26.60	0.27	-26.88	-22.44
14	-43	144	28.80	31.35	15	-4322	-162	-32.40	-0.53	-31.88	-26.62
16	-5722	124	24.80	27.15	17	-2640	-158	-31.60	-2.23	-29.38	-24.53

Temperature dependence correction applied to SG readings (micro strain units):-53.

Table H.11: Wall mounted strain gauge results, east section, December 10, 1986.

"Inner" Column				Outer Column				Axial Stress (MPa)	Bending Stress (MPa)	Moment (kN m)	
SG Number	Strain (E-6)	Net Strain	Stress (MPa)	Adjusted Stress	SG Number	Strain (E-6)	Net Strain				Stress (MPa)
2	-3830	86	17.20	19.10	3	-3788	-142	-28.40	-4.65	-23.75	-19.83
4	-617	93	18.60	19.55	5	-461	-21	-4.20	7.67	-11.87	-9.92
6	-835	105	21.00	22.37	7	-2332	-59	-11.80	5.28	-17.08	-14.26
8	-1563	95	19.00	20.72	9	-4525	-111	-22.20	-0.74	-21.46	-17.92
10	-533	48	9.60	10.86	11	-750	-103	-20.60	-4.87	-15.73	-13.13
12	-5680	132	26.40	28.62	13	-3113	-135	-27.00	0.81	-27.81	-23.22
14	-93	128	25.60	28.01	15	-4355	-161	-32.20	-2.10	-30.10	-25.14
16	-5740	140	28.00	30.54	17	-2681	-165	-33.00	-1.23	-31.77	-26.53

Temperature dependence correction applied to SG readings (micro strain units):-19.

Table H.12: Wall mounted strain gauge results, east section, February 16, 1987.

SG Number	"Inner" Column					Outer Column				Axial Stress (MPa)	Bending Stress (MPa)	Moment (kN m)
	Strain (E-6)	Net Strain	Stress (MPa)	Adjusted Stress	SG Number	Strain (E-6)	Net Strain	Stress (MPa)				
2	-3839	82	16.40	18.34	3	-3802	-151	-30.20	-5.93	-24.27	-20.27	
4	-626	89	17.80	18.77	5	-472	-27	-5.40	6.68	-12.08	-10.09	
6	-847	98	19.60	20.98	7	-2346	-68	-13.60	3.69	-17.29	-14.44	
8	-1572	91	18.20	19.99	9	-4543	-124	-24.80	-2.40	-22.40	-18.70	
10	-540	46	9.20	10.59	11	-773	-121	-24.20	-6.80	-17.40	-14.53	
12	-5679	138	27.60	29.96	13	-3128	-145	-29.00	0.48	-29.48	-24.62	
14	-106	120	24.00	26.44	15	-4372	-173	-34.60	-4.08	-30.52	-25.48	
16	-5752	133	26.60	29.20	17	-2700	-179	-35.80	-3.30	-32.50	-27.14	

Temperature dependence correction applied to SG readings (micro strain units):-14.

Table H.13: Wall mounted strain gauge results, east section, March 25, 1987.

"Inner" Column				Outer Column				Axial Stress (MPa)	Bending Stress (MPa)	Moment (kN m)
SG Number	Strain (E-6)	Net Strain	Stress (MPa)	Adjusted Stress	SG Number	Strain (E-6)	Net Strain			
22	-1231	0	0.0	0.0	23	-67	0	0.0	0.0	0.0
24	-1165	0	0.0	0.0	25	1156	0	0.0	0.0	0.0
26	-2522	0	0.0	0.0	27	-3935	0	0.0	0.0	0.0
28	-4036	0	0.0	0.0	29	-3849	0	0.0	0.0	0.0
30	-452	0	0.0	0.0	31	-2028	0	0.0	0.0	0.0
32	-1347	0	0.0	0.0	33	-1835	0	0.0	0.0	0.0
36	-2367	0	0.0	0.0	37	-6580	0	0.0	0.0	0.0
38	-2011	0	0.0	0.0	39	-5170	0	0.0	0.0	0.0

Temperature dependence correction applied to SG readings (micro strain units): 0.

Table H.14: Wall mounted strain gauge results, west section, June 20, 1984.

"Inner" Column				Outer Column				Axial Stress (MPa)	Bending Stress (MPa)	Moment (kN m)
SG Number	Strain (E-6)	Net Strain	Stress (MPa)	Adjusted Stress	SG Number	Strain (E-6)	Net Strain			
22	-1238	-7	-1.40	-1.37	23	-77	-10	-2.00	-0.31	-0.26
24	-1167	-2	-0.40	-0.38	25	1152	-4	-0.80	-0.21	-0.17
26	-2518	4	0.80	0.97	27	-3952	-17	-3.40	-2.19	-1.83
28	-4028	8	1.60	1.84	29	-3870	-21	-4.20	-3.02	-2.52
30	-408	44	8.80	9.52	31	-2070	-42	-8.40	-8.96	-7.48
32	-1235	112	22.40	24.29	33	-1950	-115	-23.00	-23.65	-19.74
36	-2339	28	5.60	6.35	37	-6642	-62	-12.40	-9.38	-7.83
38	-1977	34	6.80	7.40	39	-5208	-38	-7.60	-7.50	-6.26

Temperature dependence correction applied to SG readings (micro strain units): 0.

Table H.15: Wall mounted strain gauge results, west section, June 21, 1984.

"Inner" Column				Outer Column				Axial Stress (MPa)	Bending Stress (MPa)	Moment (kN m)	
SG Number	Strain (E-6)	Net Strain	Stress (MPa)	Adjusted Stress	SG Number	Strain (E-6)	Net Strain				Stress (MPa)
22	-1217	51	10.20	10.70	23	-113	-9	-1.80	4.45	-6.25	-5.22
24	-1138	64	12.80	13.61	25	1086	-33	-6.60	3.50	-10.10	-8.44
26	-2491	68	13.60	14.37	27	-3997	-25	-5.00	4.69	-9.69	-8.09
28	-3994	79	15.80	16.55	29	-3897	-11	-2.20	7.18	-9.38	-7.83
30	-393	96	19.20	20.26	31	-2096	-31	-6.20	7.03	-13.23	-11.05
32	-1230	154	30.80	32.87	33	-1967	-95	-19.00	6.94	-25.94	-21.66
36	-2344	60	12.00	12.62	37	-6631	-14	-2.80	4.91	-7.71	-6.44
38	-1985	63	12.60	13.06	39	-5199	8	1.60	7.33	-5.73	-4.78

Temperature dependence correction applied to SG readings (micro strain units): 37.

Table H.16: Wall mounted strain gauge results, west section, July 10, 1984.

"Inner" Column				Outer Column				Axial Stress (MPa)	Bending Stress (MPa)	Moment (kN m)	
SG Number	Strain (E-6)	Net Strain	Stress (MPa)	Adjusted Stress	SG Number	Strain (E-6)	Net Strain				Stress (MPa)
22	-1227	-1	-0.20	0.26	23	-118	-56	-11.20	-5.47	-5.73	-4.78
24	-1143	17	3.40	3.67	25	1145	-16	-3.20	0.24	-3.44	-2.87
26	-2488	29	5.80	6.65	27	-4003	-73	-14.60	-3.98	-10.62	-8.87
28	-3988	43	8.60	9.45	29	-3903	-59	-11.80	-1.18	-10.62	-8.87
30	-382	65	13.00	14.23	31	-2106	-83	-16.60	-1.18	-15.42	-12.87
32	-1236	106	21.20	23.12	33	-1954	-124	-24.80	-0.84	-23.96	-20.01
36	-2351	11	2.20	2.70	37	-6624	-49	-9.80	-3.55	-6.25	-5.22
38	-1997	9	1.80	2.07	39	-5189	-24	-4.80	-1.36	-3.44	-2.87

Temperature dependence correction applied to SG readings (micro strain units): -5.

Table H.17: Wall mounted strain gauge results, west section, August 5, 1984.

"Inner" Column										Outer Column				Axial Stress (MPa)	Bending Stress (MPa)	Moment (kN m)
SG Number	Strain (E-6)	Net Strain	Stress (MPa)	Adjusted Stress	SG Number	Strain (E-6)	Net Strain	Stress (MPa)		Stress (MPa)						
22	-1204	47	9.40	10.33	23	-152	-65	-13.00		-13.00		-1.33	-11.67	-9.74		
24	-1119	66	13.20	14.42	25	1055	-81	-16.20		-16.20		-0.89	-15.31	-12.79		
26	-2456	86	17.20	18.39	27	-4012	-57	-11.40		-11.40		3.50	-14.90	-12.44		
28	-3964	92	18.40	19.51	29	-3910	-41	-8.20		-8.20		5.65	-13.85	-11.57		
30	-368	104	20.80	22.34	31	-2129	-81	-16.20		-16.20		3.07	-19.27	-16.09		
32	-1217	150	30.00	32.34	33	-1986	-131	-26.20		-26.20		5.16	-29.27	-24.44		
36	-2308	79	15.80	16.72	37	-6632	-32	-6.40		-6.40		6.32	-11.56	-9.65		
38	-1962	69	13.80	14.45	39	-5199	-9	-1.80		-1.80			-8.13	-6.78		

Temperature dependence correction applied to SG readings (micro strain units): 20.

Table H.18: Wall mounted strain gauge results, west section, October 3, 1984.

"Inner" Column										Outer Column				Axial Stress (MPa)	Bending Stress (MPa)	Moment (kN m)
SG Number	Strain (E-6)	Net Strain	Stress (MPa)	Adjusted Stress	SG Number	Strain (E-6)	Net Strain	Stress (MPa)		Stress (MPa)						
22	-1142	39	7.80	8.95	23	-116	-99	-19.80		-19.80		-5.43	-14.37	-12.00		
24	-1042	73	14.60	15.88	25	1125	-81	-16.20		-16.20		-0.16	-16.04	-13.39		
26	-2385	87	17.40	19.23	27	-4018	-133	-26.60		-26.60		-3.68	-22.92	-19.14		
28	-3909	77	15.40	16.73	29	-3882	-83	-16.60		-16.60		0.07	-16.67	-13.92		
30	-368	34	6.80	7.59	31	-2039	-61	-12.20		-12.20		-2.30	-9.90	-8.26		
32	-1188	109	21.80	23.90	33	-1928	-143	-28.60		-28.60		-2.35	-26.25	-21.92		
36	-2238	79	15.80	17.20	37	-6619	-89	-17.80		-17.80		-0.30	-17.50	-14.61		
38	-1885	76	15.20	16.28	39	-5174	-54	-10.80		-10.80		2.74	-13.54	-11.31		

Temperature dependence correction applied to SG readings (micro strain units):-50.

Table H.19: Wall mounted strain gauge results, west section, December 5, 1984.

"Inner" Column						Outer Column				Axial Stress (MPa)	Bending Stress (MPa)	Moment (kN m)
SG Number	Strain (E-6)	Net Strain	Stress (MPa)	Adjusted Stress	SG Number	Strain (E-6)	Net Strain	Stress (MPa)				
22	-1137	39	7.80	9.16	23	-136	-124	-24.80	-7.82	-16.98	-14.18	
24	-1049	61	12.20	13.60	25	1104	-107	-21.40	-3.90	-17.50	-14.61	
26	-2390	77	15.40	17.37	27	-4039	-159	-31.80	-7.22	-24.58	-20.53	
28	-3911	70	14.00	15.52	29	-3907	-113	-22.60	-3.54	-19.06	-15.92	
30	-372	25	5.00	5.90	31	-2056	-83	-16.60	-5.35	-11.25	-9.39	
32	-1170	122	24.40	26.83	33	-1950	-170	-34.00	-3.58	-30.42	-25.40	
36	-2254	58	11.60	12.77	37	-6607	-82	-16.40	-1.82	-14.58	-12.18	
38	-1897	59	11.80	12.71	39	-5165	-50	-10.00	1.35	-11.35	-9.48	

Temperature dependence correction applied to SG readings (micro strain units):-55.

Table H.20: Wall mounted strain gauge results, west section, February 11, 1985.

"Inner" Column						Outer Column				Axial Stress (MPa)	Bending Stress (MPa)	Moment (kN m)
SG Number	Strain (E-6)	Net Strain	Stress (MPa)	Adjusted Stress	SG Number	Strain (E-6)	Net Strain	Stress (MPa)				
22	-1155	79	15.80	17.82	23	-234	-164	-32.80	-7.49	-25.31	-21.14	
24	-1060	108	21.60	23.76	25	1002	-151	-30.20	-3.22	-26.98	-22.53	
26	-2397	128	25.60	27.98	27	-4096	-158	-31.60	-1.81	-29.79	-24.68	
28	-3924	115	23.00	24.79	29	-3952	-100	-20.00	2.40	-22.40	-18.70	
30	-393	62	12.40	13.81	31	-2138	-107	-21.40	-3.80	-17.60	-14.70	
32	-1224	126	25.20	27.64	33	-2005	-167	-33.40	-2.88	-30.52	-25.48	
36	-2266	104	20.80	22.32	37	-6661	-78	-15.60	3.36	-18.96	-15.83	
38	-1948	66	13.20	14.16	39	-5222	-49	-9.80	2.18	-11.98	-10.00	

Temperature dependence correction applied to SG readings (micro strain units): 3.

Table H.21: Wall mounted strain gauge results, west section, August 29, 1985.

"Inner" Column						Outer Column				Axial Stress (MPa)	Bending Stress (MPa)	Moment (kN m)
SG Number	Strain (E-6)	Net Strain	Stress (MPa)	Adjusted Stress	SG Number	Strain (E-6)	Net Strain	Stress (MPa)				
22	-1148	84	16.80	18.77	23	-220	-152	-30.40	-5.82	-24.58	-20.53	
24	-1054	112	22.40	24.40	25	1027	-128	-25.60	-0.60	-25.00	-20.88	
26	-2396	127	25.40	27.86	27	-4104	-168	-33.60	-2.87	-30.73	-25.66	
28	-3925	112	22.40	24.15	29	-3948	-98	-19.60	2.27	-21.88	-18.27	
30	-397	56	11.20	12.19	31	-2092	-53	-12.60	-0.20	-12.40	-10.35	
32	-1202	146	29.20	31.57	33	-1975	-139	-27.80	1.89	-29.69	-24.79	
36	-2276	92	18.40	19.78	37	-6655	-74	-14.80	2.49	-17.29	-14.44	
38	-1924	88	17.60	18.67	39	-5212	-41	-8.20	5.24	-13.44	-11.22	

Temperature dependence correction applied to SG readings (micro strain units): 1.

Table H.22: Wall mounted strain gauge results, west section, March 25, 1986.

"Inner" Column						Outer Column				Axial Stress (MPa)	Bending Stress (MPa)	Moment (kN m)
SG Number	Strain (E-6)	Net Strain	Stress (MPa)	Adjusted Stress	SG Number	Strain (E-6)	Net Strain	Stress (MPa)				
22	-1147	96	19.20	21.52	23	-262	-183	-36.60	-7.54	-29.06	-24.27	
24	-1051	126	25.20	27.87	25	950	-194	-38.80	-5.47	-33.33	-27.83	
26	-2385	149	29.80	32.57	27	-4130	-183	-36.60	-2.02	-34.58	-28.88	
28	-3918	130	26.00	28.07	29	-3979	-118	-23.60	2.23	-25.83	-21.57	
30	-424	40	8.00	9.27	31	-2152	-112	-22.40	-6.57	-15.83	-13.22	
32	-1258	101	20.20	22.45	33	-2016	-169	-33.80	-5.68	-28.13	-23.48	
36	-2303	76	15.20	16.30	37	-6648	-56	-11.20	2.55	-13.75	-11.48	
38	-1973	50	10.00	10.65	39	-5210	-28	-5.60	2.52	-8.13	-6.78	

Temperature dependence correction applied to SG readings (micro strain units): 12.

Table H.23: Wall mounted strain gauge results, west section, July 29, 1986.

"Inner" Column				Outer Column				Axial Stress (MPa)	Bending Stress (MPa)	Moment (kN m)	
SG Number	Strain (E-6)	Net Strain	Stress (MPa)	Adjusted Stress	SG Number	Strain (E-6)	Net Strain				Stress (MPa)
22	-1117	61	12.20	13.84	23	-150	-136	-27.20	-6.68	-20.52	-17.13
24	-1015	97	19.40	20.89	25	1127	-82	-16.40	2.25	-18.65	-15.57
26	-2366	103	20.60	22.84	27	-4048	-166	-33.20	-5.18	-28.02	-23.40
28	-3878	105	21.00	22.74	29	-3900	-104	-20.80	0.97	-21.77	-18.18
30	-336	63	12.60	13.77	31	-2053	-78	-15.60	-0.91	-14.69	-12.26
32	-1165	129	25.80	27.92	33	-1907	-125	-25.00	1.46	-26.46	-22.09
36	-2271	43	8.60	9.60	37	-6604	-77	-15.40	-2.90	-12.50	-10.44
38	-1914	44	8.80	9.41	39	-5146	-29	-5.80	1.80	-7.60	-6.35

Temperature dependence correction applied to SG readings (micro strain units):-53.

Table H.24: Wall mounted strain gauge results, west section, December 10, 1986.

"Inner" Column				Outer Column				Axial Stress (MPa)	Bending Stress (MPa)	Moment (kN m)	
SG Number	Strain (E-6)	Net Strain	Stress (MPa)	Adjusted Stress	SG Number	Strain (E-6)	Net Strain				Stress (MPa)
22	-1116	96	19.20	21.43	23	-220	-172	-34.40	-6.48	-27.92	-23.31
24	-1020	126	25.20	27.38	25	1039	-136	-27.20	0.09	-27.29	-22.79
26	-2374	129	25.80	28.52	27	-4114	-198	-39.60	-5.54	-34.06	-28.44
28	-3902	115	23.00	24.96	29	-3950	-120	-24.00	0.48	-24.48	-20.44
30	-372	61	12.20	13.35	31	-2086	-77	-15.40	-1.03	-14.38	-12.00
32	-1182	146	29.20	31.67	33	-1967	-151	-30.20	0.74	-30.94	-25.83
36	-2279	69	13.80	15.00	37	-6636	-75	-15.00	-0.00	-15.00	-12.52
38	-1926	66	13.20	14.12	39	-5196	-45	-9.00	2.56	-11.56	-9.65

Temperature dependence correction applied to SG readings (micro strain units):-19.

Table H.25: Wall mounted strain gauge results, west section, February 16, 1987.

SG Number	"Inner" Column			Adjusted Stress	SG Number	Outer Column			Axial Stress (MPa)	Bending Stress (MPa)	Moment (kN m)
	Strain (E-6)	Net Strain	Stress (MPa)			Strain (E-6)	Net Strain	Stress (MPa)			
22	-1130	87	17.40	19.63	23	-234	-181	-36.20	-8.28	-27.92	-23.31
24	-1036	115	23.00	25.27	25	1013	-157	-31.40	-3.07	-28.33	-23.66
26	-2378	130	26.00	28.84	27	-4132	-211	-42.20	-6.68	-35.52	-29.66
28	-3914	108	21.60	23.59	29	-3966	-131	-26.20	-1.30	-24.90	-20.79
30	-385	53	10.60	11.86	31	-2112	-98	-19.60	-3.87	-15.73	-13.13
32	-1204	129	25.80	28.25	33	-1986	-165	-33.00	-2.38	-30.62	-25.57
36	-2260	93	18.60	20.06	37	-6648	-82	-16.40	1.83	-18.23	-15.22
38	-1940	57	11.40	12.29	39	-5206	-50	-10.00	1.15	-11.15	-9.31

Temperature dependence correction applied to SG readings (micro strain units):-14.

Table H.26: Wall mounted strain gauge results, west section, March 25, 1987.

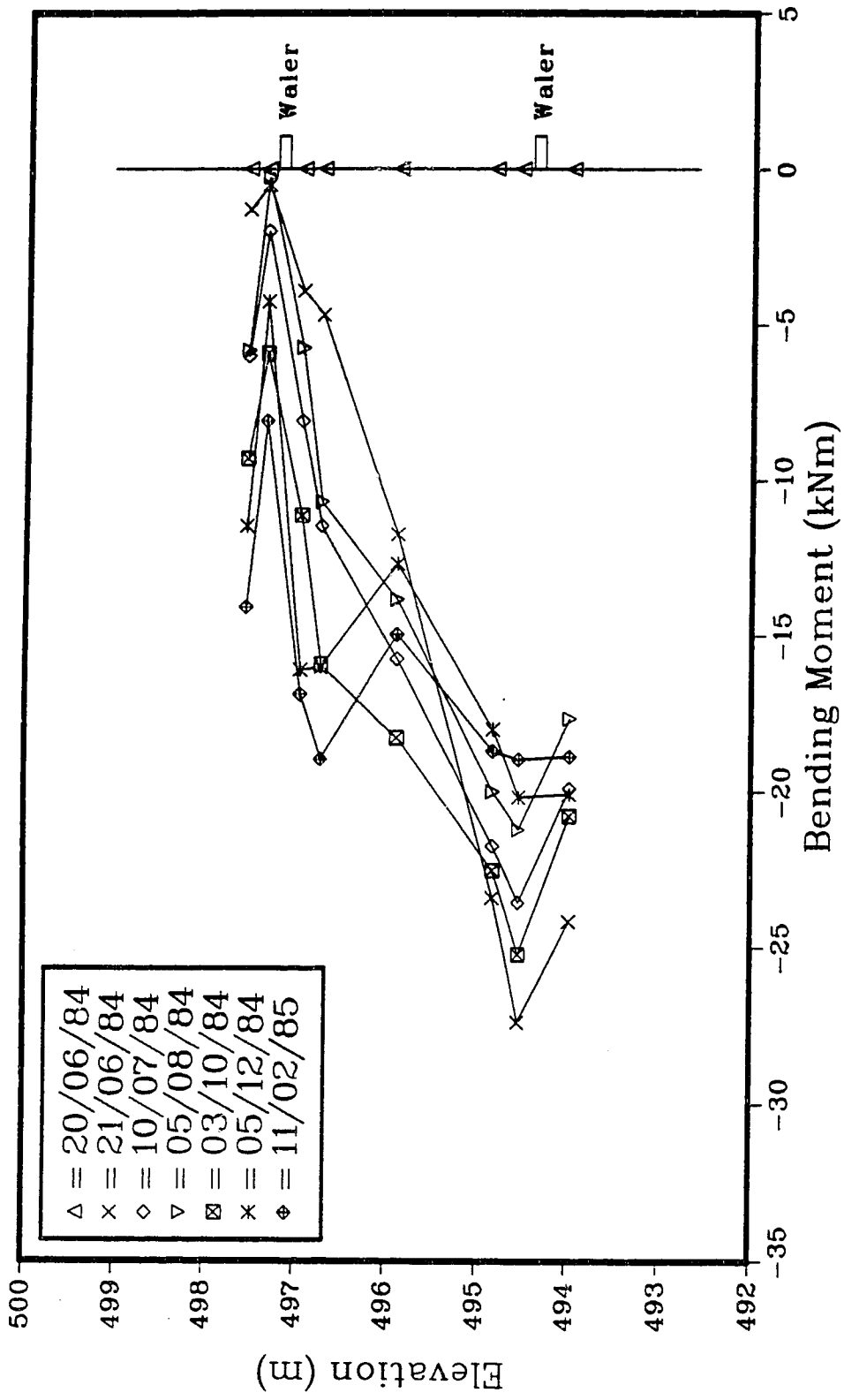


Figure H.1: Field determined moments, east section, early epochs.

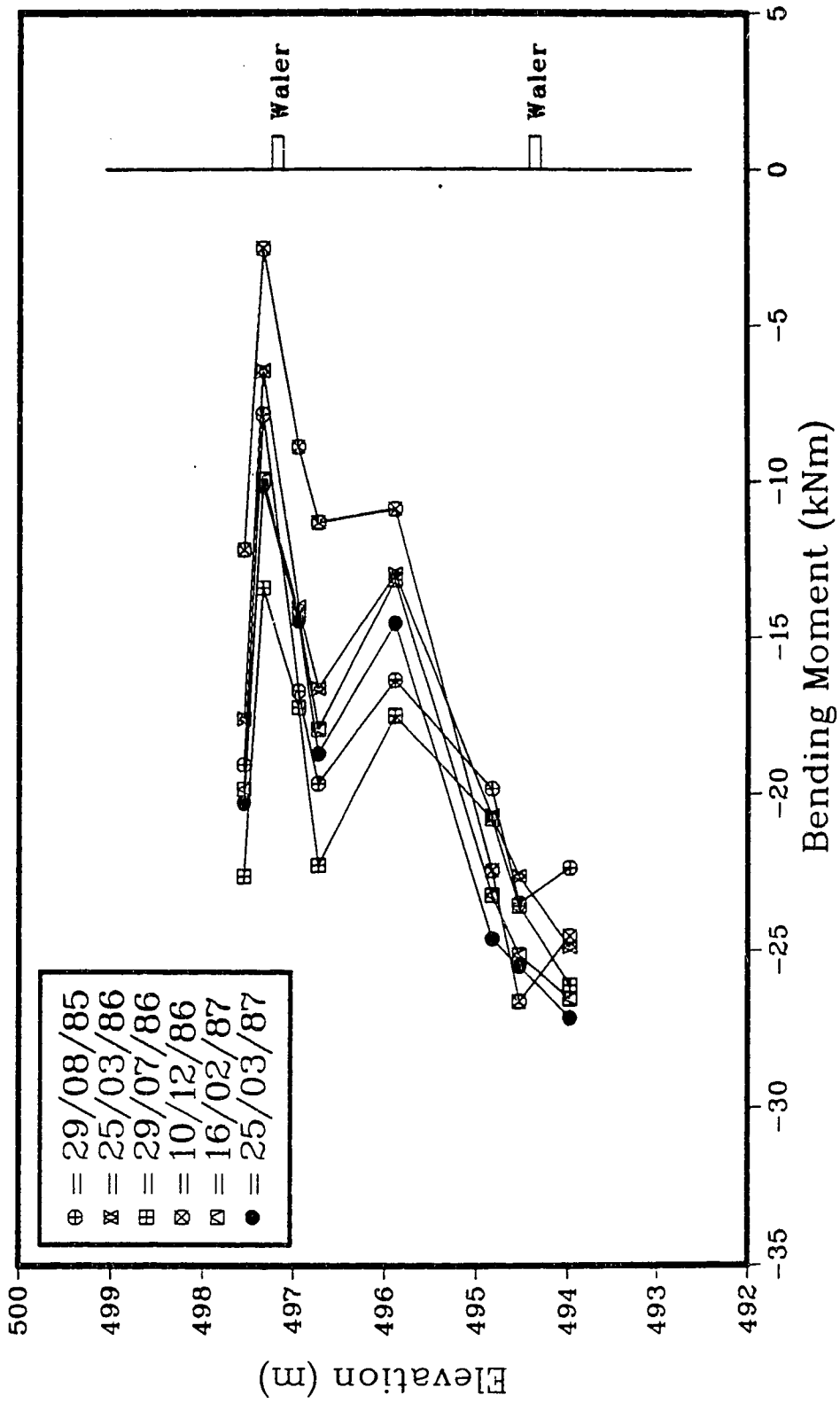


Figure H.2: Field determined moments, east section, late epochs.

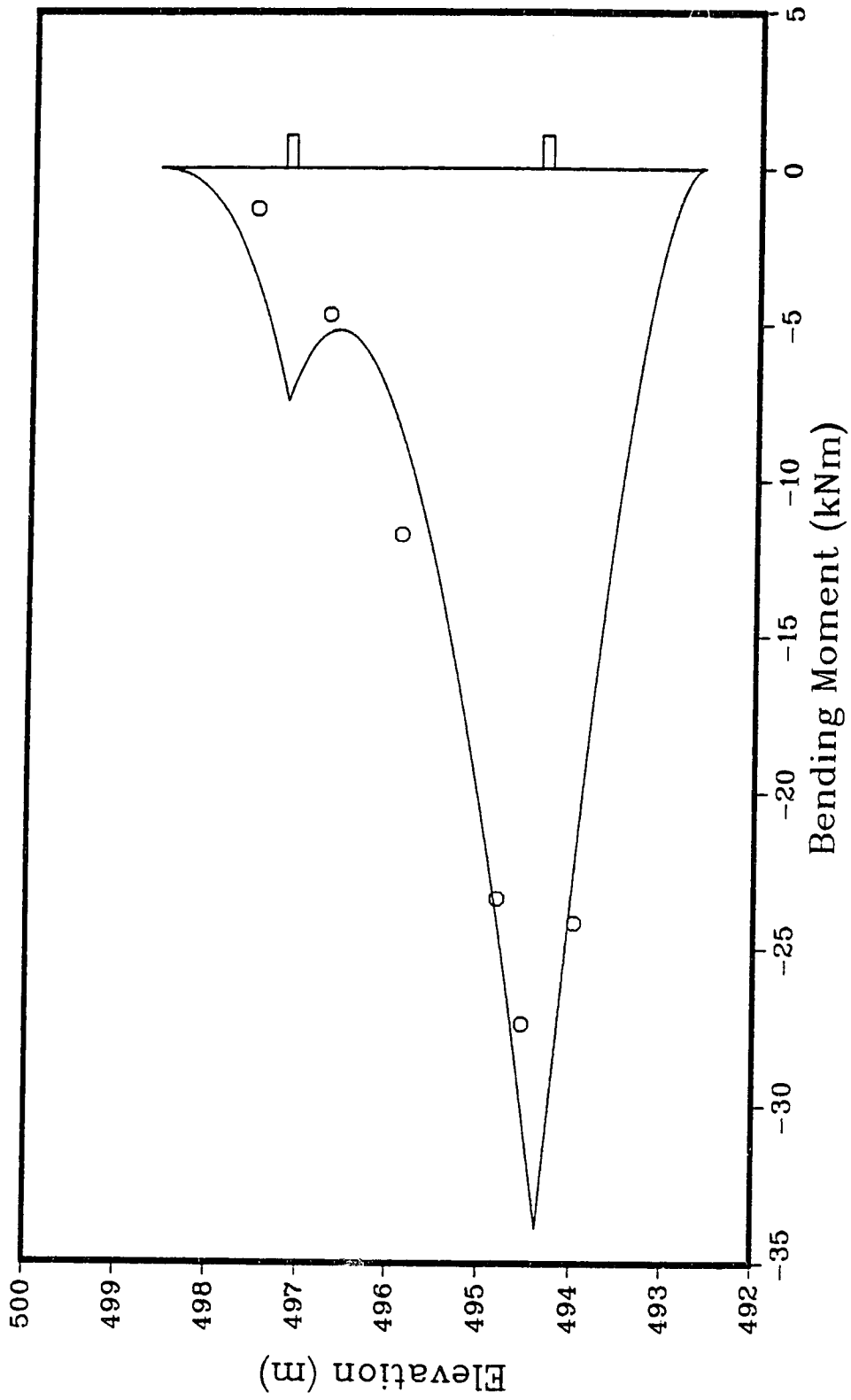


Figure H.3: Interpolated bending moment, east section, June 21, 1984.

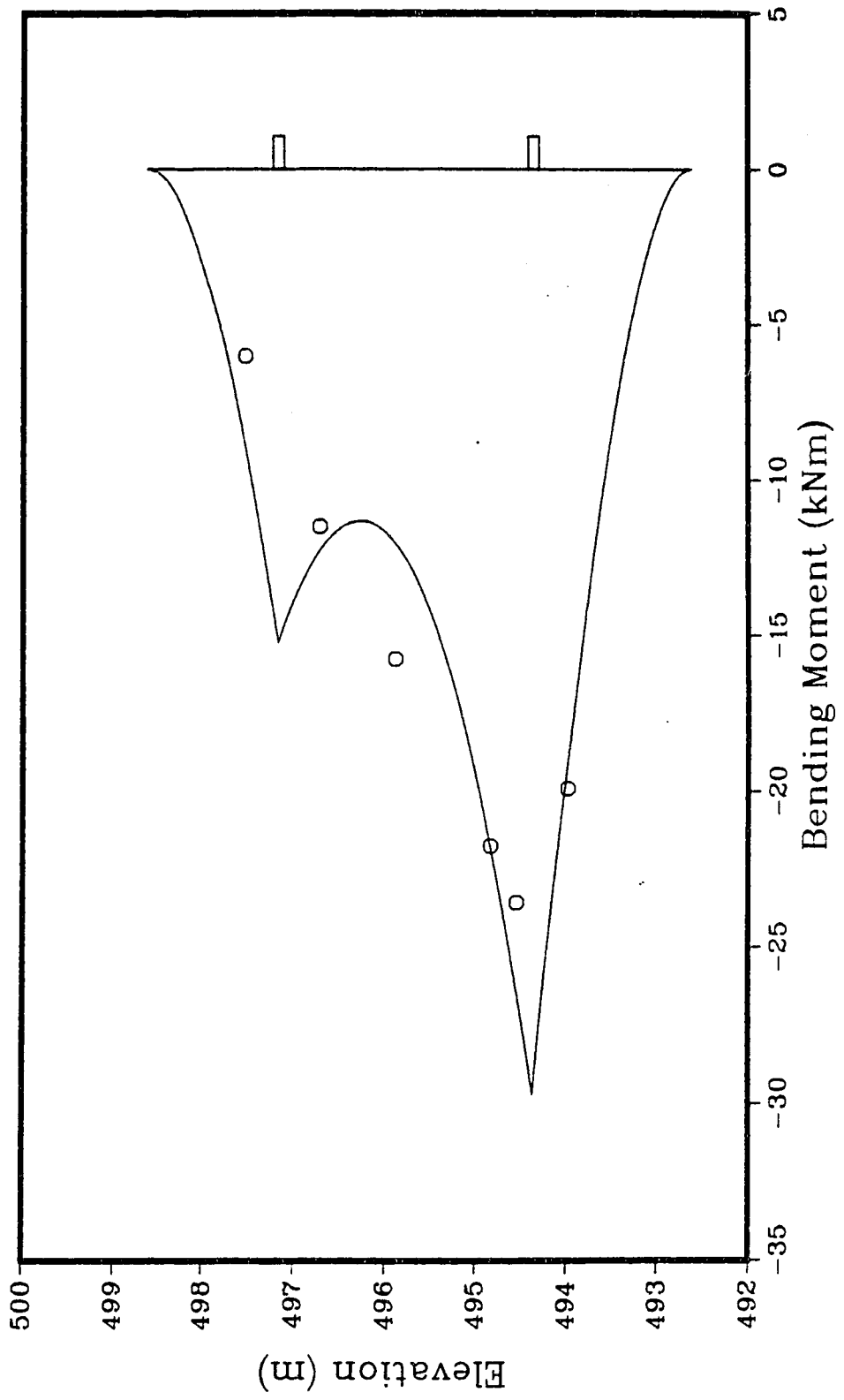


Figure H.4: Interpolated bending moment, east section, July 10, 1984.

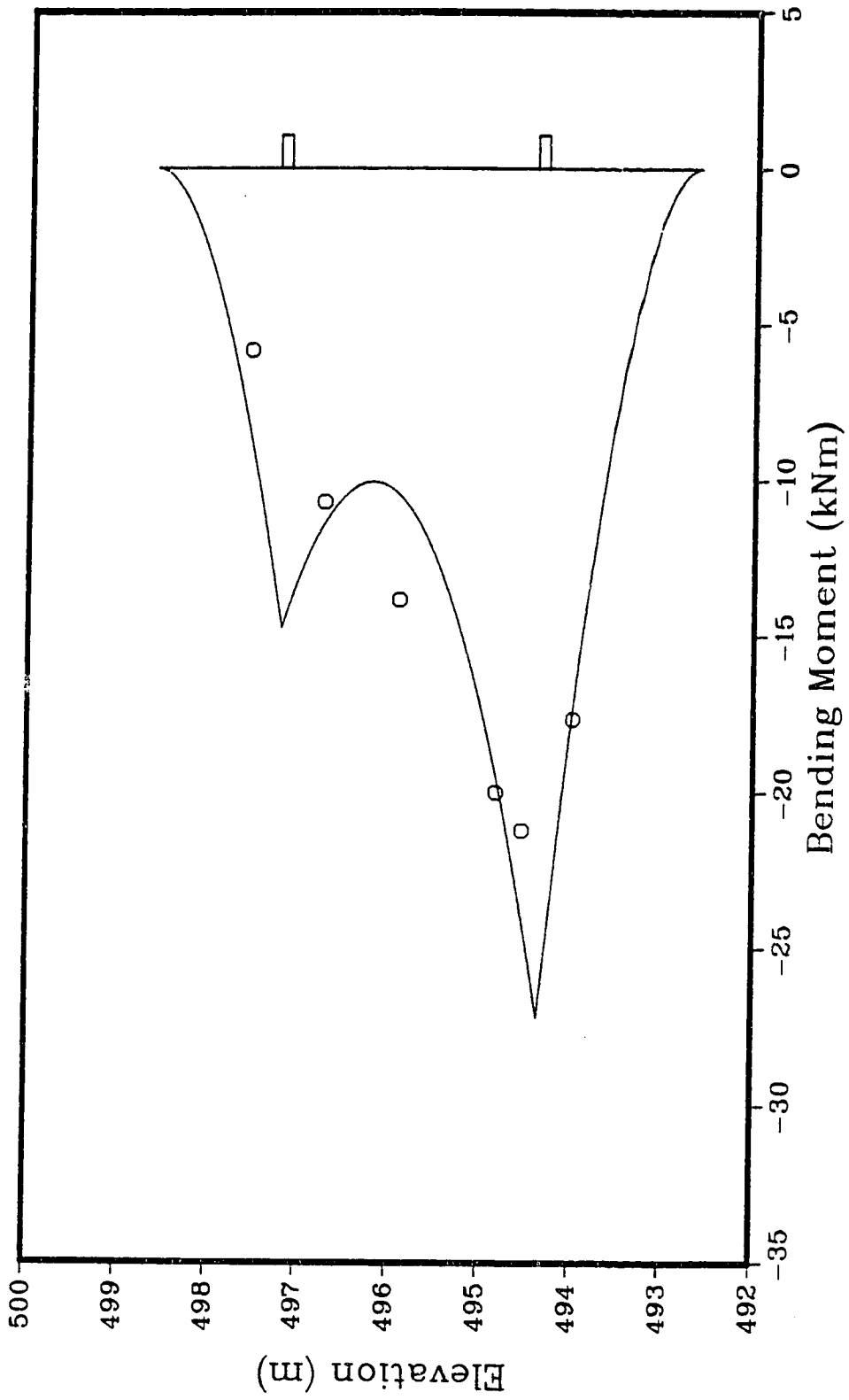


Figure H.5: Interpolated bending moment, east section, August 5, 1984.

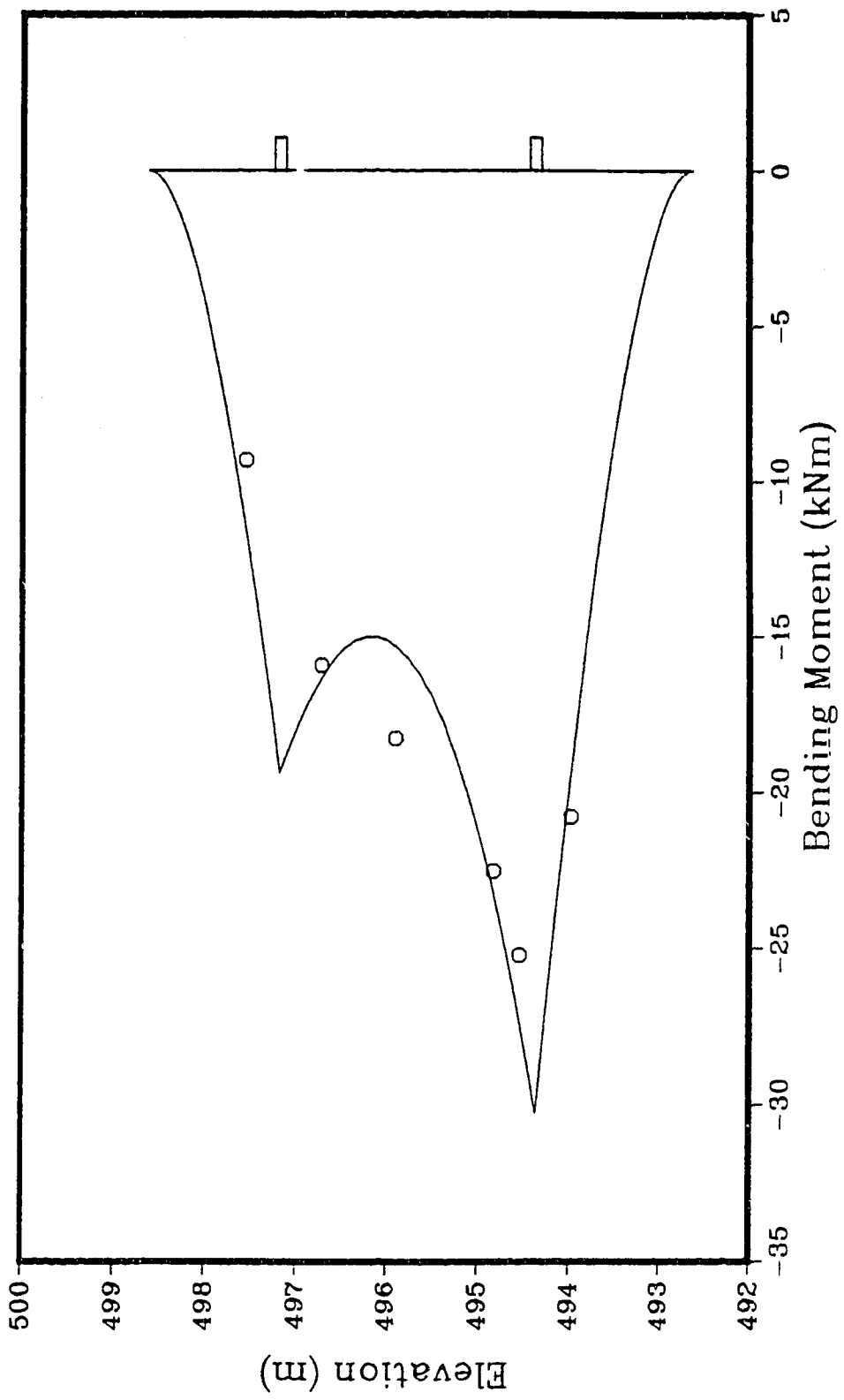


Figure H.6: Interpolated bending moment, east section, October 3, 1984.

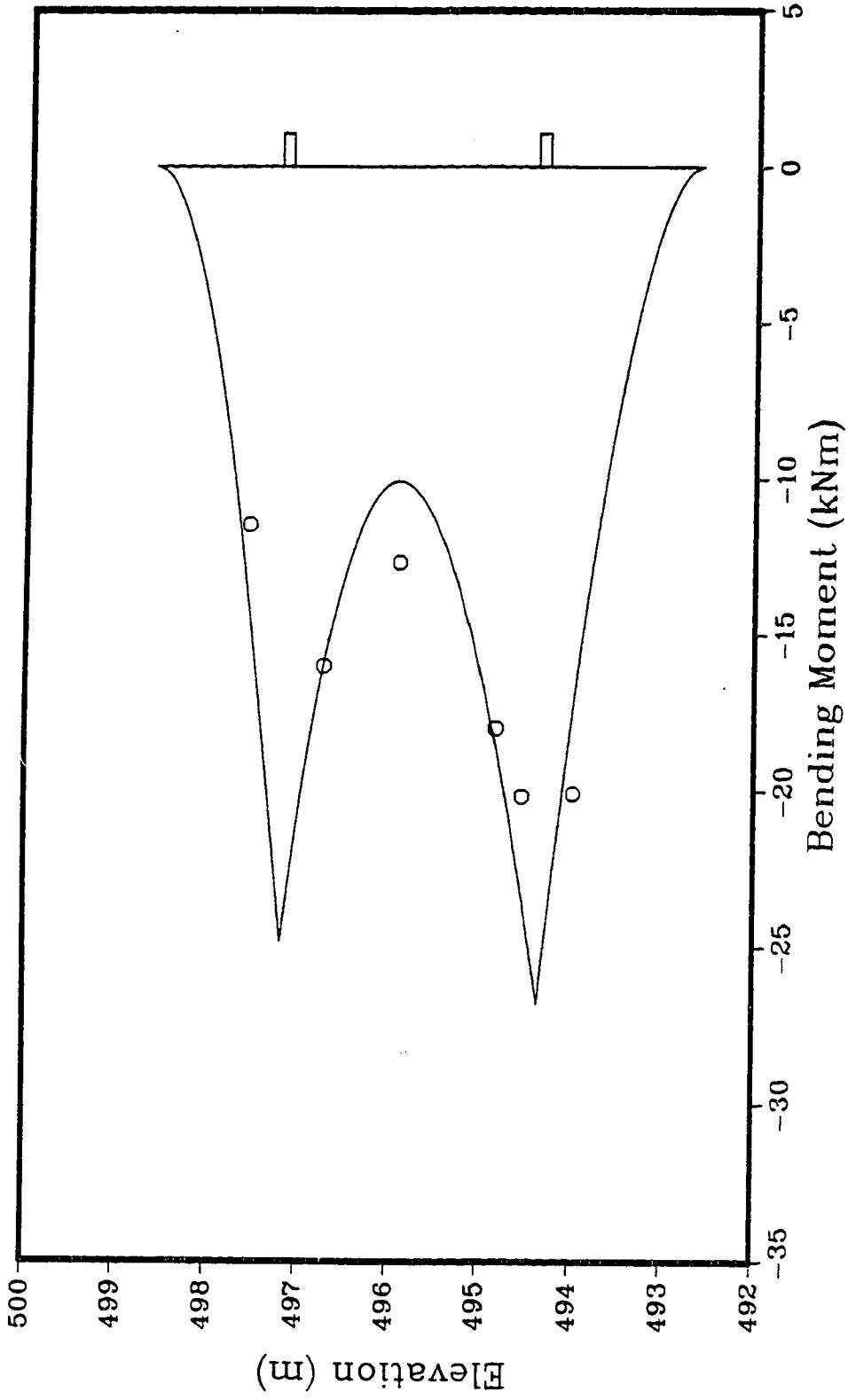


Figure H.7: Interpolated bending moment, east section, December 5, 1984.

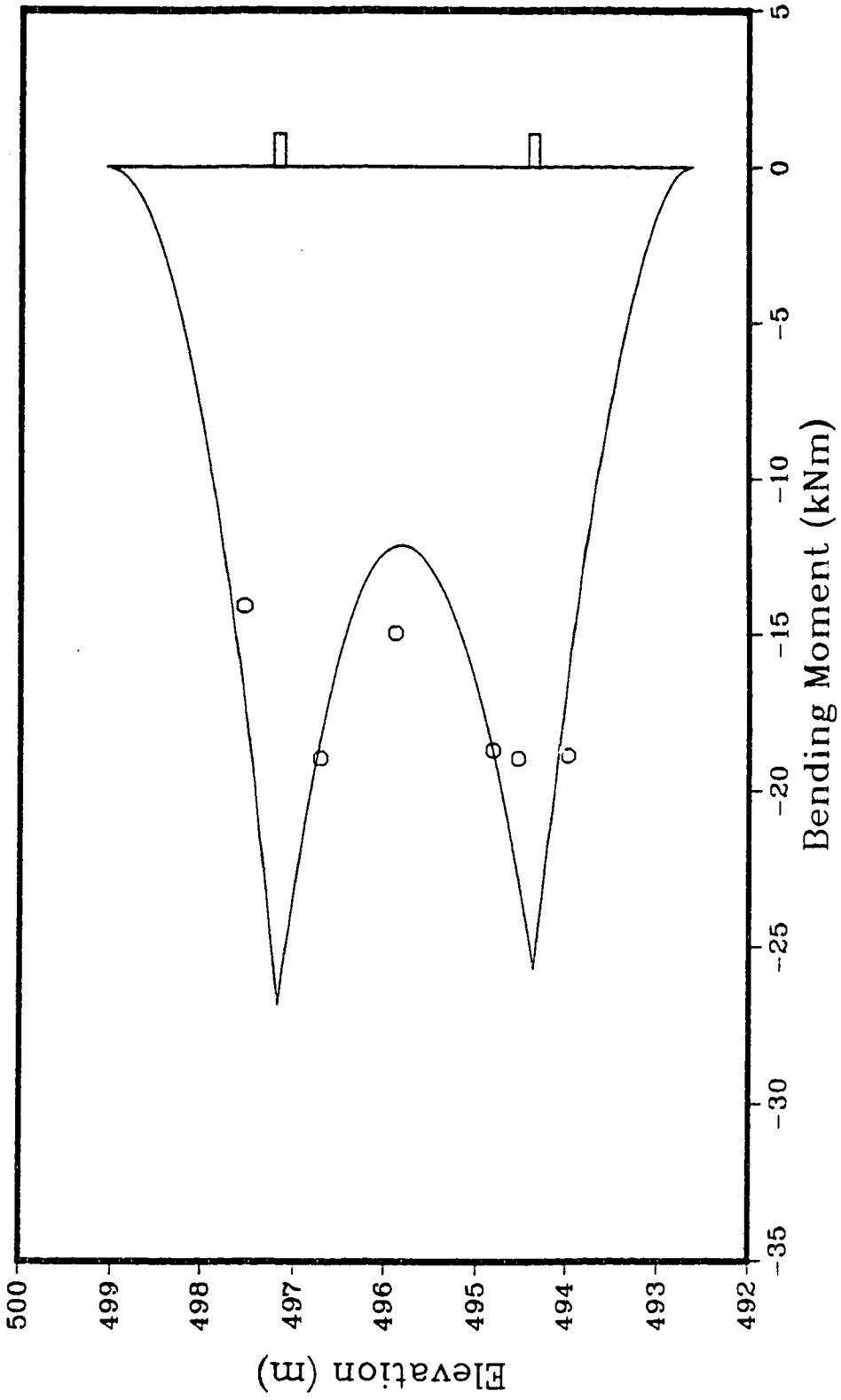


Figure H.8: Interpolated bending moment, east section, February 11, 1985.

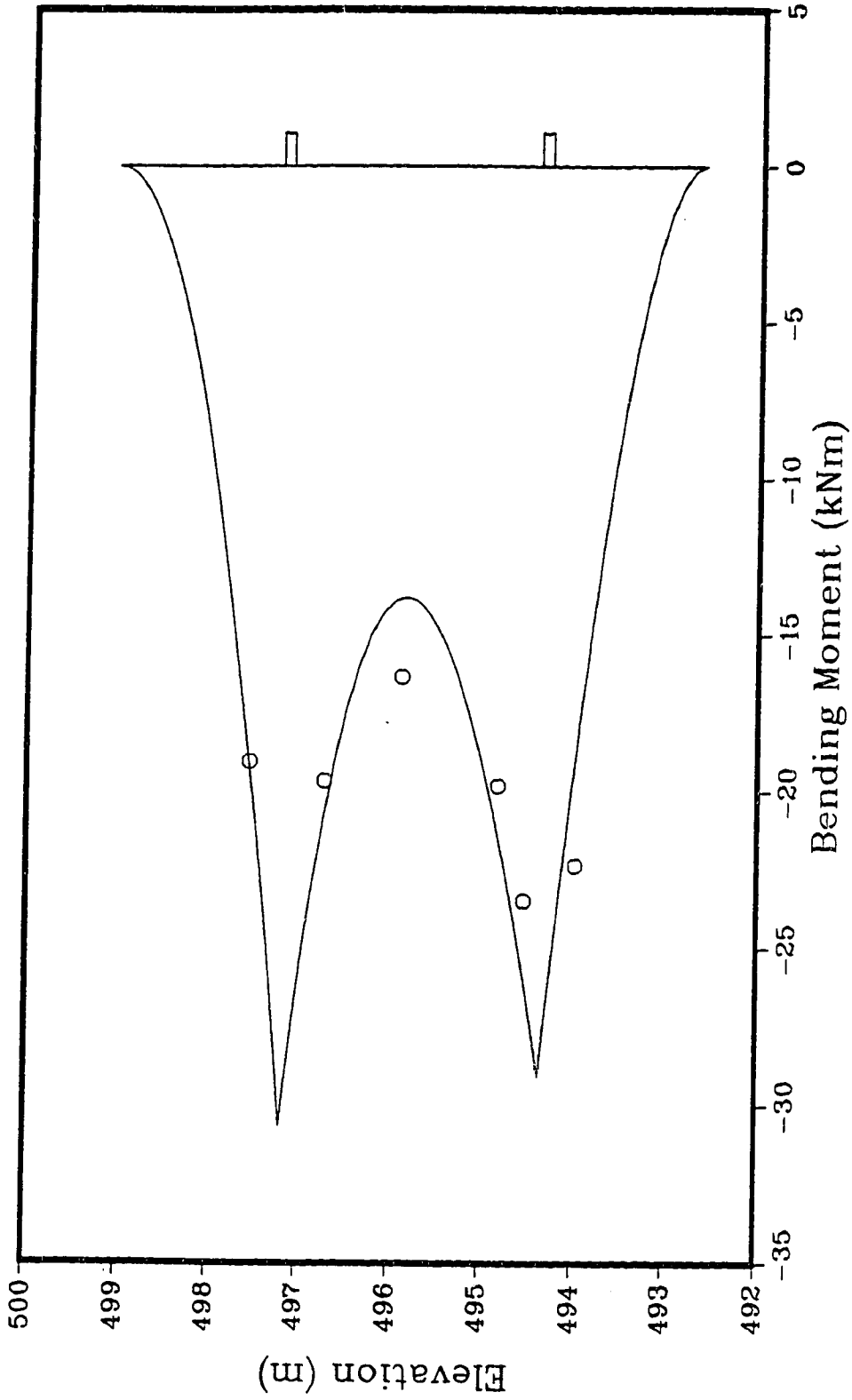


Figure H.9: Interpolated bending moment, east section, August 29, 1985.

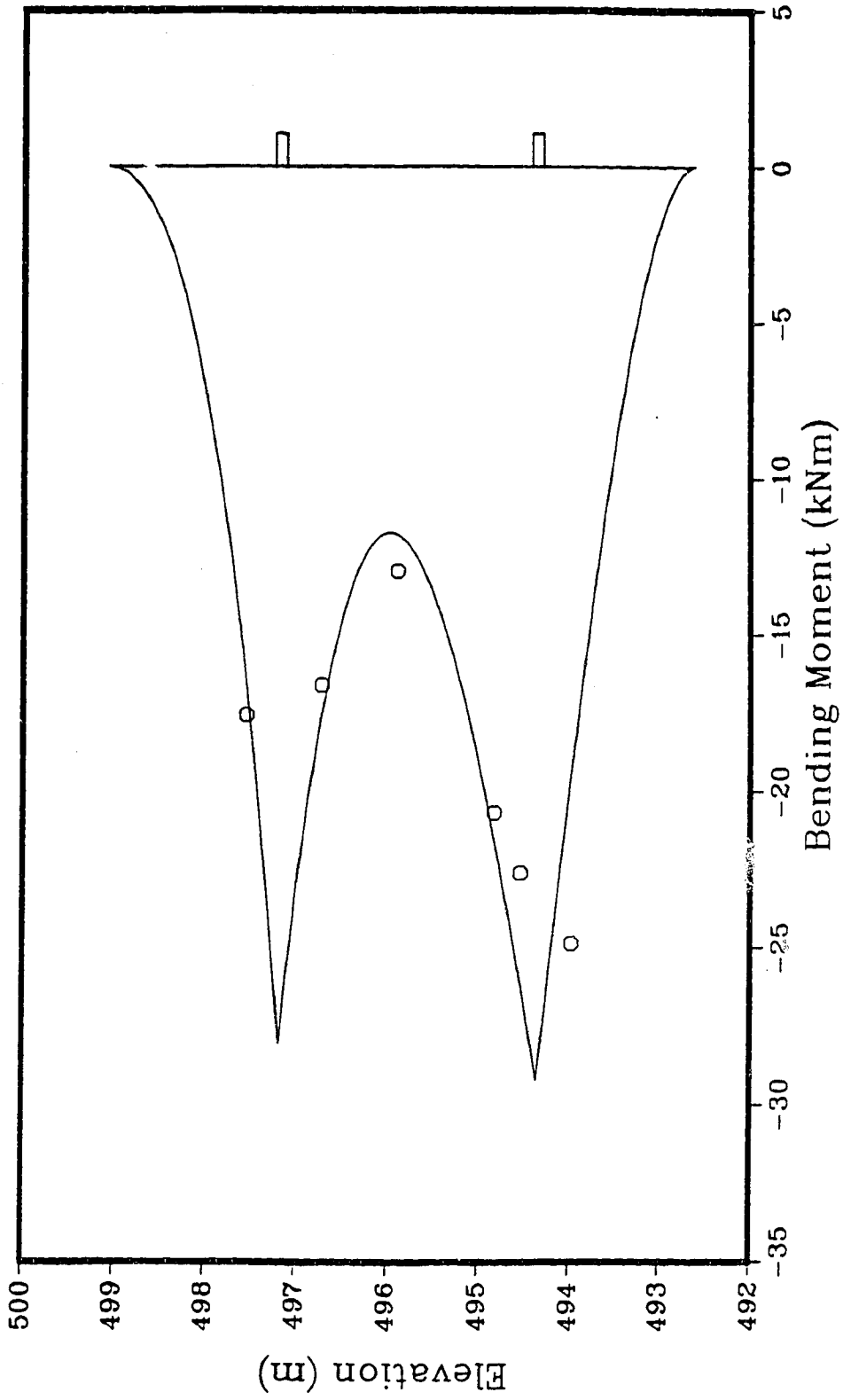


Figure H.10: Interpolated bending moment, east section, March 25, 1986.

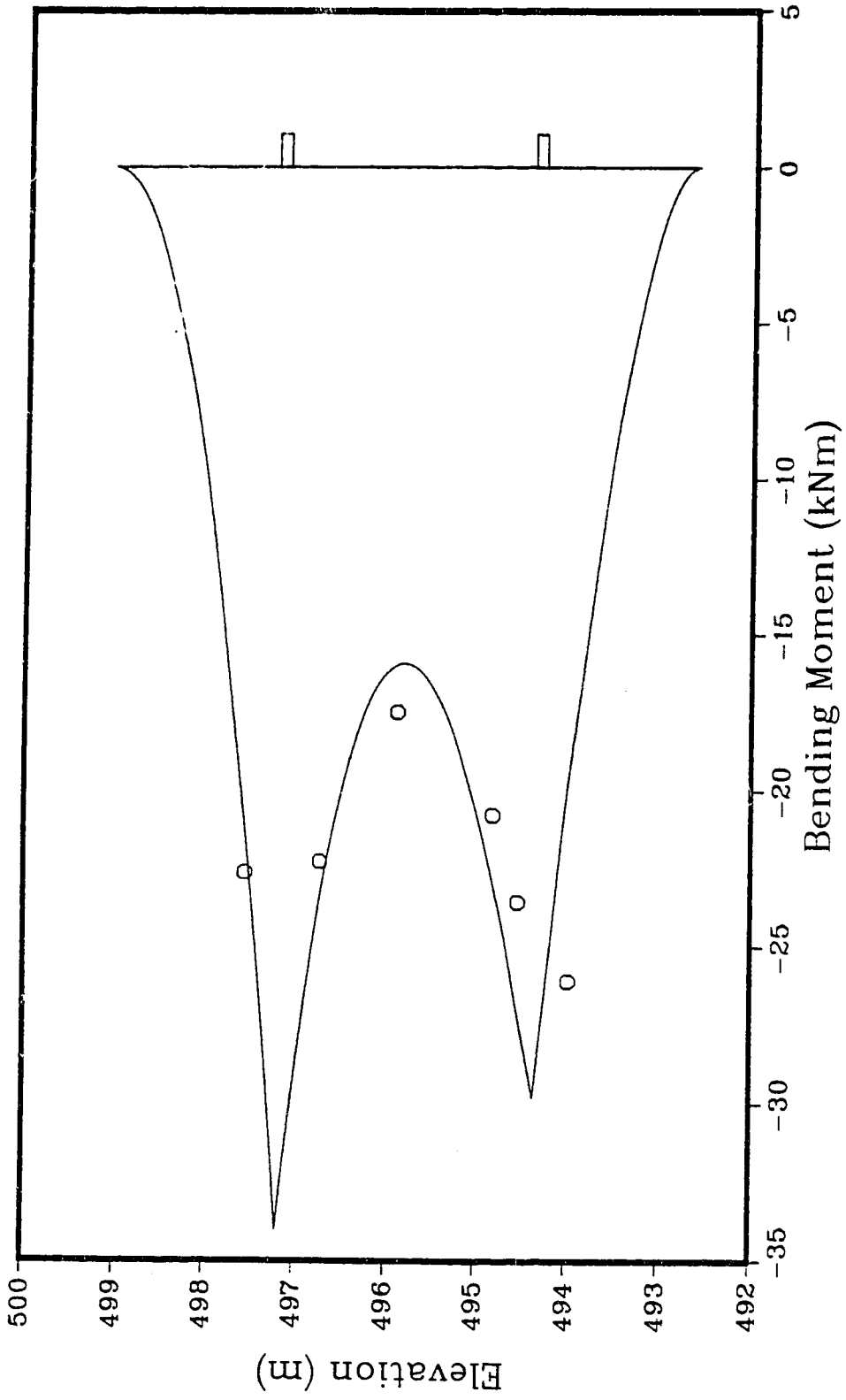


Figure H.1.1: Interpolated bending moment, east section, July 29, 1986.

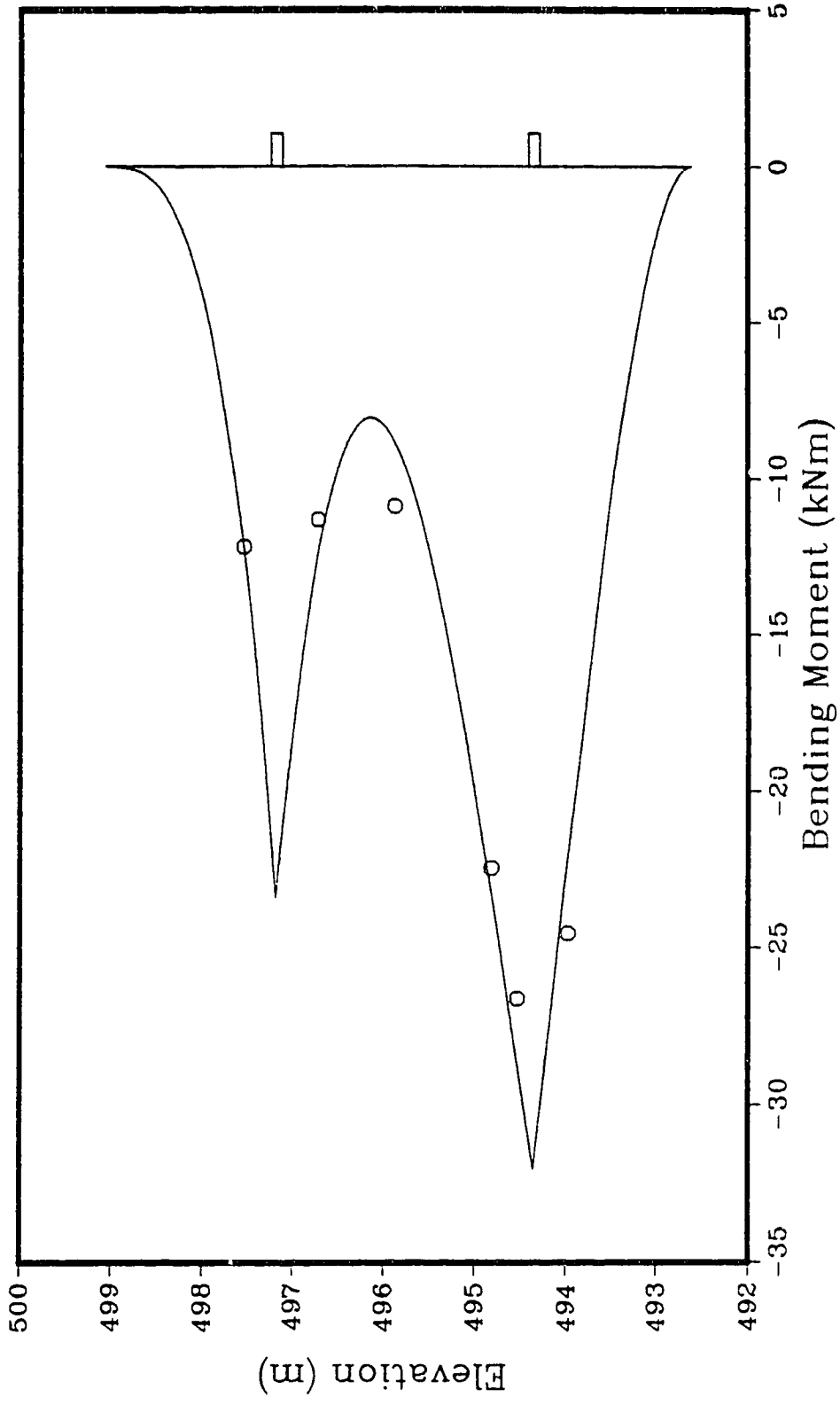


Figure H.12: Interpolated bending moment, east section, December 10, 1986.

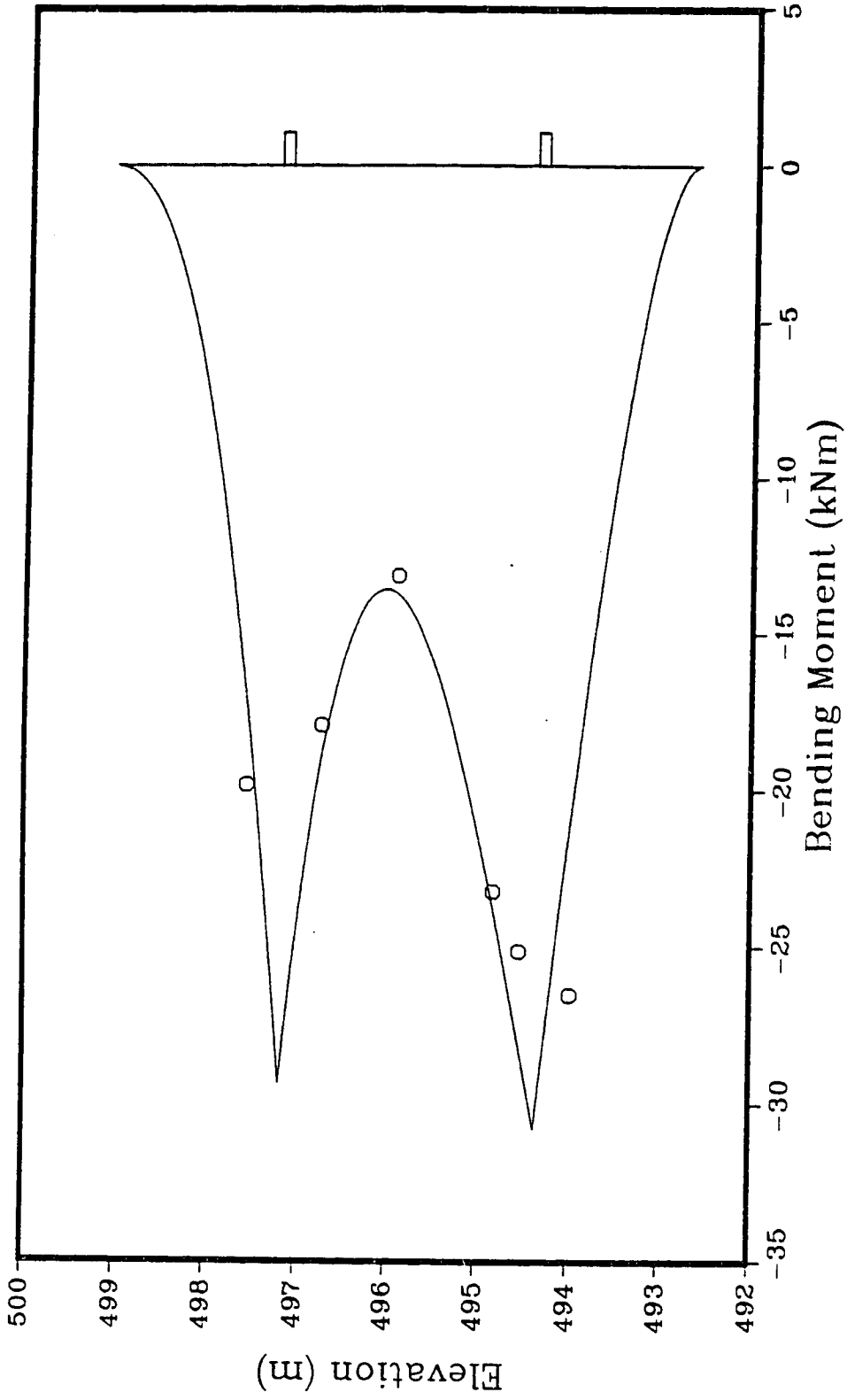


Figure H.13: Interpolated bending moment, east section, February 16, 1987.

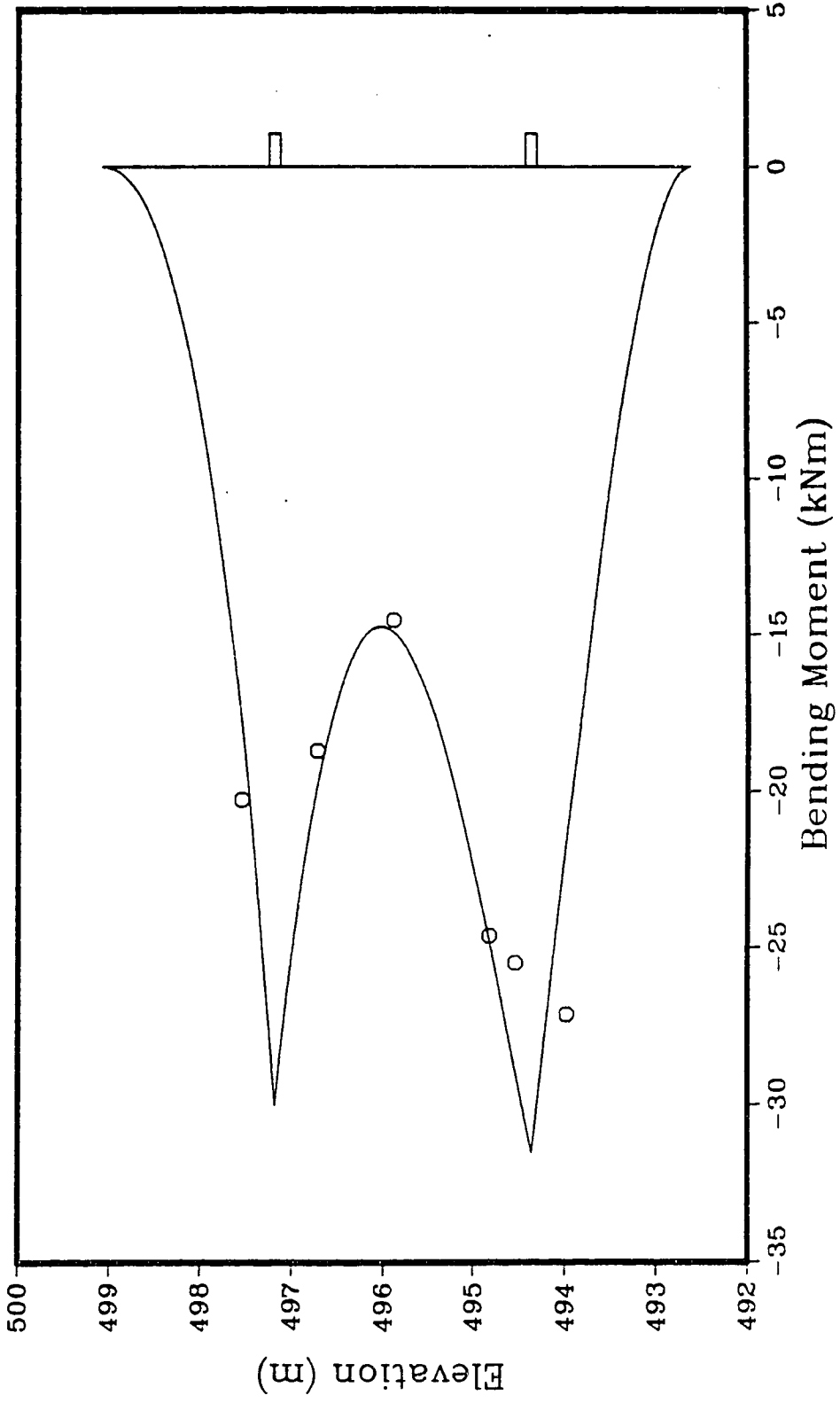


Figure H.14: Interpolated bending moment, east section, March 25, 1987.

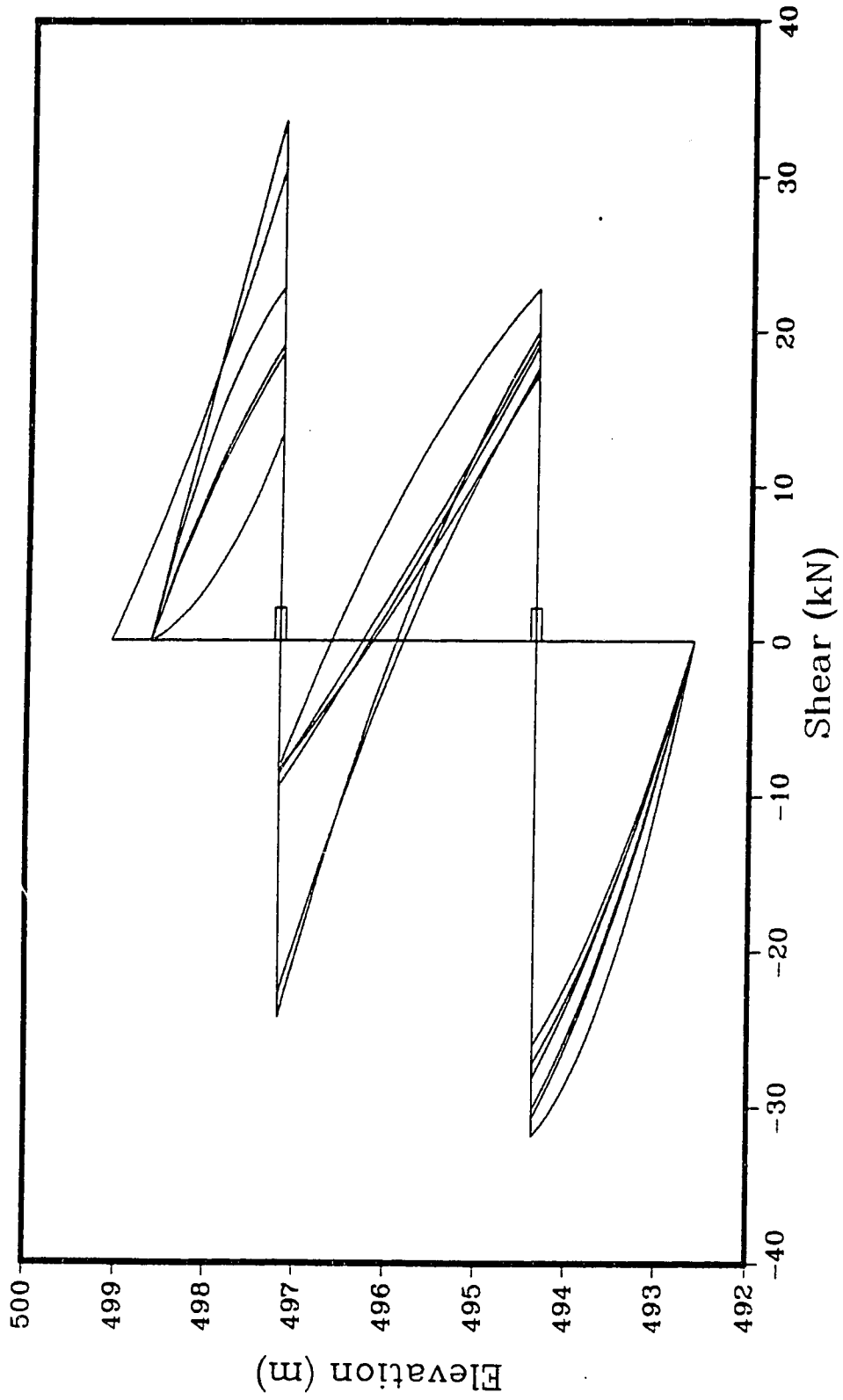


Figure H.15: Shear diagram, east section, early epochs.

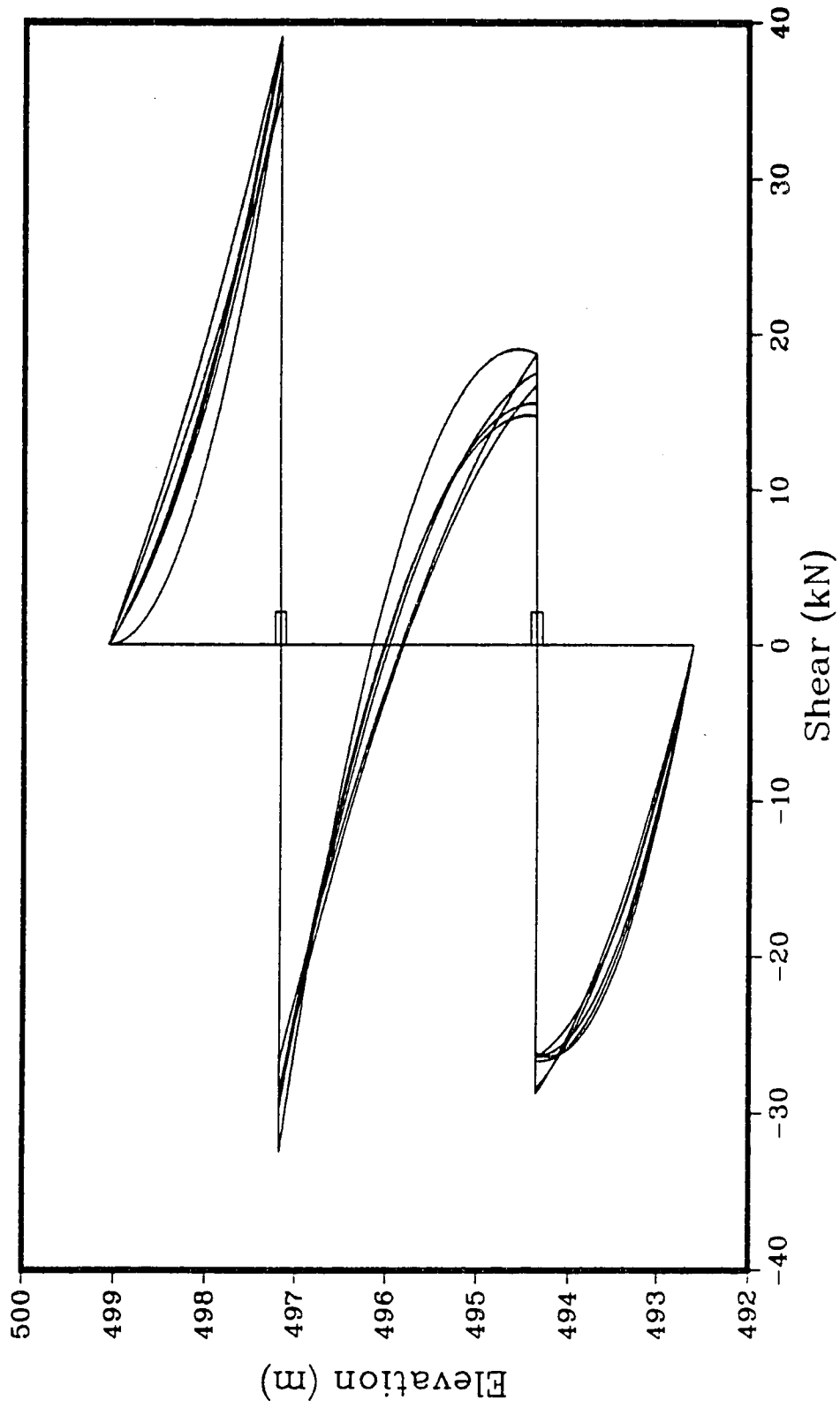


Figure H.16: Shear diagram, east section, late epochs.

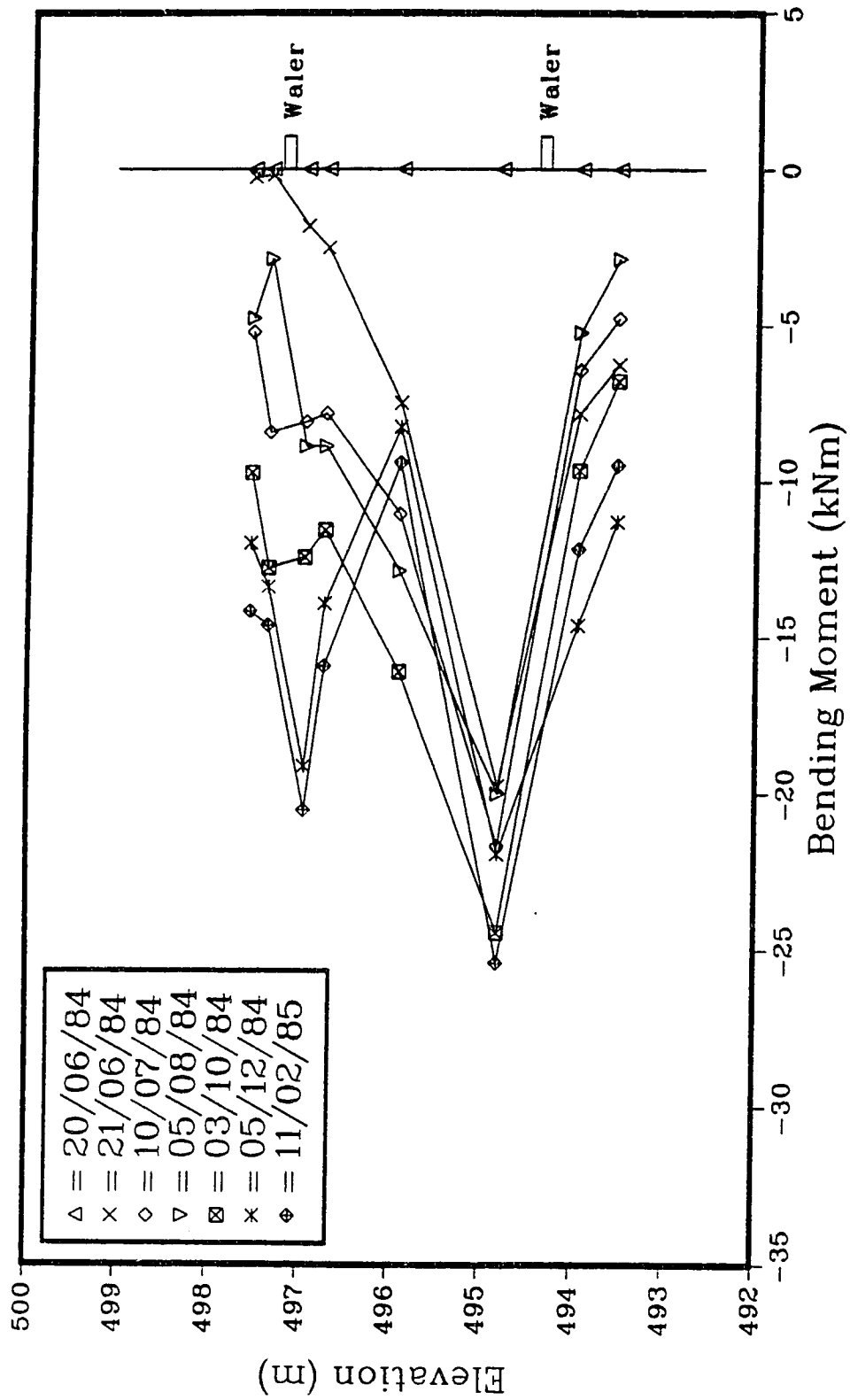


Figure H.17: Field determined moments, west section, early epochs.

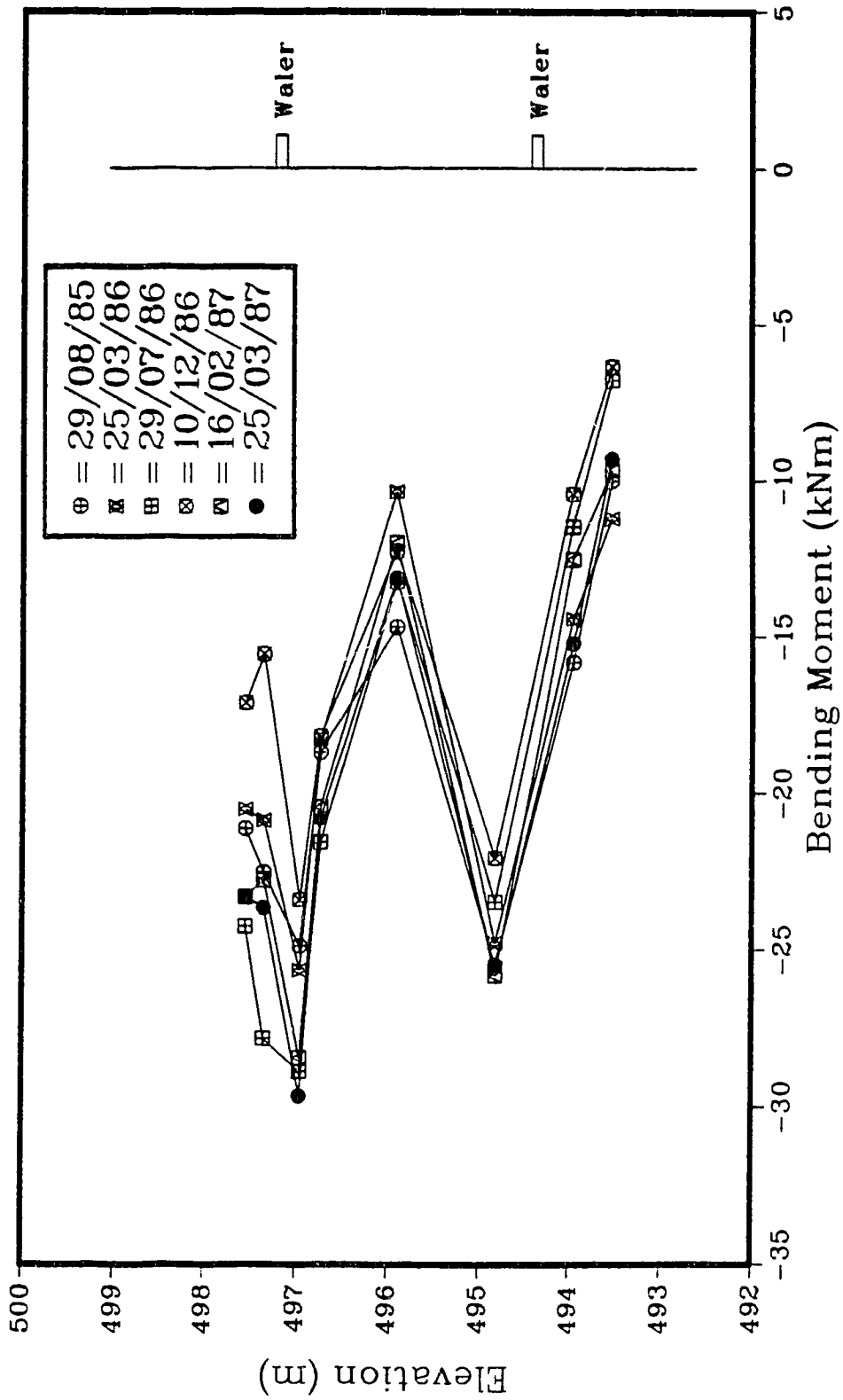


Figure H.18: Field determined moments, west section, late epochs.

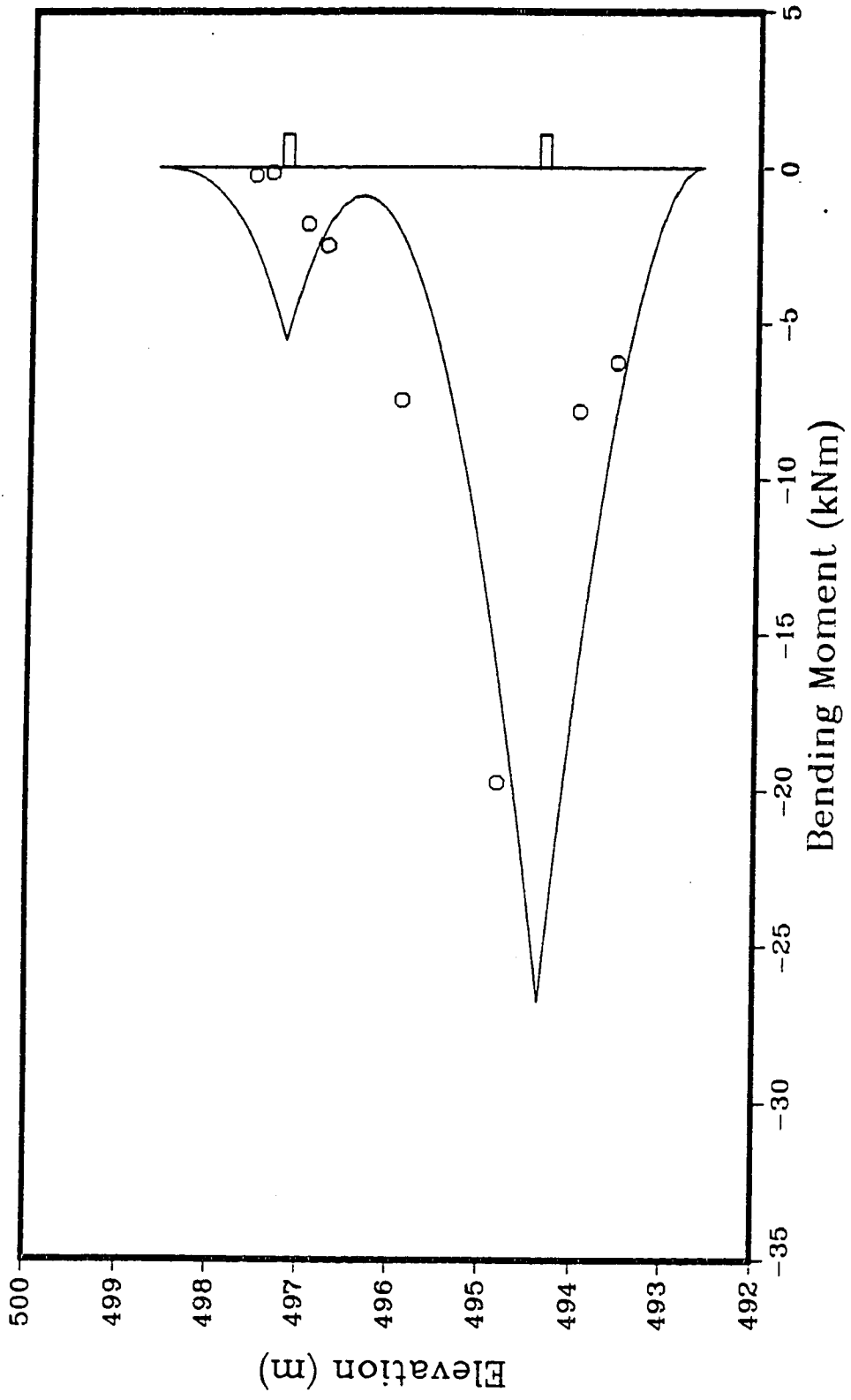


Figure H.19: Interpolated bending moment, west section, June 21, 1984.

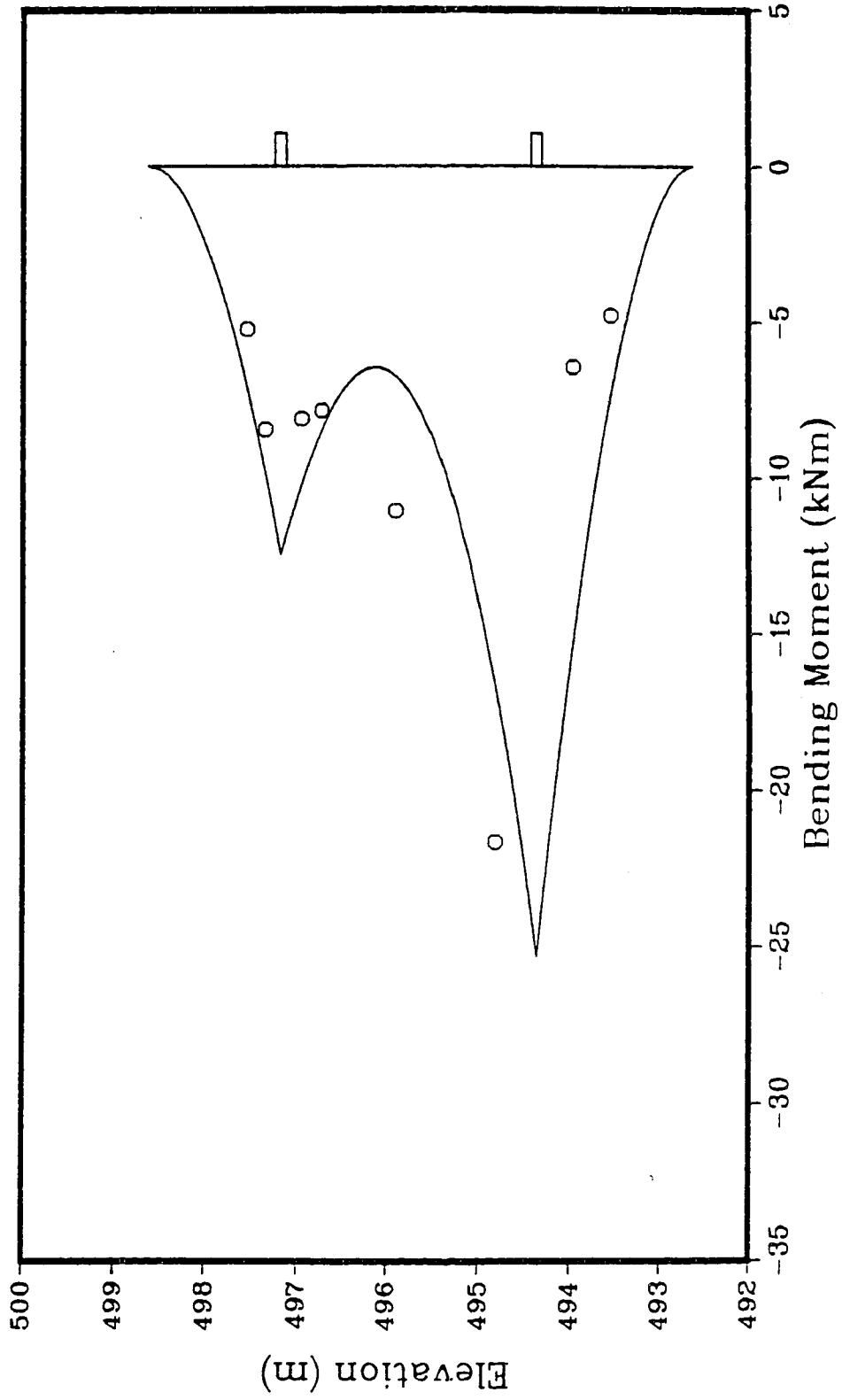


Figure H.20: Interpolated bending moment, west section, July 10, 1984.

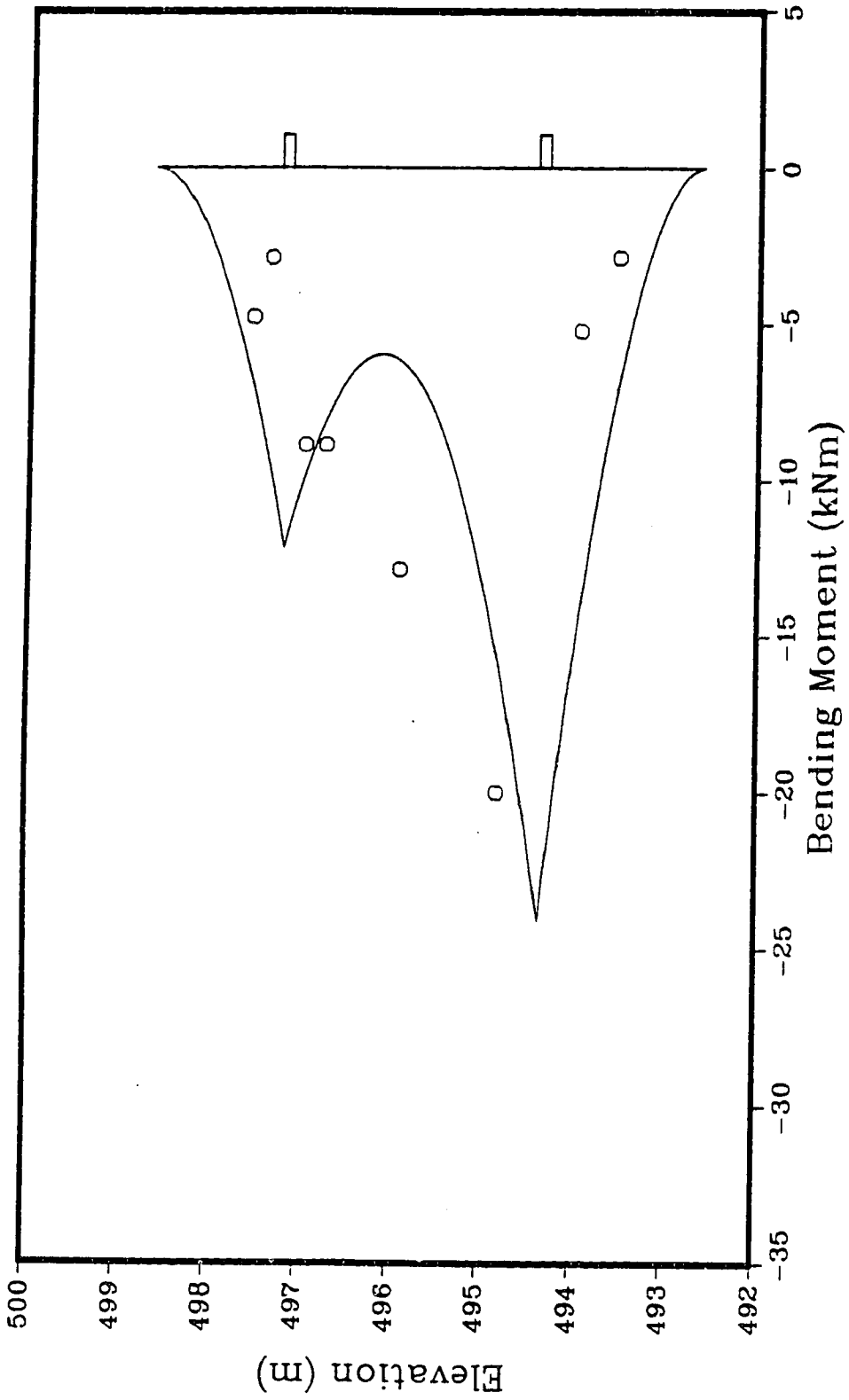


Figure H.21: Interpolated bending moment, west section, August 5, 1984.

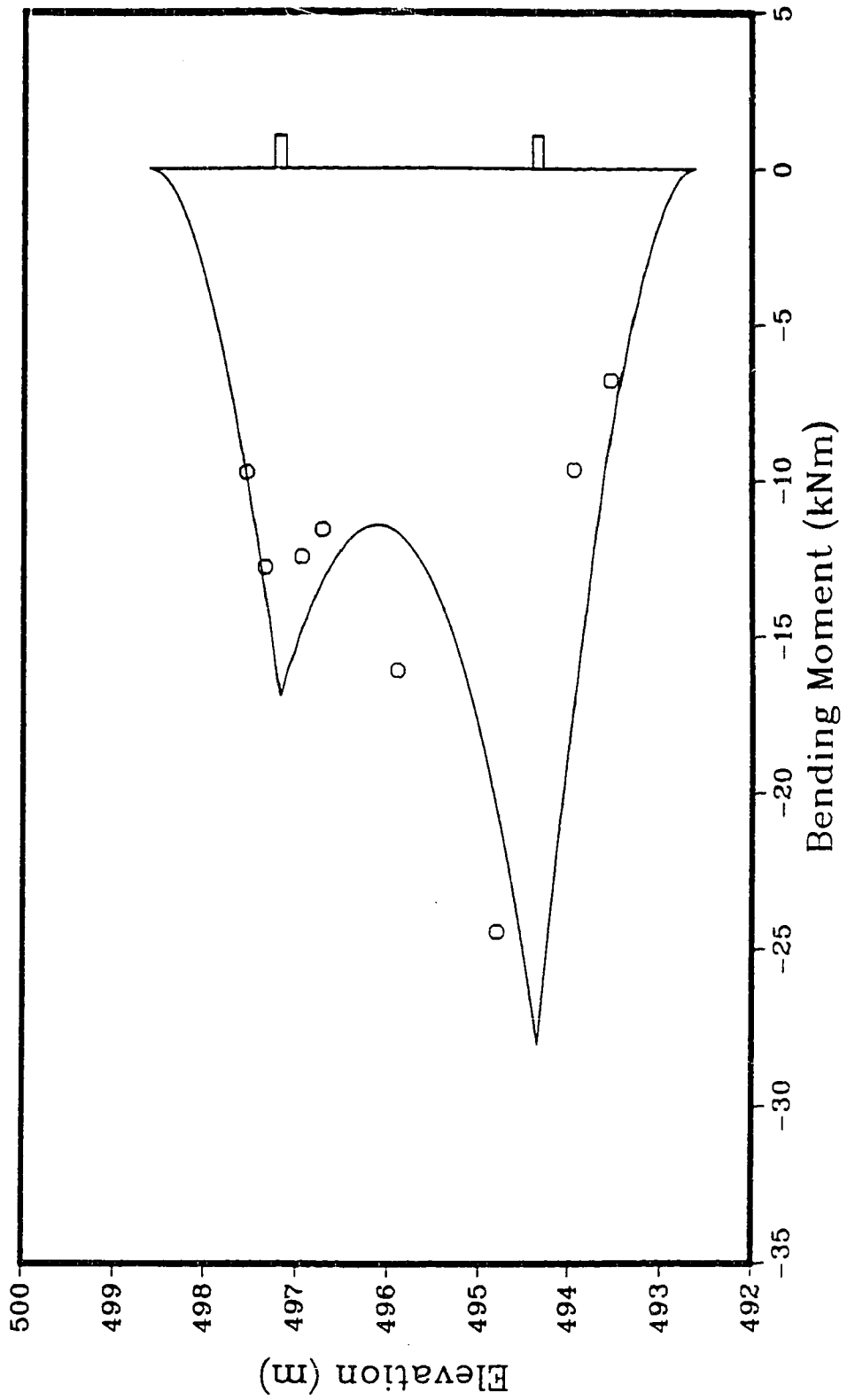


Figure H.22: Interpolated bending moment, west section, October 3, 1984.

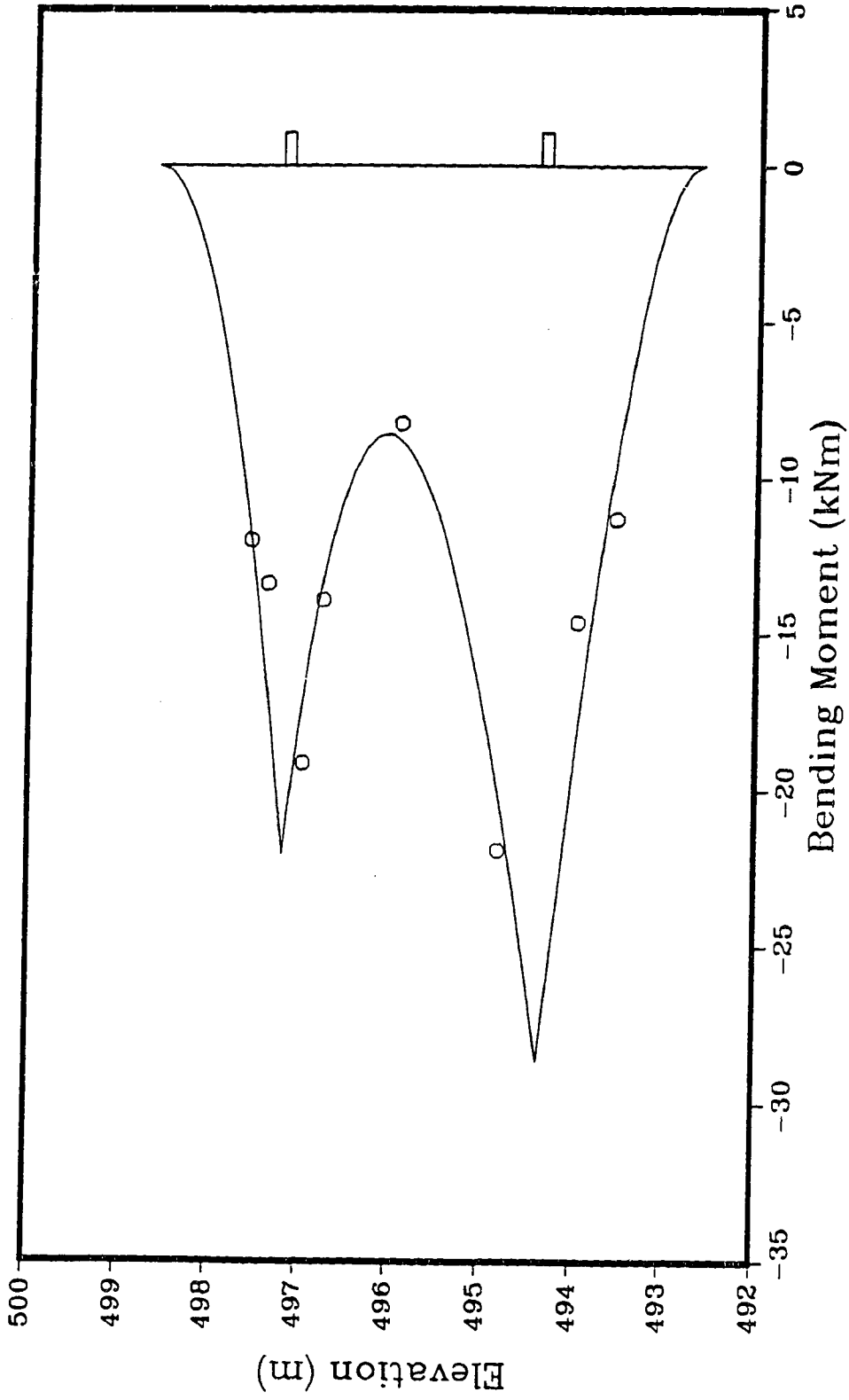


Figure H.23: Interpolated bending moment, west section, December 5, 1984.

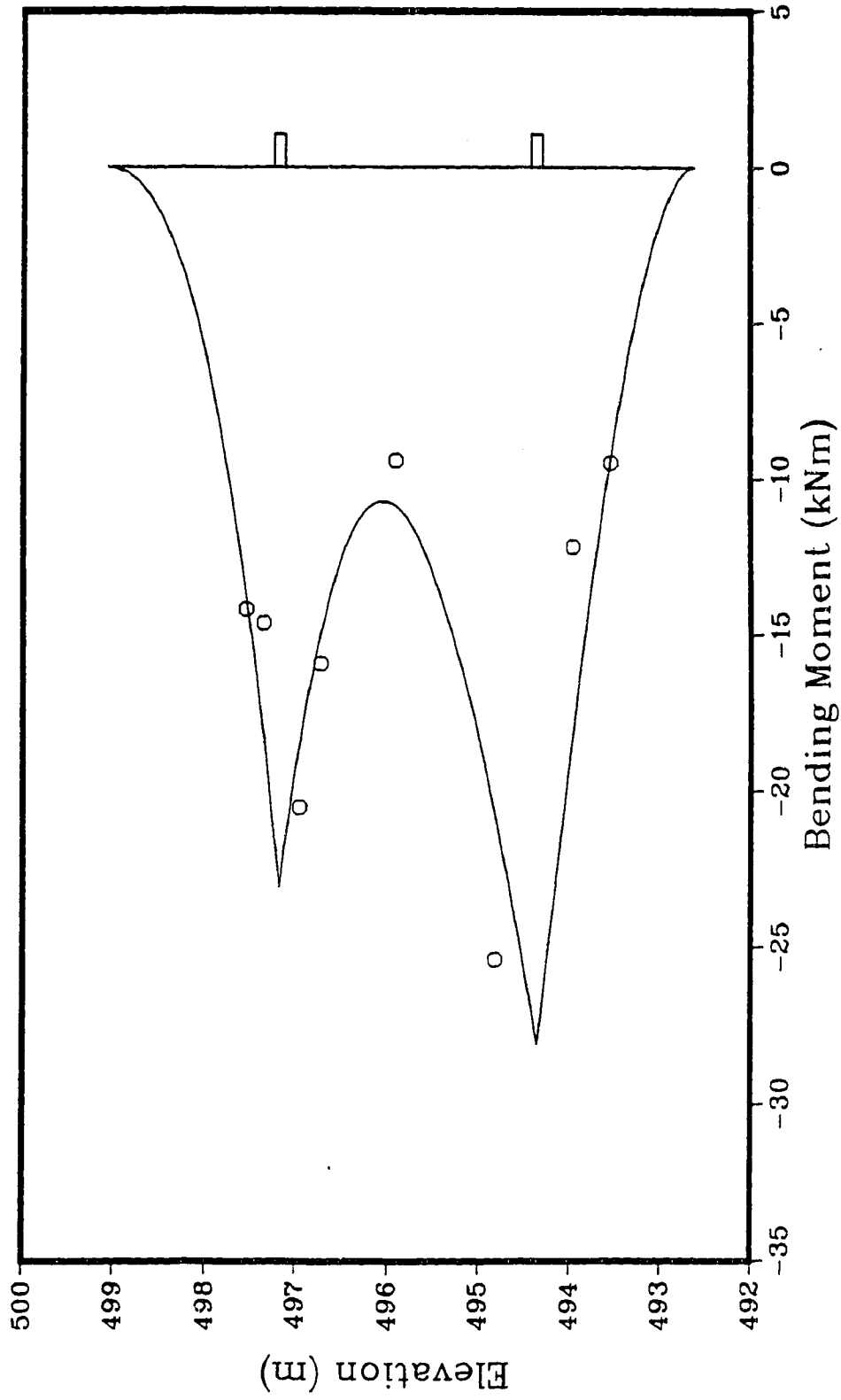


Figure H.24: Interpolated bending moment, west section, February 11, 1985.

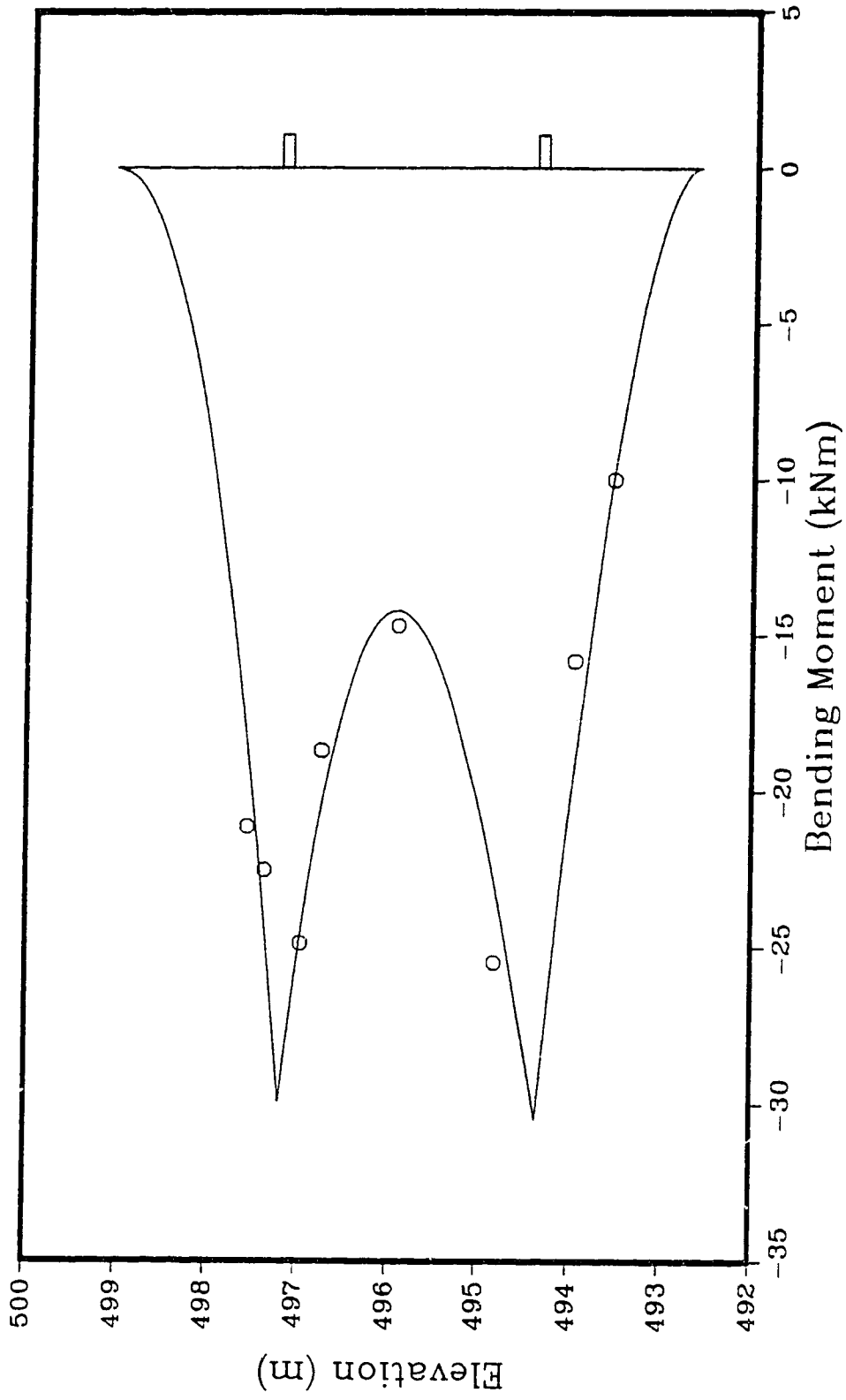


Figure H.25: Interpolated bending moment, west section, August 29, 1985.

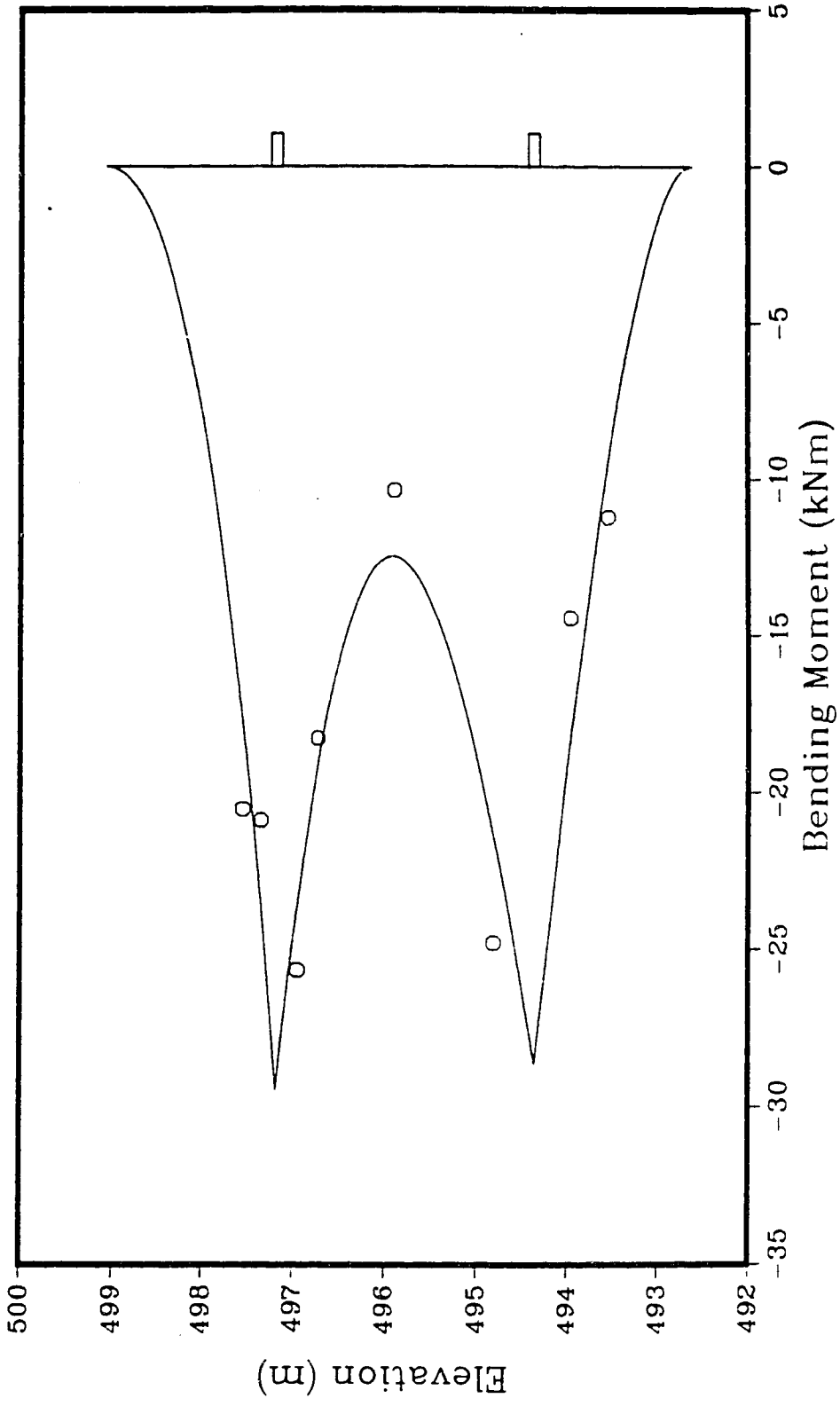


Figure H.26: Interpolated bending moment, west section, March 25, 1986.

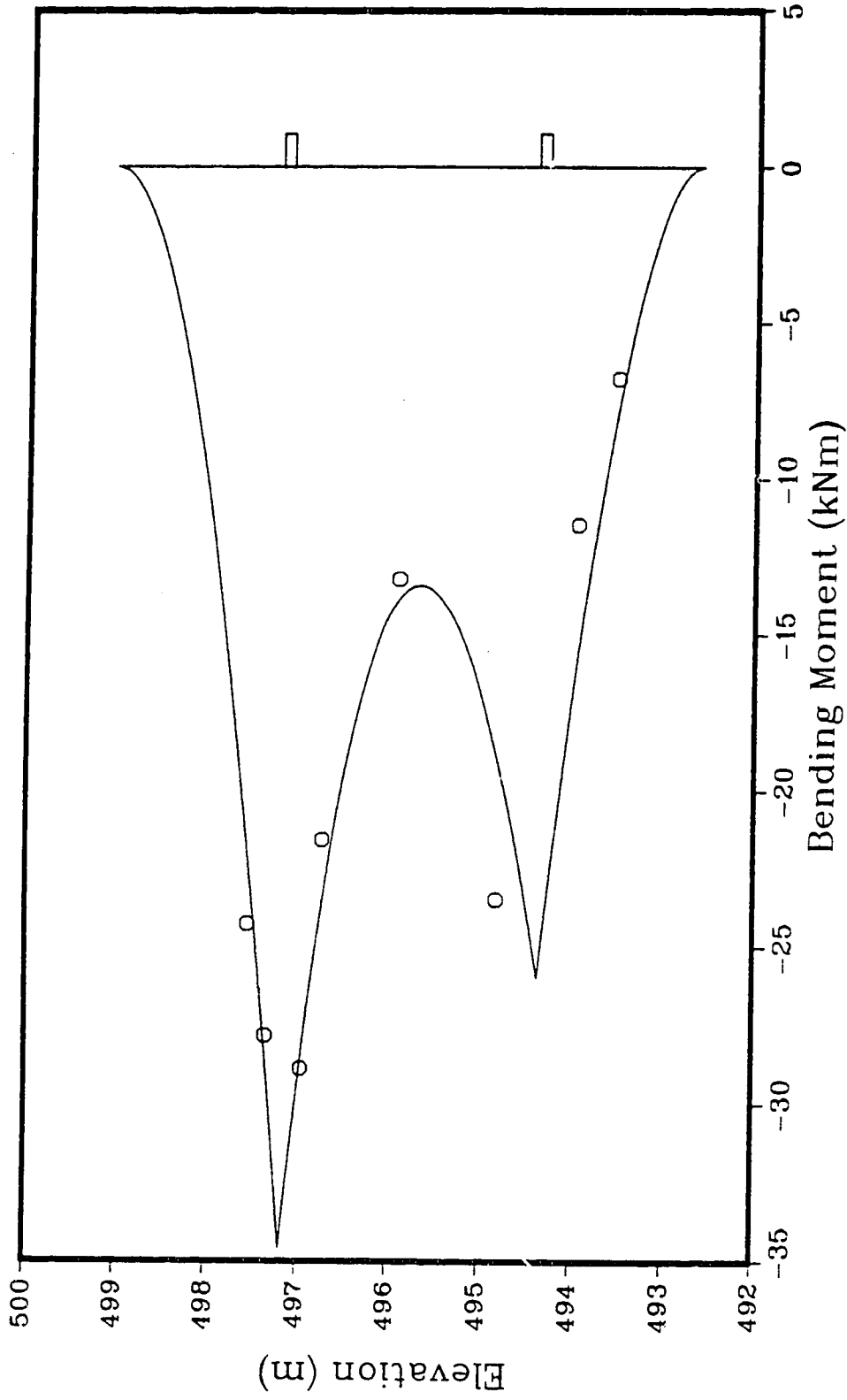


Figure H.27: Interpolated bending moment, west section, July 29, 1986.

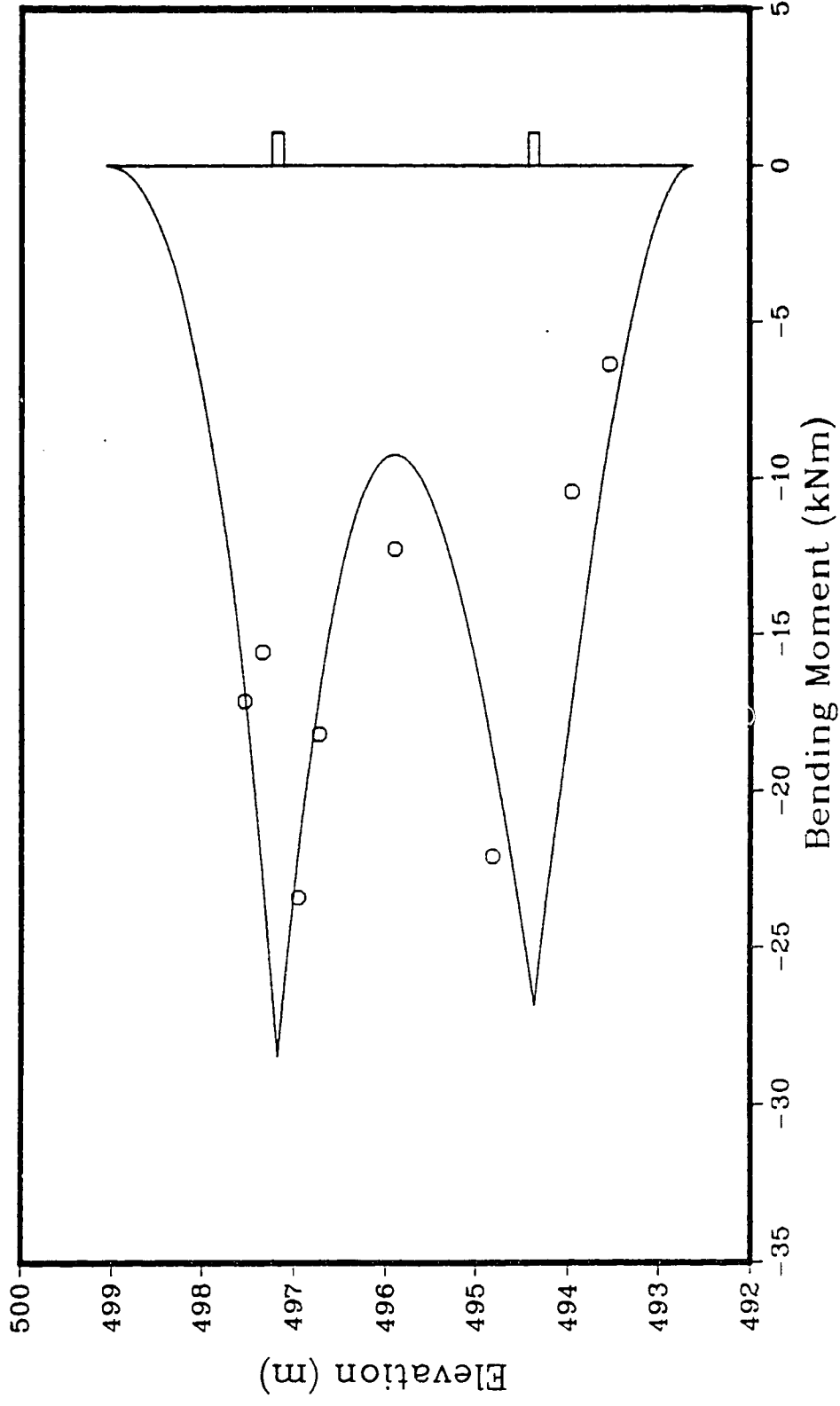


Figure H.28: Interpolated bending moment, west section, December 10, 1986. 334

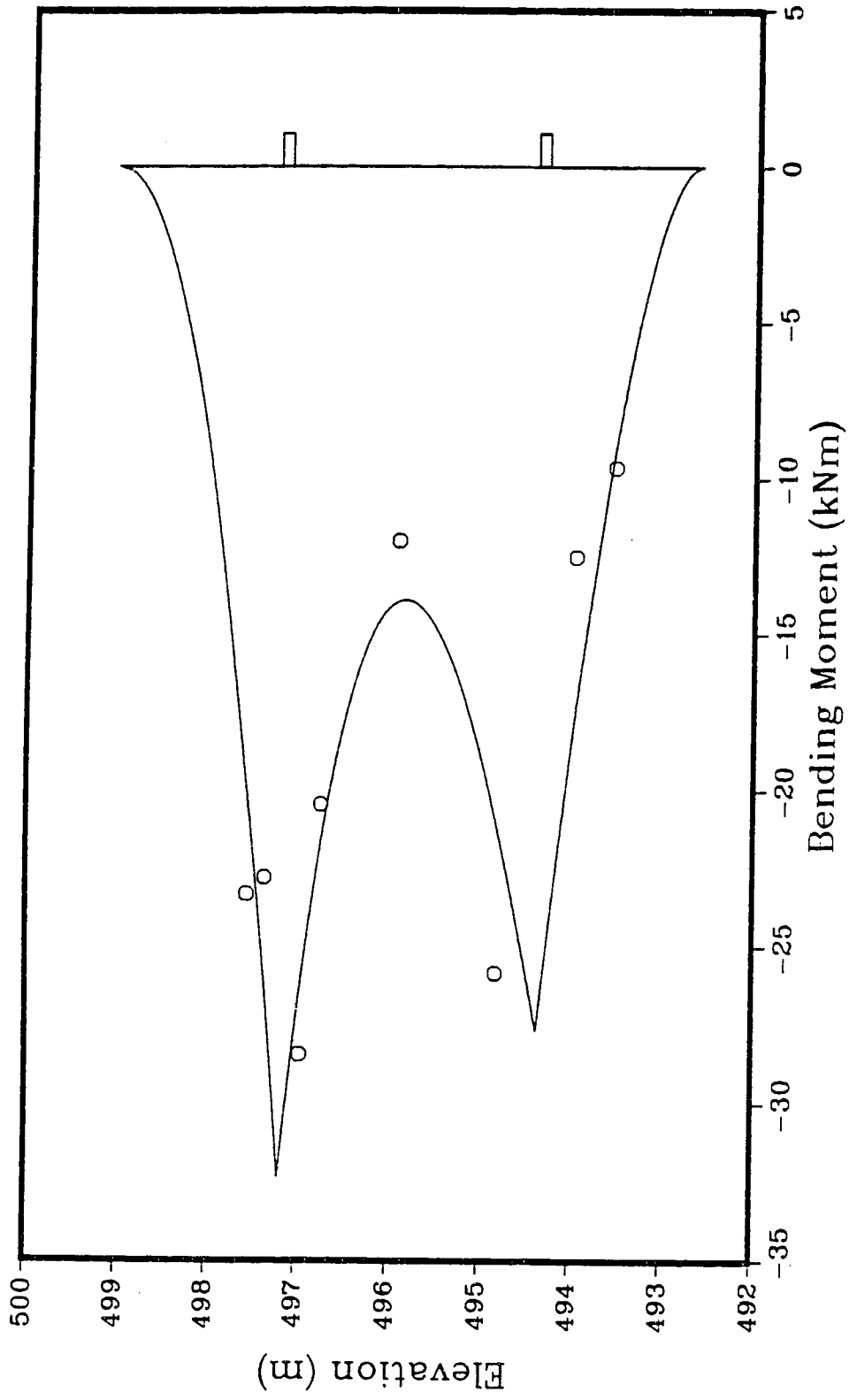


Figure H.29: Interpolated bending moment, west section, February 16, 1987.

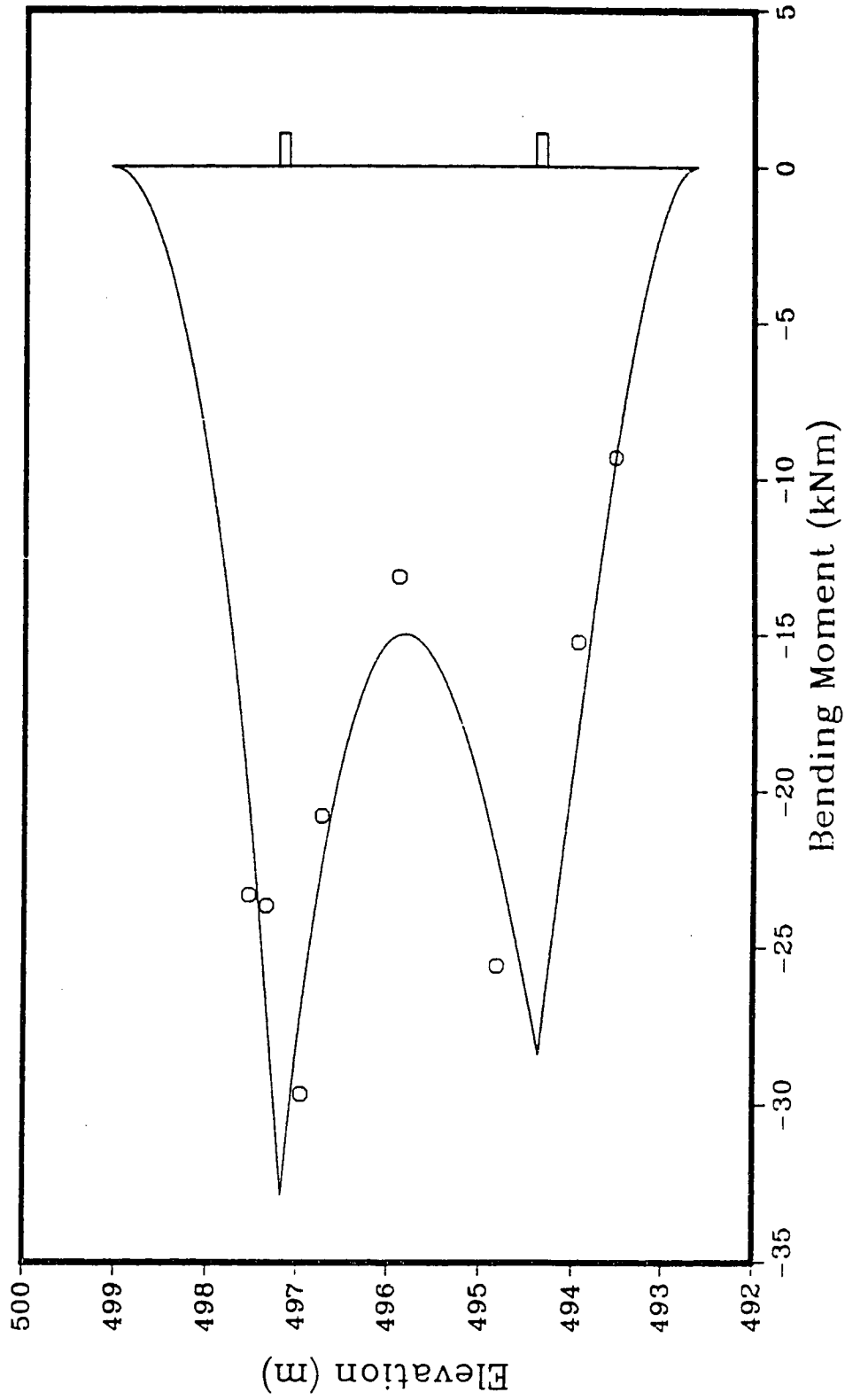


Figure H.30: Interpolated bending moment, west section, March 25, 1987.

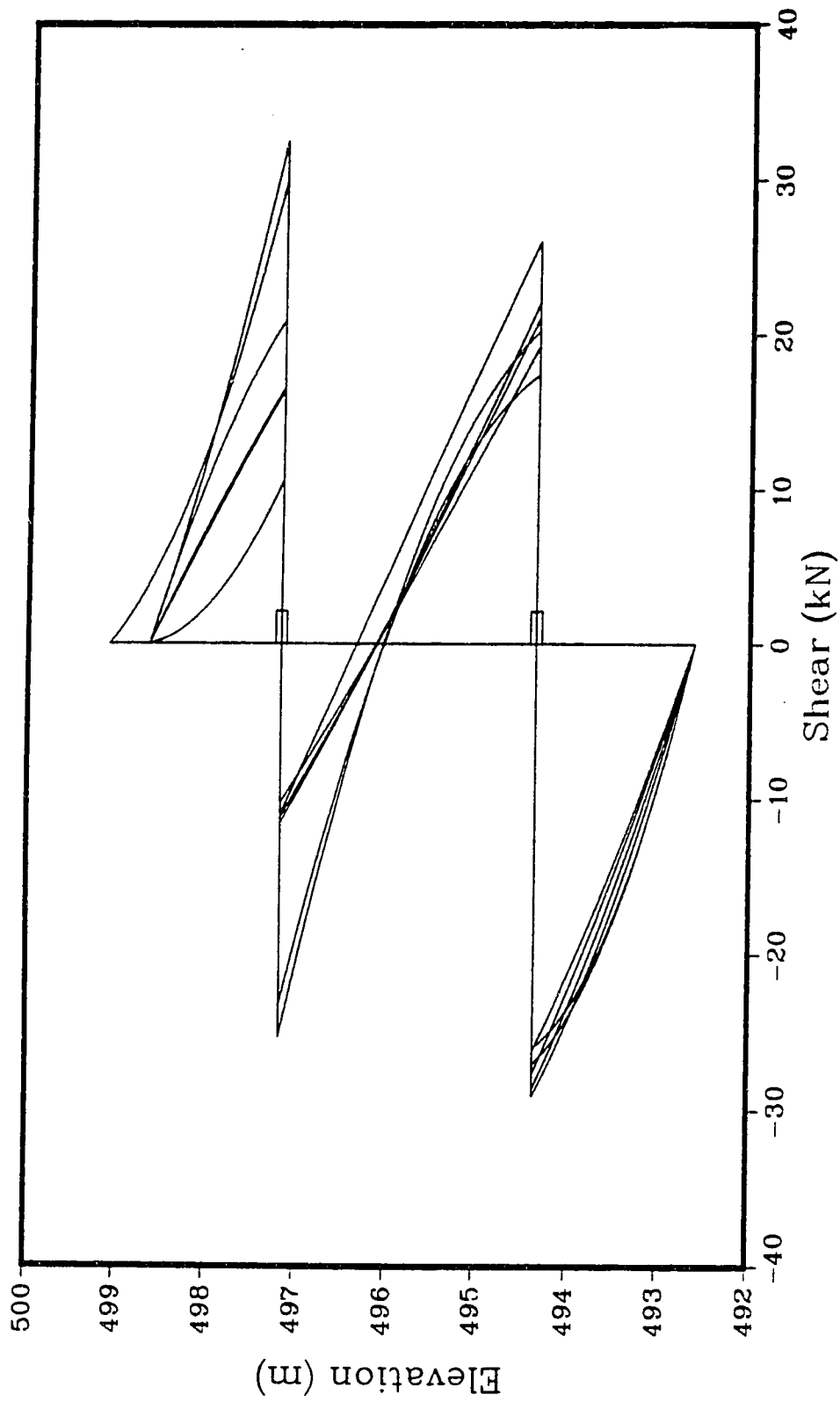


Figure H.31: Shear diagram, west section, early epochs.

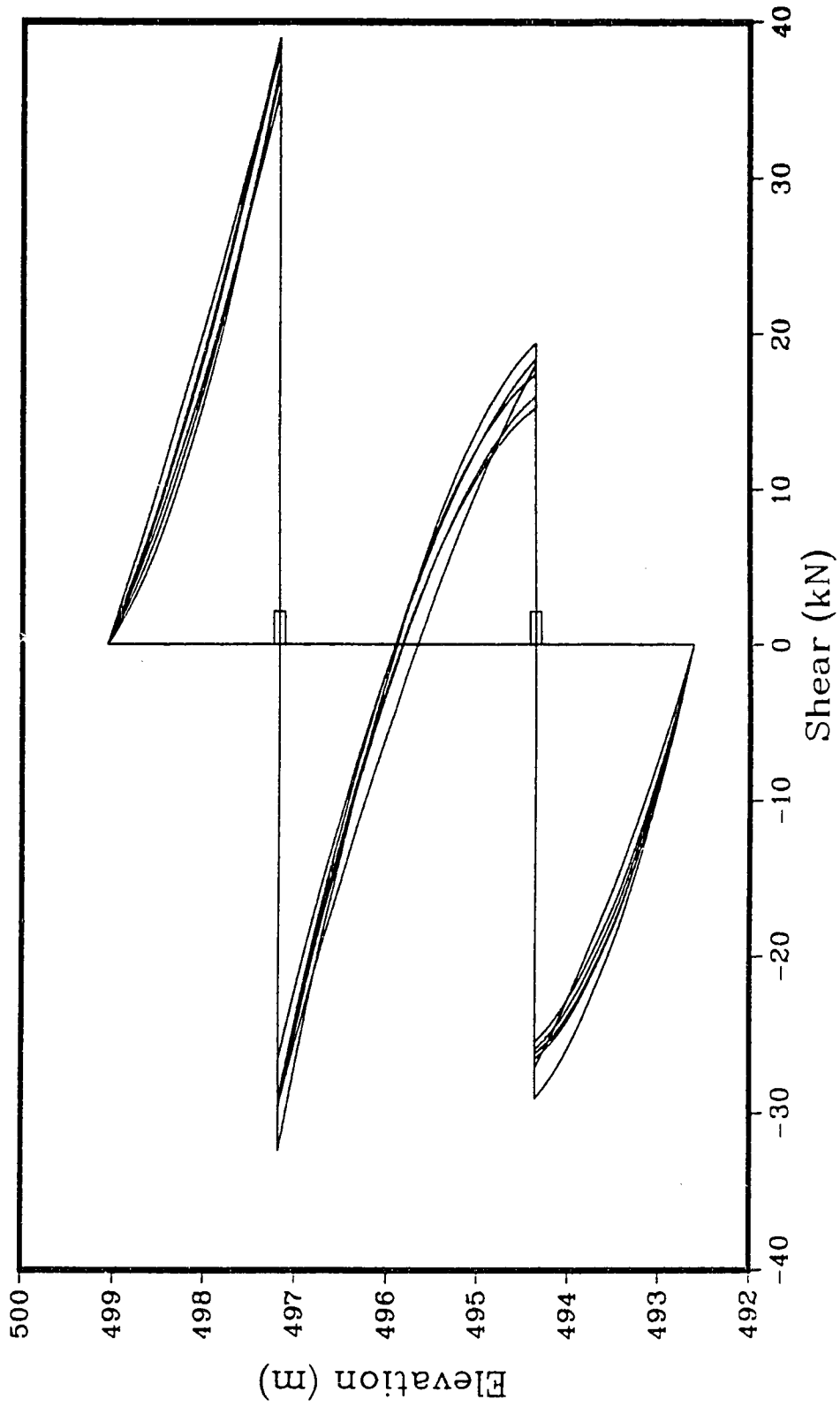


Figure H.32: Shear diagram, west section, late epochs.

Appendix I
Data Reduction Procedure for the Load Cells

1.1 Introduction

The procedure used to reduce the load cell data is incorporated into a computer program called LC-PROG. LC-PROG has the following functions:

1. Convert the load cell reading to: a force, a force per metre width of wall and a force per unit area of wall.
2. Use the stress from the anchor strain gauge results to calculate the force in the anchor. This force is also converted to a load per unit width and a load per unit area. These quantities serve as a check on the load cell results.
3. Produce a summary table for each anchor. Each table contains the load cell and anchor strain gauge results for each available epoch of data.
4. Produce plots of the loads in the anchors versus time. To facilitate comparison between anchors the load/unit area quantity is plotted. The program has the capability to produce any number of graphs with each graph including the results from any combination of anchors. As well, the load cell and/or the anchor strain gauge loads can be included on the same plot.

The calculations embodied in the program are outlined below. This is followed by an explanation of how to operate the program. Finally, the format of the datafiles is described and a program listing is provided.

1.2 Calculation Procedure

The procedure used to reduce the load cell data is based on a laboratory calibration of the instrument's response to load. The load cell, incorporating strain gauges mounted on its circumference, is subjected to a controlled loading test. A linear relationship between the response of the strain gauges and the load applied is established. This relationship, embodied in a calibration factor, is uniquely determined for each individual load cell. It is analagous to the elastic modulus except that when applied to strain, a force and not a stress is given.

The calculations involved in the data reduction process are as follows.

1. The net strain, called Δ_{strain} , between the original unloaded reading of the load cell's strain gauges and the current reading is determined.

$$\Delta_{\text{strain}} = (\text{current reading} - \text{unloaded reading}) \quad [1.1]$$

The units are $\text{mm} \times 10^{-6}/\text{mm}$ or microstrains

2. The force in the load cell is calculated by applying the calibration factor to the net strain.

$$\begin{aligned} \text{Force} &= (\Delta_{\text{strain}})(\text{calibration factor}) \quad [1.2] \\ &= A \end{aligned}$$

The units of force are kN.

3. The force in the anchor is determined from the stress in the rod. The stress used in this calculation is obtained

from the anchor strain gauge results. (The conversion of the anchor strain gauge data to stress is described in Appendix J.) The stress from the outer most strain gauge along the anchor rod is used because it will provide a load closest to that of the load cell. With increasing depth along the grouted portion of the rod the stress level reduces as load is shed to the surrounding rock. The calculation is as follows.

$$\begin{aligned} \text{Force} &= (\text{rod stress, MPa}) && \text{[I.3]} \\ &(\text{rod area, m}^2)(1000\text{kN/MN}) \\ &= A \end{aligned}$$

The units of force are again kN.

4. The anchor force per unit width of the wall is calculated. This quantity is of interest in another area of calculations.

$$\begin{aligned} \text{Force/m} &= A/\text{width, tributary area} && \text{[I.4]} \\ &= B \end{aligned}$$

The units are kN/metre.

5. The anchor force per unit area of the wall is calculated.

$$\text{Force/m}^2 = B/\text{height, tributary area} \quad \text{[I.5]}$$

The units are kN/m² or kPa.

This procedure is repeated for every anchor and epoch for which data is available.

1.3 Operating Procedure

The procedure used to produce the anchor load results is described in this section.

The data reduction program is compiled using the following command. The compiled version of the program will reside in a file called LC-PROGC.

```
$RUN *FORTGTEST SCARDS=LC-PROG SPUNCH=LC-PROGC
```

The program is run using the command given below.

```
$RUN LC-PROGC+*DISSPLA 5=LC-AH 4=LC-4 1=-1 9=-9
```

LC-AH is the file containing the load cell data. LC-4 is the file containing the anchor rod stress results. (This implies that the anchor strain gauge results must be produced before the load cell data can be processed.) File -1 is the text output file containing the load summary tables for each of the anchors. File -9 is a plot description file (PDF) containing all of the results in graphical form.

Post processing of the two output files is required to convert them to a presentable form. The text file is handled as follows.

```
$RUN CIVE:TABLE SCARDS=-1 SPRINT=-table
```

The file -table is now ready to be printed on the XEROX 9700 laser printer.

The PDF can be processed in one of two ways; either using the CALCOMPQ plotter or the graphics capability of the laser printer. To produce the results on the plotter the following command is used.

```
$RUN *CALCOMPQ PAR=FILE=-9
```

The plots can be obtained on the laser printer by running:

```
$RUN *9700PLOT SCARDS=-9 SPUNCH=-plot
```

The file -plot can be copied to the laser printer in the conventional manner.

I.4 Datafile and Program Listings

The format of datafile LC-AH is explained with an annotated version of the file which is presented below. LC-4 is a slightly modified copy of the text output file which gives the anchor strain gauge results. In this file the results for each anchor appear on a new page. Two lines of data are added to LC-4 at the top of each page. The first line specifies the number of times the anchor strain gauges have been read. The second line gives the cross sectional area of the anchor.

A listing of the program LC-PROG is provided at the end of this appendix.

Annotated version of datafile LC-AH

8. _____ Number of load cells.
 1. _____ Initial table number.

Anchor A. _____ Name of anchor.
 -4268...0909, 1.5, 2.26, 12, _____ Initial reading, calibration factor, width of tributary area
 -5170, 8, _____ of anchor, height of tributary area of anchor, number of times
 -4933, 20, _____ load cell has been read.
 -4667, 40, _____
 -4742, 65, _____
 -4726, 123, _____
 -4969, 185, _____
 -4780, 454, _____
 -4784, 662, _____
 -4757, 788, _____
 -4950, 921, _____
 -4725, 990, _____
 -4738, 1027, _____
 Anchor B. _____
 -5460...0.0877, 1.5, 2.9, 12, _____
 -3915, 8, _____
 -4136, 20, _____
 -4565, 40, _____
 -4327, 65, _____
 -4296, 123, _____
 -4044, 185, _____
 -4056, 454, _____
 -4025, 662, _____
 -3965, 788, _____
 -3984, 921, _____
 -4084, 990, _____
 -4073, 1027, _____
 Anchor C. _____
 -3809...0.0915, 4.0, 1.91, 12, _____
 -2470, 8, _____
 -2957, 20, _____
 -3260, 40, _____
 -2972, 65, _____
 -2954, 123, _____
 -2235, 185, _____
 -2369, 454, _____
 -2246, 662, _____
 -2297, 788, _____
 -2235, 921, _____

-2226,990,
-2250,1027,
Anchor D.
-3952 . . O.0901,1.5.3.07,12,
-2250,8,
-2584,20,
-2975,40,
-2742,65,
-2787,123,
-2460,185,
-2613,454,
-2510,662,
-2503,788,
-2368,921,
-2542,990,
-2560,1027,
Anchor E.
-5275 . . O.0874,1.2.2.873,12,
-4038,21,
-4191,40,
-4265,65,
-4208,123,
-4368,185,
-4450,251,
-4363,454,
-4467,662,
-4412,788,
-4510,921,
-4518,990,
-4518,1027,
Anchor F.
-4130 . . O.0907,1.673,3.132,12,
-3587,21,
-3596,40,
-3602,65,
-3623,123,
-3504,185,
-3548,251,
-3501,454,
-3513,662,
-3527,788,
-3442,921,
-3528,990,
-3544,1027,

Anchor G.
 -4770.,0.0911,3.404,3.389,12,
 -3710,21,
 -3542,40,
 -3526,65,
 -3428,123,
 -2536,185,
 -2678,251,
 -2461,454,
 -2287,662,
 -2250,788,
 -2150,921,
 -2209,990,
 -2234,1027,
 Anchor H.
 -4347.,0.0870,3.245,3.4,12,
 -3808,21,
 -3523,40,
 -3516,65,
 -3378,123,
 -2277,185,
 -2485,251,
 -2027,454,
 -1919,662,
 -1827,788,
 -1777,921,
 -1827,990,
 -1815,1027.

Number of plots.
 Title of plot.
 # of anchors on plot.
 Initial y-axis value, y interval, y maximum.
 Legend, width and height of legend box.
 1=LC, 2=ASG.
 Numerical anchor designation (1=Anchor A).

Figure A.1: Load versus time for Anchor A. —
 1, _____
 0.,20.,100., _____
 15.5,9.1,3.2,1.6, _____ x and y coordinates of
 2, _____ # of load types (1=LC or
 1,2, _____
 1, _____
 LC A _____
 ASG A _____
 Figure A.2: Load versus time for Anchor B.
 1, _____
 0.,20.,100., _____
 15.5,9.1,3.2,1.6,
 2, _____
 1,2, _____

2,
LC B
ASG B
Figure A.3: Load versus time for Anchor C.
1,
0.,20.,100.,
15.5.9.1.3.2.1.6,
2,
1,2,
3,
LC C
ASG C
Figure A.4: Load versus time for Anchor D.
1,
0.,20.,100.,
15.5.9.1.3.2.1.6,
2,
1,2,
4,
LC D
ASG D
Figure A.5: Load versus time for Anchor E.
1,
0.,20.,100.,
15.5.9.1.3.2.1.6,
2,
1,2,
5,
LC E
ASG E
Figure A.6: Load versus time for Anchor F.
1,
-20.,20.,80.,
15.5.9.1.3.2.1.6,
2,
1,2,
6,
LC F
ASG F
Figure A.7: Load versus time for Anchor G.
1,
0.,20.,100.,
15.8.9.6.2.9.1.1,
1,

1,
7,
LC G
Figure A.8: Load versus time for Anchor H.

0.,20.,100.,
15.8.9.6.2.9.1.1,
1,
1,
8,

LC H
Figure A.9: East wall load cells. — Title of plot.
4. — # of anchors on plot.
0.,20.,100., — Initial y-axis value, y interval, y maximum.
15.8.8.1.2.9.2.6. — x and y coordinates of legend, width and height of legend box.
1, — # of load types (1=LC or ASG, 2=LC and ASG).
1, — 1=LC, 2=ASG.
5, — Numerical anchor designation (5=Anchor E)
LC E — Legend Name.
6, — Numerical anchor designation (6=Anchor F)
LC F — Legend Name.
7, — Numerical anchor designation (7=Anchor G)
LC G — Legend Name.
8, — Numerical anchor designation (8=Anchor H)
LC H — Legend Name.

Figure A.10: West wall load cells.

4,
0.,20.,100.,
15.8.8.1.2.9.2.6,

1,
1,
1,

LC A

2,
LC B

3,
LC C

4,
LC D

Figure A.11: East wall ASG loads.

2,
-20.,20.,80.,
15.5.9.1.3.2.1.6,

1,
1,

2.
5.
ASG E
6.
ASG F
Figure A.12: West wall ASG loads.
4.
0.,20.,100.,
15.5,8.1,3.2,2.6.
1.
2.
1.
ASG A
2.
ASG B
3.
ASG C
4.
ASG D

```

C
C PROGRAM NAME: LC-PROG
C COMPILED VER: LC-PROGC
C
C DESCRIPTION: This program has the following functions.
C
C a) Calculates anchor loads from the LC data.
C
C b) Using the results from the program ASG-PROG
C the loads in the anchors based on the anchor
C strain gauges are determined.
C
C c) For both of the above cases the load per
C meter width of wall and the load per square
C meter of wall is also given.
C
C d) Summary tables of loads (LC and ASG) for each
C anchor are printed. These are compatible
C with CIVE:TABLE.
C
C e) The loads are plotted versus time. Any number
C of graphs can be generated each showing any
C number of anchors. As well, for each anchor
C LC loads, ASG loads or both can be plotted.
C
C NOTE: File 4 from above is the tabular output from
C ASG-PROG. Three lines of data for each anchor
C must be inserted into this file; NSG, NT, tendon
C area. This data occupies the first three lines
C of the results for each anchor.
C
C VARIABLES: LTMAT(J=1-NT,A=1-4,K=1-NCELLS,B=1-2)
C J - which epoch
C A - 1=load, 2=load/meter, 3=load/m**2, 4=day #
C K - which cell
C B - 1=load cell, 2=ASG
C
C RUN STATEMENT: $RUN LC-PROGC+*DISSPLA 5=LC-AH 4=LC-4 1=-1 9=-9
C
C PROGRAM:
C
C DIMENSION IPKRAY(100,100),DUM(20),
C .TIME(100),SG(100,100),NPLTYP(2),FIGTIT(20)
C REAL LTMAT(100,4,100,2),LOADY(100),TIMEX(100),Y1(100),
C .LOAD(100),TXTMAT(1100,7)
C INTEGER X1(100),LCELL(100)
C LOGICAL*1 TITLE(20),LEGNM(50,2),PLHED(50)
C
C Main loop which does calculations for each set of
C load cell data.
C
C READ(5,500)NCELLS
C READ(5,500)NTAB
C WRITE(1,150)
C DO 10 K=1,NCELLS

```

```

      READ(5,505)TITLE
C
C Read in initial reading, factor, and the number
C of times readings have been taken.
C
      READ(5,510)YI,XLCF,XLENG,YLENG,NT
C
C Writes output file headings.
C
      WRITE(1,100)
      WRITE(1,105)
      WRITE(1,110)
      WRITE(1,115)
      WRITE(1,120)
      WRITE(1,122)
C
C Read loadcell value & day #. Calculate load.
C
      DO 15 J=1,NT
      READ(5,515)Y1(J),X1(J)
      DUMMY=ABS(Y1(J)-YI)*XLCF
      Y1(J)=DUMMY
      LTMAT(J,1,K,1)=Y1(J)
      LTMAT(J,2,K,1)=Y1(J)/XLENG
      LTMAT(J,3,K,1)=Y1(J)/(XLENG*YLENG)
      LTMAT(J,4,K,1)=X1(J)
15 CONTINUE
C
C For anchors G and H there are no ASG readings, skip next section.
C
      IF (K .GT. 6) GOTO 20
C
C Read in ASG data and calculate load.
C
      READ(4,400)NTASG
      READ(4,405)AREA
      DO 25 I=1,35
      READ(4,505)DUM
25 CONTINUE
      DO 30 J=1,NTASG
      READ(4,410)TIME(J),SG(1,J)
      LOAD(J)=SG(1,J)*AREA*1000
      LTMAT(J,1,K,2)=LOAD(J)
      LTMAT(J,2,K,2)=LOAD(J)/XLENG
      LTMAT(J,3,K,2)=LOAD(J)/(XLENG*YLENG)
      LTMAT(J,4,K,2)=TIME(J)
30 CONTINUE
      DO 55 I=1,6
      READ(4,505)DUM
55 CONTINUE
C
C Initialize matrix which stores text output.
C
20 DO 60 I=1,1100

```

```

        DO 65 J=1,7
          TXTMAT(I,J)=-123.
65 CONTINUE
60 CONTINUE
C
C Write day numbers and loads for both LC and ASG into
C the text matrix. Accounts for the fact that day numbers
C do not exactly correspond between each set of measurements.
C
      M=1
      DO 70 I=1,2
        IF (I .EQ. 1) N=NT
        IF (I .EQ. 2) N=NTASG
        DO 75 J=1,N
          DAYNUM=LTMAT(J,4,K,I)
          TXTMAT(DAYNUM,1)=DAYNUM
          TXTMAT(DAYNUM,M+1)=LTMAT(J,1,K,I)
          TXTMAT(DAYNUM,M+2)=LTMAT(J,2,K,I)
          TXTMAT(DAYNUM,M+3)=LTMAT(J,3,K,I)
75 CONTINUE
        M=M+3
70 CONTINUE
C
C Print out the text matrix.
C
      DO 76 I=1,1100
        IF (TXTMAT(I,1) .EQ. -123.)GOTO 76
C
        IF (TXTMAT(I,2) .EQ. -123. .AND. TXTMAT(I,5) .NE. -123.)
          .WRITE(1,125)TXTMAT(I,1),TXTMAT(I,5),TXTMAT(I,6),TXTMAT(I,7)
C
        IF (TXTMAT(I,2) .NE. -123. .AND. TXTMAT(I,5) .EQ. -123.)
          .WRITE(1,130)TXTMAT(I,1),TXTMAT(I,2),TXTMAT(I,3),TXTMAT(I,4)
C
        IF (TXTMAT(I,2) .NE. -123. .AND. TXTMAT(I,5) .NE. -123.)
          .WRITE(1,135)TXTMAT(I,1),TXTMAT(I,2),TXTMAT(I,3),TXTMAT(I,4),
          .TXTMAT(I,5),TXTMAT(I,6),TXTMAT(I,7)
C
76 CONTINUE
      WRITE(1,140)
      WRITE(1,145)NTAB,TITLE
      IF (AINT(K/2.)*2 .EQ. K) WRITE(1,150)
      NTAB=NTAB+1
10 CONTINUE
C
C Plotting Routine
C
      READ(5,500)NPLOT
C
C Main plotting loop. One iteration per graph.
C Read in plot characteristics.
C
      DO 78 I=1,NPLOT
        READ(5,505)PLHED

```

```

READ(5,500)NANCH
READ(5,520)YORIG,YSTP,YMAX
READ(5,525)BX,BY,BW,BH
READ(5,500)NLDTYP
READ(5,502)(NPLTYP(J),J=1,NLDTYP)
CALL DSPDEV(' PLOTTER ')
CALL UNITS(' CM' )
CALL NOBRDR
CALL PAGE(27.94,21.59)
CALL AREA2D(19.,11.)
CALL COMPLX
CALL YNAME(' Load (kN/m**2)$' ,100)
CALL INTAXS
CALL FRAME
CALL YAXANG(0.)
CALL XREVTK
XORIG=0.
XMAX=1100.
XSTP=100.
CALL GRAF(XORIG,XSTP,XMAX,YORIG,YSTP,YMAX)
CALL BLREC(BX,BY,BW,BH,0.05)
C
C Loop 40 does one iteration for each anchor on the graph.
C
LINCNT=0
DO 80 J=1,NANCH
READ(5,500)LCELL(J)
C
C Loop 50 sets up the plot vectors for a particular curve.
C LC, ASG or both can be plotted on the same graph.
C
DO 82 L=1,NLDTYP
READ(5,505)(LEGNM(M,L),M=1,50)
IF (NPLTYP(L) .EQ. 1) NDP=NT
IF (NPLTYP(L) .EQ. 2) NDP=NTASG
DO 84 K=1,NDP
LOADY(K)=LTMAT(K,3,LCELL(J),NPLTYP(L))
TIMEX(K)=LTMAT(K,4,LCELL(J),NPLTYP(L))
84 CONTINUE
CALL CURVE(TIMEX,LOADY,NDP,1)
LINCNT=LINCNT+1
CALL LINES(LEGNM(1,L),IPKRAY,LINCNT)
82 CONTINUE
80 CONTINUE
CALL RESET(' BLNKS' )
CALL MESSAG(PLHED,100,4.,-2.75)
CALL MYLEGN(' ',1)
CALL LEGEND(IPKRAY,LINCNT,BX+0.3,BY+0.3)
CALL XGRAXS(XORIG,XSTP,XMAX,19.,' Day Number$',-100,0.,19.)
CALL XDTAXS(840601.,' MONTH',870605.,19.,' ',1,0.,0.)
CALL ENDPL(0)
78 CONTINUE
CALL DONEPL

```

```

C
C Read format statements for LC datafile.
C
500 FORMAT(I5)
502 FORMAT(2I5)
505 FORMAT(50A1)
510 FORMAT(4F10.4,I5)
515 FORMAT(2G10)
520 FORMAT(3F8.2)
525 FORMAT(4F5.2)
C
C Read format statements for ΔSG datafile
C
400 FORMAT(I5)
405 FORMAT(E14.7)
410 FORMAT(25X,F7.0,3X,F8.2)
C
C Write format statements.
C
100 FORMAT(//)
105 FORMAT(19X,'|',13X,'|',41X,'|',41X,'|')
110 FORMAT(19X,5X,'Time',22X,'Load Cell',27X,
.'Anchor Strain Gauges')
115 FORMAT(19X,14X,6('|'),'|')
120 FORMAT(19X,4X,'(Days)',10X,'kN',8X,'kN/m Width',6X,'kN/m**2',
.9X,'kN',8X,'kN/m Width',6X,'kN/m**2')
122 FORMAT(19X,7('|'),'|')
125 FORMAT(24X,F5.0,11X,'-',2(13X,'-'),10X,F6.2,2(8X,F6.2))
130 FORMAT(24X,F5.0,3(8X,F6.2),11X,'-',2(13X,'-'))
135 FORMAT(24X,F5.0,6(8X,F6.2))
140 FORMAT(19X,7('!'),'!')
145 FORMAT(/,51X,'Table A.',I1,': Load readings for ',20A1)
150 FORMAT('$9700 skipto=nextsheet',////////)
STOP
END

```


Appendix J

Data Reduction Procedure for the Anchor Strain Gauges

J.1 Introduction

The procedure used to reduce the anchor strain gauge data is incorporated into a program called ASG-PROG.

ASG-PROG has the following functions:

1. Convert the readings of the strain gauges mounted along the grouted portions of the anchor to stress.
2. Produce a summary table for each anchor giving the net strain and stress for each strain gauge for all epochs of data.
3. Produce plots for each anchor showing the stress distribution along their grouted sections. The results for each anchor are presented in two graphs.

The calculations embodied in the program are outlined below. This is followed by an explanation of how to operate the program and a description of the datafile.

J.2 Calculation Procedure

The reduction of the anchor strain gauge data to yield the stress at the gauge location is a simple procedure. The method will be considered for a single strain gauge as the technique remains constant for all the instruments. The following steps are involved.

1. The change in strain, called Δ_{strain} , between the original unloaded reading of the strain gauge and its reading at

a particular epoch is determined.

$$\Delta_{\text{strain}} = \text{Current reading} - \text{Unloaded reading} \quad [\text{J.1}]$$

The units of the strain readings, and thus of Δ_{strain} , are $\text{mm} \times 10^{-6}/\text{mm}$.

2. The change in strain is converted to stress according to Hooke's Law (1678). In this case Young's Modulus for the anchor rod steel is 2×10^5 MPa.

$$\begin{aligned} \sigma &= E\epsilon & [\text{J.2}] \\ &= (2 \times 10^5 \text{ MPa})(\Delta_{\text{strain}} \text{ mm} \times 10^{-6}/\text{mm}) \\ &= 0.2 \times \Delta_{\text{strain}} \text{ MPa} \end{aligned}$$

The stress calculated at a particular strain gauge is plotted on a graph against its position along the grouted portion of the anchor. This procedure is carried out for each strain gauge along the anchor rod. This yields the distribution of stress along the anchor at the time the readings were taken. As measurements are repeated periodically, stress distributions through time are obtained.

Although the procedure is straightforward some comments are warranted. The strain gauges are mounted axially along the anchor rod. In addition to measuring axial strain they are susceptible to the effects of residual and bending stresses. To quantify the influence these ancilliary loads

may exert on the stress field would require strain rosettes. In their absence, however, it is reasonable to arbitrarily declare that the anchor rod, prior to loading, is at a zero stress state. This action is embodied in Step 1 of the reduction procedure, where the initial strain gauge reading is taken to represent a completely unloaded condition. This removes from later measurements the influence of any stresses, axial or otherwise, that may be present in the anchor before tensioning. It is then assumed that all subsequent changes in strain are entirely attributable to fluctuations in the axial load in the anchor.

This assumption is of course invalid if bending in the anchor occurs. Bending will contribute strain that will incorrectly be ascribed to axial load. However, it is deemed unlikely that significant bending in the grouted portion of the anchor, where the strain gauges are located, is possible. This is due to the fact that the anchor rod, embedded in a drill hole, is supported by grout and the surrounding rock. Bending in the rod could be induced by settlement of the wall or the backfill. In either case it is probable that it would occur somewhere along the ungrouted portion of the rod.

The use of Hookes' Law implies a second assumption; that the anchor rod behaves elastically. Over the range of net strains encountered, never in excess of 1,000 microstrain units, this is substantiated.

J.3 Operating Procedure

The procedure used to produce the anchor strain gauge results is given below.

The data reduction program is compiled using the following command. The compiled version of the program will reside in a file called ASG-PROGC.

```
$RUN *FORTGTTEST SCARDS=ASG-PROG SPUNCH=ASG-PROGC
```

The program is run using the command given below.

```
$RUN ASG-PROGC+*DISSPLA 5=ASG-AF 1=-1 9=-9
```

ASG-AF is the file containing the anchor strain gauge data. File -1 is the text output file containing the tables summarizing the results for each of the anchors. File -9 is a plot description file (PDF) containing all of the results in graphical form.

Post processing of the two output files is exactly the same as was outlined in Appendix I for the anchor load results.

J.4 Datafile and Program Listings

The format of the datafile, ASG-AF, is explained with an annotated version of the file. This is presented below followed by a listing of the program ASG-PROG

Annotated version of datafile ASG-AF.

1, Initial table number.
 Name of anchor.
 Plot title.
 Plot title.
 Y-axis origin, interval, maximum.
 # of strain gauges, # of sets of readings.
 Spacing of strain gauges along anchor.

Strain reading, day # of readings.

Symbol # for plotting, date.

Anchor A	Anchor B
Figure B.1: Stress vs length for Anchor A, early epochs.	Figure B.3: Stress vs length for Anchor B, early epochs.
Figure B.2: Stress vs length for Anchor A, late epochs.	Figure B.4: Stress vs length for Anchor B, late epochs.
-20..60..400..	-20..60..400..
7, 13.	7, 13.
1..2..3..4..5..6..5..8..	1..2..3..4..5..6..5..8..
312, -2362, -3160, -1580, -2865, -1857, -1330, 8,	990, -1050, -1626, -4107, -2638, -2440, -1616, 8,
902, -2042, -2740, -1076, -2374, -1325, -1262, 9,	1342, -705, -1324, -3867, -2499, -2422, -1617, 9,
782, -1934, -2737, -1149, -2468, -1430, -1078, 20,	1245, -782, -1362, -3868, -2426, -2273, -1416, 20,
724, -1958, -2766, -1187, -2507, -1476, -1078, 40,	1196, -822, -1379, -3877, -2428, -2261, -1395, 40,
675, -1969, -2785, -1208, -2531, -1504, -1076, 65,	
667, -1978, -2803, -1216, -2540, -1507, -1070, 123,	
1862, -990, -1810, -194, -1515, -463, -75, 187,	
799, -2000, -2841, -1147, -2544, -1481, -1054, 454,	
786, -1978, -2861, -1014, -2511, -1462, -1032, 662,	
784, -2004, -2934, -1006, -2532, -1477, -1045, 788,	
870, -1984, -3000, -898, -2469, -1410, -985, 921,	
785, -1980, -3037, -894, -2507, -1464, -1013, 990,	
769, -1995, -3053, -895, -2526, -1482, -1026, 1027,	
0, 08/06/84	
1, 08/06/84	
2, 20/06/84	
3, 10/07/84	
4, 05/08/84	
5, 03/10/84	
6, 05/12/84	
8, 29/08/85	
9, 25/03/86	
10, 29/07/86	
11, 10/12/86	
12, 16/02/87	
13, 25/03/87	

Anchor B

1141, -867, -1413, -3910, -2458, -2275, -1406, 65,
 1134, -878, -1420, -3921, -2471, -2271, -1395, 123,
 2333, -82, -689, -3219, -1774, -1584, -728, 187,
 1652, -761, -1346, -3880, -2452, -2215, -1358, 454,
 1704, -665, -1282, -3829, -2402, -2166, -1332, 662,
 1702, -702, -1309, -3848, -2437, -2178, -1337, 788,
 1790, -627, -1238, -3786, -2379, -2107, -1276, 921,
 1711, -659, -1269, -3814, -2400, -2130, -1296, 990,
 1711, -682, -1287, -3828, -2418, -2138, -1306, 1027,
 0.08/06/84
 1.08/06/84
 2.20/06/84
 3.10/07/84
 4.05/08/84
 5.03/10/84
 6.05/12/84
 8.29/08/85
 9.25/03/86
 10.29/07/86
 11.10/12/86
 12.16/02/87
 13.25/03/87

Anchor C
 Figure B.5: Stress vs length for Anchor C, early epochs.
 Figure B.6: Stress vs length for Anchor C, late epochs.

-20., 60., 400.,
 7, 13,
 1., 2., 3., 4., 5., 6., 5., 8.,
 -1362, -960, -4070, -2840, -1973, -5040, -3016, 8,
 -673, -479, -3313, -2177, -1638, -4896, -2965, 9,
 -930, -796, -3598, -2423, -1657, -4782, -2762, 20,
 -916, -788, -3595, -2428, -1658, -4782, -2767, 40,
 -964, -833, -3637, -2467, -1671, -4796, -2769, 64,
 -947, -828, -3620, -2456, -1664, -4793, -2767, 123,
 440, 728, -2126, -1039, -492, -3670, -1693, 187,
 -643, -370, -3236, -2161, -1498, -4667, -2690, 454,
 -572, -273, -3130, -2060, -1403, -4565, -2607, 662,
 -651, -361, -3212, -2132, -1470, -4660, -2657, 788,
 -539, -266, -3080, -2033, -1395, -4567, -2569, 921,
 -560, -293, -3100, -2047, -1402, -4578, -2566, 990,
 -586, -310, -3124, -2066, -1426, -4595, -2586, 1027,
 0.08/06/84
 1.08/06/84
 2.20/06/84

3.10/07/84
 4.05/02/84
 5.03/10/84
 6.05/12/84
 8.29/08/85
 9.25/03/86
 10.29/07/86
 11.10/12/86
 12.16/02/87
 13.25/03/87

Anchor D

Figure B.7: Stress vs length for Anchor D, early epochs.

Figure B.8: Stress vs length for Anchor D, late epochs.

-20..60..400..

7,13,
 1.,2.,3.,4.,5.,6.,5.,8.,,
 716.,-2699.,-2362.,-3692.,-5589.,-1592.,-663.,8.,
 1375.,-2172.,-1876.,-3510.,-5550.,-1505.,-660.,9.,
 1248.,-2248.,-1932.,-3454.,-5469.,-1433.,-490.,20.,
 1227.,-2302.,-1944.,-3442.,-5449.,-1415.,-474.,40.,
 1165.,-2348.,-1987.,-3463.,-5465.,-1428.,-485.,65.,
 1157.,-2363.,-2003.,-3462.,-5461.,-1424.,-482.,123.,
 1966.,-1632.,-1288.,-2779.,-4788.,-750.,188.,187.,
 1263.,-2338.,-2022.,-3451.,-5438.,-1411.,-460.,454.,
 1317.,-2290.,-1954.,-3400.,-5407.,-1367.,-424.,662.,
 1300.,-2360.,-2012.,-3430.,-5426.,-1390.,-444.,788.,
 1375.,-2292.,-1950.,-3365.,-5356.,-1325.,-378.,921.,
 1320.,-2274.,-1959.,-3363.,-5387.,-1354.,-401.,990.,
 1308.,-2295.,-1977.,-3396.,-5404.,-1368.,-412.,1027.,
 0.08/06/84
 1.08/06/84
 2.20/06/84
 3.10/07/84
 4.05/08/84
 5.03/10/84
 6.05/12/84
 8.29/08/85
 9.25/03/86
 10.29/07/86
 11.10/12/86
 12.16/02/87
 13.25/03/87

Anchor E
 Figure B.9: Stress vs length for Anchor E, early epochs.

Figure B.10: Stress vs length for Anchor E, late epochs.

-30.,30.,120.,
 6, 13,
 1., 3., 4., 5., 6., 5., 8.,
 -2905,998,-1203,-970,-780,-780,-2821,20,
 -2367,1315,-1016,-916,-788,-2827,21,
 -2461,1282,-1032,-922,-783,-2827,40,
 -2505,1270,-1040,-928,-792,-2830,65,
 -2505,1276,-1041,-933,-807,-2830,123,
 -2471,1367,-948,-856,-730,-2775,185,
 -2526,1371,-937,-839,-715,-2769,251,
 -2568,1327,-1006,-900,-787,-2823,454,
 -2575,1378,-969,-863,-748,-2806,662,
 -2589,1357,-992,-887,-786,-2821,788,
 -2536,1422,-942,-839,-709,-2788,921,
 -2608,1404,-975,-866,-743,-2805,990,
 -2626,1410,-993,-876,-753,-2813,1027,
 0,20/06/84
 2,21/06/84
 3,10/07/84
 4,05/08/84
 5,03/10/84
 6,05/12/84
 7,11/02/85
 8,29/08/85
 9,25/03/86
 10,29/07/86
 11,10/12/86
 12,16/02/87
 13,25/03/87

Figure B.11: Stress vs length for Anchor F, early epochs.

-30.,30.,120.,
 7, 13,
 1., 2., 3., 4., 5., 6., 5., 8.,
 1786,176,-849,944,67,-1064,478,20,
 1695,155,-818,978,76,-1063,475,21,
 1694,148,-839,967,73,-1065,472,40,
 1687,147,-851,958,71,-1074,471,65,
 1698,167,-864,950,65,-1090,458,123,
 1852,309,-745,1015,142,-1036,510,185,
 1826,308,-742,996,158,-1036,513,251,
 1796,270,-790,913,107,-1152,465,454,

1816.309, -805.900, 146, -1148.482, 662,
1799.291, -825.863, 127, -1195.482, 788,
1909.339, -798.913, 182, -1146.542, 921,
1849.290, -854.886, 156, -1176.509, 990,
1824.272, -883.872, 144, -1185.496, 1027,
0.20/06/84
2.21/06/84
3.10/07/84
4.05/08/84
5.03/10/84
6.05/12/84
7.11/02/85
8.29/08/85
9.25/03/86
10.29/07/86
11.10/12/86
12.16/02/87
13.25/03/87

```

C
C PROGRAM NAME:  ASG-PROG
C COMPILED VER:  ASG-PROGC
C
C DESCRIPTION:   REDUCES ANCHOR STRAIN GAUGE READINGS
C                TO STRESSES.
C
C VARIABLES:    TIT1(I) - TITLE IDENTIFYING ANCHOR
C                NSG - THE NUMBER OF STRAIN GAUGES ON THE
C                ANCHOR.
C                NT - THE NUMBER OF TIMES THE ANCHOR HAS
C                BEEN READ.
C                SP(J) - THE POSITIONS OF THE STRAIN GAUGES
C                ALONG THE ANCHOR.
C                YI(N,J) - STRAIN GAUGE READING AT PARTICULAR
C                TIME AND POSITION.
C                YIS(N,J) - STRESS AT PARTICULAR TIME AND LOCATION
C                ALONG THE ANCHOR.
C                TI(N) - VECTOR CONTAINING DAY NUMBERS.
C
C RUN: $RUN ASG-PROGC+DISPLA 5=ASG-AF 1=ASG-TOUT 9=ASG-POUT
C
C PROGRAM:
C   DIMENSION X(100),YI(100,100),YIS(100,100),SP(10),
C   .TIT1(8),STRY(100),LEGNM(25),IPKRAY(100,100),
C   .BY(2),BH(2),NCB(2),NCE(2),YINET(100,100)
C   INTEGER TI(100)
C   LOGICAL*1 FIGTIT(75,2)
C
C Read in title, number of strain gauges, strain
C gauge positions and anchor designation.
C
C   READ(5,495)NTAB
C   DO 5 K=1,6
C   READ(5,500)TIT1
C   READ(5,501)(FIGTIT(I,1),I=1,75)
C   READ(5,501)(FIGTIT(I,2),I=1,75)
C   READ(5,502)YORIG,YSTP,YMAX
C   READ(5,505)NSG,NT
C   IF (NSG .EQ. 6) GO TO 10
C   READ(5,510)(SP(J),J=1,NSG)
C   GO TO 15
C 10 READ(5,515)(SP(J),J=1,NSG)
C
C Set up the text output tables.
C
C 15 WRITE(1,100)
C   IF (NSG .EQ. 6) GO TO 20
C   WRITE(1,105)
C   WRITE(1,110)
C   WRITE(1,115)
C   WRITE(1,120)
C   WRITE(1,125)
C   GO TO 25
C 20 WRITE(1,140)

```

```

WRITE(1,145)
WRITE(1,150)
WRITE(1,155)
WRITE(1,160)
C
C Read in the strain gauge readings for each time period.
C Calculate net strain and write results to a table.
C
25 DO 30 I=1,NT
   IF (NSG .EQ. 6) GO TO 35
   READ(5,525)(YI(I,J),J=1,NSG),TI(I)
   DO 32 J=1,NSG
     YINET(I,J)=YI(I,J)-YI(1,J)
32 CONTINUE
   WRITE(1,130)TI(I),(YINET(I,J),J=1,NSG)
   GO TO 30
35 READ(5,530)(YI(I,J),J=1,NSG),TI(I)
   DO 37 J=1,NSG
     YINET(I,J)=YI(I,J)-YI(1,J)
37 CONTINUE
   WRITE(1,165)TI(I),(YINET(I,J),J=1,NSG)
30 CONTINUE
   IF (NSG .EQ. 6) GO TO 45
   WRITE(1,135)
   GO TO 50
45 WRITE(1,170)
C
C Calculate stress from strain for each time period and position.
C
50 IF (NSG .EQ. 6) GO TO 55
   WRITE(1,105)
   WRITE(1,175)
   WRITE(1,115)
   WRITE(1,120)
   WRITE(1,125)
   GO TO 60
55 WRITE(1,140)
   WRITE(1,180)
   WRITE(1,150)
   WRITE(1,155)
   WRITE(1,160)
C
C Do the calculation for each strain gauge.
C
60 DO 65 I=1,NT
   DO 70 J=1,NSG
     YIS(I,J)=YINET(I,J)*0.2
70 CONTINUE
   IF (NSG .EQ. 6) GO TO 75
   WRITE(1,185)TI(I),(YIS(I,J),J=1,NSG)
   GO TO 80
75 WRITE(1,190)TI(I),(YIS(I,J),J=1,NSG)
80 CONTINUE
65 CONTINUE

```

```

      IF (NSG .EQ. 6) GO TO 85
      WRITE(1,135)
      GO TO 90
85  WRITE(1,170)
90  WRITE(1,192)NTAB,TIT1
      WRITE(1,195)
      NTAB=NTAB+1
C
C  Plotting routine (DISSPLA)
C
      NCB(1)=1
      NCE(1)=7
      NCB(2)=8
      NCE(2)=13
      BY(1)=12.85
      BH(1)=4.35
      BY(2)=13.31
      BH(2)=3.84
      DO 92 L=1,2
      NLINES=0
      CALL DSPDEV(' PLOTTER ')
      CALL UNITS(' CM' )
      CALL PAGE(21.5,28.0)
      CALL NOBRDR
      CALL PHYSOR(5.9,6.85)
      CALL AREA2D(13.0,17.5)
      CALL COMPLX
      CALL XNAME(' Grouted Anchor Length (m)$' ,100)
      CALL YNAME(' Stress (MPa)$' ,100)
      CALL INTAXS
      CALL FRAME
      CALL YAXANG(0.)
      XORIG=0.
      XMAX=9.
      XSTP=1.
      CALL GRAF(XORIG,XSTP,XMAX,YORIG,YSTP,YMAX)
      CALL BLREC(8.5,BY(L),4.2,BH(L),0.05)
      NLB=NCB(L)
      NLE=NCE(L)
      DO 95 I=NLB,NLE
      READ(5,535)ISYM,LEGNM
      DO 99 J=1,NSG
      STRY(J)=YIS(I,J)
99  CONTINUE
      CALL MARKER(ISYM)
      CALL CURVE(SP,STRY,NSG,1)
      NLINES=NLINES+1
      CALL LINES(LEGNM,IPKRAY,NLINES)
95  CONTINUE
      CALL RESET(' BLNKS' )
      CALL MYLEGN(' ',1)
      CALL LEGEND(IPKRAY,NT,8.8,BY(L)+0.3)
      CALL MESSAG(FIGTIT(1,L),100,-1.8,-3.25)
      CALL ENDPL(0)

```

```

92 CONTINUE
5 CONTINUE
CALL DONEPL

```

```

C
C Read format statements.

```

```

C
495 FORMAT(I5)
500 FORMAT(8A1)
501 FORMAT(75A1)
502 FORMAT(3F10.3)
505 FORMAT(2I5)
510 FORMAT(7F5.2)
515 FORMAT(6F5.2)
525 FORMAT(7F10.2,I5)
530 FORMAT(6F10.2,I5)
535 FORMAT(I5,25A4)

```

```

C
C Write (FILE 1) format statements.

```

```

C
100 FORMAT(/////////)
105 FORMAT(25X,'|',8X,'|',76X,'|')
110 FORMAT(25X,' Time',30X,'Net Strain (mmE-6/mm)')
115 FORMAT(34X,'|',7(10X,'|'))
120 FORMAT(27X,'(Days)',5X,'SG 1',7X,'SG 2',7X,'SG 3',7X,'SG 4',
+7X,'SG 5',7X,'SG 6',7X,'SG 7')
125 FORMAT(25X,'|',85X,'|')
130 FORMAT(25X,I7,4X,7(F7.0,4X))
135 FORMAT(25X,'|',8X,7('!',10X),'!',////)
140 FORMAT(25X,'|',8X,'|',65X,'|')
145 FORMAT(25X,' Time',25X,'Net Strain (mmE-6/mm)')
150 FORMAT(34X,'|',6(10X,'|'))
155 FORMAT(27X,'(Days)',5X,'SG 1',7X,'SG 2',7X,'SG 3',7X,'SG 4',
+7X,'SG 5',7X,'SG 6')
160 FORMAT(25X,'|',74X,'|')
165 FORMAT(25X,I7,4X,6(F7.0,4X))
170 FORMAT(25X,'|',8X,6('!',10X),'!',////)
175 FORMAT(25X,' Time',35X,'Stress (MPa)')
180 FORMAT(25X,' Time',30X,'Stress (MPa)')
185 FORMAT(25X,I7,3X,7(F8.2,3X))
190 FORMAT(25X,I7,3X,6(F8.2,3X))
192 FORMAT(45X,'Table B.',I1,' : Strain gauge results for ',
.8A1,' ')
195 FORMAT('$9700 SKIPTO=NEXTSHEET')
STOP
END

```

Appendix K

Data Reduction Procedure for the Wall Mounted Strain Gauges

K.1 Introduction

As was outlined in Section 3.3 strain gauges are mounted on the surface of the sheet pile wall in four vertical columns. Two columns each are placed on neighbouring sections of pile, called simply the east and west sections. On each pile one column of strain gauges is placed on what is referred to as the outer face; the other is on the inner face. Note that both of these locations are on the exposed side of the sheet pile. The terms "outer" and "inner" refer to the corrugated nature of the sheet pile.

As one progresses down the pile section, outer and inner face strain gauges are located at approximately equal elevations. For calculation purposes horizontally adjacent strain gauges on one pile are considered as a pair.

K.2 Calculation Procedure

The data reduction procedure is based on modelling each of the instrumented pile sections as a beam. Note that each section is considered independently. The following information is obtained for each epoch of available strain gauge data.

1. The bending stress, the axial stress and the bending moment at each pair of strain gauges along the pile.
2. An estimate of the bending moment distribution over the

length of the pile consistent with the anchor loads measured by the load cells and the known behavior of the wall.

3. The distribution of shear and pressure over the pile.
4. A prediction of the displacement of the wall based on its deflection due to bending and the elastic yield of the anchor rods.

The data reduction procedure is embodied in a computer program called SG-PROG. Most of the quantities dealt with in the program are stored in one or two dimensional arrays. To emphasize the serial nature of the calculations the vector and matrix notation is maintained in the following discussion. The vectors have elements representing a quantity at different times or epochs. The same holds true for the matrices but the first element identifies the strain gauge pair being considered. As well, some of the variable names contain a subscript, i , which takes a value of either 1 or 2. The former associates the variable with the outer face of the pile; 2 relates the quantity to the inner face.

K.2.1 Calculation of the bending and axial stresses and the bending moments

The following series of calculations is performed on each pair of strain gauges.

1. Calculation of the net strain.

For each strain gauge in the pair its initial unloaded reading is subtracted from its current value.

Because a dummy strain gauge, not subjected to any load, shows temperature dependent response, a temperature correction is applied to all the readings as well. The calculations are as follows.

$$\Delta\text{Strain}(J,K)_i = \left[\text{Strain}_i(J,K) + \text{ICOR}(K) \right] - \left[\text{Strain}_i(J,1) + \text{ICOR}(1) \right] \quad [\text{K.1}]$$

where:

$\Delta\text{Strain}(J,K)_i$ = net strain for the J^{th} strain gauge, K^{th} epoch, on the outer and inner face in microstrains

$\text{ICOR}(K)$ = temperature correction to strain gauge at k^{th} epoch in microstrains

2. Convert the net strain to stress.

The net strains are sufficiently low to warrant use of Hookes' elasticity relation. Therefore;

$$\begin{aligned} \sigma_i(J,K) &= \Delta\text{Strain}_i(J,K) \times E \times 10^{-6} & [\text{K.2}] \\ &= (\text{mm/mm}) \times \text{MPa} \\ &= \text{MPa} \end{aligned}$$

3. Determine the extreme fibre stress on the earth side of the wall.

Before further calculations can proceed, a

prediction of the stress immediately opposite $\sigma_2(J,K)$ on the earth side of the wall, is required. The stress at this location is called $\sigma_{2a}(J,K)$ where the "a" signifies adjusted. The equation used to predict σ_{2a} is given below.

$$\begin{aligned}\sigma_{2a}(J,K) &= \left[(\sigma_2(J,K) - \sigma_1(J,K)) / (AH - AT) \right] * AH \\ &\quad + \sigma_1(J,K) \qquad \qquad \qquad [K.3] \\ &= \text{MPa}\end{aligned}$$

where AH = depth of sheet pile section

AT = thickness of sheet pile

4. Determine the bending stress.

The two stresses, $\sigma_1(J,K)$ and $\sigma_{2a}(J,K)$, on opposite sides of the sheet pile wall will not necessarily be equal in magnitude or opposite in sign. Much more likely are: unequal magnitudes of stress with opposite signs; unequal stresses of like sign. However, a single representative value of the bending stress is desired.

In dealing with the above inequalities it is worthwhile to consider their cause. The strain gauges from which the stresses are calculated are separated by a horizontal distance. Therefore, at least some of the difference in the stresses may be due to a variation in the degree of bending along the wall. As the separation of the outer and inner strain gauge columns is less than 1 metre, however, the variation is likely minimal.

Alternatively, the presence of axial load on the wall will ensure that σ_1 and σ_{2a} will not have equal magnitudes nor necessarily opposite signs. Axial load results from friction which may develop between the inside of the wall and the backfill.

The bending and axial stresses can be calculated by attributing any difference in the absolute values of σ_1 and σ_{2a} to axial load on the wall. The bending and axial stresses are calculated according to the following equations.

$$\sigma_{\text{axial}}(J,K) = \left[\sigma_1(J,K) + \sigma_{2a}(J,K) \right] / 2 \quad [\text{K.4}]$$

$$\sigma_{\text{ibend}}(J,K) = \sigma_1(J,K) - \sigma_{\text{axial}}(J,K) \quad [\text{K.5}]$$

Note that σ_{ibend} signifies the bending stress acting on the outer exposed side of the wall.

5. Calculate the Bending Moment.

The bending moment at each horizontally adjacent pair of strain gauges can be calculated using the bending stress determined from above. The equation employed is as follows.

$$\begin{aligned} M(J,K) &= \sigma_{\text{ibend}}(J,K) \times S \times 1\text{m} \\ &= (\text{N/mm}^2) (\text{mm}^3/\text{m}) (\text{m}) \\ &= \text{Nmm} \\ &= 10^{-6} \text{ kNm} \end{aligned}$$

Therefore,

$$M(J,K) = \sigma_{\text{bend}}(J,K) \times S \times 1\text{m} \times 10^{-6} \quad [\text{K.6}]$$

where $M(J,K)$ = bending moment in kNm

S = section modulus in mm^3/m

σ_{bend} = bending stress in MPa

A note concerning the section modulus is required. The manufacturer of the sheet pile specifies this quantity per unit length of wall. In the above calculation a one metre section of wall was assumed. The bending stress on the other hand was determined by assuming that a single sheet pile acts as a beam. This suggests an apparent inconsistency because the width of a sheet pile is 550mm. No discrepancy exists, however, as the width of wall to consider is arbitrary. The bending moment calculated for a particular width simply reflects that required to induce the calculated bending stress over that distance.

Note that all the results discussed thus far are included as output in tabular form. One table for each epoch of data is produced. As well, two plots of elevation versus the calculated bending moments are prepared. The first shows the early epochs, the second the later ones.

K.2.2 Establish a bending moment distribution over the height of the wall

Bending moments are currently established at each of the eight pairs of strain gauges along a sheet pile section. It is desired, however, to have a continuous distribution of

bending moment over the complete height of the wall.

The wall is acted upon by some distributed load from the backfill countered by two anchor forces. If the anchors are considered as point loads the resulting moment distribution is continuous but composed of three separate curves. These curves are located above the upper waler, between the walers and below the lower waler. Each zone is referred to respectively by the subscripts "t", "m" and "b" signifying the top, middle and bottom sections of wall.

Three cubic polynomials are postulated to define the bending moment distribution over the height of the wall. One equation for each of the three sections of the wall is used.

$$M_t(x) = A_t x^3 + B_t x^2 + C_t x + D_t \quad [K.7]$$

$$M_m(x) = A_m x^3 + B_m x^2 + C_m x + D_m \quad [K.8]$$

$$M_b(x) = A_b x^3 + B_b x^2 + C_b x + D_b \quad [K.9]$$

The twelve unknown coefficients incorporated in these equations are determined using the available moment data points and a number of boundary conditions. The boundary conditions specify known behavior of the wall and are listed below.

1. The wall is free at its upper edge and also has zero embedment depth at its base. Therefore, it is known that the bending moment and shear at each end of the wall is zero.

$$M_t(x_1) = 0 \quad [K.10]$$

$$M_b(x_0) = 0 \quad [K.11]$$

$$M_t'(x_1) = 0 \quad [K.12]$$

$$M_b'(x_0) = 0 \quad [K.13]$$

where x_1 = elevation at top of wall

x_0 = elevation at bottom of wall

$M'(x)$ = first derivative of the moment
function

= shear function

2. The moment distribution, although composed of three sections, must be continuous over the entire height of the wall. The walers mark the boundary between each pair of adjacent moment functions. At these locations continuity of the bending moments must be enforced.

$$M_t(x_2) = M_m(x_2) \quad [K.14]$$

$$M_m(x_3) = M_b(x_3) \quad [K.15]$$

where x_2 = elevation at top waler

x_3 = elevation at bottom waler

3. The anchor forces, being represented by point loads, will introduce discontinuities into the shear distribution for the wall at the walers. The magnitudes of these breaks will be equal to the anchor loads. Thus at the walers a simple relationship between the first derivatives of adjacent moment functions can be specified. These are as follows.

$$A_1 = M'_t(x_2) - M'_m(x_2) \quad [K.16]$$

$$A_2 = M'_m(x_3) - M'_b(x_3) \quad [K.17]$$

A_1 and A_2 are the forces in the top and bottom anchors respectively.

Further explanation of the anchor forces used in the above equations is warranted. Recall that the bending moments were calculated on the basis of a one metre width of wall. To maintain consistency this necessitates use of anchor forces per unit width of wall. The average quantities from the anchors located adjacent to the wall mounted strain gauges are used.

4. The load distribution acting on the wall can be expected to be continuous over the wall's entire height.

Therefore, at the walers, continuity of the second derivatives of adjacent moment functions must occur. In mathematical terms this can be specified as follows.

$$M''_t(x_2) = M''_m(x_2) \quad [K.18]$$

$$M''_m(x_3) = M''_b(x_3) \quad [K.19]$$

where $M''(x)$ = second derivative of the
moment function
= pressure function

This brings the number of boundary conditions to ten. At the west section sheet pile there are eight moment data

points available. At the east section there are six usable moment values. (Although eight pairs of strain gauges are present, the readings from the two pairs adjacent to the upper waler are erroneous (Elwi, 1987)).

For both sections, therefore, the number of constraints plus data observations exceeds the number of unknowns; the twelve polynomial coefficients. This necessitates the use of least squares regression. Lagrangian multipliers are employed to enforce the boundary conditions on the least squares calculations. The complete procedure is described in detail for the west section in the following. The solution technique is identical for both sections; however, the calculations differ slightly because the west section contains more data points.

The governing equation for solution of the polynomial coefficients is as follows.

$$U = \sum_{j=1}^8 v_j^2 + \sum_{i=1}^{10} C_i \quad [\text{K.20}]$$

where:

$$\begin{aligned} v_1^2 &= \left[q_1 - (A_t p_1^3 + B_t p_1^2 + C_t p_1 + D_t) \right]^2 \\ v_2^2 &= \left[q_2 - (A_t p_2^3 + B_t p_2^2 + C_t p_2 + D_t) \right]^2 \\ v_3^2 &= \left[q_3 - (A_m p_3^3 + B_m p_3^2 + C_m p_3 + D_m) \right]^2 \\ v_4^2 &= \left[q_4 - (A_m p_4^3 + B_m p_4^2 + C_m p_4 + D_m) \right]^2 \\ v_5^2 &= \left[q_5 - (A_m p_5^3 + B_m p_5^2 + C_m p_5 + D_m) \right]^2 \\ v_6^2 &= \left[q_6 - (A_m p_6^3 + B_m p_6^2 + C_m p_6 + D_m) \right]^2 \\ v_7^2 &= \left[q_7 - (A_b p_7^3 + B_b p_7^2 + C_b p_7 + D_b) \right]^2 \\ v_8^2 &= \left[q_8 - (A_b p_8^3 + B_b p_8^2 + C_b p_8 + D_b) \right]^2 \end{aligned}$$

$$C_1 = L_1(A_t x_1^3 + B_t x_1^2 + C_t x_1 + D_t)$$

$$C_2 = L_2(3A_t x_1^2 + 2B_t x_1 + C_t)$$

$$C_3 = L_3(A_t x_2^3 + B_t x_2^2 + C_t x_2 + D_t \\ - A_m x_2^3 - B_m x_2^2 - C_m x_2 - D_m)$$

$$C_4 = L_4(3A_t x_2^2 + 2B_t x_2 + C_t \\ - 3A_m x_2^2 - 2B_m x_2 - C_m \\ - \text{upper anchor})$$

$$C_5 = L_5(6A_t x_2 + 2B_t - 6A_m x_2 + 2B_m)$$

$$C_6 = L_6(A_b x_4^3 + B_b x_4^2 + C_b x_4 + D_b)$$

$$C_7 = L_7(3A_b x_4^2 + 2B_b x_4 + C_b)$$

$$C_8 = L_8(A_m x_3^3 + B_m x_3^2 + C_m x_3 + D_m \\ - A_b x_3^3 - B_b x_3^2 - C_b x_3 - D_b)$$

$$C_9 = L_9(3A_m x_3^2 + 2B_m x_3 + C_m \\ - 3A_b x_3^2 - 2B_b x_3 - C_b \\ - \text{lower anchor})$$

$$C_{10} = L_{10}(6A_m x_3 + 2B_m - 6A_b x_3 + 2B_b)$$

Terms not previously defined are:

L_i = unknown Lagrangian multipliers

q_j = moment data point $M(J,K)$

p_j = elevation of moment data point $M(J,K)$

v_j represents the square of the distance along the ordinate between the moment data point and that predicted by the bending moment interpolation function. The ten C_i terms embody the ten boundary conditions discussed earlier.

The next step in the solution involves differentiating Equation K.20 with respect to each of the unknowns it

contains. This yields a total of 22 equations; one for each of the 12 unknown polynomial coefficients and the 10 unknown Lagrangian multipliers. These equations are arranged into a matrix. Solving this matrix provides the values of the unknown polynomial coefficients. The bending moment interpolation functions are now defined.

The program SG-PROG carries out these calculations for every epoch of available data and plots the results. This is carried out by sampling the three moment polynomials at 0.01 metre intervals. This yields a large number of elevation/bending moment coordinates which, when plotted, give smooth curves. The interpolated bending moment distribution for each epoch appears on a separate page along with the moment data points used to establish the curves.

K.2.3 Determine the shear and pressure distributions

The bending moment distributions for each epoch are composed of three polynomials. Shear and pressure profiles can be determined by differentiation of each of these functions once and twice respectively. All the coefficients in these equations are known as they were obtained by the procedure outlined Section K.2.2.

$$\begin{aligned} V_t(x) &= 3A_t x^2 + 2B_t x + C_t & [K.21] \\ &= M'_t(x) \end{aligned}$$

$$\begin{aligned} V_m(x) &= 3A_m x^2 + 2B_m x + C_m & [K.22] \\ &= M'_m(x) \end{aligned}$$

$$\begin{aligned} V_b(x) &= 3A_b x^2 + 2B_b x + C_b & [K.23] \\ &= M_b'(x) \end{aligned}$$

$$\begin{aligned} q_t(x) &= 6A_t x + 2B & [K.24] \\ &= M_t''(x) \end{aligned}$$

$$\begin{aligned} q_m(x) &= 6A_m x + 2B & [K.25] \\ &= M_m''(x) \end{aligned}$$

$$\begin{aligned} q_b(x) &= 6A_b x + 2B & [K.26] \\ &= M_b''(x) \end{aligned}$$

These equations represent the shear and pressure functions for one particular epoch of data. They can be sampled just as the moment polynomials were to yield coordinates which can be plotted. For the shear results, two graphs are produced, one for the early epochs and one for the late epochs. The pressure distributions are plotted three epochs per page.

A note concerning the units involved with the shear and pressure distributions is required. Recall that the bending moments had units of kNm and were based on a one metre width of wall. The first derivative of the bending moments, representing the slope of the moment distribution, will have units of kNm/m or kN per metre width of wall. The second derivative of the bending moments, or the pressure, is equivalent to the slope of the shear distribution. The units applicable here are kN/m per metre width of wall. This is equivalent to kN/m² or kPa.

K.2.4 Determine the theoretical bending deflection of the wall

Double integration of the bending moment distribution for a particular epoch will yield the theoretical bending deflection of the sheet pile section. The governing equation is as follows.

$$v(x) = \frac{1}{EI} \iint M(x) dx^2 \quad [K.27]$$

where $v(x)$ = the deflection function

E = modulus of elasticity

I = moment of inertia

Applying Equation K.27 to the three bending moment functions represented by Equations K.7 to K.9 gives rise to:

$$v_t(x) = \frac{1}{EI} \left[\frac{1}{20} A_t x^5 + \frac{1}{12} B_t x^4 + \frac{1}{6} C_t x^3 + \frac{1}{2} D_t x^2 + C_{t1} x + C_{t2} \right] \quad [K.28]$$

$$v_m(x) = \frac{1}{EI} \left[\frac{1}{20} A_m x^5 + \frac{1}{12} B_m x^4 + \frac{1}{6} C_m x^3 + \frac{1}{2} D_m x^2 + C_{m1} x + C_{m2} \right] \quad [K.29]$$

$$v_b(x) = \frac{1}{EI} \left[\frac{1}{20} A_b x^5 + \frac{1}{12} B_b x^4 + \frac{1}{6} C_b x^3 + \frac{1}{2} D_b x^2 + C_{b1} x + C_{b2} \right] \quad [K.30]$$

Each of the three deflection functions includes two constants of integration, C_{i1} and C_{i2} . Solving for these six unknowns requires six boundary conditions. The following are available.

1. The anchors which support the wall provide two positions where the displacement of the wall is known. It is

assumed that the movement of the wall at these locations is equal to the elastic deformation of the anchor rods.

$$\begin{aligned} v_t(x_2) &= \text{elastic yield of top anchor} & [K.31] \\ &= \Delta_t \end{aligned}$$

$$\begin{aligned} v_m(x_3) &= \text{elastic yield of bottom anchor} & [K.32] \\ &= \Delta_b \end{aligned}$$

$$\text{where } \Delta_i = \frac{P_i L_i}{A_i E}$$

P_i = change in anchor load/m width
since initial loading

L_i = ungrouted length of anchor

A_i = anchor rod area/metre
width of wall

Using only the change in load in the anchors since they were initially loaded is consistent with convention. All displacements have been referenced to the epoch immediately following tensioning of the anchors.

2. Each of the adjacent deflection functions must predict the same deflection at the walers. This provides two additional boundary conditions.

$$v_t(x_2) = v_m(x_2) \quad [K.33]$$

$$v_m(x_3) = v_b(x_3) \quad [K.34]$$

3. Similarly, the adjacent functions must give rise to deflected shapes which have the same slope at the walers. In mathematical terms these constraints can be

written as follows:

$$v'_t(x_2) = v'_m(x_2) \quad [K.35]$$

$$v'_m(x_3) = v'_b(x_3) \quad [K.36]$$

Each of these constraints is applied in turn to Equations K.28 through K.30. This produces six equations which can be arranged into a matrix which is subsequently solved. The values of the six integration constants are thus obtained. The three deflection functions are now fully defined.

Sampling these equations allows the deflected shape of the sheet pile to be plotted. Repeating this entire procedure gives rise to the deflected shape for every epoch. In this case the early epochs are plotted on one graph and the later ones on another.

K.2.5 Comments on the data reduction procedure

The approximate nature of the results calculated by the procedures discussed above must be emphasized. A number of assumptions are inherent in the calculations. Considering the sheet pile sections as beams is an estimate of actual conditions. The wall likely behaves more as a plate.

The manner in which the axial and bending stresses are calculated assumes ideal behavior of the strain gauges and uniform bending of the sheet pile.

Finally, the interpolation of the bending moment data to produce bending moment distributions is an approximate

endeavor. Numerous interpolation schemes were experimented with giving a wide variation of results. The interpolation procedure settled on was deemed the most reasonable. However, the results can at best be considered only as an approximation of actual conditions.

K.3 Operating Procedure

The procedure used to produce the results is given below. The data reduction program is compiled using the following command.

```
$RUN NEW:FORTTRANVS SCARDS=SG-PROG+Z-GAUSS1 SPUNCH=SG-PROGC
```

The file Z-GAUSS1 contains a subroutine for solving matrices. The compiled version of the program resides in SG-PROGC. The program is run with the following command.

```
$RUN SG-PROGC+*DISSPLA 5=datafile 4=-4  
6=-6 7=text output 8=-8 9=plot output
```

File 4 is used by the program only for writes and reads. File 6 is used by DISSPLA, the plotting routine, for writing messages. File 8 contains the results of equilibrium checks performed by the program. Note that the program is run once for each of the two instrumented sheet pile sections.

Post processing of the text and plot output files is identical to the procedure outlined in Appendix I.

K.4 Datafile and Program Listings

Two datafiles, one for the east section and one for the west section, are used. The east section datafile is called SG-DATAA; the west section datafile is called SG-DATAB. These files have the same format. An explanation is provided by an annotated version of SG-DATAA. This is presented below followed by a listing of the program SG-PROG and the subroutine Z-GAUSS1.

Annotated version of datafile SG-DATAA.

Wall Mounted Strain Gauge Data and Results for the East Section
 O. Title.
 0=east, 1=west section

Figure H.1: Field determined moments, east section, early epochs.
 Figure H.2: Field determined moments, east section, late epochs.
 Figure H.15: Shear diagram, east section, early epochs.
 Figure H.16: Shear diagram, east section, late epochs.
 Figure 6.2: Pressure distributions based on wall mounted strain gauges, reference epochs, east section.
 Figure F.1: Theoretical displacement (sheet pile only), east section, early epochs.
 Figure F.2: Theoretical displacement (sheet pile only), east section, late epochs.
 Figure F.5: Theoretical displacement versus time, east section.
 Figure 6.4: Displacements based on wall mounted strain gauges, reference epochs, east section.

-35.,5.,5..
 -40.,10.,40..
 -60.,5.,20..
 -5.,5.,15..
 2.0E+05,835E+03,200,8,
 13,8,1,
 2, -0.155, 497.547, 3, -0.130, 497.547,
 4, -0.155, 497.360, 5, -0.130, 497.320,
 6, -0.130, 496.936, 7, -0.115, 496.956,
 8, -0.135, 496.710, 9, -0.110, 496.729,
 10, -0.140, 495.853, 11, -0.115, 495.922,
 12, -0.155, 494.789, 13, -0.112, 494.858,
 14, -0.132, 494.543, 15, -0.130, 494.523,
 16, -0.150, 493.952, 17, -0.128, 494.001,
 June 20, 1984.

20.,1,20/06/84
 O.
 O..O..
 2, -3935, 3, -3665,
 4, -729, 5, -459,
 6, -959, 7, -2292,
 8, -1677, 9, -4433,
 10, -600, 11, -666,
 12, -5831, 13, -2997,
 14, -240, 15, -4213,
 16, -5899, 17, -2535,
 June 21, 1984.
 21.,2,21/06/84

X axis start, interval and stop for moment, shear, pressure and displacement plots.
 Elastic mod, section mod, section depth, sheet thickness.
 # of data sets, # of measurements/set, initial table #.
 2 sets of SG #, horiz offset from reference sheet pile joint, elevation.
 Date (for table).
 Day #, symbol # (for plots), Date (for legend).
 Temperature correction.
 Top anchor load/m, bottom anchor load/m.

2 sets of SG #, strain reading.

0. -14,
 21. 62, 54, 64, 3, -3678,
 2. -3933, 3, -3678,
 4. -726, 5, -462,
 6. -954, 7, -2332,
 8. -1659, 9, -4469,
 10. -550, 11, -751,
 12. -5709, 13, -3144,
 14. -112, 15, -440C,
 16. -5783, 17, -2697,
 July 10, 1984,
 40. .3, 10/07/84
 37.
 27. 67, 49, 71,
 2. -3906, 3, -3705,
 4. -690, 5, -443,
 6. -914, 7, -2340,
 8. -1619, 9, -4507,
 10. -530, 11, -777,
 12. -5714, 13, -3130,
 14. -129, 15, -4373,
 16. -5806, 17, -2671,
 August 5, 1984,
 66. .4, 05/08/84
 -5.
 27. 98, 47, 28,
 2. -3911, 3, -3708,
 4. -693, 5, -426,
 6. -913, 7, -2312,
 8. -1617, 9, -4496,
 10. -544, 11, -769,
 12. -5720, 13, -3116,
 14. -142, 15, -4359,
 16. -5816, 17, -2655,
 October 3, 1984,
 125. .5, 03/10/84
 20.
 31. 14, 48, 35,
 2. -3883, 3, -3720,
 4. -666, 5, -464,
 6. -881, 7, -2342,
 8. -1590, 9, -4529,
 10. -525, 11, -801,
 12. -5712, 13, -3137,

14. -127, 15, -4390,
 16. -5802, 17, -2677,
 December 5, 1984,
 185. .6, 05/12/84
 -50,
 57. 82, 47, 24,
 2. -3822, 3, -3684,
 4. -597, 5, -376,
 6. -812, 7, -2330,
 8. -1538, 9, -4478,
 10. -497, 11, -709,
 12. -5679, 13, -3052,
 14. -83, 15, -4288,
 16. -5752, 17, -2619,
 February 11, 1985,
 251. .7, 11/02/85
 53. 15, 43, 37,
 2. -3812, 3, -3704,
 4. -594, 5, -417,
 6. -814, 7, -2341,
 8. -1533, 9, -4507,
 10. -492, 11, -730,
 12. -5684, 13, -3065,
 14. -94, 15, -4285,
 16. -5758, 17, -2611,
 August 29, 1985,
 455. .8, 29/08/85
 3.
 62. 13, 47, 49,
 2. -3853, 3, -3802,
 4. -640, 5, -460,
 6. -861, 7, -2386,
 8. -1580, 9, -4562,
 10. -552, 11, -806,
 12. -5719, 13, -3113,
 14. -131, 15, -4374,
 16. -5793, 17, -2686,
 March 25, 1986,
 662. .9, 25/03/86
 1.
 65. 94, 43, 95,
 2. -3856, 3, -3788,
 4. -642, 5, -446,

6. -856, 7, -2350,
 8. -1578, 9, -4525,
 10. -549, 11, -764,
 12. -5704, 13, -3108,
 14. -120, 15, -4353,
 16. -5766, 17, -2688,
 July 29, 1986,
 788. .10, 29/07/86
 67. 65, 45, 18,
 2. -3840, 3, -3830,
 4. -621, 5, -505,
 6. -842, 7, -2373,
 8. -1561, 9, -4573,
 10. -540, 11, -807,
 12. -5709, 13, -3114,
 14. -134, 15, -4378,
 16. -5771, 17, -2707,
 December 10, 1986,
 922. .11, 10/12/86
 -53.
 69. 68, 44, 88,
 2. -3848, 3, -3718,
 4. -619, 5, -378,
 6. -826, 7, -2261,
 8. -1556, 9, -4442,
 10. -497, 11, -688,
 12. -5653, 13, -3077,
 14. -43, 15, -4322,
 16. -5722, 17, -2640,
 February 16, 1987,
 991. .12, 16/02/87
 -19,
 68. 22, 41, 93,
 2. -3830, 3, -3788,
 4. -617, 5, -461,
 6. -835, 7, -2332,
 8. -1563, 9, -4525,
 10. -533, 11, -750,
 12. -5680, 13, -3113,
 14. -93, 15, -4355,
 16. -5740, 17, -2681,
 March 25, 1987,
 1028. .13, 25/03/87

68. 03, 41, 41,
 2. -3839, 3, -3802,
 4. -626, 5, -472,
 6. -847, 7, -2346,
 8. -1572, 9, -4543,
 10. -540, 11, -773,
 12. -5679, 13, -3128,
 14. -106, 15, -4372,
 16. -5752, 17, -2700,

```

C
C Program Name: SG-PROG
C Compiled Ver: SG-PROGC
C
C Description: Program calculates stress and moment from
C              the wall mounted strain gauge readings and
C              plots the results. The measured moments are
C              interpolated using non-linear least squares
C              regression. Lagranian multipliers are used to
C              enforce the boundary conditions.
C              Cubic polynomial interpolation functions are
C              used. These functions, once established, are
C              differentiated to yield shear and pressure
C              distributions. The moment functions are also
C              integrated to yield a deflection profile.
C
C Compile:      $RUN NEW:FORTRANVS SCARDS=SG-PROG+Z-GAUSS1
C              SPUNCH=SG-PROGC
C
C Run Statement: $RUN SG-PROGC+*DISSPLA 5=SG-DATAi 4=-4 6=-6
C              7=SG-iTOUT 8=-8 9=SG-iPOUT
C
C Run Files:    4 - used by program only for write and read
C              5 - data file
C              6 - DISSPLA writes messages to this file
C              7 - tabular output
C              8 - contains listing of equilibrium checks
C              9 - plot file written to by DISSPLA
C
C Variables:
C
C          TITLE - IDENTIFIES SECTION OF WALL.
C          YE - MODULUS OF ELASTICITY.
C          AS - SECTION MODULUS.
C          AH - HEIGHT OF SECTION.
C          AT - THICKNESS OF SECTION.
C          NT - # OF TIMES STRAIN GAUGES ON WALL HAVE BEEN READ.
C          NL - # OF DATALINES FOR EACH SET OF READINGS.
C          NSG1(I) - VECTOR CONTAINING STRAIN GAUGE NUMBERS ALONG
C              OUTER COLUMN.
C          NSG2(I) - STRAIN GAUGE NUMBERS ALONG INNER COLUMN.
C          XL1(I)
C          YL1(I) - X AND Y COORDINATES FOR NSG1(I) AND NSG2(I)
C          XL2(I) STRAIN GAUGES.
C          YL2(I)
C          ICOR(NT) - TEMPERATURE CORRECTION FOR A PARTICULAR EPOCH.
C          DATE - DATE AT WHICH READINGS WERE TAKEN.
C          LEPS1(I,J) - STRAIN GAUGES READINGS FOR NSG1(I).
C          LEPS2(I,J) - " " " " NSG2(I).
C          ICHS1 - LEPS1(I,J)-LEPS1(I,1).
C          ICHS2 - LEPS2(I,J)-LEPS2(I,1).
C          SIG1(I,J) - STRESS AT EACH NSG1(I).
C          SIG2(I,J) - " " " NSG2(I).
C          TAP - SIG2(I,J)-SIG1(I,J)

```

```

C   SIG2A(I,J) - SIG2(I,J) ADJUSTED.
C   SIGAV(I,J) - AVERAGE OF SIG1(I,J) AND SIG2A(I,J).
C   XMOM(I,J) - MOMENT FOR EACH PAIR OF NSG1(I,J) AND NSG2(I,J).
C   PLTITL - TITLE OF PLOT.
C   LEGNM - NAME OF EACH CURVE ON PLOT FOR LEGEND.
C   MOMX(I) - VECTOR STORING MOMENTS USED IN PLOTTING.
C   ELEV(I) - VECTOR STORING ELEVATIONS USED IN PLOTTING.
C
C PART A: Moment Calculation
C
C Moments are calculated from the strain gauge readings and plotted
C with elevations. (Elevation Y, Moment X)
C
C   DIMENSION LEPS1(100,100),LEPS2(100,100),NSG1(20),NSG2(20),
C   .IPKRAY(100,100),NS1(100),NS2(100),ICOR(20),NCB(2),NCE(2),
C   .ISYM(20),JCURVE(4),DAYNUM(20)
C
C   REAL XPLOT(900),YPLOT(900)
C
C   REAL*8 MOM(900,20),ELE(900,20),PLOAD(3),B(4),POLYCO(4,3,20),
C   .XL1(100),XL2(100),YL1(100),YL2(100),BH(2),BOXY(2),
C   .SHEAR(900,20),PRESS(900,20),ANCH(2,20),YA(100),DEFLEC(900,20),
C   .SIG1(100,20),SIG2(100,20),SIG2A(100,20),SIGBND(100,20),
C   .AM(22,22),CM(22),RM(22),MOMF(20,20),PT,PB,DELT,DELB
C
C   LOGICAL*1 FIGTIT(80,13),DATE(19,20),TITLE(80),LEGNM(10,20)
C   CHARACTER*15 LGNM(4)
C
C Read in title, plot axis parameters and the properties
C of the sheet pile section. Output these properties to a table.
C
C   READ(5,505)(TITLE(I),I=1,80)
C   WRITE(7,700)(TITLE(I),I=1,80)
C   READ(5,522)ISECT
C   DO 10 L=1,13
C   READ(5,505)(FIGTIT(I,L),I=1,80)
10 CONTINUE
C   READ(5,507)XORIG1,XSTP1,XMAX1
C   READ(5,507)XORIG2,XSTP2,XMAX2
C   READ(5,507)XORIG3,XSTP3,XMAX3
C   READ(5,507)XORIG4,XSTP4,XMAX4
C   READ(5,510)YE,AS,AH,AT
C   WRITE(7,702)
C   WRITE(7,704)
C   WRITE(7,706)YE
C   WRITE(7,708)AS
C   WRITE(7,710)AH
C   WRITE(7,712)AT
C   WRITE(7,714)
C
C Read in NT, NL and the strain gauge coordinates. Output
C the coordinates to a table.
C
C   READ(5,515)NT,NL,NTAB

```

```

WRITE(7,716)
WRITE(7,718)
WRITE(7,720)
WRITE(7,722)
WRITE(7,718)
DO 20 I=1,NL
READ(5,520)NSG2(I),XL2(I),YL2(I),NSG1(I),XL1(I),YL1(I)
YA(I)=(YL1(I)+YL2(I))/2
WRITE(7,724)NSG2(I),XL2(I),NSG1(I),XL1(I),YA(I)
20 CONTINUE
WRITE(7,726)
WRITE(7,728)
C
C Read in the date of the readings. Set up table to handle the
C results.
C
DO 30 J=1,NT
READ(5,500)(DATE(I,J),I=1,19)
READ(5,502)DAYNUM(J),ISYM(J),(LEGNM(I,J),I=1,10)
READ(5,522)ICOR(J)
READ(5,526)ANCH(1,J),ANCH(2,J)
WRITE(7,732)
WRITE(7,734)
WRITE(7,736)
WRITE(7,738)
WRITE(7,740)
WRITE(7,742)
C
C Read in strain readings and calculate stress from strain.
C The stress on the inner face has to be adjusted to obtain
C the corresponding stress on the earth side of the wall.
C
DO 40 I=1,NL
READ(5,530)NS2(I),LEPS2(I,J),NS1(I),LEPS1(I,J)
ICHS1=(LEPS1(I,J)+ICOR(J))-(LEPS1(I,1)+ICOR(1))
ICHS2=(LEPS2(I,J)+ICOR(J))-(LEPS2(I,1)+ICOR(1))
SIG1(I,J)=YE*(ICHS1)*0.000001
SIG2(I,J)=YE*(ICHS2)*0.000001
TAP=(SIG2(I,J)-SIG1(I,J))
SIG2A(I,J)=((TAP/(AH-AT))*AH)+SIG1(I,J)
C
C Separate the axial component of stress from the bending component.
C
SIGAXL=(SIG1(I,J)+SIG2A(I,J))/2
SIGBND(I,J)=SIG1(I,J)-SIGAXL
SIGTST=SIG2A(I,J)-SIGAXL
C
C Calculate moment and write all results to the table.
C
MOM(I,J)=SIGBND(I,J)*AS*0.000001
MOMF(I,J)=MOM(I,J)
WRITE(7,744)NS2(I),LEPS2(I,J),ICHS2,SIG2(I,J),SIG2A(I,J),
+NS1(I),LEPS1(I,J),ICHS1,SIG1(I,J),SIGAXL,SIGBND(I,J),
.MOM(I,J)

```

```

40 CONTINUE
  WRITE(7,746)
  WRITE(7,747)ICOR(J)
  IF (ISECT .EQ. 0) THEN
    IF (NTAB .LT. 10) THEN
      WRITE(7,748)NTAB,(DATE(I,J),I=1,19)
    ELSE
      WRITE(7,750)NTAB,(DATE(I,J),I=1,19)
    ENDIF
  ELSE
    WRITE(7,752)NTAB,(DATE(I,J),I=1,19)
  ENDIF
  IF (AINT(J/2.)*2 .EQ. J) WRITE(7,728)
  NTAB=NTAB+1
30 CONTINUE

```

C
C Plotting routine. Elevation versus calculated moments. (DISSPLA)
C

```

  NCB(1)=1
  NCE(1)=7
  NCB(2)=8
  NCE(2)=13
  BH(1)=4.3
  BOXY(1)=6.4
  BH(2)=3.8
  BOXY(2)=6.9
  DO 50 L=1,2
  NLINES=0
  CALL DSPDEV(' PLOTTER ')
  CALL UNITS(' CM' )
  CALL NOBRDR
  CALL PAGE(28.0,21.5)
  CALL AREA2D(19.0,11.0)
  CALL COMPLX
  CALL PHYSOR(5.5,6.)
  CALL XNAME(' Bending Moment (kNm)$' ,100)
  CALL YNAME(' Elevation (m)$' ,100)
  CALL INTAXS
  CALL FRAME
  CALL YAXANG(0.)
  YORIG=492.
  YMAX=500.
  YSTP=1.
  CALL GRAF(XORIG1,XSTP1,XMAX1,YORIG,YSTP,YMAX)
  NLB=NCB(L)
  NLE=NCE(L)
  DO 60 J=NLB,NLE
  CALL MARKER(ISYM(J))
  DO 70 I=1,NL
  XPLOT(I)=MOM(I,J)
  YPLOT(I)=YA(I)
70 CONTINUE
  CALL CURVE(XPLOT,YPLOT,NL,1)
  CALL RESET(' MARKER' )

```

```

NLINES=NLINES+1
CALL LINES(LEGNM(1,J),IPKRAY,NLINES)
60 CONTINUE
CALL MYLEGN(' ',1)
IF (L .EQ. 2 .AND. ISECT .EQ. 1) THEN
    CALL LEGEND(IPKRAY,NT,11.3,BOXY(L)+0.3)
    CALL BLREC(11.,BOXY(L),4.15,BH(L),0.05)
ELSE
    CALL LEGEND(IPKRAY,NT,0.55,BOXY(L)+0.3)
    CALL BLREC(0.3,BOXY(L),4.15,BH(L),0.05)
ENDIF
CALL MESSAG(FIGTIT(1,L),100,0.4,-3.25)
CALL RLVEC(0.,492.61,0.,499.07,0000)
CALL BLREC(16.625,3.16,0.5,0.17,0.015)
CALL BLREC(16.625,7.0375,0.5,0.17,0.015)
CALL HEIGHT(0.25)
CALL MESSAG('Water$',100,17.38,3.095)
CALL MESSAG('Water$',100,17.38,6.973)
CALL RESET('HEIGHT')
CALL ENDPL(0)
50 CONTINUE
NCB(1)=2
C
C PART B: Moment Polynomials
C
C Moment data is considered in 3 sections. 3th order
C polynomials fit to top, middle and bottom sections.
C
C B corresponds to elevation (X) which is artificially reduced
C to allow for more more accurate computations.
C
    B(2)=497.18-492.61
    B(3)=494.36-492.61
    B(4)=492.61-492.61
    DO 75 M=1,8
        DUMMY=YA(M)-492.61
        YA(M)=DUMMY
    75 CONTINUE
C
C Polynomial determination.
C
    DO 80 J=2,NT
        IF (J .LE. 6) THEN
            B(1)=498.63-492.61
        ELSE
            B(1)=499.07-492.61
        ENDIF
C
C Initialize the matrix containing the polynomial coefficients.
C
    DO 90 I=1,4
        DO 100 M=1,3
            POLYCO(I,M,J)=0.
    100 CONTINUE

```

```

90 CONTINUE
C
C Set up the matrix used to solve for the 12 polynomial
C coefficients and the 10 Lagrangian multipliers.
C
  DO 110 L=1,22
    CM(L)=0.000
  DO 120 M=1,22
    AM(L,M)=0.000
120 CONTINUE
110 CONTINUE
C
C If east section (ISECT=0) use data points 1, 4, 5, 6, 7 and 8.
C
  IF (ISECT .EQ. 0) THEN
C
  AM(1,1)=2.*YA(1)**6.
  AM(1,2)=2.*YA(1)**5.
  AM(1,3)=2.*YA(1)**4.
  AM(1,4)=2.*YA(1)**3.
  AM(1,13)=B(1)**3.
  AM(1,14)=3.*B(1)**2.
  AM(1,15)=B(2)**3.
  AM(1,16)=3.*B(2)**2.
  AM(1,17)=6.*B(2)
C
  AM(2,1)=2.*YA(1)**5.
  AM(2,2)=2.*YA(1)**4.
  AM(2,3)=2.*YA(1)**3.
  AM(2,4)=2.*YA(1)**2.
  AM(2,13)=B(1)**2.
  AM(2,14)=2.*B(1)
  AM(2,15)=B(2)**2.
  AM(2,16)=2.*B(2)
  AM(2,17)=2.
C
  AM(3,1)=2.*YA(1)**4.
  AM(3,2)=2.*YA(1)**3.
  AM(3,3)=2.*YA(1)**2.
  AM(3,4)=2.*YA(1)
  AM(3,13)=B(1)
  AM(3,14)=1.
  AM(3,15)=B(2)
  AM(3,16)=1.
C
  AM(4,1)=2.*YA(1)**3.
  AM(4,2)=2.*YA(1)**2.
  AM(4,3)=2.*YA(1)
  AM(4,4)=2.
  AM(4,13)=1.
  AM(4,15)=1.
C
  AM(5,5)=2.*(YA(4)**6.+YA(5)**6.+YA(6)**6.+YA(7)**6.)
  AM(5,6)=2.*(YA(4)**5.+YA(5)**5.+YA(6)**5.+YA(7)**5.)

```

$AM(5,7)=2.*(YA(4)**4.+YA(5)**4.+YA(6)**4.+YA(7)**4.)$
 $AM(5,8)=2.*(YA(4)**3.+YA(5)**3.+YA(6)**3.+YA(7)**3.)$
 $AM(5,15)=-B(2)**3.$
 $AM(5,16)=-3.*B(2)**2.$
 $AM(5,17)=-6.*B(2)$
 $AM(5,20)=B(3)**3.$
 $AM(5,21)=3.*B(3)**2.$
 $AM(5,22)=6.*B(3)$

C

$AM(6,5)=2.*(YA(4)**5.+YA(5)**5.+YA(6)**5.+YA(7)**5.)$
 $AM(6,6)=2.*(YA(4)**4.+YA(5)**4.+YA(6)**4.+YA(7)**4.)$
 $AM(6,7)=2.*(YA(4)**3.+YA(5)**3.+YA(6)**3.+YA(7)**3.)$
 $AM(6,8)=2.*(YA(4)**2.+YA(5)**2.+YA(6)**2.+YA(7)**2.)$
 $AM(6,15)=-B(2)**2.$
 $AM(6,16)=-2.*B(2)$
 $AM(6,17)=-2.$
 $AM(6,20)=B(3)**2.$
 $AM(6,21)=2.*B(3)$
 $AM(6,22)=2.$

C

$AM(7,5)=2.*(YA(4)**4.+YA(5)**4.+YA(6)**4.+YA(7)**4.)$
 $AM(7,6)=2.*(YA(4)**3.+YA(5)**3.+YA(6)**3.+YA(7)**3.)$
 $AM(7,7)=2.*(YA(4)**2.+YA(5)**2.+YA(6)**2.+YA(7)**2.)$
 $AM(7,8)=2.*(YA(4)+YA(5)+YA(6)+YA(7))$
 $AM(7,15)=-B(2)$
 $AM(7,16)=-1.$
 $AM(7,20)=B(3)$
 $AM(7,21)=1.$

C

$AM(8,5)=2.*(YA(4)**3.+YA(5)**3.+YA(6)**3.+YA(7)**3.)$
 $AM(8,6)=2.*(YA(4)**2.+YA(5)**2.+YA(6)**2.+YA(7)**2.)$
 $AM(8,7)=2.*(YA(4)+YA(5)+YA(6)+YA(7))$
 $AM(8,8)=8.$
 $AM(8,15)=-1.$
 $AM(8,20)=1.$

C

$AM(9,9)=2.*YA(8)**6.$
 $AM(9,10)=2.*YA(8)**5.$
 $AM(9,11)=2.*YA(8)**4.$
 $AM(9,12)=2.*YA(8)**3.$
 $AM(9,18)=B(4)**3.$
 $AM(9,19)=3.*B(4)**2.$
 $AM(9,20)=-B(3)**3.$
 $AM(9,21)=-3.*B(3)**2.$
 $AM(9,22)=-6.*B(3)$

C

$AM(10,9)=2.*YA(8)**5.$
 $AM(10,10)=2.*YA(8)**4.$
 $AM(10,11)=2.*YA(8)**3.$
 $AM(10,12)=2.*YA(8)**2.$
 $AM(10,18)=B(4)**2.$
 $AM(10,19)=2.*B(4)$
 $AM(10,20)=-B(3)**2.$
 $AM(10,21)=-2.*B(3)$


```

AM(10,22)=-2.
C
AM(11,9)=2.*YA(8)**4.
AM(11,10)=2.*YA(8)**3.
AM(11,11)=2.*YA(8)**2.
AM(11,12)=2.*YA(8)
AM(11,18)=B(4)
AM(11,19)=1.
AM(11,20)=-B(3)
AM(11,21)=-1.
C
AM(12,9)=2.*YA(8)**3.
AM(12,10)=2.*YA(8)**2.
AM(12,11)=2.*YA(8)
AM(12,12)=2.
AM(12,18)=1.
AM(12,20)=-1.
C
CM(1)=2.*(YA(1)**3.)*MOM(1,J)
CM(2)=2.*(YA(1)**2.)*MOM(1,J)
CM(3)=2.*YA(1)*MOM(1,J)
CM(4)=2.*MOM(1,J)
C
CM(5)=2.*((YA(4)**3.)*MOM(4,J)+(YA(5)**3.)*MOM(5,J)
      +(YA(6)**3.)*MOM(6,J)+(YA(7)**3.)*MOM(7,J))
CM(6)=2.*((YA(4)**2.)*MOM(4,J)+(YA(5)**2.)*MOM(5,J)
      +(YA(6)**2.)*MOM(6,J)+(YA(7)**2.)*MOM(7,J))
CM(7)=2.*(YA(4)*MOM(4,J)+YA(5)*MOM(5,J)
      +YA(6)*MOM(6,J)+YA(7)*MOM(7,J))
CM(8)=2.*(MOM(4,J)+MOM(5,J)+MOM(6,J)+MOM(7,J))
C
CM(9)=2.*(YA(8)**3.)*MOM(8,J)
CM(10)=2.*(YA(8)**2.)*MOM(8,J)
CM(11)=2.*YA(8)*MOM(8,J)
CM(12)=2.*MOM(8,J)
C
C If west section use points 1 through 8.
C
ELSE
C
AM(1,1)=2.*(YA(1)**6.+YA(2)**6.)
AM(1,2)=2.*(YA(1)**5.+YA(2)**5.)
AM(1,3)=2.*(YA(1)**4.+YA(2)**4.)
AM(1,4)=2.*(YA(1)**3.+YA(2)**3.)
AM(1,13)=B(1)**3.
AM(1,14)=3.*B(1)**2.
AM(1,15)=B(2)**3.
AM(1,16)=3.*B(2)**2.
AM(1,17)=6.*B(2)
C
AM(2,1)=2.*(YA(1)**5.+YA(2)**5.)
AM(2,2)=2.*(YA(1)**4.+YA(2)**4.)
AM(2,3)=2.*(YA(1)**3.+YA(2)**3.)
AM(2,4)=2.*(YA(1)**2.+YA(2)**2.)

```

$AM(2,13) = B(1)**2.$
 $AM(2,14) = 2.*B(1)$
 $AM(2,15) = B(2)**2.$
 $AM(2,16) = 2.*B(2)$
 $AM(2,17) = 2.$

C

$AM(3,1) = 2.*(YA(1)**4.+YA(2)**4.)$
 $AM(3,2) = 2.*(YA(1)**3.+YA(2)**3.)$
 $AM(3,3) = 2.*(YA(1)**2.+YA(2)**2.)$
 $AM(3,4) = 2.*(YA(1)+YA(2))$
 $AM(3,13) = B(1)$
 $AM(3,14) = 1.$
 $AM(3,15) = B(2)$
 $AM(3,16) = 1.$

C

$AM(4,1) = 2.*(YA(1)**3.+YA(2)**3.)$
 $AM(4,2) = 2.*(YA(1)**2.+YA(2)**2.)$
 $AM(4,3) = 2.*(YA(1)+YA(2))$
 $AM(4,4) = 4.$
 $AM(4,13) = 1.$
 $AM(4,15) = 1.$

C

$AM(5,5) = 2.*(YA(3)**6.+YA(4)**6.+YA(5)**6.+YA(6)**6.)$
 $AM(5,6) = 2.*(YA(3)**5.+YA(4)**5.+YA(5)**5.+YA(6)**5.)$
 $AM(5,7) = 2.*(YA(3)**4.+YA(4)**4.+YA(5)**4.+YA(6)**4.)$
 $AM(5,8) = 2.*(YA(3)**3.+YA(4)**3.+YA(5)**3.+YA(6)**3.)$
 $AM(5,15) = -B(2)**3.$
 $AM(5,16) = -3.*B(2)**2.$
 $AM(5,17) = -6.*B(2)$
 $AM(5,20) = B(3)**3.$
 $AM(5,21) = 3.*B(3)**2.$
 $AM(5,22) = 6.*B(3)$

C

$AM(6,5) = 2.*(YA(3)**5.+YA(4)**5.+YA(5)**5.+YA(6)**5.)$
 $AM(6,6) = 2.*(YA(3)**4.+YA(4)**4.+YA(5)**4.+YA(6)**4.)$
 $AM(6,7) = 2.*(YA(3)**3.+YA(4)**3.+YA(5)**3.+YA(6)**3.)$
 $AM(6,8) = 2.*(YA(3)**2.+YA(4)**2.+YA(5)**2.+YA(6)**2.)$
 $AM(6,15) = -B(2)**2.$
 $AM(6,16) = -2.*B(2)$
 $AM(6,17) = -2.$
 $AM(6,20) = B(3)**2.$
 $AM(6,21) = 2.*B(3)$
 $AM(6,22) = 2.$

C

$AM(7,5) = 2.*(YA(3)**4.+YA(4)**4.+YA(5)**4.+YA(6)**4.)$
 $AM(7,6) = 2.*(YA(3)**3.+YA(4)**3.+YA(5)**3.+YA(6)**3.)$
 $AM(7,7) = 2.*(YA(3)**2.+YA(4)**2.+YA(5)**2.+YA(6)**2.)$
 $AM(7,8) = 2.*(YA(3)+YA(4)+YA(5)+YA(6))$
 $AM(7,15) = -B(2)$
 $AM(7,16) = -1.$
 $AM(7,20) = B(3)$
 $AM(7,21) = 1.$

C

$AM(8,5) = 2.*(YA(3)**3.+YA(4)**3.+YA(5)**3.+YA(6)**3.)$

$AM(8,6) = 2. * (YA(3)**2. + YA(4)**2. + YA(5)**2. + YA(6)**2.)$
 $AM(8,7) = 2. * (YA(3) + YA(4) + YA(5) + YA(6))$
 $AM(8,8) = 8.$
 $AM(8,15) = -1.$
 $AM(8,20) = 1.$

C

$AM(9,9) = 2. * (YA(7)**6. + YA(8)**6.)$
 $AM(9,10) = 2. * (YA(7)**5. + YA(8)**5.)$
 $AM(9,11) = 2. * (YA(7)**4. + YA(8)**4.)$
 $AM(9,12) = 2. * (YA(7)**3. + YA(8)**3.)$
 $AM(9,18) = B(4)**3.$
 $AM(9,19) = 3. * B(4)**2.$
 $AM(9,20) = -B(3)**3.$
 $AM(9,21) = -3. * B(3)**2.$
 $AM(9,22) = -6. * B(3)$

C

$AM(10,9) = 2. * (YA(7)**5. + YA(8)**5.)$
 $AM(10,10) = 2. * (YA(7)**4. + YA(8)**4.)$
 $AM(10,11) = 2. * (YA(7)**3. + YA(8)**3.)$
 $AM(10,12) = 2. * (YA(7)**2. + YA(8)**2.)$
 $AM(10,18) = B(4)**2.$
 $AM(10,19) = 2. * B(4)$
 $AM(10,20) = -B(3)**2.$
 $AM(10,21) = -2. * B(3)$
 $AM(10,22) = -2.$

C

$AM(11,9) = 2. * (YA(7)**4. + YA(8)**4.)$
 $AM(11,10) = 2. * (YA(7)**3. + YA(8)**3.)$
 $AM(11,11) = 2. * (YA(7)**2. + YA(8)**2.)$
 $AM(11,12) = 2. * (YA(7) + YA(8))$
 $AM(11,18) = B(4)$
 $AM(11,19) = 1.$
 $AM(11,20) = -B(3)$
 $AM(11,21) = -1.$

C

$AM(12,9) = 2. * (YA(7)**3. + YA(8)**3.)$
 $AM(12,10) = 2. * (YA(7)**2. + YA(8)**2.)$
 $AM(12,11) = 2. * (YA(7) + YA(8))$
 $AM(12,12) = 4.$
 $AM(12,18) = 1.$
 $AM(12,20) = -1.$

C

$CM(1) = 2. * ((YA(1)**3.) * MOM(1, J) + (YA(2)**3.) * MOM(2, J))$
 $CM(2) = 2. * ((YA(1)**2.) * MOM(1, J) + (YA(2)**2.) * MOM(2, J))$
 $CM(3) = 2. * (YA(1) * MOM(1, J) + YA(2) * MOM(2, J))$
 $CM(4) = 2. * (MOM(1, J) + MOM(2, J))$

C

$CM(5) = 2. * ((YA(3)**3.) * MOM(3, J) + (YA(4)**3.) * MOM(4, J) + (YA(5)**3.) * MOM(5, J) + (YA(6)**3.) * MOM(6, J))$
 $CM(6) = 2. * ((YA(3)**2.) * MOM(3, J) + (YA(4)**2.) * MOM(4, J) + (YA(5)**2.) * MOM(5, J) + (YA(6)**2.) * MOM(6, J))$
 $CM(7) = 2. * (YA(3) * MOM(3, J) + YA(4) * MOM(4, J) + YA(5) * MOM(5, J) + YA(6) * MOM(6, J))$
 $CM(8) = 2. * (MOM(3, J) + MOM(4, J) + MOM(5, J) + MOM(6, J))$

```
C
CM(9)=2.*((YA(7)**3.)*MOM(7,J)+(YA(8)**3.)*MOM(8,J))
CM(10)=2.*((YA(7)**2.)*MOM(7,J)+(YA(8)**2.)*MOM(8,J))
CM(11)=2.*(YA(7)*MOM(7,J)+YA(8)*MOM(8,J))
CM(12)=2.*(MOM(7,J)+MOM(8,J))
C
ENDIF
C
CM(16)=ANCH(1,J)
CM(21)=ANCH(2,J)
C
AM(13,1)=B(1)**3.
AM(13,2)=B(1)**2.
AM(13,3)=B(1)
AM(13,4)=1.
C
AM(14,1)=3.*B(1)**2.
AM(14,2)=2.*B(1)
AM(14,3)=1.
C
AM(15,1)=B(2)**3.
AM(15,2)=B(2)**2.
AM(15,3)=B(2)
AM(15,4)=1.
AM(15,5)=-B(2)**3.
AM(15,6)=-B(2)**2.
AM(15,7)=-B(2)
AM(15,8)=-1.
C
AM(16,1)=3.*B(2)**2.
AM(16,2)=2.*B(2)
AM(16,3)=1.
AM(16,5)=-3.*B(2)**2.
AM(16,6)=-2.*B(2)
AM(16,7)=-1.
C
AM(17,1)=6.*B(2)
AM(17,2)=2.
AM(17,5)=-6.*B(2)
AM(17,6)=-2.
C
AM(18,9)=B(4)**3.
AM(18,10)=B(4)**2.
AM(18,11)=B(4)
AM(18,12)=1.
C
AM(19,9)=3.*B(4)**2.
AM(19,10)=2.*B(4)
AM(19,11)=1.
C
AM(20,5)=B(3)**3.
AM(20,6)=B(3)**2.
AM(20,7)=B(3)
AM(20,8)=1.
```

```

AM(20,9)=-B(3)**3.
AM(20,10)=-B(3)**2.
AM(20,11)=-B(3)
AM(20,12)=-1.
C
AM(21,5)=3.*B(3)**2.
AM(21,6)=2.*B(3)
AM(21,7)=1.
AM(21,9)=-3.*B(3)**2.
AM(21,10)=-2.*B(3)
AM(21,11)=-1.
C
AM(22,5)=6.*B(3)
AM(22,6)=2.
AM(22,9)=-6.*B(3)
AM(22,10)=-2.
C
C Solve the matrix and store the 12 polynomial coefficients
C in a 4x3xNT matrix.
C
CALL GAUSS1(AM,CM,RM,22)
IJ=1
DO 130 M=1,3
DO 132 I=1,4
POLYCO(I,M,J)=RM(IJ)
IJ=IJ+1
132 CONTINUE
130 CONTINUE
C
C From the calculated polynomials determine moment data points.
C
N=1
DO 170 M=1,3
ELE(N,J)=B(M)
190 IF (ELE(N,J) .LT. B(M+1)) ELE(N,J)=B(M+1)
X=ELE(N,J)
MOM(N,J)=(POLYCO(1,M,J)*(X**3))+(POLYCO(2,M,J)*(X**2))
+(POLYCO(3,M,J)*X)+POLYCO(4,M,J)
IF (ELE(N,J) .EQ. B(M+1)) GOTO 180
N=N+1
ELE(N,J)=ELE(N-1,J)-0.01
GOTO 190
180 N=N+1
170 CONTINUE
80 CONTINUE
C
C Plot interpolated moment curve.
C
IF (ISECT .EQ. 0) THEN
IFIG=3
ELSE
IFIG=19
ENDIF
DO 200 J=2,NT

```

```

CALL UNITS(' CM' )
CALL NOBRDR
CALL PAGE(28.0,21.5)
CALL AREA2D(19.0,11.0)
CALL PHYSOR(5.5,6.)
CALL COMPLX
CALL XNAME(' Bending Moment (kNm)$' ,100)
CALL YNAME(' Elevation (m)$' ,100)
CALL INTAXS
CALL FRAME
CALL YAXANG(0.)
YORIG=492.
YMAX=500.
YSTP=1.
CALL GRAF(XORIG1,XSTP1,XMAX1,YORIG,YSTP,YMAX)
DO 210 I=1,N
XPLOT(I)=MOM(I,J)
YPLOT(I)=ELE(I,J)+492.61
210 CONTINUE
C
C Plot moment data points over interpolated moment curves.
C
CALL CURVE(XPLOT,YPLOT,N,0)
IF (ISECT .EQ. 0) THEN
  IC=0
  DO 220 I=1,NL
    IF (I .EQ. 2 .OR. I .EQ. 3) GOTO 220
    IC=IC+1
    XPLOT(IC)=MOMF(I,J)
    YPLOT(IC)=YA(I)+492.61
220  CONTINUE
    CALL CURVE(XPLOT,YPLOT,NL-2,-1)
  ELSE
    DO 222 I=1,NL
      XPLOT(I)=MOMF(I,J)
      YPLOT(I)=YA(I)+492.61
222  CONTINUE
      CALL CURVE(XPLOT,YPLOT,NL,-1)
    ENDIF
    IF (ISECT .EQ. 0) THEN
      IF (IFIG .GE. 10) THEN
        WRITE(4,442)IFIG,(DATE(I,J),I=1,18)
      ELSE
        WRITE(4,448)IFIG,(DATE(I,J),I=1,18)
      ENDIF
    ELSE
      IF (IFIG .GE. 10) THEN
        WRITE(4,443)IFIG,(DATE(I,J),I=1,18)
      ELSE
        WRITE(4,449)IFIG,(DATE(I,J),I=1,18)
      ENDIF
    ENDIF
    IFIG=IFIG+1
    BACKSPACE 4

```

```

READ(4,505)(TITLE(I),I=1,80)
CALL MESSAG(TITLE(1),100,-1.0,-3.25)
IF (J .LE. 6) THEN
  CALL RLVEC(0.,492.61,0.,498.63,0000)
ELSE
  CALL RLVEC(0.,492.61,0.,499.07,0000)
ENDIF
CALL BLREC(16.625,3.16,0.5,0.17,0.015)
CALL BLREC(16.625,7.0375,0.5,0.17,0.015)
CALL ENDPL(0)
200 CONTINUE
C
C PART C: Shear and Pressure
C
C Calculate shear and pressure distributions by differentiating
C each section of the moment polynomials. At the location of the
C moment discontinuity, f'n above and below the elevation are
C evaluated (ie same elevation has 2 shear values). Note that
C the difference between these two values equals the anchor load
C at that location.
C
DO 230 J=2,NT
IF (J .LE. 6) THEN
  B(1)=498.63-492.61
ELSE
  B(1)=499.07-492.61
ENDIF
N=1
DO 240 M=1,3
FLAG=1
ELE(N,J)=B(M)
260 IF (ELE(N,J) .LT. B(M+1)) ELE(N,J)=B(M+1)
X=ELE(N,J)
SHEAR(N,J)=(3*POLYCO(1,M,J)*(X**2))+(2*POLYCO(2,M,J)*X)
+POLYCO(3,M,J)
IF ((FLAG .EQ. 1) .AND. (M .GT. 1))
.PLOAD(M)=SHEAR(N-1,J)-SHEAR(N,J)
IF (ELE(N,J) .EQ. B(M+1)) GOTO 250
N=N+1
ELE(N,J)=ELE(N-1,J)-0.01
FLAG=0
GOTO 260
250 N=N+1
240 CONTINUE
WRITE(8,800)PLOAD(2),PLOAD(3)
230 CONTINUE
C
C Plot shear diagram.
C
DO 270 L=1,2
CALL UNITS('CM')
CALL NOBRDR
CALL PAGE(28.,21.5)
CALL AREA2D(19.0,11.0)

```

```

CALL PHYSOR(5.5,6.)
CALL COMPLX
CALL YNAME('Elevation (m)$',100)
CALL XNAME('Shear (kN)$',100)
CALL INTAXS
CALL FRAME
CALL YAXANG(0.)
YORIG=492.
YMAX=500.
YSTP=1.
CALL GRAF(XORIG2,XSTP2,XMAX2,YORIG,YSTP,YMAX)
CALL RLVEC(0.,492.61,0.,499.07,0000)
NLB=NCB(L)
NLE=NCE(L)
DO 280 J=NLB,NLE
DO 290 I=1,N
XPLOT(I)=SHEAR(I,J)
YPLOT(I)=ELE(I,J)+492.61
290 CONTINUE
CALL CURVE(XPLOT,YPLOT,N,0)
280 CONTINUE
CALL MESSAG(FIGTIT(1,L+2),100,2.,-3.25)
CALL BLREC(9.5,3.16,0.5,0.17,0.015)
CALL BLREC(9.5,7.0375,0.5,0.17,0.015)
CALL ENDPL(0)
270 CONTINUE
C
C Calculate pressure by double differentiation of moment.
C
DO 300 J=2,NT
IF (J.LE. 6) THEN
B(1)=498.63-492.61
ELSE
B(1)=499.07-492.61
ENDIF
SUMPOS=PLOAD(2)+PLOAD(3)
SUMNEG=0.00
SUMMOM=PLOAD(2)*(B(1)-B(2))
+PLOAD(3)*(B(1)-B(3))
N=1
DO 310 M=1,3
ELE(N,J)=B(M)
330 IF (ELE(N,J) .LT. B(M+1)) ELE(N,J)=B(M+1)
X=ELE(N,J)
PRESS(N,J)=(6*POLYCO(1,M,J)*X)+2*POLYCO(2,M,J)
IF (PRESS(N,J) .LT. 0.) SUMNEG=SUMNEG+PRESS(N,J)*0.01
IF (PRESS(N,J) .GT. 0.) SUMPOS=SUMPOS+PRESS(N,J)*0.01
SUMMOM=SUMMOM+PRESS(N,J)*0.01*(499.07-492.61-ELE(N,J))
DIFF=SUMPOS+SUMNEG
IF (ELE(N,J) .EQ. B(M+1)) GOTO 320
N=N+1
ELE(N,J)=ELE(N-1,J)-0.01
GOTO 330
320 N=N+1

```



```

310 CONTINUE
C
C Write out equilibrium checks.
C
  WRITE(8,810)J,SUMPOS
  WRITE(8,820)J,SUMNEG
  WRITE(8,830)DIFF
  WRITE(8,840)J,SUMMOM
300 CONTINUE
C
C Plot the pressure diagrams (three epochs per page).
C
  J=2
  IF (ISECT .EQ. 0) THEN
    IFIG=1
  ELSE
    IFIG=6
  ENDIF
C
C Set up the plot page.
C
340 CALL UNITS('CM' )
  CALL NOBRDR
  CALL PAGE(28.,21.5)
  CALL AREA2D(19.0,11.0)
  CALL PHYSOR(5.5,6.)
  CALL COMPLX
  CALL YNAME('Elevation (m)$',100)
  CALL XNAME('Pressure (kPa)$',100)
  CALL INTAXS
  CALL FRAME
  CALL YAXANG(0.)
  YORIG=492.
  YMAX=500.
  YSTP=1.
  CALL GRAF(-XORIG3,XSTP3,-XMAX3,YORIG,YSTP,YMAX)
C
C Plot three epochs on each plot page.
C
  DO 342 IJ=1,3
    XPLOT(1)=0.
    YPLOT(1)=ELE(1,J)+492.61
  DO 350 I=1,N
    XPLOT(I+1)=-PRESS(I,J)
    YPLOT(I+1)=ELE(I,J)+492.61
350 CONTINUE
  CALL LEGLIN
  IF (IJ .EQ. 2) THEN
    CALL DOT
  ELSEIF (IJ .EQ. 3) THEN
    CALL DASH
  ENDIF
  CALL CURVE(XPLOT,YPLOT,N+1,0)
  CALL LINES(LEGNM(1,J),IPKRAY,IJ)

```

```

J=J+1
342 CONTINUE
CALL RESET('DASH')
IF (ISECT.EQ. 0) THEN
  WRITE(4,444)IFIG
ELSE
  WRITE(4,445)IFIG
ENDIF
IFIG=IFIG+1
BACKSPACE 4
READ(4,505)(TITLE(I),I=1,80)
CALL MESSAG(TITLE(1),100,2.,-3.25)
CALL BLREC(14.25,3.16,0.5,0.17,0.015)
CALL BLREC(14.25,7.0375,0.5,0.17,0.015)
IF (J.LE. 6) THEN
  CALL RLVEC(0.,492.61,0.,498.63,0000)
ELSE
  CALL RLVEC(0.,492.61,0.,499.07,0000)
ENDIF
CALL MYLEGN(' ',1)
CALL LEGEND(IPKRAY,3,0.6,8.8)
CALL BLREC(0.3,8.5,4.2,2.2,0.05)
CALL HEIGHT(0.25)
CALL MESSAG('Wall',4,14.77,5.4)
CALL MESSAG('Exposed Side',12,14.75,5.0)
CALL RESET('HEIGHT')
CALL ENDPL(0)
CALL RESET('LEGLIN')
CALL RESET('DASH')
CALL RESET('DOT')
IF (J.LT. NT) GOTO 340
C
C Plot all pressure distributions on the same graph.
C
CALL UNITS('CM')
CALL NOBRDR
CALL PAGE(28.,21.5)
CALL AREA2D(19.0,11.0)
CALL PHYSOR(5.5,6.)
CALL COMPLX
CALL YNAME('Elevation (m)$',100)
CALL XNAME('Pressure (kPa)$',100)
CALL INTAXS
CALL FRAME
CALL YAXANG(0.)
YORIG=492.
YMAX=500.
YSTP=1.
CALL GRAF(-XORIG3,XSTP3,-XMAX3,YORIG,YSTP,YMAX)
CALL RLVEC(0.,492.61,0.,499.07,0000)
DO 352 J=2,NT
XPLOT(1)=0.
YPLOT(1)=ELE(1,J)+492.61
DO 354 I=1,N

```

```

XPLOT(I+1)=-PRESS(I,J)
YPLOT(I+1)=ELE(I,J)+492.61
354 CONTINUE
CALL CURVE(XPLOT,YPLOT,N+1,0)
352 CONTINUE
IF (ISECT .EQ. 0) THEN
  WRITE(4,446)IFIG
ELSE
  WRITE(4,447)IFIG
ENDIF
IFIG=IFIG+1
BACKSPACE 4
READ(4,505)(TITLE(I),I=1,80)
CALL MESSAG(TITLE(1),100,-0.4,-3.25)
CALL BLREC(14.25,3.16,0.5,0.17,0.015)
CALL BLREC(14.25,7.0375,0.5,0.17,0.015)
CALL HEIGHT(0.25)
CALL MESSAG('Wall',4,14.75,5.4)
CALL MESSAG('Exposed Side',12,14.75,5.0)
CALL RESET('HEIGHT')
CALL ENDPL(0)
C
C Plot reference epoch pressure distributions.
C
JCURVE(1)=2
JCURVE(2)=6
JCURVE(3)=11
CALL UNITS('CM')
CALL NOBRDR
CALL PAGE(28.,21.5)
CALL AREA2D(19.0,11.0)
CALL PHYSOR(5.5,6.)
CALL COMPLX
CALL YNAME('Elevation (m)$',100)
CALL XNAME('Pressure (kPa)$',100)
CALL INTAXS
CALL FRAME
CALL YAXANG(0.)
YORIG=492.
YMAX=500.
YSTP=1.
CALL GRAF(-XORIG3,XSTP3,-XMAX3,YORIG,YSTP,YMAX)
CALL RLVEC(0.,492.61,0.,499.07,0000)
DO 356 J=1,3
XPLOT(1)=0.
YPLOT(1)=ELE(1,JCURVE(J))+492.61
DO 358 I=1,N
XPLOT(I+1)=-PRESS(I,JCURVE(J))
YPLOT(I+1)=ELE(I,JCURVE(J))+492.61
358 CONTINUE
CALL LEGLIN
IF (J .EQ. 2) THEN
  CALL DOT
ELSEIF (J .EQ. 3) THEN

```

```

        CALL DASH
    ENDIF
    CALL CURVE(XPLOT,YPLOT,N+1,0)
    CALL LINES(LEGNM(1,JCURVE(J)),IPKRAY,J)
356 CONTINUE
    CALL MYLEGN(' ',1)
    CALL LEGEND(IPKRAY,3,0.6,8.8)
    CALL BLREC(0.3,8.5,4.2,2.2,0.05)
    CALL MESSAG(FIGTIT(1,5),100,1.3,-3.)
    CALL MESSAG(FIGTIT(1,6),100,1.3,-3.6)
    CALL BLREC(14.25,3.16,0.5,0.17,0.015)
    CALL BLREC(14.25,7.0375,0.5,0.17,0.015)
    CALL HEIGHT(0.25)
    CALL MESSAG('Wall',4,14.75,5.4)
    CALL MESSAG('Exposed Side',12,14.75,5.0)
    CALL RESET('HEIGHT')
    CALL RESET('DASH')
    CALL ENDPL(0)
    CALL RESET('LEGLIN')
C
C PART D: Deflection
C
C Integrate the moment functions twice to yield the theoretical
C wall deflections. Two integration constants must be calculated
C for each of the three functions. Set up the matrix to solve
C for these six constants.
C
    DO 360 J=2,NT
    DO 370 I=1,6
    CM(I)=0.000
    RM(I)=0.000
    DO 380 K=1,6
    AM(I,K)=0.000
    380 CONTINUE
    370 CONTINUE
C
C Determine anchor stretch to provide two known positions
C for the deflection profile.
C
    PT=ANCH(1,J)-ANCH(1,2)
    PB=ANCH(2,J)-ANCH(2,2)
    DELT=- (PT*3650.)/(242.4624D-6*YE*1000.)
    DELB=- (PB*4150.)/(706.8683D-6*YE*1000.)
C
C Establish matrix coefficients.
C
    AM(1,1)=B(2)
    AM(1,2)=1.
    AM(2,3)=B(3)
    AM(2,4)=1.
    AM(3,1)=B(2)
    AM(3,2)=1.
    AM(3,3)=-B(2)
    AM(3,4)=-1.

```

AM(4,3)=B(3)
 AM(4,4)=1.
 AM(4,5)=-B(3)
 AM(4,6)=-1.
 AM(5,1)=1.
 AM(5,3)=-1.
 AM(6,3)=1.
 AM(6,5)=-1.

C
 CM(1)=-((1./20.)*POLYCO(1,1,J)*(B(2)**5))
 . -((1./12.)*POLYCO(2,1,J)*(B(2)**4))
 . -((1./6.)*POLYCO(3,1,J)*(B(2)**3))
 . -((1./2.)*POLYCO(4,1,J)*(B(2)**2))
 . +(DELT/(1.D12/(YE*83.5D6)))

C
 CM(2)=-((1./20.)*POLYCO(1,2,J)*(B(3)**5))
 . -((1./12.)*POLYCO(2,2,J)*(B(3)**4))
 . -((1./6.)*POLYCO(3,2,J)*(B(3)**3))
 . -((1./2.)*POLYCO(4,2,J)*(B(3)**2))
 . +(DELB/(1.D12/(YE*83.5D6)))

C
 CM(3)=(((1./20.)*POLYCO(1,2,J)*(B(2)**5))
 . +((1./12.)*POLYCO(2,2,J)*(B(2)**4))
 . +((1./6.)*POLYCO(3,2,J)*(B(2)**3))
 . +((1./2.)*POLYCO(4,2,J)*(B(2)**2))
 . -((1./20.)*POLYCO(1,1,J)*(B(2)**5))
 . -((1./12.)*POLYCO(2,1,J)*(B(2)**4))
 . -((1./6.)*POLYCO(3,1,J)*(B(2)**3))
 . -((1./2.)*POLYCO(4,1,J)*(B(2)**2)))

C
 CM(4)=(((1./20.)*POLYCO(1,3,J)*(B(3)**5))
 . +((1./12.)*POLYCO(2,3,J)*(B(3)**4))
 . +((1./6.)*POLYCO(3,3,J)*(B(3)**3))
 . +((1./2.)*POLYCO(4,3,J)*(B(3)**2))
 . -((1./20.)*POLYCO(1,2,J)*(B(3)**5))
 . -((1./12.)*POLYCO(2,2,J)*(B(3)**4))
 . -((1./6.)*POLYCO(3,2,J)*(B(3)**3))
 . -((1./2.)*POLYCO(4,2,J)*(B(3)**2)))

C
 CM(5)=(((1./4.)*POLYCO(1,2,J)*(B(2)**4))
 . +((1./3.)*POLYCO(2,2,J)*(B(2)**3))
 . +((1./2.)*POLYCO(3,2,J)*(B(2)**2))
 . + (POLYCO(4,2,J)*B(2))
 . -((1./4.)*POLYCO(1,1,J)*(B(2)**4))
 . -((1./3.)*POLYCO(2,1,J)*(B(2)**3))
 . -((1./2.)*POLYCO(3,1,J)*(B(2)**2))
 . - (POLYCO(4,1,J)*B(2)))

C
 CM(6)=(((1./4.)*POLYCO(1,3,J)*(B(3)**4))
 . +((1./3.)*POLYCO(2,3,J)*(B(3)**3))
 . +((1./2.)*POLYCO(3,3,J)*(B(3)**2))
 . + (POLYCO(4,3,J)*B(3))
 . -((1./4.)*POLYCO(1,2,J)*(B(3)**4))
 . -((1./3.)*POLYCO(2,2,J)*(B(3)**3))

```

      .      -((1./2.)*POLYCO(3,2,J)*(B(3)**2))
      .      -      (POLYCO(4,2,J)*B(3))
C
C Solve the matrix for the integration constants.
C
      CALL GAUSS1(AM,CM,RM,6)
C
C Apply the integration constants in the calculation of the
C deflections. Since deflections are later referenced to 2nd
C epoch when wall is short deflections are calculated for
C unextended height of wall only for all epochs.
C
      MM=1
      N=1
      B(1)=498.63-492.61
      DO 390 M=1,3
      ELE(N,J)=B(M)
410 IF (ELE(N,J) .LT. B(M+1)) ELE(N,J)=B(M+1)
      X=ELE(N,J)
      DEFLEC(N,J)=-(((1./20.)*POLYCO(1,M,J)*(X**5))
      .          +((1./12.)*POLYCO(2,M,J)*(X**4))
      .          +((1./6.)*POLYCO(3,M,J)*(X**3))
      .          +((1./2.)*POLYCO(4,M,J)*(X**2))
      .          +RM(MM)*X + RM(MM+1))
      .          *(1.E12/(YE*83.5E6))
      IF (ELE(N,J) .EQ. B(M+1)) GOTO 400
      N=N+1
      ELE(N,J)=ELE(N-1,J)-0.01
      GOTO 410
400 N=N+1
      MM=MM+2
390 CONTINUE
360 CONTINUE
C
C Plot the calculated deflection curves.
C
      LL=1
      DO 415 L=1,2
      NLINES=0
      CALL UNITS(' CM' )
      CALL NOBRDR
      CALL PAGE(28.0,21.5)
      CALL AREA2D(19.0,11.0)
      CALL PHYSOR(5.5,6.)
      CALL COMPLX
      CALL XNAME(' Displacement, Positive Outward (mm)$',100)
      CALL YNAME(' Elevation (m)$',100)
      CALL INTAXS
      CALL FRAME
      CALL YAXANG(0.)
      YORIG=492.
      YMAX=500.
      YSTP=1.
      CALL GRAF(XORIG4,XSTP4,XMAX4,YORIG,YSTP,YMAX)

```

```

DO 420 J=NCB(L),NCE(L)
NP=N-1
DO 430 I=1,NP
XPLOT(I)=DEFLEC(I,J)-DEFLEC(I,2)
YPLOT(I)=ELE(I,J)+492.61
430 CONTINUE
CALL MARKER(ISYM(J))
CALL CURVE(XPLOT,YPLOT,NP,800)
NLINES=NLINES+1
CALL LINES(LEGNM(1,J),IPKRAY,NLINES)
420 CONTINUE
CALL MYLEGN(' ')
CALL LEGEND(IPKRAY,NT,14.85,0.6)
CALL BLREC(14.55,0.3,4.15,3.8,0.05)
CALL MESSAG(FIGTIT(1,LL+6),100,1.3,-3.0)
CALL MESSAG(FIGTIT(1,LL+7),100,1.3,-3.6)
CALL RLVEC(0.,492.61,0.,499.07,0000)
CALL BLREC(4.75,3.16,0.5,0.17,0.015)
CALL BLREC(4.75,7.0375,0.5,0.17,0.015)
CALL HEIGHT(0.25)
CALL MESSAG('Wall',4,8.0,5.5)
CALL MESSAG('Exposed Side',12,8.0,5.1)
CALL RESET('HEIGHT')
CALL ENDPL(0)
LL=LL+2
415 CONTINUE
C
C Plot deflection vs time for top and bottom of SPW and at walers.
C
LGNM(1)=' SPW Top$'
LGNM(2)=' Upper Waler$'
LGNM(3)=' Lower Waler$'
LGNM(4)=' SPW Base$'
JCURVE(1)=1
JCURVE(2)=146
JCURVE(3)=429
JCURVE(4)=605
CALL RESET('MARKER')
CALL PHYSOR(5.5,6.)
CALL AREA2D(19.,11.)
CALL YNAME('Deflection (mm)$',100)
CALL RESET('XNAME')
CALL XREVTK
CALL FRAME
CALL GRAF(0.,100.,1100.,XORIG4,XSTP4,XMAX4)
CALL BLREC(0.3,7.9,5.05,2.6,0.05)
DO 435 I=1,4
DO 440 J=2,NT
XPLOT(J-1)=DAYNUM(J)
YPLOT(J-1)=DEFLEC(JCURVE(I),J) - DEFLEC(JCURVE(I),2)
440 CONTINUE
CALL CURVE(XPLOT,YPLOT,NT-1,1)
CALL LINES(LGNM(I),IPKRAY,I)
435 CONTINUE

```

```

CALL RESET('BLNKS')
CALL MYLEGN(' ',1)
CALL LEGEND(IPKRAY,4,0.6,8.2)
CALL XGRAXS(0.,100.,1100.,19.,'Day Number$',-100,0.,11.)
CALL XDTAXS(840601.,'MONTH',870605.,19.,',',1,0.,0.)
CALL RLVEC(0.,0.,1100.,0.,0000)
CALL MESSAG(FIGTIT(1,11),100,0.7,-3.25)
CALL ENDPL(0)

```

```

C
C Plot deflection profiles for reference epochs.
C

```

```

    JCURVE(1)=2
    JCURVE(2)=6
    JCURVE(3)=11
    CALL UNITS('CM')
    CALL NOBRDR
    CALL PAGE(28.0,21.5)
    CALL AREA2D(19.0,11.0)
    CALL PHYSOR(5.5,6.)
    CALL COMPLX
    CALL XNAME('Displacement, Positive Outward (mm)$',100)
    CALL YNAME('Elevation (m)$',100)
    CALL INTAXS
    CALL FRAME
    CALL YAXANG(0.)
    YORIG=492.
    YMAX=500.
    YSTP=1.
    CALL GRAF(XORIG4,XSTP4,XMAX4,YORIG,YSTP,YMAX)
    CALL RLVEC(0.,492.61,0.,499.07,0000)
    DO 460 J=1,3
    NP=N-1
    DO 465 I=1,NP
    XPLOT(I)=DEFLEC(I,JCURVE(J))-DEFLEC(I,2)
    YPLOT(I)=ELE(I,JCURVE(J))+492.61
465 CONTINUE
    CALL LEGLIN
    IF (J.EQ. 2) THEN
        CALL DOT
    ELSEIF (J.EQ. 3) THEN
        CALL DASH
    ENDIF
    CALL CURVE(XPLOT,YPLOT,NP,0)
    CALL LINES(LEGNM(1,JCURVE(J)),IPKRAY,J)
460 CONTINUE
    CALL MYLEGN(' ')
    CALL LEGEND(IPKRAY,3,14.7,8.8)
    CALL BLREC(14.4,8.5,4.3,2.2,0.05)
    CALL MESSAG(FIGTIT(1,12),100,1.6,-3.0)
    CALL MESSAG(FIGTIT(1,13),100,1.6,-3.6)
    CALL BLREC(4.75,3.16,0.5,0.17,0.015)
    CALL BLREC(4.75,7.0375,0.5,0.17,0.015)
    CALL HEIGHT(0.25)
    CALL MESSAG('Wall',4,8.0,5.5)

```



```

CALL MESSAG('Exposed Side',12,8.0,5.1)
CALL RESET('HEIGHT')
CALL DONEPL

```

```

C
C File 5 read format statements.

```

```

C
500 FORMAT(19A1)
502 FORMAT(F7.1,I5,10A1)
505 FORMAT(80A1)
507 FORMAT(3F10.3)
510 FORMAT(4E10.3)
515 FORMAT(3I5)
520 FORMAT(8G20.8)
522 FORMAT(I5)
526 FORMAT(2F10.3)
530 FORMAT(5I9)

```

```

C
C File 4 write format statements

```

```

C
442 FORMAT('Figure H.',I2,': Interpolated bending moment,',
. ' east section.',18A1,'$')
443 FORMAT('Figure H.',I2,': Interpolated bending moment,',
. ' west section.',18A1,'$')
444 FORMAT('Figure C.',I1,': Earth pressure distributions,',
. ' east section.$')
445 FORMAT('Figure C.',I1,': Earth pressure distributions,',
. ' west section.$')
446 FORMAT('Figure C.',I2,': Summary of all east section,',
. ' earth pressure distributions.$')
447 FORMAT('Figure C.',I2,': Summary of all west section,',
. ' earth pressure distributions.$')
448 FORMAT('Figure H.',I1,': Interpolated bending moment,',
. ' east section.',18A1,'$')
449 FORMAT('Figure H.',I1,': Interpolated bending moment,',
. ' west section.',18A1,'$')

```

```

C
C File 7 write format statements.

```

```

C
700 FORMAT(//////////,15X,80A1)
702 FORMAT(///,15X,'Wall Properties',//)
704 FORMAT(15X,'|',29X,'|')
706 FORMAT(15X,' Modulus of Elasticity (MPa) ',10X,F8.0)
708 FORMAT(15X,' Section Modulus (mm**3/m) ',10X,F8.0)
710 FORMAT(15X,' Height (mm) ',10X,F8.0)
712 FORMAT(15X,' Thickness (mm) ',10X,F8.0)
714 FORMAT(15X,'!',29X,'!')
716 FORMAT(///,15X,'Strain Gauge Coordinates',//)
718 FORMAT(15X,'|',10X,'|',12X,'|',10X,'|',12X,'|',11X,'|')
720 FORMAT(20X,'SG',10X,'X',11X,'SG',10X,'X',9X,'Average')
722 FORMAT(18X,'Number',4X,'Coordinate',4X,'Number',4X,
+ 'Coordinate',3X,'Elevation')
724 FORMAT(15X,I7,5X,F9.3,I10,5X,F9.3,4X,F9.3)
726 FORMAT(15X,'!',10X,'!',12X,'!',10X,'!',12X,'!',11X,'!')
728 FORMAT(' 9700 SKIPTO=NEXTSHEET',//////////)

```

```

732 FORMAT(///// ,10X,'|',46X,'|',35X,'|',8X,'|',9X,'|',8X,'|')
734 FORMAT(27X,' "Inner" Column',28X,'Outer Column',14X,'Axial',
.4X,'Bending')
736 FORMAT(10X,4('|',8X),'|',10X,4('|',8X),'@ Stress Stress',4X,
.'Moment')
738 FORMAT(14X,'SG',5X,'Strain',4X,'Net',5X,'Stress',3X,
.'Adjusted',5X,'SG',5X,'Strain',4X,'Net',5X,'Stress',
.22X,'(kN m)')
740 FORMAT(12X,'Number',3X,'(E-6)',4X,'Strain',3X,'(MPa)',5X,
.'Stress',4X,'Number',3X,'(E-6)',4X,'Strain',3X,'(MPa)',
.4X,'(MPa)',5X,'(MPa)')
742 FORMAT(10X,'|',110X,'|')
744 FORMAT(10X,I6,I11,I8,F10.2,F10.2,I8,I11,I8,F10.2,F9.2,F10.2,
.F9.2)
746 FORMAT(10X,4('!',8X),',!',10X,5('!',8X),',!',9X,',!',8X,',!')
747 FORMAT(/10X,'Temperature dependence correction applied',
.' to SG readings (micro strain units):',I3,',')
748 FORMAT(//,30X,'Table H.',I1,': Wall mounted strain gauge',
.' results, east section,',19A1)
750 FORMAT(//,30X,'Table H.',I2,': Wall mounted strain gauge',
.' results, east section,',19A1)
752 FORMAT(//,30X,'Table H.',I2,': Wall mounted strain gauge',
.' results, west section,',19A1)

```

C
C File 8 write format statements.

```

C
800 FORMAT(//,'Calculated anchor loads: ',2G10.2)
810 FORMAT(/,'Sum of positive horiz forces for epoch ',I2,' is: ',
.G11.5,' kN')
820 FORMAT('Sum of negative horiz forces for epoch ',I2,' is: ',
.G11.5,' kN')
830 FORMAT(' The diff between positive and negative is: ',
.G11.5,' kN')
840 FORMAT('Sum of moment at top of wall for epoch ',I2,' is: ',
.G11.5,' kNm',/)
STOP
END

```

```

C
C Subroutine Name:  GAUSS1
C
C Description:      Matrix solver.
C
SUBROUTINE GAUSS1(A,B,C,N)
IMPLICIT REAL*8(A-H,O-Z)
DIMENSION A(22,22),B(22),C(22)
N1=N-1
DO 100 I=1,N1
AL=DABS(A(I,I))
NM=I
DO 30 J=I,N
IF(DABS(A(J,I)).LE.AL) GO TO 30
NM=J
AL=DABS(A(J,I))
30 CONTINUE
IF(NM.EQ.I) GO TO 50
BB=B(I)
B(I)=B(NM)
B(NM)=BB
DO 40 J=I,N
AA=A(I,J)
A(I,J)=A(NM,J)
40 A(NM,J)=AA
50 CONTINUE
NP=I+1
B(I)=B(I)/A(I,I)
DO 60 J=NP,N
B(J)=B(J)-B(I)*A(J,I)
A(I,J)=A(I,J)/A(I,I)
DO 60 L=NP,N
60 A(L,J)=A(L,J)-A(I,J)*A(L,I)
100 CONTINUE
C(N)=B(N)/A(N,N)
N1=N-1
DO 200 I=1,N1
NP=N-I
NP1=N-I+1
BB=0.0
DO 110 J=NP1,N
BB=BB+A(NP,J)*C(J)
110 CONTINUE
200 C(NP)=B(NP)-BB
RETURN
END

```

Appendix L

Data Reduction Procedure for the Survey

L.1 Introduction

The survey consists of a network of positions to which distance and/or direction measurements are made. These measurements yield the horizontal coordinates of the points involved. The coordinates can be used to calculate deflection profiles for the wall, the ultimate objective of the survey program. A three stage procedure is involved in obtaining these results. The first is a preliminary step which prepares the raw measurements for use as input in a Department of Civil Engineering computer program. Executing the program, called Plane Adjustment by Least Squares or PALS, constitutes the second step. PALS incorporates a technique called least squares adjustment which determines position coordinates on the basis of statistical considerations. Another program, called S-PROG, extracts from the PALS output the information necessary to plot deflection profiles for the wall. This makes up the third step of the survey data reduction procedure.

L.2 Calculation Procedure

The complete data reduction procedure is described in the following sections. Considerable attention is devoted to the theory employed by the PALS program. It is relatively complex and makes up the largest portion of the survey data

reduction process.

L.2.1 Survey Data Preparation

The steps involved in preparing the raw survey measurements for use as data in PALS are described below.

L.2.1.1 Horizontal Angles

The procedure used to measure the horizontal angles from the two survey monuments to the backsights and wall targets was described in 4.3. All the directions are reduced assuming that the line of sight from M1 to M2 is at 90° azimuth. The opposite measurement from M2 to M1 has the reciprocal azimuth, 270° . The reduction of horizontal angle measurements is straightforward and is best illustrated by example. Consider that the mean of the left face observations from M1 to M2 is $90^\circ 00' 19''$. Thus a $19''$ adjustment is required to produce a reduced mean of $90^\circ 00' 00''$. Assume that the mean for the right face observations is $270^\circ 00' 24''$. Subtracting $180^\circ 00' 24''$ will produce a right face reduced mean of $90^\circ 00' 00''$.

Thus for all subsequent measurements from M1 to the remaining survey targets, $19''$ is subtracted from the mean of the left face observations. Similarly, $180^\circ 00' 24''$ is subtracted from the mean of the right face observations. When such a subtraction produces a negative result 360° is added to produce the appropriate value.

The final step has the left and right face reduced means for sightings to a particular target averaged to produce the "mean of sets". It is this quantity which is used as the direction input in the PALS program. The exception to this occurs for measurements to the backsights and pins. According to the surveying procedure adopted, four "mean of sets" are produced for each of these locations. The average is taken for use as input into the PALS program.

The procedure described above is identical for reducing directions measured from M2. In this case, however, the left and right face adjustments are calculated to produce "reduced means" of $270^{\circ} 00' 00''$ for the measurements to M1.

L.2.1.2 Vertical Angles

Vertical angles are measured using the theodolite and are used for the reduction of slope distances to horizontal distances. Several left and right face measurements of the angle are made. The average of each set is taken and the two results summed. Comparison of this value to 360° reveals the vertical circle index error. If the sum exceeds 360° one half of the excess is subtracted from the average of the left face readings. If the sum is less than 360° one half of the shortfall is added to the average of the left face reading. For left face measurements the horizontal lies at 90° ; 0° represents a vertical angle straight up.

L.2.1.3 Chained Distances

Distances measured using the steel tape must be corrected for sag, temperature, elastic strain and the elevation difference between the two points involved (Davis *et al.*, 1981).

The sag correction, C_s , is calculated from the following equation and is subtracted from the average length determined at a particular strength of pull.

$$C_s = w^2L^3/24P^2 \quad [L.1]$$

where:

w = weight of the tape in kg/m

L = unsupported length of tape in metres

P = pull on tape in kilograms

The tape is calibrated to give accurate readings at a particular temperature. Any deviation from this temperature requires adjustment for the thermally induced strains which will alter the standard length of the tape. The correction, C_t , is calculated as follows.

$$C_t = aL(T-T_s) \quad [L.2]$$

where:

a = coefficient of thermal expansion
in mm/mm/ °C

L = measured length of line

T = tape temperature at time of
measurement in °C

T_s = tape temperature at
standardization

Note that this correction reduces the measured length when T is less than T_s and increases it when T is greater than T_s . It should also be noted that the tape temperature was not directly measured. The tape, held at close to ambient conditions at all times, was assumed to be at the same temperature as the air.

The tape undergoes elastic strain when it is pulled for a measurement. It is calibrated for a standard pull of 20 pounds or approximately 89 newtons. Deviation from this must be compensated according to the formula:

$$C_{\text{strain}} = \frac{(P - P_s)}{AE} L \quad [\text{L.3}]$$

where;

P = pull in newtons

P_s = standard pull in newtons

A = cross sectional area of the tape

E = elastic modulus of tape

L = measured length of line

For a particular strength of pull the measured length D can be corrected to yield the true slope distance D_s as follows.

$$D_s = D - C_s + C_t + C_{\text{strain}} \quad [\text{L.4}]$$

The horizontal distance, D_h , between the points in question can be determined as follows.

$$D_h = (D_s^2 - \Delta H^2)^{1/2} \quad [L.5]$$

ΔH can be determined from levelling or by using a vertical angle if it has been measured between the two points. In this case, however, adjustment for the height of the theodolite must be made. This was necessary because the theodolite is some 300mm higher than the pin used when taping measurements were made.

L.2.1.4 Distance Measured with the Wild Distomat (DI4)

The Wild Distomat is an electronic distance measuring device. It determines distance by measuring the travel time of a beam of light aimed at a target prism. Atmospheric conditions affect the Distomat results and must be accounted for.

The instrument has switch settings which can be set according to the ambient air pressure and temperature. With the appropriate settings atmospheric correction is automatically applied by the instrument. Standard practice at Boston Bar, however, was to use switch settings of 8+0, which is equivalent to zero atmospheric correction. The required correction is obtained by applying an equation provided by Wild.

$$\Delta D = 28.2 - \frac{0.029p}{1+0.0037t} \quad [L.6]$$

where:

ΔD = atmospheric correction in mm/100 metres

p = pressure in mb

t = temperature in °C

With ΔD calculated, the adjusted slope distance D_s can be found using:

$$D_s = \left[\frac{D}{100} \Delta D \right] + D \quad [L.7]$$

where:

D = average distomat distance obtained
with setting 8+0

The horizontal distance can be found according to equation L.5.

L.2.2 Least Squares Adjustment

The measurement of any quantity will involve some error. Human limitations, instrument imperfections and instabilities in nature are common sources of error. Errors are classified into two categories: systematic and random. The former refers to errors caused by a known source for which compensations can be applied. An example is the sag of the taping chain. Random errors, on the other hand, do not follow physical laws and cannot be eliminated. They remain after systematic errors have been removed and are an indeterminate quantity. From this it follows that the true or exact value of the measured quantity is also indeterminate.

The least squares adjustment technique provides a means of approximating both the exact value of a measured quantity and the error associated with it. These approximations are called respectively the most probable value (MPV) and the

residual. The residual, commonly denoted by the letter v , represents the difference between the most probable value and the magnitude of the observation. This relationship is called an observation equation.

$$v = \text{MPV} - \text{observation (containing random error only)} \quad [\text{L.8}]$$

The most probable value, as its name suggests, is the quantity which has the highest probability based on the measurements which have been made. This definition carries with it an important implication; namely that the MPV is calculated from more than one measurement. This is in fact the basis of the least squares adjustment procedure.

Assume that a certain quantity, x , has been measured a number of times. Each measurement has a residual associated with it. The residuals are defined by Equation L.8, the observation equation. The MPV for x is calculated by minimizing the sum of the squares of each measurement's residual.

$$U = \sum_{i=1}^n (v_i)^2$$

$$= \text{minimum} \quad [\text{L.9}]$$

where:

$$v_i = \text{MPV} - L_i$$

$$L_i = i^{\text{th}} \text{ measurement of unknown quantity } x.$$

If the measurements involved have unequal weights Equation L.9 assumes the following form.

$$U = \sum_{i=1}^m p_i v_i^2 \quad [L.10]$$

The term p_i is the weight associated with each observation. It can be arbitrarily established based on considerations of the relative accuracy of the measurements. Alternatively, p_i can be set equal to one over the s^2 where s is the standard deviation of the measurement in question.

The sum of the squares of the residuals is minimized by differentiating the U function with respect to the unknown quantity x . The result is set equal to zero as follows.

$$\frac{dU}{dx} = \frac{d}{dx} \sum_{i=1}^m p_i v_i^2 = 0 \quad [L.11]$$

As long as the number of measurements exceeds the number of unknowns the least squares adjustment procedure can be applied to solve for any number of most probable values. Thus the above example could be expanded to include measurements of quantities x , y and z . For each available measurement of these three quantities an observation equation is written. Each of these equations is squared and summed to yield the U function. This function is minimized by taking partial derivatives with respect to each of the unknowns it incorporates, namely x , y and z in this case. The resulting equations, each equated to zero, are called the normal equations. These can be solved to yield the most probable values for the unknowns.

For large systems of measurements solution for the most probable values is formulated using matrices. The general matrix form of least squares adjustment will be outlined in

the following.

Consider the m observation equations containing n unknowns ($m > n$) shown below. Note that these equations are linear; a convenience for the least squares solution. Note also that the observations are considered to have unequal weights.

$$v_1 = a_1A + b_1B + \dots + n_1B - L_1$$

$$v_2 = a_2A + b_2B + \dots + n_2B - L_2$$

$$v_m = a_mA + b_mB + \dots + n_mB - L_m$$

where:

a_i, b_i, \dots, n_i = known coefficients

A, B, \dots, N = unknown MPV

L_i = measurements or observations

v_i = observation residuals

These equations are readily put into matrix form:

$$\begin{bmatrix} a_1 & b_1 & \dots & n_1 \\ a_2 & b_2 & \dots & n_2 \\ \vdots & \vdots & & \vdots \\ a_m & b_m & \dots & n_m \end{bmatrix} \begin{bmatrix} A \\ B \\ \vdots \\ N \end{bmatrix} - \begin{bmatrix} L_1 \\ L_2 \\ \vdots \\ L_m \end{bmatrix} = \begin{bmatrix} v_1 \\ v_2 \\ \vdots \\ v_m \end{bmatrix}$$

or in shortened notation;

$$[A][X] - [L] = [V] \quad [L.12]$$

Equation L.12 represents the observation equations in matrix form. Applying Equation L.10 and taking partial derivatives with respect to each of the unknowns A, B, \dots, N yields n

normal equations. These have the following form.

$$p_i a_i a_i A + p_i a_i b_i B + \dots + p_i a_i n_i N = p_i a_i L_i$$

$$p_i b_i a_i A + p_i b_i b_i B + \dots + p_i b_i n_i N = p_i b_i L_i$$

$$p_i n_i a_i A + p_i n_i b_i B + \dots + p_i n_i n_i N = p_i n_i L_i$$

where:

$$p_i a_i a_i = p_1 a_1 a_1 + p_2 a_2 a_2 + \dots + p_m a_m a_m$$

$$p_i b_i L_i = p_1 b_1 L_1 + p_2 b_2 L_2 + \dots + p_m b_m L_m$$

Close scrutiny of these equations reveals that they can be written in matrix form as follows.

$$[A]^T [P] [A] [X] = [A]^T [P] [L] \quad [L.13]$$

The matrix [P] has the measurement weights p_i along its diagonal. All the off diagonal entries are ordinarily taken as zero.

Equation L.13 can be solved for [X], the vector of MPV, as follows.

$$[X] = ([A]^T [P] [A])^{-1} [A]^T [P] [L] \quad [L.14]$$

The residuals can be calculated by back substitution of [X] into equation L.12.

The calculations are now complete. However, it is possible to evaluate statistics for the solution. The equations involved are given below without proofs. The reader is referred to Wolf (1980) for complete derivations.

The standard deviation corresponding to unit weight for the adjustment is:

$$S_o = \left[\frac{[V]^T [P] [V]}{r} \right] \quad [L.15]$$

The r term represents the degrees of freedom and is equal to the number of observations (m) minus the number of unknowns (n). The standard deviations for each of the adjusted quantities is given by:

$$Sx_i = S_o \sqrt{Qx_i x_i} \quad [L.16]$$

Sx_i is the standard deviation of the i^{th} adjusted quantity (in the i^{th} row of the $[X]$ vector). $Qx_i x_i$ is the quantity in the i^{th} row and column of the cofactor matrix where the cofactor matrix equals $([A]^T [P] [A])^{-1}$.

The interpretation of the standard deviation is that the adjusted quantity has a 0.68 probability of lying within plus or minus Sx_i of its calculated value.

In surveying the quantities being adjusted are the x and y coordinates of points in space and they have a joint statistical distribution. The two standard deviations associated with the coordinates of a particular point will define a rectangle. It will be centered around the point and is called the standard error rectangle. For this situation there would be an approximate probability of 0.68^2 that the adjusted coordinates will lie within the standard error rectangle.

A more appropriate representation of accuracy in this situation involves use of the standard error ellipse (Wolf, 1980). It is inscribed inside the standard error rectangle and can be oriented in any direction along axes identified as U and V. However, the orientation which yields the maximum and minimum values respectively for the semi-major and semi-minor axes of the ellipse are normally selected. This ellipse is defined by the following equations. All the terms involved are from the cofactor matrix [Q].

$$\tan(2t) = \frac{2Q_{xy}}{Q_{yy} - Q_{xx}} \quad [L.17]$$

t = angle between U and Y axes

$$S_o^2 Q_{uu} = \text{Variance along U axis} \quad [L.18]$$

$$(S_o^2 Q_{uu})^{1/2} = \text{Semi-major axis} \quad [L.19]$$

$$S_o^2 Q_{vv} = \text{Variance along V axis} \quad [L.20]$$

$$(S_o^2 Q_{vv})^{1/2} = \text{Semi-minor axis} \quad [L.21]$$

where:

$$Q_{uu} = 0.5(Q_{xx} + Q_{yy} + k)$$

$$Q_{vv} = 0.5(Q_{xx} + Q_{yy} - k)$$

$$k = [(Q_{yy} - Q_{xx})^2 + 4(Q_{xy})^2]^{1/2}$$

The locations of the terms Q_{xx} , Q_{yy} and Q_{xy} in the cofactor matrix requires clarification. Assume that the above statistics are to be evaluated for the i^{th} point in the adjustment. Therefore:

Q_{xx} is from row $2i - 1$, column $2i - 1$ of [Q].

Q_{yy} is from row $2i$, column $2i$ of [Q].

Q_{xy} is from row $2i - 1$, column $2i$ of $[Q]$.

The complete least squares solution including calculation of statistics has been presented. As yet, however, only the statistical calculations have been specifically referenced to survey results. The least squares adjustment was dealt with in general terms only. Applying the method to surveying entails formulating observation equations in the pattern given by Equation L.8 for each type of survey measurement. Two types of survey measurements have been made at Boston Bar; distance and direction.

The distance between two points is a non-linear function of the coordinates of the points involved according to the following equation.

$$\begin{aligned} S_{ij} &= [(x_j - x_i)^2 + (y_j - y_i)^2]^{1/2} && \text{[L.22]} \\ &= f(x_i, y_i, x_j, y_j) \end{aligned}$$

The distance function must be linearized if it is to be incorporated into the least squares adjustment. This can be achieved through the use of the Taylor Series. This is shown below for a function with four independent variables and with second and higher order terms ignored.

$$\begin{aligned} f(x_i, y_i, x_j, y_j) &= f(x_i, y_i, x_j, y_j) + \frac{\delta}{\delta x_i} f(x_i, y_i, x_j, y_j) dx_i \\ &\quad + \frac{\delta}{\delta y_i} f(x_i, y_i, x_j, y_j) dy_i \\ &\quad + \frac{\delta}{\delta x_j} f(x_i, y_i, x_j, y_j) dx_j \end{aligned}$$

$$+ \frac{\delta}{\delta y_j} f(x_i, y_i, x_j, y_j) dy_j \quad [L.23]$$

The dotted variables signify approximate values of the function's arguments. The distance equation, L.22 will be expanded using the Taylor Series to yield its linear equivalent. Each of the terms in Equation L.23 will be considered individually.

$$\begin{aligned} f(x_i, y_i, x_j, y_j) &= S_{ij} \\ &= L_{ij} + v_{ij} \end{aligned} \quad [L.24]$$

where S_{ij} = MPV for distance between i and j

L_{ij} = observation

$$\begin{aligned} f(x_i, y_i, x_j, y_j) &= [(x_j - x_i)^2 + (y_j - y_i)^2]^{1/2} \quad [L.25] \\ &= S_{ij} \\ &= \text{distance based on} \\ &\quad \text{approximate coordinates} \end{aligned}$$

$$\begin{aligned} \frac{\delta}{\delta x_i} f(x_i, y_i, x_j, y_j) &= \frac{\delta}{\delta x_i} [(x_j - x_i)^2 + (y_j - y_i)^2]^{1/2} \\ &= -[(x_j - x_i)/S_{ij}] \\ &= a_{11} \end{aligned} \quad [L.26]$$

$$\begin{aligned} \frac{\delta}{\delta y_i} f(x_i, y_i, x_j, y_j) &= -[(y_j - y_i)/S_{ij}] \\ &= a_{12} \end{aligned} \quad [L.27]$$

$$\begin{aligned} \frac{\delta}{\delta x_j} f(x_i, y_i, x_j, y_j) &= [(x_j - x_i)/S_{ij}] \\ &= a_{13} \end{aligned} \quad [L.28]$$

$$\begin{aligned} \frac{\delta}{\delta y_j} f(x_i, y_i, x_j, y_j) &= [(y_j - y_i)/S_{ij}] \\ &= a_{14} \end{aligned} \quad [L.29]$$

Each of the terms in Equation L.23 is replaced by its equivalent as given by L.24 through L.29. This gives rise to a linearized version of the distance expression.

$$(L_{ij} - S'_{ij}) + v_{ij} = a_{11}dx_i + a_{12}dy_i + a_{13}dx_j + a_{14}dy_j \quad [L.30]$$

Equation L.30 represents the length observation equation. It can be readily put into vector form as follows:

$$K_{ij} + v_{ij} = [a_{11} \ a_{12} \ a_{13} \ a_{14}] \begin{bmatrix} dx_i \\ dy_i \\ dx_j \\ dy_j \end{bmatrix} \quad [L.31]$$

Each application of the length observation equation to a different measured distance yields one equation of the above form. Each of these can be assembled as successive rows into the matrix relation given by equation L.12. The coefficients a_{11} to a_{14} are placed in the columns of [A] which ensure that each is multiplied by the appropriate dx or dy in the [X] vector. Note that the order of the points in the [X] vector is arbitrary. However, once established it does affect the positioning of the a coefficients in each row of the [A] matrix.

The direction observation equation is derived in a manner exactly analogous to that described above for the length observation equation. For the exact procedure the reader is referred to Mikhail and Gracie (1981).

The use of the Taylor Series to obtain observation equations specific to survey measurements introduces some changes in the solution procedure. The [L] vector, containing the measured quantities, in equation L.12 is replaced by [K]. Each term in this new vector represents the difference between the measured quantity, be it a length or direction, and that same quantity based on approximate coordinates. This requires that approximate coordinates for the points in the survey network be available. These can be calculated using some of the available measurements and geometry. They become an input into the least squares solution.

The [X] vector, once obtained by solving the normal equations, does not contain probable values for the coordinates but rather adjustments to the approximate coordinates initially assumed. New approximate coordinates can be calculated using these adjustments and the entire solution can be repeated. Iterations can continue until the adjustments which are calculated become sufficiently small.

L.2.3 Calculation of the Deflection Profile

The PALS program is run for every epoch of data. The results are appended together to produce a file containing the coordinates of all the points involved in the survey through time. This file serves as the input for the program S-PROG. This program compares the coordinates of the wall positions at each epoch to the coordinates at time zero to

calculate the deflection of the wall. For every time interval a deflection profile is plotted for each of the four columns of wall survey positions. The deflection of each wall survey positions through time is also plotted. These appear on four additional graphs, one for each column of positions.

L.3 Operating Procedure

The procedure used to operate PALS is documented in a manual prepared by Professor A.E. Peterson, the developer of the program. Professor Peterson is a staff member of the Department of Civil Engineering at the University of Alberta.

The results provided by PALS are plotted and summarized with a program called S-PROG. S-PROG is compiled as follows:

```
$RUN NEW:FORTRANVS SCARDS=S-PROG SPUNCH=S-PROGC
```

The program is run with the following command.

```
$RUN S-PROGC+*DISSPLA 5=datafile 6=-6  
7=-7 8=text output 9=plot output
```

File 5 is the datafile which consists of selected results taken from successive runs of PALS appended together. File 6 is used by DISSPLA, the plotting routine, for writing messages. File 7 is used by the program only for writes and reads. File 8 a summary table of wall deflection results. File 9 is the plot description file.

Post processing of the text and plot output files is identical to the procedure outlined in Appendix I.

L.4 Datafile and Program Listings

An annotated version of the datafile for S-PROG, called S-T15, is provided below. This is followed by a listing of the program S-PROG.

Annotated version of datafile S-T15.

Figure D.1: Survey displacements, Column A.
 Figure D.2: Survey displacements, Column B.
 Figure D.3: Survey displacements, Column C.
 Figure D.4: Survey displacements, early epochs, Column D.
 Figure D.6: Survey displacements with time, Column A.
 Figure D.7: Survey displacements with time, Column B.
 Figure D.8: Survey displacements with time, Column C.
 Figure D.9: Survey displacements with time, Column D.
 Figure D.5: Survey displacements, late epochs, Column D.
 -5..5..15..492..1..500..
 0..100..1100..-5..5..15..

Plot titles.

x & y axis scale info for ele/defl plots & def1/time plots.

Legend names.

A1
 A2
 A3
 A4
 A5
 A6
 A7
 A8
 A9
 B1
 B2
 B3
 B4
 B5
 B6
 B7
 B8
 B9
 C1
 C2
 C3
 C4
 C5
 C6
 C7
 C8
 C9
 D1
 D2
 D3
 D4
 D5

D6
D7
D8
D9
9,
20,

Legend names.	# of data sets.	Symbol #, date.	Day #.
0, 20/06/84			
311	999.9115	1060.9071	101
312	999.8198	1060.9071	101
313	999.7530	1060.9071	101
314	999.6118	1060.9086	101
315	999.4369	1060.9119	101
316	999.2912	1060.9206	101
317	999.1866	1060.9053	101
318	999.1044	1060.9027	101
321	999.6000	1061.2724	101
322	999.4091	1061.2724	101
323	999.2365	1061.2587	101
324	999.1454	1061.2640	101
325	998.9643	1061.2453	101
331	999.6029	1061.5514	101
332	999.4072	1061.5514	101
333	999.2333	1061.5458	101
334	999.1375	1061.5525	101
335	998.9544	1061.5629	101
341	999.9079	1061.7661	101
342	999.8059	1061.7661	101
343	999.7424	1061.7819	101
345	999.6089	1061.7661	101
344	999.6569	1061.7661	101
347	999.2718	1061.7955	101
348	999.1678	1061.7902	101
349	999.0930	1061.7836	101
102	1000.0000	1108.1791	101
101	1000.0000	1000.0000	102
411	999.9091		
412	999.8159		
413	999.7473		
414	999.6097		
415	999.4365		
416	999.2899		
417	999.1862		
418	999.1044		
422	999.4055		

Survey point ID, northing coordinate,
2 unnecessary #s.

Survey point ID	northing coordinate	flag
423	999.2343	
424	999.1439	
425	998.9671	
432	999.4029	
433	999.2312	
434	999.1381	
435	998.9589	
441	999.9004	
442	999.7988	
443	999.7360	
444	999.6497	
445	999.6027	
446	999.4275	
447	999.2715	
448	999.1709	
449	999.0928	
201	1006.0490	102
202	986.3837	1417.3249 102
203	967.3668	810.7369 102
204	982.9844	1002.9971 102
205	982.4830	1105.1019 102 1
1, 10/07/84		
40,		
101	1000.0066	999.9998 102
102	999.9979	1108.1783 101
412	999.8132	
413	999.7455	
414	999.6057	
415	999.4326	
416	999.2885	
417	999.1855	
421	999.5925	
422	999.4023	
423	999.2325	
424	999.1428	
425	998.9668	
432	999.4011	
431	999.5925	
433	999.2288	
434	999.1357	
435	998.9598	
441	999.8982	
442	999.7950	
443	999.7319	

Survey point ID, northing coordinate,
 2 unnecessary #s. Last line ends in
 flag of "1".

446	999.4242						
447	999.2707						
448	999.1696						
449	999.0925						
201	1006.0490						
202	986.3837						
203	967.3668						
204	982.9844						
205	982.4830						
2.05/08/84							
66,							
101	1000.0131						
102	999.9987						
412	999.8176						
413	999.7498						
414	999.6083						
415	999.4348						
416	999.2905						
417	999.1868						
418	999.1080						
421	999.5973						
422	999.4049						
423	999.2337						
424	999.1448						
425	998.9686						
432	999.4024						
431	999.5968						
433	999.2317						
434	999.1381						
435	988.9612						
441	999.9007						
442	999.7988						
443	999.7357						
444	999.6498						
445	999.6015						
446	999.4260						
447	999.2720						
448	999.1709						
449	999.0941						
201	1006.0490						
202	986.3837						
203	967.3668						
204	982.9844						
205	982.4830						
3.03/10/84							
125,							
101	1586.6056						
102	1417.3249						
432	810.7369						
431	1002.9971						
434	1105.1019						
435	999.9660						
442	999.8011						
446	999.4289						
447	999.2755						
448	999.1753						
449	999.0979						
201	1006.0490						
202	986.3837						
203	967.3668						
204	982.9844						
205	982.4830						
4.05/12/84							
185,							
101	1000.0296						
102	1000.0098						
432	999.4096						
431	999.6038						
433	999.2373						
434	999.1433						
435	998.9655						
436	998.9045						
441	999.9078						
442	999.8048						
446	999.4313						
447	999.2768						
448	999.1747						
449	999.0980						
201	1006.0490						
202	986.3837						
203	967.3668						
204	982.9844						
205	982.4830						
6.25/08/85							
451,							
102	1586.6056						
102	1417.3249						
102	810.7369						
102	1002.9971						
102 1	1105.1019						
999.9998							
1108.1791							
1000.0197							
1000.0005							
999.4052							
999.5985							
999.2345							
999.1408							
999.9660							
999.8011							
999.4289							
999.2755							
999.1753							
999.0979							
1006.0490							
986.3837							
967.3668							
982.9844							
982.4830							
1000.0296							
1000.0098							
999.4096							
999.6038							
999.2373							
999.1433							
998.9655							
998.9045							
999.9078							
999.8048							
999.4313							
999.2768							
999.1747							
999.0980							
1006.0490							
986.3837							
967.3668							
982.9844							
982.4830							
1000.0364							
1000.0226							
999.9989							
1108.1594							
102							
101							

411	999.9174				
412	999.8212				
413	999.7533				
414	999.6109				
415	999.4378				
416	999.2909				
417	999.1886				
418	999.1089				
423	999.2366				
424	999.1471				
425	998.9695				
431	999.5996				
433	999.2331				
434	999.1384				
435	998.9618				
436	998.8991				
442	999.8005				
445	999.6034				
446	999.4273				
447	999.2721				
448	999.1712				
449	999.0916				
202	986.3837				
203	967.3668				
204	982.9971				
205	982.4830				
202	986.3873				
203	967.3693				
204	982.9847				
205	982.4824				
8.30/07/86					
789.					
101	1000.0506				
102	1000.0224				
411	999.9189				
412	999.8226				
413	999.7553				
414	999.6133				
415	999.4381				
416	999.2918				
417	999.1916				
418	999.1110				
423	999.2380				
424	999.1467				
101	1000.0013				
101	1108.1651				
102	1417.3249				
102	810.7369				
102	1002.9971				
102	982.9971				
102	1105.1019				
102	1417.3284				
102	810.7570				
102	1002.9968				
102 1	1105.0997				
9.10/12/86					
925.					
101	1000.0559				
102	1000.0435				
411	999.9193				
412	999.8235				
413	999.7549				
414	999.6131				
415	999.4380				
416	999.2917				
417	999.1895				
418	999.1105				
421	999.6037				
422	999.4091				
423	999.2379				
424	999.1483				
425	998.9719				
432	999.4079				
431	999.6039				
433	999.2355				
434	999.1415				
435	998.9632				
436	998.9013				
442	999.8037				
443	999.7389				
444	999.6520				
425	999.9706				
431	999.6018				
432	999.4066				
433	999.2357				
434	999.1416				
435	998.9629				
436	998.9002				
442	999.8041				
445	999.6059				
446	999.4292				
447	999.2740				
448	999.1710				
449	999.0947				
202	986.3837				
203	967.3668				
204	982.9844				
205	982.4830				
206	1003.7001				
1417.3249					102
810.7369					102
1002.9971					102
1105.1019					102
1588.6558					102 1
1000.0559					102
1000.0435					101
999.9193					
999.8235					
999.7549					
999.6131					
999.4380					
999.2917					
999.1895					
999.1105					
999.6037					
999.4091					
999.2379					
999.1483					
998.9719					
999.4079					
999.6039					
999.2355					
999.1415					
998.9632					
998.9013					
999.8037					
999.7389					
999.6520					

445	999.6047		
446	999.4277		
447	999.2725		
448	999.1707		
449	999.0931		
202	986.3837	1417.3249	102
203	967.3668	810.7369	102
204	982.9844	1002.9971	102
205	982.4830	1105.1019	102
206	1003.7001	1588.6558	102 1
11.28/03/87			
1028.			
101	1000.0588	1000.0041	102
102	1000.0511	1108.1834	101
411	999.9159		
412	999.8212		
413	999.7543		
414	999.6115		
415	999.4371		
416	999.2905		
417	999.1886		
418	999.1087		
421	999.6021		
422	999.4096		
423	999.2363		
424	999.1468		
425	998.9699		
432	999.4069		
431	999.6020		
433	999.2341		
434	999.1393		
435	998.9616		
436	998.9004		
442	999.8034		
443	999.7385		
444	999.6513		
445	999.6042		
446	999.4264		
447	999.2717		
448	999.1701		
449	999.0926		
202	986.3837	1417.3249	102
203	967.3668	810.7369	102
204	982.9844	1002.9971	102
205	982.4830	1105.1019	102
206	1003.7001	1588.6558	102 1

```

C
C Program Name:      S-PROG
C
C Compiled Version:  S-PROGC
C
C Run Statement:     RUN S-PROGC+*DISSPLA 5=s-t15 7=-7
C                                     8=text output 9=plot file
C
C Description:       Program plots the survey results using DISSPLA.
C                   The input file is composed of the -t15 files
C                   (one obtained for each epoch for every run of
C                   PALS) appended together. Several lines are
C                   added to this file including the plot titles
C                   and the epoch dates. As well, a flag is added
C                   on the end of the last line of data for each
C                   epoch. See S-T15 as an example.
C
C Program:
C
C   REAL ELEV(449),DC(60,2),COORD(20,449),DEFLEC(20,449),
C   .PDEFL(20),PELEV(20),
C   .XORIG(2),XSTP(2),XMAX(2),YORIG(2),YSTP(2),YMAX(2),X(20),Y(20)
C   INTEGER DAYNUM(20),NCB(2),NCE(2)
C   DIMENSION IPKRAY(100,100),ISYM(20),IPK(100,100)
C   LOGICAL*1 TITL(70,9),DATE(10,20),LEGNM(4,36)
C   CHARACTER*5 STORE(9)
C
C Read in plot titles and plot parameters.
C
C   DO 10 I=1,9
C     READ(5,500)(TITL(J,I),J=1,70)
C   10 CONTINUE
C
C   DO 15 I=1,2
C     READ(5,501)XORIG(I),XSTP(I),XMAX(I),YORIG(I),YSTP(I),YMAX(I)
C   15 CONTINUE
C
C   DO 20 I=1,36
C     READ(5,503)(LEGNM(J,I),J=1,4)
C   20 CONTINUE
C
C Set elevations. The vertical measurements taken in July/86
C will be used to establish elevations. The reference elevation
C is arbitrarily taken as 500m at the top of pin 1 (excluding the
C pin). The top of the SPW at the reference joint has ele 498.63m.
C
C   ELEV(411)=493.048
C   ELEV(412)=493.509
C   ELEV(413)=493.952
C   ELEV(414)=494.819
C   ELEV(415)=495.902
C   ELEV(416)=496.828
C   ELEV(417)=497.448
C   ELEV(418)=497.960
C   ELEV(421)=493.736

```

```

ELEV(422)=494.917
ELEV(423)=495.991
ELEV(424)=496.542
ELEV(425)=497.645
ELEV(431)=493.755
ELEV(432)=494.917
ELEV(433)=495.971
ELEV(434)=496.532
ELEV(435)=497.645
ELEV(436)=498.039
ELEV(441)=493.051
ELEV(442)=493.607
ELEV(443)=494.001
ELEV(444)=494.494
ELEV(445)=494.789
ELEV(446)=495.853
ELEV(447)=496.808
ELEV(448)=497.448
ELEV(449)=497.941
READ(5,505)NT
C
C Initialize coordinate and deflection matrices.
C
DO 25 I=1,20
PDEFL(I)=0.
PELEV(I)=0.
DO 30 J=1,449
COORD(I,J)=0.
DEFLEC(I,J)=-12345.
30 CONTINUE
25 CONTINUE
C
C Read in data.
C
DO 35 I=1,NT
READ(5,510)ISYM(I),(DATE(J,I),J=1,10)
READ(5,512)DAYNUM(I)
NL=0
40 NL=NL+1
READ(5,515)DC(NL,1),DC(NL,2),DUM1,DUM2,FLAG
IF (FLAG.NE.1) GOTO 40
DO 45 J=1,NL
IDESIG=DC(J,1)
COORD(I,IDESIG)=DC(J,2)
45 CONTINUE
35 CONTINUE
C
C Calculate deflections.
C
DO 50 I=1,NT
DO 55 J=411,449
IF (COORD(I,J).LT.800.OR.COORD(1,J).LT.800) GOTO 55
DEFLEC(I,J)=COORD(I,J)-COORD(1,J)
55 CONTINUE

```

```

50 CONTINUE
C
C Write deflection results to a table:
C
WRITE(8,800)
WRITE(8,805)
WRITE(8,810)
WRITE(8,815)((DATE(J,I),J=1,8),I=1,9)
WRITE(8,820)(DAYNUM(I),I=1,9)
WRITE(8,825)
NLEG=0
NSDES=411
NEDES=419
DO 60 L=1,4
DO 65 J=NSDES,NEDES
C
C First initialize STORE character array, then if data write to it.
C
DO 70 I=1,9
STORE(I)=' - '
70 CONTINUE
PFLAG=0
IF (J .EQ. 431)WRITE(8,827)
IF((J.EQ.421).OR.(J.EQ.441))WRITE(8,830)
NLEG=NLEG+1
DO 75 I=1,NT
IF (DEFLEC(I,J) .EQ. -12345.) GOTO 75
PFLAG=1
VALUE=DEFLEC(I,J)*1000.
WRITE(7,700)VALUE
BACKSPACE 7
READ(7,705)STORE(I)
75 CONTINUE
C
C If deflection data in the STORE array write it out. First
C write statement simply adds '(mm)' in front of data.
C
IF (J .EQ. 432 .AND. PFLAG .EQ. 1) THEN
WRITE(8,832)(LEGNM(I,NLEG),I=1,2),ELEV(J),(STORE(K),K=1,9)
ELSEIF (PFLAG .EQ. 1) THEN
WRITE(8,835)(LEGNM(I,NLEG),I=1,2),ELEV(J),(STORE(K),K=1,9)
ENDIF
65 CONTINUE
C
C Increment counters to move to next column of survey points.
C
NSDES=NSDES+10
NEDES=NEDES+10
60 CONTINUE
WRITE(8,840)
WRITE(8,845)
C
C Plotting routine for elevation/deflection curves.
C

```

```

NSDES=411.
NEDES=419.
NCB(1)=1
NCE(1)=9
NCB(2)=0
NCE(2)=0
LOOPST=1
M=1
DO 80 L=1,4
IF (L .EQ. 4) THEN
NCB(1)=1
NCE(1)=5
NCB(2)=6
NCE(2)=9
LOOPST=2
ENDIF
DO 83 NN=1,LOOPST
CALL DSPDEV(' PLOTTER ')
CALL UNITS(' CM' )
CALL PAGE(27.94,21.59)
CALL NOBRDR
CALL PHYSOR(5.,5.5)
CALL AREA2D(19.0,11.0)
CALL COMPLX
CALL YNAME(' Elevation (m)$' ,100)
CALL XNAME(' Displacement, Positive Outward (mm)$' ,100)
CALL INTAXS
CALL FRAME
CALL YAXANG(0.)
CALL GRAF(XORIG(1),XSTP(1),XMAX(1),YORIG(1),YSTP(1),YMAX(1))
CALL RLVEC(0.,492.82,0.,499.17,0000)
CALL BLREC(4.75,3.16,0.5,0.17,0.015)
CALL BLREC(4.75,7.0375,0.5,0.17,0.015)
CALL RESET(' BLNKS' )
N=0
DO 85 I=NCB(NN),NCE(NN)
CALL HEIGHT(0.25)
K=0
DO 90 J=NSDES,NEDES
IF (DEFLEC(I,J) .EQ. -12345.) GOTO 90
K=K+1
PDEFL(K)=DEFLEC(I,J)*1000
PELEV(K)=ELEV(J)
IF (I .EQ. 1 .OR. I .EQ. 9) THEN
MM=M+J-NSDES
YH=ELEV(J)-0.075
CALL RLMESS(LEGNM(1,MM),2,-4.85,YH)
ENDIF
90 CONTINUE
IF (K .EQ. 0) GOTO 85
N=N+1
CALL MARKER(ISYM(I))
CALL CURVE(PDEFL,PELEV,K,1)
CALL RESET(' HEIGHT' )

```



```

      CALL LINES(DATE(1,1),IPKRAY,N)
85  CONTINUE
      CALL RESET('HEIGHT')
      IF (L .EQ. 4 .AND. NN .EQ. 1) THEN
      CALL MESSAG(TITL(1,4),100,2.,-3.)
      ELSEIF (L .EQ. 4 .AND. NN .EQ. 2) THEN
      CALL MESSAG(TITL(1,9),100,2.,-3.)
      ELSE
      CALL MESSAG(TITL(1,L),100,3.35,-3.)
      ENDIF
      BOXHI=N*0.5+0.83
      YB=10.7-BOXHI
      CALL BLREC(14.45,YB,4.25,BOXHI,0.05)
      CALL RESET('BLNKS')
      CALL MYLEGN(' ',1)
      CALL LEGEND(IPKRAY,N,14.7,YB+0.3)
      CALL ENDPL(0)
83  CONTINUE
      NSDES=NSDES+10
      NEDES=NEDES+10
      M=M+9
80  CONTINUE
C
C Plotting routine for deflection/time graphs.
C
      NSDES=411
      NEDES=419
      NTT=NT+1
      NLEG=0
      DO 95 L=1,4
      CALL PHYSOR(5.,5.)
      CALL AREA2D(19.,11.)
      CALL YNAME('Deflection (mm)$',100)
      CALL RESET('XNAME')
      CALL RESET('MARKER')
      CALL XREVTK
      CALL FRAME
      CALL GRAF(XORIG(2),XSTP(2),XMAX(2),YORIG(2),YSTP(2),YMAX(2))
C
C Create legend.
C
      MSYM=0
      NCURVE=0
      DO 100 J=NSDES,NEDES
      NLEG=NLEG+1
      IF (DEFLEC(1,J) .EQ. -12345.) GOTO 100
      NCURVE=NCURVE+1
      XX=-100.
      YY=-100.
      CALL MARKER(MSYM)
      CALL CURVE(XX,YY,1,-1)
      CALL LINES(LEGNM(1,NLEG),IPK,NCURVE)
      MSYM=MSYM+1
100 CONTINUE

```

```

      CALL MYLEGN(' ',1)
C
C Legend for column A.
C
      IF (L .EQ. 1) THEN
      CALL BLREC(0.3,7.84,4.35,2.76,0.05)
      CALL RESET('BLNKS')
      CALL LEGEND(IPK,4,0.6,8.14)
      DO 105 NN=1,4
      CALL DELLEG(NN)
105 CONTINUE
      CALL LEGEND(IPK,8,2.6,8.14)
C
C Legend for columns B and C.
C
      ELSEIF ((L .EQ. 2) .OR. (L .EQ. 3)) THEN
      CALL BLREC(0.3,7.84,2.4,2.76,0.05)
      CALL RESET('BLNKS')
      CALL LEGEND(IPK,4,0.6,8.14)
C
C Legend for column D.
C
      ELSE
      CALL BLREC(0.3,7.30,4.35,3.3,0.05)
      CALL RESET('BLNKS')
      CALL LEGEND(IPK,5,0.6,7.6)
      DO 110 NN=1,5
      CALL DELLEG(NN)
110 CONTINUE
      CALL LEGEND(IPK,9.2.6,8.1)
      ENDIF
C
C Plot data. Purpose of flag is to only increment the legend
C symbol if a curve has been drawn.
C
      MSYM=0
      DO 115 J=NSDES,NEDES
      NPTS=0
      FLAG=0
      DO 120 I=1,NTT
      IF (DEFLEC(I,J) .EQ. -12345.) GOTO 125
      NPTS=NPTS+1
      Y(NPTS)=DEFLEC(I,J)*1000.
      X(NPTS)=DAYNUM(I)
      GOTO 120
125 IF (NPTS .EQ. 0) GOTO 120
      FLAG=1
      CALL MARKER(MSYM)
      CALL CURVE(X,Y,NPTS,1)
      NPTS=0
120 CONTINUE
      IF (FLAG .EQ. 0) GOTO 115
      MSYM=MSYM+1
115 CONTINUE

```

```

C
C Secondary axes and title.
C
  CALL XGRAXS(XORIG(2),XSTP(2),XMAX(2),19.,'Day Number$',
.-100,0.,11.)
  CALL XDTAXS(840601.,'MONTH',870605.,19.,' ',1,0.,0.)
  CALL RLVEC(0.,0.,1100.,0.,0000)
  CALL MESSAG(TITL(1,L+4),100,2.2,-3.)
  CALL ENDPL(0)
  NSDES=NSDES+10
  NEDES=NEDES+10
95 CONTINUE
  CALL DONEPL
C
C Read format statements.
C
500 FORMAT(70A1)
501 FORMAT(6F10.3)
503 FORMAT(4A1)
505 FORMAT(I5)
510 FORMAT(I3,10A1)
512 FORMAT(I7)
515 FORMAT(F10.0,2F15.4,F10.0,F2.0)
C
C Write format statements.
C
700 FORMAT(F5.1)
705 FORMAT(A5)
800 FORMAT(//////////,13X,'|',13X,'|',93X,'|')
805 FORMAT(17X,'Survey',45X,'Date (Day Number)')
810 FORMAT(16X,'Position',3X,9('|',10X),'|')
815 FORMAT(29X,9(8A1,3X))
820 FORMAT(15X,'(Elevation)',4X,9('(',14,')',5X))
825 FORMAT('|',12X,'|',13X,'|',9(10X,'|'))
827 FORMAT(2X,'Deflection',|',112X,'|')
830 FORMAT(13X,'|',112X,'|')
832 FORMAT(5X,'(mm)',6X,2A1,' (',F6.2,')',4X,A5,8(6X,A5))
835 FORMAT(15X,2A1,' (',F6.2,')',4X,A5,8(6X,A5))
840 FORMAT('!',12X,'!',13X,'!',9(10X,'!'),///)
845 FORMAT(42X,'Table D.1: Survey displacement results, east wall.')
  STOP
  END

```

Appendix M

Data Reduction Procedure for the Slope Indicator

M.1 Introduction

The slope indicator data is reduced by a program called SI-PROG. It yields deflection profiles over the height of an instrument's casing in two orthogonal directions. SI-PROG was developed specifically as an improvement on an existing program, CIVE:SLOPIND. The new program incorporates an up to date plotting package and presents the printed results in straightforward tables. It also allows for the deflection of any point or points along the casing to be plotted against time. Most importantly, however, it includes the option of positioning the deflected profile anywhere in space. This is necessary to determine absolute displacements for casings which are free to move over their entire length. This is the case for VSI1, mounted along the outside of the east sheet pile wall. A complete description of the calculations involved in reducing the data is given below.

M.2 Calculation Procedure

The first step in reducing the slope indicator data is to decide on the sign convention to be used. This decision is made prior to running the reduction program when the field data is entered into an input file. Recall from section 4.5 that the probe is run up the slope indicator casing twice. The orientation of the fixed wheels on the

probe, defining the A plane and perpendicular to the wall, is rotated 180° between the two runs. Thus, two sets of measurements for the A and B direction inclinations are obtained.

The user can choose which direction in the A plane will be considered positive. At Boston Bar this has been declared to be outwards from the wall and towards the river (west). This automatically establishes the positive B direction to the north.

The data reduction can be made consistent with the chosen convention by ensuring the following: the data obtained with the fixed wheels in the chosen positive direction is considered as the first set, or A1 and B1. Therefore, the data obtained with the fixed wheels of the probe in the negative A direction are referred to as A2 and B2. In the data file the slope indicator readings for a particular time and depth are entered as A1, B1, A2, B2. The reading for the deepest level appear first with successive lines representing shallower readings.

As an additional note the decimals in the slope indicator readings are ignored. This is equivalent to multiplying the measurements by 10^4 and is done out of convenience. The appropriate correction of 10^{-4} is applied when the data is reduced.

The slope indicator readout provides readings of $2\sin\theta$ where θ is the angle of inclination of the probe in the casing. This angle is formed relative to the two foot

spacing of the probe's support wheels and the vertical. Therefore, by simple trigonometry, the value of $2\sin\theta$ represents the horizontal displacement of the top wheels relative to the bottom wheels.

Integrating this distance at every two foot interval allows the profile over the complete height of the casing to be determined. Note that in this procedure the base of the casing is assumed to be stationary. If this is not satisfied the shape of the casing remains the same but its absolute position in space is unknown.

The procedure outlined above is essentially the method adopted by the program SI-PROG. Two important differences exist, however. The program does not calculate the shape of the casing at a particular time. Rather, it determines the change in shape by comparing the profile at various times to an initial state. The initial configuration of the casing is considered zero displacement. In this manner the movements of points along the casing through time can be determined.

The second difference relates to the fact that two sets of measurements, each corresponding to one run of the probe in the casing, are available. The calculation procedure used by the program effectively considers the average of the two data sets. The method, described for the A direction only (it remains identical for the B direction) is described below.

Several quantities required to convert the slope indicator readings to deflection are calculated in a series

of steps.

1. Calculate the difference in the calibration readings at each depth. Note that the calibration readings represent the initial measurements taken at time zero.

$$\text{CALDIF}(J,1) = \text{CAL}(J,1) - \text{CAL}(J,3) \quad [\text{M.1}]$$

where:

$\text{CAL}(J,1)$ = initial A1 reading at measurement point J along the casing

$\text{CAL}(J,3)$ = initial A2 reading at measurement point J along the casing

Ideally the values of A1 and A2 should be equal in magnitude but opposite in sign. In practice the magnitudes are usually slightly different. This step is analogous to the first step involved in calculating an average where the available measurements are summed. The second step, dividing by the number of measurements, in this case two, is delayed until later in the calculations.

2. The same procedure is repeated for data from the epochs after the initial one.

$$\text{DIFF}(J,1) = \text{D}(J,1) - \text{D}(J,3) \quad [\text{M.2}]$$

where:

$\text{D}(J,1)$ = A1 reading at point J

$\text{D}(J,3)$ = A2 reading at point J

3. The change between the initial and subsequent difference

values at each depth is determined.

$$\text{CHNG}(J) = \text{DIFF}(J) - \text{CALDIF}(J,1) \quad [\text{M.3}]$$

Because DIFF and CALDIF are composed of the sum of two sets of readings the quantity CHNG is roughly twice what it would be if only one set of data was relied upon.

4. The quantity CHNG(J) is accumulated from the base of the casing to each particular depth along the casing.

$$\text{SOC}(J+1) = \text{SOC}(J) + \text{CHNG}(J) \quad [\text{M.4}]$$

SOC(J+1) represents the sum of the quantities CHNG(J) from the base of the casing to measurement point J. SOC(J) equals the accumulated sum of CHNG to measurement point J-1. Note that SOC(1) corresponds to the base of the casing and equals 0 (this implies fixity of the base of the casing).

All the quantities necessary to calculate deflections are now available. The deflection equation is derived below.

$$\theta = \sin^{-1} \left[\frac{\text{Slope indicator reading}}{2 \times 10^4} \right] \quad [\text{M.5}]$$

θ is the angle between the vertical and the line formed by the support wheels of the probe. The term "2" arises from the wheel spacing in feet along the probe. The "10⁴" term is the correction applied for considering the slope indicator readings as whole numbers and not as fractions.

The change in inclination can be calculated by using the quantity CHNG(J).

$$\Delta\theta = \sin^{-1}\left[\frac{\text{CHNG}(J)}{2 \times 2 \times 10^4}\right] \quad [\text{M.6}]$$

$\Delta\theta$ is the change in inclination between the current reading and the original reading at measurement point J. Recall that CHNG(J) is based on two sets of readings. This explains the second "2" term in the above equation. This completes the "averaging" of the two sets of data referred to earlier.

The amount of local deflection that has occurred since time zero at a particular depth can be calculated using $\Delta\theta$. It represents the net horizontal separation between the top and bottom support wheels since the initial period.

$$\begin{aligned} \text{Local deflection} &= 2\sin\Delta\theta \\ &= 2\sin\left[\sin^{-1}\left[\frac{\text{CHNG}(J)}{4 \times 10^4}\right]\right] \text{ feet} \\ &= 25.4 \times 24 \left[\frac{\text{CHNG}(J)}{4 \times 10^4}\right] \text{ mm} \\ &= \text{CHNG}(J) \times 25.4 \times 6 \times 10^{-4} \quad [\text{M.7}] \end{aligned}$$

The global deflection refers to the net movement between a point along the casing and the base at a particular time. It can be calculated using an equation identical in form to M.7 above except that CHNG(J) is replaced by SOC(J).

$$\text{DEF}(I, J, 1) = \text{SOC}(J+1) \times 25.4 \times 6 \times 10^{-4} \quad [\text{M.8}]$$

DEF(I, J, 1) is the global deflection at measurement point J along the casing at time I since time zero in millimeters. The index "1" refers to the A direction.

The conventional reduction of the slope indicator data is now complete. The calculations described above are carried out for all measurement points along a casing and for every epoch of data. The program SI-PROG produces summary tables of the data and the results as well as elevation/deflection plots. These plots show the deflected shape of the casing at the various times measurements were made. The program can also produce plots of deflection versus time. These plots allow the movement of selected points along the casing to be charted through time.

The conventional data reduction procedure gives deflections relative to the base of the casing. When the base is not fixed the absolute position of the casing in space is not revealed. The deflection results remain relative. The program SI-PROG incorporates the option of fixing the location of the casing in space so that absolute displacements can be determined. This option is required for VSI1. The survey results are relied upon to provide the casing position. However, this data is only available in a direction perpendicular to the wall. Therefore, absolute displacements are obtained for the A direction movements of VSI1 only. The procedure involved in the calculations is described below.

Ideally, the slope indicator casing would have been directly surveyed at a point coincident with the location of a probe measurement. Call this point P. The survey may have revealed, for example, that point P has displaced 10mm from

its original position. The slope indicator results may show that P has experienced 6mm of movement relative to the base of the casing. This implies that the bottom of the casing has moved 4mm. This quantity is referred to as a correction. Adding the correction to each slope indicator deflection translates the casing to its actual position in space. The calculation would proceed as follows.

$$\text{CORR} = \text{ABDIS} - \text{DEF}(\text{I}, \text{FIXPT}, 1) \quad [\text{M.9}]$$

$$\text{DEF}(\text{I}, \text{J}, 1) = \text{DEF}(\text{I}, \text{J}, 1) + \text{CORR} \quad [\text{M.10}]$$

CORR is the correction to be applied to the slope indicator relative deflections. ABDIS is the absolute displacement of a point along the casing referred to by the number FIXPT. DEF(I, FIXPT, 1) is the relative deflection of point FIXPT as given by the slope indicator results.

Unfortunately, VSI1 has not been directly surveyed. Thus, the quantity ABDIS is not directly available for any point along VSI1's casing. Reliance must be made on the surveying of the wall target positions in close proximity to the slope indicator. The horizontal separation between VSI1 and the nearest column of survey positions is approximately 250mm. It is assumed that the movement of the survey position used in the calculations is representative of the slope indicator casing at the same elevation. This necessarily introduces error as full satisfaction of this assumption is unlikely. Nevertheless, reference to the survey results for columns B and C indicate similar results.

This endorses the approach used as columns B and C are located on either side of VSI1.

An additional complication remains, however. In general, there will be a vertical separation between the survey position used to establish ABDIS and FIXPT, the nearest slope indicator measurement point. Therefore, Equation M.9 must be replaced by the following slightly modified expression.

$$\text{CORR} = \text{ABDIS} - \text{DEF}(I, \text{FIXPT}_{\text{INT}}, 1) \quad [\text{M.11}]$$

$\text{DEF}(I, \text{FIXPT}_{\text{INT}}, 1)$ represents the interpolated deflection of the slope indicator casing at a point called $\text{FIXPT}_{\text{INT}}$. The elevation of $\text{FIXPT}_{\text{INT}}$ is equal to the elevation of the survey position which provides ABDIS. The magnitude of $\text{DEF}(I, \text{FIXPT}_{\text{INT}}, 1)$ is determined using the slope indicator deflections immediately above and below it. The calculation is as follows.

$$\text{DEF}(I, \text{FIXPT}_{\text{INT}}, 1) = \left[\frac{A - B}{C - D} \right] E + B \quad [\text{M.12}]$$

where:

$$\begin{aligned} A &= \text{DEF}(I, J, 1) \\ B &= \text{DEF}(I, J-1, 1) \\ C &= \text{ELE}(J) \\ D &= \text{ELE}(J-1) \\ E &= \text{ELE}(\text{FIXPT}_{\text{INT}}) - D \end{aligned}$$

One last consideration concerns the fact that the survey measurements have not been made as frequently as the

slope indicator readings. This means that at an epoch where survey data is unavailable an interpolated value of absolute deflection must be used to locate the slope indicator. The interpolation is linear and uses the survey results from earlier and later epochs.

M.3 Operating Procedure

The procedure used to produce the results is given below. The data reduction program is compiled using the following command.

```
$RUN NEW:FORTTRANVS SCARDS=SI-PROG SPUNCH=SI-PROGC
```

The program is run with the following command.

```
$RUN SI-PROGC+*DISSPLA 5=datafile 1=text output 9=plot ouput
```

Post processing of the text and plot output files is identical to the procedure outlined in Appendix I.

M.4 Datafile and Program Listings

The data for each slope indicator appears in a separate file. The three files are called SI-VSI1, SI-VSI2 and SI-VSI3. An annotated version of SI-VSI1 is given below to illustrate the format of the data. This is followed by a listing of the program SI-PROG.

Annotated version of datafile SI-VSI1.

VSI1	Title	Number of plots.
0.		
0.4, Figure E.1:	VSI1, A direction absolute displacements, early epochs.	
0.55, Figure E.2:	VSI1, A direction absolute displacements, late epochs.	
1.65, Figure E.3:	VSI1, B direction displacements, early epochs.	
1.85, Figure E.4:	VSI1, B direction displacements, late epochs.	
1.5, Figure E.5:	VSI1, A direction absolute displacements/time.	
2.75, Figure E.6:	VSI1, B direction displacements/time.	
1.		
2.		
1.5.		
6.10.		
27.94, 21.59.		
19., 19.,		
11.,		
-5., 5., 15.,		
-10., 10., 110.,		
492., 1., 500.,		
4.75, 1.583,		
0., 100., 1100.,		
8.10.		
1.3.4., 494.92.		
498.353, 10.,		
21/06/84		
-3268, 154, 3306, -128,		
-3226, 151, 3262, -116,		
-3204, 119, 3236, -89,		
-3143, 179, 3159, -152,		
-3208, 52, 3260, -7,		
-3214, 86, 3238, -51,		
-3156, 104, 3182, -62,		
-3110, 90, 3144, -54,		
2.05/08/84		
66,		
-0.5,		
-3275, 154, 3309, -158,		
-3226, 134, 3268, -126,		
-3209, 162, 3245, -153,		
-3138, 198, 3163, -181,		
-3200, 25, 3249, -6,		
-3185, 77, 3219, -70,		
-3123, 123, 3140, -104,		
-3046, 94, 3090, -72,		

Title
Number of plots.

x position of plot title,
plot title.

Initial table #.
Early and late epochs split.
#s of 1st & last epoch on 1st plot.
#s of 1st & last epoch on 2nd plot.
x & y axis page lengths.
x axis lengths for ele/def1 & def1/time plots.
y axis length on plots.
Scale info, x axis A & B direction ele/def1
plots, y axis A & B def1/time plots.
y axis ele/def1 plots.
x location of waters.
x axis def1/time plots.
of depths & # of sets of readings.
See * at end of file.
Elevation of top of & angle of casing.
Calibration date.

Calibration readings,
A1, B1, A2, B2.

Symbol #, date.
Day #.
Absolute position.

A1, B1, A2, B2.

3.03/10/84				7.25/03/86	
125,				662,	
2.3,				4.4,	
-3285,	175,	3328,	-128,	-3283,	483,
-3230,	164,	3276,	-138,	-3196,	450,
-3210,	180,	3251,	-154,	-3170,	486,
-3147,	218,	3177,	-189,	-3116,	495,
-3203,	38,	3259,	-9,	-3214,	336,
-3193,	100,	3224,	-79,	-3204,	399,
-3120,	135,	3144,	-111,	-3123,	436,
-3047,	122,	3096,	-101,	-3049,	372,
4.05/12/84				8.29/07/86	
185,				788,	
6.7,				3.7,	
-3273,	260,	3306,	-268,	-3283,	438,
-3206,	235,	3246,	-251,	-3200,	427,
-3180,	274,	3214,	-292,	-3196,	436,
-3221,	309,	3144,	-315,	-3123,	484,
-3203,	129,	3258,	-136,	-3209,	286,
-3190,	187,	3212,	-208,	-3213,	374,
-3115,	252,	3138,	-274,	-3127,	406,
-3048,	231,	3088,	-238,	-3056,	417,
5.11/02/85				9.09/12/86	
251,				922,	
5.9,				5.0,	
-3282,	286,	3324,	-277,	-3256,	565,
-3208,	265,	3247,	-257,	-3172,	499,
-3180,	293,	3218,	-295,	-3148,	543,
-3127,	318,	3157,	-315,	-3088,	553,
-3215,	135,	3262,	-128,	-3175,	409,
-3207,	192,	3234,	-192,	-3155,	465,
-3117,	245,	3148,	-251,	-3083,	504,
-3033,	205,	3078,	-209,	-3048,	416,
6.29/08/85				10.16/02/87	
455,				991,	
5.2,				4.5,	
-3302,	388,	3332,	-332,	-3286,	561,
-3213,	340,	3250,	-300,	-3187,	534,
-3190,	376,	3218,	-352,	-3164,	551,
-3137,	400,	3151,	-359,	-3112,	564,
-3224,	207,	3272,	-163,	-3197,	410,
-3220,	301,	3242,	-280,	-3205,	456,
-3140,	344,	3162,	-301,	-3122,	501,
-3082,	304,	3118,	-261,	-3048,	434,
				3090,	-429,
				3330,	-543,
				3236,	-496,
				3198,	-545,
				3139,	-546,
				3252,	-394,
				3235,	-445,
				3148,	-484,
				3090,	-429,

11,25/03/87

1028.

4.0, 545, 3328, -539,
 -3273, 519, 3240, -516,
 -3182, 540, 3211, -543,
 -3163, 550, 3143, -551,
 -3109, 392, 3262, -375,
 -3194, 463, 3238, -460,
 -3195, 492, 3150, -518,
 -3118, 408, 3096, -430,
 -3039, 14.4,0.3,4.3,3.3,0.05,

4, _____
 2,ELE. 494.09 ; _____
 4,ELE. 495.31 ; _____
 7,ELE. 497.13 ; _____
 8,ELE. 497.75 ; _____
 5.3.7.85,4.75,2.75,0.05, _____

x & y of LL corner, width height, line thickness of legend box.
 # of positions on defl/time plots.

Position # & elevation of point on defl/time plot.

Same as above but for defl/time legend box.

* Explanation for line 22.

'1' = Relative displacements converted to absolute.

'3' & '4' are SI measurement points above and below elevation of survey position used to specify the absolute displacement.

'494.92' = elevation of survey point used to specify absolute displacement.


```

C
C Program name: SI-PROG
C Compiled ver: SI-PROGC
C
C Description: Program reduces slope indicator data to deflections
C and plots the results. The results are also
C tabulated in written form.
C
C Plot parameters can be input; ie axis length,
C axis scales, page orientation.
C
C Relative or absolute deflections can be plotted.
C ie. each curve can be positioned horizontally.
C This positioning can be done by referencing
C an absolute displacement to any point on the
C casing.
C Run Statement: $RUN SI-PROGC+*DISSPLA 5=input 1=output 9=plot
C file file file
C Variables:
C
C * NDEP - Number of positions along the casing at which
C readings have been taken. (Integer)
C
C * NT - Number of times the hole has been read. Note
C that the initial calibration reading is not
C included in the NT total. (Integer)
C
C * DATE - Character string that contains the date at
C which the hole was read. (Real)
C
C DEPY(NDEP) - Vector containing the depths in the hole at
C which readings have been taken. Vector has
C ndep number of elements. (Real)
C
C * CAL(NDEP,4) - Matrix containing the calibration readings with
C ndep rows and 4 columns; A1, A2, B1, B2 with
C each successive row representing a shallower
C depth. (Integer)
C CALDIF(NDEP,2) - Matrix containing the difference in calibration
C values. A1-A2 in column one and B1-B2 in column
C two. (integer)
C
C * D(NDEP,4) - Matrix containing the readings of SI data; same
C format as CAL(NDEP,4). (Integer)
C
C DIFF - Variable containing alternatively
C D(NDEP,1)-D(NDEP,2), ie A1-A2, and then
C D(NDEP,3)-D(NDEP,4), ie B1-B2. (Integer)
C
C CHNG - Variable containing alternatively
C DIFF-CALDIF(NDEP,1) and DIFF-CALDIF(NDEP,2).
C (Integer)
C

```

```

C
C      SOC - Variable containing the accumulated sum of CHNG
C      for each value of NDEP. SOC is reset to zero
C      for each new set of data. (Integer)
C
C      DEF(NT,NDEP,2) - Array storing the calculated deflection for each
C      set of readings at every depth for both the A
C      and B directions. (Real)
C
C      DEFX(NDEP) - 1d array extracted from DEF(NT,NDEP,2) containing
C      the deflection at each depth at a particular time
C      and for a particular direction, A or B. (Real)
C
C      I,J,K,L,M,N - Counters. (integer)
C
C Program:
C
C      REAL DEPY(100),DEF(100,100,2),DEFX(100),XAXIS(2),
C      .XORIG(2),XSTP(2),XMAX(2),YOR(2),YST(2),YMA(2),Y(100),
C      .X(100),WALX(2),TPOS(10)
C      INTEGER DISTYP,CAL(100,4),CALDIF(100,2),DAYNUM(100),
C      .D(100,4),DIFF(100),CHNG(100),SOC(100),WCHCRV(100),NCB(10),
C      .NCE(10),ISYM(20),FIXPT1,FIXPT2
C      DIMENSION IPKRAY(100,100),IPK(100,100)
C      CHARACTER*4 TITLE
C      CHARACTER*15 DATE(20),LGNM(20)
C      CHARACTER*75 PLOTIT(6)
C
C      Read in text and figure titles for elevation/deflection plots.
C
C      READ(5,500)TITLE
C      READ(5,510)NPLOT
C      DO 5 I=1,NPLOT
C      READ(5,502)TPOS(I),PLOTIT(I)
C      5 CONTINUE
C      READ(5,505)ITAB
C      READ(5,505)NDIV
C      DO 7 I=1,NDIV
C      READ(5,510)NCB(I),NCE(I)
C      7 CONTINUE
C
C      Read in plotting parameters.
C
C      READ(5,515)XPAGE,YPAGE
C      READ(5,515)XAXIS(1),XAXIS(2)
C      READ(5,520)YAXIS
C      READ(5,525)XORIG(1),XSTP(1),XMAX(1)
C      READ(5,525)XORIG(2),XSTP(2),XMAX(2)
C      READ(5,525)YORIG,YSTP,YMAX
C      READ(5,515)WALX(1),WALX(2)
C      READ(5,525)XOR,XST,XMA
C
C      Read in hole characteristics.
C

```

```

      READ(5,510)NDEP,NT
      READ(5,512)DISTYP, FIXPT1, FIXPT2, ELEABD
      READ(5,515)TOPELE, VANGLE
C
C Read in calibration values and set up depth vector.
C
      N=NDEP
      READ(5,500)DATE(1)
      DO 10 I=1,NDEP
      READ(5,530)(CAL(I,J),J=1,4)
      DEPY(I)=TOPELE-(N*2*0.3048)*COS(VANGLE*3.14159/180.)
      N=N-1
10 CONTINUE
      J=1
      L=1
      M=3
C
C Loop 15 sets up the tables into which the calibration data
C and results are written. The first iteration considers the
C A direction, the second works on the B direction.
C
      DO 15 K=1,2
      IF (K .EQ. 1) THEN
      WRITE(1,105)
      WRITE(1,110)
      WRITE(1,115)
      WRITE(1,110)
      ELSE
      WRITE(1,120)
      WRITE(1,110)
      WRITE(1,125)
      WRITE(1,110)
      ENDIF
C
C Loop 20 calculates the difference in calibration values and
C writes the results.
C
      DO 20 I=1,NDEP
      CALDIF(I,J)=CAL(I,L)-CAL(I,M)
      WRITE(1,130)DEPY(I),CAL(I,L),CAL(I,M),CALDIF(I,J)
20 CONTINUE
      J=J+1
      L=L+1
      M=M+1
      WRITE(1,135)
      WRITE(1,140)
15 CONTINUE
      IF (ITAB .LT. 10) THEN
      WRITE(1,142)ITAB,TITLE,DATE(1)
      ELSE
      WRITE(1,143)ITAB,TITLE,DATE(1)
      ENDIF
      ITAB=ITAB+1
C

```

```

C Main loop which does calculations on each set of data.
C
  DO 25 I=1,NT
C
C Read in set of data for a particular trip.
C
  READ(5,535)ISYM(I),DATE(I)
  READ(5,505)DAYNUM(I)
  IF (DISTYP .EQ. 1) THEN
  READ(5,520)ABDIS
  ENDIF
  WRITE(1,145)
  DO 30 K=1,NDEP
  READ(5,530)(D(K,J),J=1,4)
30 CONTINUE
C
C Loop 45 works first on the A data and then on the B data.
C It also sets up the table into which the results are written.
C
  L=1
  M=3
  DO 35 K=1,2
  IF (K .EQ. 1) THEN
  WRITE(1,150)
  WRITE(1,155)
  WRITE(1,160)
  WRITE(1,155)
  ELSE
  WRITE(1,165)
  WRITE(1,155)
  WRITE(1,170)
  WRITE(1,155)
  ENDIF
C
C Loop 60 calculates the deflections at each depth and writes
C the results.
C
  SOC(1)=0.
  DO 40 J=1,NDEP
  DIFF(J)=D(J,L)-D(J,M)
  CHNG(J)=DIFF(J)-CALDIF(J,K)
  SOC(J+1)=SOC(J)+CHNG(J)
  DEF(I,J,K)=SOC(J+1)*0.0006*25.4
40 CONTINUE
C
C Determine absolute deflections if required.
C
  IF (DISTYP .EQ. 1 .AND. K .EQ. 1) THEN
  DEFINT=((DEF(I, FIXPT2, 1)-DEF(I, FIXPT1, 1)))/
  .(DEPY(FIXPT2)-DEPY(FIXPT1)))
  .*(ELEABD-DEPY(FIXPT1))
  .+DEF(I, FIXPT1, 1)
  CORR=ABDIS-DEFINT
  DO 45 J=1,NDEP

```

```

DEF(I,J,1)=DEF(I,J,1)+CORR
45 CONTINUE
ENDIF
C
C Print the intermediate results and the deflections.
C
DO 50 J=1,NDEP
WRITE(1,175)DEPY(J),D(J,L),D(J,M),DIFF(J),CHNG(J),
.SOC(J+1),DEF(I,J,K)
50 CONTINUE
L=L+1
M=M+1
WRITE(1,180)
WRITE(1,140)
35 CONTINUE
DATE(I)(9:9)='.'
IF (ITAB .LT. 10) THEN
WRITE(1,185)ITAB,TITLE,DATE(I)
ELSE
WRITE(1,190)ITAB,TITLE,DATE(I)
ENDIF
ITAB=ITAB+1
25 CONTINUE
C
C Plotting routine for elevation/deflection graphs.
C
IJK=1
READ(5,540)XB,YB,BW,BH,TH
DO 55 K=1,2
DO 60 M=1,NDIV
NLines=0
CALL DSPDEV('PLOTTER ')
CALL UNITS('CM')
CALL PAGE(XPAGE,YPAGE)
CALL PHYSOR(5.,5.5)
CALL NOBRDR
CALL AREA2D(XAXIS(K),YAXIS)
CALL COMPLX
CALL YNAME('Elevation (m)$',100)
IF (K .EQ. 1) THEN
CALL XNAME('Displacement, Positive Outward (mm)$',100)
ELSE
CALL XNAME('Displacement, Positive Northward (mm)$',100)
ENDIF
CALL INTAXS
CALL FRAME
CALL YAXANG(0.)
CALL GRAF(XORIG(K),XSTP(K),XMAX(K),YORIG,YSTP,YMAX)
CALL BLREC(XB,YB,BW,BH,TH)
DO 65 I=NCB(M),NCE(M)
DO 70 J=1,NDEP
DEFX(J)=DEF(I,J,K)
70 CONTINUE
CALL MARKER(ISYM(I))

```

```

CALL CURVE(DEFX,DEPY,NDEP,1)
NLINES=NLINES+1
DATE(I)(9:9)='$'
CALL LINES(DATE(I),IPKRAY,NLINES)
65 CONTINUE
CALL RESET('BLNKS')
CALL MYLEGN(' ',1)
CALL LEGEND(IPKRAY,NT,XB+0.3,YB+0.3)
CALL RLVEC(0.,492.61,0.,499.07,0000)
CALL BLREC(WALX(K),7.0375,0.5,0.17,0.015)
CALL BLREC(WALX(K),3.16,0.5,0.17,0.015)
CALL MESSAG(PLOTIT(IJK),100,TPOS(IJK),-3.0)
CALL ENDPL(0)
IJK=IJK+1
60 CONTINUE
55 CONTINUE
C
C Plotting routine for deflection/time graphs.
C
CALL RESET('MARKER')
READ(5,505)NCURV
DO 75 J=1,NCURV
READ(5,535)WCHCRV(J),LGNM(J)
75 CONTINUE
READ(5,540)XB,YB,BW,BH,TH
DO 80 K=1,2
CALL PHYSOR(5.,5.)
CALL AREA2D(XAXIS(K),YAXIS)
CALL YNAME('Deflection (mm)$',100)
CALL RESET('XNAME')
CALL XREVTK
CALL FRAME
CALL GRAF(XOR,XST,XMA,XORIG(K),XSTP(K),XMAX(K))
CALL BLREC(XB,YB,BW,BH,TH)
DO 85 J=1,NCURV
DO 90 I=1,NT
X(I)=DAYNUM(I)
Y(I)=DEF(I,WCHCRV(J),K)
90 CONTINUE
CALL CURVE(X,Y,NT,1)
CALL LINES(LGNM(J),IPK,J)
85 CONTINUE
CALL RESET('BLNKS')
CALL MYLEGN(' ',1)
CALL LEGEND(IPK,NCURV,XB+0.3,YB+0.3)
CALL XGRAXS(XOR,XST,XMA,XAXIS(K),'Day Number$',-100,0.,YAXIS)
CALL XDTAXS(840601.,'MONTH',870605.,XAXIS(K),' ',1,0.,0.)
CALL RLVEC(0.,0.,1100.,0.,0000)
CALL MESSAG(PLOTIT(IJK),100,TPOS(IJK),-3.0)
CALL ENDPL(0)
IJK=IJK+1
80 CONTINUE
CALL DONEPL
C

```

C Read format statements.

C

```
500 FORMAT(A)
502 FORMAT(F6.3,A)
505 FORMAT(I10)
510 FORMAT(2I5)
512 FORMAT(3I5,F8.4)
515 FORMAT(2F8.3)
520 FORMAT(F8.3)
525 FORMAT(3F8.3)
530 FORMAT(4I10)
535 FORMAT(I5,A)
540 FORMAT(5F6.2)
```

C

C Write format statements.

C

```
105 FORMAT(////,43X,'A Direction',/)
110 FORMAT(43X,'|',11X,'|',10X,'|',10X,'|',11X,'|')
115 FORMAT(45X,'Elev. (m)',6X,'A1',9X,'A2',8X,'A1-A2')
120 FORMAT(43X,'B Direction',/)
125 FORMAT(45X,'Elev. (m)',6X,'B1',9X,'B2',8X,'B1-B2')
130 FORMAT(47X,F6.2,6X,I5,6X,I5,7X,I5)
135 FORMAT(43X,'!',11X,'!',10X,'!',10X,'!',11X,'!')
140 FORMAT(//)
142 FORMAT(43X,'Table E.',I1,': ',A,', calibration values, ',A,')
143 FORMAT(43X,'Table E.',I2,': ',A,', calibration values, ',A,')
145 FORMAT(' 9700 skipto=nextsheet')
150 FORMAT(////,29X,'A Direction',/)
155 FORMAT(29X,'|',11X,'|',8X,'|',8X,'|',9X,'|',8X,'|',8X,'|',13X
+, '|')
160 FORMAT(31X,'Elev. (m)',5X,'A1',7X,'A2',6X,'A1-A2',4X,
+'CHANGE',5X,'SOC',4X,'Deflec (mm)')
165 FORMAT(29X,'B Direction',/)
170 FORMAT(31X,'Elev. (m)',5X,'B1',7X,'B2',6X,'B1-B2',4X,
+'CHANGE',4X,'SOC',5X,'Deflec (mm)')
175 FORMAT(30X,F8.2,5X,I5,4X,I5,5X,I5,4X,I5,3X,I6,6X,F6.2)
180 FORMAT(29X,'!',11X,'!',8X,'!',8X,'!',9X,'!',8X,'!',8X,'!',13X
+, '!')
185 FORMAT(45X,'Table E.',I1,': ',A,', results from ',A)
190 FORMAT(45X,'Table E.',I2,': ',A,', results from ',A)
STOP
END
```

Appendix N

Data Reduction Procedure for the Extensometer

N.1 Introduction

As was outlined in Section 4.6 the extensometer is a simple audio device which measures the depths of vertically aligned magnets buried in the earth. The magnets are located via a probe lowered down a casing which passes through the magnets. The depth of a magnet relative to a benchmark, usually the top of the casing, is given by a measuring tape.

The data obtained from an extensometer consists of pairs of depth readings for each of the magnets mounted along the instrument. Each pair of numbers refers to the depths of the top and bottom of a magnet.

The procedure used to reduce the extensometer data is incorporated into a program called EXT-PROG. EXT-PROG reduces the data and plots the results. The calculations embodied in the program are outlined below. This is followed by an explanation of how to operate the program and a description of the datafile.

N.2 Calculation Procedure

Average values of the data for each magnet are first calculated.

$$\text{READAV}(I,J) = 0.5(\text{READTOP}(I,J) + \text{READBOT}(I,J)) \quad [\text{N.1}]$$

where:

$$I = 1 \text{ to total \# of epochs}$$

$J = 1$ to total # of magnets
 $READTOP(I,J)$ = tape reading at the top of
 the J^{th} magnet at epoch I

Note that $J=1$ refers to the lowest magnet.

The elevations of each magnet are then determined with respect to the lowest magnet in the hole. The lowest magnet is assumed to be stationary through time at a fixed elevation of zero.

$$ELE(I,J) = READAV(I,1) - READAV(I,J) \quad [N.2]$$

Note that when $J=1$, $ELE(I,1)$ is calculated as 0 which is consistent with the above assumptions.

The above calculations are carried out for every epoch of data and for every magnet along the instrument. Thus a history of the elevations of all the magnets through time is provided. More informative, however, are the changes in elevation experienced by the magnets. This is calculated as follows.

$$\Delta ELE(I) = ELE(I,J) - ELE(1,J) \quad [N.3]$$

Equation N.3 is performed for all the epochs for each magnet in turn. When all of the epochs have been dealt with $\Delta ELE(I)$ will contain the elevation changes for a particular magnet. $\Delta ELE(I)$ is then plotted against time. When this is complete Equation D.3 moves on to the next magnet.

N.3 Operating Procedure

The procedure used to produce the extensometer results is given below.

The data reduction program is compiled using the following command. The compiled version of the program will reside in a file called EXT-PROGC.

```
$RUN *FORTGTEST SCARDS=EXT-PROG SPUNCH=EXT-PROGC
```

The program is run using the command given below.

```
$RUN ASG-PROGC+*DISSPLA 5=EXT-DATA 9=-9
```

EXT-DATA is as its name suggest the file containing the extensometer data. File -9 is a plot description file (PDF) containing the results in graphical form.

Post processing of the output files is exactly the same as was outlined in Appendix I for the anchor load results.

N.4 Datafile and Program Listings

The format of EXT-DATA is explained with an annotated version of the file. This is presented below followed by a listing of the program EXT-PROG

Annotated version of EXT-DATA.

	# of epochs, # of readings/epoch.
3.6.	
Initial ele 490.002m	
Initial ele 491.395m	
Initial ele 492.453m	
Initial ele 494.290m	
Initial ele 497.278m	
Initial ele 497.875m	
123.	
8.635, 8.675,	
7.240, 7.280,	
6.180, 6.225,	
4.340, 4.390,	
1.355, 1.400,	
0.760, 0.800,	
990.	
28.4675, 28.4795,	
27.0800, 27.1120,	
26.0220, 26.0540,	
24.2600, 24.2915,	
21.4035, 21.4360,	
20.8045, 20.8360,	
1027,	
8.2940, 8.3235,	
6.9065, 6.9367,	
5.8475, 5.8780,	
4.0860, 4.1160,	
1.2317, 1.2613,	
0.6315, 0.6615,	

Legend names.

Day #.

Tape readings at magnet.

```

C
C Program Name:   EXT-PROG
C
C Compiled Ver:   EXT-PROGC
C
C Run Statement:  $RUN EXT-PROGC+*DISSPLA 5=input 9=plot file
C
C Description:    Program reduces and plots extensometer data.
C                 Plots change in depth of magnet with time.
C
C Program:
C
C   DIMENSION NDAY(20), READAV(20,20), ELE(20,20),
C     .XPLOT(20), YPLOT(20), IPKRAY(100,100)
C     LOGICAL*1 LEGNM(25,6)
C
C Read in the data.  Deepest reading are read first.
C
C   READ(5,500)NTIME,NDEP
C   DO 5 I=1,NDEP
C     READ(5,510)(LEGNM(J,I),J=1,25)
C 5  CONTINUE
C   DO 10 I=1,NTIME
C     READ(5,505)NDAY(I)
C     DO 15 J=1,NDEP
C       READ(5,515)READB,READT
C       READAV(I,J)=0.5*(READB+READT)
C 15  CONTINUE
C 10  CONTINUE
C
C Calculate the elevations w.r.t. the base (assumed to have
C zero elevation).
C
C   DO 20 I=1,NTIME
C     DO 25 J=1,NDEP
C       ELE(I,J)=READAV(I,1)-READAV(I,J)
C 25  CONTINUE
C 20  CONTINUE
C
C Plot the results.
C
C   CALL DSPDEV(' PLOTTER ')
C   CALL UNITS(' CM' )
C   CALL NOBRDR
C   CALL PAGE(27.94,21.59)
C   CALL PHYSOR(5.,5.5)
C   CALL AREA2D(19.,11.)
C   CALL COMPLX
C   CALL YNAME(' Change in elevation (mm)$',100)
C   CALL INTAXS
C   CALL YAXANG(0.)
C   CALL FRAME
C   XORIG=0.
C   XSTP=200.
C   XMAX=1100.

```

```
YORIG=-300.  
YSTP=50.  
YMAX=100.  
CALL GRAF(XORIG,XSTP,XMAX,YORIG,YSTP,YMAX)  
DO 30 J=1,NDEP  
DO 35 I=1,NTIME  
XPLOT(I)=NDAY(I)  
YPLOT(I)=(ELE(I,J)-ELE(1,J))*1000.  
35 CONTINUE  
CALL CURVE(XPLOT,YPLOT,NTIME,1)  
CALL LINES(LEGNM(1,J),IPKRAY,J)  
30 CONTINUE  
CALL XDTAXS(840601.,'MONTH',870605.,19.,' ',1,0.,0.)  
CALL MYLEGN(' ',1)  
CALL LEGEND(IPKRAY,NDEP,0.6,0.6)  
CALL BLREC(0.3,0.3,7.4,3.8,0.05)  
CALL MESSAG('Figure G.1: Extensometer results.$',100,4.8,-3.0)  
CALL DONEPL  
C  
C FORMAT STATEMENTS  
C  
500 FORMAT(2I5)  
505 FORMAT(I5)  
510 FORMAT(25A1)  
515 FORMAT(2F10.4)  
STOP  
END
```

Appendix 0
Earth Pressure Results

0.1 Introduction

This Appendix presents in tabular form the results from the earth pressure and force polygon calculations discussed in Chapter 6. Standardized tables have been produced which are applicable for all of the methods. Included are terms for:

ϕ , the internal angle of friction of the backfill.

γ , the soil unit weight in kN/m^3 .

δ , the angle of friction between the wall and the backfill.

K_a , the coefficient of lateral earth pressure.

P_a , the total active earth thrust in kN.

Three sample earth pressures; p_1 , p_2 and p_3 from the top of the wall, midway between the walers and the bottom of the wall respectively. Units are kPa.

A_1 and A_2 , the upper and lower anchor forces per metre width of wall respectively, in kN.

Only those columns appropriate to a particular solution are used.

Recall that calculations were carried out for the wall prior to extension and after its height was increased. The two conditions are identified as the low wall and the high wall in the table titles.

As well, for the earth pressure methods two additional cases were considered: the height of soil above the top of the wall was both ignored and accounted for. This was done because of uncertainty concerning whether the shallow sloping backfill above the wall would influence the earth pressures. The former case is identified in the tabular results as "no soil surcharge", the latter as "soil surcharge".

Finally, for the force polygon methods, which can account for surface point loads, calculations were done both with and without train loads. The force polygon solutions account directly for any effects of the sloping backfill. Therefore, it is unnecessary to consider the soil surcharge and no soil surcharge cases.

ϕ	γ	K_a	P_1	P_2	P_3	A_1	A_2
30.	17.	0.270	0.0	13.14	27.86	18.61	63.48
30.	18.	0.270	0.0	14.89	30.91	20.88	70.86
30.	21.	0.270	0.0	18.23	29.17	22.88	78.43
35.	17.	0.208	0.0	10.18	21.40	14.31	48.11
35.	18.	0.208	0.0	11.36	23.91	16.00	54.68
35.	21.	0.208	0.0	12.88	26.43	17.88	60.66
40.	17.	0.158	0.0	7.70	16.21	10.84	37.20
40.	18.	0.158	0.0	8.61	18.12	12.12	41.58
40.	21.	0.158	0.0	9.51	20.02	13.40	46.95
45.	17.	0.117	0.0	5.67	11.84	7.89	27.61
45.	18.	0.117	0.0	6.34	13.38	8.83	30.84
45.	21.	0.117	0.0	7.01	14.78	9.87	33.66
50.	17.	0.083	0.0	4.03	8.47	5.87	19.45
50.	18.	0.083	0.0	4.50	9.47	6.34	21.74
50.	21.	0.083	0.0	4.97	10.47	7.00	24.03

Table 0.1: Rankine earth pressure results, low wall, no soil surcharge.

ϕ	γ	K_a	P_1	P_2	P_3	A_1	A_2
30.	17.	0.270	0.0	15.16	28.88	24.84	69.78
30.	18.	0.270	0.0	16.98	32.17	27.84	77.92
30.	21.	0.270	0.0	18.73	36.87	30.44	86.20
35.	17.	0.208	0.0	11.73	22.86	18.06	53.97
35.	18.	0.208	0.0	13.11	25.86	21.30	60.32
35.	21.	0.208	0.0	14.48	28.36	23.84	68.97
40.	17.	0.158	0.0	8.88	17.39	14.44	40.88
40.	18.	0.158	0.0	9.93	19.46	16.14	45.70
40.	21.	0.158	0.0	10.88	21.48	17.83	50.51
45.	17.	0.117	0.0	6.35	12.82	10.84	30.13
45.	18.	0.117	0.0	7.32	14.32	11.89	33.67
45.	21.	0.117	0.0	8.09	16.83	13.14	37.22
50.	17.	0.083	0.0	4.85	9.08	7.88	21.38
50.	18.	0.083	0.0	5.16	10.16	8.44	23.88
50.	21.	0.083	0.0	5.74	11.23	9.33	26.41

Table 0.2: Rankine earth pressure results, high wall, no soil surcharge.

Φ	γ	K_a	P_1	P_2	P_3	A_1	A_2
30.	17.	0.270	5.24	16.38	32.80	33.26	76.79
30.	19.	0.270	6.68	20.64	36.77	37.17	86.16
30.	21.	0.270	8.47	22.70	40.64	41.08	96.68
35.	17.	0.208	4.05	14.22	28.45	28.73	61.72
35.	19.	0.208	4.93	18.66	28.44	28.76	68.94
35.	21.	0.208	6.00	17.56	31.43	31.78	76.24
40.	17.	0.166	3.07	10.77	18.28	18.48	48.78
40.	19.	0.166	3.43	12.04	21.85	21.76	52.25
40.	21.	0.166	3.76	13.30	23.61	24.07	57.78
45.	17.	0.117	2.26	7.94	14.20	14.36	34.45
45.	19.	0.117	2.93	8.67	18.46	18.05	38.90
45.	21.	0.117	3.78	9.60	17.55	17.74	42.86
50.	17.	0.083	1.60	6.63	10.08	10.19	24.45
50.	19.	0.083	1.76	6.29	11.27	11.36	27.32
50.	21.	0.083	1.86	6.96	12.45	12.56	30.20

Table 0.3: Rankine earth pressure results, low wall, soil surcharge.

Φ	γ	K_a	P_1	P_2	P_3	A_1	A_2
30.	17.	0.270	3.22	16.38	32.80	35.08	76.79
30.	19.	0.270	3.89	20.64	36.77	39.22	86.16
30.	21.	0.270	3.97	22.70	40.64	43.35	96.68
35.	17.	0.208	2.48	14.22	28.45	27.14	61.72
35.	19.	0.208	2.76	18.66	28.44	30.34	68.94
35.	21.	0.208	3.07	17.56	31.43	33.53	76.24
40.	17.	0.166	1.86	10.77	18.28	20.66	48.78
40.	19.	0.166	2.11	12.04	21.85	22.96	52.25
40.	21.	0.166	2.33	13.30	23.61	26.40	57.78
45.	17.	0.117	1.39	7.94	14.20	16.15	34.45
45.	19.	0.117	1.95	8.67	18.46	16.83	38.90
45.	21.	0.117	1.72	9.60	17.55	16.72	42.86
50.	17.	0.083	0.98	6.63	10.08	10.76	24.45
50.	19.	0.083	1.10	6.29	11.27	12.02	27.32
50.	21.	0.083	1.22	6.96	12.45	13.28	30.20

Table 0.4: Rankine earth pressure results, high wall, soil surcharge.

Φ	γ	δ	P_u	P_1	P_2	P_3	A_1	A_2
30.	17.	0.0	102.41	0.0	18.88	30.83	28.02	78.87
30.	17.	18.00	80.88	0.0	16.24	26.70	21.80	66.22
30.	17.	20.00	67.87	0.0	14.76	24.36	20.89	62.56
30.	19.	0.0	116.46	0.0	18.65	34.23	27.86	84.26
30.	19.	18.00	101.66	0.0	17.03	27.22	24.01	74.01
30.	19.	20.00	87.87	0.0	16.80	27.22	23.48	69.93
30.	21.	0.0	128.51	0.0	20.43	37.83	30.91	87.55
30.	21.	18.00	112.27	0.0	18.48	31.78	27.06	81.80
30.	21.	20.00	108.17	0.0	18.23	30.08	26.83	77.28
38.	17.	0.0	77.87	0.0	12.43	24.26	18.44	60.73
38.	17.	19.00	68.60	0.0	11.26	21.50	16.83	61.31
38.	17.	23.33	67.87	0.0	10.84	20.52	16.08	46.56
38.	19.	0.0	87.14	0.0	13.68	27.11	20.60	67.64
38.	19.	17.80	78.01	0.0	12.88	24.03	17.68	67.38
38.	19.	23.33	78.41	0.0	12.22	22.93	16.65	54.30
38.	21.	0.0	96.31	0.0	15.38	29.88	22.77	78.02
38.	21.	17.80	86.22	0.0	13.81	26.88	19.66	63.38
38.	21.	23.33	83.34	0.0	13.51	26.38	18.63	60.02
40.	17.	0.0	57.78	0.0	9.08	18.38	12.44	45.21
40.	17.	20.00	51.72	0.0	8.16	16.28	11.77	37.84
40.	17.	26.67	48.88	0.0	7.80	16.87	10.77	35.06
40.	19.	0.0	64.88	0.0	10.12	20.51	15.03	50.82
40.	19.	20.00	57.81	0.0	9.12	18.17	12.71	42.48
40.	19.	26.67	58.87	0.0	8.83	17.81	12.03	40.08
40.	21.	0.0	71.38	0.0	11.19	22.87	16.61	65.64
40.	21.	20.00	63.00	0.0	10.04	20.08	14.06	48.92
40.	21.	26.67	61.78	0.0	9.78	19.38	13.30	44.30
48.	17.	0.0	41.37	0.0	6.47	13.38	9.59	32.41
48.	17.	22.80	37.17	0.0	5.61	12.00	8.04	27.14
48.	17.	30.00	36.03	0.0	5.62	11.86	7.57	25.55
48.	19.	0.0	48.24	0.0	7.23	14.86	10.72	36.23
48.	19.	22.80	41.88	0.0	6.50	13.41	8.88	30.22
48.	19.	30.00	40.18	0.0	6.38	12.82	8.48	28.88
48.	21.	0.0	61.10	0.0	7.88	16.83	11.88	40.04
48.	21.	22.80	48.82	0.0	7.18	14.22	9.93	33.83
48.	21.	30.00	44.38	0.0	6.84	14.28	9.38	31.88
50.	17.	0.0	28.84	0.0	4.48	8.23	6.82	22.38
50.	17.	28.00	28.71	0.0	4.02	8.32	6.61	18.82
50.	17.	33.33	28.88	0.0	3.88	8.04	6.16	17.44
50.	19.	0.0	31.90	0.0	4.88	10.32	7.40	24.88
50.	19.	28.74	28.74	0.0	4.48	9.30	6.16	20.81
50.	19.	33.33	27.77	0.0	4.34	8.88	6.77	18.50
50.	21.	0.0	35.28	0.0	5.61	11.41	8.18	27.82
50.	21.	28.00	31.78	0.0	4.97	10.26	6.81	23.00
50.	21.	33.33	30.88	0.0	4.80	9.82	6.38	21.88

Table 0.5: Coulomb earth pressure results, low wall, no train.

ϕ	γ	δ	P_a	P_1	P_2	P_3	A_1	A_2
30	17	0.0	188.48	0.0	36.26	37.82	73.42	117.84
30	17	18.00	182.37	0.0	31.42	28.71	64.67	92.66
30	17	20.00	188.02	0.0	30.02	27.80	62.02	88.90
30	18	0.0	189.82	0.0	36.32	40.84	78.38	126.87
30	18	18.00	172.07	0.0	33.23	32.12	67.24	96.60
30	18	20.00	184.38	0.0	31.78	28.87	64.48	92.37
30	21	0.0	211.21	0.0	40.36	43.86	78.27	138.20
30	21	18.00	181.87	0.0	36.06	34.86	69.61	106.93
30	21	20.00	173.74	0.0	33.61	32.14	66.68	98.63
38	17	0.0	146.12	0.0	31.66	22.18	46.84	100.97
38	17	17.80	128.02	0.0	28.07	25.86	44.36	78.77
38	17	23.33	123.68	0.0	27.01	23.86	42.68	74.02
38	18	0.0	187.07	0.0	33.26	34.87	51.93	107.86
38	18	18.00	136.42	0.0	28.84	27.82	48.11	88.80
38	18	23.33	131.04	0.0	28.44	26.78	44.38	78.37
38	21	0.0	186.02	0.0	34.83	37.18	63.82	114.68
38	21	17.80	146.81	0.0	31.09	28.87	47.66	81.23
38	21	23.33	138.80	0.0	28.82	27.87	46.88	84.71
40	17	0.0	112.28	0.0	27.87	27.48	28.06	88.88
40	17	20.00	88.80	0.0	26.88	22.40	26.27	68.87
40	17	28.87	88.70	0.0	24.86	20.88	24.36	64.81
40	18	0.0	118.08	0.0	28.01	28.88	28.17	91.73
40	18	20.00	108.81	0.0	26.80	26.16	26.28	74.40
40	18	28.87	101.47	0.0	26.08	22.82	26.32	68.33
40	21	0.0	126.88	0.0	30.28	31.87	30.28	87.80
40	21	20.00	111.81	0.0	28.04	28.86	27.28	78.72
40	21	28.87	107.28	0.0	27.31	26.28	26.28	73.78
48	17	0.0	78.74	0.0	6.47	23.82	8.88	71.26
48	17	28.80	78.38	0.0	6.61	18.82	6.04	60.36
48	17	30.00	68.88	0.0	6.01	18.83	7.68	66.86
48	18	0.0	88.88	0.0	7.23	28.38	10.72	78.14
48	18	28.80	78.88	0.0	6.80	21.40	6.88	62.88
48	18	30.00	78.18	0.0	6.28	20.22	6.48	59.81
48	21	0.0	88.37	0.0	7.88	27.08	11.88	78.80
48	21	22.80	61.02	0.0	7.18	22.86	6.83	68.78
48	21	30.00	78.41	0.0	6.84	21.83	6.36	62.82
50	17	0.0	68.82	0.0	4.48	20.37	6.82	42.77
50	17	28.00	48.31	0.0	4.02	18.00	5.81	37.84
50	17	33.33	48.20	0.0	3.88	17.23	5.18	36.87
50	18	0.0	82.82	0.0	4.88	21.78	7.08	48.08
50	18	28.00	48.11	0.0	4.48	18.26	6.18	38.82
50	18	33.33	47.83	0.0	4.34	18.64	5.77	37.82
50	21	0.0	88.82	0.0	5.81	23.20	8.10	48.30
50	21	28.30	51.81	0.0	4.87	20.82	6.10	41.48
50	21	33.33	50.88	0.0	4.80	18.86	6.38	38.72

Table 0.6: Coulomb earth pressure results, low well, train.

ϕ	γ	δ	P_a	P_1	P_2	P_3	A_1	A_2
30.	17.	0.0	107.44	0.0	17.03	31.42	38.86	60.11
30.	17.	18.00	86.40	0.0	16.36	26.46	34.98	67.61
30.	17.	20.00	81.83	0.0	14.92	26.11	33.07	63.66
30.	18.	0.0	120.08	0.0	19.03	38.12	32.38	68.64
30.	18.	18.00	108.63	0.0	17.18	30.89	27.93	76.46
30.	18.	20.00	102.76	0.0	16.68	28.07	28.88	71.38
30.	21.	0.0	122.72	0.0	21.03	36.61	36.40	86.66
30.	21.	18.00	117.68	0.0	19.00	32.71	30.86	83.38
30.	21.	20.00	113.67	0.0	18.43	31.02	28.46	78.67
38.	17.	0.0	82.23	0.0	12.49	24.33	21.64	61.58
38.	17.	17.50	73.27	0.0	11.66	21.64	18.02	61.66
38.	17.	23.33	70.76	0.0	11.16	20.77	17.66	60.11
38.	18.	0.0	91.80	0.0	14.41	27.30	26.32	68.78
38.	18.	17.50	81.68	0.0	13.48	24.07	20.92	67.96
38.	18.	23.33	78.10	0.0	12.48	23.21	19.76	64.38
38.	21.	0.0	101.87	0.0	16.82	30.06	27.11	76.04
38.	21.	17.50	90.61	0.0	14.37	26.61	23.01	64.06
38.	21.	23.33	87.43	0.0	13.41	26.64	21.84	60.66
40.	17.	0.0	81.47	0.0	9.99	18.42	16.32	48.10
40.	17.	20.00	64.79	0.0	8.96	16.31	13.66	36.66
40.	17.	26.67	62.68	0.0	8.27	15.71	12.93	36.38
40.	18.	0.0	88.71	0.0	10.71	20.99	18.24	51.62
40.	18.	20.00	81.23	0.0	9.67	18.22	16.30	43.12
40.	18.	26.67	68.10	0.0	8.24	17.68	14.46	40.67
40.	21.	0.0	76.94	0.0	11.64	22.76	20.16	56.88
40.	21.	20.00	67.68	0.0	10.66	20.14	18.62	47.66
40.	21.	26.67	66.32	0.0	10.21	19.60	18.67	44.66
48.	17.	0.0	44.88	0.0	6.86	12.64	11.62	33.44
48.	17.	22.50	38.93	0.0	6.21	12.01	9.66	27.66
48.	17.	30.00	36.46	0.0	6.88	11.68	8.26	26.17
48.	18.	0.0	48.82	0.0	7.76	15.02	12.22	37.38
48.	18.	22.50	44.92	0.0	6.84	13.62	11.00	31.12
48.	18.	30.00	42.66	0.0	6.69	12.98	10.34	28.26
48.	21.	0.0	66.07	0.0	8.66	18.60	14.67	41.31
48.	21.	22.50	68.20	0.0	7.67	14.62	12.16	34.40
48.	21.	30.00	47.48	0.0	7.40	14.32	11.43	32.32
50.	17.	0.0	31.70	0.0	6.66	9.99	4.26	23.37
50.	17.	28.00	27.89	0.0	6.38	9.23	4.66	16.74
50.	17.	33.33	28.68	0.0	6.20	8.12	4.41	16.74
50.	18.	0.0	34.82	0.0	6.42	10.60	8.24	26.12
50.	18.	28.00	31.24	0.0	4.87	8.06	7.66	21.66
50.	18.	33.33	30.16	0.0	4.70	8.06	7.17	20.27
50.	21.	0.0	38.48	0.0	6.00	11.60	12.21	26.67
50.	21.	28.00	34.23	0.0	5.36	10.41	4.46	23.64
50.	21.	33.33	33.32	0.0	5.18	10.06	7.62	22.40

Table B.7: Coulomb earth pressure results, high wall, no train.

ϕ	γ	δ	P_2	P_1	P_2	P_3	A_1	A_2
30.	17.	0.0	194.65	0.0	37.26	38.32	76.22	121.43
30.	17.	18.00	167.71	0.0	32.32	30.20	67.16	86.46
30.	17.	20.00	160.24	0.0	30.66	28.10	64.62	84.48
30.	18.	0.0	208.40	0.0	38.47	41.46	76.51	120.49
30.	18.	18.00	178.19	0.0	34.24	31.78	70.96	102.71
30.	18.	20.00	170.25	0.0	32.78	30.50	67.20	89.28
30.	21.	0.0	218.88	0.0	41.87	46.68	82.80	138.84
30.	21.	18.00	188.68	0.0	38.20	38.31	72.82	108.86
30.	21.	20.00	180.28	0.0	34.62	32.69	66.64	102.02
35.	17.	0.0	162.91	0.0	32.48	32.38	61.71	103.66
35.	17.	17.50	133.26	0.0	28.91	26.90	48.08	82.26
35.	17.	23.33	127.68	0.0	27.62	24.17	44.14	76.30
35.	18.	0.0	162.46	0.0	34.20	35.02	62.88	111.02
35.	18.	17.50	141.81	0.0	30.83	28.08	47.93	86.28
35.	18.	23.33	136.66	0.0	28.40	26.18	46.04	81.66
38.	21.	0.0	172.01	0.0	38.10	37.66	66.16	116.48
38.	21.	17.50	148.93	0.0	32.16	30.20	48.92	84.31
38.	21.	23.33	143.62	0.0	30.87	28.21	47.88	87.88
40.	17.	0.0	116.60	0.0	24.80	27.55	30.85	66.72
40.	17.	28.67	102.66	0.0	28.28	22.86	28.02	71.86
40.	17.		88.78	0.0	28.68	21.18	28.08	67.08
40.	18.	0.0	123.02	0.0	30.68	28.72	30.11	64.82
40.	18.	20.00	108.10	0.0	27.32	24.37	27.14	76.86
40.	18.	28.67	104.66	0.0	27.00	22.67	24.17	71.72
40.	21.	0.0	130.28	0.0	31.61	31.90	31.25	100.92
40.	21.	20.00	116.91	0.0	28.07	28.19	28.37	81.96
40.	21.	28.67	111.12	0.0	28.22	24.89	27.28	78.41
45.	17.	0.0	82.08	0.0	8.98	23.61	11.82	71.52
45.	17.	22.60	74.46	0.0	6.21	18.90	6.88	60.42
45.	17.	30.00	72.08	0.0	6.88	16.63	6.26	67.18
45.	18.	0.0	87.22	0.0	7.76	26.21	12.22	78.26
45.	18.	22.60	78.12	0.0	6.84	21.64	11.00	62.66
45.	18.	30.00	76.68	0.0	6.88	20.28	10.24	60.24
45.	21.	0.0	82.34	0.0	6.88	27.10	14.61	78.18
45.	21.	25.80	83.76	0.0	7.97	22.84	12.68	69.18
45.	21.	30.00	81.10	0.0	7.40	21.78	11.82	62.21
50.	17.	0.0	50.68	0.0	4.88	20.08	6.28	43.41
50.	17.	26.00	47.82	0.0	4.26	17.60	6.88	37.74
50.	17.	33.33	46.40	0.0	4.20	17.06	6.41	36.61
50.	18.	0.0	64.07	0.0	6.42	21.64	6.24	48.68
50.	18.	25.00	60.46	0.0	4.87	16.08	7.68	38.72
50.	18.	33.33	48.30	0.0	4.70	16.20	7.19	37.68
50.	21.	0.0	67.24	0.0	6.00	22.88	10.21	47.82
50.	21.	25.00	63.46	0.0	5.28	20.28	8.66	41.70
50.	21.	33.33	62.20	0.0	5.18	19.66	7.92	38.97

Table 6.8: Coulomb earth pressure results, high wall, train.

ϕ	γ	δ	P_a	P_1	P_2	P_3	A_1	A_2
30	17	0.0	110.84	0.0	23.46	16.08	35.43	76.61
30	17	15.00	97.23	0.0	20.43	14.23	30.46	62.60
30	17	20.00	83.44	0.0	20.11	13.70	28.32	56.84
30	18	0.0	123.84	0.0	26.24	17.86	38.60	85.84
30	18	15.00	108.67	0.0	23.26	16.60	34.38	71.08
30	18	20.00	104.43	0.0	22.48	16.31	32.77	66.66
30	21	0.0	126.68	0.0	28.01	19.67	42.77	94.68
30	21	15.00	120.11	0.0	25.72	17.68	37.65	78.66
30	21	20.00	116.43	0.0	24.64	16.82	36.22	73.62
35	17	0.0	66.18	0.0	18.44	8.82	28.10	58.47
35	17	17.50	76.00	0.0	17.11	8.18	22.68	48.71
35	17	23.33	73.61	0.0	16.47	8.64	22.78	46.64
35	18	0.0	86.22	0.0	21.72	11.08	31.40	68.41
35	18	17.50	86.82	0.0	18.12	10.37	28.80	58.86
35	18	23.33	82.48	0.0	18.41	10.00	28.47	52.37
35	21	0.0	108.47	0.0	24.01	12.38	34.71	73.40
35	21	17.50	94.32	0.0	21.13	11.38	28.62	61.40
35	21	23.33	91.18	0.0	20.38	11.08	28.16	67.68
40	17	0.0	55.48	0.0	15.85	4.78	22.02	44.68
40	17	20.00	58.28	0.0	13.80	4.78	18.61	37.11
40	17	26.67	58.24	0.0	13.40	4.72	17.60	34.66
40	18	0.0	73.18	0.0	17.28	6.38	24.62	56.70
40	18	20.00	66.14	0.0	16.64	6.22	20.68	41.48
40	18	26.67	62.68	0.0	14.98	6.37	18.68	36.96
40	21	0.0	80.68	0.0	19.21	8.82	27.21	64.82
40	21	20.00	72.00	0.0	17.16	8.48	22.66	48.16
40	21	26.67	68.67	0.0	16.68	8.82	21.61	43.16
45	17	0.0	46.82	0.0	12.24	0.87	17.22	21.95
45	17	22.60	43.16	0.0	10.42	1.36	14.18	26.68
45	17	30.00	41.68	0.0	10.42	1.48	12.31	26.08
45	18	0.0	64.32	0.0	13.84	1.08	18.24	35.71
45	18	22.60	64.32	0.0	12.08	1.02	16.88	28.62
45	18	30.00	68.88	0.0	11.64	1.62	14.68	28.03
45	21	0.0	88.41	0.0	16.12	1.20	21.27	36.47
45	21	22.60	83.26	0.0	12.28	1.68	17.83	32.66
45	21	30.00	81.48	0.0	12.67	1.78	16.48	30.68
50	17	0.0	34.84	0.0	8.68	-1.62	12.34	21.62
50	17	28.00	20.88	0.0	6.38	-1.02	10.64	16.22
50	17	33.33	23.88	0.0	6.08	-0.86	10.08	17.10
50	18	0.0	38.72	0.0	10.68	-1.62	14.91	24.40
50	18	28.00	34.63	0.0	8.38	-1.18	12.11	20.38
50	18	33.33	33.40	0.0	8.00	-0.88	11.26	18.11
50	21	0.0	42.18	0.0	11.41	-2.02	17.48	28.97
50	21	28.00	38.21	0.0	10.37	-1.27	13.38	22.62
50	21	33.33	36.61	0.0	8.88	-1.08	12.47	21.12

Table 0.9: Oubrove earth pressure results. low wall, no train.

Φ	γ	δ	P_0	P_1	P_2	P_3	A_1	A_2
30.	17.	0.0	201.67	0.0	45.31	12.60	104.14	100.88
30.	17.	18.00	173.21	0.0	37.23	10.90	88.43	74.06
30.	17.	20.00	143.86	0.0	31.03	10.43	64.38	72.08
30.	18.	0.0	214.06	0.0	47.86	14.18	108.28	108.04
30.	18.	18.00	162.82	0.0	38.48	12.34	82.37	64.60
30.	18.	20.00	132.60	0.0	31.17	11.70	67.76	78.18
30.	21.	0.0	223.26	0.0	60.66	18.71	112.43	117.31
30.	21.	18.00	182.91	0.0	41.78	13.67	88.80	91.14
30.	21.	20.00	163.64	0.0	36.32	13.22	81.11	84.31
38.	17.	0.0	161.68	0.0	40.64	6.97	62.98	61.42
38.	17.	17.60	138.34	0.0	32.73	6.78	70.74	63.30
38.	17.	23.33	133.00	0.0	31.78	6.87	67.10	66.41
38.	18.	0.0	171.98	0.0	42.86	6.87	66.27	66.04
38.	18.	17.60	147.78	0.0	35.88	6.88	72.96	66.96
38.	18.	23.33	141.03	0.0	33.68	6.82	68.77	63.32
38.	21.	0.0	181.43	0.0	48.28	7.97	68.87	64.68
38.	21.	17.60	164.17	0.0	37.68	7.86	78.37	73.66
38.	21.	23.33	148.07	0.0	35.63	7.40	72.40	66.23
40.	17.	0.0	128.40	0.0	28.68	0.45	62.38	64.88
40.	17.	20.00	110.42	0.0	21.03	1.31	54.28	61.10
40.	17.	26.67	108.76	0.0	20.38	1.81	61.46	47.20
40.	18.	0.0	134.03	0.0	28.67	0.68	68.68	70.21
40.	18.	20.00	117.08	0.0	22.76	1.62	66.42	66.30
40.	18.	26.67	112.18	0.0	21.02	2.02	63.61	61.10
40.	21.	0.0	161.86	0.0	40.68	1.80	66.40	76.44
40.	21.	20.00	123.76	0.0	34.48	2.26	68.88	68.60
40.	21.	26.67	118.83	0.0	32.68	2.83	68.88	68.01
48.	17.	0.0	94.27	0.0	33.30	-4.36	44.86	50.76
48.	17.	22.50	84.04	0.0	28.88	-2.82	38.88	47.84
48.	17.	30.00	80.90	0.0	27.68	-2.40	36.82	37.84
48.	18.	0.0	98.85	0.0	38.00	-4.24	48.77	54.74
48.	18.	22.50	88.11	0.0	30.48	-2.68	40.44	43.68
48.	18.	30.00	85.70	0.0	29.10	-2.23	38.39	40.67
48.	21.	0.0	108.66	0.0	36.70	-4.12	48.80	53.72
48.	21.	22.50	96.18	0.0	31.68	-2.48	41.88	47.18
48.	21.	30.00	90.87	0.0	30.64	-2.06	38.80	43.70
50.	17.	0.0	64.87	0.0	20.38	-6.70	27.66	28.12
50.	17.	20.00	68.18	0.0	27.64	-6.81	24.16	21.24
50.	17.	33.33	67.36	0.0	26.68	-6.37	23.00	28.16
50.	18.	0.0	68.87	0.0	31.62	-6.87	28.64	40.98
50.	18.	28.00	62.72	0.0	26.68	-7.08	28.12	23.72
50.	18.	33.33	60.62	0.0	27.66	-6.62	23.62	31.42
50.	21.	0.0	72.48	0.0	32.26	-6.23	38.74	43.88
50.	21.	28.00	68.30	0.0	28.16	-7.23	28.08	26.11
50.	21.	33.33	68.28	0.0	28.16	-6.67	24.64	23.66

Table 6.10: Dubrova earth pressure results, low wall, train.

ϕ	γ	δ	P_a	P_1	P_2	P_3	A_1	A_2
30.	17.	0.0	107.46	0.0	23.08	12.22	39.89	69.21
30.	17.	18.00	98.40	0.0	20.33	11.31	34.12	66.26
30.	17.	20.00	91.92	0.0	18.60	11.02	32.62	65.21
30.	18.	0.0	120.08	0.0	25.80	12.67	44.98	77.28
30.	18.	18.00	108.62	0.0	22.73	12.64	38.14	66.26
30.	18.	20.00	102.75	0.0	21.61	12.32	36.34	61.70
30.	21.	0.0	122.72	0.0	28.62	15.11	48.28	85.99
30.	21.	18.00	117.85	0.0	26.12	13.86	42.17	72.11
30.	21.	20.00	113.57	0.0	24.21	13.62	40.17	68.20
35.	17.	0.0	82.22	0.0	18.78	8.81	32.28	51.21
35.	17.	17.50	72.27	0.0	16.92	8.94	27.15	43.22
35.	17.	23.23	70.78	0.0	15.86	8.60	25.72	41.07
35.	18.	0.0	81.80	0.0	21.00	6.48	36.08	57.24
35.	18.	17.50	81.86	0.0	18.64	6.82	30.28	48.42
35.	18.	23.23	79.11	0.0	17.66	6.48	28.75	45.90
35.	21.	0.0	101.57	0.0	23.21	7.16	39.68	62.27
35.	21.	17.50	90.82	0.0	20.64	7.21	33.64	52.82
35.	21.	23.23	87.42	0.0	18.74	7.16	31.77	50.72
40.	17.	0.0	61.47	0.0	15.08	1.02	26.97	38.48
40.	17.	20.00	54.78	0.0	13.27	1.89	21.48	30.82
40.	17.	28.87	52.88	0.0	12.77	1.70	20.18	29.14
40.	18.	0.0	68.71	0.0	16.67	1.16	28.02	40.74
40.	18.	20.00	61.22	0.0	14.82	1.78	23.86	34.48
40.	18.	28.87	59.10	0.0	14.27	1.60	22.86	32.97
40.	21.	0.0	78.84	0.0	18.84	1.27	32.08	48.02
40.	21.	20.00	67.66	0.0	16.78	2.10	26.60	38.08
40.	21.	28.87	66.22	0.0	15.78	2.10	24.92	36.00
45.	17.	0.0	48.58	0.0	12.01	-2.21	20.71	24.58
45.	17.	22.80	38.95	0.0	10.48	-1.48	18.88	20.84
45.	17.	30.00	38.42	0.0	10.07	-1.28	18.78	19.87
45.	18.	0.0	48.62	0.0	13.42	-2.58	22.15	27.44
45.	18.	25.80	44.82	0.0	11.72	-1.82	18.04	22.26
45.	18.	30.00	42.66	0.0	11.28	-1.60	17.61	21.86
45.	21.	0.0	58.07	0.0	14.64	-2.68	26.88	30.22
45.	21.	22.80	49.20	0.0	12.86	-1.80	20.82	25.74
45.	21.	30.00	47.48	0.0	12.44	-1.68	19.68	24.20
50.	17.	0.0	31.18	0.0	8.44	-4.44	16.22	15.22
50.	17.	28.00	27.88	0.0	6.22	-3.42	12.12	12.11
50.	17.	33.23	26.98	0.0	7.87	-3.18	12.18	12.27
50.	18.	0.0	34.82	0.0	10.58	-4.98	18.24	17.12
50.	18.	28.00	31.24	0.0	9.18	-3.62	14.68	14.65
50.	18.	33.23	30.18	0.0	8.00	-3.82	12.81	12.82
50.	21.	0.0	38.48	0.0	11.68	-5.48	20.18	18.02
50.	21.	28.00	34.82	0.0	10.18	-4.22	16.21	16.18
50.	21.	33.23	32.22	0.0	9.72	-3.60	16.08	16.28

Table 0.11: Dubrova earth pressure results, high wall, no train.

Φ	γ	δ	P_a	P_1	P_2	P_3	A_1	A_2
30	17	0.0	184.88	0.0	42.80	6.90	108.88	66.98
30	17	15.00	187.71	0.0	38.18	6.83	82.71	66.81
30	17	20.00	180.24	0.0	34.03	6.76	68.08	64.83
30	18	0.0	208.60	0.0	48.64	6.12	112.35	86.64
30	18	15.00	178.18	0.0	38.47	7.93	88.71	76.06
30	18	20.00	170.28	0.0	36.24	7.83	81.88	70.87
30	21	0.0	218.88	0.0	49.38	9.34	118.04	104.20
30	21	15.00	188.88	0.0	40.78	9.04	100.72	82.21
30	21	20.00	180.28	0.0	38.44	8.80	95.88	76.32
38	17	0.0	182.81	0.0	38.82	0.08	82.81	66.87
38	17	17.80	182.28	0.0	32.28	1.23	72.28	64.38
38	17	23.33	127.88	0.0	30.88	1.82	70.88	60.82
38	18	0.0	182.48	0.0	41.28	0.71	80.38	74.83
38	18	17.80	181.81	0.0	34.38	1.88	77.08	68.17
38	18	23.33	128.88	0.0	32.48	2.24	73.08	64.82
38	21	0.0	172.02	0.0	43.68	1.38	84.08	80.88
38	21	17.80	148.82	0.0	36.38	2.88	60.22	63.88
38	21	23.33	143.82	0.0	34.38	2.88	78.11	68.42
40	17	0.0	118.80	0.0	34.70	-5.88	88.18	51.41
40	17	20.00	102.88	0.0	28.41	-3.60	68.88	41.28
40	17	28.87	98.78	0.0	27.87	-3.08	63.78	38.38
40	18	0.0	123.03	0.0	36.72	-8.87	88.04	58.88
40	18	20.00	108.10	0.0	31.18	-2.40	68.14	44.88
40	18	26.87	104.88	0.0	28.83	-2.85	68.08	41.8
40	21	0.0	130.28	0.0	38.72	-8.48	71.88	60.28
40	21	20.00	118.81	0.0	32.18	-2.18	61.81	48.81
40	21	28.87	111.12	0.0	31.18	-2.82	68.40	48.82
48	17	0.0	82.08	0.0	31.08	-10.42	47.02	36.22
48	17	22.80	74.48	0.0	27.08	-8.38	40.84	28.82
48	17	30.00	72.08	0.0	26.86	-7.88	38.81	27.83
48	18	0.0	87.22	0.0	32.77	-11.18	48.08	38.81
48	18	27.80	78.12	0.0	28.60	-4.87	42.42	32.87
48	18	37.80	78.88	0.0	27.31	-7.82	40.27	30.22
48	21	0.0	92.38	0.0	34.47	-11.48	51.08	42.88
48	21	22.80	82.78	0.0	30.11	-8.78	44.17	38.11
48	21	30.80	81.10	0.0	28.78	-8.01	41.84	32.80
50	17	0.0	80.88	0.0	27.88	-18.87	26.88	22.81
50	17	28.00	47.83	0.0	26.31	-12.28	28.32	18.28
50	17	33.33	48.40	0.0	24.48	-12.87	24.10	18.12
50	18	0.0	88.07	0.0	28.32	-18.22	30.11	24.82
50	18	28.00	80.80	0.0	28.81	-12.82	28.81	20.87
50	18	33.33	48.30	0.0	28.72	-13.18	28.14	18.71
50	21	0.0	87.24	0.0	30.78	-17.08	31.38	28.78
50	21	28.00	82.48	0.0	27.82	-14.84	27.80	22.88
50	21	33.33	82.20	0.0	26.88	-13.74	26.18	21.21

Table 0.12: Dubrova earth pressure results, high wall, train.

ϕ	γ	δ	k_a	ρ_1	A_1	A_2
30	17	0.0	0.270	22.12	49.21	55.75
30	17	15.00	0.237	18.76	41.71	47.25
30	17	20.00	0.232	17.63	38.64	44.80
30	18	0.0	0.270	24.72	55.00	62.20
30	18	15.00	0.237	20.85	46.51	52.15
30	18	20.00	0.232	19.52	44.30	50.15
30	21	0.0	0.270	27.24	60.75	68.85
30	21	15.00	0.237	22.17	51.52	58.35
30	21	20.00	0.232	21.02	48.95	55.47
35	17	0.0	0.208	17.12	38.05	42.12
35	17	17.50	0.184	14.31	31.68	36.12
35	17	23.33	0.180	13.88	30.18	34.15
38	18	0.0	0.208	19.12	42.54	48.15
38	18	17.50	0.184	16.03	36.84	40.37
38	18	23.33	0.180	15.15	33.71	38.15
38	21	0.0	0.208	21.14	47.02	52.25
38	21	17.50	0.184	17.71	39.36	44.82
38	21	23.33	0.180	16.75	37.25	42.20
40	17	0.0	0.155	12.97	26.43	27.55
40	17	20.00	0.140	10.77	22.85	24.14
40	17	26.67	0.138	10.14	22.55	23.55
40	18	0.0	0.155	14.49	32.22	36.51
40	18	20.00	0.140	12.04	26.75	30.22
40	18	26.67	0.138	11.34	25.21	28.55
40	21	0.0	0.155	16.02	38.42	40.35
40	21	20.00	0.140	13.71	29.95	32.52
40	21	26.67	0.138	12.82	27.85	31.57
45	17	0.0	0.117	9.55	21.25	24.07
45	17	22.50	0.104	7.80	17.55	19.55
45	17	30.00	0.104	7.41	16.47	18.65
45	18	0.0	0.117	10.65	23.75	26.50
45	18	22.50	0.104	8.53	19.52	22.25
45	18	30.00	0.104	8.25	18.40	20.55
45	21	0.0	0.117	11.50	26.25	29.72
45	21	22.50	0.104	9.78	22.45	24.57
45	21	30.00	0.104	9.15	20.34	23.05
50	17	0.0	0.082	6.75	15.05	17.05
50	17	25.00	0.075	5.55	12.42	14.05
50	17	33.33	0.075	5.22	11.62	13.15
50	18	0.0	0.082	7.55	16.55	18.05
50	18	25.00	0.075	6.25	13.50	15.74
50	18	33.33	0.075	5.84	12.65	14.71
50	21	0.0	0.082	8.25	18.52	21.10
50	21	25.00	0.075	6.81	15.25	17.40
50	21	33.33	0.075	6.45	14.35	16.25

Table 0.13: Terzaghi and Peck (1968) earth pressure results. low wall, no soil surcharge.

ϕ	γ	δ	k_a	P_1	A_1	A_2
30.	17.	0.0	0.270	23.76	62.06	66.78
30.	17.	18.00	0.237	20.13	52.60	48.63
30.	17.	20.00	0.222	18.13	49.99	47.38
30.	18.	0.0	0.270	26.54	66.37	68.71
30.	18.	16.00	0.237	22.69	56.79	55.68
30.	18.	20.00	0.232	21.38	55.66	52.93
30.	21.	0.0	0.270	28.22	78.67	72.82
30.	21.	16.00	0.237	24.66	66.98	61.88
30.	21.	20.00	0.232	23.53	61.76	58.50
35.	17.	0.0	0.208	16.37	46.01	45.57
35.	17.	17.50	0.184	15.28	40.22	38.10
35.	17.	23.33	0.160	14.28	36.04	36.03
35.	18.	0.0	0.208	20.33	53.65	50.92
35.	18.	17.50	0.184	17.20	44.66	42.58
35.	18.	23.33	0.160	16.27	42.61	40.27
35.	21.	0.0	0.208	22.89	59.20	56.17
35.	21.	17.50	0.184	19.01	49.66	47.06
35.	21.	23.33	0.160	17.96	46.66	44.61
40.	17.	0.0	0.158	13.81	36.37	34.45
40.	17.	20.00	0.140	11.66	30.22	28.82
40.	17.	26.67	0.128	10.86	28.46	26.65
40.	19.	0.0	0.158	16.95	40.95	38.60
40.	19.	20.00	0.140	13.82	32.77	31.19
40.	19.	26.67	0.128	12.17	31.60	30.12
40.	21.	0.0	0.158	17.19	44.92	42.95
40.	21.	20.00	0.140	14.28	37.33	35.38
40.	21.	26.67	0.128	13.48	36.14	33.28
45.	17.	0.0	0.117	10.25	26.60	25.38
45.	17.	22.50	0.104	8.47	22.16	20.88
45.	17.	30.00	0.104	7.96	20.77	19.67
45.	19.	0.0	0.117	11.46	29.66	28.37
45.	19.	22.50	0.104	9.47	24.78	23.45
45.	19.	30.00	0.104	8.66	23.21	21.89
45.	21.	0.0	0.117	12.67	32.10	31.26
45.	21.	22.50	0.104	10.47	27.36	26.82
45.	21.	30.00	0.104	9.62	26.06	24.30
50.	17.	0.0	0.082	7.26	18.02	16.01
50.	17.	25.00	0.076	6.00	16.64	15.65
50.	17.	33.33	0.076	5.61	14.88	13.86
50.	19.	0.0	0.082	8.12	21.25	20.12
50.	19.	25.00	0.076	6.71	17.53	16.60
50.	19.	33.33	0.076	6.27	16.36	15.61
50.	21.	0.0	0.082	9.89	23.49	22.25
50.	21.	25.00	0.076	7.41	18.37	16.36
50.	21.	33.33	0.076	6.92	16.10	14.14

Table 0.14: Terzaghi and Peck (1948) earth pressure results, high wall, no soil surcharge.

ϕ	γ	δ	k_a	p_i	A_1	A_2
30.	17.	0.0	0.270	26.22	73.36	63.26
30.	17.	15.00	0.237	22.31	72.16	61.05
30.	17.	30.00	0.232	21.30	66.06	61.02
30.	18.	0.0	0.270	26.42	61.88	70.80
30.	18.	15.00	0.237	24.82	60.48	60.01
30.	18.	30.00	0.232	23.89	66.04	67.02
30.	21.	0.0	0.270	32.51	60.82	76.26
30.	21.	15.00	0.237	27.58	71.61	68.32
30.	21.	30.00	0.232	26.18	73.00	63.02
35.	17.	0.0	0.208	20.36	66.74	48.00
35.	17.	17.50	0.184	17.08	47.84	41.08
35.	17.	33.33	0.180	16.13	44.66	36.62
35.	18.	0.0	0.208	22.76	62.42	64.76
35.	18.	17.50	0.184	18.06	63.13	48.68
35.	18.	33.33	0.180	16.02	60.26	42.36
35.	21.	0.0	0.208	28.16	70.08	60.82
35.	21.	17.50	0.184	21.07	68.72	50.71
35.	21.	33.33	0.180	16.83	66.64	47.66
40.	17.	0.0	0.166	16.42	42.86	37.12
40.	17.	20.00	0.160	12.81	39.91	30.44
40.	17.	26.67	0.138	12.06	33.02	28.04
40.	18.	0.0	0.166	17.24	48.04	41.48
40.	18.	20.00	0.160	15.82	38.02	34.47
40.	18.	26.67	0.138	13.48	37.56	32.45
40.	21.	0.0	0.166	18.06	63.10	48.66
40.	21.	20.00	0.160	14.12	44.12	36.10
40.	21.	26.67	0.138	14.00	41.64	35.67
45.	17.	0.0	0.117	11.36	31.97	27.36
45.	17.	22.50	0.104	9.39	28.16	22.61
45.	17.	30.00	0.104	8.61	26.66	21.20
45.	18.	0.0	0.117	12.70	36.00	30.57
45.	18.	22.50	0.104	10.80	28.00	26.27
45.	18.	30.00	0.104	9.64	27.44	23.66
45.	21.	0.0	0.117	14.06	36.12	32.76
45.	21.	22.50	0.104	10.66	32.36	27.92
45.	21.	30.00	0.104	10.66	30.32	26.18
50.	17.	0.0	0.082	8.06	22.66	19.41
50.	17.	28.00	0.076	6.96	18.52	16.00
50.	17.	33.33	0.076	6.21	17.32	14.66
50.	18.	0.0	0.082	9.01	26.12	21.69
50.	18.	28.00	0.076	7.43	20.11	17.66
50.	18.	33.33	0.076	6.64	18.36	16.71
60.	21.	0.0	0.062	9.86	27.76	22.86
60.	21.	28.00	0.076	6.21	22.60	18.77
60.	21.	33.33	0.076	7.66	21.36	18.47

Table 6.15: Terzaghi and Peck (1966) earth pressure results, low wall, soil surcharge.

Φ	δ	k_a	P_1	A_1	A_2
30.	17.	0.270	25.32	60.64	63.38
30.	17.	0.237	23.31	64.36	63.38
30.	17.	0.232	21.20	64.98	61.03
30.	18.	0.270	26.42	60.18	70.80
30.	18.	0.237	24.83	76.43	60.01
30.	18.	0.232	23.66	72.64	67.03
30.	21.	0.270	32.61	68.67	76.28
30.	21.	0.237	27.86	66.48	66.32
30.	21.	0.232	26.19	60.28	63.03
35.	17.	0.208	20.36	62.41	49.00
35.	17.	0.184	17.08	62.28	41.08
35.	17.	0.180	16.12	48.48	38.62
35.	18.	0.208	22.78	66.78	66.76
35.	18.	0.184	18.06	66.78	48.96
35.	18.	0.180	18.03	62.27	43.38
38.	21.	0.208	28.15	77.08	60.53
38.	21.	0.184	21.07	66.88	60.71
38.	21.	0.180	18.93	61.08	47.88
40.	17.	0.188	16.42	47.26	37.12
40.	17.	0.140	12.61	38.28	30.64
40.	17.	0.138	12.08	36.98	28.04
40.	18.	0.188	17.24	62.64	41.48
40.	18.	0.140	14.32	43.80	34.47
40.	18.	0.138	13.48	41.34	32.45
40.	21.	0.188	19.08	68.40	48.36
40.	21.	0.140	16.63	48.82	38.10
40.	21.	0.138	14.60	45.69	35.67
45.	17.	0.117	11.38	26.46	27.26
45.	17.	0.104	8.26	21.98	21.20
45.	17.	0.104	6.61	21.00	21.20
45.	18.	0.117	12.70	38.84	30.67
45.	18.	0.104	10.60	32.18	25.27
45.	18.	0.104	9.84	30.18	23.69
45.	21.	0.117	14.04	42.02	32.78
45.	21.	0.104	11.60	36.67	27.62
45.	21.	0.104	10.68	32.36	26.18
50.	17.	0.083	6.08	24.72	18.41
50.	17.	0.078	6.68	20.38	16.00
50.	17.	0.078	6.21	18.08	14.86
50.	18.	0.083	8.01	27.62	21.68
50.	18.	0.078	7.43	22.78	17.68
50.	18.	0.078	6.84	21.28	16.71
50.	21.	0.083	8.86	30.56	23.96
50.	21.	0.078	8.21	28.18	18.77
50.	21.	0.078	7.68	25.63	16.47

Table 0.16: Terzaghi and Peck (1948) earth pressure results, high wall, soil surcharge.

ϕ	γ	K_a	P_i	A_1	A_2
30.	17.	0.270	17.98	50.64	55.86
30.	18.	0.270	20.09	56.80	62.32
30.	21.	0.270	22.21	62.86	68.12
35.	17.	0.208	13.81	38.17	43.28
35.	18.	0.208	15.54	42.78	48.37
35.	21.	0.208	17.18	48.38	53.46
40.	17.	0.158	10.64	28.87	32.78
40.	18.	0.158	11.77	33.18	38.64
40.	21.	0.158	13.01	38.88	44.60
45.	17.	0.117	7.78	21.87	24.18
45.	18.	0.117	8.68	24.46	27.00
45.	21.	0.117	9.59	27.01	29.64
50.	17.	0.083	5.81	16.82	17.14
50.	18.	0.083	6.16	17.34	18.16
50.	21.	0.083	6.80	18.17	21.16

Table 0.17: Terzaghi and Peck (1967) earth pressure results, low wall, no soil surcharge.

ϕ	γ	K_a	P_i	A_1	A_2
30.	17.	0.270	18.28	62.70	68.01
30.	18.	0.270	21.86	70.08	77.11
30.	21.	0.270	23.63	77.45	84.17
35.	17.	0.208	14.82	48.50	54.64
35.	18.	0.208	16.66	54.20	61.80
35.	21.	0.208	18.43	60.81	67.37
40.	17.	0.158	11.21	38.74	43.18
40.	18.	0.158	12.64	41.08	46.32
40.	21.	0.158	13.87	46.38	51.48
45.	17.	0.117	8.22	27.07	28.02
45.	18.	0.117	9.21	30.26	31.97
45.	21.	0.117	10.28	33.44	36.02
50.	17.	0.083	6.01	18.21	18.40
50.	18.	0.083	6.61	21.47	20.86
50.	21.	0.083	7.30	23.73	25.72

Table 0.18: Terzaghi and Peck (1967) earth pressure results, high wall, no soil surcharge.

ϕ	γ	K_a	P_1	A_1	A_2
30.	17.	0.270	21.38	50.23	66.95
30.	19.	0.270	23.90	67.32	74.38
30.	21.	0.270	26.42	74.40	82.21
35.	17.	0.208	16.64	46.66	51.47
35.	19.	0.208	18.48	52.07	57.83
35.	21.	0.208	20.43	57.66	63.59
40.	17.	0.162	12.53	36.26	38.89
40.	19.	0.156	14.00	38.44	43.66
40.	21.	0.156	15.46	42.80	48.17
45.	17.	0.117	9.23	26.01	26.73
45.	19.	0.117	10.32	28.07	32.11
45.	21.	0.117	11.41	32.12	35.49
50.	17.	0.083	6.55	16.46	20.38
50.	19.	0.083	7.32	20.92	22.78
50.	21.	0.083	8.08	22.80	25.19

Table 0.19: Terzaghi and Peck's (1967) earth pressure results, low wall, soil surcharge.

ϕ	γ	K_a	P_1	A_1	A_2
30.	17.	0.270	21.38	69.50	66.95
30.	19.	0.270	23.80	77.87	74.38
30.	21.	0.270	26.42	86.68	82.21
35.	17.	0.208	16.64	53.76	51.47
35.	19.	0.208	18.48	60.08	57.83
35.	21.	0.208	20.43	66.40	63.59
40.	17.	0.166	12.53	40.72	38.89
40.	19.	0.166	14.00	45.81	43.56
40.	21.	0.158	15.46	50.30	48.17
45.	17.	0.117	9.23	30.91	28.73
45.	19.	0.117	10.32	33.84	32.11
45.	21.	0.117	11.41	37.07	35.49
50.	17.	0.083	6.55	21.26	20.38
50.	19.	0.083	7.32	23.60	22.78
50.	21.	0.083	8.08	26.30	25.19

Table 0.20: Terzaghi and Peck (1967) earth pressure results, high wall, soil surcharge.

γ	P_1	A_1	A_2
17.	16.37	41.27	41.26
18.	16.30	46.12	46.10
21.	20.23	60.67	60.66

Table 0.21: Tscheboterloff (1951) earth pressure results, low wall, no soil surcharge.

γ	P_1	A_1	A_2
17.	17.67	51.61	52.90
19.	19.84	67.66	68.82
21.	21.71	83.64	83.74

Table 0.22: Tscheboterloff (1951) earth pressure results, high wall, no soil surcharge.

γ	P_1	A_1	A_2
17.	18.46	54.05	56.57
19.	21.77	61.21	62.39
21.	24.06	67.76	67.90

Table 0.23: Tscheboterloff (1951) earth pressure results, low wall, soil surcharge.

γ	P_1	A_1	A_2
17.	19.46	63.29	66.67
19.	21.77	70.72	62.39
21.	24.06	76.16	67.90

Table 0.24: Tscheboterloff (1951) earth pressure results, high wall, soil surcharge.

γ				P_1		A_1	A_2
17.				20.47		87.85	83.70
18.				22.86		84.43	71.10
21.				25.23		71.21	78.88

Table 0.23: Tscheboterloff (1973) earth pressure results, low wall, no soil surcharge.

γ				P_1		A_1	A_2
17.				21.86		71.28	88.35
18.				24.85		79.76	78.38
21.				27.13		88.18	84.43

Table 0.26: Tscheboterloff (1973) earth pressure results, high wall, no soil surcharge.

γ				P_1		A_1	A_2
17.				24.34		88.87	78.78
18.				27.21		78.82	84.67
21.				30.07		84.70	83.88

Table 0.27: Tscheboterloff (1973) earth pressure results, low wall, soil surcharge.

γ				P_1		A_1	A_2
17.				24.34		78.11	78.78
18.				27.21		88.42	84.67
21.				30.07		87.73	83.88

Table 0.28: Tscheboterloff (1973) earth pressure results, high wall, soil surcharge.

Φ	γ	k	ρ_1	A_1	A_2
30.	17.	0.385	25.62	72.12	76.73
30.	19.	0.385	26.63	60.66	66.11
30.	21.	0.385	31.96	66.14	66.49
35.	17.	0.316	21.14	69.83	66.76
35.	19.	0.316	23.62	66.56	72.62
35.	21.	0.316	26.11	72.64	61.35
40.	17.	0.286	17.15	48.30	53.37
40.	19.	0.286	19.17	52.96	59.65
40.	21.	0.258	21.18	59.67	66.62
45.	17.	0.205	12.62	36.37	42.40
45.	19.	0.205	15.23	42.88	47.36
45.	21.	0.205	16.63	47.40	62.37
50.	17.	0.168	10.64	39.97	32.79
50.	19.	0.168	11.76	22.17	26.64
50.	21.	0.158	13.01	26.66	40.60

Table 0.29: Manna & Metallene earth pressure results. low wall, no soil surcharge.

Φ	γ	k	ρ_1	A_1	A_2
30.	17.	0.385	27.48	69.35	65.56
30.	19.	0.385	30.73	66.66	61.62
30.	21.	0.385	33.66	110.37	105.69
35.	17.	0.316	22.66	72.71	70.66
35.	19.	0.316	25.35	62.36	76.69
35.	21.	0.316	28.02	91.06	67.19
40.	17.	0.266	16.40	69.60	67.27
40.	19.	0.256	20.67	66.66	64.00
40.	21.	0.256	22.73	72.66	70.74
45.	17.	0.205	14.62	47.61	45.66
45.	19.	0.205	16.34	63.10	60.66
45.	21.	0.205	16.06	66.69	60.20
50.	17.	0.158	11.31	36.74	36.16
50.	19.	0.158	12.64	41.07	26.22
50.	21.	0.158	13.97	45.38	43.66

Table 0.30: Manna & Metallene earth pressure results. high wall, no soil surcharge.

ϕ	γ	K	ρ_1	A_1	A_2
30.	17.	0.285	30.47	86.02	86.43
30.	19.	0.285	34.08	96.92	105.88
30.	21.	0.285	37.64	108.02	117.14
35.	17.	0.318	28.14	79.81	78.23
35.	19.	0.318	29.10	79.14	87.44
35.	21.	0.318	31.05	87.47	98.64
40.	17.	0.268	20.40	87.48	82.47
40.	19.	0.258	22.60	84.21	70.84
40.	21.	0.238	26.20	79.88	76.41
45.	17.	0.205	16.20	48.84	60.42
45.	19.	0.205	18.11	61.01	66.38
45.	21.	0.205	20.02	60.36	62.28
50.	17.	0.158	12.53	39.29	38.00
50.	19.	0.158	14.01	38.48	42.88
50.	21.	0.158	15.46	42.80	48.17

Table 0.31: Hanna & Metalliana earth pressure results, low wall, soil surcharge.

ϕ	γ	K	ρ_1	A_1	A_2
30.	17.	0.285	30.47	86.02	86.43
30.	19.	0.285	34.08	110.68	106.88
30.	21.	0.285	37.64	122.37	117.14
35.	17.	0.318	28.14	61.70	78.23
35.	19.	0.318	26.10	61.31	67.44
35.	21.	0.318	31.06	100.82	96.64
40.	17.	0.258	20.40	86.28	82.47
40.	19.	0.258	22.60	74.08	70.84
40.	21.	0.258	26.20	61.88	76.41
45.	17.	0.205	16.20	52.66	50.42
45.	19.	0.205	18.11	59.69	56.38
45.	21.	0.205	20.02	68.08	62.28
50.	17.	0.158	12.53	40.72	38.00
50.	19.	0.158	14.01	45.82	42.88
50.	21.	0.158	15.46	50.31	48.17

Table 0.32: Hanna & Metalliana earth pressure results, high wall, soil surcharge.

Appendix P
Factor of Safety Analyses

P.1 Sliding Factor of Safety

A factor of safety analysis based on sliding failure was carried out in conjunction with the prediction calculations presented in Chapter 6. The results were of use in characterizing which backfill parameters, from the ranges of values considered, were most appropriate. The analysis is described in the following.

The procedure examines a wedge of soil and the forces acting on it. An example is illustrated in Figure P.1a. The factor of safety against sliding is given by Hoek and Bray (1981) as:

$$FS = \frac{(W_n + A_n) \tan \phi}{W_s - A_s} \quad [P.1]$$

where W_n = the weight component of the wedge normal to the sliding surface

A_n = the component of the total anchor force normal to the sliding surface

W_s = the component of weight parallel to the sliding surface

A_s = the component of the total anchor force parallel to the sliding surface

Several assumptions are inherent in applying this equation. The wedge is assumed to behave rigidly. Despite this, however, it is assumed that wall friction, if it

exists, does not contribute any component normal or parallel to the sliding surface. The full anchor loads are assumed to be acting on the shear plane, ie; load is not lost along the anchor shaft through friction.

Note that in the Figure P.1b no forces are shown acting at the original wall boundary. In reality this will not happen until failure occurs and the wedge separates from the timber wall. To simplify the analysis all of the reaction to the anchor and gravity forces is assumed to occur at the lower slip surface.

A large number of analyses were carried out for the east wall cross-section illustrated in Figure 3.4. Different geometries, backfill parameters and anchor forces were used. Sliding surfaces at various inclinations were tested in both of the configurations shown in Figure P.1. The same combinations of ϕ , γ and δ that were discussed in Chapter 6 were repeated as well. The anchor forces were varied according to the loads present at the reference epochs. Finally, cases both with and without train loads were considered.

The calculations involved in this procedure have been incorporated into a computer program called S-FS which is listed at the end of this appendix.

P.2 Factor of Safety based on Force Equilibrium

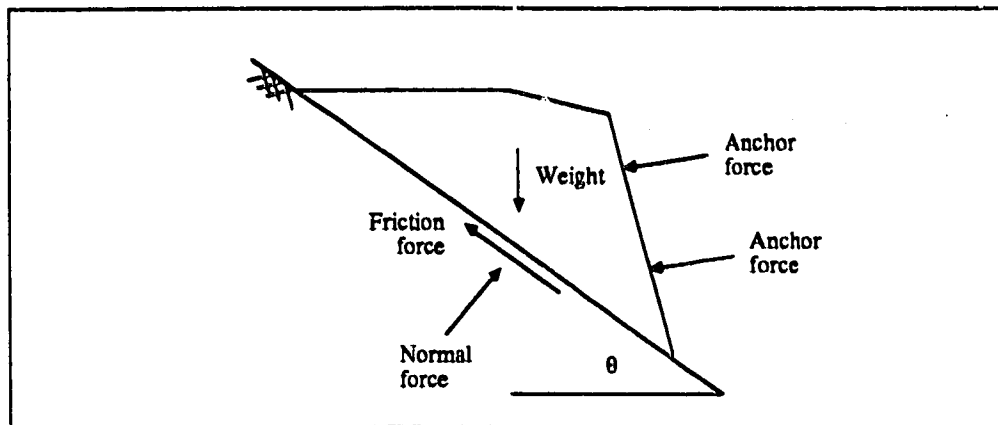
This analysis is based on the assumption that the original retaining wall has an influence on the loads the new wall experiences. Factors of safety are calculated within the context of this assumption.

The wedge of soil shown in Figure P.2 has been considered. The forces RDE, RBE and RAE and their inclinations are unknown. Their magnitudes and orientations are determined so that force equilibrium with the known anchor loads is maintained. Because of the number of unknowns, an iterative approach is adopted. A ϕ mobilized is assumed to establish the force inclinations. Equilibrium calculations then proceed in two stages. First the upper wedge BCDE is considered for calculation of forces RDE and RBE. Then the lower wedge is considered to solve for RAE and the two anchor forces, A_1 and A_2 . Because of an excess of unknowns a relationship, based on the actual anchor loads, is established between A_1 and A_2 . Once these forces are calculated they are compared to the measured anchor forces. If the results do not compare within a tolerance of 1% ϕ is adjusted slightly and the process is repeated. When the calculated anchor forces match the measured loads the mobilization of ϕ required to satisfy force equilibrium has been found. Comparing this angle to the available friction allows a factor of safety to be calculated.

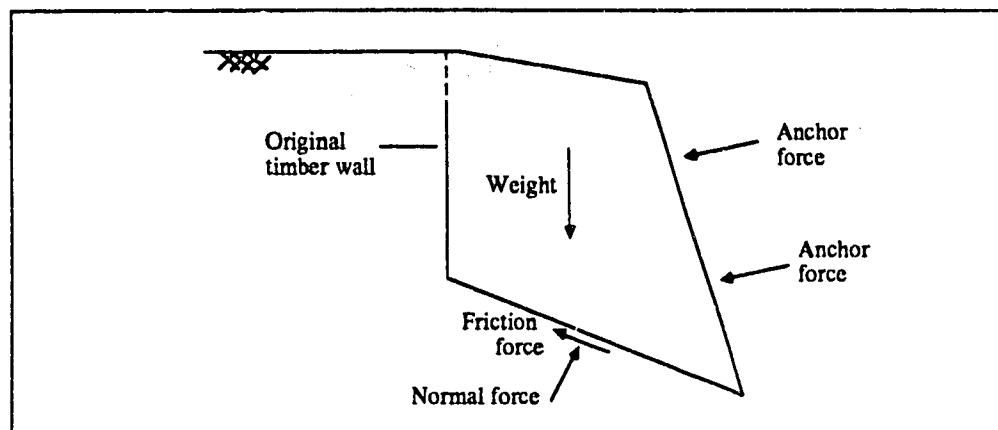
Analyses were carried out for various inclinations of AE. The ranges of backfill parameters referred to in Chapter

6 were again used as were the reference epoch anchor loads. Cases both with and without train loads were also considered.

The program which carries out these calculations, called FE-FS, is listed at the end of this appendix.



(a)



(b)

Figure P.1: Forces involved in sliding factor of safety analysis; a) general case, b) with the original timber retaining wall considered.

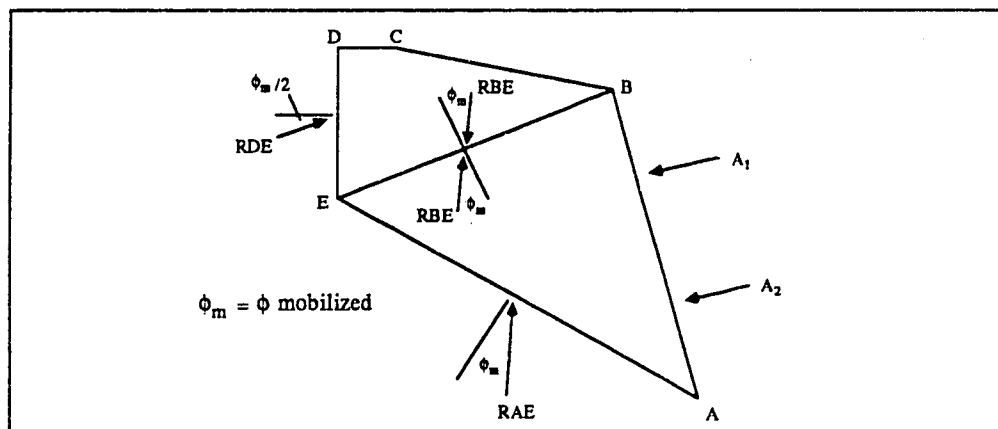


Figure P.2: Forces involved with factor of safety analysis based on force equilibrium.


```

C
C Program Name: S-FS
C Compiled Ver: S-FSC
C
C Description: Calculates sliding factor of safety for a
C wedge acted upon by two anchor forces
C and optional train load. Wedge can have
C linear or bilinear sliding surface.
C
C Run Statement: $RUN S-FSC 4=input 6=output
C Data is also requested from the screen.
C
C Program:
C
C IMPLICIT REAL(A-I,L-Z)
C
C READ(4,400)ALPHA,H,L1,BETA1,L2,BETA2,WALL,L3
C WRITE(6,600)
C READ(5,500)JTR
C PI=3.14159265
C ALPHA=ALPHA*PI/180.
C BETA1=BETA1*PI/180.
C BETA2=BETA2*PI/180.
C
C Write output table headings.
C
C WRITE(7,700)
C WRITE(7,705)
C WRITE(7,710)
C WRITE(7,705)
C
C Calculate corner coordinates and ground surface line equations.
C
C BX=H*TAN(ALPHA)
C BY=H
C CX=BX+L1*COS(BETA1)
C CY=BY+L1*SIN(BETA1)
C DX=CX+L2*COS(BETA2)
C DY=CY+L2*SIN(BETA2)
C EX=DX
C EY=DY-L3
C SLPBC=TAN(BETA1)
C INTBC=BY-SLPBC*BX
C SLPCD=TAN(BETA2)
C INTCD=CY-SLPCD*CX
C
C Calculate angles to points C and D on the backslope.
C
C ANGC=ATAN(CY/CX)
C ANGCD=ATAN(DY/DX)
C
C Loop 10 considers different PHIs.
C
C DO 10 M=1,5
C GAMMA=17.

```

```

READ(4,405)PHI,THETA
PHI=PHI*PI/180.
THETA=THETA*PI/180.
SLPSS=TAN(THETA)
C
C Loop 15 considers defferent GAMMAS
C
DO 15 N=1,3
C
C Based on which section of backslope the slip surface
C intersects calculate the area of the wedge.
C
IF (THETA .GE. ANGC) THEN
BCSSX=INTBC/(SLPSS-SLPBC)
BCSSY=SLPBC*BCSSX+INTBC
TH=SQRT(BX**2+BY**2)*SIN(PI/2.-ALPHA-THETA)
TB=SQRT(BCSSX**2+BCSSY**2)
TA=0.5*TB*TH
C
C Slip surface hits ground in front of old wall.
C
ELSEIF (THETA .GE. ANGD) THEN
CDSSX=INTCD/(SLPSS-SLPCD)
CDSSY=SLPCD*CDSSX+INTCD
BAC=ARSIN(SIN(PI/2.+ALPHA+BETA1)*
SQRT((CX-BX)**2+(CY-BY)**2)/SQRT(CX**2+CY**2))
TH1=SQRT(BX**2+BY**2)*SIN(BAC)
TB1=SQRT(CX**2+CY**2)
TH2=SQRT(CX**2+CY**2)*SIN(PI/2.-ALPHA-BAC-THETA)
TB2=SQRT(CDSSX**2+CDSSY**2)
TA=0.5*(TH1*TB1+TH2*TB2)
C
C Shallow slip surface but old wall not considered.
C
ELSEIF (THETA .LT. ANGD .AND. WALL .EQ. 0) THEN
CDSSX=INTCD/(SLPSS-SLPCD)
CDSSY=SLPCD*CDSSX+INTCD
BAC=ARSIN(SIN(PI/2.+ALPHA+BETA1)*
SQRT((CX-BX)**2+(CY-BY)**2)/SQRT(CX**2+CY**2))
TH1=SQRT(BX**2+BY**2)*SIN(BAC)
TB1=SQRT(CX**2+CY**2)
TH2=SQRT(CX**2+CY**2)*SIN(PI/2.-ALPHA-BAC-THETA)
TB2=SQRT(CDSSX**2+CDSSY**2)
TA=0.5*(TH1*TB1+TH2*TB2)
C
C Old wall considered, slip surface intersects old wall.
C
ELSE
DESSX=DX
DESSY=DX*TAN(THETA)
BAC=ARSIN(SIN(PI/2.+ALPHA+BETA1)*
SQRT((CX-BX)**2+(CY-BY)**2)/SQRT(CX**2+CY**2))
TH1=SQRT(BX**2+BY**2)*SIN(BAC)
TB1=SQRT(CX**2+CY**2)

```

```

      TH2=SQRT(CX**2+CY**2)*SIN(PI/2-ALPHA-ANGD-BAC)
      TB2=SQRT(DX**2+DY**2)
      TH3=DX
      TB3=DY-DESSY
      TA=0.5*(TH1*TB1 + TH2*TB2 + TH3*TB3)
    ENDIF
  C
  C Calculate the force vectors.
  C
    IF (JTR .EQ. 1 .AND. THETA .LT. 58.9) THEN
      W=TA*GAMMA+150.
    ELSE
      W=TA*GAMMA
    ENDIF
    WN=W*COS(THETA)
    WS=W*SIN(THETA)
  C
  C Loop 20 considers different anchor loads.
  C
    DO 20 JJ=1,3
      IF (JJ .EQ. 1) THEN
        ANCTOP=21.62
        ANCBOT=54.64
      ELSEIF (JJ .EQ. 2) THEN
        ANCTOP=27.98
        ANCBOT=47.28
      ELSE
        ANCTOP=69.68
        ANCBOT=44.88
      ENDIF
      AN=(ANCTOP+ANCBOT)*SIN(THETA+ALPHA)
      AS=(ANCTOP+ANCBOT)*COS(THETA+ALPHA)
  C
  C Calculate the factor of safety and print the results.
  C
    FS=((WN+AN)*TAN(PHI))/(WS-AS)
    WRITE(7,715)PHI*180./PI,GAMMA,ANCTOP,ANCBOT,FS
    IF (JJ .EQ. 3 .AND. N .LT. 3) WRITE(7,720)
  20 CONTINUE
    GAMMA=GAMMA+4
  15 CONTINUE
    IF (M .LT. 5) THEN
      WRITE(7,705)
    ELSE
      WRITE(7,725)
    ENDIF
  10 CONTINUE
  C
  C FORMAT STATEMENTS
  C
  400 FORMAT(8F9.5)
  405 FORMAT(2F9.5)
  500 FORMAT(I5)
  600 FORMAT(' Input 0 if no train, 1 if train')

```

```
700 FORMAT(//////)
705 FORMAT(2(' |',8X),2(' |',9X),' |',10X,3(' |',9X),2(' |',10X),
. |',8X, |')
710 FORMAT(/)
715 FORMAT(4X,F3.0,7X,F3.0,65X,2(F6.2,5X),F4.2)
720 FORMAT(9X,' |',8X,2(' |',9X),' |',10X,3(' |',9X),2(' |',10X),
. |',8X, |')
725 FORMAT(2(' !',8X),2(' !',9X),' !',10X,3(' !',9X),2(' !',10X),
. !',8X, '!')
STOP
END
```

```

C
C Program Name: FE-FS
C Compiled Ver: FE-FSC
C
C Description: Limit equilibrium for a wedge on a bilinear
C slip surface. Calculates factor of safety
C based on input anchor loads.
C Solution is iterative.
C
C Run Statement: $RUN FE-FSC+CIVE:STRULIB 4=input 6=output
C
C Program:
C
C REAL AM(2,2),CM(2,1),RMO(2,1),L1,L2,L3,N
C READ(4,400)ALPHA,H,L1,BETA1,L2,BETA2,L3
C READ(4,405)ANCT,ANCB,TRAIN
C WRITE(6,600)
C WRITE(6,405)ANCT,ANCB,TRAIN
C WRITE(6,610)
C N=ANCB/ANCT
C PI=3.141592654
C ALPHA=(ALPHA*PI)/180.
C BETA1=(BETA1*PI)/180.
C BETA2=(BETA2*PI)/180.
C
C Calculate coordinates of corners of wedge.
C
C BX=H*TAN(ALPHA)
C BY=H
C CX=BX+L1*COS(BETA1)
C CY=BY+L1*SIN(BETA1)
C DX=CX+L2*COS(BETA2)
C DY=CY+L2*SIN(BETA2)
C EX=DX
C EY=DY-L3
C
C THETA is inclination of lower wedge slip surface.
C CHI is inclination of upper wedge slip surface.
C
C THETA=ATAN(EY/EX)
C CHI=ATAN((BY-EY)/(EX-BX))
C
C Calculate the area of the upper wedge.
C
C A1S=0.5*(DX-CX)*(DY-EY)
C A1B=0.5*SQRT((EX-BX)**2+(BY-EY)**2)*SIN(BETA1+CHI)*L1
C
C Calculate the area of the lower wedge.
C
C A2=0.5*SQRT(EX**2+EY**2)*SIN(PI/2-ALPHA-THETA)
C .*SQRT(BX**2+BY**2)
C
C Loop 10 considers different GAMMAs.
C
C PHIU=(4.9*PI/180.)

```

```

      GAMMA=17.
      DO 10 I=1,3
15  PHIU=PHIU+0.1*PI/180.
C
C Calculate forces on the upper wedge.
C
      IF (TRAIN .EQ. 1) THEN
          W1=(A1S+A1B)*GAMMA+150.
      ELSE
          W1=(A1S+A1B)*GAMMA
      ENDIF
C
C If PHIU GE CHI then use CHI.  PHIU is PHI utilized.
C PHIT is inclination of resultant not in excess of CHI.
C
      IF (PHIU .GE. CHI) THEN
          PHIT=CHI
      ELSE
          PHIT=PHIU
      ENDIF
C
C Sum the x forces on the upper wedge.
C
      AM(1,1)=-COS(PHIT/2)
      AM(1,2)=COS(PHIT+PI/2-CHI)
      CM(1,1)=0.
C
C Sum the y forces on the upper wedge.
C
      AM(2,1)=SIN(PHIT/2)
      AM(2,2)=SIN(PHIT+PI/2-CHI)
      CM(2,1)=W1.
C
C Solve the matrix for the forces RDE and RBE.
C
      CALL SIMQ(AM,CM,RMO,2,KS)
      IF (KS .NE. 0) WRITE(7,700)KS
      RDE=RMO(1,1)
      RBE=RMO(2,1)
C
C Calculate the forces on the lower wedge.
C
      W2=A2*GAMMA
C
C If PHIU is greater THEATA then use THETA.
C
      IF (PHIU .GE. THETA) THEN
          PHIB=THETA
      ELSE
          PHIB=PHIU
      ENDIF
C
C Sum the x forces on the lower wedge.
C

```

```

AM(1,1)=COS(ALPHA)*(1+N)
AM(1,2)=-COS(PHIB+PI/2-THETA)
CM(1,1)=RBE*COS(PHIT+PI/2-CHI)
C
C Sum the y forces on the lower wedge.
C
AM(2,1)=-SIN(ALPHA)*(1+N)
AM(2,2)=SIN(PHIB+PI/2-THETA)
CM(2,1)=RBE*SIN(PHIT+PI/2-CHI)+W2
C
C Solve the matrix for the forces A1 and RAE.
C
CALL SIMQ(AM,CM,RMO,2,KS)
IF (KS .NE. 0) WRITE(7,700)KS
A1C=RMO(1,1)
RAE=RMO(2,1)
C
C Test calculated results against measured results.
C
IF (ABS((A1C/ANCT)-1) .GT. 0.01) GOTO 15
C
C Otherwise calculate FS for different PHI availables and
C print the results.
C
PHIAV=30.
DO 20 J=1,5
WRITE(6,615)GAMMA,PHIAV,PHIB*180./PI,A1C,N*A1C,
.TAN(PHIAV*PI/180.)/TAN(PHIB)
PHIAV=PHIAV+5.
20 CONTINUE
WRITE(6,620)
GAMMA=GAMMA+2
10 CONTINUE
C
C Format Statements
C
400 FORMAT(7F10.5)
405 FORMAT(3F7.2)
600 FORMAT(//,' ANCT ANCB TRAIN' )
610 FORMAT(/,' GAMMA PHIAV PHIB A1 A2=NA1 FS' )
615 FORMAT(6F8.3)
620 FORMAT(/)
700 FORMAT(' KS = ' ,I1,' IF KS=0 THEN CORRECT SOLUTION' ,/)
STOP
END

```

Appendix Q

Miscellaneous Computer Programs

This appendix includes the listings for two of the computer programs used in Chapter 6. The first, called FP-PROG, performs the force polygon calculations for the Coulomb and Dubrova earth pressure predictions. The second, called B-PROG, is an implementation of the modified Boussinesq solution described in Section 6.3.7.


```

C
C Program Name:  FP-PROG
C
C Description:   Program does a force polygon solution for
C               Coulomb (PHI constant) or Dubrova (PHI a
C               function of z).  Program can account for
C               presence or absence of train load on outer
C               most rail.  PHI=30 to 50, GAMMA=17 to 19,
C               DELTA=0, 1/2, 2/3 of PHI.
C
C               JANAL = '0' if Coulomb, '1' if Dubrova
C               JTRAIN = '0' if no train, '1' if train.
C
C Run Statement: run -hope**displa 4=input 7=text output 9=pdf
C               8=sample pressure data points for plotting
C
C Program:
C
C   IMPLICIT REAL(A-I,L-Z)
C   DIMENSION P(5,3,3,55),PP(55),PRESS(5,3,3,55),ELE(55),
C   .JPKRAY(100,100)
C   LOGICAL*1 TITLE(70,2)
C
C   READ(4,400)(TITLE(I,1),I=1,70)
C   READ(4,400)(TITLE(I,2),I=1,70)
C   READ(4,405)ALPHA,H,ELET,L1,BETA1,BETA2
C   READ(4,410)JANAL,JTRAIN
C   PI=3.14159265
C   ALPHA=ALPHA*PI/180.
C   BETA1=BETA1*PI/180.
C   BETA2=BETA2*PI/180.
C   PHI=30.*PI/180.
C
C Write output table headings.
C
C   WRITE(7,700)
C   WRITE(7,705)
C   WRITE(7,710)
C   WRITE(7,705)
C
C Loop 10 determines pressure distribution for different PHIs.
C Loop 12 considers different GAMMAs, 14, different DELTAs.
C
C   DO 10 M=1,5
C   GAMMA=17.
C   DO 12 MM=1,3
C   DO 14 MJ=1,3
C   IF (MJ .EQ. 1) DELTA=0.0
C   IF (MJ .EQ. 2) DELTA=PHI/2.
C   IF (MJ .EQ. 3) DELTA=2.*PHI/3.
C   Z=0.00
C
C Loop 15 considers wall from z=0 to z=H.
C
C   DO 15 J=1,46

```

```

PAMAX=0.0
THEMAX=0.0
IF (JANAL .EQ. 0) THEN
  CPHI=PHI
ELSE
  CPHI = PHI * (0.019179133*(Z**2) - 0.1238972*Z + 1)
ENDIF

C
C Calculate coordinates.
C
  BX=Z*TAN(ALPHA)
  BY=Z
  CX=BX+L1*COS(BETA1)
  CY=BY+L1*SIN(BETA1)
  ANGZTR=ATAN(CY/(CX+0.18))
  ANGZC=ATAN(CY/CX)
  SLPBC=TAN(BETA1)
  INTBC=BY-SLPBC*BX
  SLPCC=TAN(BETA2)
  INTCC=CY-SLPCC*CX
  IF (Z .GT. 0) THEN
    ITHETA=PI/2.-ALPHA-(9.9*PI/180.)
  ELSE
    ITHETA=BETA1
  ENDIF

C
C Loop 20 calculates maximum earth thrust for a wedge at a
C particular elevation.
C
  K=0
  20 K=K+1
  THETA=ITHETA-(K)*(0.1*PI/180.)
  SLPSS=TAN(THETA)
  BCSSX=INTBC/(SLPSS-SLPBC)
  BCSSY=SLPBC*BCSSX+INTBC
  CCSSX=INTCC/(SLPSS-SLPCC)
  CCSSY=SLPCC*CCSSX+INTCC
  DBCSS=SQRT(BCSSX**2+BCSSY**2)
  DCCSS=SQRT(CCSSX**2+CCSSY**2)

C
C Calculate wedge area.
C
  IF (Z .EQ. 0) THEN
    IF (THETA .GE. BETA1) THEN
      TA=0.
    ELSE
      TH=SQRT(CX**2+CY**2)*SIN(BETA1-THETA)
      TB=DCCSS
      TA=0.5*TB*TH
    ENDIF
  ELSE
    IF (THETA .GE. ANGZC) THEN
      TH=SQRT(BX**2+BY**2)*SIN(PI/2.-ALPHA-THETA)
      TB=DBCSS
    
```

```

      TA=0.5*TB*TH
    ELSE
      BAC=ARSIN(SIN(PI/2.+ALPHA+BETA1)*
      SQRT((CX-BX)**2+(CY-BY)**2)/SQRT(CX**2+CY**2))
      TH1=SQRT(BX**2+BY**2)*SIN(BAC)
      TB1=SQRT(CX**2+CY**2)
      TH2=SQRT(CX**2+CY**2)*SIN(PI/2.-ALPHA-BAC-THETA)
      TB2=SQRT(CCSSX**2+CCSSY**2)
      TA=0.5*(TH1*TB1+TH2*TB2)
    ENDIF
  ENDIF
C
C Calculate the weight and lateral thrust of the trial wedge.
C
  IF (JTRAIN .EQ. 1 .AND. THETA .LT. ANGZTR) THEN
    W=TA*GAMMA+150.
  ELSE
    W=TA*GAMMA
  ENDIF
  PA=W*SIN(THETA-CPHI)/
  .SIN(PI/2.-ALPHA+DELTA-THETA+CPHI)
C
C Test if PA is maximum.
C
  IF (PA .GT. PAMAX) THEN
    PAMAX=PA
    THEMAX=THETA*180./PI
  ENDIF
  IF (THETA .GT. (ANGZTR-(5.*PI/180.))) GOTO 20
C
C When all trial slip surfaces at particular Z have been tried
C store max thrust and increment Z.
C
  P(M,MM,MJ,J)=PAMAX
  Z=Z+H/45.0
15 CONTINUE
14 CONTINUE
  GAMMA=GAMMA+2.
12 CONTINUE
  PHI=PHI+5.*PI/180.
10 CONTINUE
C
C Calculate horizontal component of pressure over wall height.
C
  DLEN=(H/45.)/COS(ALPHA)
  PHI=30.
  DO 30 M=1,5
    GAMMA=17.
    DO 40 MM=1,3
      DO 50 MJ=1,3
        IF (MJ .EQ. 1) DELTA=0.
        IF (MJ .EQ. 2) DELTA=PHI/2.
        IF (MJ .EQ. 3) DELTA=2.*PHI/3.
        RDELTA=DELTA*PI/180.

```

```

DO 60 J=2,46
DELFOR=P(M,MM,MJ,J)-P(M,MM,MJ,J-1)
PRESS(M,MM,MJ,J-1)=(DELFOR/DLEN)*COS(RDELTA-ALPHA)
ELE(J-1)=ELET+(0.5*H/45.)-(J-1)*H/45.)
60 CONTINUE
C
C Calculate anchor forces. Extract pressures half way between
C walers, at top and at bottom. Calculate total horiz thrust.
C
IF (H .EQ. 6.02) THEN
  PMID=PRESS(M,MM,MJ,22)
  ANCT=0.5*(P(M,MM,MJ,22)+P(M,MM,MJ,23))*COS(RDELTA)
ELSE
  PMID=0.5*(PRESS(M,MM,MJ,23)+PRESS(M,MM,MJ,24))
  ANCT=P(M,MM,MJ,24)*COS(RDELTA)
ENDIF
ANCB=(P(M,MM,MJ,46)*COS(RDELTA)) - ANCT
PTOP=0.0
PBOT=PRESS(M,MM,MJ,45)
THRUST=P(M,MM,MJ,46)*COS(RDELTA-ALPHA)
C
C Write out the results.
C
WRITE(7,715)PHI,GAMMA,DELTA,THRUST,PTOP,PMID,PBOT,ANCT,ANCB
IF (MJ .EQ. 3 .AND. MM .LT. 3) WRITE(7,720)
50 CONTINUE
GAMMA=GAMMA+2
40 CONTINUE
PHI=PHI+5.
IF (M .LT. 5) THEN
  WRITE(7,705)
ELSE
  WRITE(7,725)
ENDIF
30 CONTINUE
WRITE(7,730)(TITLE(IJ,2),IJ=1,70)
C
C Plot sample pressure distributions (GAM=19, DEL=PHI/2)
C
CALL DSPDEV(' PLOTTER ')
CALL UNITS(' CM ')
CALL NOBRDR
CALL PAGE(27.94,21.59)
CALL PHYSOR(5.,6.)
CALL AREA2D(19.,11.)
CALL COMPLX
CALL YNAME(' Elevation (m)$',100)
CALL XNAME(' Pressure (kPa)$',100)
CALL INTAXS
CALL YAXANG(0.)
CALL FRAME
XORIG=60.
XSTP=5.
XMAX=-20.

```

```

YORIG=492.
YSTP=1.
YMAX=500.
CALL GRAF(XORIG,XSTP,XMAX,YORIG,YSTP,YMAX)
DO 70 I=1,5
DO 80 K=1,45
PP(K)=PRESS(1,2,2,K)
80 CONTINUE
CALL CURVE(PP,ELE,45,1)
CALL MESSAG(TITLE(1,1),100,3.,-2.5)
70 CONTINUE
CALL DONEPL
C
C Output pressures for PHI=40, GAMMA=19, DELTA=20
C
WRITE(8,800)(TITLE(IJ,2),IJ=1,70)
DO 90 K=1,45
WRITE(8,805)ELE(K),PRESS(3,2,2,K)
90 CONTINUE
C
C FORMAT STATEMENTS
C
400 FORMAT(70A1)
405 FORMAT(6F12.4)
410 FORMAT(2I3)
700 FORMAT(////////)
705 FORMAT(2(' '|',8X),2(' '|',9X),'|',10X,3(' '|',9X),2(' '|',10X),
.' '|',8X, '|')
710 FORMAT(/)
715 FORMAT(4X,F3.0,6X,F3.0,5X,F5.2,15X,F6.2,4X,3(F6.2,4X),
.1X,2(F6.2,5X))
720 FORMAT(9X,' '|',8X,2(' '|',9X),'|',10X,3(' '|',9X),2(' '|',10X),
.' '|',8X, '|')
725 FORMAT(2('!' ,8X),2('!' ,9X),'|!',10X,3('!' ,9X),2('!' ,10X),
.'!' ,8X, '|')
730 FORMAT(///,30X,70A1)
800 FORMAT(//,70A1,/)
805 FORMAT(2F12.3)
STOP
END

```

```

C
C Program Name:   B-PROG
C
C Compiled Ver:   B-PROGC
C
C Description:    Calculates pressure distribution due to line
C                loads according to the Boussinesq procedure.
C
C Run Statement:  $run b-progc+*displa 5=b-dat 7=-7 8=-8 9=-9
C
C Program:
C
C   REAL M(4),SIG(5,200),ELE(200),XPLOT(200),YPLOT(200),
C   .IPKRAY(100,100)
C   LOGICAL*1 LEGNM(20,5),FIGTIT(70,2)
C
C Establish constants. Vector M gives horizontal
C distances from rails to top of wall.
C
C   QL=150.
C   M(1)=3.18
C   M(2)=4.615
C   M(3)=7.78
C   M(4)=9.215
C
C Read in height of wall, distance of top of wall below
C surface and titles.
C
C   READ(5,500)HW,HT
C   READ(5,510)(FIGTIT(I,1),I=1,70)
C   READ(5,510)(FIGTIT(I,2),I=1,70)
C   DO 5 J=1,5
C   READ(5,520)(LEGNM(I,J),I=1,20)
C   5 CONTINUE
C
C Calculate pressure from each rail of the two tracks.
C
C   DO 10 I=1,4
C   WRITE(7,700)
C
C Set Z so that first pressure calculation is carried out
C at the top of the wall.
C
C   Z=HT
C   N=0
C   20 N=N+1
C   ELE(N)=499.77-Z
C   D=(M(I)+(Z-0.7)*TAN(0.1745329252))/HW
C   ZN=Z/HW
C   TOP=1.28*(D**2)*ZN*QL
C   BOT=((D**2+ZN**2)**2)*HW
C   SIG(I,N)=TOP/BOT
C
C Write out the results.
C

```

```

FLAG=((N-7)/5.)-AINT((N-7)/5.)
IF ((FLAG .EQ. 0) .OR. (N .EQ. 1) .OR. (N .EQ. 130))
.WRITE(7,710)N,Z,ELE(N),SIG(I,N)
C
C Increment Z and compare to depth below surface of wall base.
C
Z=Z+0.0500
IF (Z .LT. 7.16) GOTO 20
10 CONTINUE
C
C Integrate pressure from outer rail to calculate contribution
C to anchor loads.
C
TOTF=0.000
IF (HW .EQ. 6.02) THEN
NUMPRS=121
ELSE
NUMPRS=130
ENDIF
NUMINT=NUMPRS-1
DO 35 I=1,NUMINT
FINT=0.5*(SIG(1,I)+SIG(1,I+1))*0.05
TOTF=TOTF+FINT
IF (HW .EQ. 6.02 .AND. I .EQ. 57) ATOP=TOTF
IF (HW .EQ. 6.46 .AND. I .EQ. 66) ATOP=TOTF
35 CONTINUE
ABOT=TOTF-ATOP
WRITE(8,800)ATOP,ABOT
C
C Write out all results from outer rail to file 8.
C
IF (HW .EQ. 6.02) THEN
WRITE(8,805)
ELSE
WRITE(8,810)
ENDIF
DO 25 J=1,N
WRITE(8,500)ELE(J),SIG(1,J)
25 CONTINUE
C
C Calculate the sum of the pressure from the outer 2 rails.
C
DO 30 J=1,N
SIG(5,J)=SIG(1,J)+SIG(2,J)
30 CONTINUE
C
C Plot the pressure distributions.
C
CALL DSPDEV(' PLOTTER ')
CALL UNITS(' CM' )
CALL NOBRDR
CALL PAGE(27.94,21.59)
CALL PHYSOR(5.5,6.)
CALL AREA2D(19.,11.)

```

```

CALL COMPLX
CALL YNAME('Elevation (m)$',100)
CALL XNAME('Pressure (kPa)$',100)
CALL INTAXS
CALL YAXANG(0.)
CALL FRAME
XORIG=60.
XSTP=5.
XMAX=-20.
YORIG=492
YSTP=1.
YMAX=500.
CALL GRAF(XORIG,XSTP,XMAX,YORIG,YSTP,YMAX)
DO 40 I=1,5
DO 50 J=1,N
XPLOT(J)=SIG(I,J)
YPLOT(J)=ELE(J)
50 CONTINUE
CALL CURVE(XPLOT,YPLOT,N,140)
CALL LINES(LEGNM(1,I),IPKRAY,I)
40 CONTINUE
CALL MESSAG(FIGTIT(1,1),100,1.70,-3.)
CALL MESSAG(FIGTIT(1,2),100,1.70,-3.6)
IF (HW .EQ. 6.02) THEN
CALL RLVEC(0.,492.61,0.,498.63,0000)
ELSE
CALL RLVEC(0.,492.61,0.,499.07,0000)
ENDIF
CALL BLREC(14.25,3.1600,0.5,0.17,0.015)
CALL BLREC(14.25,7.0375,0.5,0.17,0.015)
CALL MYLEGN(' ',1)
CALL LEGEND(IPKRAY,5,0.6,7.75)
CALL BLREC(0.3,7.45,5.4,3.25,0.05)
CALL DONEPL

C
C FORMAT STATEMENTS
C
500 FORMAT(2F12.3)
510 FORMAT(70A1)
520 FORMAT(20A1)
700 FORMAT(/,'      N          Z          ELE          SIG')
710 FORMAT(I5,3F10.2)
800 FORMAT(/,' Top anchor   Bottom anchor: ',2F10.3,/)
805 FORMAT(/,' Boussinesq press, outer rail; low wall. '//)
810 FORMAT(/,' Boussinesq press, outer rail; high wall. '//)
STOP
END

```